

WD-A185 113

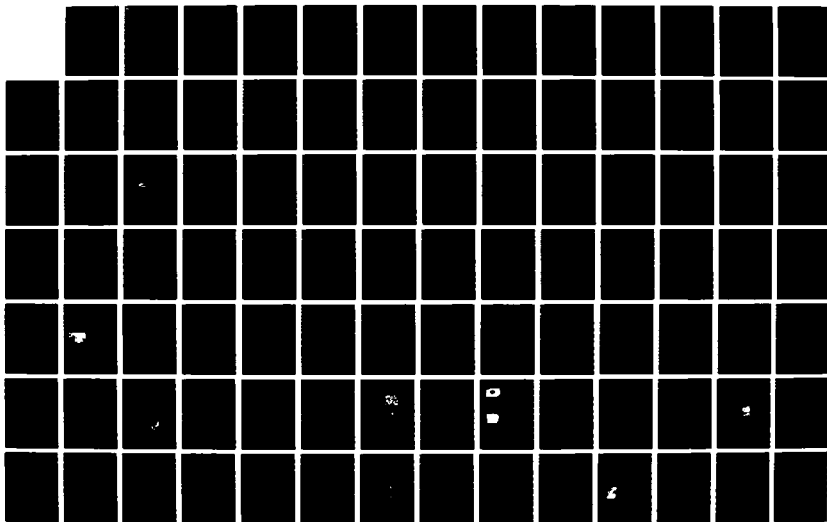
UNITED STATES - JAPAN WORKSHOP ON DIELECTRIC AND
PIEZOELECTRIC CERAMICS ((3RD)) HELD IN TOYAMA JAPAN ON
NOVEMBER (9)-(12) (1986)(U) KEIO UNIV TOKYO (JAPAN)
30 JUL 87

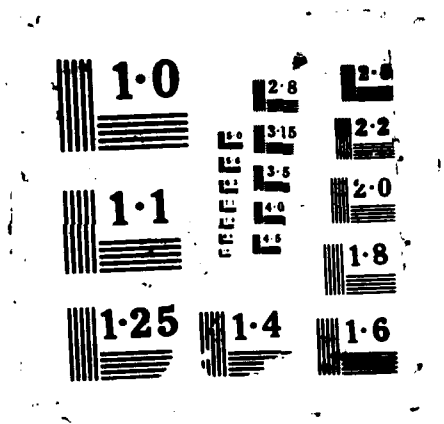
1/3

UNCLASSIFIED

F/G 11/2

NL





DTIC FILE COPY

12

AD-A185 113

THIRD U.S. - JAPAN WORKSHOP

ON DIELECTRIC AND PIEZOELECTRIC CERAMICS

NOVEMBER 9-12, 1986
TOYAMA JAPAN

Prepared For: The Office of Naval Research

July 30, 1987

SEP 25 1987

A

Approved
for sale, its
content is
unclassified

87 0 012

DISCLAIMER NOTICE

**THIS DOCUMENT IS BEST QUALITY
PRACTICABLE. THE COPY FURNISHED
TO DTIC CONTAINED A SIGNIFICANT
NUMBER OF PAGES WHICH DO NOT
REPRODUCE LEGIBLY.**

THIRD U.S. - JAPAN WORKSHOP

ON DIELECTRIC AND PIEZOELECTRIC CERAMICS

NOVEMBER 9-12, 1986
TOYAMA JAPAN

Prepared For: The Office of Naval Research

July 30, 1987

TABLE OF CONTENTS

INTRODUCTION

SUGGESTIONS FOR FUTURE WORKSHOPS

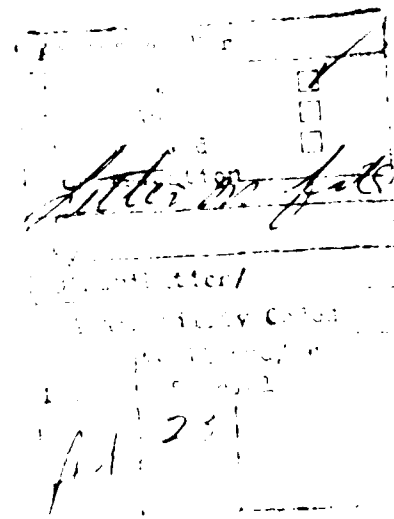
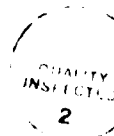
PERSPECTIVE ON RESEARCH AND DEVELOPMENT

ABSTRACTS

POSTERS

TRIP REPORTS

LISTS OF PARTICIPANTS



INTRODUCTION

The Third U.S.-Japan Workshop on Dielectric and Piezoelectric Materials was held in Toyama, Japan, November 9-12, 1986. There were approximately 85 attendees, 25 from the U.S. and 60 from Japan. A large percentage (~N 75) of the Japanese representatives were from industry, while industrial representation in the U.S. delegation was quite small (~N 20%). The purpose of this series of workshops has been the fostering of an exchange of scientific information between individual researchers from the two countries. To this end, the Workshop was organized to provide as much time as possible for informal discussions.

Other than for two invited review presentations by Professor Eric Cross and Professor Noboru Ichinose, the papers consisted of a four minute summary and a poster presentation by each attendee. The attendees were asked to present the results of recent research rather than review material. Copies of the abstracts of each of the papers as well as the material presented in the posters are included in a later section of this report. In addition to the poster papers, four roundtable discussion sessions were held in parallel. These roundtable discussions were held in the areas of dielectrics, piezoelectrics, processing, and mechanical properties. Discussion leaders from the U.S. and Japan supplied topics and helped to guide the conversations. Finally, a meeting for U.S. attendees only was held in Japan at the close of the Workshop to discuss what was learned regarding the important new areas of Japanese research and development as well as the industrial and economic aspects of these materials. In addition many of the U.S. attendees visited government, university, and industrial research laboratories, both before and after the formal portion of the Workshop. In some instances, these trips were arranged by the individual, but there were tour series set up by the Japanese, as well.

↓
The value of this series of workshops on dielectric and piezoelectric materials to the United States is twofold:

First, the discussions, both formal and private, have provided a source of new research ideas for the individual scientist. In a number of instances, these ideas have evolved into new directions for research as well as collaborative programs with the Japanese.

Second, the collective knowledge gained by the U.S. attendees, individuals having many different areas of expertise, has aided the Navy in focussing on the newest and most important research directions which the Japanese are taking on these materials. It is clear that the components and devices based on these materials have played an ever increasing role in Naval applications as well as the U.S. technology as a whole. A summary of the newest areas of Japanese research and development on these dielectric and piezoelectric materials is presented in the next section of this report.

SUGGESTIONS FOR FUTURE WORKSHOPS

Based upon the successful exchange of information in the previous three Workshops, we have made preliminary plans to hold a fourth meeting in the United States in the Fall of 1988. The tentative arrangement is that this Workshop would be held at the National Bureau of Standards in Gaithersburg, MD. We do have a number of suggested changes in the format of the meeting, which we believe will increase its value to both the Navy as well as U.S. industry:

1. The post-Workshop meeting for the U.S. attendees should be lengthened considerably, perhaps to as much as half a day. This meeting provides a way to obtain a collective view of Japanese R&D from the perspectives of industrial, university, and government researchers. We should take this opportunity to help form an overall picture of where the Japanese are going in terms of their developments in dielectric and piezoelectric ceramics.

2. In connection with the above, we should make a much stronger attempt to encourage U.S. industrial representatives to attend, and contribute to this Workshop.

3. One way of obtaining more industrial participation may be to eliminate the formal plant visits which have been associated with this Workshop in the past. These plant visits, however, can be important sources of information. Thus, it is suggested that such visits be arranged on an individual basis.

4. Any roundtable discussion sessions should be more highly structured. Individuals from both countries should be asked to prepare advanced lists of specific topics and questions.

We believe that these modifications should help improve the Workshop, and help provide an even greater exchange of information.

DIELECTRIC AND PIEZOELECTRIC CERAMICS: A PERSPECTIVE ON RESEARCH
AND DEVELOPMENT IN JAPAN

Stephen W. Freiman

National Bureau of Standards
Gaithersburg, MD 20899

and

Robert C. Pohanka

Office of Naval Research
Arlington, VA 22217

BACKGROUND

This summary represents the observations and opinions of a number of material scientists regarding the current status and most exciting topics in Japanese research and development on dielectric and piezoelectric ceramics. These scientists include many of the U.S. attendees at the Third U.S.-Japan Workshop on Dielectric and Piezoelectric Materials held November 9-12, 1986, in Toyama, Japan. The Workshop itself consisted of poster presentations by each of the U.S. and Japanese participants as well as four roundtable discussion sessions. Also, many of the U.S. attendees visited Japanese industrial and university laboratories both before and after the Workshop.

The report is divided into two sections, the first describing work on dielectric ceramics, followed by a section on piezoelectric materials. A number of application areas for each class of material are discussed.

DIELECTRICS

The primary application and certainly the current major market for ceramics as dielectric materials is in multilayer capacitors. The focus of much of the current attention of the Japanese is on capacitors containing lower cost electrodes. Two types of electrode systems are being considered. In the first, capacitor compositions are chosen in which Ag:Pd electrodes containing a large Ag/Pd ratio can be used. Lowering the Pd content in the electrode reduces the cost of the capacitor, but also reduces the temperature at which the capacitor must be fired in order to prevent electrode degradation. These "low fire" compositions are widely used in Japan. The second approach involves the use of Ni electrodes. The stability of the Ni electrodes is directly related to the partial pressure of oxygen in the firing atmosphere. These capacitors are doped with Ca to achieve the correct stoichiometry in the ceramic, which permits them to be fired in a low oxygen partial pressure. The Japanese advances in this area would seem to have occurred primarily through an experimental approach. However, the Japanese have made good use of fundamental research carried out in the U.S., Europe, and elsewhere. For instance, the understanding of the role of the Ca in base metal, i.e. Ni, electrode compositions was

based, in part, on the work of Professor Don Smyth at Lehigh University.

Another area of Japanese activity in multilayer capacitors observed during plant visits to TDK Corporation was the screen printing of dielectrics. Screen printing allows the formation of very thin layers of ceramic, giving rise to better homogeneity and reducing the tendency to bowing in thick specimens with a large number of layers. The improved homogeneity results in high capacitor reliability. Mitsubishi Mining and Cement Corporation has commercialized this process.

The Japanese are also interested in the use of relaxor compositions for multilayer capacitors in order to obtain materials with a high dielectric constant, low firing temperature and compatibility to electronic packaging materials. They reported on the properties of lead zinc niobate and suggested that this material is a promising candidate for capacitor applications. A major producer of relaxor materials is NEC Corporation, who can put capacitors directly on substrates. The development of these kinds of components involves understanding the mechanical compatibility of the capacitors and substrates, as well as the processing behavior of materials having different chemical compositions and physical properties. Finally, private discussions with individuals from Murata suggest that there may be serious cracking problems in ceramic capacitors made from relaxor compositions. It is not completely clear at present whether these problems arise because of an intrinsic weakness in the relaxor materials or are due to other causes such as processing defects.

The use of Pb injected electrodes in multilayer capacitors was briefly discussed. While there are some advantages to this system, the Japanese and U.S. representatives agreed that their use is not practical.

There did not appear to be a great deal of effort in Japan on determining the mechanical properties of capacitors. The one paper in this area was presented by Mr. Kishimoto Koumoto and Professor Yanagida from The University of Tokyo. Based on the similarity in Weibull distributions, these investigators concluded that a direct correlation exists between fracture strength and dielectric strength in fine grain size barium titanate. The correlation for larger grain size material was not as good.

In a related area, it was reported that TDK has developed a thermal shock testing technique which can be used to detect delaminations in capacitors.

The other major application for dielectric ceramics is in products used at microwave frequencies, e.g. tuned waveguides used in cellular telephones and satellite television communication systems. These waveguides are tuned to specific frequencies by varying the permittivity and dimensions of the dielectric resonator. There were four papers on microwave applications presented by Japanese companies at the Workshop. It was pointed out that the critical parameters for optimum performance are a relatively high dielectric constant at microwave frequencies, a very high Q for signal discrimination

and to reduce power losses. A zero or negative temperature coefficient of the resonant frequency is also required. Most of the Japanese work appears to be quite empirical; compositions are varied and properties determined. The work reported by Murata was less empirical. In their work, the dielectric loss was matched with the infrared spectra of the materials. They considered changes in properties based on order/disorder in the structure. In the case of the work reported by Narumi China Corp., the microwave properties were altered by changes in the crystalline phases in the material. The "optimum" properties reported by Narumi China were $\epsilon' = 38$ and $Q = 9000$ at 4GHz, and $T_c = 2\text{ppm}/^\circ\text{C}$. It is also apparent that the U.S. is doing virtually nothing in the microwave ceramics area.

PIEZOELECTRICS/ELECTROSTRICTIVES

One of the important research topics on piezoelectric materials is in the area of ceramic/polymer composites. Applications for this relatively new class of materials include improved sensitivity transducers for medical applications, which have a better impedance match to human tissue, as well as improved loudspeakers. One way of creating a piezoelectric composite with a controlled impedance is to produce a material having a gradient in filler concentration. There are approximately five Japanese companies involved in piezoelectric composite development. They do not seem too concerned with new materials but are concentrating on producing known compositions. They appear to be behind the U.S. in the theory of piezoelectric composites, but are neck and neck on the practical aspects of the industrial development of these materials.

One of the exciting new areas in which the Japanese are well ahead of the U.S. is in the development of practical piezoelectric and electrostrictive actuators and motors. These devices are based on materials such as PZT and lead magnesium niobate. In general, these applications are best formulated from hard piezoelectric materials having low hysteresis, low aging, and a high fracture toughness. A high Q increases the potential efficiency of the motor. Since one wants the largest possible strains in the material for a given applied voltage, piezoelectric compositions near morphotropic phase boundaries appear to be the most attractive.

There were six papers on motors and actuators presented by the Japanese at the Workshop. Professor Kenji Uchino at Sofia University continues to be an innovator in this field. His review paper on these devices, published in the Proceedings of the Sixth IEEE International Symposium on Applications of Ferroelectrics (1986), is particularly informative with regard to potential applications and material property requirements. Professor Uchino has recently become concerned with the mechanical reliability of the materials involved in these motors, and has been doing work on the fracture of PLZT, which is a good electrostrictive material. He has observed that the critical fracture toughness increases as the grain size decreases for three different lanthanum concentrations. Matsushita and Toyo

Soda (among others) are apparently developing a whole family of small, low speed, high torque, piezoelectric motors. These motors can be made cheaply. In general, these motors have a high efficiency. Applications for these motors include precision machining, robotics, ink-jet printers, and pneumatic control valving.

Thin film pyroelectric sensors for use as quick monitors of temperature are also of interest to the Japanese. Deposition is mainly accomplished by magnetron sputtering using various control parameters. The papers at the workshop discussed the effect of alkaline earth substitutions in lead titanate ceramics on their pyroelectric and piezoelectric properties. PZT was also discussed as a candidate material for thin film sensors. A significant growth in the use of thin film materials for electrooptic applications was predicted.

ACKNOWLEDGEMENTS

The authors would like to acknowledge the help of a number of the other participants at this Workshop for their aid in identifying the key Japanese research and development areas, particularly Manfred Kahn, Harlan Anderson, Relva Buchanan, and Eric Cross.

The Third U.S. : Japan Seminar on
Dielectric and Piezoelectric Ceramics

PROGRAM and ABSTRACTS

Co-chairman T. Yamaguchi, Keio University
Co-chairman S. W. Freiman, National Bureau of Standards

Chairman of Program Committee, H. Banno, NGK Spark Plug Co.
Chairman of Financial Committee, K. Wakino, Murata MFG. Co.
Chairman of Tour Committee, N. Ichinose, Waseda University
Chairman of Executive Committee, A. Okamoto, TDK Electronics
Secretary, T. Kimura, Keio University

November 9-12, 1986
YKK Conference Hall
Toyama, Japan

Sunday 9th November 1986

4:00 pm	Registration	(NEW OTANI HOTEL)
to		
6:00 pm		
6:00 pm	Dinner	
7:30 pm	Cocktail Party: Reception	

Monday 10th November 1986

8:30 am	(Bus leaves Hotel)	
		(YKK Conference Hall)
9:20 am	Welcome to 3rd U.S:Japan Seminar	K. Wakino
		Murata MFG. Co.
	Opening Remarks	S. Freiman, NBS
	Announcements	T. Yamaguchi, Keio Univ.

Technical Program

Overviews

9:40 am	Perspectives on Dielectric and Piezoelectric Ceramics
	L. E. Cross, Penn State Univ.

10:40 am	Coffee
----------	--------

11:00 am	Recent Progress of Electronic Ceramics in Japan
	N. Ichinose, Waseda Univ., I. Sakabe, Murata MGF. Co.

12:00 am	Lunch
----------	-------

1:30 pm	<u>Poster Session I</u>
	Processing and Dielectrics I
5:00 pm	(Bus leaves YKK)

(NEW OTANI HOTEL)

6:00 pm	Dinner
---------	--------

7:30 pm	<u>Roundtable Discussions</u>
	Mechanical Properties
	Piezoelectrics
	Dielectrics
	Processing

TECHNICAL PROGRAM
U.S.:JAPAN SEMINAR ON DIELECTRIC AND PIEZOELECTRIC CERAMICS
NOVEMBER 9-12, 1986, TOYAMA, JAPAN

Overviews (Monday Morning) Session Chair: S. Shirasaki (NIRIM)

"Perspectives on Dielectric and Piezoelectric Ceramics"

L. E. Cross, Pennsylvania State University, Materials Research Lab.

"Recent Progress of Electronic Ceramics in Japan"

N. Ichinose, Waseda University

I. Sakabe, Murata MFG Co. Ltd.

Roundtable Discussions (Monday Evening)

1) Mechanical Properties: S. W. Freiman, B. Koepke and R. C. Pohanka,
K. Niihara and K. Uchino

2) Piezoelectrics: L. E. Cross, J. Dougherty, M. P. Harmer, N. Ichinose
and H. Takekuchi

3) Dielectrics: I. Burn, H. U. Anderson, D. Payne, D. A. Smyth,
H. Yanagida and K. Wakino

4) Processing: R. Buchanan, G. Haertling, R. W. Vest, T. Yamaguchi and
S. Hirano

Poster Sessions

Poster Session I (Monday Afternoon) Session Chair; D. A. Payne (Univ. of
Illinois), S. Hirano (Nagoya Univ.)
Processing and Dielectrics I

Poster Session II (Tuesday Morning) Session Chair; R. C. Pohanka (ONR),
H. Yanagida (Tokyo Univ.)
Dielectrics II, Pyroelectrics, Mechanical Properties and Electro-optic and
PLZT

Poster Session III (Wednesday Morning) Session Chair; W. A. Schultz (Alfred
Univ.), K. Uchino (Sophia Univ.)
Piezoelectrics, Actuator and Miscellaneous

Tuesday 11th November 1986

8:00 am (Bus leaves Hotel) (YKK Conference Hall)

8:50 am Poster Session II
DielectricsII, Pyroelectrics, Mechanical Properties and
Electro-optic and PLZT

12:00 am Lunch

12:40 pm (Bus leaves YKK)
1:45 pm (Bus leaves Hotel)
2:00 pm Excursion (NEW OTANI HOTEL)

6:30 pm Party : Courtesy of DuPont Japan

Wednesday 12th November 1986

8:30 am (Bus leaves Hotel) YKK Conference Hall

9:20 am Poster Session III
Piezoelectrics, Actuator and Others

12:00 am Closing Remarks K. Okazaki
Nat. Defense Acad.

1:00 pm Farewell Party: Courtesy of YKK

2:00 pm U. S. Reflection Meeting

Poster Session I (Monday Afternoon)

Processing

- M-1 Sol-Gel Processing of PbTiO_3 , PZT and PLZT
D. A. Payne, K. D. Budd and S. K. Dey, University of Illinois
- M-2 Preparation and Properties of Ferroelectric Films from Metallo-organic Precursors
R. W. Vest, Purdue University
- M-3 Fabrication of Grain-Orientated $\text{K}_2\text{Sr}_2\text{Nb}_5\text{O}_{15}$ Ceramics
T. Kimura, Y. Ogino and T. Yamaguchi, Keio University
- M-4 Properties of Sub-micron BaTiO_3 with Additives for Low Firing Temperature
K. Abe, M. Aoki, K. Fukai and K. Hidaka, Sakai Chemical Industry Co., Ltd.
- M-5 Effect of MgTiO_3 on the Grain Growth of $(\text{Ba,Ca})(\text{Ti,Zr})\text{O}_3$ Ceramics
S. Itoh, T. Noguchi and T. Ogasawara, TDK Corporation
- M-6 Machining of PZT, PT, and $(\text{MnZn})\text{Fe}_2\text{O}_4$ Ceramics by Laser-Induced Chemical Etching
T. Shiosaki and A. Kawabata, Kyoto University
- M-7 Synthesis and Properties of Alkoxy-derived $\text{Zr}_x\text{Ti}_y\text{Sn}_z\text{O}_4$ Ceramics
S. Hirano, T. Hayashi and A. Hattori, Nagoya University
- M-8 Effect of Agglomerated Particles on Properties of Ceramic Green Sheets
T. Ueyama, N. Kaneko and Y. Machii, Hitachi Chemical Co., Ltd.
- M-9 Sinterability of High-Packing Density BaTiO_3 Green Sheets
T. Ueyama, S. Yamana and N. Kaneko, Hitachi Chemical Co., Ltd.

Dielectrics I

- M-10 An Investigation of the Low Voltage Failure Mechanism in Multilayer Ceramic Capacitors
C. J. Brannon and H. U. Anderson, University of Missouri-Rolla
- M-11 Additive Effects on Microstructure and Properties of BaTiO_3
R. Buchanan, University of Illinois
- M-12 Barium Titanate-Based Dielectrics for MLC's with High K and Low Firing Temperature
I. Burn and M. T. Secaur, E. I. du Pont de Nemours & Co.
- M-13 Electrical Conduction in BaTiO_3 -Based Ceramic
L. C. Burton and H. Y. Lee, Virginia Polytechnic Institute and State University
- M-14 Dielectric and Piezoelectric Ceramics Historical Developments: Current Status and Future Prospects
L. E. Cross, Pennsylvania State University
- M-15 Operationally Induced Thermal Stress gradients in Multilayer Capacitors
J. Dougherty, Advanced Materials Technologies
- M-16 Microstructure and Nanostructures of Relaxor Ferroelectrics
M. P. Harmer, Lehigh University
- M-17 Dielectric Properties of Fine-Grained BaTiO_3 Derived From $\text{BaTiO}(\text{C}_2\text{O}_4) \cdot 4\text{H}_2\text{O}$
T. Enomoto, T. Uno and N. Okada, Central Glass Co., Ltd.
- M-18 Low Temperature Fired Glass-Ceramics Dielectric Material

- W-7 Electromechanical Properties of Planar Vibrational mode in
PZT/Polymer Piezoelectric Composites
H. Takeuchi and C. Nakaya, Hitachi Ltd.
- W-8 Anisotropic Piezoelectric Coupling Factor of
[Pbx(Bi_{1-x}Na_{2x})_{1-x}]TiO₃ Ceramics
S. Tashiro, Y. Oikawa, H. Igarashi and K. Okazaki,
National Defense Academy
- W-9 Effects of Shape and Volume Fraction of Closed Pore on
Dielectric Loss, Mechanical Quality Factor and
Electromechanical Coupling Factor of Dielectric and
Piezoelectric Ceramics-A Theoretical Approach-
H. Banno, NGK Spark Plug Co., Ltd.

Actuator

- W-10 Efficiency of Piezoelectric Ceramic Actuator
S. Takahashi, NEC Corp.
- W-11 Ceramic Green Sheet Puncher Using Piezoelectric Actuator
T. Yoshiura, K. Yoshida, I. Kagaya, Y. Shimada and S.
Takahashi, NEC Corp.
- W-12 Monomorph Actuators Using Semiconductive Piezoelectrics
K. Uchino, M. Yoshizaki, H. Yamamura*, K. Kasai*, N. Sakai*
and H. Asakura*, Sophia University, *Toyo Soda
Manufacturing Co., Ltd.
- W-13 Development of Electrostrictive Ceramics
S. Jomura and K. Maruta, Hitachi Metals Co., Ltd.
- W-14 Temperature Dependence of Electrostriction Under a High
Electric Field
K. Abe., O. Furukawa, M. Katura and K. Inagaki*
Toshiba Corp, *Marucon Electronics Co. Ltd.
- W-15 Preparation and Characteristics of New Monomorph Actuator
N. Sakai, K. Kasai and H. Yamamura, Toyo Soda Manufacturing
Co., Ltd.

Miscellaneous

- W-16 Laser Patterning of Polymers for Electronic Packaging
H. S. Cole, Y. S. Liu, H. R. Philipp and L. M. Levinson,
General Electric Corporate Research and Development
- W-17 Characterization of the Role of Excess Magnesium Oxide and
Lead Oxide in Lead Magnesium Niobate
H. C. Wang and W. A. Schulze, Alfred University
- W-18 Trivalent Impurities in BaTiO₃
K. Takada, R. Y. Lee, S. R. Witek and D. M. Smyth, Lehigh
University
- W-19 Line-focus-beam Acoustic Microscope System for
Nondestructive Evaluation of Acoustic Inhomogeneity on PTZ
Wafer for SAW Devices
N. Chubachi and J. Kushibiki, Tohoku University
- W-20 Electrical Properties of (Sr,Ca)TiO₃ Based Ceramic
Varistors
M. Masuyama, J. Funayama and N. Yamaoka, Taiyo Yuden Co.,
Ltd.
- W-21 Defect Structure and Electrical Property of La-Doped
Barium Titanate
S. Shirasaki, H. Haneda and M. Sugimoto*, National
Institute for Research in Inorganic Materials, *TDK Corp.
- W-22 Determination of a Compositional Fluctuation in Perovskite
Ternary Systems
K. Kakegawa and Y. Sasaki, Chiba University
- W-23 Properties of AlN Ceramics
T. Takahashi, K. Anzai, N. Takada and K. Shinozaki, New
Materials Department, Toshiba Corp.

- M-19 M. Takabatake, K. Kawakami and M. Sakai, Asahi Glass Co.
Low Temperature Fired Multilayer Ceramic Capacitor with Ni Electrodes
H. Kishi, T. Wada, S. Murai and H. Chazono, and N.Yamaoka, Taiyo Yuden Co., LTD.
- M-20 Barium Titanate Ceramics for Base Metal Monolithic Ceramic Capacitors
Y. Sakabe, T. Takagi and K. Wakino, Murata Manufacturing Co., Ltd.
- M-21 Temperature Stable Barium Titanate Ceramics for Base Metal Multilayer Capacitors
N. Fujikawa, N. Yokoe and F. Hamano, Kyocera Corp.
- M-22 Barium Modified Lead Zinc Niobate Dielectrics for Multilayer Ceramic Capacitor
K. Inagaki, Y. Yamashita and K. Yuuki, Marucon Electronics Co. Ltd.
- M-23 Dielectric Relaxation Studies in Some Polymer-PZT Composites
A. M. Varaprasad, Naval Dockyard, India (Sophia University)

Poster Session II (Tuesday Morning)

Dielectrics II (Microwave)

- T-1 Microwave Dielectric Properties of $\text{Pb}(\text{Zr,Ce})\text{O}_3$ Ceramics
K. Murano, K. Tatuki, S. Nishigaki*, S. Yano*, and H. Kato*, Sony Corp., *Narumi China Corp.
- T-2 High Dielectric Constant Ceramics for Microwave Resonators
H. Sato, K. Ayusawa, M. Saito and K. Kawamura, OKI Electric Industry CO. Ltd.
- T-3 High-Q Dielectric Resonator Material for Millimeters-Wave Frequencies
H. Tamura, D. A. Sagara, M. Murata and K. Wakino, Murata Manufacturing Co., Ltd.
- T-4 Dielectric Properties of $\text{BaO-TiO}_2\text{WO}_3$ System at Microwave Frequency
S. Nishigaki, S. Yano, H. Kato and T. Nonomura, Narumi China Corp.

Pyroelectrics

- T-5 Ferroelectric and Pyroelectric Properties of Sputter-deposited PZT and PT Films
M. Adachi, T. Shiosaki and A. Kawabata, Kyoto University
- T-6 Pyroelectric and Electrical Properties of Modified Lead Titanate Ceramics
N. Ichinose, Waseda University
- T-7 Properties of Hot-Pressed Lead Germanate Silicate Ceramics
K. Nagata and K. Okazaki, National Defense Academy

Mechanical Properties

- T-8 Comparison: Thermal and Mechanical Properties of Barium Titanate Versus Lead Perovskite Dielectrics
A. E. Brown and C. R. Koripella, Union Carbide Corp.
- T-9 Fracture Behavior of Capacitor Ceramics
S. W. Freiman and T. L. Baker, National Bureau of Standards
- T-10 Compositional Influences on PLZT Switching Properties
B. Koepke, F. Wallenhorst and J. Kyonka, Honeywell Inc.

- T-11 Electromechanical Failure Predictions
R. C. Pohanka, P. L. Smith and S. W. Freiman*, Office of Naval Research, *National Bureau of Standards
- T-12 The Relation of Anisotropy Between Crack Length and Fracture Toughness in Poled PLZT and Modified PbTiO_3 Ceramics
T. Yamamoto, H. Igarashi and K. Okazaki, National Defense Academy
- T-13 Mechanical and Dielectric Failure of BaTiO_3 Ceramics
A. Kishimoto, K. Koumoto and H. Yanagida, The University of Tokyo
- T-14 Ceramic Toughening by Crack-Stacking Faults Interactions
K. Niihara and T. Hirai*, National Defense Academy, Tohoku University

Electrooptics & PLZT

- T-15 Electrooptic Materials for Integrated Optic Device Applications
R. L. Holman, Battelle Columbus Laboratories
- T-16 Growth and Applications of Tungsten Bronze Family Crystals
R. R. Neurgaonkar, W. K. Cory, J. R. Oliver and W. F. Hall, Rockwell International Science Center
- T-17 Photoferroelectric Effect in PLZT Ceramics
G. Haertling, Motorola, Inc.
- T-18 Photodriven Relay Using PLZT Ceramics
K. Uchino, T. Sada and M. Inoue, Sophia University
- T-19 PLZT Thin Film on $\text{MgAl}_2\text{O}_4/\text{Si}$ Substrate
S. Matsubara, Y. Miyasaka, N. Shohata and M. Yonezawa, NEC Corp.
- T-20 Some Electrooptic Properties of PLZT Ceramics
K. Hikita, M. Hirama, Y. Tanaka and M. Ono, Mitsubishi Mining & Cement Co., Ltd.
- T-21 Dielectric Properties of Sputtered Polycrystalline $(\text{Pb},\text{La})(\text{Zr},\text{Ti})\text{O}_3$ Thin Films
K. Wasa, H. Adachi and T. Mitsuyu, Matsushita Electric Ind. Co., Ltd.

Poster Session III (Wednesday Morning)

Piezoelectrics

- W-1 Preparation and Performance of Ceramic-Air Composites for Hydrostatic Sensing
M. Kahn, A. Dalzell and B. Kovel, U. S. Naval Research Laboratory
- W-2 A Resonance Technique for Measuring the Complex Elastic, Dielectric and Piezoelectric Coefficients of Composite Materials
X. Q. Chang, A. R. Ramachandran and R. E. Newnham, Pennsylvania State University
- W-3 Ferroelectric Composite Transducers
B. A. Auld, Stanford University
- W-4 Piezoelectric Properties of Some New Hydrophone Materials
R. Y. Ting, U. S. Naval Research Laboratory.
- W-5 Dielectric and Piezoelectric Properties of PbZrO_3 -PZ($\text{Zn}_{1/3}\text{Nb}_{2/3}$) O_3 Ceramics
K. Sakata and T. Takenaka, Science University of Tokyo
- W-6 Piezoelectric Properties of $(\text{Na}, \text{Li})\text{NbO}_3$ Ceramics
T. Honda, I. Kawamata, H. Watarai and T. Ido, Mitsubishi Electric Corp.

POSTER SESSION I

M-1

SOL-GEL PROCESSING OF PbTiO_3 , PZT AND PLZT

D. A. PAYNE, K. D. RUDD AND S. K. DEY

Department of Ceramic Engineering and Materials Research Laboratory,
University of Illinois at Urbana-Champaign, 105 S. Goodwin Avenue,
Urbana, Illinois 61801, U.S.A.

ABSTRACT: Dielectric thin-films of PbTiO_3 based materials were prepared by the spin-casting of a Pb,Ti-methoxyethoxide solution onto platinum, silicon and a variety of substrate materials. The resulting gel layers densified at relatively low temperatures ($< 350^\circ\text{C}$) with crystallization to the perovskite phase at $450 - 700^\circ\text{C}$, depending upon composition. The films were transparent and had electric strengths in excess of $100 \text{ V}/\mu\text{m}$. Ferroelectric hysteresis loops were obtained for $1 \mu\text{m}$ layers with grain sizes of $0.1 \mu\text{m}$. PZT 53/47 had $P_R = 32.5 \mu\text{C}/\text{cm}^2$, with $E_C = 30 \text{ KV}/\text{cm}$; and the relative permittivity of PLZT 10/65/35 was 1700.

1. INTRODUCTION

An upset technology is in the making for the fabrication of dielectric thin-films by polymeric sol-gel processing. This novel processing route avoids powder (and attendant problems), and produces films of exceptional quality, at relatively low temperatures. The present study reports on recent measurements on ferroelectric and dielectric properties.

2. EXPERIMENTAL

2.1 Materials

Precursor solutions of a complex Pb-Ti alkoxide were prepared by reacting lead acetate with titanium isopropoxide in methoxyethanol. A complex Pb,Ti-methoxyethoxide formed by alcohol exchange with Ti-isopropoxide, and subsequent reaction with a dehydrated Pb-acetate solution. Alkoxides of Zr and La were also incorporated into the system. The importance of hydrolysis conditions, condensation reactions, and thermal processing conditions, on film formation and microstructure development, are summarized in reference 2.

2.2 Measurements

A parallel-plate capacitor geometry was used to determine relative permittivities, dissipation factors, and electric strengths. The counter electrodes were sputtered gold. Scaling of capacitance with area was taken to be a proper indication of the absence of contact problems. Hysteresis measurements were made on a modified Sawyer-Tower Circuit.

3. RESULTS

Table 1 summarizes relative permittivities and dissipation factors for sol-gel derived films on Pt. The results are in good agreement with values reported in the literature for bulk samples and hot-pressed parts. Figure 1 illustrates the dependence of relative permittivity on heat treatment

a) Details of the processing route are given in references 1 and 2.

conditions and crystallization behavior. The dielectric strengths were in excess of 10^8 V/cm. Hysteresis loops were observed, confirming ferroelectricity (Figure 2).

4. DISCUSSION

Sol-gel processing is an attractive method for the fabrication of high quality thin-films of complex dielectric materials. Applications include the direct integration of capacitors onto semiconductors and substrates, piezoelectric and ferroelectric devices, and optical connectors.

Table 1. Dielectric Properties of Sol-Gel Derived Thin-Films

composition	crystallinity	permittivity	dissipation factor
PbTiO ₃	amorphous	28 - 42	0.003 - 0.010
PbTiO ₃	crystalline	155 - 185	0.006 - 0.030
PZT 53/47	amorphous	35	0.005 - 0.010
PZT 53/47	crystalline	300 - 1200	0.020 - 0.070
PLZT 10/65/35	amorphous	35	0.005 - 0.010
PLZT 10/65/35	crystalline	300 - 1700	0.020 - 0.090

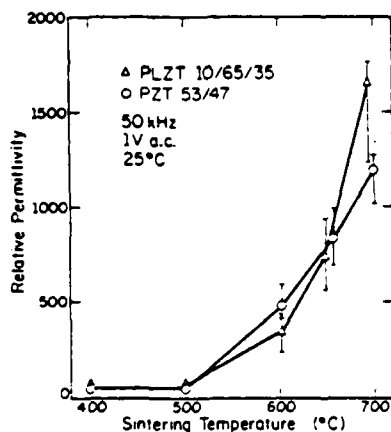


Fig. 1. Effect of heat-treatment on permittivity of high-K thin films.

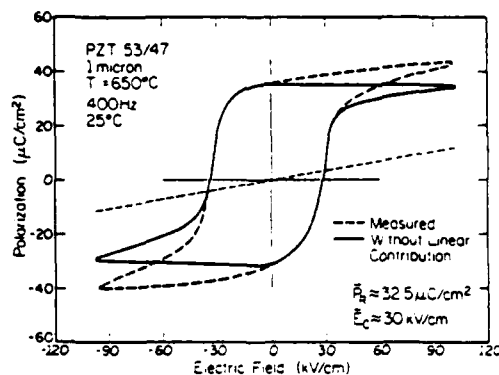


Fig. 2. Ferroelectric hysteresis for PZT 53/47, 1 μ m thin-film.

ACKNOWLEDGEMENTS

This work was supported by the U.S. Department of Energy, Division of Materials Sciences, under contract DE-AC02-76SR01198.

REFERENCES

1. K. D. Rudd, S. K. Dey and D. A. Payne, Brit. Cer. Proc., **36**, 107 (1985).
2. K. D. Rudd, S. K. Dey and D. A. Payne, "Better Ceramics Through Chemistry II," Vol. 73, p. 711, Materials Research Society, Pittsburgh, PA (1986).

M-2

PREPARATION AND PROPERTIES OF FERROELECTRIC FILMS FROM METALLO-ORGANIC PRECURSORS

R.W. VEST

Purdue University, West Lafayette, Indiana, 47907, U.S.A.

ABSTRACT: Ferroelectric PbTiO_3 and $(\text{PbSr})\text{TiO}_3$ films 0.5 to 5.0 μm thick were prepared by the metallo-organic decomposition (MOD) process using multilayer spinning with firing temperatures of 490 to 700°C. Both Pt and ITO electrodes were also prepared by the MOD process, and dielectric properties were measured as a function of temperature. The films were near theoretical density and defect free over 2 cm \times 2 cm areas.

1. INTRODUCTION

The MOD process for preparing ferroelectric films has a number of advantages over conventional processes. These include rapid formation of compounds in films and lower temperature processing of equilibrium phases.

2. EXPERIMENTAL

Lead neodecanoate $[\text{Pb}(\text{C}_9\text{H}_{19}\text{COO})_2]$, strontium neodecanoate $[\text{Sr}(\text{C}_9\text{H}_{19}\text{COO})_2]$ and titanium di-methoxy-di-neodecanoate $[(\text{CH}_3\text{O})_2\text{Ti}(\text{C}_9\text{H}_{19}\text{COO})_2]$ were the precursors used for the ferroelectric films. These compounds were dissolved in an appropriate solvent, the solutions mixed to achieve the desired stoichiometry, and the resulting solution spun onto substrates which had previously been provided with Pt or ITO electrodes by the MOD process. The samples were fired at a programmed rate to temperatures from 490 to 700°C, either with or without an electric field present.

The crystal structure was studied using x-ray diffraction analyses, and the microstructure was studied using SEM and TEM. The temperature dependences of D.C. resistivity, dielectric constant, dissipation factor and spontaneous polarization were measured.

3. RESULTS AND DISCUSSION

For a given time-temperature profile, it was determined that the film must be below some critical thickness in order to sustain the volume change of as much as a factor of 30 without cracking. It was shown that multiple spinning and firing of films below this critical thickness can be used to produce any desired final film thickness. The reliability for the specimens, defined as the percent of the 143 planner capacitors in a 4 cm² area which gave equivalent dielectric properties with an applied field of 100 kV/cm, was found to depend on factors such as the choice of substrate, the purity of the metallo-organic precursors, and the process cleanliness in addition to the time-temperature firing profile and the single layer thickness. Currently, 2 cm \times 2 cm dielectric films can be made with 100 percent reliability if all these factors are properly controlled.

It was found that the c/a ratio for PbTiO_3 films varied with the firing temperature and with single layer thickness, but in all cases was smaller than that of bulk tetragonal PbTiO_3 . For the same thickness PbTiO_3 films fired at the same temperature, it was found that the c/a values for those films fired in a D.C. electric field at temperatures below T_c were smaller compared to those fired without a field, and that the effect increased with increasing field strength.

The grain size of the PbTiO_3 films was found to increase with increasing firing temperature and single layer thickness, but in all cases was very small (14 to 25 nm). This small grain size was responsible for the small spontaneous polarization ($\sim 5 \mu\text{C}/\text{cm}^2$) values observed. At lower firing temperatures ($< 550^\circ\text{C}$), the grain orientation in polycrystalline tetragonal films was random. For firing temperatures higher than 600°C , a strong tendency for preferred orientation with the c axis perpendicular to the substrate surface was observed.

The dielectric constant of the PbTiO_3 films was 100 \sim 110 at temperatures below 300°C , and reached a maximum value of 3×10^4 at the Curie point (493 to 495°C). The dissipation factor remained almost constant until 250°C and then increased rapidly with further increase in temperature. The temperature dependence of dielectric constant was found to be a function of the c/a ratio, which could be modified by either control of the single layer thickness or the strength of an applied D.C. field during film preparation below the Curie temperature. The dielectric strength for 0.5 to 2.0 μm thick films was greater than 100 kV/cm.

Solid solutions of PbTiO_3 and SrTiO_3 were formed, and compositions to give T_c in the neighborhood of room temperature were extensively studied. The dielectric constant was found to be a strong function of electric field for these films.

M-3

FABRICATION OF GRAIN-ORIENTED $\text{KSr}_2\text{Nb}_5\text{O}_{15}$ CERAMICS

T. KIMURA, Y. OGINO and T. YAMAGUCHI

Faculty of Science and Technology, Keio University, Yokohama, Japan

ABSTRACT: The morphology of powder particles obtained by molten salt synthesis was examined for alkali-alkaline earth niobate $\text{AB}_2\text{Nb}_5\text{O}_{15}$, where A=Na or K and B=Sr or Ba. Rod-like particles suitable for the preparation of grain-oriented ceramics were obtained in $\text{KSr}_2\text{Nb}_5\text{O}_{15}$. The crystallographic direction of the rod-axis was determined to be [001] by X-ray diffraction analysis of extruded and sintered compacts.

1. INTRODUCTION

Grain-oriented ceramics are prepared by normal sintering of plate- or rod-like powders made by molten salt synthesis. Alkali-alkaline earth niobate $\text{AB}_2\text{Nb}_5\text{O}_{15}$ (A and B are alkali and alkaline earth ions respectively) has tetragonal tungsten bronze-related structure and its polar axis is parallel to [001]. Particle morphology depends on the anisotropy of growth rate in molten salt. Rod-like powder particles with rod-axis parallel to [001] are suitable for preparing grain-oriented ceramics. This paper deals with the preparation of $\text{AB}_2\text{Nb}_5\text{O}_{15}$ (A=Na or K; B=Sr or Ba) powders in the presence of molten chloride.

2. EXPERIMENTAL

Mixtures of alkali carbonate A_2CO_3 , alkaline earth carbonate BCO_3 , niobium oxide Nb_2O_5 and alkali chloride ACl were heated at a desired temperature between 700° and 1200°C for 1h. The products were washed with hot water to remove the chloride. The crystalline phases and morphology of the resultant powders were examined by X-ray diffraction analysis (XRD) and scanning electron microscopy (SEM) respectively.

Rod-like $\text{KSr}_2\text{Nb}_5\text{O}_{15}$ powder particles were mixed with methyl cellulose, polyethylene oxide and water in a roll-mill and extruded through a nozzle 1 mm in diameter. The resulting rods were cut to 3 cm long rods, which were aligned in a square die (3x3 cm) and pressed at 98 MPa. The compacts were cut to small pieces (1x1x0.2 cm) and heated slowly up to 500°C in air to burn out the organic ingredients. The green compact was sintered at 1350°C for 1h. Orientation of particles and grains in green and sintered compacts was examined by XRD.

3. RESULTS AND DISCUSSION

Particle morphology of the powders obtained at 1200°C was examined by SEM. For $\text{NaSr}_2\text{Nb}_5\text{O}_{15}$ and $\text{NaBa}_2\text{Nb}_5\text{O}_{15}$, mixtures of rod-like and equiaxed particles were obtained. For $\text{KSr}_2\text{Nb}_5\text{O}_{15}$ and $\text{KBa}_2\text{Nb}_5\text{O}_{15}$, the powders consisted of only rod-like particles. $\text{KSr}_2\text{Nb}_5\text{O}_{15}$ particles were selected because of their large aspect ratio.

Figure 1a shows the XRD pattern of a green compact made by extruding of the rod-like powder. Comparison with the XRD pattern for equiaxed powder (Fig. 1b) indicates that intensities of (230), (400) and (140) for the compact of the rod-

like powder are larger than those for the equiaxed powder. SEM observation of the compact revealed that many particles aligned with their c -axis parallel to the extrusion direction. These results indicate that the c -axis is parallel to $[001]$.

Figure 2 shows the XRD patterns of a sintered compact. Sintering increased the intensities of $(hk0)$ reflections from the plane parallel to the extrusion direction (compare Figs. 1a and 2a). Only (001) and (002) were intense peaks from the plane perpendicular to the extrusion direction. The sintered compact was characterized by anisotropic microstructure; the rod-like grains were aligned in the direction parallel to the extrusion direction. These results indicate that grain-oriented ceramics with aligned polar axis are obtained.

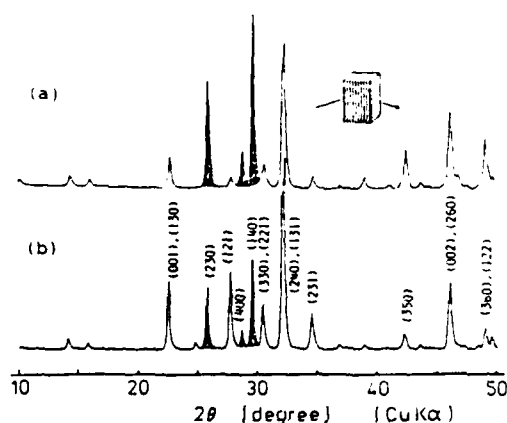


Fig. 1 X-ray diffraction patterns of (a) green compact and (b) equiaxed powder.

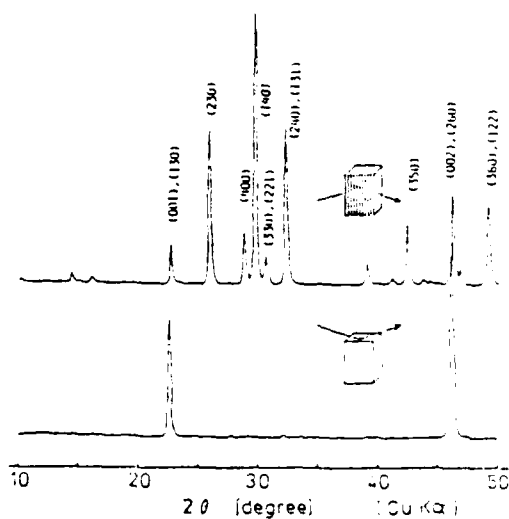


Fig. 2 X-ray diffraction patterns of sintered compact.

M-4

PROPERTIES OF SUB-MICRON BaTiO_3 WITH ADDITIVES FOR LOW FIRING TEMPERATURE

K. ABE, M. AOKI, K. FUKAI, K. HIDAKA

Research and Development Division, Sakai Chemical Industry Co., Ltd., Sakai,
Osaka 590, Japan

ABSTRACT: Sintering properties, electrical properties and crystal structure of three kind of BaTiO_3 with an additive for low firing temperature were studied.

Comparisons were made among three powder production methods, i.e. the hydrothermal synthesis method, the oxalate method and the calcination method, and among various additives for low firing temperature. As a result, it was found that the hydrothermal synthesis method provides the most excellent sintering and electrical properties for BaTiO_3 with an additive for low firing temperature.

1. INTRODUCTION

Payne et al.¹⁾ and Chowdary et al.²⁾ attempted to reduce firing temperature by adding glassy materials to BaTiO_3 powder. It is expected that sintering temperature will be further reduced by adding such an additive for low firing temperature to easily sinterable BaTiO_3 obtained by the hydrothermal synthesis method.

2. EXPERIMENTAL

2.1. Sample Powders and additives

The following three BaTiO_3 powders were used as samples:

- 1) Powder produced by the hydrothermal synthesis method
- 2) Commercially available powder produced by the oxalate method
- 3) Powder produced by the calcination method, which is calcined at 1150°C using high-purity fine BaCO_3 and TiO_2 (both Sakai Chemical).

Five kinds of additives (A,B,C,D,E) were used. Each additive was added to each BaTiO_3 in a specified amount (see table 2). Mixing was carried out in a polyethylene pot containing zirconia balls and acetone overnight.

2.2 Measurement

After sample powders were granulated, 2.2g of the granules were placed in dies 20mm in diameter, pressed 1000 kg/cm² for 1min. Resulting green molds were fired for 3 hours at specified temperature between 800°C and 1300°C . Fired products were subjected to measurement of sintered density electrical properties.

3. RESULTS AND DISCUSSION

Properties of BaTiO_3 powders without an additive are shown in Table 1. Table 1 shows that there are no significant differences among the three in

purity, although the powder produced by the hydrothermal synthesis is the most excellent in particle shape (spherical), fine particle size (0.1 μ m) and particle size distribution (uniform).

Figures 1-3 show typical temperature dependence of sintered density. As shown in these figures, the BaTiO₃ powder produced by the hydrothermal synthesis method is the most easily sinterable independent of whether or not an additive is added. Based on this finding, it is thought that the low temperature sinterability of the main raw material rather than the effect of additives is an important factor for low temperature firing.

Table 3 shows electrical properties of sintered products obtained at minimum firing temperature for sintering. As shown in this table, it is found that additive A is a most effective additive for low firing temperature, because this additive makes it possible to perform sintering at 1000°C even though it is added in a small amount (1.0 mol%), thus having a less effect on electrical properties of the sintered product.

REFERENCES

1. D.A.Payne and S.M.Park, USP 4,218,723
2. K.R.Chowdary and E.C.Subbarao, Ferroelectrics, **37**, 689-692 (1981)

Table 1 powder properties

method	Hydrothermal	Oxalate	Calcination
BET surface area (m ² /g)	1.2	2.2	1.0
Bulk density	0.59	0.72	0.83
TEM mean particle size (μ m)	0.1	0.3	1.2
Ba/Ti mol ratio	1.01	1.00	1.01

Table 2 Addition ratio

Additive	ratio
A	1 mol%
B	1 mol%
C	10 vol%
D	5 vol%
E	5 vol%

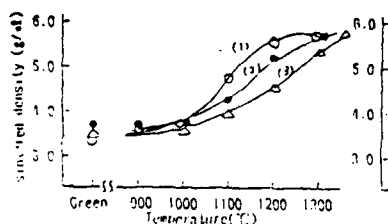


Fig. 1 Sintering curves of BaTiO₃ without an additive.
(1) Hydrothermal synthesis (2) Oxalate method (3) Calcination method

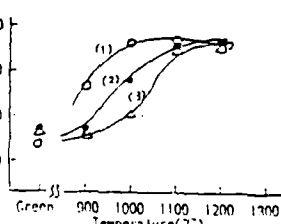


Fig. 1 Sintering curves of BaTiO₃ with an additive A.
(1) Hydrothermal synthesis (2) Oxalate method (3) Calcination method

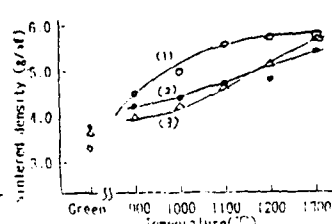


Fig. 1 Sintering curves of BaTiO₃ with an additive D.
(1) Hydrothermal synthesis (2) Oxalate method (3) Calcination method

Table 3 Properties of sintered products obtained at minimum firing temperature necessary for sintering, by Archimedes's method

Production method	Additive	Firing Temperature	Sintered density (g/cc)	Grain size (μ)	$\epsilon_{20^\circ\text{C}}$ (at kHz)	$\tan \delta$ (at kHz)	Curie point ($^\circ\text{C}$)	ρ_{max} (at kHz)	Resistivity ($\Omega \cdot \text{cm}$)
Hydrothermal Synthesis	no	1200	5.83	2.1	3208	0.01	125	6100	1.9×10^{11}
	A	1000	5.82	0.8	2817	1.10	122	3783	2.4×10^{12}
	D	1100	5.50	0.3	1210	3.27	110	2095	3.8×10^{10}
Oxalate method	no	1300	5.83	4.3	3117	3.28	120	10188	6.7×10^{11}
	A	1100	5.78	2.8	2930	1.81	127	1516	1.5×10^8
	D	1200	5.53	2.8	1712	2.87	129	6564	2.3×10^8
Calcination method	no	1300	5.81	7.7	2018	1.51	121	9127	1.9×10^{12}
	A	1100	5.05	12	2118	1.12	116	6210	2.0×10^{12}
	D	1200	5.01	2.5	1477	3.01	122	6310	2.3×10^{12}

M-5

EFFECT OF MgTiO_3 ON THE GRAIN GROWTH OF $(\text{Ba,Ca}) (\text{Ti,Zr})\text{O}_3$ CERAMICS

S. ITOH, T. NOGUCHI, T. OGASAWARA
CERAMIC COMPONENTS MFG DIVISION, TDK CORPORATION

1. INTRODUCTION

For the manufacturing of ceramics, it is important to clarify the relation between characteristics and phenomena which occurs during firing. In $(\text{Ba,Ca}) (\text{Ti,Zr})\text{O}_3$ ceramics, which is widely used for ceramic capacitors, we have investigated the effect of MgTiO_3 and microstructural changes during firing. And we have found that the final grain size was strongly depend on the firing profile, especially on the cooling curve.

2. EXPERIMENTAL

2.1. Samples

The composition and the preparation method of samples are shown in Table-I.

2.2. Rapid Cooling Experiments

Samples were fired along the temperature profile shown in Fig.1, and were air quenched from various points of this profile. Microstructural changes were examined to those samples by SEM and EPMA.

3. RESULTS AND DISCUSSION

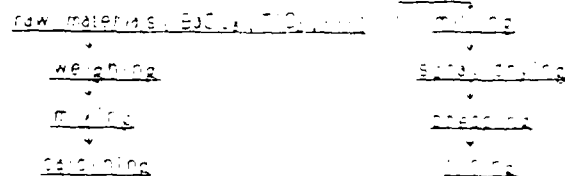
From the result shown in Fig.1, it was found that the addition of MgTiO_3 retards the grain growth, and grain growth was occurred at cooling zone in sample B. Photo 1 (a) and (b) shows the microstructure of samples containing 4% MgTiO_3 quenched from 1380°C and 1250°C respectively. Photo 1 (a) shows second phase, which is observed as dark phase, wets grains and exists at grain boundary. On the contrary, in the sample quenched from 1250°C (Photo 1 (b)), the second phase was observed as a granule. Fig.2. shows the change of the angle of contact between matrix and this second phase. Fig.3. shows the DTA data of sample C at cooling zone and it was found that exso-thermic process was occurred.

From these results, we inferred that this second phase was liquid at high temperature (T_1) and grains were surrounded by this liquid, at cooling zone (T_2), this liquid was solidified and disappear from grain boundary, so grain growth was occurred.

Table 1. a) Composition of samples (mol%)

Sample	BaTiO_3	BaZrO_3	CaTiO_3	MgTiO_3
A	800	115	5.5	0
B	770	110	5.0	4.0
C	400	60	4.0	500

b) Preparation method of samples



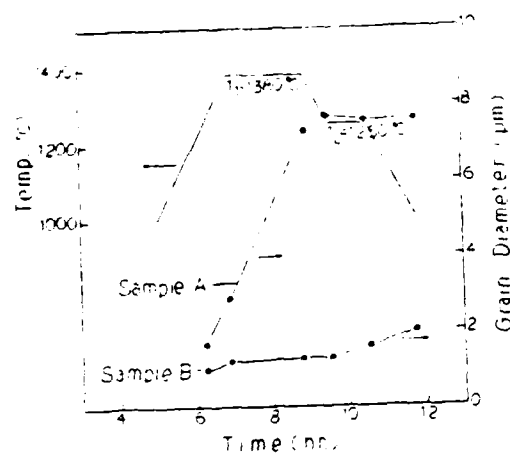


Fig. 1. Change of grain sizes of sample A and B by Rapid Cooling Experiment

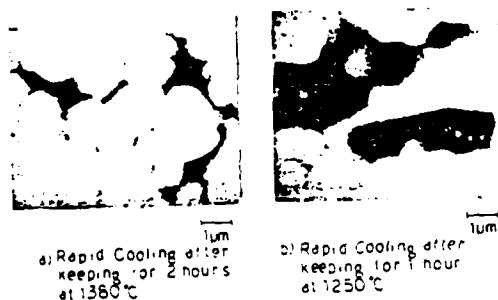


Photo 1. Microstructures of sample B observed by SEM (Composition Image)

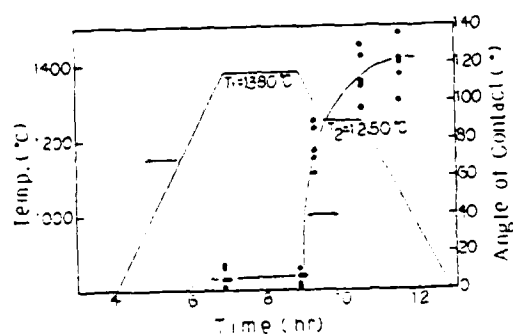


Fig. 2. Angle of contact by Rapid Cooling Experiment (sample B)

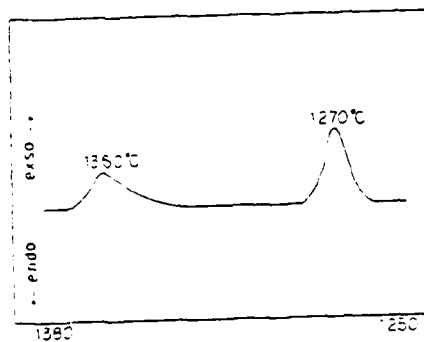


Fig. 3. DTA data during cooling (sample C)

REFERENCES

1. D. Hennings and H. Schreinemacher, *Mat. Res. Bull.*, **12**, 1221-1226 (1977).
2. D. Hennings and A. Schreier, *J. Am. Ceram. Soc.*, **65**, 539-544 (1982).

MACHINING OF PZT, PT, AND (Mn, Zn)Fe₂O₄ CERAMICS BY LASER-INDUCED CHEMICAL ETCHING

I. SHIOSAKI and A. KAWABATA

Department of Electronics, Faculty of Engineering, Kyoto University,
Kyoto, 606, Japan

ABSTRACT: Laser-enhanced chemical etching of PbTiO₃, PZT and (Mn-Zn)-ferrite ceramics is reported. The KOH solution of 10 mol/l is suitable for the laser enhanced inter-granular etching of the PbTiO₃ and PZT with depth etching rate higher than 100 $\mu\text{m/s}$ in the initial laser irradiation period of Ar⁺ laser of 1W output. The KOH and NaOH solutions are also suitable for the inter-granular etching of (Mn-Zn)-ferrite. The H₃PO₄ solution of 6 mol/l is suitable for the laser enhanced trans-granular etching of (Mn-Zn)-ferrite with the depth etching rate of about 10 $\mu\text{m/s}$ in the initial irradiation period of an Ar⁺ laser of 1W output.

1. INTRODUCTION

A number of interesting new schemes for localized etching of semiconductors and ceramics using lasers have been reported over the last years. The laser plays a dual role in the etching process through the thermal or optical excitation to the etchant and/or workpiece. The one is to initiate or enhance the etching process and the other is to define the etch pattern by the area irradiated.

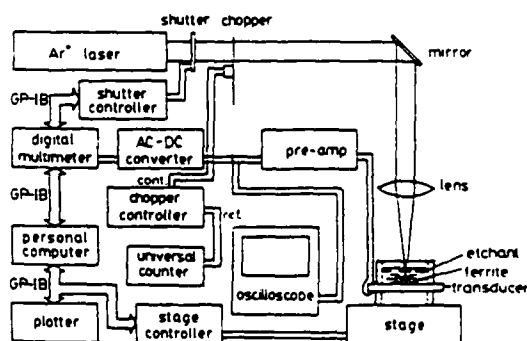


Fig.1 Experimental set-up for laser-induced chemical etching. The photo-acoustic emission detected by the transducer is used for the automatic focussing.

In the present paper, the laser enhanced etching of ceramics of PT: (Pb_{0.76}Ca_{0.24})(Ti_{0.96}(Co_{1/2}W_{1/2})_{0.04})O₃ from Toshiba, PZT: Pb(Sn_{1/2}Sb_{1/2})_{0.05}Ti_{0.47}Zr_{0.48}O₃ from Murata, and Mn-Zn ferrite (Fe₂O₃ 52.4 mol%, MnO 26.5 mol%, ZnO 21.1mol%) from Sumitomo Special Metal in alkaline and acid solutions without external electromotive driving sources is described.

2. EXPERIMENTAL

Figure 1 is the set-up for the laser enhanced etching. When a new material is introduced as a new workpiece of the laser enhanced etching, experiments are started with the selection of etchants and their concentration. The depth and width etching rates are measured for various laser output power levels (maximum 1W) and the surface morphology and appearance of etched holes and slots are examined in several etchants and in air and a pure water.

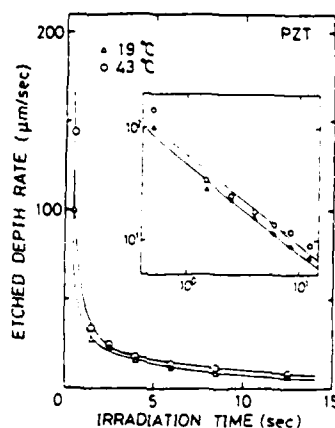


Fig.2 The relation between the laser-induced etching rate and the laser irradiation time. The laser output is 1W and the focal length of the lens is 30mm. KOH solution is 10mol/l.

4. RESULTS

The etching rates of the PI and PZT without laser irradiation in 10 mol/l KOH which is the most suitable etchant for these are almost equal and less than 3×10^{-5} $\mu\text{m/s}$. This means area without laser irradiation remains virtually unchanged during the process. The relation between the laser irradiation time and etched depth rate for PZT is shown in Fig.2. The etching rate is enhanced from less than 3×10^{-5} $\mu\text{m/s}$ to 150 $\mu\text{m/s}$ by 5×10^6 times.

The scanning electron micrographs of laser machined workpieces show that the hole made in air has a peripherally smooth contour with some voids typical of a material that has once melted and refrozen. The upper periphery of the hole is surrounded by a ridge of refrozen material. The results when the laser is incident on the sample submerged in water are similar to those in air, but somewhat less material is removed. The dimpling and splashing of materials on the surface indicates local melting and refreezing. In both machining in air and water, cracks are frequently observed after laser irradiation. All the acid etchants are not suitable because their etching rate is low, machined surface appearance is not good, and the acid gas is vaporized and condensed on the lens. Only in the presence of KOH around 10 mol/l in water, the hole wall is uniform in texture, and the top surface at the hole's periphery is smooth and even, both being similar to the texture of the unetched surface of the ceramics. Similarly, slots etched in the 10 mol/l KOH solution contain no lip or melted and refrozen ridges in contrast to those formed in air or water. The 10 mol/l KOH solution gives the highest etching rate and excellent surface appearances. Taking all the results into account, 10 mol/l KOH water solution is decided to be the most suitable etchant for the Ar^+ laser etching of the present PZT and PT.

The X-ray diffraction pattern of the powders which are collected from the etchant

after laser enhanced etching of PZT is shown in Fig.3, together with the pattern of the PZT ceramic plate. These patterns are identical and show that the laser enhanced etching is an inter-granular etching by removing the ceramic grains one after another and not by melting, dissolving or vaporizing the grains. This inter-granular etching mechanism is confirmed by observing the etched surface of PZT ceramics.

The above mentioned inter-granular etching mechanism takes place also in the laser enhanced etching of the (Mn-Zn)-ferrite in the NaOH solution. The laser enhanced etching of (Mn-Zn)-ferrite ceramic in H_3PO_4 solution is concluded as trans-granular etching by observing the etched surface. The H_3PO_4 solution is known as a mirror etchant of the (Mn-Zn)-ferrite ceramic.

The piezoelectric and magnetic properties are supposed to remain unchanged because the surface temperature is kept below the boiling point around 100°C of etchants and the grains are not melted.

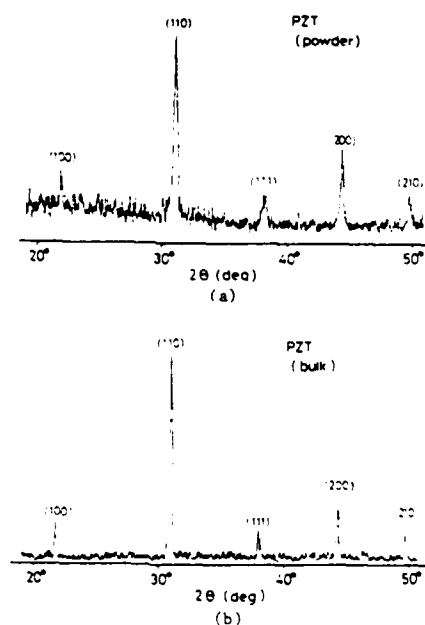


Fig.3 The X-ray diffraction patterns of the powders (a) and bulk (b) of PZT. The PZT powders are collected from the etchant.

SYNTHESIS AND PROPERTIES OF ALKOXY-DERIVED $Zr_xTi_ySn_zO_4$ CERAMICS

S. HIRANO, T. HAYASHI, and A. HATTORI

Department of Applied Chemistry, Faculty of Engineering, Nagoya University,
Nagoya, Japan

ABSTRACT: Monosized spherical particles of $Zr_xTi_ySn_zO_4$ ($x+y+z=2$) with an average diameter of about 0.3 μm were synthesized by the controlled hydrolysis of alkoxides. The as-prepared particles were formed directly without any sintering aid and sintered into bodies with > 96.0 % of theoretical density at 1600°C for 3 hrs. The pure sintered body of $Zr_{0.80}Ti_{0.20}SnO_4$ showed the dielectric constant of about 40 and the Q value of about 5300 at 10 GHz.

1. INTRODUCTION

Many kinds of dielectric materials have been developed for microwave applications. Among them, the compound in the system Zr-Ti-Sn-O, $Zr_xTi_ySn_zO_4$ ($x+y+z=2$), is known to have a high dielectric constant, a low dielectric loss and a low temperature coefficient of resonance frequency¹⁾. The compound has been sintered with the sintering aids like ZnO, NiO, Fe_2O_3 and La_2O_3 ^{1,2)}.

This study was carried out in order to characterize the monosized spherical particles of $Zr_xTi_ySn_zO_4$ ($y=1$) prepared by the controlled hydrolysis of metal alkoxides from the view-point of the dielectric properties.

2. EXPERIMENTAL PROCEDURE

Zirconium n-propoxide, titanium isopropoxide and tin isopropoxide were weighed in desired amounts according to the formula $Zr_xTi_ySn_zO_4$ and were mixed into absolute n-propanol. The mixture of alkoxides was refluxed in dry N_2 for 24 hrs and then hydrolyzed at a refluxing temperature or room temperature. The precipitates were aged and ultrafiltered. The amorphous as-precipitated $ZrTiO_4$ and $Zr_xTi_ySn_zO_4$ were calcined for 5 hrs at the crystallization temperature of 700°C and 650°C, respectively, and then pressed into the disks, or pressed into the disks directly and then preheated at 690°C for 5 hrs, followed by sintering at 1600°C for 3 hrs. The dielectric properties of dense sintered bodies at microwave frequency were measured by the resonant cavity method in $TE_{01\delta}$.

3. RESULTS AND DISCUSSION

The effect of hydrolysis conditions on the particle size and morphology of as-precipitated particles of $Zr_{0.80}Ti_{0.20}SnO_4$ is shown in TABLE 1. The particle size and morphology of as-precipitated particles did depend on the temperature during hydrolysis, especially for the composition of $Zr_{0.80}Ti_{0.20}SnO_4$. The higher the hydrolysis temperature, the size of the precipitated particles became larger. The spherical particles could be prepared by the hydrolysis of the solution at a refluxing temperature or of the lower concentration of 0.025 mol/l. The as-precipitated powders were found to be the monosized unagglomerated particles of about 0.3 μm with narrow particle size distribution (Fig.').

Calcined ZrTiO_4 powders were densified to fully dense bodies by sintering at 1600°C for 3 hrs, while the densification of $\text{Zr}_{0.80}\text{TiSn}_{0.20}\text{O}_4$ particles depended strongly on the processing, i.e. the process A (as-precipitates \rightarrow directly forming \rightarrow crystallization \rightarrow sintering) or the process B (as-precipitates \rightarrow calcination \rightarrow forming \rightarrow sintering), as shown in TABLE 2. The density of the sintered body through the process A was higher than that through the process B, though the green densities with both processes were the same. The finer particles ($0.1 - 0.2 \mu\text{m}$) yielded the higher density of the sintered body, compared with that from the powders ($0.3 - 0.4 \mu\text{m}$).

Dielectric properties of the dense sintered bodies at 10 GHz are shown in TABLE 3. $\text{Zr}_{0.80}\text{TiSn}_{0.20}\text{O}_4$ ceramics showed lower dielectric constant than ZrTiO_4 , but higher Q value of about 5300 at 10 GHz, and the lower temperature coefficient of resonance frequency of about 4 ppm/ $^\circ\text{C}$, which were superior to those of ZrTiO_4 ceramics.

TABLE 1. Effect of hydrolysis conditions on particle size and morphology of as-precipitates, $\text{Zr}_{0.80}\text{TiSn}_{0.20}\text{O}_4$

Conc. (mol/l)	Hydrolysis Temp.	Particle Size (μm)	Morphology
0.05	room temp.	< 0.1	irregular
0.05	reflux	0.3-0.4	spherical
0.025	room temp.	0.1-0.2	spherical
0.025	reflux	0.3-0.4	spherical

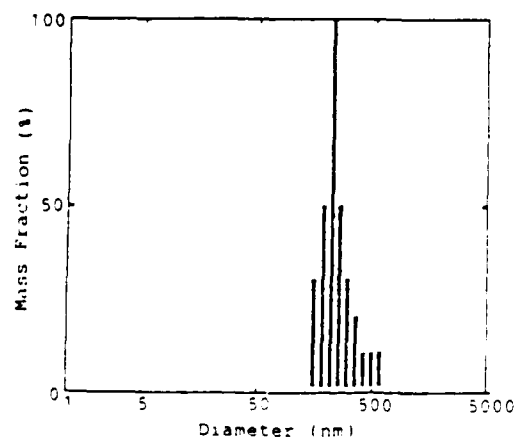


Fig. 1. Particle size distribution of alkoxy-derived $\text{Zr}_x\text{Ti}_y\text{Sn}_2\text{O}_4$

TABLE 2. Effect of processing on sintering of $\text{Zr}_{0.80}\text{TiSn}_{0.20}\text{O}_4$

Particle Size (μm)	Process *	R.D. (%)	
		Before Sinter.	After Sinter.
0.1-0.2	A	49	96
0.3-0.4	A	55	92
0.3-0.4	B	55	80

*Process A; As-precipitates \rightarrow Consolidation \rightarrow Crystallization \rightarrow Sintering
 Process B; As-precipitates \rightarrow Calcination \rightarrow Forming \rightarrow Sintering

TABLE 3. Properties of bodies sintered at 1600°C for 3 hrs

	R.D. (%)	ϵ_r	Q	τ_f (ppm/ $^\circ\text{C}$)
ZTS	96	39.5	5323	3.7
ZTS	92	35.7	5387	3.3
2T	100	45.4	2712	72.4
2T	100	45.6	2761	64.3

2T; ZrTiO_4 ZTS; $\text{Zr}_{0.80}\text{TiSn}_{0.20}\text{O}_4$

REFERENCES

1. K. Wakino and H. Tamura, J. Ceram. Soc. Jap., **88**, 475 (1980).
2. G. Wolfram and H. E. Goebel, Mat. Res. Bull., **16**, 1455 (1981).

EFFECT OF AGGLOMERATED PARTICLES ON PROPERTIES OF CERAMIC GREEN SHEETS

TAMOTSU UYEYAMA, NAOYA KANEKO, and YŌICHI MACHII

Shimodate Research Laboratory, Hitachi Chemical Co., Ltd. 1380-1 Tarazaki,
Katsuta, Ibaraki, 312 Japan.

ABSTRACT: Packing density of dielectric powders in ceramic green sheets was investigated. The packing density was changed by agglomerated particle size and binder content. The smaller agglomerated particle size and/or binder content is, the higher the packing density becomes.

1. INTRODUCTION

In manufacturing dielectric ceramic green sheets, it is very important to decrease scatter of packing density of green sheets. Scatter of packing density causes that of firing shrinkage. Particularly, when packing density becomes low, many pores tend to be generated in sintered body.

We have investigated slurry manufacturing technique and developed the new technique of dielectric powders. Using this technique, agglomerated particles can be pulverized primary particles without mechanical destruction, and as the result of it, scatter of packing density decrease remarkably.

In this report, the relationship between agglomerated particle size and packing density of green sheets, which are manufactured by the new manufacturing technique, is described. Moreover, the relationship between binder content and packing density of dielectric powders is discussed.

2. EXPERIMENTAL

As dielectric powders, Al_2O_3 and $BaTiO_3$ was used in this work. Table 1 and 2 gives the typical composition of green sheets.

Table 1 Typical composition of Al_2O_3 green sheets

Material	weight parts
Al_2O_3	100
Binder (Poly vinyl Buty rate)	6
Plasticizer (Bulyul Benzil phthalate)	3
Solvent (Chlorinated Hydrocarbon & Alcohol Mixture)	Proper Quantity

Table 2 Typical composition of $BaTiO_3$ green sheets

Material	weight parts
$BaTiO_3$	100
Binder (Poly methyl methacrilat)	12.4
Plasticizer (Bulyul Benzil phthalate)	1.4
Solvent (Chlorinated Hydrocarbon & Keton Mixture)	Proper Quantity

Slurries were produced using new advanced ballmilling technologies. In new advanced technique, agglomerated powders can be pulverized to primary particles.

Dielectric ceramic green sheets were produced by the doctor blading process.

3. Result and Discussion

3.1 Agglomerates size and packing density

Result are shown in Fig. 1, 2. When agglomerates are pulverized the packing density gradually increases, and reaches the saturation value when the size of the primary particles is attained. This value is almost equal to the packing density of 60.45 vol% calculated with monosized powders cast without pressure.

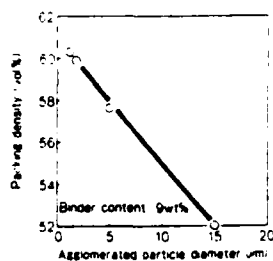


Fig 1 Relationship between agglomerated particle diameter and packing density of Al_2O_3 green sheet

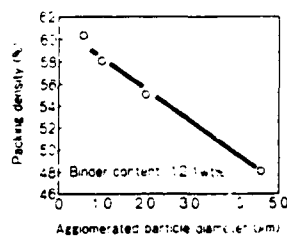


Fig 2 Relationship between agglomerated particle diameter and packing density of BaTiO_3 green sheet

3.2 Binder Content, Packing density and packing forms of monosized balls.

Figure 3 indicates the relation between packing arrangement and packing density of monosized balls. When monosized powders are packed without external force like doctor blading process, it can be presumed that maximum coordination number of powders is 8. Therefore, theoretically, maximum packing density of monosized powders in green sheets is 60.45 vol%, which is the value of single stagger arrangement in Fig. 3.

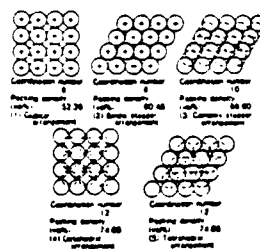


Fig 3 Packing forms of monosized balls

Figure 4, 5 shows the relationship between binder content and packing density; the smaller the agglomerates diameter and/or binder content, the higher the packing density of Al_2O_3 and BaTiO_3 powders.

The maximum packing density of dielectric powders, which was obtained in this work, is nearly equal to this theoretical packing density of monosized powders.

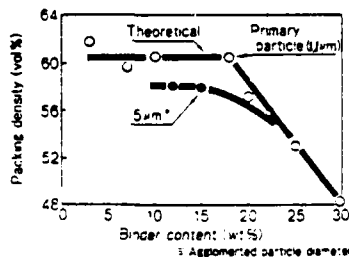


Fig 4 Relationship between binder content and packing density of Al_2O_3 green sheet

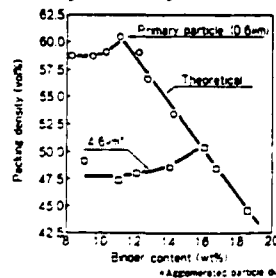


Fig 5 Relationship between binder content and packing density of BaTiO_3 green sheet

4. CONCLUSIONS

1. Packing density in the green sheets increases at decreasing agglomerate size, and reaches the saturation value of 60.4 vol% when the size of agglomerates reaches the primary particle size.
2. The saturation value of 60.4 vol% is well matched with the packing density of 60.45 vol% corresponding to a coordination number 8 for monosized particles in single stagger arrangement.
3. Especially, in the case of BaTiO_3 green sheet, when agglomerates are pulverized packing density reaches a maximum at a definite binder content, and decreases when the binder content deviates from this level, either downward or upward.
4. The packing density decrease which occurs when the binder content in the green sheets is too small is assumed to derive from a weaker bonding force of the polymethyl methacrylate binder which incompletely fills interparticle voids.

SINTERABILITY OF HIGH-PACKING DENSITY BaTiO_3 GREEN SHEETS

Tamotsu Ueyama,*Shozo Yamana, and Naoya Kaneko
Shimodate Research Laboratory, Hitachi Chemical Co., Ltd. 1380-1 Tarazaki
Katsuta, Ibaraki, 312 Japan

ABSTRACT: Sintering properties was discussed regarding BaTiO_3 green sheets which packing densities were different. The sinterability of BaTiO_3 dependent greatly on agglomerates size rather than on the packing density of powder. The larger the agglomerates size are, the more the optimum firing temperature which are vanished of open pores was shifts toward the high-temperature side, and the firing density then is diminished significantly. On the other hand, green sheets which are pulverized into primary particles have the firing density fixed at the constant value 5.8 and does not change at all even when the packing density is significantly lowered by varying the amount of binder.

1. INTRODUCTION

The low temperature sintering of dielectric ceramic is study by using fine powder and Liquid phase.

We developed technique to pulverize agglomerated fine powder gradually into primary particles in the slurry.

By using this slurry, production of green sheets which packing density is almost equal to theoretical packing density is enabled.

This report describes the relationship between the agglomerates size and packing density and sinterability on the green sheets of BaTiO_3 which was manufactured by this technique.

2. EXPERIMENTS

As dielectric material, BaTiO_3 was used in this work. Table 1 gives the chemical composition of BaTiO_3 powder. Dielectric green sheets were produced by the doctor blading process. Samples were sintered in the range 700 - 1,300°C in an atmosphere.

Table 1 Characterization of BaTiO_3 powder*

Item	Density	Specific surface area	Average particle Diameter	Chemical composition											
				Ba	Ti	Pb	Zn	Nb	Bi	Co	Si	Mn	Al	Sr	Ni
Unit	g/cm ³	m ² /g	μm	%											
Observation	6.01	2.52	0.6	52.1	19.1	1.63	0.84	0.75	0.45	0.20	0.13	0.02	0.02	0.03	0.01

* TANTRON CERAMICS

3. RESULT AND DISCUSSION

3.1 Agglomerates and Firing Density

Result are shown in Fig. 1.

The increase in the density of BaTiO_3 which are pulverized into primary particles at between 1120 - 1200°C is very slowly. In the case of BaTiO_3 when agglomerates size is large, the increase in this density is comparatively large. The large agglomerates size is, the larger this tendency of increasing in the density is.

3.2 Agglomerates Size and Open Pore Vanishing Temperature

Result are shown in Fig. 2. As shown in Fig. 2, the smaller the agglomerates size is, the lower the firing temperature is.

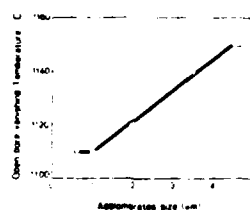
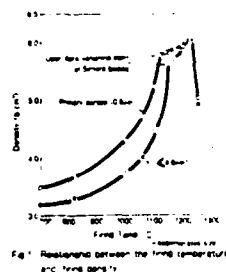


Fig. 2 Relationship between the open pore vanishing temperature of sintered body and agglomerates size of BaTiO_3

3.3 Effect of Packing Density and Agglomerates Size on the Firing Density

Result are shown in Fig. 3.

Sintering density of the BaTiO_3 is decided not by packing density but by the agglomerates size of powder in the green sheets. Possible reasons for this is that the extra voids are made because agglomerated particles are disturbed in the arrangement condition of powder by steric hindrance and further pores are made in the sintered body because sintering progresses with closed voids left in agglomerated particles.

Fig. 4 shown the relationship between the agglomerates size and the density of the sintered body which are fired at open pore vanished temperature. The density of a sintered body increases rapidly when agglomerated particles are pulverized into small agglomerates size, and at the primary particle diameter, saturation is carried out at the Maximum value 5.8 g/cm^3 .

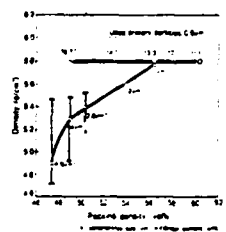


Fig. 3 Relationship between the packing density and firing density when sintered at open pore vanishing temperature

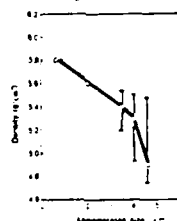


Fig. 4 Relationship between the agglomerates size and firing density when sintered at open pore vanishing temperature

4. CONCLUSION

1. Sinterability is improved lowering the open pores vanishing temperature when agglomerates size diminishes.
2. When agglomerated particles are pulverized into primary particles, the firing density of BaTiO_3 at the open pore vanishing temperature becomes a fixed value of 5.8 g/cm^2 .
3. This value does not change at all even when the amount of binder in the green sheets is varied and the packing density is changed within the range of $49 \sim 60.4\%$. The reason for this considered is that the sinterability becomes the same because the packing density becomes the same value 60.4% after debinding.
4. The firing density changes greatly depending on agglomerates size rather than the packing density. For instance, it becomes 4.9 g/cm^3 when the agglomerates size of BaTiO_3 is $4.6 \mu\text{m}$. This value becomes 5.4 g/cm^3 at $3.5 \mu\text{m}$ and 5.6 g/cm^3 at $2.5 \mu\text{m}$.

Possible reasons for this is: numerous pores are made within the sintered body because agglomerates size is disturbed in the packing arrangement due to steric hindrance making extra voids between agglomerated particles and further sintering progresses with closed voids left within the agglomerated particles.

M-10

AN INVESTIGATION OF THE LOW VOLTAGE FAILURE MECHANISM* IN MULTILAYER
CERAMIC CAPACITORS

C. JOHN BRANNON and H.U. ANDERSON

Department of Ceramic Engineering, University of Missouri-Rolla, Rolla,
Missouri 65401, U.S.A.

ABSTRACT: Increased leakage current was induced into multilayer ceramic capacitors by the introduction of cracks reaching from the surface through the electrode layers by means of thermal shock and then exposing the capacitors to a low voltage bias and a humid atmosphere. Results indicated that electrolytic conduction may be responsible for the increased conduction and that the proposed dendritic growth mechanisms may be more complex than necessary.

1. INTRODUCTION

In recent years a problem has been identified which concerns the insulation resistance failure of ceramic capacitors which are biased well below their rated voltages. This is a significant problem, and a research effort has focused on determining the cause of low voltage failures as well as developing a testing procedure to effectively detect those capacitors that might be prone to low voltage failures. It is a generally recognized among observers of low voltage failure that failure tends to occur only in the presence of moisture and most often in capacitors having such structural defects as voids, delaminations, or cracks extending from the surface through the electrode layers.

The dominant theory of low voltage failure in ceramic capacitors involves the growth of a dendrite of electrode material that connects two electrode layers and thus produces a short in the capacitor. According to this theory, the electrode material is dissolved in the water that condenses in the present defects which allows the dendrite to grow along the defect connecting two electrode layers.¹⁾ The conducting dendrite grows either by electroconduction or by precipitation. This kind of low voltage failure may be cleared by the application of a voltage high enough to vaporize the dendrite. This study reports on the interrelationship between cracks, moisture, temperature and applied voltage on the low voltage failure of multilayer ceramic capacitors.

2. EXPERIMENTAL

2.1. Materials

Special X7R, multilayer capacitors were prepared by Presidio Components, Inc., San Diego, California. The capacitors consisted of two Pd electroded 0.003 cm dielectric layers which were buried 0.0076 cm from each surface

*Study sponsored by the Office of Naval Research

and separated by 0.088 cm. The separation of the layers enabled cracks to be introduced from the surface through an electrode pair without structurally damaging the capacitor.

2.1. Measurements

To insure their integrity, the entire lot, 128 units, was subjected to the methanol test.²⁾

Structural defects in the form of cracks were introduced into one half of the capacitors by thermal shocking. Trial and error experimentation revealed that a temperature gradient of approximately 770°C would introduce cracks extending from the surface of the capacitor through the electrode layers without otherwise damaging the properties of the capacitor.

The cracked and reference capacitors were subjected to a variation of the standard 85/85 test in which the atmosphere was allowed to be either dry or to contain 85% RH, usually in a 4 hours dry, 4 hours wet, and 4 hours dry pattern. Voltages were applied to the capacitors (0.5 to 70 VDC) and the leakage current monitored for times up to 20 days at temperatures ranging from 85 to 115°C.

3. RESULTS

In almost all cases in which low voltage failure occurred, a "sawtooth" pattern of failure was observed. With a dry atmosphere, and 1.5 VDC current density would typically hold steady at approximately 10^{-11} amps/cm². When a 85% RH atmosphere was introduced, the leakage current would typically smoothly rise about 2 orders of magnitude and begin to level off at a current "plateau". The leakage current would then abruptly jump anywhere from 1 to 6 orders of magnitude and then smoothly decrease to the "plateau" level. The current level would then abruptly jump again, thus repeating the cycle until the moisture was removed from the atmosphere. The period of this cycle was usually seen to be between 20 and 45 minutes.

Low voltage failure was found to be dependent upon the voltage level on the capacitor. When a bias of 0.5 volts was introduced, no difference was observed between the leakage current of the cracked and the reference, uncracked specimen. However, at a bias from 1.0 to 20 VDC low voltage failure clearly occurred with the same "sawtooth" behavior as previously observed.

Lifetests were extended to up to 20 days with no change in the "sawtooth" pattern which was observed at 85% RH and 85°C. During these tests when the moisture was removed all of the failing capacitors showed a slow decrease of the leakage currents until they matched the reference capacitors. In a series of tests temperature was varied. The leakage current was low in the dry 85°C atmosphere, and increased dramatically when the humidity was raised. When, with the humidity still at 85% RH, the temperature was raised to 115°C, the leakage current returned to its original, lower level and the "sawtooth" pattern could no longer be observed. This supports the idea that water which condenses into the cracks in the capacitor plays the dominant role in low-voltage breakdown.

4. DISCUSSION

The low voltage current induced in the capacitors of this study exhibits the "classical" low voltage failure characteristics, i.e. the presence of

structural defects in the capacitors and the ability of high voltages to "clear" shorts in the capacitors. The "sawtooth" pattern of failure is peculiar to this study, although this behavior has been seen in porous disc capacitors exposed to similar voltages and humid atmospheres.³⁾

The "sawtooth" behavior and the absence of excess electrode material being found anywhere in the cracks suggests that dendrites are not responsible for the failure. Breakdown ceased immediately after the moisture was removed from the atmosphere which suggests that dendrites cannot be the source of the increased leakage current. Even if dendrites require water to grow in the defects, once grown they should continue to exist and facilitate breakdown.

It is much more likely that ionic conduction causes the increased leakage current. If electrolytic impurities such as chlorine or bromine salts were present conduction between the electrode layers could have occurred by means of electrolytic solution. Any soluble impurity ions could conceivably take part in this mechanism. Also, water undergoes dissociation to H^+ and OH^- at 0.87 volts, which could increase conductivity. The fact that the onset of the "sawtooth" behavior occurs at voltages greater than 0.5 VDC supports this suggestion. At higher voltages the increased currents could generate enough localized heat to facilitate the evaporation of the aqueous conductor. This could also account for the "sawtooth effect" with the rapid rise in current producing enough heat to effectively halt itself.

Electrolytic conduction is a much simpler breakdown mechanism than dendritic growth, and does not require as narrow a range of conditions in order to take place. Furthermore, conditions postulated to be necessary for dendritic growth, such as the presence of moisture in existing defects and the presence of Cl ions, are ideally suited for the facilitation of an electrolytic solution as the conduction mechanism.

5. REFERENCES

- 1.K. Sato, et al., "A Low-Voltage Screening of Ceramic Capacitors From Leakage Failures", Proceedings of the International Symposium for Testing and Failure Analysis, 1981.
- 2.R.C. Chittick, E. Gray and J.H. Alexander, "Non-Destructive Screening for Low-Voltage Failure in Multilayer Capacitors", Proceedings of the 3rd Annual Capacitor and Resistor Technology Symposium, March 1983.
- 3.W. Huebner, Unpublished Research Conducted at the University of Missouri-Rolla, 1983.

Third US-Japan Seminar on Dielectric and Piezoelectric Materials

Additive Effects on Microstructure and Properties of BaTiO_3

R.C. Buchanan

University of Illinois at Urbana-Champaign

Abstract

Sintered ZrO_2 doped BaTiO_3 compacts were prepared with and without flux addition (≤ 2 wt%) from the $\text{CaO} \cdot \text{Al}_2\text{O}_3 \cdot \text{B}_2\text{O}_3$ system. In ZrO_2 doped samples (≤ 1.0 wt% ZrO_2) solid solubility was found to be significantly reduced when BaTiO_3 was densified ($>93\%$ ThD) at temperatures $\leq 1300^\circ\text{C}$. The added oxide was found to exist as a grain boundary phase, which constrained discontinuous grain growth, giving a uniform fine-grained microstructure, and an essentially flat dielectric constant/ temperature profile and low dissipation factor ($<1\%$) over the temperature range -30 to $+110^\circ\text{C}$. As the sintering temperature was increased by steps from 1300 to $1350^\circ\text{C}/1\text{-}2\text{h}$ soak, STEM EDS measurements showed a progressive Zr flux towards the grain centers and apparent counter migration of Ti ions, resulting in increased grain size and reappearance of the sharply peaked dielectric constant profile at the Curie temperature. Effectiveness of the peak suppression depended on the type of ZrO_2 used. With Ca-stabilized ZrO_2 additions, greater densification was achieved at equivalent temperatures, and some PTC effect was noted with Yttria stabilized, compared to the unstabilized ZrO_2 additions.

In fluxed samples near theoretical densities were achieved at temperatures $<1175^\circ\text{C}$. Microstructural analysis showed nearly uniform grain sizes ($<1\mu\text{m}$) and properties consistent with unfluxed BaTiO_3 . X-ray analysis of both fluxed and unfluxed BaTiO_3 showed a decrease in the axial ratio with increasing ZrO_2 content up to 2.0 wt%, with the BaTiO_3 becoming

progressively more pseudo-cubic in structure. Accompanying the decrease in tetragonality was a lower dissipation factor and an increase in the dielectric constant. No significant ion flux across the grain boundaries was noted for these samples, attributed to the relatively low sintering temperature.

Dielectric behavior of the ZrO_2 doped and fluxed samples suggested the existence of a low dielectric constant boundary phase which constrained grain development, resulting in an expected preponderance of 90° domains adjacent to the grain boundary regions. Increased dielectric constant (small grain size), suppression of polarization response at T_c (lattice strain), low dissipation factor (small grain size, second phase) and low aging rate would be the expected result. Data on microstructure, and grain boundary structure and lattice parameter changes support these observations.

M-12

BARIUM TITANATE-BASED DIELECTRIC FOR MLC'S WITH HIGH K AND LOW FIRING TEMPERATURE

I. BURN and M.T. SECAUR

E.I. du Pont de Nemours & Co. (Inc.), Photosystems and Electronic Products Department, Electronic Materials Division, Wilmington, Delaware 19898, U.S.A.

ABSTRACT: A barium titanate-based dielectric has been developed which combines high volumetric efficiency, high reliability and low electrode cost. The dielectric has been formulated with controlled A/B site cation stoichiometry, a balance of donor and acceptor dopants, and a small amount (<1.5 wt%) of a specially prepared flux. The material is intended for Z5U/Y5U applications at thicknesses <25 microns and has a dielectric constant at 25°C of 9000-10,000 together with low aging rate and low losses. Silver electrodes containing <30% Pd can be used. Results of life-tests and fracture toughness measurements indicate the suitability of this dielectric for applications demanding high reliability.

1. INTRODUCTION

At the present time, a variety of techniques exist for making multilayer ceramic capacitors with high volumetric efficiency and low electrode cost; these include lead injection, nickel electrodes, and the use of lead-based relaxor systems. Much of the motivation for developing these technologies has resulted from the fact that dielectrics based on barium titanate, which were compatible with low-cost high silver content electrodes, had relatively low dielectric constant. The low dielectric constant is a consequence of the addition of glass or flux to the barium titanate to reduce its sintering temperature below the melting point of silver-palladium alloys. Substantial decrease in dielectric constant can result from dilution of the high K phase, or by unwanted chemical interaction between the glass or flux and the barium titanate. These problems have been avoided in a new barium titanate-based dielectric, known as XL103.

2. EXPERIMENTAL

Submicron barium titanate was blended with additives to shift the Curie temperature to 15-20°C, and to broaden the Curie peak to fit Z5U/Y5U temperature limits (e.g. a change in K <56% between 25 and 85°C). The composition contained a relatively small amount of lead and this was fully reacted so that it was retained completely in the ceramic during processing. No bismuth or cadmium compounds were used. A minimum of glass-forming oxides (silica, boron oxide etc.), and no fluorides, were added to aid sintering. The A/B site stoichiometry was carefully adjusted by considering the composition of the ceramic and flux as a whole; this minimized unwanted minor phases and controlled grain development.

The composition was designed for use with Du Pont 5200 binder solution to make tape (following the manufacturer's instructions) and 70% Ag/30% Pd electrodes (Du Pont 4772D). Organic binders were thoroughly removed by bake-out to 400°C, or bisque firing at 750°C. MLC's were fired on setters or in saggers at 1100°C for about 2 hours.

3. RESULTS

Typical results for MLC's of different styles are given in Table 1. Dielectric constant was 9300 to 10,000 with low DF at 1 volt/mil. TCC is tight at 85°C but K 10,000 is possible with Z5U or Y5U characteristics with careful processing, as illustrated in Fig. 1. A low aging rate of 3.0% per decade and low DF at ambient temperature and above result from operation on the paraelectric side of the Curie peak. As can be seen from Fig. 2, DF does not increase with frequency (in contrast, for example, to most relaxor dielectrics that are used for high K applications).

Finally, all the test data indicate that this is a very reliable dielectric. The material has a fracture toughness of 0.9 MPa.m^{1/2}, typical of dielectrics based on barium titanate, and has survived various DC bias and humidity/bias tests as summarized in Table 2.

4. CONCLUSION

Low-firing dielectrics based on barium titanate are safe and easy to process, and have an established reputation for reliability. Competitive K's for Z5U or Y5U applications are now possible.

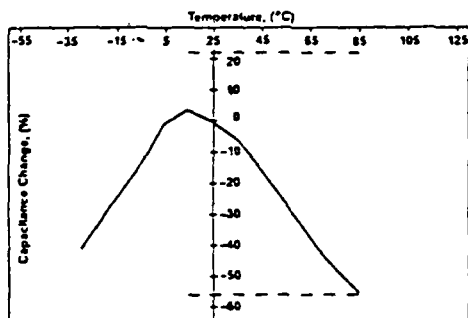


Fig. 1. TCC of XL103 (K = 10,000 ± 500)

TABLE 1. Electrical Properties of XL103

Firing Temp. (°C)	Effective K	1 VRMS % DF	$\Delta C @ 85^\circ C$ (%)	RxC 25°	RxC 85°
(0.5 μF 2225 Size 5 Active Layers)					
1100	10,000	1.00%	-61.9	11500	2100
1080	9,700	1.20%	-55.9	10900	2000
(0.17 μF 1209 Size 10 Active Layers)					
1100	10,000	1.30%	-56.9	10000	1000
1080	9,300	1.40%	-54.5	10000	1000

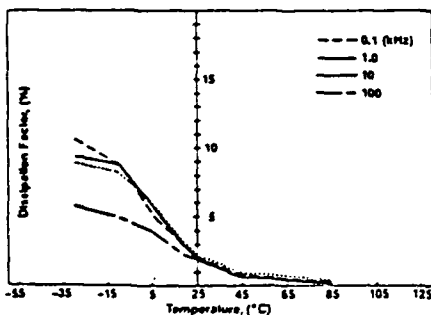


Fig. 2. DF vs. Frequency (1V/mil)

TABLE 2. MLC Life-Test Performance (25 μm layers)

Volts	Temp. (°C)	Time (h)	Result
100	85	1000	No degradation
200	125	24	No degradation
50	85/85 R.H.	1000	No degradation

ELECTRICAL CONDUCTION IN BaTiO_3 -BASED CERAMIC

L. C. BURTON and H. Y. Lee

College of Engineering, Virginia Polytechnic Institute and State University,
Blacksburg, VA 24061

ABSTRACT: The physics of electron conduction in BaTiO_3 -based ceramic is reviewed. Measurements related to a conductivity anomaly near the Curie temperature for high resistance BaTiO_3 ceramic are presented. Contributions of donor ionization energy, crystallographic transition, and grain boundary barrier are discussed.

1. INTRODUCTION

We have established, for some specific types of BaTiO_3 -based ceramic, that current is caused by electrons, with a near-exponential time increase that can be attributed to ionic movement and/or grain boundary impedance reduction.⁽¹⁾ The contribution of grain boundaries to impedance of high resistance BaTiO_3 -based ceramic ($> 10^{13}$ ohm-cm) is, however, still not clear. This study is intended to help clarify this issue.

2. EXPERIMENTAL

Galvanic, thermoelectric and leakage current measurement techniques we have used on BaTiO_3 -based samples are described in the literature.^(2,3) These measurements were performed mostly at elevated temperatures. In an effort to improve understanding of conduction in high resistance ceramic near room temperature, we have extended dielectric constant and conductivity measurements to below 70°C . Samples are BaTiO_3 -based discs with guard ring electrodes, measured under low voltage (ohmic) bias.

3. RESULTS AND DISCUSSION

Galvanic, thermoelectric and current measurements versus temperature, voltage and time have been reported elsewhere.⁽¹⁻³⁾ Some of these results will be presented.

A conductivity versus inverse temperature plot for a high resistance BaTiO_3 ceramic disc is shown in Figure 1. This characteristic has at least two salient features: a) linear regions below and above the Curie temperature, with activation energies of about 0.66eV and 1.11eV respectively; b) a striking discontinuity near the Curie temperature. Such features do not resemble those of PTC or low resistance single crystal material. A somewhat similar spike (although much less prominent) has been reported for single crystal BaTiO_3 ,⁽⁴⁾ and for polycrystalline material,⁽⁵⁾ although those curves differ from that of Fig. 1 in other ways.

The causes of the conductivity peak have not been conclusively established. Since such a peak has been reported for single crystal material, it may not be totally a grain boundary effect for our case. However, the size of the peak in Figure 1 coincides with the large increase in permittivity, and a decrease in grain boundary barrier height would be expected. Another

possible mechanism is a reduction in conduction electron ionization energy, since such energies in general vary inversely with permittivity. More extensive measurements on polycrystalline samples, with varying grain size for example, will be necessary to clarify these points.

1. H. Y. Lee and L. C. Burton, to be published in IEEE-CHMT Transactions (Dec. 1986).
2. H. Y. Lee, K. C. Lee, J. N. Schunke and L. C. Burton, IEEE Transactions CHMT-7, 443 (1984).
3. L. C. Burton, IEEE Transactions CHMT-8, 517 (1985).
4. A. Branwood and R. H. Tredgold, Proc. Phys. Soc. 76, 93 (1960).
5. K. Lehovic and G. A. Shirn, J. Appl. Phys. 33, 2036 (1962).

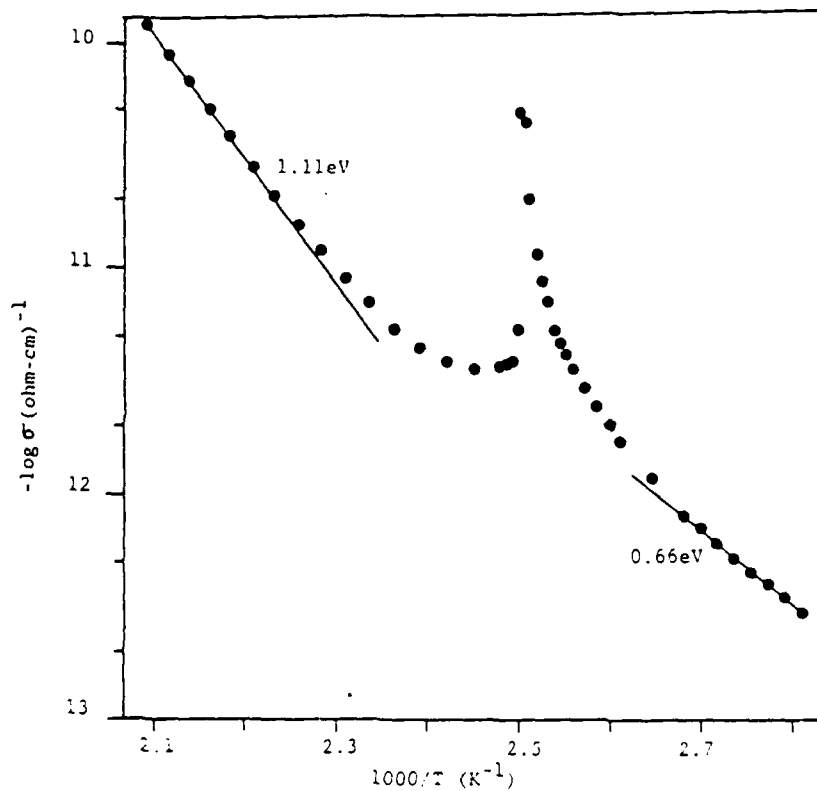


Figure 1. Electrical conductivity versus inverse temperature for BaTiO_3 ceramic disc. Conductivity spike occurs at Curie temperature.

M-14

DIELECTRIC AND PIEZOELECTRIC CERAMICS: HISTORICAL DEVELOPMENTS, CURRENT STATUS AND FUTURE PROSPECTS

L. ERIC CROSS

Materials Research Laboratory, The Pennsylvania State University, University Park, PA 16802

ABSTRACT: The present generation of dielectric and piezoelectric ceramics which are used in capacitors, transducers, actuators, and PTC thermistors draw heavily upon the phenomena of ferroelectricity and ferroelasticity. In this talk, the evolution in understanding of these phenomena will be traced and the ongoing interplay between basic understanding and 'serendipitous' technological innovation underscored.

The historical groundwork for the discovery of ferroelectricity was laid in the last century by famous crystal physicists Weiss, Pasteur, Pockels, Hooke, Groth, Voigt and the brothers Curie were major contributors. Beginning with the pioneer work upon Rochelle salt and KDP, the study of ferroelectricity accelerated rapidly during World War II with the simultaneous discovery of barium titanate in the U.S., Japan and the Soviet Union. There followed in the 1950's and early 60's a period of very rapid proliferation with more than 100 new ferroelectrics identified. Over this period, many Japanese scientists made major contributions both in Japan and to groups in the USA. In the following decade, the concepts of soft modes and order parameters lead to the age of "high science" in the sixties. Neutron experiments soon authenticated the soft mode concept and lead to the discovery of a number of peculiar improper ferroelectrics such as gadolinium molybdate. It was at this time that Aizu in Japan and Shuvalov in the USSR, using symmetry arguments, began to point up the possibilities of ferroelastic and of secondary ferroic phenomena.

In the seventies came the age of diversification in which the electro-^{tic} properties, defect chemistry and transport behavior in polycrystal ceramics were more fully explored, but much theoretical work diverged strongly from practical objectives following the fascinating structures with incommensurate phases, lock in transitions, improper, pseudo proper and coupled phase changes.

In the decade of the 80's, however, one discerns a convergence again between practical and theoretical with renewed focus upon "glassy ferroelectrics," 'ferroelectric relaxors' and other nanocomposite systems. New needs for very tough ceramics are driving more practical interest in ferroelastics and improper ferroelectrics, and renewed interest in the physics of martensitic metals begins to draw upon the lattice dynamic and phenomenological tools of the ferroelectrician.

For the technological thrusts in this decade, we are witnessing the beginnings of electroceramic integration, ferroelectric capacitors and piezoelectrics being integrated into multilayer ceramic packages along with metal interconnect circuitry and ceramic resistors. Following the trends clearly evident in semiconductors, we may look forward to further integration and miniaturization in the years ahead as the sophistication of new processing methods becomes more fully applied.

M-15

OPERATIONALLY INDUCED THERMAL STRESS GRADIENTS IN MULTILAYER CAPACITORS

JOSEPH P. DOUGHERTY

Advanced Materials Technologies, Niles, Michigan 48120, U.S.A.

1. INTRODUCTION

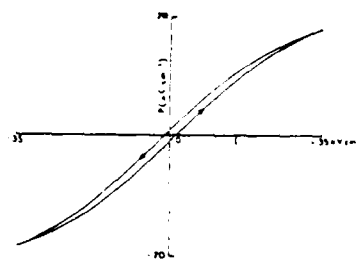
High permittivity multilayer capacitors are widely used in electronic digital and analog circuit designs. These ceramic capacitors are the engineering choice for many applications because of their compact size and low loss factors at high frequencies.

The ceramics used to manufacture multilayer capacitors are ferroelectric materials. Ferroelectrics are unique in that they have a spontaneous polarization that can be reversed or reoriented. It is this unique property of polarization reversal that gives ferroelectric ceramic materials the high permittivity properties that make them desirable.

2. HYSTERETIC HEATING

In addition to contributing to the permittivity, domain reversal also contributes to the dielectric losses. The hysteretic losses per cycle are equal to the area enclosed in the polarization/field or charge/voltage hysteresis loop. The result of the hysteretic effects is a self-heating mechanism. A typical example of a dielectric hysteresis loop is shown in Figure 1. These data were obtained using a computer controlled test apparatus that performed the function of the Sawyer-Tower Circuit but allowed for precise quantitative data interpretation.

The hysteretic heating and dielectric saturation effects are directly proportional to the magnitude of the spontaneous polarization. Thus, the Curie temperature acts as an upper limit on the heating effects produced by dielectric hysteresis. Figure 2 shows the temperature dependence of dielectric hysteresis in a Z5U ferroelectric ceramic capacitor.



TYPICAL LOOP FOR Z5U TYPE MATERIALS

EFFECTIVE DISSIPATION FACTOR

$$D_{eff} = W_d / W_s$$

W_d = Energy lost/cycle
= area of hysteresis loop

W_s = Energy stored/cycle
= $Q_{max} \cdot V_{max}$

Figure 1

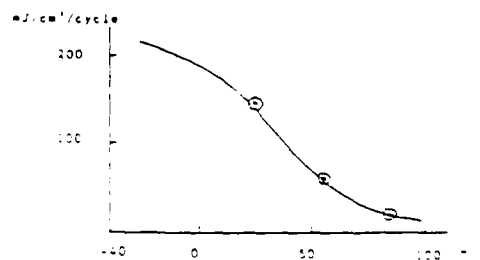


Figure 2

TEMPERATURE DEPENDENCE of HYSTERETIC LOSSES

Z5U TYPE 18a CAPS OF Q_D
CURIE TEMPERATURE = 40°C

3. THERMAL STRESS GRADIENTS IN MULTILAYER CAPACITORS

When an alternating voltage is applied to a high dielectric constant, multilayer ceramic chip capacitor, the component will self-heat due to the hysteretic effects intrinsic to the ferroelectric nature of the material. The high temperature itself is not intrinsically harmful to the ceramic capacitor. However, due to the manner in which multilayer capacitors are manufactured, the heat is not uniformly distributed in the capacitor. The hysteretic heating effects only occur in the ceramic material that is between two electrode layers. This leaves a dead zone near the end terminations that has no electric field and therefore, no dielectric heating (Fig 3). The result of this situation is to set up a thermal gradient that couples through thermal expansion to set up a stress gradient in the ceramic.

4. CALCULATED HEATING RATE AND STRESSES

Using the temperature dependent dielectric heating data shown in Figure 2, it is possible to make an approximate calculation of the heating rate for a multilayer chip capacitor using operating voltages seen in typical circuit applications. The calculations use the thermal properties of barium titanate and the dimensions of a typical chip capacitor. Using these data we can calculate the chip heating rate that occurs when the circuit starts operation from a cold ambient condition. The heat input, Q , is given by:

$$Q = W_d \times \text{volume}$$

where W_d is the energy per unit volume dissipated on each cycle of the circuit voltage. The temperature rise, dT , is given by:

$$dT = Q/C_v$$

where C_v is the volume specific heat.
For the test conditions of:

$$W_d = 150 \text{ mJ/cc}$$

$$\text{volume} = 5.2 \times 10^{-3} \text{ cc}$$

$$C_v = 3.0 \text{ J/}^\circ\text{C-cc}$$

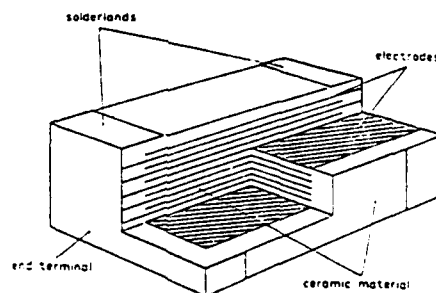


Figure 3

we find that $dT = 0.055^\circ\text{C/cycle}$. If the circuit is operating at a 1 kHz frequency, and we assume that heat cannot be quickly lost to the outside, the heating rate can approach 55°C/sec .

The highest stress condition for multilayer capacitors may occur during circuit start-up conditions at ambient temperatures. In fact, a colder ambient will produce higher stresses. An MLC with a 100°C gradient from hysteretic heating can attain a peak stress of 400 kg/cm^2 , and the MLC can reach this level in less than 10 seconds.

MICROSTRUCTURES AND NANOSTRUCTURES OF RELAXOR FERROELECTRICS

MARTIN P. HARMER

Department of Materials Science and Engineering, Lehigh University, Bethlehem, PA 18015, USA

ABSTRACT: In order to better understand and exploit the properties of relaxor ferroelectrics it is imperative to develop a deeper understanding of the microstructure and microchemistry of these materials. Since many fundamental properties of relaxors have been traced to events taking place on a nanoscopic scale, analytical and transmission electron microscopy (AEM and TEM) are ideal techniques for investigating these materials further. The present work describes the results of detailed TEM and AEM studies of several important classes of lead-based relaxor ferroelectric systems.

1. LEAD SCANDIUM TANTALATE $\text{Pb}(\text{Sc}_{1/2}\text{Ta}_{1/2})\text{O}_3$

Lead scandium tantalate (PST) is an attractive model system in which to study relaxor behavior because of the degree of control over the B-site cation ordering that can be achieved by heat treatment. Setter and Cross¹⁾ have studied extensively the dielectric properties of PST as a function of the degree of ordering (S) of the Sc^{3+} and Nb^{5+} ions. In our work on PST we have studied the microstructure as a function of the degree of cation ordering²⁾. Single crystals of ordered (S=0.8) and disordered (S=0.35) PST were found to contain ordered microchemical domains ≈ 20 -60 nm in size dispersed within a disordered matrix²⁾. No microstructural changes were observed after the single crystals were annealed for 24 hr at 1000°C. In sintered polycrystals aged similarly, however, the domains did coarsen considerably producing non-uniform structures containing anti-phase domain boundaries (APB's) separating domains which varied in size from ≈ 20 -400nm. Anomalous (1/2,1/2,0) superlattice reflections were observed in the selected area diffraction (SAD) patterns in all samples. This reflection is forbidden for a perfect NaCl-type ordered structure. It was postulated that these anomalous reflections originated from small regions (≈ 1 nm) of short range order having a primitive type of unit cell.

2. LEAD MAGNESIUM NIOBATE $\text{Pb}(\text{Mg}_{1/3}\text{Nb}_{2/3})\text{O}_3$

Microchemical ordering, ferroelectric domains and secondary phases have been characterized in $\text{Pb}(\text{Mg}_{1/3}\text{Nb}_{2/3})\text{O}_3$ (PMN) and $\text{PMN:10}\% \text{PbTiO}_3$ ³⁾. A substantial degree of ordering between the Mg^{2+} and Nb^{5+} ions in single crystal and polycrystalline PMN and PMN:PT was revealed by the presence of (1/2,1/2,1/2) superlattice reflections in the SAD patterns. Dark field imaging using the (1/2,1/2,1/2) reflection provided direct evidence of microchemical ordering on a scale of ≈ 2 -5nm. One interpretation of the SAD patterns is that the Mg^{2+} and Nb^{5+} ions order, on a nanostructural scale, in the same manner that Sc^{3+} and Ta^{5+} order in PST. A NaCl-type ordering arrangement in PMN, however, would upset the local stoichiometry and introduce a charge imbalance that would, as a consequence, be expected to limit the domains to very small sizes. A hint that this may indeed be the case comes from observations that the domains in PMN do strongly resist coarsening during prolonged heat treatments. Alternatively, the ordering could take place as alternating (111) layers with Nb^{5+} ions in one layer and a mixture of Nb^{5+} + Mg^{2+} ions in the other. Microchemical analysis is required to distinguish between these models.

Ferroelectric domains were observed only in PMN containing 10% PbTiO_3 and only at temperatures less than -120°C . The domain boundaries were found to lie on (100) and (110) which is consistent with the formation of 70° and 109° domain boundaries in the rhombohedral system. The angle α in the rhombohedral unit cell was determined to be $89.95^\circ \pm 0.01^\circ$.

A cubic pyrochlore phase in the form of large isolated grains of composition $\text{Pb}_2\text{Nb}_{1.75}\text{Mg}_{0.25}\text{O}_{6.62}$ was detected in sintered samples made via the mixed oxide method. Samples made from reagent grade starting oxides contained second phase films over a significant proportion of the grain boundaries. The films were rich in lead and phosphorus. The use of ultra high purity starting powders minimized the amount of intergranular impurity phase present, leading to much improved dielectric properties.

3. LEAD LANTHANUM MAGNESIUM NIOBATE $\text{Pb}_{1-x}\text{La}_x\text{Mg}_{(1+x)/3}\text{Nb}_{(2-x)/3}\text{O}_3$

A family of compositions referred to as PLMN were studied in which Mg:Nb was adjusted closer to 1:1 in order to enhance the degree of $\text{Mg}^{2+}:\text{Nb}^{5+}$ ordering; the excess magnesium was internally charge compensated by doping with La^{3+} on the Pb^{2+} sites. The following range of compositions were studied: $0.01 < x < 0.5$. For $x \lesssim 0.05$ isolated microchemical domains $\approx 10\text{nm}$ in size were observed. For $x \gtrsim 0.1$ complete ordering was observed along with the appearance of APB's. The microdomain size increased with increasing x ; domains as large as 500nm were observed. Strong $(1/2, 1/2, 1/2)$ superlattice reflections were observed in the x-ray diffraction patterns as well as in the SAD patterns. Evidence for a ferroelectric domain structure at -185°C was obtained.

4. LEAD ZINC NIOBATE:LEAD TITANATE $\text{Pb}(\text{Zn}_{1/3}\text{Nb}_{2/3})\text{O}_3:10\%\text{PbTiO}_3$

Flux grown single crystals of PZN:10%PT were studied by TEM; this composition falls on the tetragonal:rhombohedral morphotropic phase boundary at room temperature. The material was confirmed to be perovskite by SAD. Very faint $(1/2, 1/2, 1/2)$ superlattice reflections were observed in the SAD patterns indicating a slight tendency for ordering (much less than in PMN however).

Ferroelectric domains were visible at room temperature and below. The domain width was very small ($<10\text{nm}$) and the domain configurations were consistent with rhombohedral symmetry.

ACKNOWLEDGEMENTS

The author gratefully acknowledges valuable collaboration with H.M. Chan, J. Chen, A. Gorton, D.M. Smyth, L.E. Cross and A. Bhalla as well as the financial support of the Materials Research Division of the National Science Foundation and the E.I. DuPont de Nemours Company.

REFERENCES

1. N. Setter and L.E. Cross, J. Appl. Phys., 51:4356 (1980).
2. H.M. Chan, M.P. Harmer, A. Bhalla and L.E. Cross, Jap. J. Appl. Phys., Vol. 24, Supplement 24-2, pp. 550-552 (1985).
3. M.H. Chan and M.P. Harmer, in "Ceramic Microstructures '86: Role of Interfaces," by J.A. Pask and A.G. Evans, Plenum (in press).

DIELECTRIC PROPERTIES OF FINE-GRAINED BaTiO_3 CERAMICS DERIVED FROM
 $\text{BaTiO}(\text{C}_2\text{O}_4)_2 \cdot 4\text{H}_2\text{O}$

T. Enomoto, T. Ono and N. Okada

Ube research center, Central Glass Co., Ltd.

ABSTRACT: FINE-GRAINED BaTiO_3 powder was produced by coprecipitation method using oxalic acid. The effect of BaO/TiO_2 mole ratio and sintering parameters on the dielectric properties of the products were studied. At the BaO/TiO_2 mole ratio = 1.000, dielectric constant value at room temperature (K25) and at curie temperature (K125) were 6500 and 14000 respectively.

1. INTRODUCTION

The process of manufacturing BaTiO_3 powder which is used as a raw material of capacitors include both solid phase reaction and reaction in solution. $\text{BaTiO}(\text{C}_2\text{O}_4)_2 \cdot 4\text{H}_2\text{O}$ was initially prepared by reaction in solution from TiCl_4 , BaCl_2 and $(\text{COOH})_2$. The effect of BaO/TiO_2 mole ratio and sintering parameters on the dielectric properties of fine-grained BaTiO_3 derived from $\text{BaTiO}(\text{C}_2\text{O}_4)_2 \cdot 4\text{H}_2\text{O}$ were studied.

2. EXPERIMENTAL

2.1 MATERIALS

$\text{BaTiO}(\text{C}_2\text{O}_4)_2 \cdot 4\text{H}_2\text{O}$ prepared by coprecipitation in a mixed solution of TiCl_4 , BaCl_2 and oxalic acid was calcined at 800 C for 1 Hr in air. Calcined BaTiO_3 powders were pressed into pellet at uniaxial pressures of 1000 Kg/cm^2 and sintered for 1.5 - 2.0 Hrs in air. BaO/TiO_2 mole ratio of $\text{BaTiO}(\text{C}_2\text{O}_4)_2 \cdot 4\text{H}_2\text{O}$ was controlled by the mole ratio of raw materials such as $\text{TiCl}_4/(\text{COOH})_2$ and $\text{TiCl}_4/\text{BaCl}_2$, method of admixing, pH of solution and so on.

2.2 MEASUREMENT

The relative dielectric constant was measured as a function of temperature at 1 kHz using a low frequency impedance analyzer Hewlett Packard 4192 A. Indium-Gallium electrode were placed on both surfaces of the samples by painting.

3. RESULTS

BaTiO_3 powders produced in such a process were 0.2 - 0.3 μm in diameter of grain size and impurity level was less than 100 wt PPM. Effect of BaO/TiO_2 mole ratio and sintering temperature on the dielectric constant, dissipation factor,

relative density, grain size of ceramics are shown in Table I, and Fig. 1. Temperature dependence of the dielectric constant of BaTiO_3 ceramic with BaO/TiO_2 mole ratio = 1.000 is shown in Fig. 2.

TABLE I. Effect of mole ratio and sintering temperature on the dielectric properties, density and grain size.

BaO/TiO_2	Sintering temp ($^{\circ}\text{C}$)	K25	K125	$\tan\delta^{25^{\circ}\text{C}}$ (%)	S.D. (%)	Grain size (μm)
0.991	1250	2750	6120	6.2	82	- 60
	1300	2190	12860	0.3	95	- 100
0.995	1250	6300	13310	5.4	94	2 - 5
1.000	1200	6420	12580	2.8	91	1 - 2
	1250	6470	13860	2.5	95	1 - 2
	1300	4660	13900	3.2	97	3 - 10
1.004	1200	6580	14416	3.7	96	2 - 4
	1250	6060	13500	4.1	93	2 - 5
1.007	1150	5770	11270	2.0	97	1
	1200	4230	13440	3.0	98	1 - 3
	1250	3890	13690	4.5	97	1 - 4

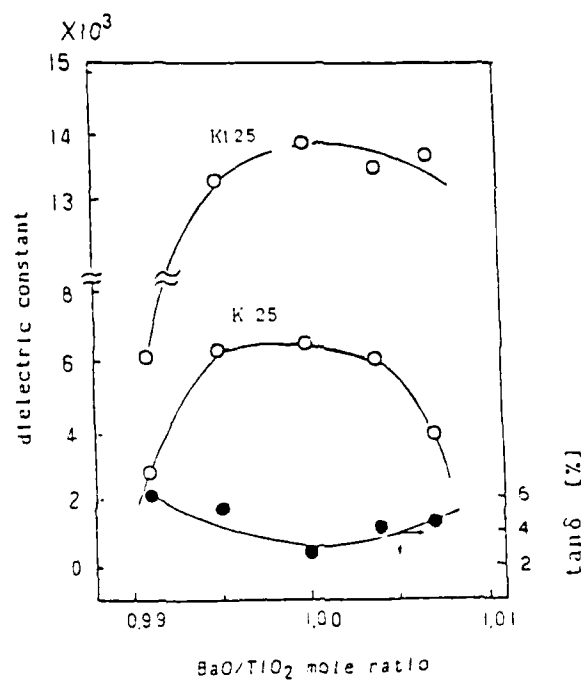


FIG. 1. Effect of BaO/TiO_2 mole ratio on dielectric properties at 1250°C .

4. DISCUSSION

The density and microstructure of the sintered body are significantly influenced by the BaO/TiO_2 mole ratio. BaO/TiO_2 mole ratio above 1.0 causes lowering of sintering temperature. On the other hand, when BaO/TiO_2 mole ratio is below 1.0, it is difficult to obtain dense ceramic. This is due to the fact that raising of firing temperature causes remarkable grain growth on account of the liquid phase sintering of BaTiO_3 . BaO/TiO_2 mole ratio of 1.00 gives dense and fine grained ceramics. It was also found that the dielectric property was strongly effected by the BaO/TiO_2 mole ratio. $\text{BaO/TiO}_2 = 1.000 \pm 0.005$ resulted in the highest dielectric constant. When the BaO/TiO_2 mole ratio was 1.000, quite high values of dielectric constant at room temperature (K25) and at Curie temperature (K125) were obtained, that is 6500 and 14000 respectively (Fig. 2). These very high dielectric constant may be interpreted by the internal stress model reported by G. Arlt, D. Hennings et.al.⁽¹¹⁾ and authors also confirmed this.

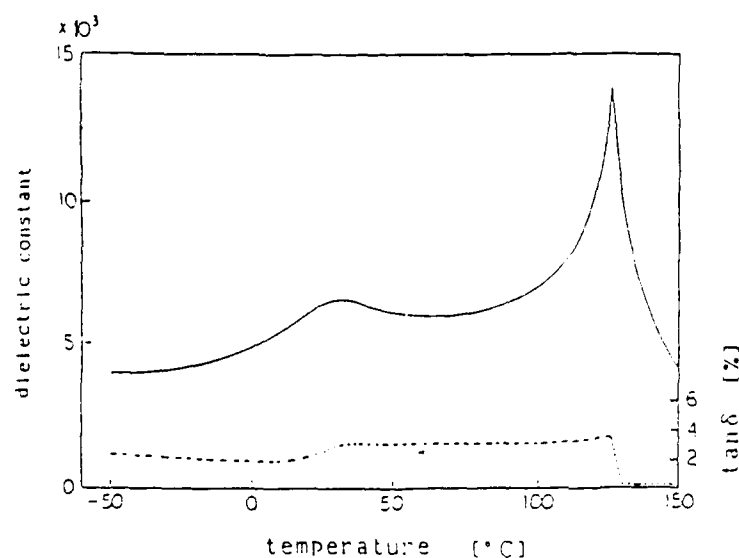


FIG. 2. Temperature dependence of the dielectric properties of BaTiO_3 ceramic with BaO/TiO_2 mole ratio = 1.000

REFERENCES

1. G. Arlt, H. Hennings, G. Heilich, J. Appl. Phys., **58**, 1619 (1985)

LOW TEMPERATURE FIRED GLASS-CERAMICS DIELECTRIC MATERIAL

M. TAKABATAKE, K. KAWAKAMI, and M. SASAKI

Research and Development Division, Asahi Glass Company, Yokonama, Japan.

ABSTRACT: Sintering process of glass- Al_2O_3 - $2\text{MgO}\cdot\text{SiO}_2$ system and glass- Al_2O_3 system between 800°C to 900°C were investigated. At glass- Al_2O_3 system, glass and Al_2O_3 don't react, while, at glass- Al_2O_3 - $2\text{MgO}\cdot\text{SiO}_2$ system, $2\text{MgO}\cdot\text{SiO}_2$ dissolves in the glass and, as the result, B_2O_3 in the glass react with Al_2O_3 , and new crystal $2\text{Al}_2\text{O}_3\cdot\text{B}_2\text{O}_3$ occurs. This process is effective for dense sintering and chemical resistance.

1. INTRODUCTION

A low temperature fired multilayer ceramic technology has been developed for hybrid circuits.

The low temperature fired ceramic is composed of glass phases and refractory filler materials. Relative amount of the glass and filler phases are adjusted to give dense, hermetic fired structures.

The present study reports the interaction between borosilicate glass and ceramics, and the effect of $2\text{MgO}\cdot\text{SiO}_2$ additives.

2. EXPERIMENTAL

2.1. Materials

Several kinds of glass- Al_2O_3 and glass- Al_2O_3 - $2\text{MgO}\cdot\text{SiO}_2$ films were made by a doctor blade method, and sintered at 900°C for 2h in air, and boiled in 90°C hot water to test the chemical stability.

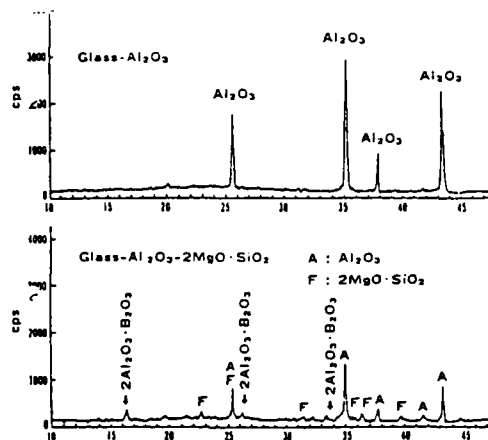
2.2. Measurements

Mechanical and electrical properties were measured. X-ray diffraction, Scanning Electron Microscope and Transmission Electron Microscope observations were carried out on the sintered samples which are before and after boiling.

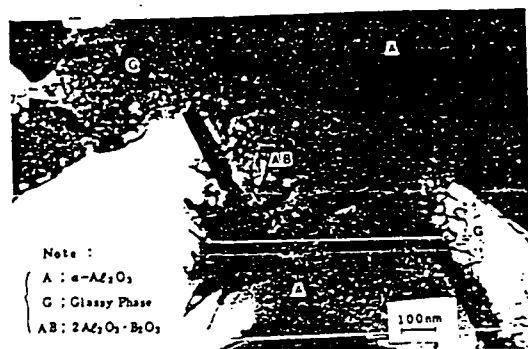
3. RESULTS and DISCUSSION

At glass- Al_2O_3 binary system, glass and Al_2O_3 did not react at 900°C. At glass- Al_2O_3 - $2\text{MgO}\cdot\text{SiO}_2$ ternary system, major part of $2\text{MgO}\cdot\text{SiO}_2$ dissolved in the glass and as the result, B_2O_3 in the glass reacted with Al_2O_3 and new needle like crystal $2\text{Al}_2\text{O}_3\cdot\text{B}_2\text{O}_3$ occurred in the grain boundary of glass and Al_2O_3 . It was clarified that the process and the structure is effective for dense sintering and chemical resistance. The reasons are considered as follows:

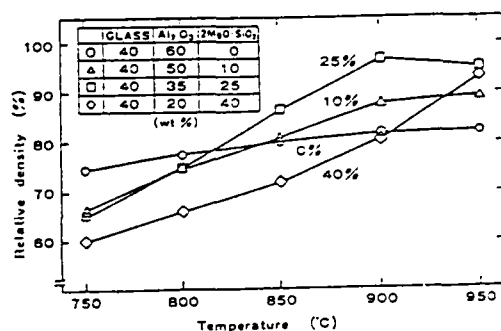
- (1) $2\text{Al}_2\text{O}_3\cdot\text{B}_2\text{O}_3$ crystallization is effective for sintering agent
- (2) Relative amount of B_2O_3 in the glass phase are reduced, which has good resistance to water.



X-ray diffraction patterns of various compositions sintered at 900°C



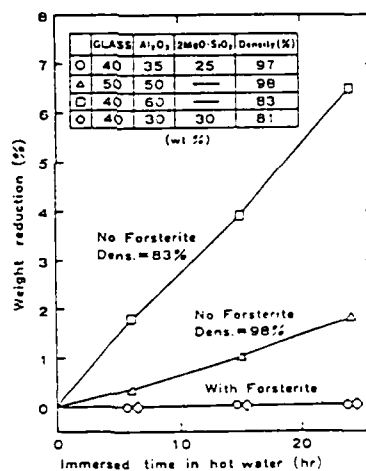
Transmission Electron Microscope Observation



Relative density of various glass-Al₂O₃-2MgO·SiO₂ compositions with temperature.

Properties

	GLASS-Al ₂ O ₃ -2MgO·SiO ₂
Sintering Temperature (°C)	900
Flexural Strength (kg/cm ²)	2000
Thermal conductivity (cal/deg·cm·sec)	0.007
Thermal Expansion Coefficient (deg ⁻¹)	60×10 ⁻⁷
Dielectric Constant (100kHz)	6.5
Dissipation Factor (100kHz)	1.5×10 ⁻³
Volume Resistivity (Ω·cm)	> 10 ¹⁴
Surface Roughness (μRa)	0.5



Corrosion resistance to hot water at 92°C
(sample dimension: 17mm×17mm×5mm)

M-19

LOW TEMPERATURE FIRED MULTILAYER CERAMIC CAPACITOR WITH NI ELECTRODES

H. KISHI, T. WADA, S. MURAI, H. CHAZONO, and N. YAMAOKA

Central Research Institute, Taiyo Yuden Co., LTD., Gunma, Japan

ABSTRACT: Dielectric ceramics based on barium titanate and glass components for multilayer ceramic capacitor with nickel electrodes has been developed. The ceramics could be fired at temperature less than 1200 °C in an atmosphere of low oxygen partial pressure, exhibited high dielectric constant (ϵ_r : 10000-12000, $\tan \delta$: 2700-3300) and high resistivity (above $10^{12} \Omega \text{cm}$). The multilayer chip capacitors with nickel electrodes using these dielectric materials have good characteristics.

1. INTRODUCTION

Conventional multilayer ceramic capacitors employ electrodes of noble metals such as Pd or Ag. For replacing Pd or Ag by cheaper alternatives, multilayer ceramic capacitors with base metal electrodes have been reported. In this work, we presents the dielectric materials which can be fired at low temperature in reduced atmosphere. Then we shows their application to multilayer chip capacitors with Ni electrodes.

2. EXPERIMENTAL PROCEDURE

The starting materials for the basic perovskite compounds were BaCO_3 , SrCO_3 , CaCO_3 , TiO_2 and ZrO_2 . They were weighed according to the general formula, $(\text{Ba}_{1-x-y}\text{Sr}_x\text{Ca}_y)(\text{Ti}_{1-z}\text{Zr}_z)\text{O}_3$ and ball-milled in water. After drying, the powder was calcined in air at 1200 °C for 2 hours. The glass components (alkaline earth lithiumsilicate glass, were then added to the calcined perovskite powders. Disk samples were formed by ordinary technique.

An In-Ga alloy electrode was then attached to the both surfaces of the sintered disk.

Multilayer chip capacitors were prepared as shown in Fig. 1. Nickel metal was used as both of internal and terminal electrodes and co-fired in the firing process of ceramic bodies. The samples were fired in a low oxygen atmosphere controlled by N_2 and H_2 gasses.

Dielectric constant and dissipation factor were measured by LCR meter at 1kHz with 1V rms. Insulation resistance was measured with a high-resistance meter in one minute after applying 100VDC.

3. RESULTS and DISCUSSION

3.1 Dielectric materials

The samples with glass components added were fired with full densification at 1100 °C to 1200 °C. Fig. 1 shows insulation resistance of the samples sintered in an atmosphere of N_2 and H_2 at 1100 °C.

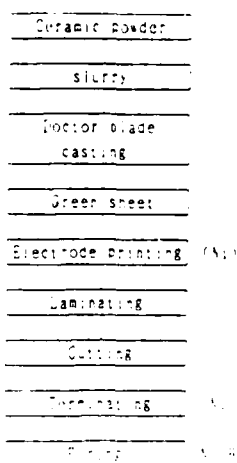


Fig. 1 Flow chart for multilayer chip capacitor.

Insulation resistance increase markedly on addition of glass components. The insulation resistance is higher than $10^{12} \Omega \text{cm}$.

Fig.3(a),(b) shows temperature characteristics of dielectric constant. The system of $(\text{Ba}_{1-x-y}\text{Sr}_x\text{Ca}_y)(\text{Ti}_{1-z}\text{Zr}_z)\text{O}_3$ -glass components shows various temperature characteristics according to their compositions and exhibit high dielectric constant 10000-12000 for Y5V specification, 2700-3300 for X7R specification.

3.2 Properties of chip capacitor

The characteristics for multilayer chip capacitors with nickel electrodes are shown in Table 1. The capacitors are compactly designed and have large capacitance and satisfy EIA standard specification. The multilayer chip capacitors with nickel electrodes using the dielectric materials of this system are as reliable as those with precious metal electrodes.

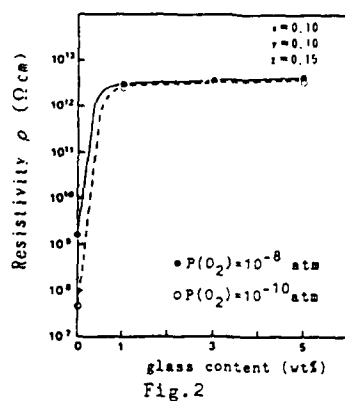


Fig.2. Resistivity v.s. glass content.

Fig.3 (a),(b). Temperature dependence of dielectric constant for various composition.

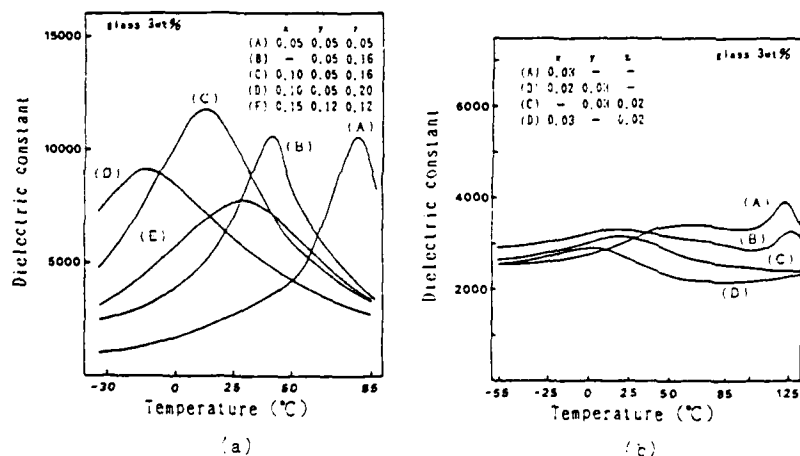


Fig.3

	chip size(mm)					dielectric characteristics				TCC(%)			
	L	W	T	t*	n**	Cap.(nF)	D.F.(%)	XIR(V/Ω)	BDV(V)	-55℃	-30℃	85℃	125℃
Y5V	3.2	1.6	1.25	13	60	1170	2.3	2×10^4	500	-	-30	-75	-
X7R	3.2	1.6	1.25	18	35	116	2.0	1×10^4	700	-12	-9	-7	-3

* t: thickness of dielectric layer (μm).

** n: numbers of effective dielectric layer

Table 1.
Characteristics of multilayer chip capacitors with nickel electrodes

BARIUM TITANATE CERAMICS FOR BASE METAL MONOLITHIC CERAMIC CAPACITORS

Y. SAKABE, H. TAKAGI, and K. WAKINO

Research and Development Department V, Murata Manufacturing Co., Ltd.,
2-26-10 Tenjin, Nagaokakyo-shi, Kyoto 617, Japan

ABSTRACT: Barium titanate ceramics doped with SiO_2 , CaO and ZrO_2 were fired under several low oxygen partial pressures, and their dielectric properties were measured. The dielectrics yielded a high dielectric constant ($k=14,000$) and high resistivity ($\sim 10^{12} \Omega\text{-cm}$) when they were fired with an nickel electrode in a reducing atmosphere of 10^{-13} – 10^{-11} MPa. The dielectrics are suitable for large-capacitance monolithic ceramic capacitors with nickel electrodes.

1. INTRODUCTION

Advanced dielectrics and firing technologies for monolithic ceramic capacitors have been developed in order to be able to substitute base metals, such as Ni, for noble metal electrodes¹⁻⁴). In this case, the firing of the capacitors should be carried out under low oxygen atmosphere, since nickel electrodes oxidize completely when fired in air. In this study, newly developed dielectrics were fired under several $P(\text{O}_2)$ atmospheres in order to realize practical firing conditions of nickel electrode monolithic capacitors.

2. EXPERIMENTAL

2.1. Materials

Two dielectric materials "A" and "B" were prepared by the conventional powder process. "A" is a new composition and "B" is a normal one.

A: $[(\text{Ba}_{0.82}\text{Sr}_{0.08}\text{Ca}_{0.10})\text{O}]_{1.005}[(\text{Ti}_{0.82}\text{Zr}_{0.18})\text{O}_2] + 0.1\text{at}\%\text{MnO}_2$

B: $\text{Ba}(\text{Ti}_{0.82}\text{Zr}_{0.18})\text{O}_3$

The test samples were prepared in disc form (14 mm in diameter by 1.0 mm thick). The discs, with and without Ni-paste on the surface, were sintered under $P(\text{O}_2)$ ranges of 10^{-2} to 10^{-16} MPa.

2.2. Measurements

An In-Ga alloy was applied as a conducting electrode on the sintered disc. Resistance was measured at room temperature on a megohmmeter at 500 V dc or on a resistance meter with low voltage. Capacitance was measured on an LF impedance analyzer at 1 V and 1 kHz.

3. RESULTS

Figure 1 shows the resistivity at room temperature vs sintering $P(\text{O}_2)$. The "A" dielectrics yielded high resistivity ($\sim 10^{12} \Omega\text{-cm}$), when $P(\text{O}_2)$ was higher than 3×10^{-13} MPa. At $P(\text{O}_2)$ lower than 10^{-14} MPa, the samples were converted to dark-colored semiconductors. This marginal $P(\text{O}_2)$ was close to the equilibrium one for Ti_2O_3 - TiO_2 (e.g., 5×10^{-14} MPa at 1300°C). The dielectrics "B" always showed low resistivity.

Figure 2 shows the dependence of the dielectric constant on the sintering atmosphere. The "A" dielectrics sintered in the $P(\text{O}_2)$ range of 10^{-13} to

10^{-11} MPa showed a very high dielectric constant (14,000) and low dissipation factor (1.5%). At the $P(O_2)$ regions higher than 10^{-11} MPa, the dielectric constant of the Ni-electroded disc decreased with increasing $P(O_2)$. The dependence of the dielectric constant on temperature for the "A" dielectrics co-fired with the nickel electrode in various $P(O_2)$ atmospheres is shown in Fig. 3. The temperature which shows maximum dielectric constant was not affected by the sintering atmosphere.

4. DISCUSSION

The equilibrium $P(O_2)$ for Ni-NiO at 1300°C is 2×10^{-8} MPa. But even in the lower $P(O_2)$ regions (to 10^{-11} MPa), nickel metal on the dielectric ceramics was partially oxidized and reacted with ceramics, resulting in a degradation of the dielectric properties. Firing atmosphere for the nickel-electrode monolithic ceramic capacitors with "A" dielectrics has to be controlled accurately within the $P(O_2)$ ranges of 10^{-11} to 10^{-13} MPa.

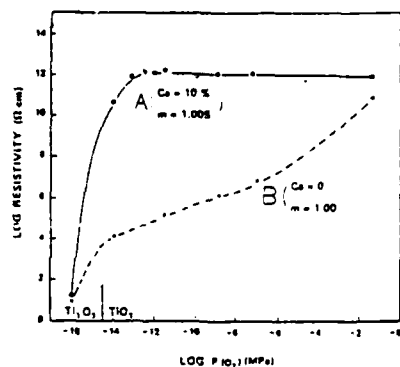


Fig. 1. Resistivity of the "A" and "B" dielectrics sintered under various $P(O_2)$ at 1300°C and 1400°C, respectively, for 2 h.

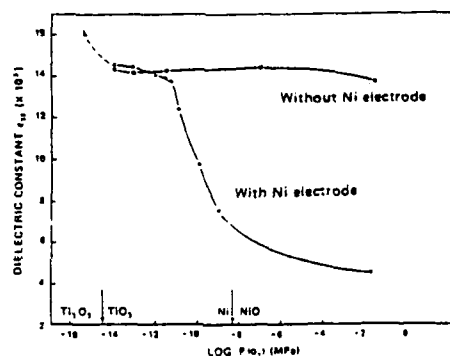


Fig. 2. Dielectric constant of the "A" dielectrics sintered with and without Ni-electrode under various $P(O_2)$ atmosphere at 1300°C for 2 h.

REFERENCES

1. J. M. Herbert, Trans. Brit. Soc., **62**, [8], 645-58 (1963).
2. I. Burn and G. M. Maher, J. Mat. Sci., **10**, 633-40 (1975).
3. H. J. Hageman and D. Hennings, J. Am. Ceram. Soc., **64**, [10], 590-94 (1981).
4. Y. Sakabe, K. Minai, and K. Wakino, Jpn. J. Appl. Phys. Supplement **20-4**, **20**, 147-50 (1981).

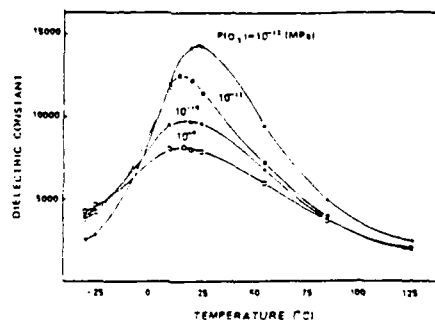


Fig. 3. Temperature dependence of dielectric constant of the "A" dielectrics sintered with Ni-electrode under low oxygen partial pressures at 1300°C for 2 h.

M-21

TEMPERATURE STABLE BARIUM TITANATE CERAMICS FOR BASE METAL MULTILAYER CAPACITORS

N. FUJIKAWA, N. YOKOI, and P. HAMANO

Central Research Laboratory, Kyocera Corp., Japan

ABSTRACT: In order to develop X7R multilayer ceramic capacitor with base metal electrodes, the system of $\text{BaTiO}_3\text{-CaZrO}_3\text{-MnO-Y}_2\text{O}_3$ was studied. These dielectric ceramics are sintered in an atmosphere of low oxygen partial pressure to yield a high resistivity ($10^{12}\Omega\text{cm}$), a high dielectric constant (2700-3300) and a flat dielectric temperature characteristic. The multilayer ceramic capacitors with nickel electrodes fabricated using the dielectrics have good characteristics that meet X7R.

1. INTRODUCTION

Multilayer ceramic capacitors have been increasingly used in electronic circuits. However, the material costs of the capacitor are high because of precious metal electrodes such as palladium. Several methods are proposed to reduce the material costs.¹⁻³ One way to achieve low cost is to use base metal such as nickel and copper for internal electrodes. The present study reports the dielectric materials that can be fired in a low oxygen atmosphere and have a flat dielectric temperature characteristic that meets X7R, and their application to multilayer ceramic capacitors with base metal electrodes.

2. EXPERIMENTAL PROCEDURE

2.1. Dielectric Materials

Given quantities of BaTiO_3 , CaZrO_3 , MnCO_3 and Y_2O_3 were weighed, and they were mixed with 3% PVA binder and water. After drying, the powder was pressed into a disk 12 mm in diameter and 1.2 mm in thickness. The disk was baked at 500 °C in air to burn out binder, then it was fired at 1270-1350 °C in a low oxygen atmosphere controlled by H_2 and H_2O gasses. An In-Cu electrode was attached to the surface of the sintered disk.

Capacitance and dissipation factor were measured by a digital LCR meter (YHP-4274A) at 1 kHz with 1 Vrms. Dielectric constant was calculated from a capacitance and a dimension of a disk. Insulation resistance was measured after applying 35V Vdc for 1 minute.

2.2. Multilayer Ceramic Capacitor

Green chips were fabricated using green dielectric sheets with 35 μm thickness and a nickel electrode ink in the conventional green sheet method. These chips were fired in a low oxygen atmosphere. One termination was formed by applying nickel alloy electrode on each end of the chip and fired at 800 °C in H_2 .

Capacitance and dissipation factor were measured in the same way as the disk samples. Insulation resistance was measured after applying 50 Vdc for 1 minute.

3. RESULTS AND DISCUSSION

Figure 1 and 2 show temperature characteristics of dielectric constant as a function of CaZrO_3 or Y_2O_3 content. Temperature characteristic curves shift clockwise with increasing CaZrO_3 content, and become flat with increasing Y_2O_3 content. However, ceramics containing more than 1 mol% Y_2O_3 are not well sintered even at 1350 °C. The optimum contents of CaZrO_3 and Y_2O_3 for a flat temperature characteristic (within $\pm 5\%$) are in the range of 1.0 - 1.5 mol% CaZrO_3 and 0.5 - 1.0 mol% Y_2O_3 .

Figure 3 shows dielectric constant and insulation resistance as a function of Y_2O_3 content.

Dielectric constant decreases with increasing Mn content, but these compositions have relatively high dielectric constant (>2700). Insulation resistance is higher than $10^{12} \Omega \text{ cm}$ when the ceramics contain more than 1.5 mol% Mn. The increase of insulation resistance on addition of MnO can be understood by the compensation action of the acceptor type dopant.

Figure 4 shows the insulation resistance of ceramics related to the conventional $\text{BaTiO}_3 - \text{Nb}_2\text{O}_5$ system and the new developed system when they are fired in several oxygen atmospheres. Insulation resistance of the conventional system decreases remarkably with decreasing oxygen partial pressure. On the other hand, the new developed system keeps high insulation resistance in low oxygen partial pressure ($3 \times 10^{-10} - 3 \times 10^{-5} \text{ atm.}$). In order to make a nickel electrodes multilayer ceramic capacitor, green chips should be fired under low oxygen partial pressure less than that of the Ni-NiO equilibrium at firing temperature. Since the oxygen partial pressure of the Ni-NiO equilibrium at 1350°C is about 10^{-5} atm. , the new developed ceramics are usable for this purpose.

The dielectric material of this system was applied to the multilayer ceramic capacitor with nickel electrodes. The characteristics of capacitors are listed in Table 1. These capacitors meet X7R and show no degradation under the load life test (125°C , 100 Vdc, 1000 Hr).

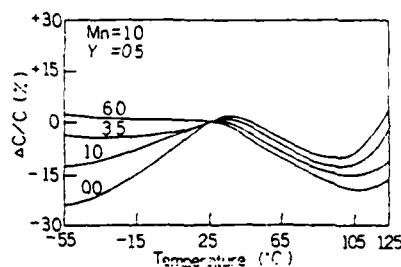


Fig. 1 TCC as a function of CaZrO_3 content.

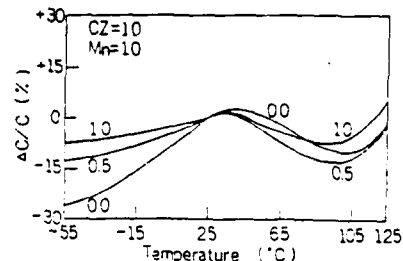


Fig. 2 TCC as a function of Y_2O_3 content.

Table 1 Characteristics of MLC with Ni electrodes.
Chip size: $3.2 \times 1.6 \text{ mm}$
Green thickness of dielectric layer: $35 \mu\text{m}$

CHARACTERISTICS	20 LAYERS	40 LAYERS
CAPACITANCE (nF)	53.4	110.5
D.F. (%)	2.2	2.0
IR (GΩ)	25	12
CR PRODUCT (nF)	1300	1300
BDV (VDC min.)	500	400
TCC (EIA)	X7R	X7R

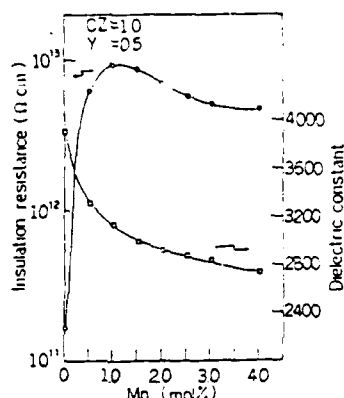


Fig. 3 IR and dielectric constant v.s MnO.

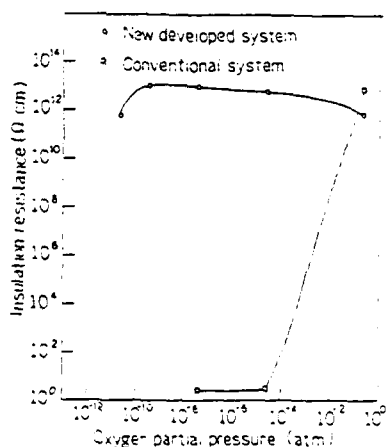


Fig. 4 IR v.s firing atmosphere (PO_2).

REFERENCES

1. Y. Sakabe, K. Minai and K. Wakino, Jpn. J. Appl. Phys., **20**(suppl. 2C-4), 147 (1981).
2. T. O. Butt and J. A. Stynes, IEEE Trans. Hybrids & Packag., **PH-2**, 144 (1973).

BARIUM MODIFIED LEAD ZINC NIOBATE DIELECTRICS FOR MULTILAYER CERAMIC CAPACITOR

K. INAGAKI, Y. YAMASHITA and K. YUUKI

Engineering Department, Marcon Electronics Co. Ltd., 1-1 Saiwai-cho, Nagai,
Yamagata 993, Japan

ABSTRACT: Substitution effects for lead zinc niobate based ceramic by barium and titanium have been systematically investigated. It was found that the partially substituted lead zinc niobate dielectric by barium and titanium has shown to be a promising candidate for multilayer ceramic capacitor.

1. INTRODUCTION

In order to improve disadvantages of $BaTiO_3$ based dielectric material, studies of new high dielectric constant relaxor materials are widely carried out. The authors have succeeded in easily synthesizing perovskite type lead zinc niobate as a ceramic form, by means of partial substitution by strontium and titanium¹⁻²⁾. In the present study, dielectric properties of the lead zinc niobate based compositions, in which the dielectric constant maxima show around the room temperature, has been investigated by the adjustment of the amount of barium and titanium substitution.

2. EXPERIMENTAL PROCEDURE

The studied compositions were of the general formula,
 $(Pb_{1-x}Ba_x)((Zn_{1/3}Nb_{2/3})_yTi_2)O_3$ which hereafter is abbreviated as PBZT 100x/100y/100z. Dielectric powder preparation was carried out by conventional method. The disks were fired in a magnesia crucible at 980 to 1,150°C for 2 hours. Then they were formed to 1.0mm thick, printed silver paste as electrodes on both surfaces and fired at 700°C.

3. EXPERIMENTAL RESULTS

The sintered bodies were crashed into powders and measured a relative amount of perovskite phase (P.A.) by X-ray diffraction method with $CuK\alpha$ radiation. The results are shown in Fig. 1. It can be seen that the composition partially substituted by barium and titanium represents high (P.A.) ratio.

Figure 2 shows temperature dependences of relative dielectric constant and dissipation factor in PBZT 27/60/40 compared to Y5T characteristics $BaTiO_3$ based dielectric. In all temperature regions, the PBZT 27/60/40 shows gentle and high dielectric constant curve compared to the $BaTiO_3$ based dielectric owing to diffuse phase transition effect.

Figure 3 shows tolerance factor t in the PBZT system. It can be found that (P.A.) tends to high with increasing in substitution ratio of barium

and titanium. Furthermore, perovskite crystal structure has an ionic bond. As a scale of amount of ionic bond component, electronegativity proposed by Pauling is well known. According to this, the amount of ionic bond component between two atoms P_{AB} are expressed as

$$P_{AB} = 1 - \exp[-1/4(\chi_A - \chi_B)^2].$$

Figure 4 shows the amount of ionic character in the PBZT system. Since the amount of ionic character becomes larger when P_{AB} tends to unity, it is explained that barium and titanium substitution is effective for perovskite phase formation of lead zinc niobate ceramics.

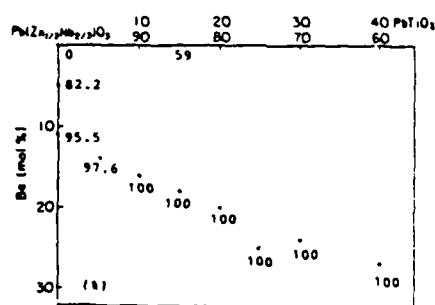


Fig. 1. Relative amount of perovskite phase for the PBZT system.

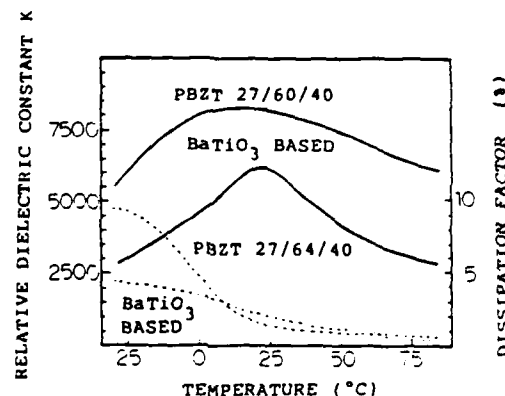


Fig. 2. Dielectric properties for the PBZT 27/60/40 and conventional YST characteristics $BaTiO_3$ based dielectric.

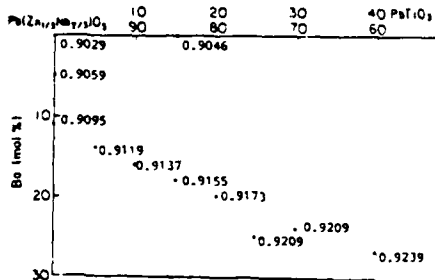


Fig. 3. Tolerance factor for the PBZT system.

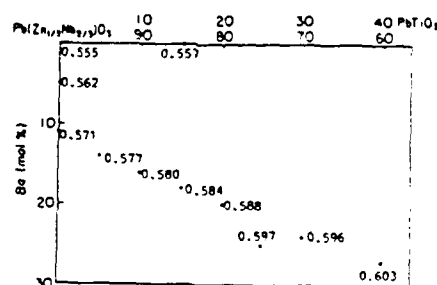


Fig. 4. Amount of ionic character for the PBZT system.

REFERENCES

1. O. Furukawa, Y. Yamashita, M. Harata, T. Takahashi and K. Inagaki, Proc. of FMA-5th, Kyoto, 1985, Jpn. J. Appl. Phys., Suppl., 24-2, 96 (1985).
2. Y. Yamashita, O. Furukawa, M. Harata, T. Takahashi and K. Inagaki, Proc. of IMF-6th, Kobe, 1985, Jpn. J. Appl. Phys., Suppl., 24-2, 1027 (1985).

M-23

DIELECTRIC RELAXATION STUDIES IN SOME POLYMER - PZT COMPOSITES

A. M. VARAPRASAD

Naval Chemical and Metallurgical Laboratory, Naval Dockyard, Bombay - 400023, India

Present address :

Department of Physics, Sophia University, Kioi-cho, Chiyoda-ku, Tokyo 102, Japan

Due to the rapid increase in application of ferroelectrics in electronic industry, ferroelectric titanate and niobate materials have been studied extensively [1,2] and composite materials made up of such ferroelectric particles dispersed in a polymer matrix have attracted the attention of materials technologists due to its ease of preparation, higher sensitivities and favourable economics. Anomalous piezo- / pyro- electric properties have been noticed [3] in composites, basically due to the changes in the molecular motion of the polymer. In the present study, dielectric relaxation studies were therefore planned on composites between PZT and certain mechanically sound polymeric materials to unfold the effect of composite formation on the molecular motion of the polymer phase.

The polymer materials used for the composite formation were vinyl acetate - vinyl chloride (VA-VC) co-polymer, amide cured epoxy (ACE), nitrile rubber - poly vinyl chloride (NR-PVC) blend and piezoelectric poly vinylidene fluoride (PVDF). The base materials for VA-VC, ACE and NR-PVC were obtained from Calico Products (Bombay). The PVDF material used was Kynar grade film as supplied by Pennwalt USA. The starting material was of pure trans form (TTTT configuration).

Free films of the composite materials were formed on a motorized film applicator between 75 micron PZT particles (composition : $\text{Pb}_{0.94}\text{La}_{0.04}\text{Zr}_{0.51}\text{Ti}_{0.49}\text{O}_3$) 55vol% and the VA-VC, ACE and NR-PVC polymers. PZT - PVDF composite was formed by pressing a pre-formed PZT film against the Kynar PVDF film at about 80 C. The thickness of the films were limited to the size of PZT particles (about 75 microns).

Dielectric measurements were performed using a Wayne-kerr autobalance capacitance bridge, in the temperature range 30 to 150 C. A silicon oil thermostat was used for the temperature variation studies.

The variation of dielectric loss ($\tan \delta$) with temperature (t C) plots were depicted in figures 1 and 2 for the pure polymers and composites respectively. New dielectric relaxation peaks were observed in the case of VA-VC and PVDF composites below glass transition temperature. In VA-VC composite the observed relaxation was attributed to the segmental motion of the VA and VC segments. In the case of pure VA-VC polymer the relaxation was known to occur below room temperature (-20 C). Owing to coupling of the polymer segments with the polarization charge of PZT particles it could be possible that the relaxation of the segmental motion has been shifted to higher temperatures.

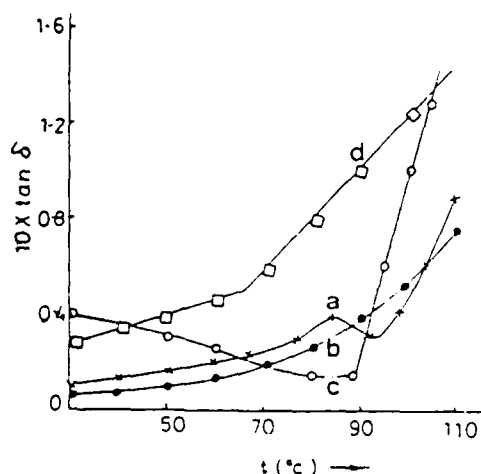


Fig.1. Dielectric relaxations in some polymers used for composite formation (a)VA-VC (b)PVDF (c)ACE (d)NR-PVC

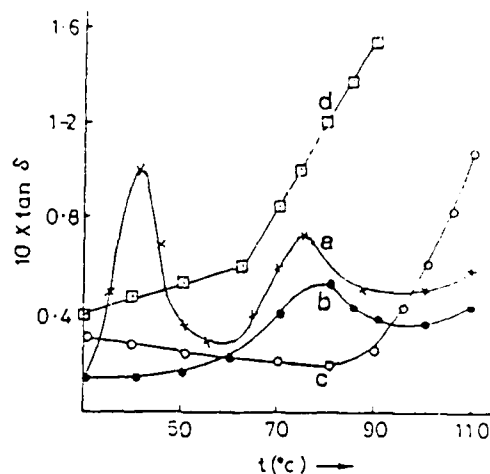


Fig.2. Dielectric relaxations in the composites (a)VA-VC (b)PVDF (c)ACE (d)NR-PVC

In the case of PVDF, a relaxation around 70 C was known to occur due to the segmental motion in the TGTG configuration. No such relaxation was however, known for the all trans (TTTT) configuration. In fact, the starting PVDF material (fig.1b) didnot show any relaxation peak around this temperature. The observation of new relaxation peak in the composite at about 80 C (fig.2b) was therefore ascribed to the partial conversion of the TTTT to the TGTG configuration. Relaxation due to the segmental motion of NR-PVC and ACE composites were not observed in the experimental range of temperature viz 30 to 150 C. The high temperature α -relaxation owing to the motion of the main polymer chain near glass transition was mostly unchanged in the composites.

REFERENCES

- 1.Kenji Uchino, Am. Ceram. Soc. Bull., 65, 647 (1986)
- 2.A.M.Varaprasad, Jap. J. Appl. Phys., 24Suppl.,361(1985)
- 3.J.Mort and G.Pfister, Electronic Properties of Polymers, Wiley-Interscience, New York, pp 109-160 (1982)

POSTER SESSION II

MICROWAVE DIELECTRIC PROPERTIES OF $\text{Pb}(\text{Zr,Ce})\text{O}_3$ CERAMICS

K. MURANO, K. TATSUKI

Sony Development Center, Sony Corp. Tokyo, Japan

S. NISHIGAKI, S. YANO, H. KATO

Narumi Technical Lab. Narumi China Corp. Nagoya, Japan

ABSTRACT: We developed $\text{Pb}(\text{Zr,Ce})\text{O}_3$ ceramics having a high dielectric constant (ϵ_r), a high Q and a negative temperature coefficient of the resonant frequency (T_f). Combining this with a conventional dielectric ceramic, we made a ceramic which exhibited $\epsilon_r=170$, $Q=1200$, and $T_f=80\text{ppm}/^\circ\text{C}$ at 3GHz.

1. INTRODUCTION

The ceramic required to make a good microwave resonator must have three important dielectric properties.

- (1) A high ϵ_r to miniaturize the size of resonator in proportion to $1/f_r\sqrt{\epsilon_r}$. (f_r is the resonant frequency)
- (2) A high Q factor to keep the power loss as low as possible.
- (3) A low T_f to stabilize the resonant frequency.

We investigated microwave resonators at 3GHz which need high ϵ_r because the frequency of 3GHz is a rather long wavelength for microwaves. There are some conventional ceramics having high ϵ_r , high Q and a large positive T_f at microwave frequencies. It is conceivable that ceramics having negative T_f , can be combined with the conventional ceramics to produce a resonator having an extremely small T_f . The purpose of our study was to develop ceramic compositions having high ϵ_r , high Q and a large negative T_f .

2. EXPERIMENTAL

2.1. Sample Preparation

All the starting materials- PbO , ZrO_2 and CeO_2 with a purity of above 99.8%- were weighed to give the compositions in Fig.1. These materials were ball milled for 16 hrs, then dried and calcined at 850°C for 1 hr. The product was reground in a ball mill, then dried. The powder was pressed into disks and hot pressed at 1250°C for 4 to 10 hrs under a pressure of 100 to $250\text{Kg}/\text{cm}^2$. The hot-pressed disks were cut into a form having a resonant frequency of approximately 3GHz.

2.2. Measurements

Dielectric properties at microwave frequencies were measured by the resonant cavity method in the TE_{012} mode. A sample was inserted into a wave guide which acted as a band rejection filter, resulting in a dip curve on the network analyzer display. The unloaded Q was calculated from the resonant curve. The ϵ_r was calculated using the value of the f_r and the size of the sample. The T_f was measured in a temperature range from -20°C to 60°C .

3. RESULTS AND DISCUSSION

Figure 2 shows the relation between E_r , Q and T_f as a function of the Pb/Zr ratio when the CeO_2 content is constant at 5mol% from (A) to (B) in Fig.1. We found the value of E_r and Q was highest when the ratio is slightly over one. Figure 3 shows the change of the dielectric properties against CeO_2 contents from (C) to (D) in Fig.1. Hot-pressed PbZrO_3 without CeO_2 is well sintered, but has a Q so low it cannot be measured at 3GHz. The small addition of CeO_2 to PbZrO_3 improves the dielectric properties, especially the Q value. We found an excellent composition of $\text{Pb}_{1.06}(\text{Zr}_{0.98}\text{Ce}_{0.02})\text{O}_{3.06}$ ((E) in Fig.1) which has a high E_r (140), a high Q (850) and a large negative T_f (-1080ppm/ $^{\circ}\text{C}$). The microstructure of a $\text{Pb}(\text{Zr,Ce})\text{O}_3$ is shown in Fig.4 and the relation between the diameter of grains and the CeO_2 content is shown in Fig.5. It should be noted that (E) has the largest grain size and gives the best E_r and Q . We suppose that the addition of CeO_2 to PbZrO_3 increases the sinterability of PbZrO_3 and improves the dielectric properties. Table 1 shows the combination properties of a stacked ceramic formed of (E) and a conventional ceramic.

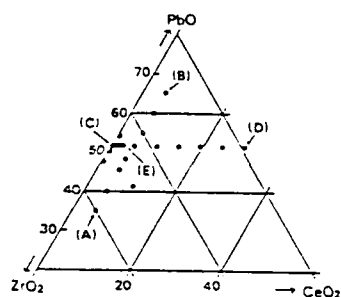


Fig. 1.
Composition diagram.

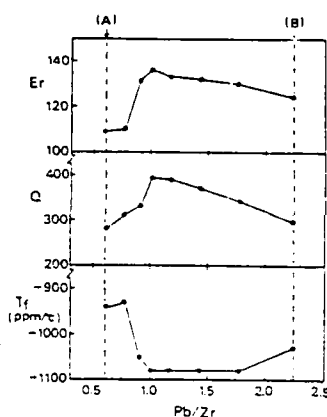


Fig. 2.
Dielectric properties
as a function of
Pb/Zr ratio at 3GHz.

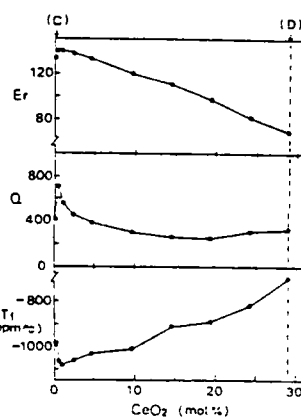


Fig. 3.
Dielectric properties
vs CeO_2 content
at 3GHz.



Fig. 4. Microstructure
of a $\text{Pb}(\text{Zr,Ce})\text{O}_3$

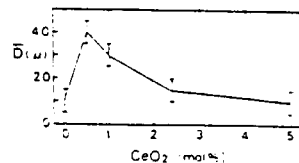


Fig. 5. The relation
between grain size
and CeO_2 content.

TABLE. 1.
Dielectric properties of
combined ceramics at 3GHz.

Comp	(1) $\text{PbZrO}_3\text{-CeO}_2$	(2) $\text{SrTiO}_3\text{-NiO}$ $\text{-Nb}_2\text{O}_5$	(1)+(2)
E_r	140	230	170
Q	850	2800	1200
T_f (ppm/ $^{\circ}\text{C}$)	-1080	1250	80

HIGH DIELECTRIC CONSTANT CERAMICS FOR MICROWAVE RESONATORS

H. SATO, K. AYUSAWA, M. SAITO, and K. KAWAMURA

Research Laboratory, OKI Electric Industry Co., Ltd. Tokyo, Japan

ABSTRACT: Dielectric ceramics consisting of $\text{BaO} \cdot \text{Sm}_2\text{O}_3 \cdot \text{CeO}_2 \cdot \text{La}_2\text{O}_3 \cdot \text{TiO}_2$ were investigated for applying microwave dielectric resonators. The material developed has the following properties: dielectric constant (ϵ_r): 75.5, unloaded Q(Q_u): 1870 at 5GHz, and temperature coefficient of resonant frequency, (T_f): 0 ppm/ $^\circ\text{C}$. X-ray analysis shows that the main compound of the ceramics are $\text{Ba}(\text{RE})_2\text{Ti}_5\text{O}_{14}$: RE = Sm, Ce, La. The addition of CeO_2 makes this material susceptible to $\text{HF} + \text{HNO}_3$ mixed acid.

1. INTRODUCTION

Dielectric ceramics having a high values of ϵ_r and Q_u , and a small value of T_f are necessary for miniaturizing microwave devices such as dielectric resonators. BaTi_4O_7 has a high value of ϵ_r , however T_f is not 0 ppm/ $^\circ\text{C}$. We have investigated the effect Sm_2O_3 , CeO_2 and La_2O_3 addition in $(\text{BaO})(\text{TiO}_2)_4$ and succeeded in developing new dielectric ceramics.

2. EXPERIMENTAL PROCEDURE

The starting materials were BaCO_3 (G.R.), TiO_2 (G.R.), Sm_2O_3 (99.9%), CeO_2 (99.9%) and La_2O_3 (99.9%). They were mixed with distilled water in a pot and then dried. The mixed powder was calcined at 1080 $^\circ\text{C}$ for 2h in air. After the calcination, the sample was pulverized in a pot and dried. Calcined powder was granulated and pressed into disks and then sintered in an alumina crucible at 1250 $^\circ\text{C}$ to 1400 $^\circ\text{C}$ for 2h in air.

The microwave dielectric characteristics were measured by Hakki and Coleman's dielectric resonator method⁽¹⁾ improved by Kobayashi and Tanaka⁽²⁾.

3. RESULTS AND DISCUSSION

Figure 1 shows the diagram of the $(\text{BaO})(\text{Sm}_2\text{O}_3 \cdot \text{CeO}_2 \cdot \text{La}_2\text{O}_3)(\text{TiO}_2)_4$ system. The hatched areas I and II were examined in the present study. Figure 2 shows the dependencies of ϵ_r , Q_u and T_f on w_2 in $(\text{BaO})\{(\text{Sm}_2\text{O}_3)_{0.842} - w_2(\text{CeO}_2)_{0.158}(\text{La}_2\text{O}_3)_{w_2}\}(\text{TiO}_2)_4$ in area I. T_f increases with an increase in w_2 and becomes 0 ppm/ $^\circ\text{C}$ at $w_2 = 0.1$, where ϵ_r and Q_u are 75.5 and 1870 (5GHz), respectively. Figure 3 shows ϵ_r , Q_u and T_f as functions of a particular set of w_1 and w_2 in $(\text{BaO})\{(\text{Sm}_2\text{O}_3)_{1-w_1-w_2}(\text{CeO}_2)_{w_1}(\text{La}_2\text{O}_3)_{w_2}\}(\text{TiO}_2)_4$. In this case, T_f is almost zero (0.1 ppm/ $^\circ\text{C}$) in the whole experimental range. ϵ_r and Q_u are constant in the range, $w_1 = 0 \sim 0.175$ and $w_2 = 0.154 \sim 0.09$, $w_1 = 0 \sim 0.3$ and $w_2 = 0.154 \sim 0.045$, respectively. These findings indicate that if the compositions of the ceramics vary along the line \overline{AB} in Figure 1, they always give $T_f = 0$ ppm/ $^\circ\text{C}$. Similar experiments showed that the lines \overline{DE} and \overline{FG} in Figure 1 give the compositions corresponding to $T_f = 10$ and -10 ppm/ $^\circ\text{C}$, respectively. X-ray analysis shows that main compound of the C point ceramics was $\text{Ba}(\text{RE})_2\text{Ti}_5\text{O}_{14}$: RE = Sm, Ce, La. The chemical etching property is important for the metallization of the ceramics. Figure 4 shows the SEM photographs of samples as-sintered and etched in a $\text{HF} + \text{HNO}_3$ acid solution.

The ceramics containing CeO_2 are easily etched in this acid.

4. CONCLUSION

The $\text{BaO-Sm}_2\text{O}_3\text{-CeO}_2\text{-La}_2\text{O}_3\text{-TiO}_2$ ceramics have excellent dielectric characteristics in the microwave region. X-ray analysis shows that the most suitable ceramics for resonators are mainly consisting of $\text{Ba}(\text{RE})_2\text{Ti}_5\text{O}_{14}$: $\text{RE} = \text{Sm}, \text{Ce}, \text{La}$. The ceramics are susceptible to HF containing acid. This property makes metalization by chemical plating very easy. These ceramics, therefore, are useful for microwave resonators.

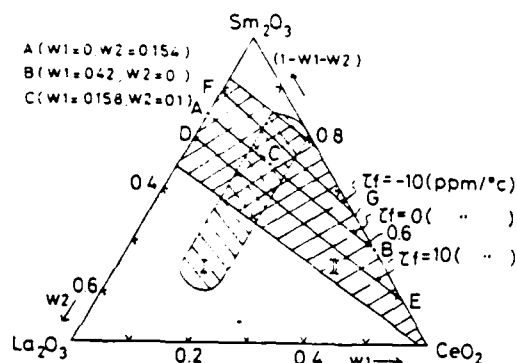


Fig.1 Diagram of the system $((\text{BaO})((\text{Sm}_2\text{O}_3)_{1-w_1-w_2}(\text{CeO}_2)_{w_1}(\text{La}_2\text{O}_3)_{w_2})(\text{TiO}_2)_4)$

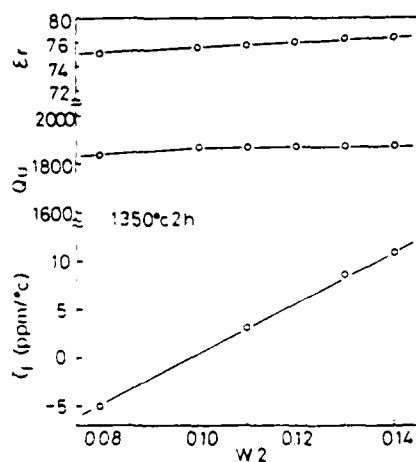


Fig.2 Dielectric characteristics of the system $((\text{BaO})((\text{Sm}_2\text{O}_3)_{0.2-w_2}(\text{CeO}_2)_{0.158}(\text{La}_2\text{O}_3)_{w_2})(\text{TiO}_2)_4)$ as functions of w_2

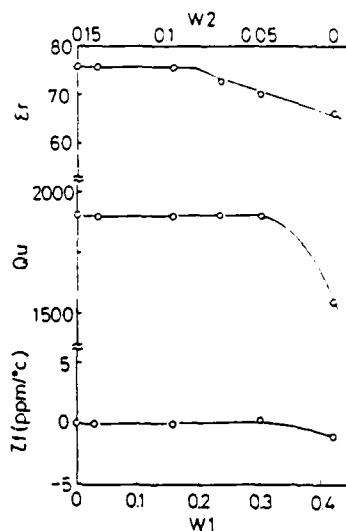


Fig.3 Dielectric characteristics of the system $((\text{BaO})((\text{Sm}_2\text{O}_3)_{1-w_1-w_2}(\text{CeO}_2)_{w_1}(\text{La}_2\text{O}_3)_{w_2})(\text{TiO}_2)_4)$ as function of w_1 and w_2



Fig.4 SEM Photographs (a) as-sintered (b) etched μm
and etched ceramics in $(\text{HF}+\text{HNO}_3)$ acid

REFERENCES

1. B.W. Hakki and P.D. Coleman, IRE Trans. Microwave Theory Techn., MTT-8, 402(1960).
2. Y. Kobayashi and S. Tanaka, The Institute of Electronics and Communication Engineers of Japan, CPM 72-33(1972).
3. Y. Ayusawa, M. Nakayama, H. Sato, M. Kazama and S. Onno, National Conference Record Communications, The Institute of Electronics and Communication Engineers of Japan, 1-64(1964).

HIGH-Q DIELECTRIC RESONATOR MATERIAL FOR MILLIMETER-WAVE FREQUENCIES

H. TAMURA, D. A. SAGALA, M. MURATA, and K. WAKINO

Research & Development Department V, Murata Manufacturing Co., Ltd., Kyoto, Japan

ABSTRACT: Microwave characteristics of the system $\text{Ba}(\text{Mg}_{1/3}\text{Ta}_{2/3})\text{O}_3\text{-BaSnO}_3$ were investigated. Although $\text{Ba}(\text{Mg}_{1/3}\text{Ta}_{2/3})\text{O}_3$ had a perovskite pseudocell and hexagonal superstructure, the superstructure was not formed after the addition of BaSnO_3 of more than about 10 mol%. Sintering of solid solution $\text{Ba}(\text{Sn}_{0.1}\text{Mg}_{0.3}\text{Ta}_{0.6})\text{O}_3$ was accelerated compared to those of $\text{Ba}(\text{Mg,Ta})\text{O}_3$ alone, and the microwave Q value was also improved. The resultant dielectric characteristics are as follows: $K=24.5$, $Q=20,000$ at 10 GHz, and temperature coefficient of resonant frequency, $\tau_f=0$ ppm/°C.

1. INTRODUCTION

Dielectric resonator ceramics have gained an important position as a key element for microwave components. Among many materials developed for dielectric resonators, those with complex perovskite structure have very high Q values¹⁻³. Complex perovskite materials of the system $\text{Ba}(\text{Mg,Ta})\text{O}_3\text{-BaSnO}_3$ are investigated here. This system presented a very high Q value and would be useful for applications of millimeter-wave frequency.

2. EXPERIMENTAL

2.1. Materials

Reagent grade BaCO_3 , MgCO_3 , Ta_2O_5 , and SnO_2 were mixed by ball-milling for 16 h. They were dried and calcined at 1200°C for 2 h. The powder was milled again with organic binder, pressed into discs 12 mm in dia. and 5 mm thick and then sintered at 1550°C for 4 h.

2.2. Measurements

The crystal structure was examined using powder X-ray diffraction, and the microwave dielectric characteristics were measured by Hakki and Coleman's dielectric resonator method.

3. RESULTS

$\text{Ba}(\text{Mg}_{1/3}\text{Ta}_{2/3})\text{O}_3$ has pseudocubic unit cells with hexagonal superstructures because the two B-site ions are of ordered configuration. Fig. 1 shows the X-ray powder diffraction patterns of this material. The Miller indices parameters in the figures are those of hexagonal superstructure, and the peaks marked by an asterisk are caused by the formation of superstructures.

This material, however, has the problem that it is difficult in sintering to dense ceramics. The addition of BaSnO_3 accelerated the sintering and improved the Q value. Fig. 2 shows that the optimum Q value is obtained by the addition of about 10 mol% BaSnO_3 . The peaks of superstructure have disappeared in the X-ray diffraction patterns of $\text{Ba}(\text{Sn}_{0.1}\text{Mg}_{0.3}\text{Ta}_{0.6})\text{O}_3$.

Fig. 3 shows the frequency dependence of this $\text{Ba}(\text{Sn,Mg,Ta})\text{O}_3$ ceramic whose τ_f is optimized to 3 ppm/°C.

4. DISCUSSION

We reported that the Q value of $\text{Ba}(\text{Zn},\text{Ta})\text{O}_3$ was improved by the addition of Ba_2rO_3 whose lattice constant is larger than that of $\text{Ba}(\text{Zn},\text{Ta})\text{O}_3^{(2)}$. In the system $\text{Ba}(\text{Mg},\text{Ta})\text{O}_3\text{-BaSnO}_3$, BaSnO_3 also has the larger lattice constant of 4.12 Å, i.e., pseudocubic unit cells of $\text{Ba}(\text{Mg},\text{Ta})\text{O}_3$ has the lattice constant of 4.08 Å. The B-site ions in the solid solution are assumed to be more strongly bonded in the oxygen octahedron than in $\text{Ba}(\text{Mg},\text{Ta})\text{O}_3$ itself. And this strong bonding seems to improve the Q value of solid solution, adding to the effect of accelerated sintering.

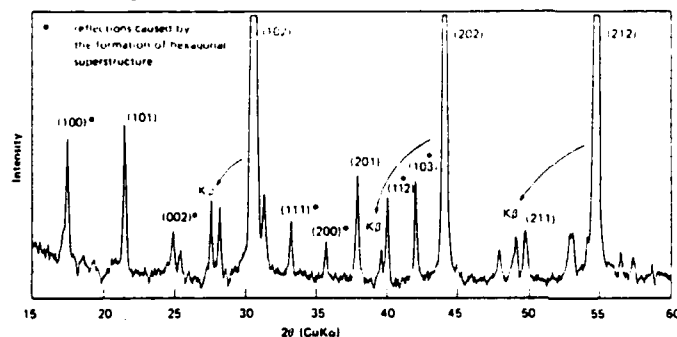


Fig. 1. X-ray powder diffraction patterns of $\text{Ba}(\text{Mg}_{1/3}\text{Ta}_{2/3})\text{O}_3$

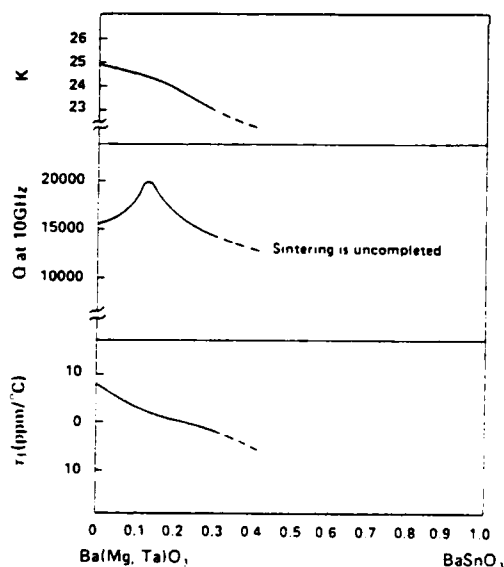


Fig. 2. Dielectric characteristics of $\text{Ba}(\text{Mg},\text{Ta})\text{O}_3\text{-BaSnO}_3$ ceramics.

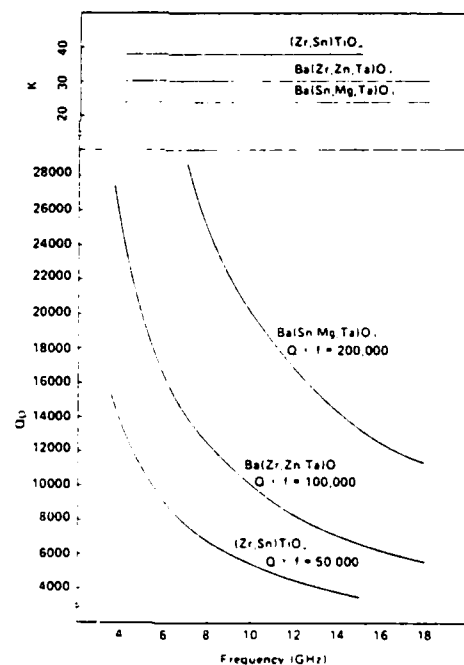


Fig. 3. Frequency vs K and Q for $\text{Ba}(\text{Sn},\text{Mg},\text{Ta})\text{O}_3$ ceramic.

REFERENCES

1. K. Wakino, K. Minai, and H. Tamura, *J. Am. Ceram. Soc.*, **67**, p. 278 (1984).
2. H. Tamura, T. Konoike, Y. Sakabe, and K. Wakino, *J. Am. Ceram. Soc.*, **67**, C-59 (1984).
3. K. Wakino, M. Morata, and H. Tamura, *J. Am. Ceram. Soc.*, **69**, p. 34 (1986).

T-4

DIELECTRIC PROPERTIES OF BaO-TiO₂-WO₃ SYSTEM AT MICROWAVE FREQUENCY

S. NISHIGAKI, S. YANO, H. KATO, and T. SONOMURA

Narumi Technical Laboratory, Narumi China Corporation, Nagoya, Japan

ABSTRACT Microwave Properties of BaO-TiO₂-WO₃ ceramic system were investigated. Addition of a small amount of WO₃ to BaO-XTiO₂ leads to an explicit improvement of Q and τ_f (temperature coefficient of resonant frequency). Microwave properties of the compositions with X=4 to 4.5 and Y=0 to 0.04 in the equation of BaO-XTiO₂·(1+X)YWO₃ were observed. With the range of X=4 to 4.5 and Y=0.02 to 0.005, higher Q values (8000~9000 at 6GHz) and lower τ_f values of nearly zero (-0.5 to 2.5 ppm/°C) with ϵ of 35~38 were obtained. These ceramics had three kinds of crystallines composed of BaTi₄O₉, Ba₂Ti₆O₂₀ and BaWO₄. It was found that these improvements seem to be attributed to BaWO₄ crystallines with a negative τ_f , which is segregated as a secondary phase by WO₃ addition in the dielectrics.

1. INTRODUCTION

Ceramics of the TiO₂ rich region of BaO-TiO₂ system such as BaTi₄O₉⁽¹⁾ and Ba₂Ti₆O₂₀⁽²⁻⁴⁾ are well known to be good dielectric resonator materials at microwave frequency. In order to improve the Q values, such methods as chemical treatment⁽⁵⁻⁶⁾ of calcined materials or addition of small amounts of Mn²⁺ were reported previously. There are, however, few data on the reduction of τ_f . The optimum of these published data for BaO-TiO₂ dielectrics are understood as following: BaTi₄O₉ (BaO-4TiO₂): ϵ =38, Q=9000 at 4GHz, (Q=6000 at 6GHz), τ_f =15~20 ppm/°C⁽¹⁾; Ba₂Ti₆O₂₀ (BaO-4.5TiO₂): ϵ =39~40, Q=8000~11,000 at 4GHz, (Q=5300~7300 at 6GHz), τ_f =2 ppm/°C⁽²⁻⁴⁾.

In our case, the segregated BaWO₄ crystallines formed by WO₃ addition have an advantage for both improvement of Q and τ_f . This paper is mainly concerned with the relation between the WO₃ amount, the microstructure and the microwave properties.

2. EXPERIMENTAL

2.1. Material and Procedure

The starting materials composed of BaCO₃, TiO₂, WO₃ and MnCO₃ powder with a purity of 99.7 to 99.9% were mixed to be the designated composition mentioned above, in which MnO was fixed to 0.1 mol%. The mixed powder was calcined at 1000°C in air for 4Hrs. Ball milled powder was cold pressed into disks and then sintered at a temperature ranging between 1360°C to 1420°C in O₂ for 2Hrs.

2.2. Measurement

The microwave properties of the dielectrics were measured by the resonant cavity method on the TE₀₁₈ mode at 6GHz. XRD, SEM and EPMA analysis were used to examine the microstructure of the dielectrics.

3. RESULT AND DISCUSSION

In order to study microwave properties for our dielectrics, we selected several points of X(4~4.5) in the composition written as BaO-XTiO₂·(1+X)YWO₃.

The properties of BaO-4TiO₂ and BaO-4.5TiO₂ with a small amount of WO₃ (Y=0~0.04) were represented typically in Fig. 1. In each case, the addition of WO₃ at Y=0.02 shows a remarkable increase of Q (7100, 5700~8000~9000), which is however saturated with further addition. It is still difficult to explain this favorable Q behavior (at Y=0.02).

On the other hand, it is well explained from Fig. 1 and the microstructure of these dielectrics (Fig. 2) that the change of ϵ and τ_f seems to depend on the segregation of BaWO₄ and Ba₂Ti₆O₂₀ in BaO-4TiO₂ or of BaWO₄ and TiO₂ in BaO-4.5TiO₂. The increase of ϵ and τ_f is due to segregation of TiO₂. The decrease of ϵ and τ_f is due to segregation of BaWO₄. It is thought from the optimum data of τ_f , -0.5 ppm/°C for BaO-4TiO₂·0.1WO₃ (Y=0.02) that BaWO₄ must have negative τ_f with smaller ϵ than Ba₂Ti₆O₂₀ and BaTi₄O₉. The segregation of Ba₂Ti₆O₂₀ is effective for ϵ increase and τ_f decrease. Therefore in order to obtain a dielectric resonator with high Q and zero τ_f with relatively high ϵ , coexistence of three kinds of crystallines of BaTi₄O₉, Ba₂Ti₆O₂₀ and BaWO₄ is required. (ϵ =35~38). The reaction equations with WO₃, which was identified by EPMA quantitative analysis for the microstructures, would be interpreted as follows. Table 1 is the summary of our study.

- (1) $\text{BaO} \cdot 4\text{TiO}_2 + \text{WO}_3 \rightarrow \text{BaTi}_4\text{O}_{10} + \text{Ba}_2\text{Ti}_8\text{O}_{20} + \text{BaWO}_4$
 $\text{BaTi}_4\text{O}_{10} + \text{Ba}_2\text{Ti}_8\text{O}_{20} + \text{BaWO}_4 + \text{WO}_3 \rightarrow \text{Ba}_2\text{Ti}_8\text{O}_{20} + \text{BaWO}_4 + \text{TiO}_2$
 (2) $\text{BaO} \cdot 4.5\text{TiO}_2 + \text{WO}_3 \rightarrow \text{Ba}_2\text{Ti}_9\text{O}_{20} + \text{BaWO}_4 + \text{TiO}_2$

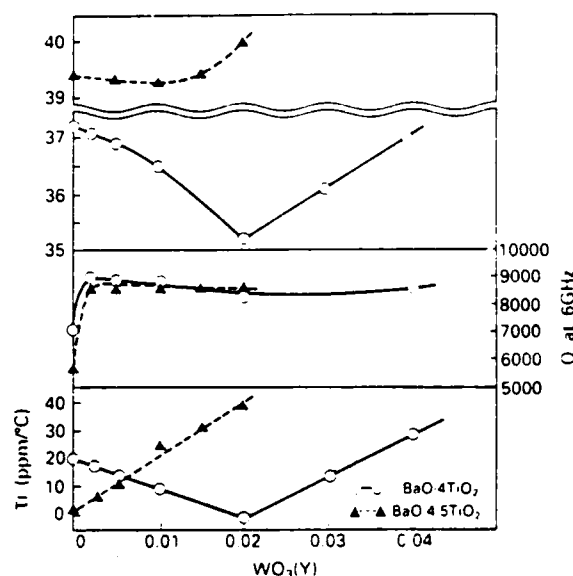
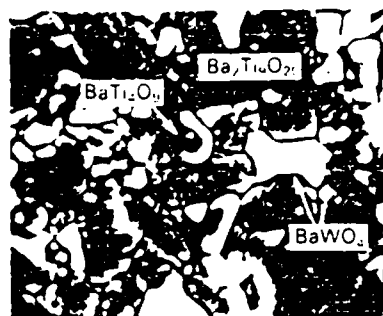


Fig. 1 Dielectric Properties of $\text{BaO} \cdot 4\text{TiO}_2 (1+4)\text{YWO}_3$ and $\text{BaO} \cdot 4.5\text{TiO}_2 (1+4.5)\text{YWO}_3$ at 6GHz

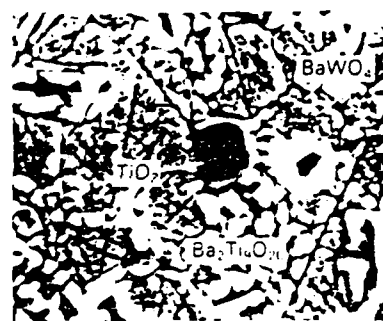
Table 1 Dielectric Properties of $\text{BaO} \cdot \text{XTiO}_2 (1+\text{X})\text{YWO}_3$

Composition	X	Y	Properties at 6GHz			Phase
			ϵ	Q	τ_f	
	4.0	—	37	7100	19	BT_4
	4.0	0.02	35	8400	-0.5	$\text{BT}_{4.5}, \text{BT}_{4.5}, \text{BW}$
	4.2	0.01	37	8800	1.6	$\text{BT}_4, \text{BT}_{4.5}, \text{BW}$
	4.3	0.005	38	8300	2.5	$\text{BT}_4, \text{BT}_{4.5}, \text{BW}$
	4.5	—	39	5700	1.4	$\text{BT}_{4.5}, \text{BW}, \text{T}$
	4.5	0.002	39	8800	4.0	$\text{BT}_{4.5}, \text{BW}, \text{T}$

$\text{BT}_4: \text{BaTi}_4\text{O}_{10}$, $\text{BT}_{4.5}: \text{Ba}_2\text{Ti}_9\text{O}_{20}$, T: TiO_2 , BW: BaWO_4



$\text{BaO} \cdot 4\text{TiO}_2 (1+4)0.02\text{WO}_3$



$\text{BaO} \cdot 4.5\text{TiO}_2 (1+4.5)0.002\text{WO}_3$

Fig. 2 Microstructure of $\text{BaO} \cdot 4\text{TiO}_2 (1+4)0.02\text{WO}_3$ and $\text{BaO} \cdot 4.5\text{TiO}_2 (1+4.5)0.002\text{WO}_3$

REFERENCES

- D.J. Masse et al., "A New Low-Loss High-K Temperature-Compensated Dielectric for Microwave Applications", proceeding of the IEEE Nov. 1628-1629 (1971).
- H.M. O'Bryan and J. Thomson, Jr., "Phase Equilibria in the TiO_2 -Rich Region of the System $\text{BaO}-\text{TiO}_2$ ", Jour. Am. Ceram. Soc., **57** [12] 522-526 (1974).
- H.M. O'Bryan and J. Thomson, Jr., "A New $\text{BaO}-\text{TiO}_2$ Compound with Temperature-Stable High Permittivity and Low Microwave Loss", Jour. Am. Ceram. Soc., **57** [10] 450-453 (1974).
- H.M. O'Bryan and J. Thomson, Jr., " $\text{Ba}_2\text{Ti}_9\text{O}_{20}$ as a Microwave Dielectric Resonator", Jour. Am. Ceram. Soc., **58** [9-10] 418-420 (1975).
- H.M. O'Bryan, Jr., J. Thomson and J.K. Plourde, "Effect of Chemical Treatment on Loss Quality of Microwave Dielectric Ceramics", Ber. Dt. Keram. Ges., **55** [7] 348-351 (1978).
- H.M. O'Bryan and J. Thomson, " $\text{Ba}_2\text{Ti}_9\text{O}_{20}$ with Improved Microwave Loss Quality", Am. Ceram. Soc. Annual Meeting, 121-E-86, May 1 (1986).
- S. Nomura, K. Tomaya and K. Kaneta, "Effect of Mn Doping on the Dielectric Properties of $\text{Ba}_2\text{Ti}_9\text{O}_{20}$ Ceramics at Microwave Frequency", Jap. Jour. Appl. Phys., **22** [7] 1125-1128 (1983).

FERROELECTRIC AND PYROELECTRIC PROPERTIES OF SPUTTER-DEPOSITED PZT AND PT FILMS

M. ADACHI, T. SHIOSAKI, and A. KAWABATA

Department of Electronics, Faculty of Engineering, Kyoto University,
Sakyo-ku, Kyoto 606, Japan

ABSTRACT: [111]-oriented PZT(90/10) films have been successfully grown with good epitaxy onto the c plane of sapphire and epitaxial Pt film substrates by the rf-magnetron sputtering method. The crystallographic identifications of these PZT and PT films are made by the X-ray and RHEED measurements. Dielectric, ferroelectric and pyroelectric properties of the films are measured. Pyroelectric coefficients at room temperature have been determined as 4.5 and $3.5 \times 10^{-8} \text{C/cm}^2\text{K}$ for epitaxial PZT and polycrystalline PT films, respectively. Epitaxial PZT(90/10) films on Pt/sapphire possess desirable properties for potential applications in pyroelectric devices.

1. INTRODUCTION

$\text{PbTiO}_3(\text{PT})$ is a tetragonal system with a point group of 4mm and its [001] axis is polar. On the other hand, the polar axis of PZT(90/10) belonging to the rhombohedral structure is parallel to the [111] axis. [100] and [111]-oriented platinum (Pt) films have been successfully grown with good epitaxy onto (100)MgO and (0001)sapphire substrates, respectively. These films are also used as lower electrodes.

In this paper, sputter-deposition of [111]-oriented epitaxial films of rhombohedral PZT(90/10) in the perovskite phase, and their dielectric, ferroelectric and pyroelectric properties are mainly described.

2. EXPERIMENTAL PROCEDURE

An rf-planar magnetron sputtering equipment was used to fabricate PZT(90/10) and PT films. The optimum sputtering conditions for these perovskite type film preparation adopted in the present experiment

were a gas content of $\text{Ar}(80\%) + \text{O}_2(20\%)$, a gas pressure of $(0.8-2) \times 10^{-2} \text{Torr}$, an rf power input of around 150W, and a substrate temperature of around 600°C . The Pt films with a thickness of about $0.3 \mu\text{m}$ were deposited epitaxially onto sapphire and MgO substrates by the same method at a substrate temperature of 450°C and also used as substrates for preparing epitaxial PZT and PT films.

3. RESULTS AND DISCUSSION

The crystalline structures of films deposited at various conditions were investigated. At substrate temperatures lower than 580°C , a metastable pyrochlore structure appeared. PZT of perovskite structure were obtained at substrate temperatures higher than about 580°C . The X-ray diffraction pattern of an epitaxial (111)PZT film sputtered on the (111)Pt/(0001)sapphire at the substrate temperature of 610°C is shown in Fig.1. Figure 2 shows a typical RHEED pattern of the epitaxial film. The epitaxial relations were found to be (111)PZT//[(111)Pt//[(0001)sapphire and $[1\bar{1}0]\text{PZT}//[1\bar{1}0]\text{Pt}//[10\bar{1}0]\text{sapphire}$. On the

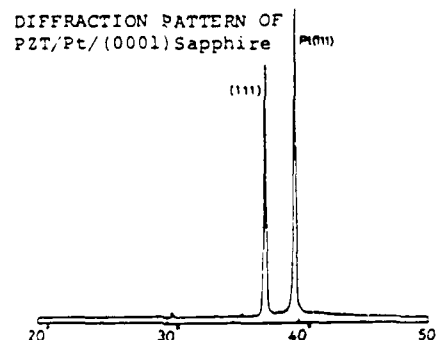


Fig.1 X-ray diffraction pattern of the epitaxial PZT(90/10) thin film on Pt/sapphire.

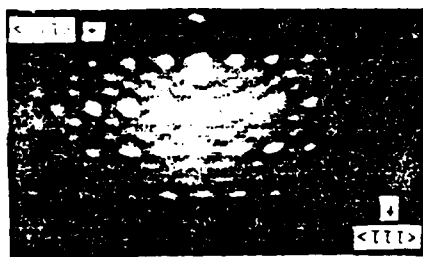


Fig.2 RHEED pattern of the epitaxial PZT(90/10) thin film on Pt/sapphire.

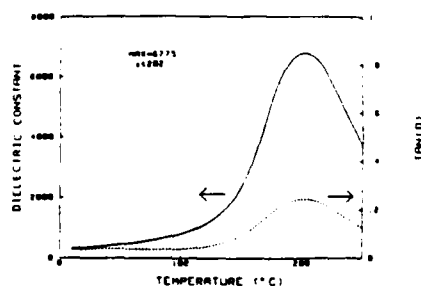


Fig.3 Temperature dependence of the dielectric constant of PZT(90/10) thin film.

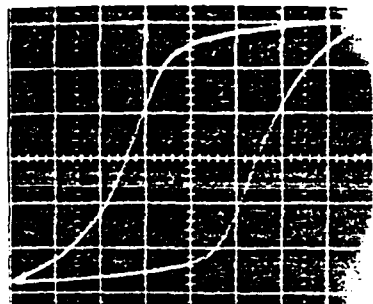


Fig.4 D-E hysteresis loop of PZT(90/10) film. The thickness is 12 μ m. Scale units: x axis: 25KV/cm/div., y axis: 15 μ C/cm²/div.

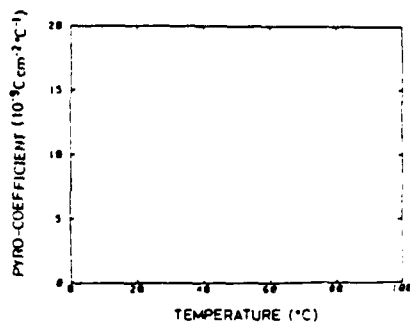


Fig.5 Temperature dependence of the pyroelectric coefficient of as-grown PZT(90/10) film without poling treatment.

other hand, [001]-oriented PT films deposited epitaxially on the (100)Pt/(100)MgO were not so reproducible in the present experiment. Figure 3 shows the temperature dependence of the dielectric constant measured for an epitaxial PZT. The constant shows an anomaly at the transition point of 202°C and its value at room temperature is 350. The dielectric constant maximum for the PZT film shows a broad temperature dependence and the T_c of the film is approximately 60°C lower than that of the PZT(90/10) ceramic. It would be considered that the disagreement of T_c between the film and the ceramic could be attributed to compositional difference of the film and/or to the thermal stress in the film caused by the difference in the thermal expansion coefficient between PZT and sapphire. D-E hysteresis loops were observed on the epitaxial PZT film as shown in Fig.4. The film thickness is 12 μ m. The coercive field E_c is 35kV/cm. E_c is remarkably larger than that of the PZT ceramic (11kV/cm). This higher E_c observed on the film is due to the small grain size and internal stress. On the other hand, the remanent polarization P_r is 35 μ C/cm² which is the same value of the PZT ceramic. Pyroelectric currents were observed in as-grown epitaxial [111]-oriented PZT films even without poling treatment and the directions were from upper to lower electrodes. Figure 5 shows the temperature dependence of the pyroelectric coefficient measured on the as-grown epitaxial film. The pyroelectric coefficient at room temperature is 3×10^{-9} C/cm²K. In addition, the phase transition from a lower temperature rhombohedral ferroelectric phase $F_R(LT)$ to a higher temperature rhombohedral ferroelectric phase $F_R(HT)$ was observed at 60°C. When the poling treatment was carried out in a direction coinciding with the direction of pre-existing internal bias, the pyroelectric coefficient increased. The pyroelectric coefficients of the epitaxial PZT and polycrystalline PT films with poling treatment were determined as 4.5 and 3.5×10^{-8} C/cm²K at room temperature, respectively. Accordingly it was concluded that the [111]-oriented epitaxial PZT(90/10) film is one of the most promising materials for pyroelectric applications.

T-6

PYROELECTRIC AND ELECTRICAL PROPERTIES OF MODIFIED LEAD TITANATE CERAMICS

N. ICHINOSE

School of Science and Engineering, Waseda University, Tokyo, Japan

ABSTRACT: Pyroelectric and electrical properties of the modified (Pb, Me)·[(Co_{1/2}Ti_{1/2}), Ti]O₃ ceramics (Me=Ba, Sr or Ca) containing small amounts of MnO and NiO have been investigated. These ceramics are characterized by high apparent density, small dielectric constant (about 200) and facility in poling procedure. Among the ceramics substituted with the alkaline earth metals, the Ca-modified ceramics show markedly excellent pyroelectric and piezoelectric properties. Various kinds of pyroelectric detectors and ultrasonic transducers have been developed by employing these modified PbTiO₃ ceramics.

1. INTRODUCTION

The modified PbTiO₃ ceramics have been regarded as good pyroelectric and electrical materials, because of their large pyroelectric coefficient, small dielectric constant and high Curie temperature. The present paper reports the pyroelectric and electrical properties of (Pb, Me)[(Co_{1/2}W_{1/2}), Ti]O₃ ceramics (Me=Ba, Sr or Ca).

2. EXPERIMENTAL

2.1. Materials

Raw materials were calcined at 900°C for 2 hours in air after weighing and mixing. The mixture were formed by die pressing and fired at 1050 - 1200°C for several hours. Because of the low firing temperature and small amount of PbO vaporization, the mixture was not fired in PbO atmosphere.

2.2. Measurements

The spontaneous polarization values were measured by the Sawyer - Tower method and relative dielectric constants were measured by ordinary method. Using the system in Fig. 1, we have measured pyroelectric coefficient values.

3. RESULTS

Figure 2 shows pyroelectric coefficient P, relative dielectric constant ε and figure of merit F_V for (Pb_{1-x}Ca_x)[(Co_{1/2}W_{1/2})_{0.96}Ti_{0.04}]O₃ as a function of Ca concentration. As Ca is introduced into PbTiO₃ ceramic, the pyroelectric coefficient increases to a great extent.

Curie temperatures and coupling factors for the (Pb_{1-x}Me_x)[(Co_{1/2}W_{1/2})_{0.96}Ti_{0.04}]O₃ system are shown in Fig. 3 and Fig. 4, respectively. From Fig. 4, it is found that these piezoelectric materials have an extremely anisotropic piezoelectric effect.

4. DISCUSSION

The improvement of pyroelectricity by the Ca introduction into PbTiO₃ host lattice may be attributed to the increase of the spontaneous polarization as shown in Fig. 5.

The large piezoelectric anisotropy of these ceramics may be understood when the piezoelectric properties are deduced from the electrostrictive coefficient and the piezoelectric constant d_{31} disappears for a particular ratio of the electrostrictive coefficients and a certain degree of polarization.¹⁾

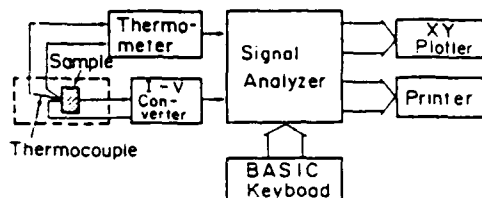


Fig. 1. Schematic diagram for measuring pyroelectric coefficient P .

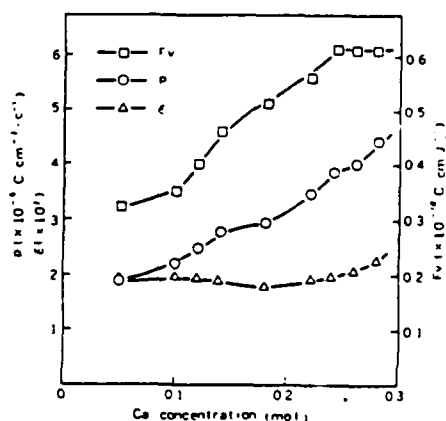


Fig. 2. Pyroelectric coefficient P , relative dielectric constant ϵ , and figure of merit F_v for $(\text{Pb}_{1-x}\text{Ca}_x)(\text{Co}_{1/2}\text{W}_{1/2})_{0.5}\text{Ti}_{0.5}\text{O}_3$ as a function of Ca concentration.

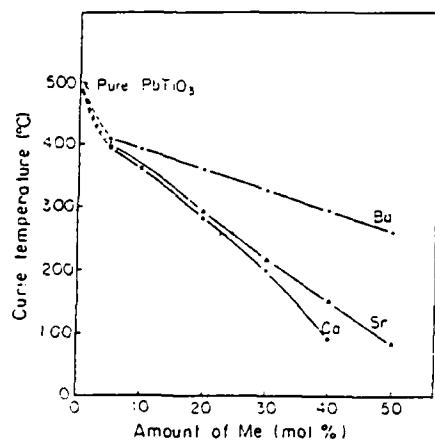


Fig. 3. Curie temperature vs amount of Me for $(\text{Pb}_{1-x}\text{Me}_x)(\text{Co}_{1/2}\text{W}_{1/2})_{0.5}\text{Ti}_{0.5}\text{O}_3$ system.

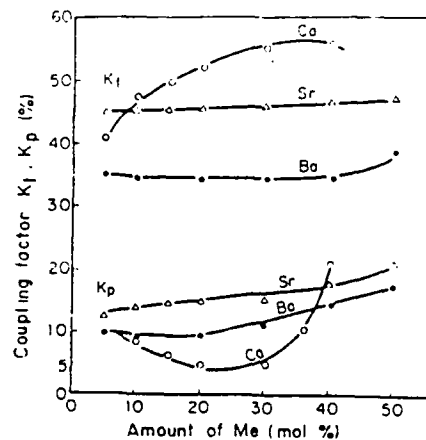


Fig. 4. Coupling factors vs amount of Me for $(\text{Pb}_{1-x}\text{Me}_x)(\text{Co}_{1/2}\text{W}_{1/2})_{0.5}\text{Ti}_{0.5}\text{O}_3$ system.

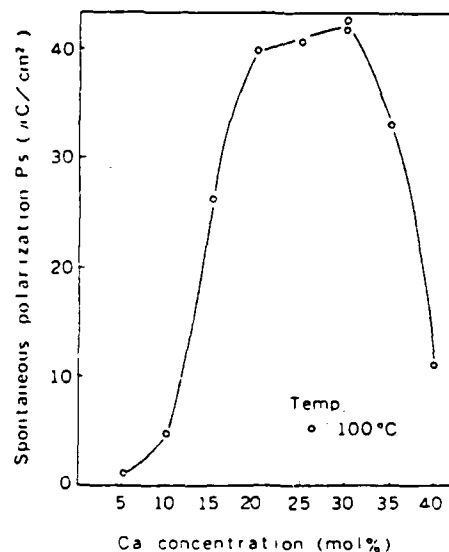


Fig. 5. Relation between spontaneous polarization P_s and Ca concentration of $(\text{Pb}_{1-x}\text{Ca}_x)(\text{Co}_{1/2}\text{W}_{1/2})_{0.5}\text{Ti}_{0.5}\text{O}_3$ ceramics.

REFERENCE

1. W. Wersing et al., ISAF, PD-21 (1986).

Properties of Hot-Pressed Lead Germanate Silicate Ceramics

K. Nagata and K. Okazaki

Department of Electrical Engineering,

The National Defense Academy, Yokosuka 239, Japan

Lead germanate ($\text{Pb}_5\text{Ge}_3\text{O}_{11}$) single crystal has large pyroelectric coefficients and relatively small dielectric constants, being expected to the use for an infrared detector.¹⁾ However, pyroelectricity and optical-activity in the ceramics have not been so much satisfactory. This is because that the lead germanate has large anisotropy of crystal-structure and that poling is difficult in the ceramics. Therefore many researchers have been studied concerning the polar-axis oriented crystal growth behaviors and substitutional effects of Si and Ba for lead germanate. K.Takahashi et al have succeeded in polar-axis oriented thick-film lead germanate silicate monocrystal by the grass-recrystallization method.²⁾ Also, G.Kirer et al have grown thin-film of lead-germanate by reactive dc-sputtering.³⁾

On the other hand, we obtained grain-oriented ferroelectric ceramics of bismuth-layer type and tungsten-bronze type by hot-pressing method.⁴⁻⁷⁾ This indicates that if the same method is applied to the lead germanate, the similar grain-oriented ceramics can be prepared. In this study, grain-oriented silicate modified lead germanate ceramics were prepared by hot-pressing. The microstructure, and the dielectric and pyroelectric properties of grain-oriented lead germanate silicate ceramics were measured and discussed.

The lead germanate silicate with the composition of $\text{Pb}_5\text{Ge}_{3-x}\text{Si}_x\text{O}_{11}$ (hereafter abbreviated to PGSO/x) were prepared, using pure grade PbO , GeO_2 and SiO_2 as starting materials. They are ball-milled and calcined for 5 h at 500°C , then melted in the alumina crucible and hold at 800°C for 10 min, and subsequently, quenched to get glassy material. The glassy material were calcined at 500°C for 30 h in air.

The powders were pressed uniaxially into compact of 15 mm in diameter and 20 mm in height under a pressure of 1000 kg/cm^2 . The green compact was hot-pressed at 600°C for 5 h under 100 kg/cm^2 pressure in the oxygen atmosphere. The hot-pressed ceramics were sliced with the normal direction to the slicing plane perpendicular ($P\perp$), or parallel ($P//$), to the direction of hot-pressing. For the measurement of the electrical properties, gold was sputtered on the both faces of the plate samples.

The temperature dependence of the relative permittivity for the hot-pressed lead germanate silicate is shown in Fig. 1. In the all composition, permittivities of $P//$ sample are 1.5 to 4 times larger than that of $P\perp$ sample. Especially, the anisotropy of about 4 times in the permittivity at Curie point was found in the PGSO/0.25 composition.

The D-E hysteresis loops for the hot-pressed PGSO/0.25 are shown in Fig. 2. A typical hysteresis loop was observed for $P//$ sample. On the other hand, a linear D-E relationship without any hysteresis was observed for $P\perp$ sample.

The remanent polarization of P// and P⊥ sample was 11 and 0 $\mu\text{C}/\text{cm}^2$, respectively.

The pyroelectric coefficient as a function of temperature for the hot-pressed $\text{Pb}_{0.5}\text{Ge}_{1.5}\text{Si}_{0.25}\text{O}_{11}$ ceramics is shown in Fig. 1. The peak of the pyroelectric coefficient at about 70°C was about $15 \times 10^{-2} \mu\text{C}/\text{cm}^2/\text{°C}$ in P// sample. On the other hand, pyroelectric coefficient of P⊥ sample was about 0 between 15 and 150°C. The pyroelectric coefficient in P// at room temperature was about $2.5 \times 10^{-2} \mu\text{C}/\text{cm}^2/\text{°C}$, was as same as that of LiTaO_3 single crystal and 3 to 4 times as large as that of LiNbO_3 single crystal.

These results indicated that the each polar-axis (c-axis) of lead germanate silicate crystals were oriented parallel to the hot-pressing direction. In the crystal growth of lead germanate single crystal, the easy crystal-growth direction is the c-plane, hexagonal plate-shaped grains are formed in the early stage of the crystal growth or glass-recrystallization.³⁾ Therefore, during hot-pressing, the plate-shaped crystallites are created in the early stage of the firing process and they are aligned perpendicular to the hot-pressing direction. In the hot-pressed lead germanate silicate, the c-axis and polar-axis of ceramics are arranged parallel to the hot-pressing direction.

REFERENCES

- 1) H. Iwasaki et al.; J. Appl. Phys., 43 (1972) 4907.
- 2) K. Takahashi et al.; Jpn. J. Appl. Phys., (1983) Suppl. 22-2, p73.
- 3) G. Kleer et al.; Ferroelectrics, 26 (1980) 757.
- 4) Y. Inoue et al.; J. Ceram. Soc. Japan, 92 (1984) 54.
- 5) K. Nagata et al.; Ferroelectrics, 38 (1981) 853.
- 6) K. Nagata et al.; Jpn. J. Appl. Phys., 22 (1983) 1353.
- 7) K. Nagata et al.; Jpn. J. Appl. Phys., (1983) Suppl. 22-2, p123.
- 8) W. Eysel et al.; J. Am. Ceram. Soc., 56 (1973) 185.

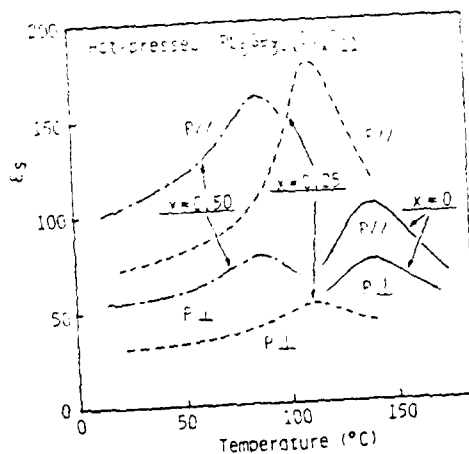


Fig. 1. Temperature dependence of dielectric constant of hot-pressed lead germanate silicate ceramics.

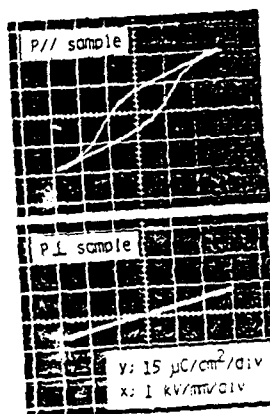


Fig. 2. D-E hysteresis loops for hot-pressed $\text{Pb}_{0.5}\text{Ge}_{1.5}\text{Si}_{0.25}\text{O}_{11}$ ceramics.

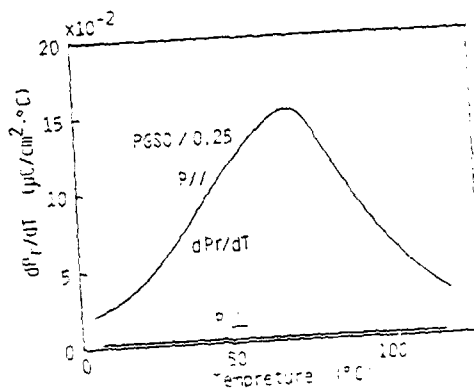


Fig. 3. Pyroelectric coefficient as a function of temperature for hot-pressed $\text{Pb}_{0.5}\text{Ge}_{1.5}\text{Si}_{0.25}\text{O}_{11}$ ceramics.

T-8

COMPARISON: THERMAL AND MECHANICAL PROPERTIES OF BARIUM TITANATE VERSUS LEAD PEROVSKITE DIELECTRICS

A. E. BROWN and C. R. KORIPELLA

Union Carbide Corporation, Greenville, S. C., USA

ABSTRACT: Thermal and mechanical properties of solid ceramic and multilayer ceramic chips were measured and the properties of barium titanate-based dielectrics were compared to a lead perovskite dielectric material. Fracture toughness and bend strength values indicate that the lead perovskite dielectrics are relatively weak. Thermal shock experiments show that thermal stresses cause unstable crack propagation in barium titanate dielectrics whereas a stable crack propagation occurs in the lead perovskite dielectrics.

1. INTRODUCTION

Recent increased use of surface mount components has placed a major emphasis on the mechanical strength and the thermal shock resistance of ceramic chips. In this study, fracture toughness and modulus of rupture values measured on barium titanate-based commercial dielectrics were compared with a lead perovskite dielectric. Using the measured physical and mechanical properties of these materials, the theoretical thermal shock resistance parameters for fracture initiation, R and R^1 , were calculated¹⁾ and compared with the experimental thermal shock results.

2. EXPERIMENTAL

Fracture toughness was measured by an indentation strength method in which the samples were precracked with a micro indenter and then fractured by a four point bend testing method²⁾. Modulus of rupture was measured by a simple three point bending technique.

Thermal shock resistance was measured by heating the chips to various elevated temperatures, quenching into room-temperature water and then measuring the three point bend strength of the quenched samples. All tests were performed on a 5819 size (14.7 x 4.8 x 1.5 mm) solid and multilayer chips.

3. RESULTS AND DISCUSSION

The experimental data show that the lead perovskite dielectric is softer and mechanically weaker than the barium titanate-based dielectric. Theoretically calculated thermal shock resistance parameters also indicate that these dielectrics are inferior to barium titanate-based dielectrics. However, experimental thermal shock results indicate that the lead perovskite dielectrics have a delayed, intermittent, and the barium titanate dielectrics. $BaTiO_3$

(C).

dielectrics show a sudden drop in strength at a critical temperature differential of approximately 75 to 100°C, whereas, the lead perovskites show a gradual decrease in strength.

Microscopic observations of the thermal shocked chips show many surface cracks in BaTiO₃ dielectrics and few or no cracks in the lead perovskite dielectrics. The experimental results suggest that in BaTiO₃ dielectrics fracture occurs by unstable crack propagation, due to thermal stresses, and in the lead perovskite dielectric, stable crack propagation occurs.

REFERENCES

1. D.P.H. Hasselman, Am. Ceram. Soc. Bull., 49, 1033-37 (1970).
2. P. Chantikul, G. R. Anstis, B. R. Lawn, D. B. Marshall, J. Am. Ceram. Soc., 64, 539-43 (1981).

FRACTURE BEHAVIOR OF CAPACITOR CERAMICS

S. W. FREIMAN and T. L. BAKER

National Bureau of Standards, Gaithersburg, Maryland 20899

ABSTRACT: Mechanical failure of ceramic capacitors is examined from the point of view of loss of components during fatigue crack growth and the effects of inservice failures. This study involves the use of optical, scanning electron, and microstructure on the fracture toughness and crack growth behavior of several ceramic materials used in multilayer capacitors. The purpose of this study is to determine whether internal stresses due to the package firing process and the transformation have an effect on the fracture of these materials and to establish correlations between strength and dielectric aging.

Six capacitor ceramics were used in this study. The materials were fired identically to actual capacitor firing conditions and the specimens were fired to avoid the complications of crack-electrode interactions. Indentation fracture tests were used to measure K_{IC} as well as to assess the possible effects of internal stresses on the fracture behavior of these materials and to correlate strength, K_{IC} , and dielectric strength. The environmentally enhanced crack growth behavior of these materials was determined by conducting dynamic fatigue tests in water of room temperature.

It is shown that the initial fracture toughness of these materials varied by as much as a factor of two from one material to another (see Table 1). The differences were ascribed to variations in the degree of trace defect or due to the firing process in the materials. Unlike the behavior of titanium nitride used in high voltage applications, little or no direct effects of internal stresses were observed in these materials, except at indentation loads of 100 g or less, where a slight increase in the material designated as having a "high" aging rate exhibited a stronger resistance to stresses than did a "low" aging rate material. No variation in these internal stress effects could be detected as a function of aging time at room temperature.

Susceptibility to moisture enhanced crack growth was also examined as a function of capacitor composition. Crack growth exponents, n , ranged from 10 to 20. The dynamic fatigue curves for the two X7R compositions suggested the existence of a crack growth limit in these materials.

TABLE 1. Compositions and Properties of Capacitor Ceramics

Designation	Major Constituent	Crack growth limit, n	K_{IC} , $\text{ksi}\sqrt{\text{in}}$	K_{IC} , $\text{MPa}\sqrt{\text{m}}$
NPO	Rare earth oxide	1-3	1.4	1.8
X7R-1	BaTiO ₃ (B1)	2-7	1.7	2.2
X7R-2	BaTiO ₃	1-7	1.7	2.2
C5U	BaTiO ₃	1-7	1.7	2.2
C5U "high" aging	BaTiO ₃	1-7	1.7	2.2
C5U "low" aging	BaTiO ₃	1-7	1.7	2.2

T-10

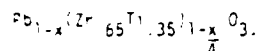
COMPOSITIONAL INFLUENCES ON PLZT SWITCHING PROPERTIES

B. JOEPKE, F. WALLENHORST and J. KYONKA
Honeywell Inc., Minneapolis, MN

ABSTRACT: Half-wave voltages, polarization and capacitance were measured for a series of PLZT samples with varying La contents and Zr/Ti ratios. These parameters, particularly half-wave voltage, are critical in the design of active PLZT optical components. Lower values of half-wave voltage are highly desirable. This work establishes that as the La content exceeds 9.4 atom % and as the Zr/Ti ratio exceeds 65/35, undesirable increases in half-wave voltage will result.

1. INTRODUCTION

PLZT materials have been extensively studied since the high transparency of the lanthanum modified lead zirconate-lead titanate family was discovered by Haertling in 1969¹⁾. These materials have been used primarily in optical shutter applications²⁾. Most of the study efforts have concerned compositions prepared to the formula



with x ranging from .090 (9.0 atom % La) to .100 (10.0 atom % La). When the compositions are used in optical shutter applications, low switching times and low half-wave voltages are both desirable. This investigation was carried out to determine if both reduced switching time and lower half-wave voltages could be found in compositions with Zr/Ti ratios above 65/35 and La contents above 9.5 atom %.

2. EXPERIMENTAL PROCEDURE

A fine-composition matrix was selected for investigation with La contents of 9.4, 9.7 or 10.0 atom percent. The Zr/Ti ratios used were 65.5/34.5, 66.5/33.5 or 67.5/32.5. Material preparation was by chemical coprecipitation. Slugs were prepared by hot pressing 1220°C for 10 hours at 100 psi (3.3 MPa). Wafer samples 5.08cm diameter were sliced from resulting slugs and polished to a high quality surface. An interdigital pattern of electrode grooves was cut into the 0.015" (3mm) thick wafers to a nominal depth of 0.022" (0.05mm) and with 0.40" (10mm) edge to edge spacing. The groove pattern was electroded by electroless deposition of nickel, followed by gold. Additional test samples of 0.030" (0.77mm) in thickness and 0.020" (0.51mm) in diameter were fabricated and electroded with full surface electrodes of 100nm silver for polarization measurements.

In the half-wave voltage tests, a white light source was used with a converging lens, Fresnel lens, and aperture to provide the testing light beam. A linear polarizer along with green and IR filters allowed only polarized light of the desired wave length to enter the PLZT sample. The PLZT sample was followed by a second polarizer, at 45° to the first, and a detector to measure transmitted light. The voltage to the PLZT sample was ramped upward until 50% transmission was achieved at each step. The voltage at maximum transmission was taken as the half-wave voltage.

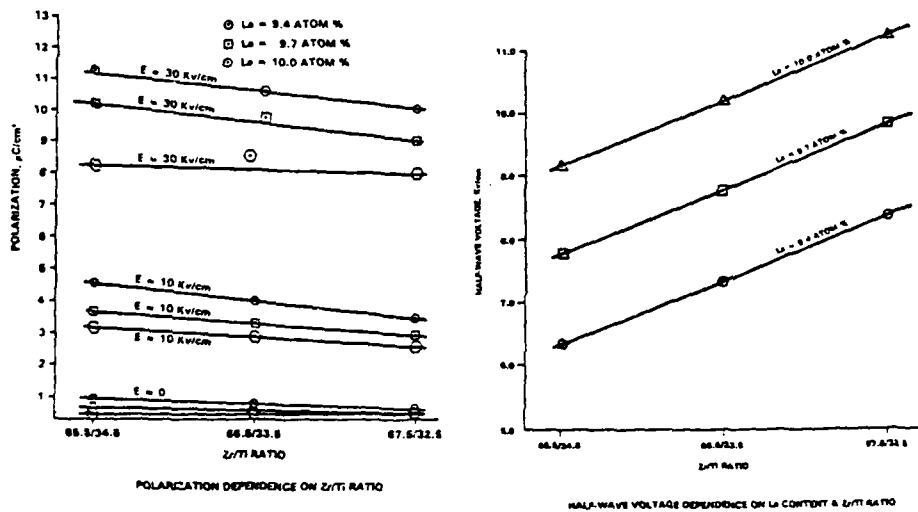
3. RESULTS

Results indicate consistent low half-wave voltage requirements with increasing La

content. In addition, it is shown that increasing Zr/Ti ratios also result in higher half-wave voltage levels.

Switching times measured in the test described above ranged from 45 to 75 microseconds over the nine compositions tested. Data scatter was such that no trends were detectable through the composition range tested. Data scatter was thought to be due to mechanical oscillations of the PLZT wafer following discharge.

Polarization is shown to be inversely related both to the Zr/Ti ratio and to the La content. Variations of the La content resulted in substantially larger changes in polarization than variations in the Zr/Ti ratio. Wafer capacitance, and therefore the material dielectric constant, is shown to be inversely related to both the La content and to the Zr/Ti ratio.



4. DISCUSSION

This work shows that, as the Zr/Ti ratio is raised above the 65/35 level, the half-wave voltage increases for 9.4 atom percent and higher La contents. Switching time measurement scatter was such that differences between samples were not detectable. The wafer capacitance and therefore dielectric constant is inversely related to both the La content and the Zr/Ti ratio. Polarization is inversely related to both La content and Zr/Ti ratio. The results of this work indicate that Zr/Ti ratios of less than 65/35 along with La contents of less than 9.4 atom percent should be explored. It appears that lower half-wave voltages can be achieved with probable minor impact on switching time but at some cost in higher dielectric constant and polarization values.

REFERENCES

1. G. H. Haertling and G. E. Land, "Hot Pressed $\text{Pb}(\text{La})\text{Zr}_{1-x}\text{Ti}_x\text{O}_3$ Ferroelectric Ceramics for Electro-optic Applications", *J. Amer. Ceram. Soc.*, **59**, 1, 1976, 1977.
2. J. T. Cutcher, J. D. Harris, Jr., and G. R. Laduna, "Applications of PLZT Electro-optic Chutters", Sandia Laboratories, Albuquerque, NM Rept. SAND-76-053.
3. J. D. Harris, Jr., and J. T. Cutcher, "Compositional Dependence of Electro-optic and Electro-optic Characteristics of 45/55 PLZT Ceramics", *J. Appl. Phys.*, **47**, 1976, 1977.
4. A. S. Khalafalla, J. Harrison and J. Harris, "Effect of Zr/Ti Ratio on the Electro-optic Characteristics of Ferroelectric PLZT", *J. Appl. Phys.*, **47**, 1976, 1977.

ELECTROMECHANICAL FAILURE PREDICTIONS

R.C. PODIANKA, P.L. SMITH
Office of Naval Research, Arlington, VA 22217
S.W. FREEMAN
National Bureau of Standards, Gaithersburg, MD 20899

ABSTRACT: Dielectric and piezoelectric ceramics such as barium titanate and PZT are known to be subject to environmentally enhanced crack growth. That is, if a static mechanical stress, σ_a , is imposed on such ceramics in the presence of water vapor, small surface flaws may extend slowly with time until they reach a size at which catastrophic fracture takes place. It has been demonstrated previously that the time to failure, t_f , under such conditions can be calculated from fracture mechanics principles and is given by the expression:

$$t_f = B S_i^{(n-2)} \sigma_a^{-n} \quad (1)$$

where B is a constant made up of a number of flaw and crack growth parameters, S_i is the initial strength of the material, and n is a constant which is a measure of the crack growth susceptibility of the material. Such an expression has been shown to accurately predict the lifetime of components under static, far field loads.

Increasingly, however, dielectric and piezoelectric ceramics are being operated under conditions, i.e., resonant cyclic fields, where more complex stresses can arise. The purpose of this paper will be to demonstrate how these more complex stress states affect the sensitivity of such ceramics to delayed failure and to begin to formulate expressions which will allow a designer to use these materials safely.

The devices being considered and types of electrical fields imposed on them are shown in Table 1. The key factors which are discussed in this paper are:

1. Effects of electrostrictive stresses local to a crack tip generated by the application of a d.c. bias field.
2. Cyclic stressing effects due to application of an a.c. field at a resonant frequency.

It will be shown that the presence of these factors can lead to complex expressions for failure time which may not be analytically determinable. Other complexities such as the presence of internal stresses in piezoelectric ceramics and mechanisms of crack growth under compressive loads will also be discussed.

Table 1
Electromechanical Conditions

<u>Device</u>	<u>Electrical Field</u>	<u>Strain Condition</u>	<u>Stress</u>
Capacitors Microdisplacive Devices	Static	Static	Stresses at Flaws increased by Electric Field Concentrations
Piezoelectric Transducers	Cyclic	Cyclic	Uniform at cross section
Electrostrictive Transducers a) biased b) non-biased	Static + Cyclic Cyclic	Cyclic + Static Cyclic	Uniform at cross section

The relation of anisotropy between crack length and fracture toughness in poled PLZT and modified PbTiO_3 ceramics

T. YAMAMOTO, H. IGARASHI and K. YAMAZAKI

Department of Electrical Engineering, National Defense Academy, Yokosuka Japan

ABSTRACT: A micro-indentation technique was applied to the poled $(\text{Pb},\text{La})(\text{Zr},\text{Ti})\text{O}_3$ and $(\text{Pb},\text{Ca})\text{TiO}_3$ ceramics. Internal stress induced by the DC application of 3KV/mm were measured as the 3.3 MN/m^2 and 65.6 MN/m^2 in the direction parallel and perpendicular to the poling field in the $(\text{Pb},\text{Ca})\text{TiO}_3$ ceramics. These anisotropies of internal stress could be also confirmed in the three point bending test. The anisotropy of crack lengths was explained by this internal stress.

1. INTRODUCTION

In general, ferroelectric ceramics were used after DC poling treatment. The electrical properties of the poled ferroelectric ceramics have been widely investigated for the practical use. Mechanical properties in the poled ferroelectric ceramics are important for an improvement of reliability in electronic components. In this paper, the internal stress was measured by using the micro-indentation (MI) technique. The relation of anisotropy between crack length and fracture toughness was discussed.

2. EXPERIMENTAL PROCEDURE

The chemical compositions of the sample for this experiment were $(\text{Pb}_{0.76}\text{Ca}_{0.24})[(\text{Co}_{1/2}\text{W}_{1/2})_{0.04}\text{Ti}_{0.96}\text{O}_3]$, $(\text{Pb},\text{Ca})\text{TiO}_3$ and $(\text{P}_{0.98}\text{La}_{0.02})(\text{Zr}_{0.5}\text{Ti}_{0.5})\text{O}_3$. PLZT 2/50/50. The sintered body was prepared by normal sintering for $(\text{Pb},\text{Ca})\text{TiO}_3$ and by hot-pressing for PLZT 2/50/50. The sample dimensions for MI measurement were 7 mm in width, 30 mm in length and 10 mm in thickness, respectively and silver electrodes were attached to the major surfaces. The side surfaces perpendicular to the electrode were finish ground with 1 μm gritt alumina and annealed at 800°C for 5 min in order to remove the residual strain induced by the mechanical polishing. The samples were poled in silicon oil at 110°C by applying DC fields of 0 to 3 KV/mm for 10 min. The micro-Vicker's hardness tester was applied as shown in Fig. 1.

3. RESULTS AND DISCUSSIONS

Figure 2 depicted the micrographs of cracks induced by the indent load of 10, 20, and 30 Kg in the poled $(\text{Pb},\text{Ca})\text{TiO}_3$ ceramics. The anisotropies of crack length caused by the indent load of 30 Kg was 1.4 times in the direction parallel and perpendicular to the poling field direction. From the length of these cracks, K_{1c} values were calculated from the following formula,

$$K_{1c} = 0.020E^{0.5}P^{0.5}a^{-0.5}(\bar{a}/\bar{c})^{-1.5}$$

where E is Young's modulus, P in the indent load, \bar{a} and \bar{c} are indent length and crack length, respectively. If the sample has a internal stress, the fracture toughness represents the effective value as shown in the following equation,

$$K_{1c} = K_{1c}^0 + 2\sigma_i\sqrt{\bar{a}}$$

where K_{Ic}^0 is an intrinsic fracture toughness and σ_1 is an internal stress. The equation can be applied when the sample has the uniform distribution of stress. Figure 3 shows the fracture toughness as a function of indent loads. The internal stress parallel, $\sigma_1(E\parallel)$ and perpendicular, $\sigma_1(E\perp)$ to the poling field direction were the compressive stress of 11.5 MN/m^2 and external stress of 26.6 MN/m^2 , respectively. As shown in micrographs in Fig. 2 and K_{Ic}^0 value measured by the indent load of 10 Kg in Fig. 3, the crack lengths parallel and perpendicular to the poling field direction are almost same and as a result the $K_{Ic}(E\parallel)$ and $K_{Ic}(E\perp)$ were almost same. Table 1 shows the crack lengths, $c(E\parallel)$ and $c(E\perp)$ and fracture toughness, $K_{Ic}(E\parallel)$ and $K_{Ic}(E\perp)$ and the ratio of crack length, $c(E\parallel)/c(E\perp)$. The anisotropy of crack lengths became larger at the heavy indent load. If the sample has no internal stress, the K_{Ic}^0 value became to a constant value at the various indent load and the internal stress was zero. Table 1 also represents the crack length parallel and perpendicular to the poling field, $c(E\parallel)$ and $c(E\perp)$ and the ratio of $c(E\parallel)$ and $c(E\perp)$ calculated from the experimental conditions that the internal stress is zero and $K_{Ic}^0(E\parallel)=2.33 \text{ MN/m}^{1.5}$ and $K_{Ic}^0(E\perp)=1.94 \text{ MN/m}^{1.5}$ at the indent load of 20 and 30 Kg. As shown at the right side in Table 1, the anisotropy of crack lengths parallel and perpendicular to the poling field was reduced. Therefore, the internal stress was induced by the rearrangement of domains by the poling field application and it could be concluded that the anisotropy of cracks was induced from the internal stress.

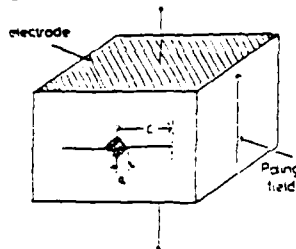


Fig. 1 sample configuration

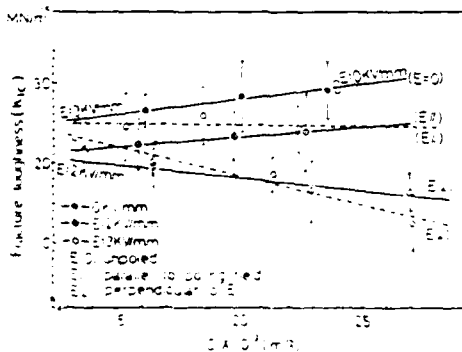


Fig. 2 Optical micrographs of crack and indent
Fig. 3 Fracture toughness as a function indent load in poled (Pb,Ca,TiO₃)

Table 1

kg	$c(E\parallel)$ (μm)	$c(E\perp)$ (μm)	$K_{Ic}(E\parallel)$ (MN/m ^{1.5})	$K_{Ic}(E\perp)$ (MN/m ^{1.5})	$c(E\parallel)/c(E\perp)$	$K_{Ic}(E\parallel)/K_{Ic}(E\perp)$
10	100	100	2.33	1.94	1.0	1.0
20	120	100	2.5	1.94	1.2	1.2
30	150	100	2.8	1.94	1.5	1.5

Indent load: 10 kg, 20 kg, 30 kg
Crack length: $c(E\parallel)$, $c(E\perp)$
Fracture toughness: $K_{Ic}(E\parallel)$, $K_{Ic}(E\perp)$
Ratio: $c(E\parallel)/c(E\perp)$, $K_{Ic}(E\parallel)/K_{Ic}(E\perp)$

MECHANICAL AND DIELECTRIC FAILURE OF BaTiO_3 CERAMICS

A. KISHIMOTO, F. KOMOTO, and M. YANAGIDA

Department of Industrial Chemistry, Faculty of Engineering,
The University of Tokyo, Tokyo, Japan

ABSTRACT: The present paper reports the alternative method to predict the mechanical failure probability of ferroelectric BaTiO_3 thick films, utilizing the analogy between mechanical and dielectric strength distributions without spending a lot of test pieces. The effects of microstructure and measurement method on the strength distributions are also discussed.

1. INTRODUCTION

It is still difficult to predict the probability of mechanical failure of ceramic materials. Usual mechanical strength test requires a lot of test pieces subjected to failure, which should be inconvenient from the technological point of view.

Mechanical failure is recognized to be microstructure-sensitive. Especially larger grains and pores are regarded to play an important role as fracture origins. On the other hand, dielectric strength is also proved to be dependent upon microstructural parameters as grain size, porosity, etc., which would lead to the scattering in dielectric strength distribution. Hence, the analogy between dielectric and mechanical strength distributions can be expected, if the fracture origins in both failures are similar.⁽¹⁾ In the present work, this concept was examined for BaTiO_3 thick films as representative ferroelectric ceramics.

2. EXPERIMENTAL

The specimens subjected to the test were fabricated by the modified doctor blade method.⁽²⁾ The final thickness of the film was in the range of 180 to 220 μm . Mechanical strengths were measured in three point flexure (12mm span). For dielectric breakdown tests, Ag pastes were attached on both sides of the film as the electrodes. The dc voltage was applied to a specimen placed in silicon oil and increased at the rate of 50V/sec. Breakdown voltage was determined by measuring the abrupt increase in current. Both the dielectric and mechanical strengths were estimated by the Weibull statistics.

3. RESULTS

Weibull plots of the sets of data of mechanical and dielectric strength obtained for the specimen sintered at 1300°C are shown in Fig. 1 as a typical example. Those for the other specimens sintered at 1350°C and 1400°C have shown similar distributions to those shown in Fig. 1.

It is seen in the figure that the distribution-shapes of both strengths are very close to each other, which indicates a similar role of microstructure in both failure, though the decisive factor for fracture is not well known.

On the other hand, Weibull plots for the specimens sintered at 1450 °C revealed different distribution shapes between mechanical and dielectric strength.

4. DISCUSSION

The present results would firmly suggest that the fracture origins in both failures are similar in a small-grained specimen but not in a larger-grained specimen. Fairly good correlation in Weibull distributions between mechanical and dielectric strengths can be utilized to predict the mechanical failure probability of a material without spending a lot of test pieces.

Similar experiments were carried out above the Curie temperature to examine if the analogy between mechanical and dielectric failure still appears. Thicker specimens were also subjected to the similar tests. Details will be presented on the poster.

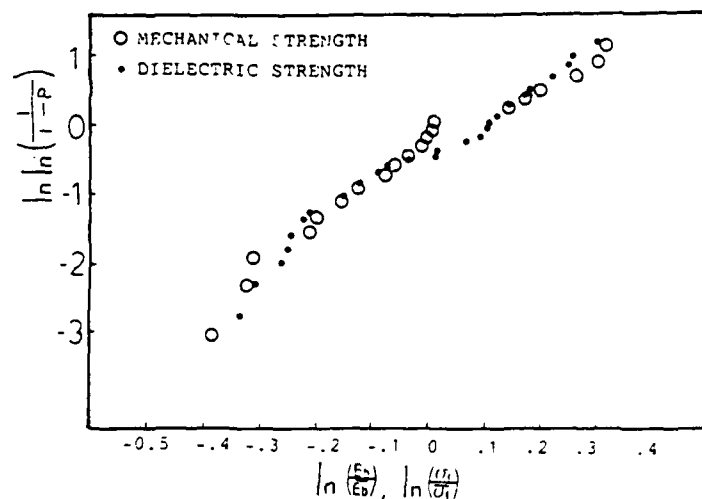


Fig. 1. The WEIBULL PLOTS of the data of dielectric and mechanical strength for the specimen of BaTiO₃ sintered at 1300°C

REFERENCES

1. Y. Yamashita, Y. Koumoto and H. Yanagida, *Comm. Am. Ceram. Soc.*, **67**, p-31 (1984)
2. M. Nagai and H. Yanagida, *Yogyo-Kyokai-shi*, **84**, 157-61 (1976)

Toughening of ceramics by crack tip/stacking faults interactions

K. NIIHARA

Physics Department, The National Defense Academy, Yokosuka 239, Japan

T. HIRAI

RIISON, Tohoku University, Sendai 980, Japan

ABSTRACT: Effects of stacking faults on fracture toughness have been investigated for highly pure and dense β -SiC ceramics prepared by CVD method. TEM observations revealed that there exist no glassy layers or secondary phases at any grain boundaries. As expected from this facts, the crack deflection by the grain boundaries was not observed for almost all cases. However, the strong crack tip deflection and/or microcrack formation associated with stacking faults were revealed by TEM observation, which suggests the fracture toughness of SiC may be improved by incorporating the stacking faults into the grains. In fact, the toughness increased from 3.2 to 6.8 MN/m^{3/2} with increase in the stacking fault density.

1. INTRODUCTION

It is well-known that the fracture toughness of Si_3N_4 and SiC can be improved by controlling the grain morphology, that is, by growing the elongated Si_3N_4 and SiC grains. However, this toughening mechanism operates only for the Si_3N_4 and SiC ceramics with the glassy phases at grain boundaries. On the other hand, Si_3N_4 and SiC ceramics with the glassy phases at grain boundaries show the rapid strength degradation at high temperatures above approximately 1000°C. Thus, it seems to be very difficult to achieve both good mechanical properties at high temperatures and high toughness at room temperature at the same time. The aim of this work is to develop new toughening mechanism without help of grain boundary for SiC ceramics. This new toughening mechanism is related with the nanostructure control within SiC grain, i.e. the control of stacking fault density inside SiC grains.

2. EXPERIMENTAL PROCEDURES

The plates (1 to 3 mm thick) of SiC were prepared by chemical vapor deposition (CVD) from a mixture of C_3H_8 and H_2 -carried SiCl_4 . The preparation conditions are as follows: deposition temperature (T_{dep}); 1500°C, total gas pressure; 30 to 760 Torr, gas flow rates of SiCl_4 , C_3H_8 and H_2 ; 170, 10 to 55, 700 cm³/min, respectively. The density of stacking faults were controlled by changing the total gass pressure in the furnace and the gas flow rate of C_3H_8 , i.e. the deposition rate. Fracture strength was evaluated by three point bending (span; 10 mm, cross head speed; 0.5 mm/min). Fracture toughness was estimated by indentation microfracture, double cantilever beam and/or compact tension techniques. Microcracks for TEM observations were introduced into thin discs of CVD-SiC by using Vickers diamond pyramid at room temperature, 800°, 1000° and 1300°C in vacuum. The observations around cracks formed by indentation were performed using a JEM 200CX.

3. RESULTS AND DISCUSSIONS

The CVD-SiC prepared are confirmed to be β phase by X-ray diffraction, however, many stacking faults were observed in the almost all grains, as shown in Fig. 1. High resolutional electron microscopy of these materials revealed that there exist no glassy layers or secondary phases at any grain boundaries and multiple-grain junctions. Thus, strength degradation was not observed up to 1500°C; the strength of SiC

increased with increasing temperature above about 800°C. Typical temperature dependence of fracture strength of CVD-SiC is indicated in Fig. 2.

The clear crack tip/stacking fault interactions were observed by TEM as shown in Fig. 3. These observations suggest that the fracture toughness of SiC may be improved by incorporating the stacking faults into the grain. Therefore, the CVD-SiC with various density of stacking faults were prepared by controlling the total gas pressure and C_3H_8 flow rate and their fracture toughness were estimated by IM, CT and DCB techniques. The results are shown in Fig. 4. The fracture toughness was found to increase remarkably with increasing stacking fault density inside grains. This new toughening mechanism is considered to make possible the development of SiC ceramics with good strength at high temperatures and high toughness at room temperature.

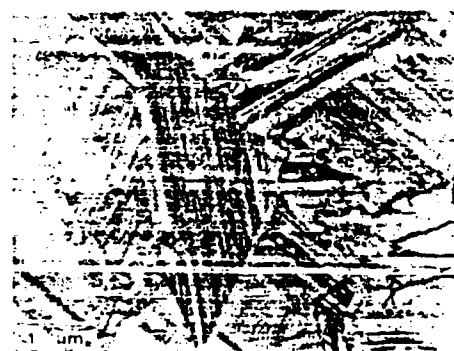


Fig. 1 Transmission electron micrograph of CVD-SiC.

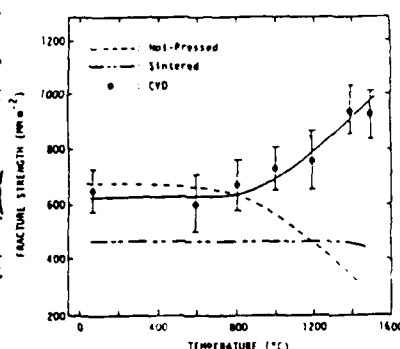


Fig. 2 High-temperature fracture strength for CVD-SiC.

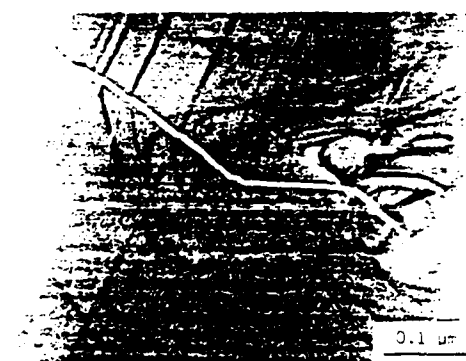


Fig. 3 Crack tip/stacking fault interaction observed for CVD-SiC.

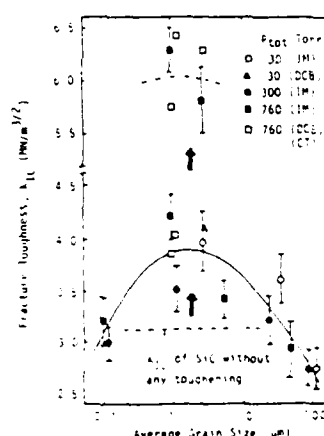
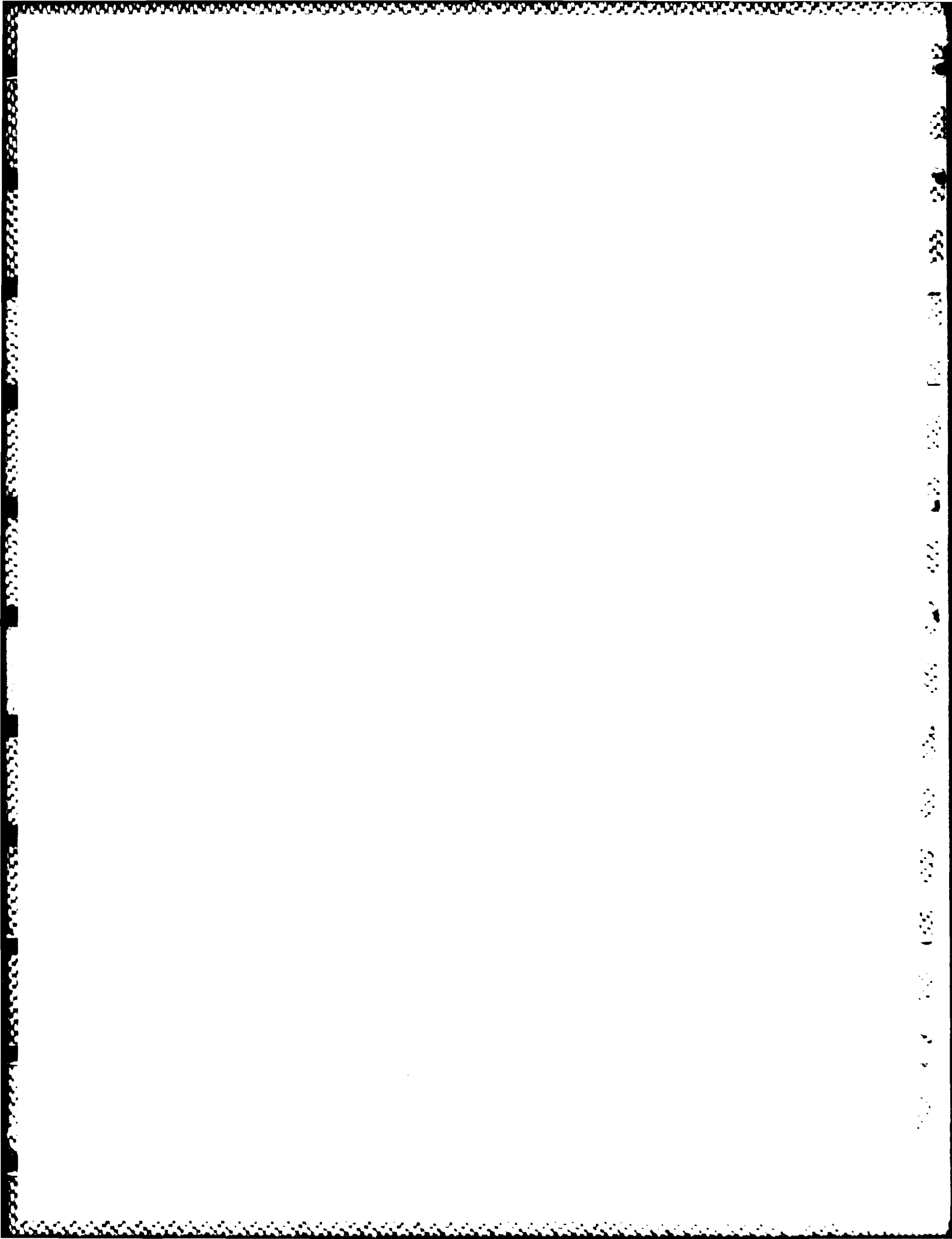


Fig. 4 Fracture toughness for CVD-SiC with various density of stacking fault.

T-15



GROWTH AND APPLICATIONS OF TUNGSTEN BRONZE FAMILY CRYSTALS

R. R. NEURGAONKAR, W. J. DORR, J. R. OLIVER, and W. F. HALL

Rockwell International Science Center
Thousand Oaks, California 91320 USA

ABSTRACT: Ferroelectric tungsten bronze (T. B.) undoped and doped crystals, specifically $\text{Sr}_{0.6}\text{Ba}_{0.4}\text{Nb}_2\text{O}_6$ (SBN:60) and $\text{Ba}_{1-x}\text{Sr}_x\text{K}_{1-y}\text{Na}_y\text{Nb}_2\text{O}_{15}$ (BSKNN), have been grown using the Czochralski technique. The optical figures-of-merit of these crystals are excellent to test photorefractive and millimeter wave device concepts.

1. INTRODUCTION

The present study reports the state-of-art of tungsten bronze family crystals for millimeter wave and photorefractive device studies in terms of their ferroelectric and optical properties.

2. EXPERIMENTAL

Both $\text{Sr}_{1-x}\text{Ba}_x\text{Nb}_2\text{O}_6$ (SBN) and $\text{Ba}_{1-x}\text{Sr}_x\text{K}_{1-y}\text{Na}_y\text{Nb}_2\text{O}_{15}$ (BSKNN) crystals were grown using the Czochralski Technique under different conditions. A variety of measurement techniques were used to evaluate these crystals for millimeter wave and photorefractive applications.

3. RESULTS AND 4. DISCUSSION

Both SBN:60 and BSKNN compositions are multicomponent systems, and there are several crystallographic sites available for large cations in tungsten bronze structure. Because of these factors, the following problems are encountered in crystal growth:

- Exchange among crystallographic sites, specifically of the 15- and 12-fold coordinated ions, and this causes severe striation problems.
- Reduction of Nb^{5+} to Nb^{4+} at growth temperature, causing severe problems with quality and composition.

In spite of these problems, Neurgaonkar et al.¹⁾ have grown undoped and Ge-doped SBN:60 and BSKNN crystals in optical quality as large as 1.5 to 2.0 cm in diameter. Bronze crystals grown along the c-axis are

NO-A105 113

UNITED STATES - JAPAN WORKSHOP ON DIELECTRIC AND
PIEZOELECTRIC CERAMICS ((3RD)) HELD IN TOYAMA JAPAN ON
NOVEMBER <9>-<12> <1986> (U) KEIO UNIV TOKYO (JAPAN)

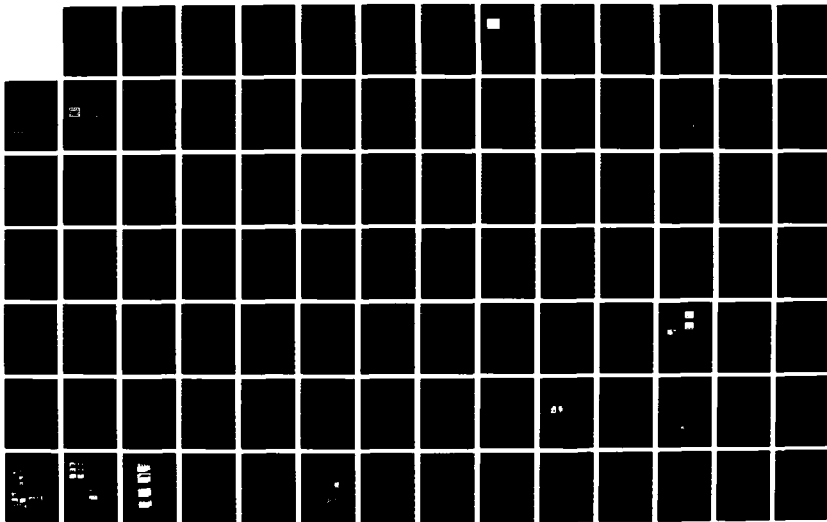
2/5

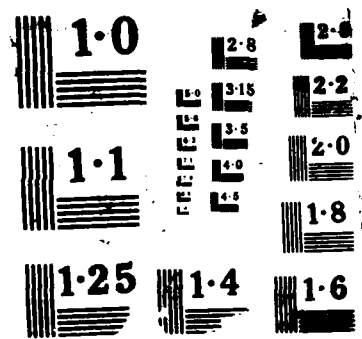
UNCLASSIFIED

30 JUL 87

F/G 11/2

ML





usually faceted, which is quite exceptional for Czochralski grown crystals.

Ce-doped SBN:60 crystals, having electro-optic coefficient $r_{33} = 420 \times 10^{-12}$ m/V, are found to be excellent hosts for device studies. The photorefractive speed for this crystal can be controlled to 1 ms, depending upon laser power, while undoped SBN:60 crystals exhibit speeds of 1000 ms. This improvement in speed and other enhanced properties such as photorefractive coupling are making this crystal attractive for device applications.

Trends in the measured millimeter wave properties of SBN:60 and BSKNN crystals have been shown to conform to simple models for the loss process and the nonlinear susceptibility²⁻³). Measurements have been made over a wide temperature range, down to 20 K, and for frequencies from 35 GHz to 125 GHz. Based on these results, crystal composition and operating temperature can now be selected to maximize particular nonlinear effects for device applications.

ACKNOWLEDGEMENT

This work was supported under the ONR and DARPA contracts.

REFERENCES

1. R. R. Neurgaonkar and W. K. Cory, J. Opt. Soc. Am., 3 (B), 274, 1986.
2. B. Bobbs, M. Matloubian, H. R. Fetterman, R. R. Neurgaonkar and W. K. Cory, Appl. Phys. Lett., 48 (24), 1642, 1986.
3. W. F. Hall, W. W. Ho, R. R. Neurgaonkar, and W. K. Cory, in Proceedings of the 1986 IEEE International Symposium on Applications of Ferroelectrics, June 8-11, 1986, at Lehigh University, Bethlehem, PA.

T-17

PHOTOFERROELECTRIC EFFECTS IN PLZT CERAMICS

GENE HAERTLING

Motorola, Inc., Albuquerque, New Mexico, 87113, U.S.A.

ABSTRACT: Several non-memory PLZT compositions were evaluated for their resistance to the combined effects of high electric field, high temperature and intense light exposure. All materials exhibited behavior which limit their performance under these conditions; however, the photoexcited space charge effects could be eliminated by means of ac rather than dc operation.

1. INTRODUCTION

Since the early 1970's when the transparent, slim-loop ferroelectric PLZT materials were first utilized in shutter devices, it was noted that these materials were limited in their performance by residual memory phenomena manifested in a time-dependent deterioration of the OFF condition. Subsequent research investigations^(1,2) have contributed greatly to an understanding of these phenomena which are generally classified as (1) residual memory effects resulting from a field-induced ferroelectric state and (2) space charge effects produced by the photoexcitation of charge carriers and their movement under the influence of an electric field. The present study reports on some observed effects in category (2) as they relate to SFE (penferroelectric) materials in transverse-mode, shutter devices.

2. EXPERIMENTAL

Hot pressed, polished and electroded samples of PLZT compositions 9/65/35, 9.5/65/35, 8/70/30 and 15/40/60 were selected for study. The vacuum deposited, Cr-Au, single-sided, surface electrodes consisted of an interdigital array of electrode widths and gaps ranging from 0.05 mm to 0.25 mm. Electrical and electrooptic measurements were made on the samples as a function of electric field, temperature, time and light exposure. A high intensity mercury arc lamp was used as the light source in conjunction with various filters ranging from 370 nm to several microns.

3. RESULTS

It was found that (1) the PLZT materials evaluated in this study were highly susceptible to the combined effects of high intensity light exposure and high electric fields, (2) the effects are more pronounced at temperatures near or above T_c (maximum in dielectric constant, 65°C for 9/65/35) and (3) the effects are time dependent and will always anneal out at a rate which is dependent on temperature and light exposure. A typical set of curves are shown in Figure 1. As noted, the virgin material is symmetric about the zero E axis, whereas the materials subjected to either a positive or negative bias while illuminated (the usual situation in a shutter device) display varying degrees of light intensity asymmetry. The relaxation time for this effect at 100°C for PLZT 9/65/35 was found to be approximately 5 seconds; consequently, an activated shutter would be totally compensated (turned OFF) by the photoexcited space charge field in this time frame. Likewise, the material could be refreshed in an equal amount of time. This suggests that if the electric field were alternated (+ to -) at a rate faster than the relaxation time, then this effect would be minimal. This, in fact, does occur and driving the shutter at 30 Hz ac was found to be

sufficient to eliminate, at all temperatures, the undesirable space charge effects.

Photoconductive effects in these materials were also studied by monitoring the voltage across a 22 M Ω resistor connected in series with the shutter and the power supply. When a bias voltage was applied to the shutter without illumination, little or no steady state voltage was developed across the resistor; however, when the light source was turned on, several volts (depending on temperature) would develop across the resistor as a result of the conduction of photoexcited space charge across the gaps of the interdigital electrodes. The voltage trace shown in Figure 2 was thus generated by mechanically shuttering the light source at the various rates indicated. This effect was found to be the largest at the short wavelengths. It was also significant across the visible spectrum but not in the IR.

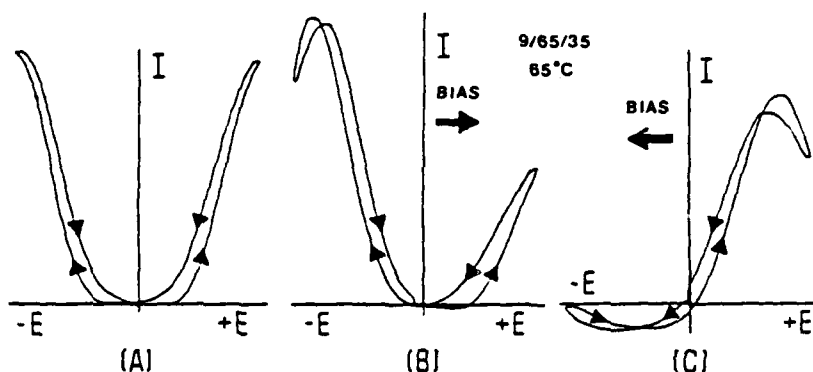


Figure 1. Variation of light intensity as a function of electric field for (A) a virgin PLZT 9/65/35 at 65°C, (B) same sample after 15 minutes light exposure with a + bias of 40 KV/cm and (C) same sample after 30 minutes light and a - bias of 40 KV/cm.

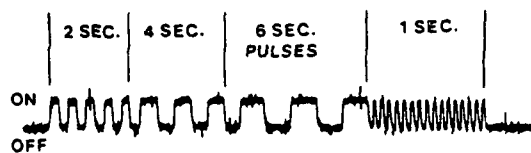


Figure 2. Photoconductivity effects in a PLZT 8/70/30 material as the light is shuttered on and off.

REFERENCES

1. F. Micheron, C. Mayeux and J. Trotier, *Appl. Optics*, **13**, 784 (1974).
2. A. Kapefeks, A. Krumins and V. Dimza, *Ferroelectric Lett.*, **44**, 189 (1982).

PHOTODRIVEN RELAY USING PLZT CERAMICS

Kenji Uchino, Toru Sada and Motoh Inoue
 Department of Physics, Sophia University
 Kioi-cho 7-1, Chiyoda-ku, Tokyo 102, Japan

Photostriction explainable by the superposition of the bulk photovoltaic effect and piezoelectricity has been investigated in the solid solution ceramics $(\text{Pb,Lu})(\text{Zr,Ti})\text{O}_3$ (3/52/48). Photostriction is strongly dependent on the sample preparation history, i.e. on grain size and remanent polarization.

Three samples were prepared; a) atmosphere sintered of oxide chemicals, b) hot-pressed of oxide chemicals, c) atmosphere sintered of coprecipitated PLZT powder. The last ceramic sample was found to reveal the largest photovoltage and photostriction (Fig. 1). As shown in Fig. 2, the photovoltage and photostriction become larger with decreasing grain size, though the piezoelectric coefficient d_{33} becomes slightly smaller. The highest photovoltage, 2.5-3.0 KV/cm, and the maximum photostriction, $1.0-1.3 \times 10^{-4}$, were obtained at the moment in the ceramic sample prepared by coprecipitation with about $1 \mu\text{m}$ grains under 4 mW/cm^2 illumination. Both the photovoltage

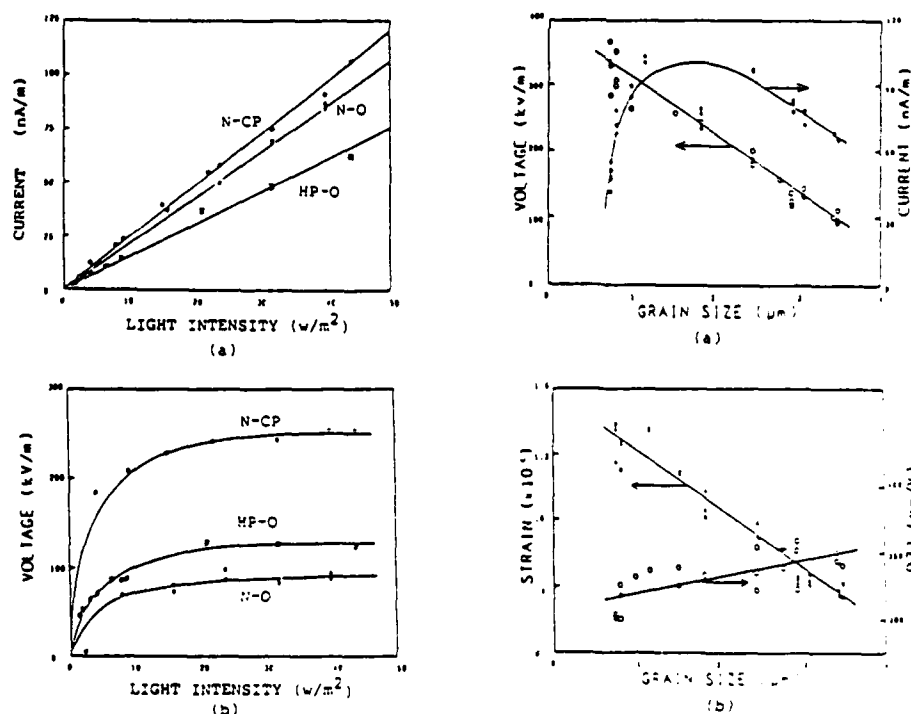


Fig.1 Photovoltaic effect in three samples N-O, HP-O and N-CP. Fig.2 Grain size dependence of photostriction

and piezoelectric coefficient d_{33} have a linear relation with the remanent polarization, so that the photostriction is proportional to the square of the remanent polarization (Fig. 3).

Using PLZT(3/52/48) ceramics, we have fabricated a photodriven relay as a trial photostrictive actuator. This relay consists of an optomechanical bimorph-type actuator and a snap action switch, as illustrated in Fig. 4. In order to obtain quick response, the "dual beam method" was applied. Tip deflection over 100 μm was observed in the bimorph with 20 mm length (Fig. 5). Though the delay time to the illumination is several seconds, we have observed primitive relay function controlled by optical irradiation. Furthermore, analysis of the relay response is proposed, giving the requirements for photostrictive material characteristics and the optimum shape of the bimorph.

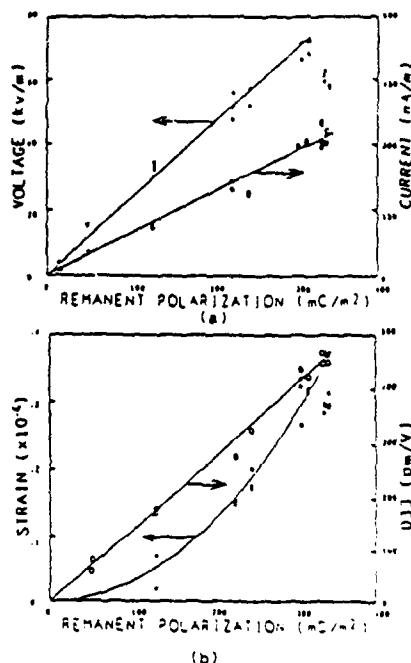


Fig.3 Remanent polarization dependence of photostriction

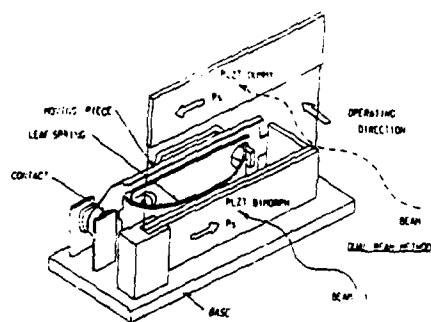


Fig.4 Structure of photodriven relay

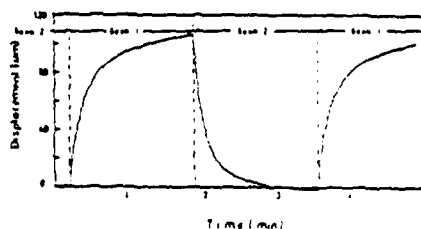


Fig.5 Tip-end deflection of bimorph to the light illumination

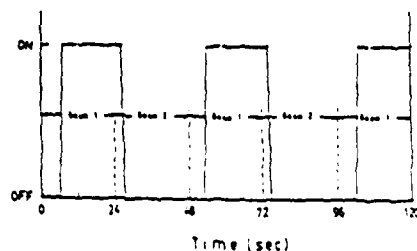


Fig.6 ON/OFF response of newly developed relay

PLZT THIN FILM ON $\text{MgAl}_2\text{O}_4/\text{Si}$ SUBSTRATES

S. MATSUBARA, Y. MIYASAKA, N. SHOHATA and M. YONEZAWA

Fundamental Res. Labs., NEC Corp., 4-1-1 Miyazaki, Miyamae-ku, Kawasaki, 213, Japan

ABSTRACT: PLZT films were sputter-deposited onto $(001)\text{MgAl}_2\text{O}_4/(001)\text{Si}$ substrates using $\text{PLZT}(x/65/35)$ powder targets with varied La contents. X-ray and electron diffraction analysis confirmed that PLZT films grew epitaxially along the 001 axis on the MgAl_2O_4 films. The crystallinity and the lattice constant depended on the La content of the target. The dielectric constant of the PLZT film was measured with a metal-insulator-semiconductor (MIS) structure, and found to be 488 for the film deposited from the $(10/65/35)$ target.

1. INTRODUCTION

Fabrication of epitaxial ferroelectric thin films on Si substrates would lead to the application of the films to various Si monolithic devices¹⁾. We reported the epitaxial growth of PbTiO_3 on $\text{MgAl}_2\text{O}_4/\text{Si}$ substrates in an earlier paper²⁾. The PLZT is also an attractive material because of its high dielectric constant, large electro-optic effect and so on. This paper reports the epitaxial growth of PLZT films on $\text{MgAl}_2\text{O}_4/\text{Si}$ substrates.

2. EXPERIMENTAL

$(001)\text{MgAl}_2\text{O}_4$ epitaxial films, 100-1000 Å thick, were grown on $(001)\text{Si}$ (n-type) wafers by CVD technique in an $\text{Al-HCl-MgCl}_2\text{-CO}_2\text{-H}_2$ gas system at 980°C. The PLZT films were deposited onto the substrates using a magnetron sputtering system under the conditions listed in Table 1. We used $\text{PLZT}(x/65/35)$ targets with varied La contents. The crystal structure and surface morphology of the films were investigated with X-ray diffraction, reflection high energy electron diffraction (RHEED) and scanning electron microscopy (SEM). The dielectric constant was measured with an Au-PLZT- $\text{MgAl}_2\text{O}_4\text{-Si}$ metal-insulator-semiconductor (MIS) structure. The electrode was 1mm x 1mm in dimension.

3. RESULTS AND DISCUSSION

X-ray diffraction patterns for PLZT films yielded only (00h)lines, which indicates that the films grew along the 001 axis. Furthermore, we observed spot diffraction patterns in RHEED, as shown in Fig.1, for all the films. Therefore, we concluded that the PLZT films grew epitaxially along the 001 axis of the MgAl_2O_4 films. The La content of the $\text{PLZT}(x/65/35)$ targets affected the films crystallinity and lattice constant, as shown in Figs.2 and 3, respectively. The crystallinity dependence on La content could be due to the lattice matching between PLZT films and MgAl_2O_4 films. In the SEM study, columnar structures in cross sections of PLZT films and mosaic patterns on the surface of the films

were observed. Figure 4 shows a typical capacitance-voltage (C-V) curve measured at 1 MHz with a Au-PLZT-MgAl₂O₄-Si-Au MIS structure. The capacitance at the accumulation region in the C-V curve corresponds to the dielectric layer consisting of the PLZT layer and the MgAl₂O₄ layer in series. The dielectric constant was estimated at 488 for the PLZT(10/65/35) films.

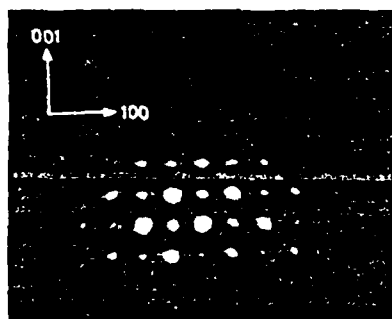


Fig.1. RHEED pattern of PLZT film

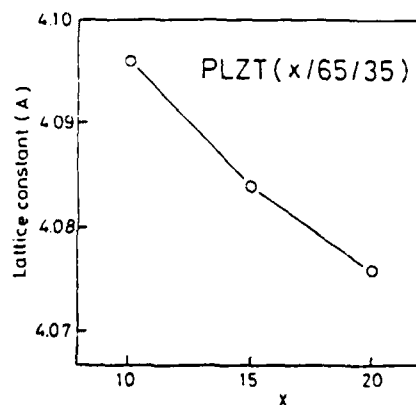


Fig.3. Lattice constant of PLZT films as a function of La content (x).

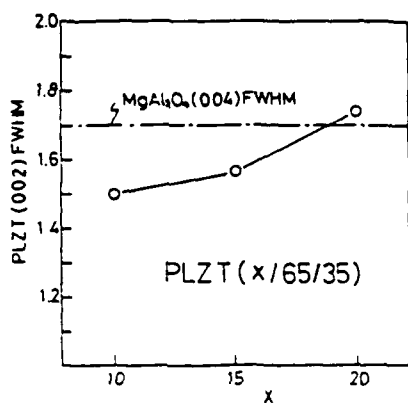


Fig.2. Crystallinity of PLZT films as a function of La content (x). FWHM of the (002) X-ray rocking curve is considered a measure of film crystallinity.

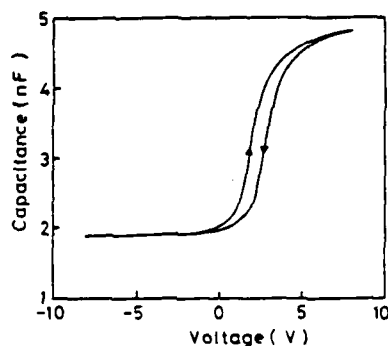


Fig.4. Typical C-V curve of MIS structure measured at 1 MHz.

Table 1. Sputtering conditions for PLZT deposition

Substrate	1001-MgAl ₂ O ₄ /1001-Si
Target	PLZT(x/65/35)-5wt%PbO
Substrate temp.	500°C
Sputtering gas	50% O ₂ + 50% Ar
Pressure	2 x 10 ⁻² torr
Input power	150 W
Deposition rate	3500 Å/h

REFERENCES

1. M. Okuyama et al., Jpn. J. Appl. Phys. Suppl. 31-1, 1982, 225.
2. S. Watsubara et al., Jpn. J. Appl. Phys. Suppl. 34-3, 1985, 12.

SOME ELECTROOPTIC PROPERTIES OF PLZT CERAMICS

K. HIKITA, M. HIRAMA, Y. TANAKA and M. ONO
 R&D Center Ceramics, Mitsubishi Mining & Cement Co., LTD.,
 Yokoze, Chichibu, Saitama, 368, JAPAN

ABSTRACT: Dielectric and electrooptic properties were studied for the hot-pressed lanthanum modified lead zirconate titanate (PLZT) ceramics near the compositions of (9/67/33), where three phase boundaries were crossed. For the series with the composition of (9/Zr/Ti), D-E hysteresis loop became slim and the quadratic electrooptic coefficients were decreased with increasing Zr/Ti ratio from (65/35) to (69/31).

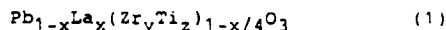
1. INTRODUCTION

According to the phase diagram of PLZT established by Haertling and Land,¹⁾ phase boundaries among two ferroelectric phases and a pseudo-cubic phase are crossed near the composition of (9/67/33), and near where the composition of (9/65/35), which is suitable for optical shutter applications, locates. However, the electrooptic properties have been scarcely studied around the crossed point, especially in both rhombohedral and pseudo-cubic phase.¹⁻³⁾ The present study reports the dielectric and electrooptic properties in this region.

2. EXPERIMENTALS

2.1. Materials

Samples with various composition were prepared according to the general formula given by following equation (1).¹⁾



where x and y were varied from 0.08 to 0.10 by 0.01, and from 0.65 to 0.69 by 0.02, respectively. PLZT ceramic powder was prepared from a mixture of Pb and La oxides with purity above 99.99% and Zr and Ti alkoxides, through hydrolysis. Prefired ceramic powder was hot-pressed by means of the two-stage method.⁴⁾

2.2. Measurements

D-E hysteresis loop was measured by applying AC electric field of 2kV/mm at 50Hz, used 5x5mm² by 0.25mm thick samples with silver electrodes on both surfaces. Birefringence (Δn) was determined from the retardation measured by a polarizing microscope with a Senarmont compensator, on a mirror-polished PLZT sample of 0.5mm thick with slit type electrodes separated by a gap of approximately 0.5mm on a surface. Quadratic electrooptic coefficient, R, was determined by following equation (2).¹⁾

$$R = (-2/n_1^3)(\Delta n/E_3^2) \quad (2)$$

where n_1 and E_3 were the refractive index and the applied field, respectively.

3. RESULTS and DISCUSSION

Figure 1 shows the D-E hysteresis loops for each composition illustrated on the PLZT phase diagram. In the system of (X/69/31), hysteresis loop changed to slim with increasing of La ratio, as reported in (X/65/35) system.¹⁾ On the other hand, in the system of (9/Y/Z) with constant La ratio, the hyste-

resis loops became slim with increasing Zr/Ti ratio from (65/35) to (69/31).

Figure 2 shows the birefringence as a function of electric field illustrated on the PLZT phase diagram. In the both systems of (X/65/35) and (X/69/31), memory effect was shown for La 3 atm, and quadratic electrooptic effect was shown as La ratio was increased. In the system of (9/Y/2), quadratic curves changed to flat as Zr/Ti ratio was increased.

Table 1 summarizes the quadratic electrooptic coefficients calculated by eq.(2). In the system of (9/Y/2), the quadratic electrooptic coefficient was increased with decreasing Zr/Ti ratio, and which was given as $1.2 \times 10^{-16} \text{ m}^2/\text{V}^2$ for (9/67/33) and $2.0 \times 10^{-16} \text{ m}^2/\text{V}^2$ for (9/65/35), respectively in tetragonal phase, however a little hysteresis was shown in birefringence. In pseudo-cubic phase, the quadratic electrooptic coefficient was smaller than that in tetragonal phase, in spite of smaller hysteresis.

The difference between the experimental results and the reference data of quadratic electrooptic coefficient, for the composition of (9/65/35) and (10/65/35), was considered due to thickness of the samples, therefore further study should be attempted for thinner samples.

TABLE 1. Quadratic electrooptic coefficient $R / (10^{-16} \text{ m}^2/\text{V}^2)$

La ratio	Zr/Ti ratio (69/31) (67/33) (65/35)			
9	0.13	1.2	2.8	(9.116) ¹⁾
10	0.13	---	0.55	(1.073) ¹⁾

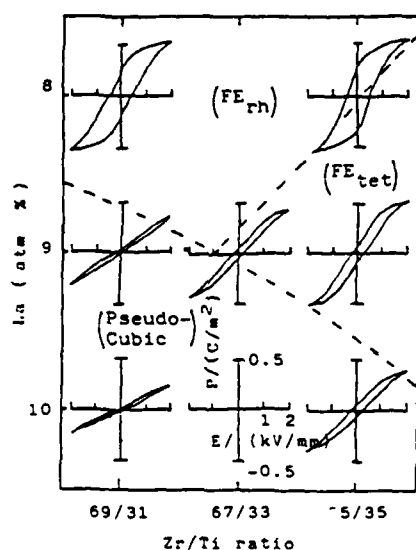


Fig. 1. D-E hysteresis loops measured at 25°C.

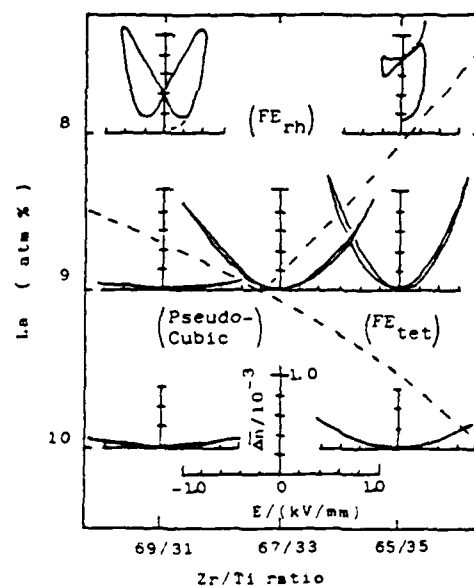


Fig. 2. Birefringence as a function of electric field at 25°C.

REFERENCE

1. G. H. Haertling and C. L. Land, *J. Amer. Ceram. Soc.*, **54**, 1 (1971).
2. J. T. Cutchen, J. O. Harris, Jr., and G. R. Laguna, 1973 *AMSCON* 3-30, Sept., (1973).
3. E. T. Keve and A. D. Annis, *Ferroelectrics*, **5**, 77 (1973).
4. K. Okazaki, I. Ohtsubo and K. Toda, *Ferroelectrics*, **10**, 195 (1976).

DIELECTRIC PROPERTIES OF SPUTTERED POLYCRYSTALLINE $(\text{Pb},\text{La})(\text{Zr},\text{Ti})\text{O}_3$ THIN FILMS

K. WASA, H. ADACHI, and T. MITSUYU

Central Research Laboratories, Matsushita Electric Ind. Co., Ltd.

3-15, Yagumo-Nakamachi, Moriguchi 570, Japan

ABSTRACT: Thin films of polycrystalline $\text{Pb}_{1-x/100}\text{La}_x/100(\text{Zr}_y/100\text{Ti}_z/100)^{1-x/400}\text{O}_3$, PLZT, were prepared on a sapphire substrate by rf-magnetron sputtering from the PLZT sintered powder target. The sputtered films show a perovskite structure and exhibit a dielectric anomaly. Dielectric properties were discussed in comparison with bulk ceramics.

1. INTRODUCTION

Thin films of ferroelectric materials are of much interest for a fabrication of novel functional devices. The single crystal films of the quaternary solid solution of $\text{Pb}_{1-x/100}\text{La}_x/100(\text{Zr}_y/100\text{Ti}_z/100)^{1-x/400}\text{O}_3$, PLZT(x,y,z), were extensively studied for making an electro-optic devices¹⁾. Recently we have prepared polycrystalline thin films of the PLZT(x/y/z) by rf-magnetron sputtering and evaluated their dielectric properties.

2. PREPARATIONS AND MEASUREMENTS

The PLZT thin films were deposited by the sputtering from sintered PLZT powder target. The sputtering conditions are shown in TABLE 1. Sapphire wafers were used as the substrates. The substrate temperature was kept at 500 to 700°C. The dielectric properties of the sputtered PLZT films were evaluated in a sandwich structure, Au thin film top electrode/sputtered PLZT films/TiN thin film base electrode, prepared on the sapphire wafers. The TiN base electrode was sputtered onto the sapphire wafer prior to the sputtering deposition of the PLZT films. The Au top electrode was deposited by a conventional vacuum deposition after the deposition of the PLZT films.

3. RESULTS AND DISCUSSIONS

The sputtered PLZT films showed a polycrystalline form with the perovskite structure. Their room temperature permittivity was ranged from 100 to 700 depending on their composition, and dielectric loss, $\tan\delta$ 0.01 to 0.1. The frequency dispersion of the permittivity was 5 to 15 % from the frequency range of 10 kHz to 1 MHz. These sputtered films exhibited a dielectric anomaly. Typical results for the PLZT films sputtered from PLZT(9/65/35) target are shown in Fig.1.

Figure 2 shows a variation of the dielectric properties with the La concentration in the target of PLZT(x/65/35). It is seen that the permittivity shows a maximum at the La concentration of about 10 %. This may suggest that there appears a phase change from rhombohedral/tetragonal/cubic by the increase of the La concentration similar to the case of bulk ceramics²⁾. The dielectric-anomaly temperature observed in the sputtered films was 220 to 280°C which was higher than the dielectric-anomaly temperature for bulk ceramics. This

is mainly due to the difference of the net composition between bulk ceramics and the sputtered films.

The sputtering process is generally believed to be the most reliable process for the deposition of the complex compounds. However, the difference of the chemical composition between the source target and the sputtered films must be taken into a consideration when the substrates are kept at the high temperature during the deposition. The effects of the stress and/or undissolved oxides on the dielectric properties should be also considered for the detailed discussions³⁾.

TABLE 1. Sputtering conditions.

Target	PLZT powder, 100%
Substrate	Sapphire
Substrate temperature	500~700 °C
Sputtering gas	Ar(60%)+O ₂ (40%)
Gas pressure	6.3×10^{-2} Torr
Rf power	160 W
Deposition rate	70~100 Å/min

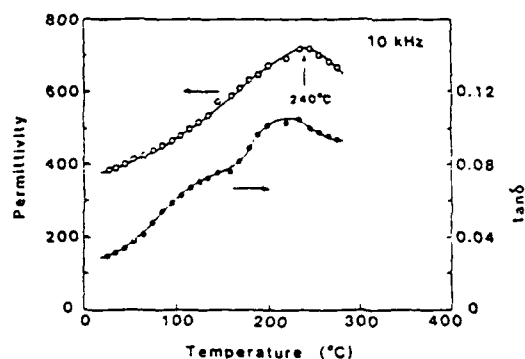


Fig. 1. Temperature dependence of dielectric properties.

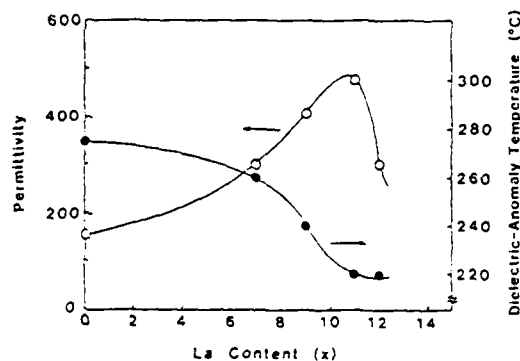


Fig. 2. Dielectric properties of PLZT thin films for various La contents.

REFERENCES

1. K. Wasa, O. Yamazaki, H. Adachi, T. Kawaguchi, and K. Setsune, IEEE J. Lightwave Tech., **LT-2**, 710 (1984).
2. G. H. Haertling and C. E. Land, J. Am. Ceram. Soc., **54**, 1 (1971).
3. C. E. Land, Private Communication.

POSTER SESSION III

W-1

PREPARATION AND PERFORMANCE OF CERAMIC-AIR COMPOSITES FOR HYDROSTATIC SENSING

M. KAHN, A. DALZELL and B. KOVEL

U.S. Naval Research Laboratory, Code 6363

Washington, D.C. 20375-5000

ABSTRACT: Arrays of ordered, flat voids are introduced into PZT ceramic through the use of tape technology, by applying computer designed patterns of fugitive ink to green tapes. These are then stacked, laminated and fired. The resulting ceramic-air composites have modified mechanical properties and exhibit a greatly enhanced hydrostatic response.

1. INTRODUCTION

The hydrostatic sensing performance of lead zirconate titanate (PZT) with internal voids has been shown to be related to their lower Poisson's ratio of PZT ceramics with ordered voids.(1) The present work documents the preparation and piezoelectric behaviour.

2. EXPERIMENTAL

2.1 Sample Preparation

A screen is masked off with a pattern through which a fugitive ink is deposited onto green ceramic tape made from PZT 5A powder. These tapes are stacked and laminated under elevated pressures and temperatures. "Blanks" were made identically, except without fugitive ink. Upon burn-out, the organic constituents of the tape, and of the ink, vaporize and diffuse out, leaving voids where the ink had been.(2) At the subsequent sintering, the ceramic around these voids consolidates to a near fully dense state. Silver electrodes were then applied and the ceramics were poled at 130°C for 10 minutes in a silicon fluid.

2.2 Procedures for testing piezoelectric behaviour.

The uniaxial piezoelectric stress constant (d_{33}) was measured on a Berlincourt CPDT 3300 d_{33} meter. An approximation of d_{31} and d_{32} was derived by using the d_{33} probes with a thin insulator to apply stress onto 2 surfaces orthogonal to the electrodes, and connecting the 2 leads from the instrument to the silver electrodes. The resultant reading is multiplied by the ratio of the area touched by the instrument probes to the area of the silver electrodes. The free field acoustic response was measured in air and in oil by comparison with a calibrated pressure sensor.

3. RESULTS AND DISCUSSION

3.1) Void shapes and volumes:

Figure 1 shows a crosssection of a ceramic containing square shaped voids 0.5mil thick and

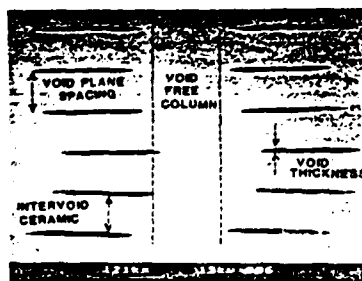
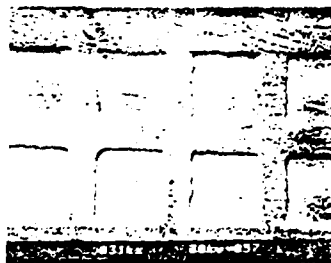


Fig. 1

Fig. 2



11mil long. Figures 2, 3 and 4 show ground top surfaces of samples with various void configurations. The porosities of these samples were 14.6% to 21.6%.

3.2) Piezoelectric Stress Coefficients and Dielectric Constants.

The d_{33} values increased with poling voltages up to 1.5 KV/mm. The table shows that after poling at 2.1 KV/mm the samples with void patterns had d_{33} values that were 13% to 35% lower than those of blanks. There was some dispersion in these d_{33} values. The $(d_{31}+d_{32})/d_{33}$ ratios ranged from 0.19 in samples with disc shaped voids to -0.09 for some of the samples with the crossed bar shaped voids. This is compared to ~ -0.4 in blanks. The calculated d_h values are shown in Figure 5. They also increased initially with poling voltage. The unpoled dielectric constants of blanks were 1183. Those of the laminates with voids ranged from below 350 to above 550. Poling raised the dielectric constants of samples with voids only by about 9% to 38% instead of the 82% increase seen in blanks. One then calculates relatively high piezoelectric voltage sensitivities, g_h , above 85 mV/m. The measured free field hydrostatic responses were 20% less than those derived from the Berlincourt d_{33} data. They were within 3 db of their 1 KHZ value up to 100 KHZ. $d_h \cdot g_h$ products above 20 000 were calculated.

Samples with voids were encapsulated in a flexible epoxy. Preliminary tests indicate no change in hydrostatic sensitivity of these samples at pressures of 100 psi and no irreversible parameter changes under pressures in excess of 3000 psi.

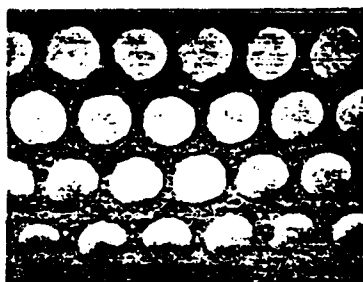


Fig. 3

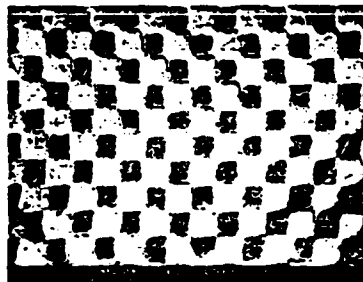
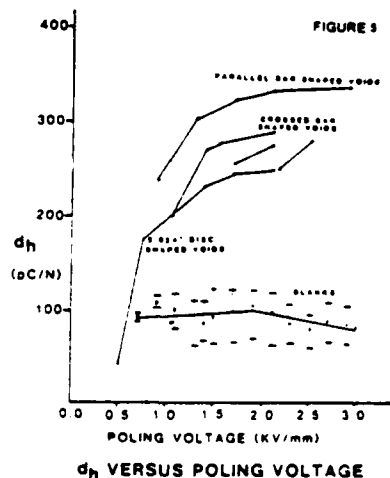


Fig. 4

TABLE I
DIELECTRIC AND PIEZOELECTRIC RESPONSE OF PZT WITH VARIOUS VOID PATTERNS

VOID CONFIGURATION	ϵ	d_{33} (pC/N)	$d_{31}+d_{32}$ (pC/N)	d_h (pC/N)	g_h (mV/m)
Blank	1183	1182	1182	1182	1182
Parallel bar shaped voids					
2.0KV 1000	110	1.22	1.22	110	110
2.1KV 1000	110	1.22	1.22	110	110
2.2KV 1000	110	1.22	1.22	110	110
2.3KV 1000	110	1.22	1.22	110	110
2.4KV 1000	110	1.22	1.22	110	110
2.5KV 1000	110	1.22	1.22	110	110
2.6KV 1000	110	1.22	1.22	110	110
2.7KV 1000	110	1.22	1.22	110	110
2.8KV 1000	110	1.22	1.22	110	110
2.9KV 1000	110	1.22	1.22	110	110
3.0KV 1000	110	1.22	1.22	110	110
3.1KV 1000	110	1.22	1.22	110	110
3.2KV 1000	110	1.22	1.22	110	110
3.3KV 1000	110	1.22	1.22	110	110
3.4KV 1000	110	1.22	1.22	110	110
3.5KV 1000	110	1.22	1.22	110	110
3.6KV 1000	110	1.22	1.22	110	110
3.7KV 1000	110	1.22	1.22	110	110
3.8KV 1000	110	1.22	1.22	110	110
3.9KV 1000	110	1.22	1.22	110	110
4.0KV 1000	110	1.22	1.22	110	110
4.1KV 1000	110	1.22	1.22	110	110
4.2KV 1000	110	1.22	1.22	110	110
4.3KV 1000	110	1.22	1.22	110	110
4.4KV 1000	110	1.22	1.22	110	110
4.5KV 1000	110	1.22	1.22	110	110
4.6KV 1000	110	1.22	1.22	110	110
4.7KV 1000	110	1.22	1.22	110	110
4.8KV 1000	110	1.22	1.22	110	110
4.9KV 1000	110	1.22	1.22	110	110
5.0KV 1000	110	1.22	1.22	110	110
5.1KV 1000	110	1.22	1.22	110	110
5.2KV 1000	110	1.22	1.22	110	110
5.3KV 1000	110	1.22	1.22	110	110
5.4KV 1000	110	1.22	1.22	110	110
5.5KV 1000	110	1.22	1.22	110	110
5.6KV 1000	110	1.22	1.22	110	110
5.7KV 1000	110	1.22	1.22	110	110
5.8KV 1000	110	1.22	1.22	110	110
5.9KV 1000	110	1.22	1.22	110	110
6.0KV 1000	110	1.22	1.22	110	110
6.1KV 1000	110	1.22	1.22	110	110
6.2KV 1000	110	1.22	1.22	110	110
6.3KV 1000	110	1.22	1.22	110	110
6.4KV 1000	110	1.22	1.22	110	110
6.5KV 1000	110	1.22	1.22	110	110
6.6KV 1000	110	1.22	1.22	110	110
6.7KV 1000	110	1.22	1.22	110	110
6.8KV 1000	110	1.22	1.22	110	110
6.9KV 1000	110	1.22	1.22	110	110
7.0KV 1000	110	1.22	1.22	110	110
7.1KV 1000	110	1.22	1.22	110	110
7.2KV 1000	110	1.22	1.22	110	110
7.3KV 1000	110	1.22	1.22	110	110
7.4KV 1000	110	1.22	1.22	110	110
7.5KV 1000	110	1.22	1.22	110	110
7.6KV 1000	110	1.22	1.22	110	110
7.7KV 1000	110	1.22	1.22	110	110
7.8KV 1000	110	1.22	1.22	110	110
7.9KV 1000	110	1.22	1.22	110	110
8.0KV 1000	110	1.22	1.22	110	110
8.1KV 1000	110	1.22	1.22	110	110
8.2KV 1000	110	1.22	1.22	110	110
8.3KV 1000	110	1.22	1.22	110	110
8.4KV 1000	110	1.22	1.22	110	110
8.5KV 1000	110	1.22	1.22	110	110
8.6KV 1000	110	1.22	1.22	110	110
8.7KV 1000	110	1.22	1.22	110	110
8.8KV 1000	110	1.22	1.22	110	110
8.9KV 1000	110	1.22	1.22	110	110
9.0KV 1000	110	1.22	1.22	110	110
9.1KV 1000	110	1.22	1.22	110	110
9.2KV 1000	110	1.22	1.22	110	110
9.3KV 1000	110	1.22	1.22	110	110
9.4KV 1000	110	1.22	1.22	110	110
9.5KV 1000	110	1.22	1.22	110	110
9.6KV 1000	110	1.22	1.22	110	110
9.7KV 1000	110	1.22	1.22	110	110
9.8KV 1000	110	1.22	1.22	110	110
9.9KV 1000	110	1.22	1.22	110	110
10.0KV 1000	110	1.22	1.22	110	110



ACKNOWLEDGEMENTS

The support of this work by the Office of Naval Research and the performance of the free field measurements by G. Le Blank at NUSC and by W. Thompson at NRL are gratefully acknowledged.

REFERENCES

1. "Acoustic and Elastic Properties of PZT Ceramics with Anisotropic Pores", M. Kahn, J. of The Amer. Cer. Soc., 68, pp. 623-28, 1985.
2. "Ceramic Matrices for Electronic Devices and Process", T. Rutt, J. Stynes, U.S. Patent #4353957, 1982.

A RESONANCE TECHNIQUE FOR MEASURING THE COMPLEX ELASTIC, DIELECTRIC AND PIEZOELECTRIC COEFFICIENTS OF COMPOSITE MATERIALS

XU QI-CHANG, A. R. RAMACHANDRAN AND R. E. NEWNHAM

Materials Research Laboratory, Pennsylvania State University, University Park, Pennsylvania 16802, U.S.A.

ABSTRACT: Many composite piezoelectric transducers made from ceramics and polymers have quality factors (Q_m and Q_e) far smaller than ceramics or single crystals. Moreover, the electromechanical coupling factors depend markedly on frequency, so that traditional measurement methods such as the IEEE standard, or the method recommended for ceramics by IEC, are not suitable for composites. Quasistatic measurements are also inadequate because they are too low in frequency.

In this paper, we describe two measurement techniques based on resonance methods. One experiment is for determining the real part of the electromechanical coupling factor appearing in the equivalent lumped circuit, and the other measures the complex coefficients through an analytical solution of a single resonant mode. These techniques have been applied successfully to single mode vibrations in low Q_m and low $k^2 Q_m$ piezoelectric materials. Results will be reported for NTK 0-3 composites, MRL fired composites, and polyvinylidene fluoride films. An LF Impedance Analyzer (HP-4192A) and Computer (HP-9121) were used to process the data with iterative times of less than three minutes for the complex measurements.

The experimental results demonstrate that

- (1) The techniques are effective even for composites with $Q_m < 4$ and $k^2 Q_m \sim 0.02$.
- (2) Errors in coupling factors can be reduced to less than 5% because the change in capacitance $(C - C_0)/C$ can be measured very accurately. In this expression C is the capacitance of the sample, and C_0 is the clamped capacitance.
- (3) Using a single disk-shaped sample, the real part of the electromechanical coupling factor can be obtained for the longitudinal length mode, the transverse length mode, the thickness mode, the planar mode, and the hydrostatic mode.
- (4) For NTK-306 composites and MRL fired composites, piezoelectric coefficient h_{33} is complex: $h''/h' = 3.4\%$ for the NTK sample, and -9.0% for the MRL composite. The assumption that h_{33} is real for all piezoelectric materials must be reconsidered.
- (5) These techniques can also be applied to single-mode vibrations of low Q_m transducers even when the transducer is immersed in a liquid or attached to a solid. In this way, it is possible to estimate the effective coupling co-

efficient, efficiency, and bandwidth of the transducer near resonance.

(6) Regarding the iterative method, we recommend using three frequencies:
 $f_1 = (1 - 0.2/Q_m)f_s$, $f_2 = (1 + 0.2/Q_m)f_s$, and $f_3 = (1 + 0.1/Q_m)f_s$. This choice is important for accurate measurements.

(7) These techniques work well for polyvinylidene fluoride films, but are unsuitable for piezoelectric ceramics with large Q_m .

(8) By altering sample size, the two methods can be used to measure coupling coefficients as a function of frequency and temperature.

W-3

FERROELECTRIC COMPOSITE TRANSDUCERS

B. A. AULD

Department of Applied Physics, Stanford University, Stanford, California 94305
U.S.A.

ABSTRACT: Ceramic/epoxy periodic composites (elastic superlattices) have important advantages over single phase ferroelectric ceramics in piezoelectric transducers for medical and NDE applications: (a) Lower acoustic impedance, (2) Higher piezoelectric coupling, (3) Suppression of lateral modes, (4) Reduction of cross-talk in imaging transducers. An overview is given of the theory of elastic superlattice vibrations needed to effectively exploit these features in the design of composite transducers.

1. INTRODUCTION

Piezoelectric composites, consisting of periodically arrayed ferroelectric ceramic inclusions in an epoxy matrix, were originally introduced for hydrophone applications¹⁾. These two-phase materials have better properties than those of either phase alone, leading to improved detection sensitivity. Piezoelectric composites are now finding applications in ultrasonic transducers, where they also provide improved performance²⁻⁷⁾. This paper explains the physical reasons for the improvements in transducer performance and gives general design rules for optimum transduction.

2. SUPERLATTICE STRUCTURE OF PIEZOELECTRIC COMPOSITES

A number of different periodic composite structures have been investigated^{1,5)}, but the standard, and most easily fabricated, form is a cross-diced ceramic with epoxy filling the saw cuts^{3,4)}. The elastic superlattice in this case consists of a square two-dimensional array of square ceramic rods in an epoxy matrix. It is a close-packed array, with the faces of each ceramic rod separated from its nearest neighbors by a small epoxy gap. The ceramic rod elements are poled along the length direction. Transducers are fabricated from composite plates, with the ceramic rods normal to the plate faces. Full face electrodes or electrode arrays are used, depending upon the application.

The transducers are designed to operate in the longitudinal thickness mode; but they can also vibrate in lateral resonances between the transducer edges. Such lateral resonances, when coupled piezoelectrically, interfere with the desired thickness mode and reduce its coupling. Lateral propagation in the transducer plate also causes mechanical crosstalk in imaging transducers. The superlattice structure of composite materials reduces these effects because, as in actual crystal lattices, wave propagation is impeded by stopbands for the lateral waves.

3. MODELING OF COMPOSITE TRANSDUCERS

A mathematical model has been constructed for elastic wave propagation in two-dimensional elastic superlattices and applied to the ceramic/epoxy composites used in transducers^{2,5)}. This model permits identification of the spurious lateral modes excited by the transducer and suggests methods for controlling them. It also predicts the widths, center frequencies and attenuation rates of the various superlattice stopbands. Because of the large impedance mismatch between the ceramic and epoxy phases, the stopbands are wide⁶⁾ and highly attenuating. Elastic damping can be incorporated into the model, and the effect of the thickness of the transducer plate can also be taken into account.

4. DESIGN CONSIDERATIONS

The superlattice model for lateral modes dictates a choice of superlattice period that is small compared with the plate thickness. As the transducer frequency is increased, this condition imposes more and more stringent fabrication tolerances. In this case, it is desirable to increase the period (i.e., to bring the spurious resonances closer to the main thickness mode), and a compromise must be made. Another condition is imposed on the choice of period by the need to trade-off the requirements for low acoustic impedance (matching into water) and optimum electro-mechanical coupling (insertion loss)⁷⁾. Current design approaches to these criteria are discussed in the references^{3,4,7)}.

REFERENCES

1. R.E. Newnham, L.J. Bowen, K.A. Klicker, and L.E. Cross, *Mat. Eng.* 2, p.93 (1980).
2. B.A. Auld, H.A. Kunkel, Y.A. Shui, and Y. Wang, *Proc. 1983 IEEE Ultrasonics Symposium*, p.554 (1984).
3. A.A. Shaulov, W.A. Smith, and B.M. Singer, *Proc. 1984 IEEE Ultrasonics Symposium*, p.545 (1985).
4. H. Takeuchi, C. Nakaya, and K. Katakura, *Proc. 1984 IEEE Ultrasonics Symposium*, p.507 (1985).
5. T.R. Gururaja, W.A. Schulze, R.E. Newnham, B.A. Auld, and Y. Wang, *IEEE Trans. Son. Ultrason.*, SU-32, p.481 (1985).
6. Y. Wang and B.A. Auld, *Proc. 1985 Ultrasonics Symposium*, p.627 (1986).
7. W.A. Smith, A.A. Shaulov, and B.A. Auld, *Proc. 1985 IEEE Ultrasonics Symposium*, p.642 (1986).

W-4

PIEZOELECTRIC PROPERTIES OF SOME NEW HYDROPHONE MATERIALS

ROBERT Y. TING

Underwater Sound Reference Detachment, U. S. Naval Research Laboratory,
P.O. Box 568337, Orlando, FL 32856-8337, U.S.A.

ABSTRACT: The application of large-area hydrophones in passive sonar systems is an interesting new concept, and has been actively pursued since large sheets of polyvinylidene fluoride (PVDF) thick-films became available. However, it is known by now that PVDF is not adequate for this purpose because of several limitations, most notably its poor thermal stability, low dielectric constant and planar anisotropy. There is, therefore, an urgent need to seek for alternative transduction materials that can meet this new hydrophone requirement. The Underwater Sound Reference Detachment (USRD) of the U.S. Naval Research Laboratory has a continued effort in this endeavor. The results of recent studies on several new material systems will be reported in terms of their piezoelectric voltage coefficients g_h in hydrostatic mode: $g_h = dE_3/dp$, where E_3 is the electric field produced in the polar direction and p the pressure. The new materials include:

(1) VDF-TrFE Copolymers: The properties of copolymers of different compositions were measured as a function of pressure and aging temperature. DSC and X-ray studies were also carried out in order to better understand the effect of thermal treatment on their piezoelectric behaviors.

% VDF	T (°C)	K_{33}^T/K_{33}^T (initial)	g_h/g_h (initial)
70	85.0	1.07	0.83
68	83.5	1.12	0.83
65	83.5	1.32	0.61
70	92.0	1.18	0.59

(2) A "1-3" Piezoceramic Composite: The sample represented a recent successful development by the Plessey Australia Ltd. The design fashioned the basic concept of Newnham et al of the Pennsylvania State University. Initial samples were tested at USRD over a wide range of frequency and pressure.

p = 35 KPa				p = 7 MPa		
f (Hz)	C (pF)	D (%)	M* (dB)	C (pF)	D (%)	M* (dB)
100	12920	2.6	-191.0	17254	2.6	-193.3
1000	12802	2.1	-191.7	16648	1.6	-193.9
2000	12708	2.1	-192.4	16754	1.7	-194.1

* dB re 1 V/ μ Pa

(3) Lead Titanate Ceramics: Samples of this new piezoelectric ceramic from three different sources have been studied, (see Fig. 1). Prototype hydrophones were designed to determine the frequency-domain response of this material. The low planar coupling of lead titanate is most interesting. The implication of this property on hydrophone applications is being investigated.

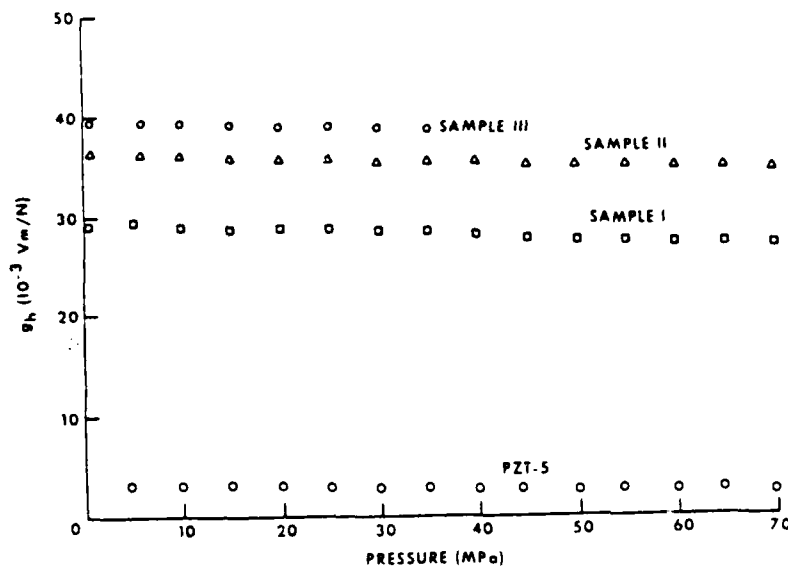


Fig. 1: Piezoelectric g_h coefficients for lead titanate samples as a function of pressure, compared with that of PZT-5.

(This work is supported by the U.S. Office of Naval Research).

DIELECTRIC AND PIEZOELECTRIC PROPERTIES OF $\text{PbZr}_x\text{Pb}_{1-x}(\text{Zn}_{1/3}\text{Nb}_{2/3})_{1-x}\text{O}_3$ CERAMICS

K. SAKATA and I. TAKENAKA

Faculty of Science and Technology, Science University of Tokyo, Noda-shi, 278 Japan

ABSTRACT: The new piezoelectric ceramic materials of the $\text{PbZr}_x(\text{Zn}_{1/3}\text{Nb}_{2/3})_{1-x}\text{O}_3$ system with compositions close to the antiferroelectric-ferroelectric phase boundary have been studied. The antiferroelectric phase changes to the ferroelectric phase at $x=0.93\sim 0.94$. Piezoelectric properties are characterized by the large coupling factor of the thickness shear mode.

1. INTRODUCTION

The antiferroelectric phase in PbZrO_3 is very critical, in the sense that its free energy is very close to that of the ferroelectric phase, especially near the curie temperature¹⁾. Thus extensive research of PbZrO_3 -based compounds has been made from the standpoint of phase transitions^{2,3)}. Recently, Takeuchi et al. found a large anisotropy in the electromechanical coupling factor of one PbZrO_3 -based ceramic⁴⁾. In this work, we have attempted to obtain basic information regarding a new piezoceramic group, from an applicational viewpoint of electronic device material. The dielectric and piezoelectric properties of the $\text{PbZr}_x(\text{Sn}_{1/3}\text{Nb}_{2/3})_{1-x}\text{O}_3$ solid solution (abbreviated to "PZZN-100x") with up to 20 mol% ($\text{Zn}_{1/3}\text{Nb}_{2/3}$) were investigated.

2. EXPERIMENTAL METHODS

The specimens were made following the standard techniques of sintering: grinding, calcination at 800°C for 1 hour, milling and sintering at 1240°C for 1 hour in a PbO atmosphere using discs of pressed $\text{Pb}_3\text{Zr}_2\text{O}_7$ powder. The curie point was determined from the temperature dependence of dielectric constant. Piezoelectric measurements are made by the resonance-antiresonance method.

3. RESULTS AND DISCUSSION

Remarkably high density samples with density ratios 92~96% of theoretical X-ray density were obtained. X-ray powder diffraction patterns indicate a single phase of the perovskite structure.

Figure 1 shows room-temperature values of ϵ_s and $\tan\delta$ in the PZZN system as a function of PbZrO_3 mol%. Both ϵ_s and $\tan\delta$ at room temperature abruptly decreased at $x=0.93\sim 0.94$, and were almost independent of increasing PbZrO_3 mol% (x) in the range $x=0.94$ to $x=1.0$. This suggests that the antiferroelectric-ferroelectric phase boundary at room temperature exists near $x=0.93\sim 0.94$.

Figure 2 gives the phase relation of the PZZN system determined from dielectric measurements and D-E hysteresis loop observations.

Typical values of the piezoelectric activities are given in Table 1. The piezoelectric constants were calculated from the coupling factor, the elastic compliance and the free permittivity. The relatively large anisotropy, k_{33}/k_{31} , as compared with that of PZT systems, has a maximum value of 4.5 at $x=0.92$.

being near the antiferroelectric to ferroelectric (AF-F) phase boundary at room temperature.

The piezoelectric properties of the PZZN system are characterized by the low free permittivity, ϵ_{11}^1 or ϵ_{33}^1 , and the large coupling factor, k_{15} , of the thickness shear mode. The free permittivity is one third of that of the conventional PZT system, and the coupling factor is two times as large as that of the PbTiO₃ system. These piezoceramic materials seem favorable for some applications such as ceramic filters or resonators operated at high frequencies using the thickness shear mode.

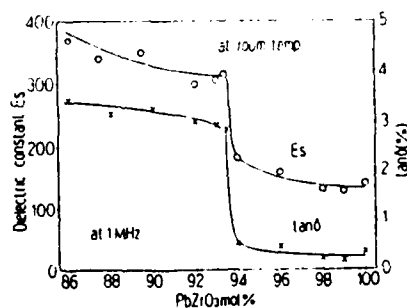


Fig. 1 Dielectric constant ϵ_s and loss tangent $\tan \delta$ at room temperature of the PZZN system.

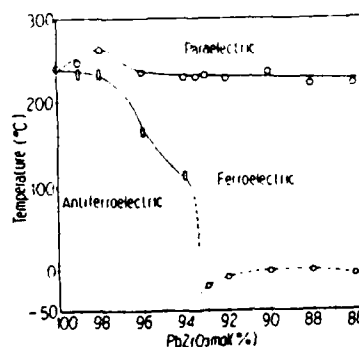


Fig. 2 The phase relation of the PZZN system.

Table 1 Piezoelectric properties of the PZZN-90 and PZZN-92.

	Dielectric const.		Loss tang-ent	Coupling factor		Frequency const.					Elastic compliance					Piezoelectric constant											
	ϵ_{11}^E	ϵ_{33}^E	$\tan \delta_{11}$	$\tan \delta_{33}$	k_{33}	k_{31}	k_t	k_p	k_{15}	N_{33}	N_{31}	N_t	N_p	N_{15}	S_{11}^E	S_{33}^E	S_{55}^E	S_{11}^P	S_{33}^P	S_{55}^P	d_{33}	d_{31}	d_{15}	g_{33}	g_{31}	g_{15}	
	10kHz		(%)		(%)					(Hz·m)					(10^{-12} m/N)					(10^{-12} C/N)					(10^{-3} Vm/N)		
PZZN-90	300	385	2.03	2.79	291	603	536	2090	2610	1520	743	198	741	427	139	359											
					7.33	8.41		2040	2710						8.10	7.40	14.1				862	16.1	40.3				
PZZN-92	262	386	2.49	3.50	292	429	592	2090	2390	1560	7.73	205	745	402	157	349											
					6.03	7.57		2050	2780						9.15	7.70	13.3				809	17.3	45.9				

REFERENCES

- (1) G. Shirane, E. Sawaguchi and Y. Takagi: J. Phys. Soc. Japan, 6, p.205 (1951).
- (2) J. Handerek, Z. Ujma and K. Roleder: Phase Transitions, 1, p.377 (1980).
- (3) K. Roleder and K. Wojcik: Ferroelectrics, 61, p.203 (1984).
- (4) H. Takeuchi, S. Jyomura and C. Nakaya: Jpn. J. Appl. Phys., 24S-2, p.30 (1985).

PIEZOELECTRIC PROPERTIES OF (Na,Li)NbO₃ CERAMICS

T. HONDA, I. KAWAMATA, H. WATARAI and T. IDO

Materials and Electronic Devices Laboratory, Mitsubishi Electric Corporation,
Sagamihara-city Miyashiro 1-1-57, Kanagawa

ABSTRACT: The dielectric and piezoelectric properties of the solid-solution (Na,Li)Nb₃ have been studied. In this system with a small amount of alumina, high density, very fine microstructure and superior piezoelectric properties were obtained even by the ordinary sintering process. Using (Na_{0.9}Li_{0.1})NbO₃ solid-solution with 0.5wt.% of alumina, ultrasonic transducers for high frequency up to 20MHz were developed.

1. INTRODUCTION

Polycrystalline piezoelectric materials in the application of ultrasonic transducers are based almost exclusively on PZT piezoelectric ceramics. For high frequency application, however, the fabrication of vibrating elements becomes difficult because of the small dimension required. Thus, another transducer materials which have the lower dielectric constant and higher sound velocity are required. (Na,Li)Nb₃ piezoelectric ceramics with lower dielectric constant and higher frequency constant is one of the candidates for such requirements, but it is well known that the dense body has not been obtained by the ordinary sintering process¹⁻³⁾. Authors investigated on the effect of Al₂O₃ addition to (Na,Li)NbO₃ ceramics to develop the transducer material for high frequency application.

2. EXPERIMENTAL

2.1. Sample Preparation

The raw materials used were sodium carbonate (99.5%), lithium carbonate (99.0%), niobium pentoxide (99.7%), and alumina (99.5%). The niobium pentoxide was commercial grade with 0.03% Ta₂O₅. For each composition, the raw materials were wet-mixed for 13 hrs in a nylon pot containing zirconia balls and ethanol, then dried and calcinated at 950 °C for 3 hrs in air. The calcinated powder was ball milled for 18 hrs using zirconia balls and pressed with PVA(2.5%) binder into tablets at 700 kg/cm². The tablets were sintered for 3 hrs at 1150-1240 °C in air. The sintered bodies were lapped to the desirable dimension and electroded by painting the body with silver paste, and then fired at 780 °C for 10 minutes.

2.2. Measurements

Samples for the microstructure analysis by the scanning electron microscopy (SEM) were prepared by polishing and thermal etching at 1050 °C for 30 minutes. Densities of sintered bodies were determined using Archimedes' method. Specimen for piezoelectric and dielectric properties were poled in silicon oil at 1000 °C for 0.5 hrs under a field of 5-6 kV/mm. More than 24 hrs after poling, the measurement was carried out by LF impedance analyzer(VHP:4192A).

3. RESULTS

Fig.1. shows the density of $(\text{Na}_{1-x}\text{Li}_x)\text{NbO}_3$ ceramics as a function of the lithium content x . Measured densities are too small compared with theoretical values deviated from the X-ray diffraction analysis. The microstructure of $(\text{Na}_{0.9}\text{Li}_{0.1})\text{NbO}_3$ ceramics containing 0.5 wt.% alumina is shown in Fig.2a. Fig.2b shows the microstructure of alumina free $(\text{Na}_{0.9}\text{Li}_{0.1})\text{NbO}_3$ ceramics. Piezoelectric and dielectric properties of $(\text{Na}_{0.9}\text{Li}_{0.1})\text{NbO}_3$ with 0.5 wt.% alumina are listed in Table I. Electron microscopy revealed that a small amount of alumina addition enhanced the sinterability without the large grain growth and the superior piezoelectric properties of $(\text{Na},\text{Li})\text{NbO}_3$ ceramics were obtained. Using $(\text{Na}_{0.9}\text{Li}_{0.1})\text{NbO}_3$ with 0.5 wt.% Al_2O_3 , ultrasonic transducers from 5 MHz up to 20 MHz have been developed.

REFERENCES

1. T.Nitta; J.Am.Ceram.Soc., **51**,626,(1968)
2. R.M.Henson et.al.; J.Am.Ceram.Soc., **60**,15,(1977)
3. R.R.Zeyfang et.al.; J.Appl.Phys., **48**,3014,(1977)

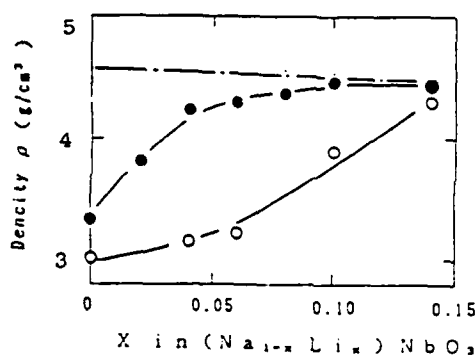


Fig.1. Measured density of $(\text{Na}_{1-x}\text{Li}_x)\text{NbO}_3$ as a function of lithium content x ;

○ : without alumina, ● : with 0.5 wt.% alumina,
--- : theoretical value.

Table.I. Piezoelectric and dielectric properties of $(\text{Na}_{0.9}\text{Li}_{0.1})\text{NbO}_3$ + 0.5 wt.% Al_2O_3 .

Dielectric Constant	
ϵ_{33}/ϵ_0	= 110 (1kHz)
Coupling Factor	k_t = 42 %
	k_p = 21
Frequency Constant	
N_t	= 2900 Hz·m
N_p	= 3700
Density	ρ = $4.5 \times 10^3 \text{ kg/m}^3$
Curie Temperature	T_c = 340 °C

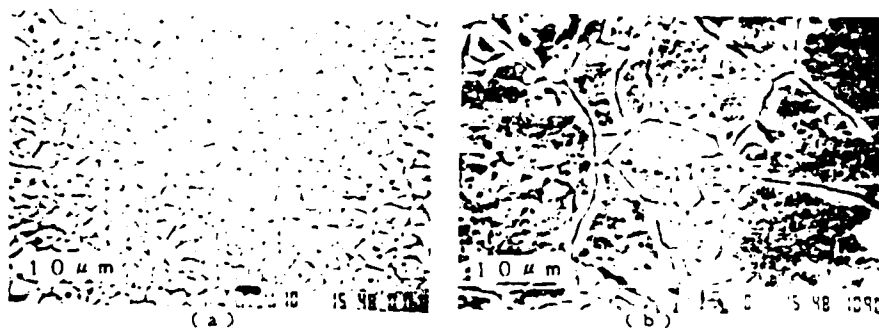


Fig.2. SEM photographs of $(\text{Na}_{0.9}\text{Li}_{0.1})\text{NbO}_3$ ceramics with 0.5 wt.% Al_2O_3 (a) and without Al_2O_3 (b).

W-7

ELECTROMECHANICAL PROPERTIES OF PLANAR VIBRATIONAL MODE IN PZT/POLYMER PIEZO-ELECTRIC COMPOSITES

HIROSHI TAKEUCHI and CHITOSE NAKAYA

Central Research Laboratory, Hitachi Ltd., Kokubunji, Tokyo 185, Japan

ABSTRACT: Electromechanical properties of planar vibrational mode in PZT/polymer 1-3 composites were determined as a function of the PZT volume fraction and PZT pillar shape. An electromechanical coupling factor k_p of 0.38 was observed when using epoxy as a polymer matrix.

1. INTRODUCTION

Recently, piezoelectric composites (PZT/polymer) having various structures have been intensively analyzed for hydrophone and medical ultrasonic probe applications. These composites can be classified according to Newnham's connectivity theory.¹⁾ The 1-3 connectivity (PZT pillar embedded in a polymer matrix) is reported to be useful for high-frequency medical ultrasonic applications.²⁻⁴⁾ Furthermore, the dynamical behavior of the thickness mode has been analyzed theoretically in the 1-3 composites.⁵⁾

However, the planar vibrational mode of 1-3 composite has not yet been investigated systematically because this mode is unwanted vibration for medical ultrasonic application. In the present work, electromechanical properties of planar vibrational mode were determined as a function of the PZT volume fraction and PZT pillar shape.

2. EXPERIMENTAL

PZT/polymer 1-3 composite disks were fabricated using a "dicing and filling" technique. The PZT pillar size and volume fraction were varied by changing the blade thickness and dicing pitch. Chromium-gold films were deposited as electrodes onto both surfaces of composite disks.

The electromechanical properties of planar vibrational mode were determined by measuring the impedance characteristics with an HP-4192A impedance analyzer. The electromechanical coupling factor k_p was determined from the following equation:

$$k_p^2 = 1.24 \frac{f_n^2 - f_m^2}{f_n f_m}$$

where f_m is the minimum-impedance-frequency, and f_n the maximum-impedance-frequency. Frequency constant N_p was approximated by

$$N_p \approx f_m a \quad (a: \text{diameter of disk}).$$

3. RESULTS AND DISCUSSION

Typical impedance characteristics of PZT/epoxy composite disk are shown in Fig. 1 together with phase characteristics. Here, the diameter and the thickness of the disk are 11mm and 0.4mm, respectively. A single resonant curve was obtained.

Frequency constant N_p and electromechanical coupling factor k_p are shown in Fig. 2 as a function of PZT volume fraction V_{PZT} . Sample thickness is 0.1mm and PZT pillar shape w/t is changed from 1 to 3. Frequency constant was found to be clearly dependent on V_{PZT} . This is because the planar vibrational mode is excited through direct mechanical interaction between PZT pillar and polymer matrix.

Electromechanical coupling factor k_p gradually decreased with a decrease in V_{PZT} . However, the value of k_p stayed as high as $0.32 \sim 0.38$ over the region $V_{PZT} = 0.25 \sim 0.7$ when using epoxy as a polymer matrix. This is large enough for lateral mode applications.

The results of this work imply that PZT/epoxy 1-3 composites are potential materials for not only thickness mode application but also flexure mode application such as a piezoelectric speaker. In addition, low acoustic impedance compared to PZT, relatively high k_p , and flexibility of these materials may also open the way to other new applications.

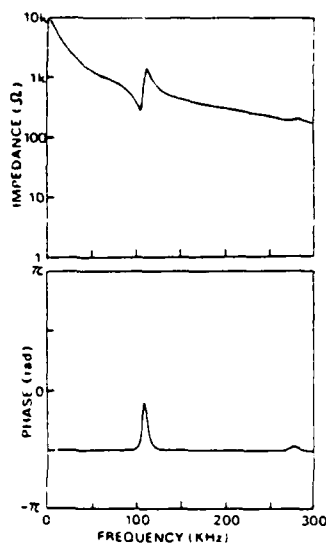


Fig. 1. Impedance and phase characteristics of PZT/epoxy composite disk (diameter: 11mm, thickness: 0.4mm). PZT volume fraction and PZT pillar shape w/t are 0.59 and 1.0, respectively.

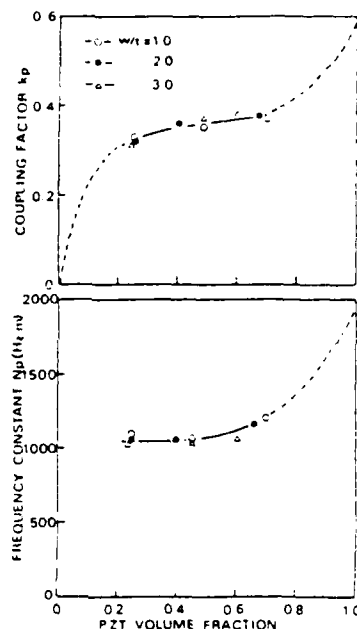


Fig. 2. Frequency constant and electromechanical coupling factor of planar vibrational mode in composite disk as a function of PZT volume fraction (sample thickness: 0.1mm).

REFERENCES

1. R. E. Newnham, D. P. Skinner and L. E. Cross, *Mat. Res. Bull.*, **13**, 525 (1978).
2. H. Takeuchi, C. Nakaya and K. Katakura, *Proc. 1984 IEEE Ultrasonics Symposium*, p. 507 (1984).
3. T. R. Gururaja, W. A. Schulze, L. E. Cross and R. E. Newnham, *Proc. 1984 IEEE Ultrasonics Symposium*, p. 523 and p. 533 (1984).
4. W. A. Smith, A. A. Shaulov and B. M. Singer, *Proc. 1984 IEEE Ultrasonics Symposium*, p. 539 and p. 545 (1984).
5. B. A. Auld and Y. Wang, *Proc. 1984 IEEE Ultrasonics Symposium*, p. 528 (1984).

Anisotropic Piezoelectric Coupling Factor of
 $[\text{Pb}_x(\text{Bi}_{1-x}\text{Na}_{1-x})_{1-x}] \text{TiO}_3$ Ceramics

Shinjiro Tashiro, Yukio Oikawa, Hideji Igarashi and Kiyoshi Okazaki

Dept. of Electrical Engineering, The National Defense Academy,
 Yokosuka 239, Japan

Alkaline earth metals (Ba, Sr, Ca) or rare earths (La, Pr, Nd, Sm, Gd) modified PbTiO_3 ceramics have been extensively investigated because of their great promise as a material for high frequency and high temperature applications, and it was found that Ca or Sm with smaller ionic radius compared with Pb ion was excellent as the substituting elements to make large piezoelectric anisotropy between longitudinal and transverse modes. Sakata et al investigated the piezoelectric properties of $(\text{Bi}_{1-x}\text{Na}_x)\text{TiO}_3$ - PbTiO_3 system near the MPB compositions.^{(1),(2),(3)} In the tetragonal phase region of their system, large anisotropy in piezoelectric properties would be expected because of the small ionic radius of Bi and Na ion. In this study, dielectric and piezoelectric properties of PbTiO_3 -($\text{Bi}_{1-x}\text{Na}_x$) TiO_3 - $\text{Pb}(\text{Fe}_{1-x}\text{Nb}_x)\text{O}_3$ system ceramics were experimentally investigated. The compositions of the ternary system were $x \cdot \text{PbTiO}_3$ - $y \cdot (\text{Bi}_{1-x}\text{Na}_x)\text{TiO}_3$ - $z \cdot \text{Pb}(\text{Fe}_{1-x}\text{Nb}_x)\text{O}_3$ with 1 mol% MnCO_3 (hereafter abbreviated to $\text{PBFN}x/y/z$).

Lattice parameters of the $\text{PBFN}(x/y/0)$ and $\text{PBFN}(x/y/5)$ as a function of PbTiO_3 content (x) are shown in Fig.1. MPB was found near $x = 18$ mol% in $\text{PBFN}(x/y/0)$ as same as reported by Sakata. By adding of 5mol% $\text{Pb}(\text{Fe}_{1-x}\text{Nb}_x)\text{O}_3$, tetragonal phase region was extended, moreover the change of

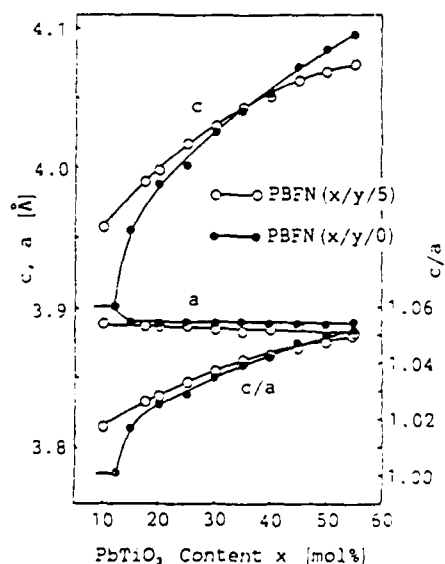


Fig. 1. Lattice parameters of the $\text{PBFN}(x/y/0)$ and $\text{PBFN}(x/y/5)$ as a function of PbTiO_3 content (x).

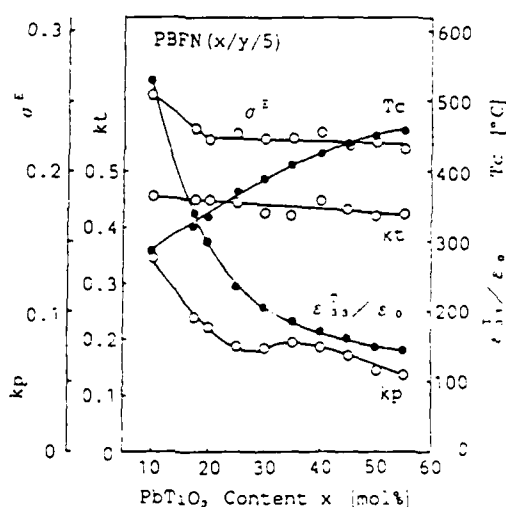


Fig. 2. Electromechanical coupling factor k_p , k_t , dielectric constant ϵ_{33}/ϵ_0 , Curie point T_c and poisson's ratio σ_E of $\text{PBFN}(x/y/5)$.

crystal tetragonality (c/a) was decreased. Figure 2 shows electromechanical coupling factor k_p, k_t , dielectric constant $\epsilon_1^T/\epsilon_\infty$, Curie point T_c and poisson's ratio σ^E of $\text{PBFN}(x/y/5)$ as a function of (x) . Thickness dilatational coupling factor k_t did not noticeably change with PbTiO_3 content (x) and had relatively large values (0.42-0.46). In contrast to k_t , planar coupling factor k_p decreased notably in the region from $x = 10$ to $x = 25$, and kept the values (0.072-0.078) from $x = 25$ to $x = 40$, and decreased again in the region greater than $x = 45$. Poisson's ratio σ^E decreased from $x = 10$ to $x = 20$, and kept the value (0.22) in the region greater than $x = 0.20$. This change is similar to that of k_p . this result suggests that anisotropy of coupling factor relates to poisson's ratio σ^E . The $\epsilon_1^T/\epsilon_\infty$ decreased rapidly with (x) and T_c increased to correspond to c/a change. $\epsilon_1^T/\epsilon_\infty$ was smaller than 200 and T_c was higher than 400°C in the region greater than $x = 30$. Figure 3 shows coupling factors k_t, k_p of $\text{PBFN}(x/y/0)$ and $\text{PBFN}(x/y/5)$. By substituting 5 mol% $\text{Pb}(\text{Fe}_{0.5}\text{Nb}_{0.5})\text{O}_3$, k_p decreased remarkably in the PbTiO_3 rich region. Figure 4 shows the correlation between σ^E and coupling factor k_p which have reported in the various kinds of PbTiO_3 ceramics. Good correlation between k_p and σ^E can be seen, and it suggests that k_p has negligibly small value if σ^E is smaller than 0.19. However, it is not enough to explain this relation theoretically because $\sigma^E = s_{11}^E/s_{11}^E$ is not an intrinsic constant to dominate k_p value.

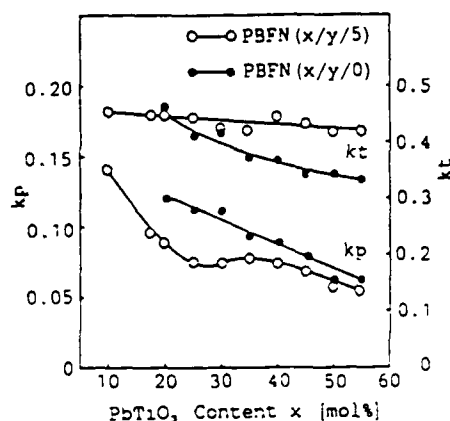


Fig. 3. Effect of substitution of 5 mol% $\text{Pb}(\text{Fe}_{0.5}\text{Nb}_{0.5})\text{O}_3$ on coupling factors k_p, k_t of $\text{PBFN}(x/y/0)$.

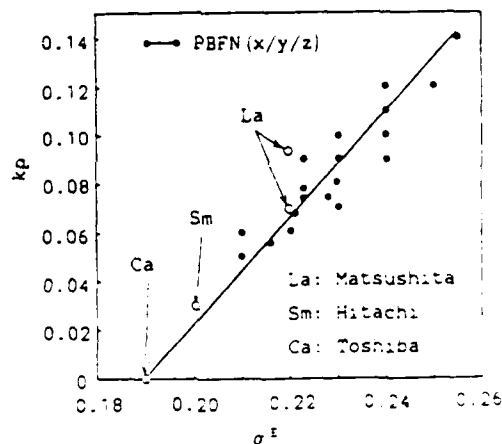


Fig. 4. Correlation between σ^E and coupling factor k_p in PbTiO_3 ceramics modified with various substituting elements.

REFERENCES

1. Y. Yamashita et al, Jpn. J. Appl. Phys. Suppl., 22-2, 40 (1983).
2. H. Takeuchi et al, Jpn. J. Appl. Phys. Suppl., 22-2, 166 (1983).
3. K. Sakata et al, Joint Convention Record of Four Institutes of Electrical Engineers, Japan, No.403, 470 (1967).

EFFECTS OF SHAPE AND VOLUME FRACTION OF CLOSED PORE ON DIELECTRIC LOSS, MECHANICAL QUALITY FACTOR AND ELECTROMECHANICAL COUPLING FACTOR OF DIELECTRIC AND PIEZOELECTRIC CERAMICS
- A THEORETICAL APPROACH -

HISAO BANNO

NGK SPARK PLUG CO., LTD. NAGOYA JAPAN

1. THEORY

Series and parallel models are schematically shown in Fig.1. Elastic properties for shear modulus G and bulk modulus K are expressed as follows:

For series model,

$$1/\bar{G} = v_1/G + v_2/G \quad (1)$$

$$1/\bar{K} = v_1/K + v_2/K \quad (2)$$

for parallel model,

$$\bar{G} = v_1 \cdot G + v_2 \cdot G \quad (3)$$

$$\bar{K} = v_1 \cdot K + v_2 \cdot K \quad (4)$$

Young's modulus E and Poisson's ratio σ are expressed as a function of G and K as follows:

$$E = 9KG/(3K+G) \quad (5) \quad \text{and} \quad \sigma = (3K-2G)/(2(3K+G)) \quad (6)$$

Combining the equations 1-6, one can obtain the equations for the Young's modulus and Poisson's ratio as follows:

For series model,

$$1/\bar{E} = v_1/E + v_2/E \quad (7) \quad \text{and} \quad \bar{\sigma} = (v_1/E) \cdot \sigma + (v_2/E) \cdot \sigma \quad (8)$$

For parallel model, Hashin discussed the elastic properties of fiber-reinforced composite and gave a very important approximation as follows:¹⁾

$$\bar{E} \sim v_1 \cdot E + v_2 \cdot E \quad (9) \quad \text{and} \quad \bar{\sigma} \sim v_1 \cdot \sigma + v_2 \cdot \sigma \quad (10)$$

where Poisson's ratio σ is with less accuracy. It is the equations 7 and 9 for the Young's modulus that Newnham et al. based on when he derived those for piezoelectric constants of the series and parallel models.²⁾

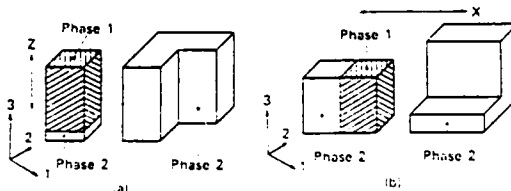
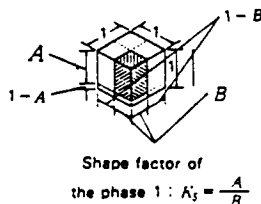
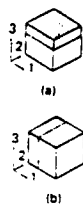


Fig.1. (a) Series and (b) parallel models.

Fig.2. Modified cubes model.

Fig.3. Schematic representation of the model which is divided into two parts for (a) Z and (b) X directions.

Mechanical quality factor Q_m and mechanical loss tangent $\tan \delta_m$ are defined as follows:

$$Q_m = 1/\tan \delta_m = s'/s'' \quad (11)$$

where s' and s'' are real and imaginary parts of complex elastic compliance $\hat{s} (=s' - j \cdot s'')$.

Combining the equations 7, 9 and 11, the theoretical equations for Q_m or $\tan \delta_m$ of series and parallel models are obtained as follows:

For Q_{m33} or $\tan \delta_{m33}$ of series model and Q_{m11} or $\tan \delta_{m11}$ of parallel model, and

$$1/\bar{Q}_m = \tan \delta_m = \frac{v_1 \cdot s' \cdot \tan \delta_{m1} + v_2 \cdot s' \cdot \tan \delta_{m2}}{v_1 \cdot s'' + v_2 \cdot s''} \quad (12)$$

for Q_{m11} or $\tan \delta_{m11}$ of series model and Q_{m33} or $\tan \delta_{m33}$ of parallel model in the case when $(\tan \delta_m)^2 \ll 1$ and $(\tan \delta_m)^2 \ll 1$,

$$1/\bar{Q}_m = \tan \delta_m = \frac{v_1 \cdot s' \cdot \tan \delta_{m1} + v_2 \cdot s' \cdot \tan \delta_{m2}}{v_1 \cdot s'' + v_2 \cdot s''} \quad (13)$$

Dielectric loss tangent is defined as follows:

$$\tan \delta = \epsilon''/\epsilon' \quad (14)$$

where ϵ' and ϵ'' are real and imaginary parts of complex dielectric constant $\hat{\epsilon} (= \epsilon' - j \cdot \epsilon'')$. This relation and the equations of dielectric constants from series and parallel models are similar to the elastic compliance's.

Accordingly one obtains the following equations:

For $\tan \delta_{33}$ of series model and $\tan \delta_{11}$ of parallel model,

$$\tan \delta = 1/\bar{Q} = \frac{v_1 \cdot \epsilon' \cdot \tan \delta_{11} + v_2 \cdot \epsilon' \cdot \tan \delta_{22}}{v_1 \cdot \epsilon'' + v_2 \cdot \epsilon''} \quad (15)$$

and for $\tan \delta_{11}$ of series model and $\tan \delta_{33}$ of parallel model in the case when $(\tan \delta)^2 \ll 1$

$$< 1 \quad \text{and} \quad (\tan \delta)^2 < 1,$$

$$\frac{\tan \delta}{1 - \tan \delta} = \frac{v_p \cdot \epsilon_p \cdot \tan \delta + v_s \cdot \epsilon_s \cdot \tan \delta}{v_p \cdot \epsilon_p + v_s \cdot \epsilon_s} \quad (16)$$

Assuming that the unit cell of the modified cubes model (Fig.2) is divided into two parts as shown in Fig.3 (a) for Z axis direction and (b) for X axis direction respectively and based on this geometry and combining theoretical equations from series and parallel models, one can derive the theory on the dielectric, elastic and electromechanical properties. The notation is used in this paper according to Newnham's.²¹

With consideration of distribution and shape of pores (shape factor K_s)²² and assuming that $\epsilon_p = 0$ and $\tan \delta_p = 0$, the theoretical equations for Young's modulus \bar{E} , elastic compliance \bar{s} and Poisson's ratio σ of the ceramics with closed pores are obtained as follows:

$$\bar{E}_{33} = 1/\bar{s}_{33} = E_{33}(1 - p^{2/3}/K_s^{2/3}) = (1/s_{33})(1 - p^{2/3}/K_s^{2/3}) \quad (17)$$

$$\bar{\sigma}_{31} = s_{31}(1 - p^{2/3}/K_s^{2/3}) \quad (18)$$

$$\bar{E}_{11} = 1/\bar{s}_{11} = E_{11}(1 - p^{2/3}/K_s^{1/3}) = (1/s_{11})(1 - p^{2/3}/K_s^{1/3}) \quad (19)$$

$$\text{and} \quad \bar{\sigma}_{12} = s_{12}(1 - p^{2/3}/K_s^{1/3}). \quad (20)$$

Theoretical equations for mechanical quality factors Q_{33} and Q_{31} or mechanical loss tangent $\tan \delta_{33}$ and $\tan \delta_{31}$ of the ceramics with closed pores are obtained as follows:

$$Q_{33} = 1/\tan \delta_{33} = 1/\tan \delta_{33} = Q_{33} \quad (21)$$

$$\text{and} \quad Q_{31} = 1/\tan \delta_{31} = 1/\tan \delta_{31} = Q_{31} \quad (22)$$

Theoretical equations for dielectric loss tangent $\tan \delta$ from series and parallel models are derived as equations 15 and 16. Assuming that the loss tangent of pore $\tan \delta_p$ is zero, the dielectric loss tangent of the ceramics with closed pores are obtained as follows:

$$\tan \delta_{33} = \tan \delta_{33} \quad (23) \quad \text{and} \quad \tan \delta_{31} = \tan \delta_{31} \quad (24)$$

The radial coupling factor k_p is expressed as follows:

$$k_p^2 = \frac{2 \cdot d_{31}^2}{\epsilon_{33} \cdot s_{11} \cdot E_{11} (1 - \sigma_{12}^2)} \quad (25)$$

As k_p is a function of ϵ_{33} , d_{31} , s_{11} and σ_{12} , one can obtain a theoretical equation for k_p as a function of volume fraction (P) and shape factor (K_s) of pores.

2. RESULTS AND DISCUSSIONS

Okazaki et al. have reported porosity dependences of resonant impedances (Z_r) and radial coupling factors (k_p) of hot-pressed piezoelectric (PZT) ceramics.⁴⁾ Comparisons between theory and experimental results are shown in Fig.4 (a) and (b).

Banno et al. have investigated the porosity dependences of dielectric loss tangent ($\tan \delta$) or electrical quality factor ($Q = 1/\tan \delta$) of microwave dielectric ceramics. Results are shown in Fig.5.⁵⁾ There is no dependence of the quality factor (Q) on porosity, which agrees well with the theoretical equations 21 and 22.

In Fig.3, the theoretical values agree well with the experimental ones in the case when the K_s value is 0.5. This results are same as those for dielectric and piezoelectric constants.²¹

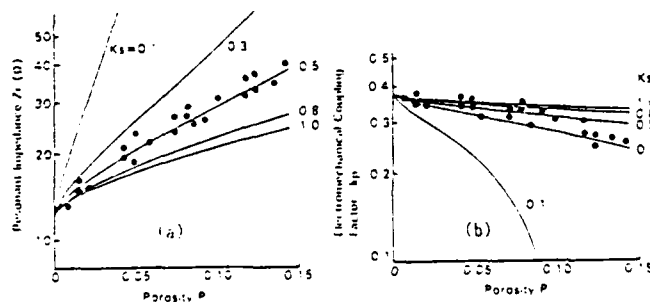


Fig.4. Comparison between the experimental and theoretical values for (a) resonant impedance Z_r and (b) electro-mechanical coupling factor k_p of hot pressed PZT.

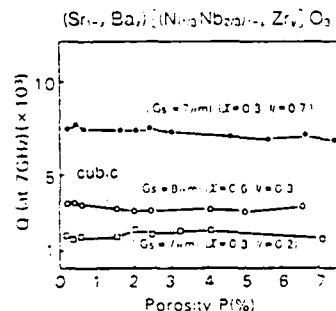


Fig.5. Electrical quality factor $Q (=1/\tan \delta)$ of microwave dielectric ceramics vs. porosity.

- REFERENCES 1) Z. Hashin, Ceramic Microstructures (ed. by R.M. Fulrath et al.) Chap.14, J. Wiley & Sons, 1986 p.313-341. 2) R.E. Newnham et al., Mater. Res. Bull., 13 (5) 525-36 (1978). 3) H. Banno, Jpn.J. Appl. Phys., 24 (1985) Suppl. 24 2 p.445-47. 4) K. Okazaki et al., Proc. 1971 Int'l Conf. on Mechanical Behavior of Materials IV p.404-12 (1972). 5) H. Banno, et al., Extended Abstract, Electronic Div. Am. Ceram. Soc. Ann. Meeting 1986 paper No.126-E-86.

W-10

EFFICIENCY OF PIEZOELECTRIC CERAMIC ACTUATOR

S. TAKAHASHI

Material Development Center, NEC Corp., Miyamae, Kawasaki-shi 213, Japan

ABSTRACT: Multilayer piezoelectric ceramic actuator efficiency for pulse mode operation was experimentally investigated. About 60 % of supplied electrical energy could be recovered for the actuator without mechanical loading, using a dc source with a series inductor. About 20 % of the supplied energy was lost in the actuator as heat.

1. INTRODUCTION

In order to operate the multilayer piezoelectric ceramic actuator¹⁾ in a pulse mode, a charge-discharge circuit has conventionally been used. In this case, unused stored energy in the actuator was wasted in every discharge cycle. The present study reports a method to recover the unused stored energy.

2. BASIC PRINCIPLE

Figure 1(a) shows a driver circuit with a series inductor L . When switch sw turned on, voltage across the actuator V_c and current I change with a time, as shown in Figs. 1(b) and (c), respectively. The actuator is charged during the first half cycle ($0 \leq t < T/2$). The amount of energy supplied from an electrical source E_s can be expressed as

$$E_s = E_0 \int_0^{T/2} I dt \quad (1)$$

where E_0 is the dc source voltage. In the second half cycle ($T/2 \leq t \leq T$), unused stored energy in the actuator can be recovered. The amount of recovered energy E_r is expressed as

$$E_r = E_0 \int_{T/2}^T |I| dt \quad (2)$$

3. RESULTS AND DISCUSSION

Current I was measured for an actuator without mechanical loading, using the driver circuit as shown in Fig. 1(a), where $E_0 = 78$ V and $L = 10$ mH. The result is shown in Fig. 2. Pertinent values for E_s and E_r are 2.7 mJ and 1.5 mJ, respectively. Fifty six percent of supplied energy is recovered.

The sum of equivalent resistances, for the inductor and the actuator $R_L + R_c$, is determined by

$$R_L + R_c = (2L/T) \ln(I_1/I_3) \quad (3)$$

where $R_L = 10 \Omega$.

Consequently, the heat energy lost in the actuator in one cycle E_L can be calculated by

$$E_L = R_c \int_0^T i^2 dt \quad (4)$$

The value is 0.58 mJ, corresponding to 21% of the supplied energy.

Actuator temperature ΔT can be expressed as

$$\Delta T = E_L \cdot f \cdot t \cdot m \cdot c \quad (5)$$

where f is repeated frequency, t is voltage application duration time, c is specific heat and m is mass. Figure 3 shows observed and calculated temperature rise ΔT values.

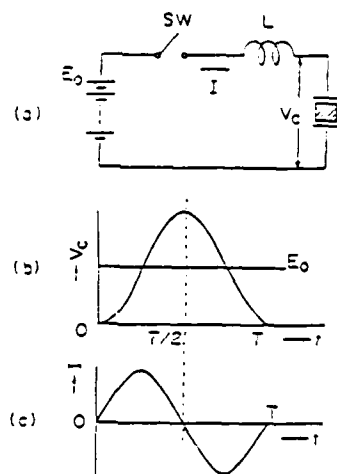


Fig.1. Actuator driving circuit with an inductor (a) circuit (b) voltage across the actuator (c) current.

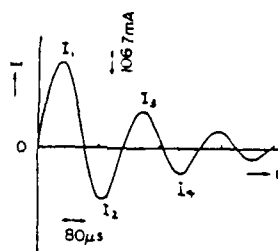


Fig.2. Observed current I with $E_0=78$ V and $L = 10$ mH.

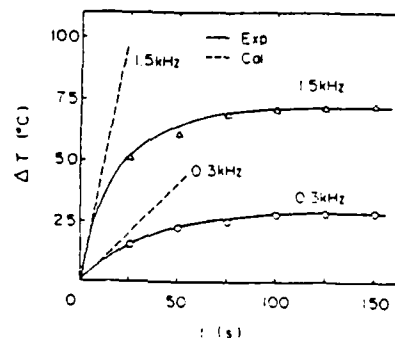


Fig.3. Actuator temperature rise ΔT during pulse driving.

REFERENCES

1. S. Takahashi, Jpn. J. Appl. Phys., 24, Supp. 24-2, 41 (1985).

CERAMIC GREEN SHEET PUNCHER USING PIEZOELECTRIC ACTUATOR

T. YOSHIURA, K. YOSHIDA, and I. KAGAYA

R&D Planning and Technical Service Division, NEC Corporation

Y. SHIMADA and S. TAKAHASHI

Material Development Center, NEC Corporation

ABSTRACT: A Ceramic Green Sheet is required to have many through holes, made by a small hole punching tool with a very small pitch. A Ceramic Green Sheet Puncher generally has a punch and die arranged in some pattern. However, a puncher which has patterned punch die, can not be used to match a variable pattern. The authors have developed a ceramic green sheet puncher, using a piezo electric actuator. It is compact and can punch through holes in a variable pattern.

MECHANICAL STRUCTURE

This ceramic green sheet puncher uses a piezoelectric actuator which takes advantage of the momentary stretch force in a piezoelectric actuator. This stretching force actuates a pin, the punch, in such a manner as to punch a through hole in a ceramic green sheet, placed between die and punch. The pin, the punch, is mounted at the center of the plate spring. Moved by the force from piezoelectric actuator, the spring is bent, the pin is moved forward until it enters the hole in the die through the ceramic green sheet. The puncher has two lines of pins drawn up in a line. Each line has 30 pins. The puncher moves laterally and ceramic green sheet moves at a right angle to the puncher. The piezoelectric actuator is driven according to instructions from the control instrument. Movements are made according to a pattern which is shown on the CRT.

ABILITY

This ceramic green sheet puncher, using a piezoelectric actuator, can punch 2400 through holes in a ceramic green sheet during a 90 second time period including the green sheet. The inner diameter of the through hole is 0.251 mm, when the ceramic green sheet is punched with a 0.250 mm diameter pin. The die has a 0.350 mm inner diameter. Sometimes the back of the ceramic green sheet breaks off putting a burr on the inner edge of the through hole. That burr causes no trouble in regard to using the punched hole as a through hole. The distance the pin moves is 1 mm, when 120 V is applied to the piezoelectric actuator and when a plate spring, 0.05 mm thick and 3 mm wide, is used the through hole pitch is 1.295 mm and pitch error is ± 0.02 mm. The puncher and ceramic green sheet feeder has 0.005 mm resolution. This equipment can punch holes in an 83 mm \times 83 mm area and 100 mm \times 100 mm ceramic green sheets can be mounted in the punch press.

MONOMORPH ACTUATORS USING SEMICONDUCTIVE FERROELECTRICS

Kenji Uchino and Mikihiro Yoshizaki

Department of Physics, Sophia University

Kioi-cho 7-1, Chiyoda-ku, Tokyo 102

Hiroshi Yamamura, Kiyoshi Kasai, Naomichi Sakai and Hiroshi Asakura

Advanced Materials Research Laboratory, Toyo Soda Manufacturing Co., Ltd.

Hayakawa 2743-1, Ayase-shi Kanagawa 252

A new actuator device is proposed using semiconductive ferroelectric ceramics. This device is a simple-plate actuator capable of bending equivalently to a piezoelectric bimorph. A significant difference is a simple structure named as a "monomorph" in comparison with a multi-stacked type in the bimorph, as illustrated in Fig. 1.

The key to obtaining the bend in the monomorph device is to realize non-uniform electric field distribution in the piezoelectric ceramics. If the ceramic plate is semiconductive as well, the ceramics-metallic electrode junction introduces a barrier to the electron energy band structure (Fig. 2(a)). When an electric voltage is applied to the semiconductive plate through the electrodes, the field is concentrated only on one side of the plate, as shown in Fig. 2(b). The combination of the piezoelectricity with the field non-uniformity causes the bend in the ceramic plate.

Figure 3 shows examples of monomorph actuators: (a) $0.8\text{PbZrO}_3\text{-}0.2(\text{K}_{1/2}\text{Bi}_{1/2})\text{ZrO}_3\text{-}1\text{mol}\%\text{Al}_2\text{O}_3$ (20mm x 10mm x 0.5mm) and (b) $\text{BaTiO}_3\text{-}0.18\text{mol}\%\text{Cy}_2\text{O}_3$ (40mm x 10mm x 0.5mm). The displacement at the top of a monomorph reaches 100 μm , comparable to the deflection of the conventional bimorphs. The slope of the displacement curve suggests the semiconductive characteristics, n- and p-type, for the samples (a) and (b), respectively. It is worth to note that the ceramic plate with ohmic-contact electrodes (InGa) reveals no significant deflection.

Figure 4 shows the composition dependence of the monomorph characteristics in the solid solution ceramics $(1-x)\text{PbZrO}_3\text{-}x(\text{K}_{1/2}\text{Bi}_{1/2})\text{ZrO}_3$ (20mm x 10mm x 0.65mm). The dopants such as Al_2O_3 and SiO_2 also affect significantly to the properties.

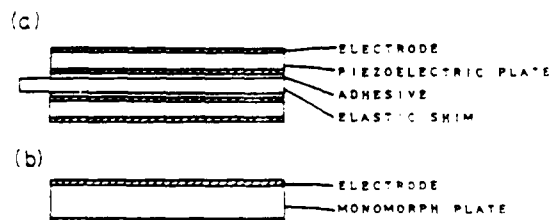


Fig. 1 Structures of a bimorph (a) and a monomorph actuator (b).

The electromechanical resonance can be observed in most of the monomorphs, as demonstrated in Fig. 5 for the PbZrO_3 -based plate: This indicates that the new monomorph actuators are applicable to buzzers, speakers, fluid pumps etc., replacing the conventional piezoelectric bimorphs.

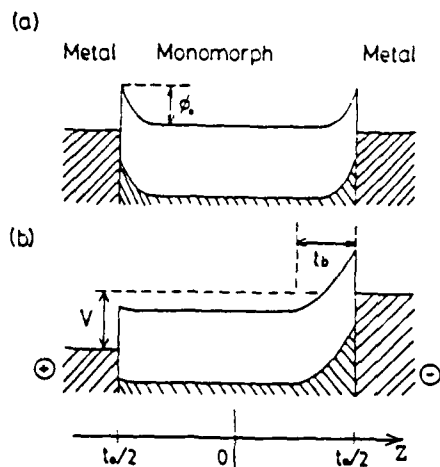


Fig. 2 Energy barrier model for a monomorph device.

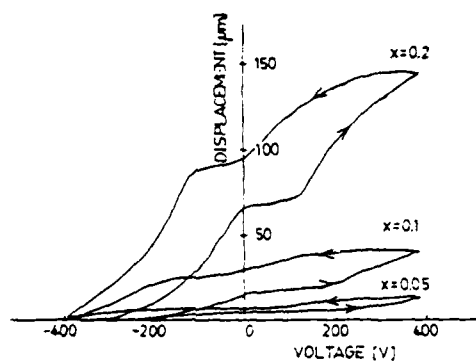


Fig. 4 Composition dependence of monomorph characteristics in the $\text{PbZrO}_3-(\text{K}_{1/2}\text{Bi}_{1/2})_2\text{ZrO}_3$ ceramics.

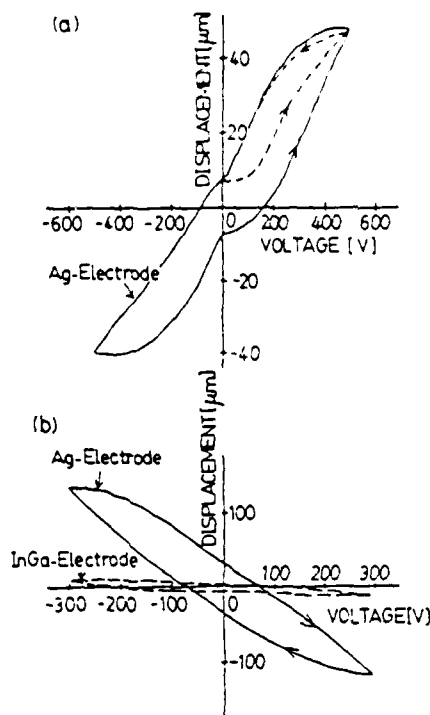


Fig. 3 Monomorph characteristics in (a) lead zirconate based and (b) barium titanate based ceramics.

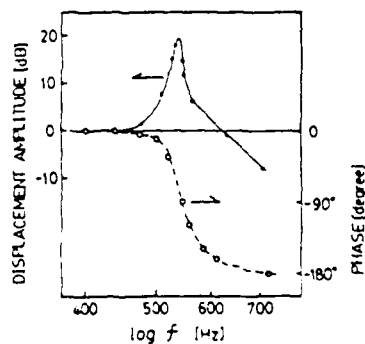


Fig. 5 Electromechanical resonance in a PbZrO_3 -based monomorph actuator.

DEVELOPMENT OF ELECTROSTRICTIVE CERAMICS

S. JOMURA, K. MARUTA and J. WATANABE

Magnetic and Electronic Materials Research Laboratory, Hitachi Metals Ltd.,
5200 Mikajiri Kumagaya, Saitama 360, Japan

ABSTRACT: Electrostrictive ceramics with a large displacement (strain) for the piezoelectric actuators have been developed. As large strain as 1×10^{-3} which is induced transversely to the applied electric field is obtained at 10 kV/cm by using electrically induced phase transitions between ferroelectric (FE) phase and antiferroelectric (AFE) one in FE-AFE coexisting ceramics.

1. INTRODUCTION

The recent developments^{1,2)} of the piezoelectric ceramics have opened the piezoelectric actuators with relatively large stroke, fast response and compact size. For these applications, the easy generations of a large stroke under low applied voltage are essential. This requirement has been partially satisfied by the use of multilayer structure³⁾, but improvement of material properties is also necessary. The present study reports the electrostrictive ceramics with a large strain.

2. EXPERIMENTAL AND RESULTS

Four types of mechanism for the piezoelectric strains are now known, that is, (1) usual piezoelectric strain proportional to piezoelectric strain constant d , (2) domain reorientation, (3) volume change accompanied with phase transitions,¹⁾ and (4) electrostriction. In order to obtain a large strain, above four types of strains should be fully utilized. In the present work, it was clarified that a large strain can be achieved using electrically induced phase transitions in the FE-AFE phases coexisting ceramics as shown in Fig.1. For example, the transverse strain such as 1×10^{-3} , normal to the applied electric field, is obtained at 10 kV/cm. It is necessary to improve several properties of this ceramic material, such as large hysteresis and temperature stability, in the case of some applications.

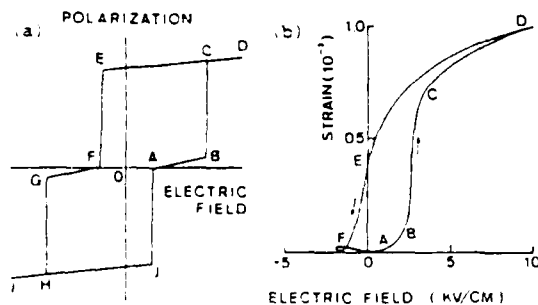


Fig.1 (a) Schematic double-hysteresis loop of a FE-AFE coexisting ceramics. Regions of G-F-O-A-B show AFE state and D-C-E and I-H-J show FE ones. (b) Strain vs. applied electric field curve of $(\text{Pb}, \text{Sr})_{1-x}(\text{Zn}, \text{Ni}, \text{Nb})\text{O}_3$ ceramic material.

REFERENCES

1. K. Uchino, Piezoelectric/electrostrictive actuator, Morikita shuppan 1986 in Japanese.
2. K. Furuta and K. Uchino, Advanced Ceram. Mater., 1, 61 (1986)
3. S. Takahashi, Jpn. J. Appl. Phys., 24, 41, (Supplement 24-2) (1985)

TEMPERATURE DEPENDENCE OF ELECTROSTRICTION UNDER A HIGH ELECTRIC FIELD

K. ABE, O. FURUKAWA and M. KATSURA

Metals and Ceramics Laboratory, Research and Development Center, Toshiba Corp. Kawasaki, 210, Japan

K. INAGAKI

Marcon Electronics Co. Ltd., Nagaoka, Yamagata, 991, Japan

ABSTRACT: A multilayer actuator, using a modified lead zinc niobate ceramic, was fabricated to investigate the temperature dependence of electrostriction under a high electric field. Temperature dependence of electrostriction under a high electric field was estimated to be less than 1.2%/°C by using dielectric stiffness, higher order stiffness and their temperature derivatives.

1. INTRODUCTION

The electrostrictive effect is suitable for micropositioner applications, because of small strain hysteresis¹⁾. However, one of the problems for electrostrictive materials is temperature dependence of strain. Since the electrostrictive coefficient Q does not change much with temperature fluctuation²⁻⁴⁾, the change in dielectric properties should be the main cause for temperature dependence of strain.

2. TEMPERATURE COEFFICIENT OF ELECTROSTRICTION

The relation between electric field E and polarization P can be approximately expressed as

$$E = \alpha P + \beta P^3 + \gamma P^5 \quad (1)$$

where α , β and γ are dielectric stiffness and higher order stiffness. The relation between electrostriction S and polarization P is expressed as

$$S = QP^2 \quad (2)$$

where Q is the electrostrictive coefficient. Under a constant electric field ($dE = 0$), the temperature coefficient of electrostriction is given by the following equation, derived from Eqs. (1) and (2).

$$\frac{1}{S} \frac{dS}{dT} = \frac{1}{Q} \frac{dQ}{dT} - \frac{2}{\alpha + 3\beta P^2 + 5\gamma P^4} \left(P \frac{d\alpha}{dT} + P^3 \frac{d\beta}{dT} + P^5 \frac{d\gamma}{dT} \right) \quad (3)$$

3. EXPERIMENTAL

A multilayer ceramic electrostrictor was fabricated by the conventional green sheet method for easy electric field application. A modified lead zinc niobate ceramic was used for the electrostrictive material, and Ag-Pd was used for the internal electrodes. Hysteresis curves for electric field vs. polarization were recorded with a Sawyer-Tower circuit under various temperature, from 9°C to 32°C.

4. RESULTS AND DISCUSSION

From the hysteresis curves, α , β and γ were calculated by the least square

method. The values of α , β and γ , under various temperatures, are plotted in Fig. 1. These values and their temperature derivatives at 20°C were used to calculate the temperature coefficient of electrostriction. The result of numerical calculation by Eq. (3) is shown in Fig. 2 for modified lead zinc niobate, as well as for modified barium titanate. For modified lead zinc niobate, the temperature coefficient shows a maximum value at $0.8 \times 10^6 \text{ V/m}$, and decreases to below $1.0 \text{ \%}/^\circ\text{C}$ at $1.0 \times 10^6 \text{ V/m}$.

5. CONCLUSION

The temperature dependence of electrostriction under a high electric field was investigated for modified lead zinc niobate in a multilayer configuration. The temperature coefficient of electrostriction was estimated to be less than $1.2 \text{ \%}/^\circ\text{C}$ for modified lead zinc niobate. It became clear that its utilization under a high electric field is favorable for temperature stability of electrostriction.

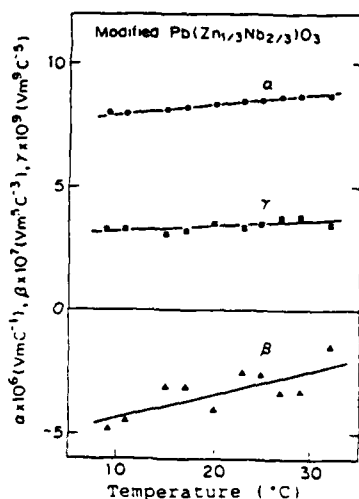


Fig. 1. Temperature dependence of α , β and γ in $E = \alpha P + \beta P^3 + \gamma P^5$.

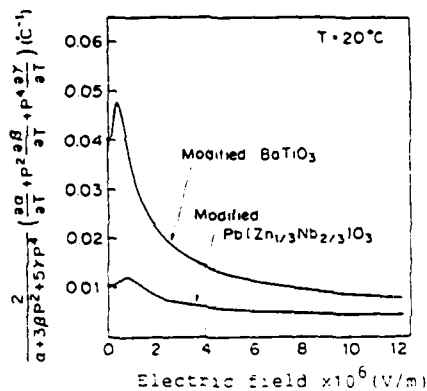


Fig. 2. Calculated curves for $\frac{1}{\alpha + 3\beta P^2 + 5\gamma P^4} \left(\frac{\partial \alpha}{\partial T} + P^2 \frac{\partial \beta}{\partial T} + P^4 \frac{\partial \gamma}{\partial T} \right)$ as function of electric field.

REFERENCES

1. K. Uchino, S. Nomura, L. E. Cross, R. E. Newnham and S. J. Jang, *J. Mat. Sci.*, **16**, 569 (1981).
2. Z. Y. Meng, U. Kumar and L. E. Cross, *J. Am. Ceram. Soc.*, **68**, 459 (1985).
3. G. Schmidt, G. Borchhardt, J. Von Clemski, D. Grutsmann, E. Purinsch and V. A. Isupov, *Ferroelectrics*, **42**, 3 (1982).
4. M. Shishineh, C. Sundius, T. Shrout and L. E. Cross, *Ferroelectrics*, **50**, 219 (1983).

PREPARATION AND CHARACTERISTICS OF NEW MONOMORPH ACTUATOR

N. SAKAI, K. KASAI, and H. YAMAMURA

Advanced Material Research Laboratory, Toyo Soda Manufacturing Co., LTD,
Kanagawa, Japan

ABSTRACT: Bending phenomenon was newly observed in a single ceramic plate of BaTiO_3 which was doped by small amount of SiO_2 and Al_2O_3 or Nb_2O_5 . The bending mode may occur by the presence of potential barrier between silver electrode and ceramic semiconductor, as a result of inhomogeneous distribution of an electric field and also by inhomogeneous polarization in oxidized surface layer.

1. INTRODUCTION

In place of usual electromagnetic drive actuator, the piezoelectric ceramic actuator is preferable to control a position for precision machining tools or optical instruments and relays, etc. There are three types of ceramic actuator, that is, multilayer, bimorph, unimorph types. First of them expands along the longitudinal direction and others have bending mode. In present study, it was found that the ceramic single plate of BaTiO_3 which was doped by small amount of SiO_2 and Al_2O_3 or Nb_2O_5 showed the bending effect by applying external field, similar with bimorph- or unimorph-type elements. It was hereafter named "monomorph". In order to clarify the bending phenomenon, a boundary effect between metal electrodes and ceramics and a role of oxidized insulate layer were investigated.

2. EXPERIMENTAL

After BaTiO_3 was ball-milled with 5mol% SiO_2 and 2-5 mol% Al_2O_3 , the powder was rubber-pressed to compacts. Sintering was preformed at 1250°C for various periods, 1 to 15 hrs, in air. BaTiO_3 doped by Nb_2O_5 (0.1 to 1 at%) was also prepared in the similar procedure above-mentioned. Metal electorodes such as Ag, Au, Ga-In were used to check the electrode effect. Bending effect was measured by both contact method using potentiometer and non-contact sensor method. The sample size measured was 40 mm length, 15 mm width, and 0.5 mm thickness. The measurement was procedured at the position of 28 mm far from the fixed end.

3. RESULTS AND DISSCUSION

A magnitude of bending was strongly influenced by sintering temperature and sintering periods. Most remarkable bending effect was observed in the SiO_2 (5 mole %) and Al_2O_3 (2 mole %) doped BaTiO_3 ceramics which were sintered for prolonged times such as 10 hrs (Fig 1). In the sample which was sintered for prolonged time, the electric resistivity was relatively low, that is, 10^7 ohm.cm and gathering of impurity phase was observed by SEM and XMA. Theremore, the bending effect was also strongly dependent on the metal electrodes. Fig.2 shows electrode dependence. It is apparent that the sample attached by silver electrode on either one side or both side produces the remarkable bending

effect. therefore, bending effect may occur by the potential barrier between semiconductive ceramics and silver electrode as a result of electric field concentration near their contact boundary.

On the other hand, it is well known that the Nb-doped BaTiO_3 shows semiconductive property, of which electric resistivity is 10^3 - 10^4 ohm.cm. It was too low resistivity to apply high voltage. Therefore, the surface of the sample was oxidized by electrolysis. Fig.3 shows electrical resistivity change as a function of distance from the oxidized surface. The resistivity was very high (10^{10} ohm.cm) near the oxidized surface and then decreased to 10^6 ohm.cm inside of the ceramic plate. the sample thus obtained showed large bending effect, regardless various electrodes (Fig.4). The electrostrictive behavior was much different from the one in the SiO_2 - Al_2O_3 doped BaTiO_3 system. This experimental fact suggests that in homogeneous distribution of polarization in oxidized surface layer may play an important role. Although similar phenomenon has been found in poly vinylidene fluoride films¹⁾, it has never been observed in ceramic single plate.

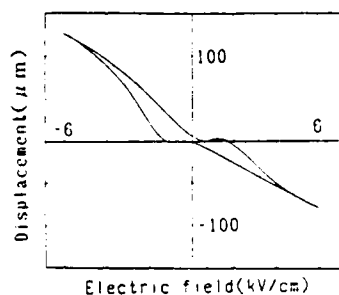


Fig.1. Displacement versus applied electric field for SiO_2 - Al_2O_3 doped BaTiO_3 .

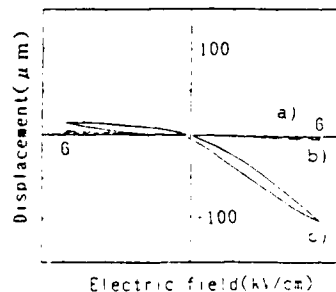


Fig.2. Effect of electrode to displacement. a) Ga-In, Ga-In b) Au, Au, c) Ag, Ga-In

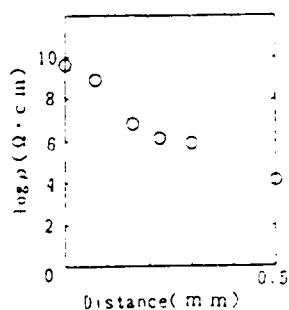


Fig.3. Resistivity change as a function of the distance from the surface.

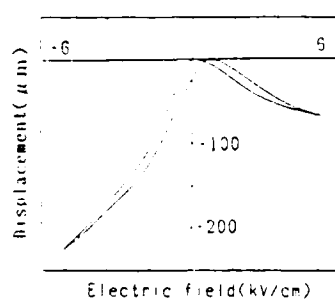


Fig.4. Displacement versus applied electric field for the Nb-doped BaTiO_3 .

REFERENCE

- 1) Michael A. Farcus, *Ferroelectrics*, 57, 203 (1984)

ACKNOWLEDGMENT

The authors very thank to Prof. K. Uchino at Sophia University for the kindly direction and the fruitful discussion.

LASER PATTERNING OF POLYMERS FOR ELECTRONIC PACKAGING

H.S. Cole, Y.S. Liu, H.R. Philipp and L.M. Levinson

General Electric Corporate Research and Development, P.O. Box 8, Schenectady, NY 12301, USA

Polymeric materials have desirable features as a packaging medium for VLSI, multichip circuitry, and as an interconnect substrate. They are inexpensive, can be formed in any desired shape, can withstand required solder temperatures, have excellent dielectric strength and, most importantly, have a very low dielectric constant, thus reducing capacitance coupling between metallization stripes. This capacitance often determines the ultimate speed or frequency limitation of packaged devices.

For hybrid wafer-scale integration, a major concern is the interconnection layout. Many chips are mounted on a substrate and a complex interconnect scheme is required to contact different metal layers to each other and to other chips. Recently, laser-activated chemistry has been shown to be a viable method to fabricate metal lines on various substrates. The production of metal lines by laser-induced deposition techniques offers several advantages over other thin-film deposition processes. The laser process is noncontact, maskless, low temperature, selective, and is relatively simple and economical. A difficulty often encountered in the use of laser-fabricated metallizations in interconnect technology is, however, the relatively high resistivity of the laser-deposited metal, usually due to hydrocarbon contamination. An approach we have adopted to solve this problem will be described. High-conductivity, thick ($\sim 5 \mu\text{m}$) metallization compatible with chip interconnect process requirements is feasible.

Excimer laser photoetching of polymers has been shown to be a convenient, fast, selective method of producing fine patterns or holes in polymeric materials. Selective etching of polymeric materials is important for discretionary rerouting of interconnects as well as for opening vias in barrier-layer coatings. For practical applications, laser photoetching must be fast, efficient, and not harmful to underlying circuitry. This includes metal bonding pads, silicon chips, and various metal interconnects. Thus, the maximum fluence available for etching polymeric layers must be safely below a level which causes damage to other components.

The effect of laser fluence on etch rates is shown in Fig. 1 for poly(methyl methacrylate). This well-studied polymer shows the general trend found for most polymeric materials. Below about 50 mJ/cm^2 , little or no photoablation occurs. This phenomenon requires that a critical number of chemical bonds be broken per unit volume and/or that a critical temperature be reached for significant etching to occur. The absolute value of the absorption coefficient, α , defines the depth within which most of the incident photons are absorbed. One might speculate that if α is low and the absorbed energy per unit volume is small, little or no etching would occur. On the other hand, if α is extremely high, the photons do not penetrate beyond the initial surface layer and the etch rate would also be low. Therefore, one would predict that at each fluence level above threshold, a maximum etch rate would exist for absorption coefficients between the above extremes. This is experimentally verified in Fig. 2. In this work, polymer blends of poly(α -methyl)styrene and poly(methyl methacrylate) and copolymer blends (styrene allyl alcohol copolymer in butylvinyl ether maleic anhydride copolymer) were prepared in order to vary the absorption coefficient over several orders of magnitude. A constant fluence of 200 mJ/cm^2 was used in one study and 100 mJ/cm^2 in the other. In both cases a maximum in etch rate was found when α was adjusted to about 10^4 cm^{-1} .

Optimization of the polymer etch rate by tailoring α will thus allow the fastest rate polymer via hole drilling without damage to the underlying circuit components.

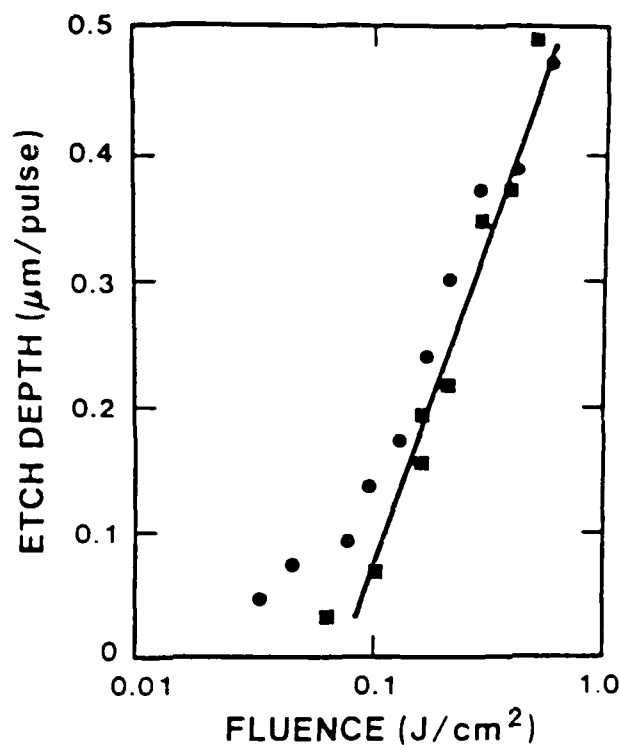


Fig. 1. Photoetching rate of PMMA at 193 nm (■ this work)

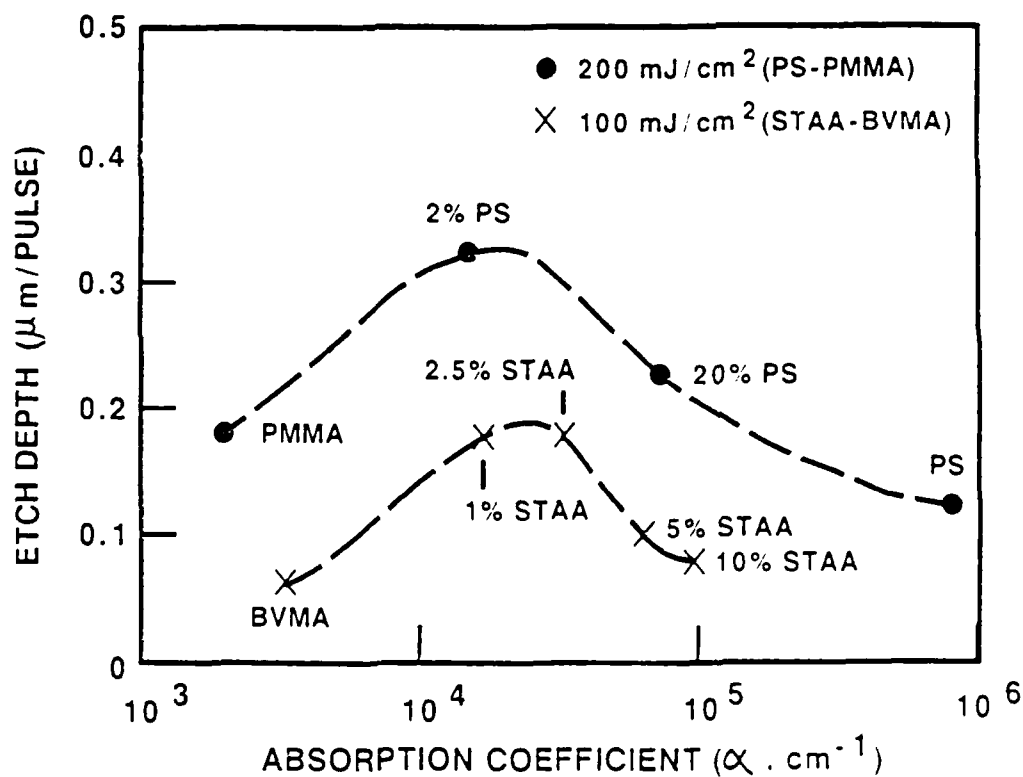


Fig. 2. Effect of absorption on photoetching rate (193 nm, 12 nsec pulse)

W-17

CHARACTERIZATION OF THE ROLE OF EXCESS MAGNESIUM OXIDE AND LEAD OXIDE IN LEAD MAGNESIUM NIOBATE

HUI-CHIEH WANG and W. A. SCHULZE

New York State College of Ceramics, Alfred University, Alfred, New York 14802, U.S.A.

ABSTRACT: $\text{Pb}(\text{Mg}_{1/3}\text{Nb}_{2/3})\text{O}_3$ (referred to as PMN) is the most studied of the diffuse phase transition or relaxor ferroelectrics. The ceramic can be prepared with peak permittivities of 25,000 (100 Hz) which suggests very "clean" or uninhibiting grain boundaries when considering electric flux continuity. This suggests that the grain boundary is either very thin or is composed of a high dielectric constant material. Alternately, the ceramic exhibits almost 100% intragranular fracture and moderate-to-low fracture strength suggesting that the PMN grain boundaries are very weak. This paper partially explores the chemistry and characteristics of these grain boundaries.

Near-phase pure PMN with MgO and PbO additives was produced by the method of Swartz and Shtrout by sintering at 1200°C. The material was characterized by SEM, x-ray diffraction, SIMS and dielectric measurements.

The microstructural studies supported the recent TEM study of Goo. Batching with excess PbO developed a continuous PbO rich phase in triple point regions of the grain boundary. Batching with MgO developed isolated inclusions of MgO rich material in the grain boundary and in the grains. Both were essentially absent in unaltered PMN. SIMS studies suggested that all modifications develop a microstructure having an increased ratio of lead in the first few hundred angstroms of the grain boundary. Quantitative analysis of the lead excess content is prevented by preferential sputtering of lead.

Dielectric measurements indicated that the highest MgO excess composition also had the highest peak dielectric constant, which was 25,000 at 100 Hz. Analysis using inverse dielectric constant versus temperature suggests that doubling the excess lead content doubles the thickness of the grain boundary. This was graphically demonstrated by parallel shifts in the high temperature curves. Excess MgO, however, gave a considerably different response. The $1/K$ equals zero intercept remained nearly constant while the slope ($1/K$ over temperature squared) decreased with increasing MgO. This seems to indicate that while MgO appears to have a very low solubility in PMN, the presence of discrete MgO particles affects the low frequency contributions to the dielectric constant. This interaction suggests that the MgO inclusions could decrease the diffuseness of the phase transition.

TRIVALENT IMPURITIES IN BaTiO_3

K. TAKADA, R. Y. LEE, S. R. WITEK, and D. M. SMYTH
Materials Research Center, No. 32
Lehigh University
Bethlehem, PA 18015, U.S.A.

ABSTRACT: The effect of small additions of trivalent metallic impurities on the electrical conductivity of BaTiO_3 has been studied for samples having an excess of either BaO or TiO_2 . The properties change gradually with the ionic radius of the impurities, indicating that those of intermediate size occupy both Ba and Ti sites in varying amounts that depend on the Ba/Ti ratio.

1. INTRODUCTION

Based on the compatibility of ionic charge, impurity cations having a charge greater than 4 are expected to occupy only the Ti sites in BaTiO_3 , while those having a charge less than 2 should occupy only the Ba sites. Trivalent impurities are a special case in that their charge is intermediate to those of Ba^{+2} and Ti^{+4} , and their site preference is expected to depend strongly on their ionic radii. The trivalent impurities Al, Sc, Y, La, Nd, Sm, Dy, Er, and Yb have been added to BaTiO_3 having an excess of either BaO or TiO_2 , and the equilibrium conductivity, measured as a function of the oxygen partial pressure at 1000°C , has been used as an indication of the site occupation.

2. EXPERIMENTAL

The samples were prepared by the liquid-mix process^{1,2)}. 1200 atomic ppm of each impurity was added to solutions having Ba/Ti ratios of 0.99, 1.00, and 1.01. The electrical conductivity was measured on sintered bars by a standard dc, 4-point technique²⁾.

3. RESULTS

Trivalent impurities substituted for Ba behave as donors, while those substituted for Ti behave as acceptors. The two situations lead to distinctly different dependences of the equilibrium conductivity on the oxygen partial pressure. By comparison of the experimental results with theoretical curves calculated for occupation of both sites in different ratios, it is possible to obtain quantitative information on the amount of impurity on each site.

The smallest impurities, Al, Sc, and Yb, show strong acceptor-doped behavior, indicating a pronounced preference for the Ti site. The largest impurities, La and Nd, appear to occupy only the Ba sites. Between these sizes, there is a steady shift from Ba sites to Ti sites with decreasing ionic radius of the impurity. The Ba/Ti ratio has the greatest effect on Y and Er, which give predominantly donor behavior in the presence of excess Ti, and acceptor behavior in the presence of excess Ba. These two impurities, with nearly identical ionic radii, can occupy either site with almost equal ease, and represent the transitional cases.

4. CONCLUSIONS

The experimental results are in general agreement with theoretical calculations of site preferences³⁾, except that there is less tendency than predicted for equal occupation of both sites to achieve self-compensation. The two transitional impurities, Y and Er, can give either semiconducting or insulating BaTiO_3 at room temperature, depending on very small differences in the Ba/Ti ratio.

5. ACKNOWLEDGEMENT

This work was supported by the Division of Materials Research of the National Science Foundation.

REFERENCES

- 1.M. Pechini, "Method of Preparing Lead and Alkaline Earth Titanates and Niobates Using the Same to Form a Capacitor", U.S. Patent 3,330,697, July 11 (1967).
- 2.N.-H. Chan, R. K. Sharma, and D. M. Smyth, J. Am. Ceram. Soc. 64[9], 556-62 (1981).
- 3.G. V. Lewis and C. R. A. Catlow, J. Phys. Chem. Solids, 47[1], 89-97 (1986).

LINE-FOCUS-BEAM ACOUSTIC MICROSCOPE SYSTEM FOR NONDESTRUCTIVE EVALUATION OF ACOUSTIC INHOMOGENEITY ON PZT WAFERS FOR SAW DEVICES

N. CHUBACHI and J. KUSHIBIKI

Department of Electrical Engineering, Faculty of Engineering,
Tohoku University, Sendai 980, Japan

ABSTRACT: The line-focus-beam acoustic microscope system has been developed which can inspect elastic properties of materials over an area of 55mm X 55mm with a measurement accuracy better than $\pm 0.03\%$ in velocity measurements. The evaluation of acoustic inhomogeneity on PZT ceramic wafers for SAW devices has been made successfully with this system. Large variations in SAW velocity have been detected on a wafer sample and also among wafers.

1. INTRODUCTION

Recently, the novel material characterization method has been established by means of a line-focus-beam acoustic microscope¹⁾. The method can be used to determine acoustic properties of materials quantitatively, viz., velocity and attenuation of leaky surface acoustic waves (SAWs) propagating along the boundary between a sample and a reference liquid of distilled water. The measurements are made nondestructively through the $V(z)$ curve analysis. The accuracy is so high that the system can be employed to detect a small change of elastic properties of materials.

In this paper, the construction and reliability of the system of line-focus-beam acoustic microscope is described that can measure the two-dimensional velocity variation on a material surface. Experiments are demonstrated for PZT ceramics, using an acoustic line-focus-beam sapphire lens at 225 MHz. The acoustic inhomogeneity on wafers detected by this system is discussed being compared with the variation of SAW device characteristics.

2. SYSTEM

Fig. 1 shows a block diagram of the system, which can be applied to acoustic inhomogeneity mapping on materials. The system consists of four main parts: 1) an acoustic probe, 2) a pulse mode measurement system of transmitting and receiving electrical signals, 3) a mechanical system of alignment and movement to record $V(z)$ curves, and 4) a computer for controlling the system and for processing the recorded curves. $V(z)$ curves are recorded into a wave-memorizer synchronized with the translation of sample driven by a stepping-motor, and then they are processed by a computer. The temperature of water and the acoustic frequency are also measured and recorded. Using a set of these data ($V(z)$ curves, temperature, and frequency), propagation properties of leaky SAWs are precisely determined.

In order to check the reliability of the measurement, the system is applied to measure the velocity for a (111)GGG wafer, which is a typical single crystal without defects. It is confirmed that the relative velocity resolution is better than $\pm 0.01\%$ and the system error for two-dimensional scanning is within $\pm 0.03\%$ over an area of 55mm X 55mm.

3. EXPERIMENTS

Experiments have been made for several PZT wafers of two-inch diameter with a grain size of 1-2 μm practically used in manufacturing SAW devices such as TV-VIF filters. For the filters, the variation of SAW velocity on wafers should be within $\pm 0.1\%$.

Fig. 2 is a typical $V(z)$ curve for a PZT wafer. By analyzing this curve according to the measurement principle, the velocity of leaky SAW is determined to be 2432 m/s. The Velocity distribution on the wafer has been measured at the center of each segmented piece with 5mm X 5mm square as shown in Fig. 3. The remarkable inhomogeneity is observed. The velocities near the center are slower than those for the periphery. The two-dimensional average velocity for the wafer is 2436 m/s with maximum difference of 0.7%.

The acoustic inhomogeneity will be discussed in detail as compared with the characteristics of SAW filters associated with device location on the wafer.

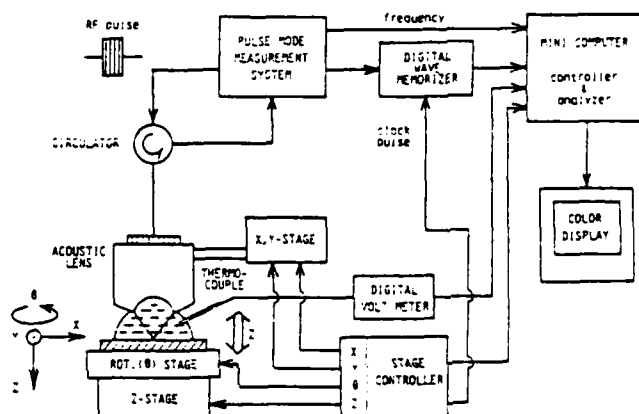


Fig. 1. Block diagram of the line-focus-beam acoustic microscope system.

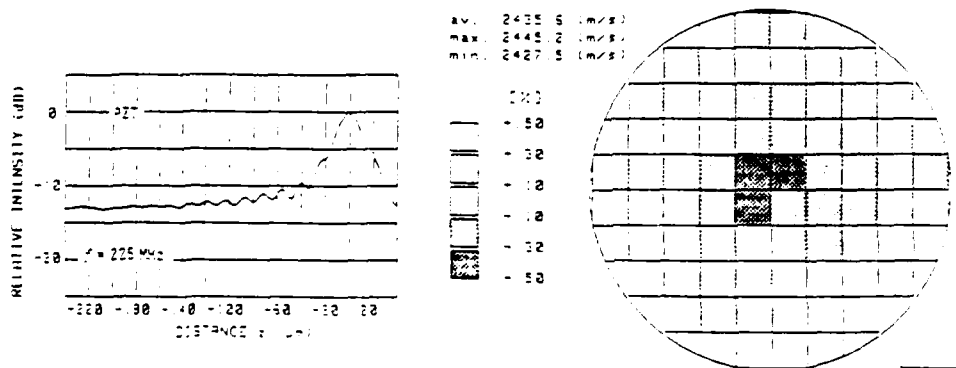


Fig. 2. Typical $V(z)$ curve measured for PZT ceramic wafer.

Fig. 3. Distribution of leaky SAW velocity on PZT ceramic wafer.

REFERENCE

1. J. Kushibiki and N. Chubachi, IEEE Trans. Sonics & Ultrason., SU-32, 189 (1986).

ELECTRICAL PROPERTIES OF $(\text{Sr,Ca})\text{TiO}_3$ BASED CERAMIC VARISTORS

M. MATSUYAMA, J. FUNAYAMA AND H. YAMAMOTO

Central Research Institute, TAIYO YUDEN CO., Ltd.

1600 Kamisatomu, Haruna-machi, Gunma-ken, Japan, 371-85.

ABSTRACT: Electrical properties of $(\text{Sr,Ca})\text{TiO}_3$ based ceramic varistors were investigated. Surge absorption characteristics of samples of which the basic semiconductive ceramics were fired in two reducing atmosphere were examined in relation to the resistivities of the based semiconductive ceramics, the impedance of the ceramic varistors and so on. The resistivity was $0.14/\text{cm}$ at sample(A), or $0.09/\text{cm}$ at sample(B), respectively. The resistivity was decreasing with increasing of H_2 concentration in the firing process. Sample(B) indicated an excellent surge absorption characteristics in the region of high impulse surge voltages compared with that of sample(A). The depressed voltage was 260V at sample(B), or 340V at sample(A), respectively, when a high impulse surge of $5000\text{V}(8/20\mu\text{s})$ was supplied to samples. The difference of this depressed voltage is originated from the resistance of the semiconductive grains.

1. INTRODUCTION

Microstructures and some electrical properties of SrTiO_3 or $(\text{Sr,Ca})\text{TiO}_3$ based ceramic varistors were reported by our previous papers¹⁻³. It is well known that $(\text{Sr,Ca})\text{TiO}_3$ based ceramic varistors have a high apparent permittivity and a high surge absorption capability. However, The varistor characteristics of these ceramic varistors are unknown in the region of a high current surge or a high voltage surge. In this work, we present the varistor characteristics in the region of a high impulse surge in the relation to the resistivity of the based semiconductive ceramics, the impedance at the resonant frequency of the varistors and so on.

2. EXPERIMENTAL

The starting materials used in this study were high purity materials of SrCO_3 , TiO_2 , CaCO_3 , Nb_2O_5 and small amount of additives. The basic components were weighed, respectively and the powder mixtures were ball-milled for 15 hours. The mixed powders, with an appropriate organic binder, were pressed into tablets under a pressure of 10^8Pa . After burning the binder, the tablets were fired at a temperature of 1360°C - 1420°C in $95\%\text{H}_2$ - $5\%\text{H}_2$ or $95\%\text{H}_2$ - $10\%\text{H}_2$ atmosphere, respectively. In order to make BL structures, a paste including AgI was printed on the surface of semiconductive ceramics. The printed specimen were heat treated at 1150°C - 1250°C in air for the grain boundary diffusion of the printed materials. In-Pb alloy were attached to the surfaces of semiconductive ceramics for the measurement of the resistivities. Silver electrodes were fired on the surfaces of the ceramics after the grain boundary diffusion. The capacitance were measured using a capacitance bridge. The impedance at various frequency were measured using an impedance analyzer (VHF: model-413). The current was measured by an ammeter meter. A standard impulse wave of $8/20\mu\text{s}$ in width was used to examine the surge capabilities of $(\text{Sr,Ca})\text{TiO}_3$ based ceramic varistors.

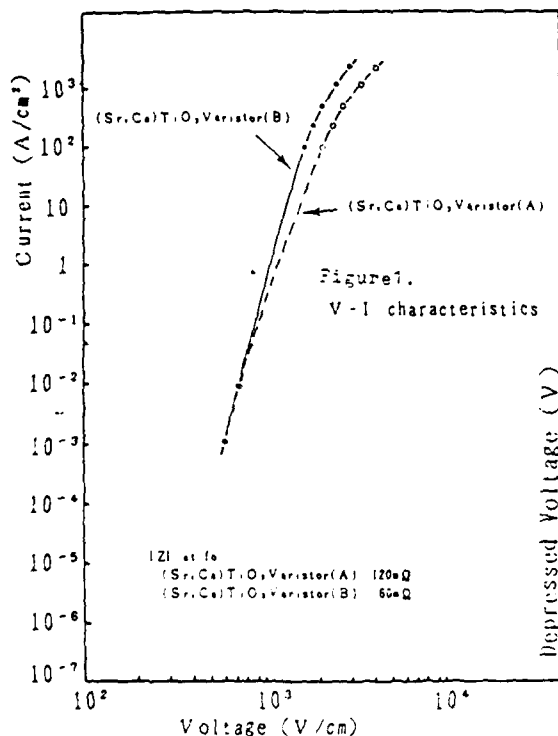
3. RESULTS AND DISCUSSION

Electrical properties of (Sr,Ca)TiO₃ based varistors and the basic semiconductive ceramics were measured. The typical values are shown in table-1. The basic semiconductive ceramics of samples were fired at 1410°C in 10%O₂-90%N₂ atmosphere at sample(A), or in 100%N₂ atmosphere at sample(B), respectively. As can be seen in table-1, the resistivity of the basic semiconductive ceramic was 0.14Ω·cm at sample(A) or 0.09Ω·cm at sample(B), respectively. The grain size of the based ceramics fired at 1410°C was 1μm in average and was almost the same each other. The impedance at the resonant frequency of samples was 120Ω at sample(A) and 65Ω at sample(B) respectively. These results seem to indicate that the resistivity of the basic semiconductive ceramic grains of sample(B) is evidently lower than that of sample(A). The Q of both samples were almost the same value.

Figure-1 shows a I-V characteristic of sample(A) and (B). The I-V curve of both samples is almost the same line in the region below 100mA. However, I-V curve of sample(B) showed a more sharp uprised line compared with that of sample(A). Surge absorption capabilities of sample(A) and sample(B) were examined respectively when various high impulse voltage (8/20μs in width) were supplied to the samples. The results are shown in figure-2. When the impulse voltage of 5000V was supplied to samples, the depressed voltage was 340V at sample(A) or 280V at sample(B), respectively. The surge absorption capability of sample(B) was higher at a supplied surge voltage above 1000V than that of sample(A). As a consequent, this difference of surge absorption capabilities between sample(A) and sample(B) is originated from the resistance of the semiconductive ceramic grains.

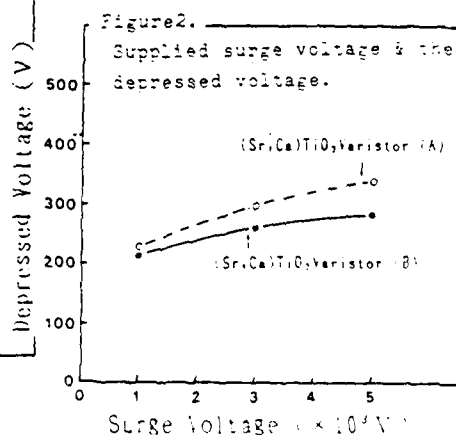
Sample No.	ρ_s	Capitance	Z ₀	Q V _{10A-V10mA}	V _{1mA}
A	0.14(Ω·cm)	19700(pF)	120(Ω)	17.2	80.0(V)
B	0.09(Ω·cm)	20100(pF)	65(Ω)	17.3	81.5(V)

table-1. Electrical Properties of (Sr,Ca)TiO₃ Varistors, (A) or (B).



4. REFERENCE

- 1). N.Yamaoka, M.Masuyama and M.Fukui: The Am. Ceram. Bull., Vol.62, No.6, PP696-701, 1983.
- 2). D.Kaino, J. Funayama and N. Yamaoka: JPN J. App. Phy. Vol.24, Supplement24-3, PP120-122, 1985.



Defect Structure and Electrical Property of La-doped barium titanate

S. SHIRASAKI and H. HANIDA

National Institute for Research in Inorganic Materials, Sakura-Mura, Niihari-Gun,
Ibaraki, Japan

M. Sugimoto

T. D. K. Co., Ichikawa, Chiba, Japan

ABSTRACT: A new semiconducting mechanism of La-doped barium titanate on firing was proposed. The relation between the degree of dissolution of La into host and resistivity as a function of firing temperature in the doped materials was examined to check reliability of the reported semiconducting mechanism in which electrons forms directly to compensate plus charge of $\text{La}_{\text{Ba}}^{+}$. The variation of resistivity with Po_2 at elevated temperatures was successfully interpreted in terms of the new mechanism.

1. INTRODUCTION

One often add intentionally aliovalent impurities into ceramics for controlling their sinterability and properties through variation of levels of point defects, electrons and holes. One of the most important defect equilibria in these doped materials is on a controlling valency mechanism. We have proposed a new semiconducting mechanism of rare-earth-doped barium titanate on firing at elevated temperatures, which is different from the interpretation in terms of such a controlling valency mechanism. The present study relates to the interpretation of the variation in resistivity as a function of Po_2 along with the new mechanism.

2. EXPERIMENTS

La-doped barium titanate of composition, " $\text{Ba}_{0.9}\text{La}_{0.1}\text{TiO}_{3.05}$ " was prepared by firing at temperatures 1050-1380 °C and then quenching down to room temperature. The electrical conductivity, σ and lattice constant as a function of firing temperature were determined. The observed and calculated densities on a basis of two different ideas were determined as a function of Po_2 at the time of firing at 1200 °C in an effort to decide the defect structure of the doped materials.

3. RESULTS and DISCUSSION

Fig.1 shows lattice constant of undoped and doped barium titanates which were prepared by quenching from the indicated temperatures down to R.T. This indicates La dissolution into host to occur completely at least at 1050 °C. Fig.2 shows σ at R.T. as a function of firing temperature for these quenched specimens. This shows that the semiconduction was achieved on firing at temperatures above ≈ 1250 °C. These two data may rule out the reported semiconducting mechanism of La-doped materials in which electrons forms directly to compensate plus charge arising from $\text{La}_{\text{Ba}}^{+}$.

It is widely known that σ in the doped n-type semiconductor decreases with increasing Po_2 at elevated temperatures. This behavior has been

interpreted in terms of tendency toward "electronic compensation" in lower P_{O_2} and "ionic compensation" in higher P_{O_2} . According to our model, on the other hand, this behavior in the doped material can be explained by further progress of thermal formation of oxygen vacancies plus electrons with decreasing P_{O_2} , in which the levels of cation vacancies formed for compensating plus charge (La_{Ba}) remain constant over a range of P_{O_2} considered. The appropriate way to decide the true defect structure controlling the variation in σ may be to determine densities directly to compare with densities calculated on a basis of the forgoing two different ideas. The density measurements were carried out with specimens prepared by firing at 1200 °C at various P_{O_2} and then quenching down to room temperature with maintaining the P_{O_2} . The results show in Fig.3, indicating our model to be plausible.

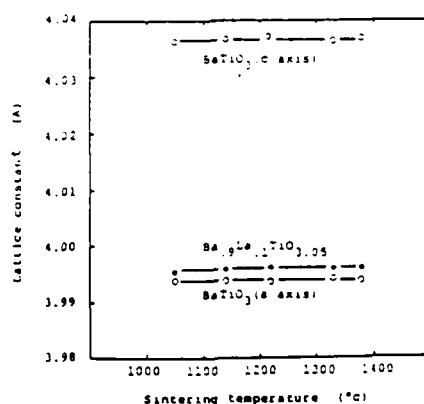


Fig. 1. Lattice constant as a function of firing temperature for $BaTiO_3$ and doped specimen of composition " $Ba_{0.9}La_{0.1}TiO_{3.05}$ ", quenched from the indicated temperatures.

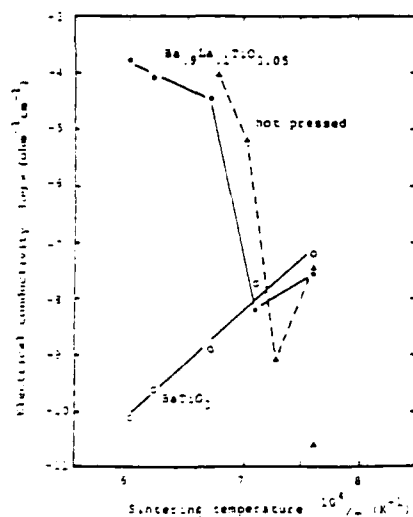


Fig.2. Electrical conductivity as a function of firing temperature for $BaTiO_3$ and doped specimens of composition " $Ba_{0.9}La_{0.1}TiO_{3.05}$ ", quenched from the indicated temperatures.

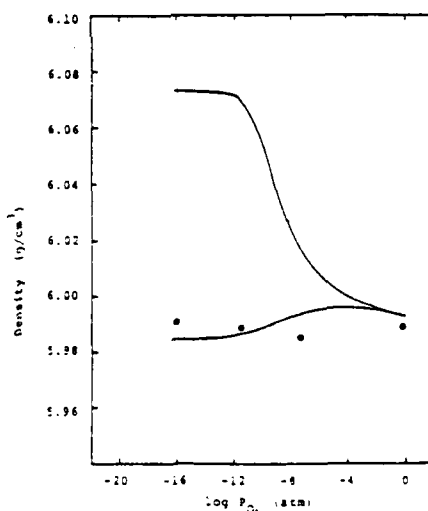


Fig.3. Observed (•) and calculated densities (—) as a function of P_{O_2} at the time of firing two different calculated densities relate to a model based on transition from "electronic compensation" to "ionic compensation" (upper line) and our model (lower line).

- REFERENCES 1) S. Shirasaki, H. Yamamura, H. Haneda, K. Kakegawa and J. Noori, J. Chem. Phys., 73, 4640 (1980).
 2) S. Shirasaki, M. Tsukioka, H. Yamamura, H. Oshima and K. Kakegawa, Solid State Commun., 19, 721 (1976).
 3) S. Shirasaki, S. Matsuda, H. Yamamura, and H. Haneda, Advance in Ceramics, Vol. 10, p. 474, The American Ceramic Society, Inc., Ohio, (1985).

DETERMINATION OF A COMPOSITIONAL FLUCTUATION IN PEROVSKITE TERNARY SYSTEMS

K. KANEHAWA, and Y. SASAKI

Faculty of Engineering, Chiba University, Chiba, Japan

ABSTRACT: It was developed to determine a region of a compositional fluctuation in perovskite ternary solid solution systems, $\text{Pb}(\text{M}_I, \text{M}_{II})\text{O}_3$ - PbZrO_3 - PbTiO_3 . The compositional fluctuation in the ternary systems extends two-dimensionally. Such a compositional fluctuation was determined from isoplethic curves of lattice spacings and fluctuations of lattice spacings in the ternary system.

1. INTRODUCTION

The authors have reported methods to determine a compositional fluctuation in perovskite solid solutions of types of $\text{A}(\text{B}_I, \text{B}_{II})\text{O}_3^{(1)}$, $(\text{A}_I, \text{A}_{II})\text{BO}_3^{(2)}$, and $(\text{A}_I, \text{A}_{II})(\text{B}_I, \text{B}_{II})\text{O}_3^{(3)}$. It was revealed that solid solutions tend to have compositional fluctuations. If a solid solution has a compositional fluctuation, many properties are affected. The compositional fluctuations can have merit in some cases and demerit in other cases. Anyway it is important to grasp the compositional fluctuation.

Ternary solid solutions of $\text{Pb}(\text{M}_I, \text{M}_{II})\text{O}_3$ - PbZrO_3 - PbTiO_3 systems are useful because the morphotropic phase boundary of them, whose compositions have excellent electrical properties, exists along a line in a ternary phase diagram. Properties of solid solutions are largely varied by a way how the compositional fluctuation extends. Thus far there were no methods to determine the compositional fluctuation in the ternary systems. In this study, a method was developed to estimate such a two-dimensional region of the compositional fluctuation.

2. THEORY

A fluctuation of lattice spacing can be determined by widths of X-ray diffraction (XRD) peak. For two-component systems, the fluctuation of lattice spacing corresponds directly to the compositional fluctuation as shown in Fig. 1. On the contrary, for the ternary systems the compositional fluctuation range can not be determined completely from the fluctuation of a lattice spacing. A schematic diagram of isopleth of a certain lattice plane is shown in Fig. 2. Now we consider that the lattice fluctuation range is estimated to be from d_1 to d_2 by the XRD measurement. Such a fluctuation of the lattice spacing can occur in either a case of (a) or (b) shown in Fig. 2. Only information which the measured fluctuation range of lattice spacing means is that the compositional fluctuation occurs within the area indicated by shaded region in this figure.

If the possible compositional fluctuation region expected from another plane is as indicated in Fig. 3, a possible compositional fluctuation range must be restricted within the common shaded area in Fig. 2 and Fig. 3. Furthermore if fluctuations of various lattice planes are measured, the common area will be more restricted and it will approach the true compositional fluctuation area.

PbO, MgO, Nb₂O₅, ZrO₂, and TiO₂ were blended in desired ratios and mixed thoroughly in an agate mortar with a pestle. The mixed oxides were pressed into powder compacts and fired at 1200°C for 1h, resulting in solid solutions of Pb(Mg_{1/3}Ta_{2/3})O₃-PbZrO₃-PbTiO₃ system (PMTZT). Lattice constants of materials having tetragonal symmetry were measured by XRD. The value of β , which is a net width of XRD peak due to a sample itself, was calculated by subtracting the effect of doublet of characteristic X-ray and the resolution of the apparatus from the measured value, using Si as a standard.

The relations between lattice constants and compositions are shown in Fig. 4 and 5, using isoplethic curves. Lattice spacings of (111), (102), and (101) were calculated from the lattice constants, and equal lattice spacing lines were drawn in the ternary system diagrams.

REFERENCES

- 1311-

PROPERTIES OF THE AlN CERAMICS

T. TAKAHASHI, F. ANZAI AND N. TAFADA

New Materials Department, Toshiba Corp. Tokyo, Japan

F. SHINGOZAKI

Metals & Ceramics Laboratory, R & D Center, Toshiba Corp. Kawasaki, Japan

ABSTRACT: Aluminium nitride ceramics were made by a doctor blade method using Y_2O_3 as a sintering additive. Some kinds of compounds which were made in the Y_2O_3 - Al_2O_3 system were observed as extra phases in the AlN ceramics. And such compound tend to correspond respectively to the thermal conductivity of the AlN ceramics. In the process of manufacturing AlN ceramics, the conditions to realize small molar fraction of Al_2O_3/Y_2O_3 are desirable for achieving the higher thermal conductivity.

1. INTRODUCTION

Yttrium oxide is well known as one of the most effective sintering additives for AlN ceramics. It reacts to Al_2O_3 impurity in AlN powder and its reactant melts during the temperature increase. This melting accelerates the AlN sintering process, and this melted compounds confined only at triple points of AlN grains. This paper studies the composition of reactants and its correlation to the thermal conductivity of the AlN ceramics.

2. EXPERIMENTATION

2.1. Materials

Aluminium nitride powder was mixed with Y_2O_3 using an organic binder. After removing the binder from the ceramic green sheets, the sintering was made at 1700-1800°C in the nitrogen atmosphere.

2.2. Measurements

Thermal conductivity was measured by the laser flash method using IR sensor at around 25°C. Samples were columnar about 10mm in diameter and 3mm thick.

3. RESULTS AND DISCUSSION

Thermal conductivity of AlN was decided dominantly by the oxygen impurity in raw material powder (Fig. 1¹⁾) and manufacturing process. The X-ray diffraction revealed there were various kinds of compounds in the sintered body, such as AlON, $3Y_2O_3 \cdot 5Al_2O_3$, $Y_2O_3 \cdot Al_2O_3$ and $2Y_2O_3 \cdot Al_2O_3$ (table 1). Increasing the thermal conductivity, decreasing the molar fraction of Al_2O_3/Y_2O_3 of the compounds. The oxygen at the grain boundaries which reduces the thermal conductivity is the remainder from impurity, which are left during sintering process.

From Fig. 1 and table 1, we think the smaller molar fraction of Al_2O_3/Y_2O_3 is, the smaller is the residual oxygen at the grain boundaries. Therefore, this molar fraction has the probability to be a good index to judge whether the manufacturing process is appropriate or not.

Table 2 shows the properties of the AlN ceramics in comparison with other materials. Thermal conductivity is 170 w/m.K, and thermal expansion coefficient is 4.8 ppm/C, which is close to the value of Silicon. BeO and SiC have higher thermal conductivity than AlN. But BeO is toxic, and SiC needs hot pressing for sintering.

As an example of its applications, AlN is very suitable for high power devices.

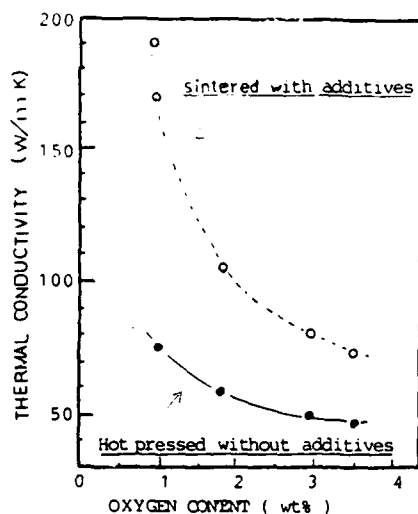


Fig. 1 Relation between oxygen content of AlN raw powder and thermal conductivity

Table 1 Compounds in the AlN ceramics which have various thermal conductivities

K-value	Compounds
110 W/m.K	YAG > AlON
140	YAG
170	YAL > YAG
190	YAM ~ YAL > YAG
235	Y ₂ O ₃ > YAM

YAG: $3Y_2O_3 \cdot 5Al_2O_3$

YAL: $Y_2O_3 \cdot Al_2O_3$

YAM: $2Y_2O_3 \cdot Al_2O_3$

Table 2 Properties of the AlN ceramics

Items	Unit	AlN	Al ₂ O ₃	BeO	SiC
Thermal conductivity	W/m.K (r.t.)	170	20	250	270
Electrical resistivity	$\Omega \cdot \text{cm}$ (r.t.)	10^{14}	10^{14}	10^{14}	10^{13}
Dielectric constant	ϵ/ϵ_0 (1MHz)	8.8	8.8	6.5	40
Dielectric loss	$\times 10^4$ (1MHz)	5-10	3	5	500
Dielectric strength	kV/cm (r.t.)	150	100	100	0.7
Thermal expansion coefficient	$10^6 / ^\circ\text{C}$ (R.T. ~ 400 C)	4.5	7.3	8	3.7
Density	g/cm ³	3.3	3.9	2.9	3.2
Young's modulus	10^{-4} kg/mm^2	2.8	3.7	3.2	4.8
Flexural strength	kg/mm ²	40-50	24-26	17-23	45

REFERENCE

1. K. Shinozaki et al, Proc. annual meeting ceramic soc. JPN, 517, (1985).

The Third U. S. : Japan Seminar on
Dielectric and Piezoelectric Ceramics

Posters

Co-chairman T. Yamaguchi, Keio University

Co-chairman S. W. Freiman, National Bureau of Standards

Chairman of Program Committee, H. Banno, NGK Spark Plug Co.

Chairman of Financial Committee, K. Wakino, Murata MFG.Co.

Chairman of Tour Committee, N. Ichinose, Waseda University

Chairman of Executive Committee, A. Okamoto, TDK Electronics

Secretary, T. Kimura, Keio University

November 9-12, 1986

YKK Conference Hall

Toyama, Japan

Poster Session I (Monday Afternoon)

Processing

- M-1 Sol-Gel Processing of PbTiO_3 , PZT and PLZT
D. A. Payne, K. D. Budd and S. K. Dey, University of Illinois 1
- M-2 Preparation and Properties of Ferroelectric Films from Metallo-organic Precursors
R. W. Vest, Purdue University 2
- M-3 Fabrication of Grain-Orientated $\text{KSr}_2\text{Nb}_2\text{O}_{10}$ Ceramics
T. Kimura, Y. Ogino and T. Yamaguchi, Keio University 7
- M-4 Properties of Sub-micron BaTiO_3 with Additives for Low Firing Temperature
K. Abe, M. Aoki, K. Fukai and K. Hidaka, Sakai Chemical Industry Co., Ltd. 9
- M-5 Effect of MgTiO_3 on the Grain Growth of $(\text{Ba,Ca})(\text{Ti,Zr})\text{O}_3$ Ceramics
S. Itoh, T. Noguchi and T. Ogasawara, TDK Corporation 19
- M-6 Machining of PZT, PT, and $(\text{MnZn})\text{Fe}_2\text{O}_4$ Ceramics by Laser-Induced Chemical Etching
T. Shiosaki and A. Kawabata, Kyoto University 21
- M-7 Synthesis and Properties of Alkoxy-derived $\text{Zr}_x\text{Ti}_{1-x}\text{Sn}_2\text{O}_8$ Ceramics
S. Hirano, T. Hayashi and A. Hattori, Nagoya University 25
- M-8 Effect of Agglomerated Particles on Properties of Ceramic Green Sheets
T. Ueyama N. Kaneko and Y. Machii, Hitachi Chemical Co., Ltd. 27
- M-9 Sinterability of High-Packing Density BaTiO_3 Green Sheets
T. Ueyama, S. Yamana and N. Kaneko, Hitachi Chemical Co., Ltd. 30

Dielectrics I

- M-10 An Investigation of the Low Voltage Failure Mechanism in Multilayer Ceramic Capacitors
C. J. Brannon and H. U. Anderson, University of Missouri-Rolla 32
- M-11 Additive Effects on Microstructure and Properties of BaTiO_3
R. Buchanan, University of Illinois 35
- M-12 Barium Titanate-Based Dielectrics for MLC's with High K and Low Firing Temperature
I. Burn and M. T. Secaur, E. I. du Pont de Nemours & Co. 39
- M-13 Electrical Conduction in BaTiO_3 -Based Ceramic
L. C. Burton and H. Y. Lee, Virginia Polytechnic Institute and State University 41
- M-14 Dielectric and Piezoelectric Ceramics Historical Developments: Current Status and Future Prospects
L. E. Cross, Pennsylvania State University 44
- M-15 Operationally Induced Thermal Stress gradients in Multilayer Capacitors
J. Dougherty, Advanced Materials Technologies 46
- M-16 Microstructure and Nanostructures of Relaxor Ferroelectrics
M. P. Harmer, Lehigh University 49

- M-17 Dielectric Properties of Fine-Grained BaTiO₃ Derived From BaTiO(C₂O₄).4H₂O
T. Enomoto, T. Uno and N. Okada, Central Glass Co., Ltd. 51
- M-18 Low Temperature Fired Glass-Ceramics Dielectric Material
M. Takabatake, K. Kawakami and M. Sakai, Asahi Glass Co. 52
- M-19 Low Temperature Fired Multilayer Ceramic Capacitor with Ni Electrodes
H. Kishi, T. Wada, S. Murai and H. Chazono, and N.Yamaoka, Taiyo Yuden Co., LTD. 54
- M-20 Barium Titanate Ceramics for Base Metal Monolithic Ceramic Capacitors
Y. Sakabe, T. Takagi and K. Wakino, Murata Manufacturing Co., Ltd. 56
- M-21 Temperature Stable Barium Titanate Ceramics for Base Metal Multilayer Capacitors
N. Fujikawa, N. Yokoe and F. Hamano, Kyocera Corp. 58
- M-22 Barium Modified Lead Zinc Niobate Dielectrics for Multilayer Ceramic Capacitor
K. Inagaki, Y. Yamashita and K. Yuuki, Marucon Electronics Co. Ltd. 60
- M-23 Dielectric Relaxation Studies in Some Polymer-PZT Composites
A. M. Varaprasad, Naval Dockyard, India (Sophia University) 62

Poster Session II (Tuesday Morning)

Dielectrics II (Microwave)

- T-1 Microwave Dielectric Properties of Pb(Zr,Ce)O₃ Ceramics
K. Murano, K. Tatuki, S. Nishigaki*, S. Yano*, and H. Kato*, Sony Corp., *Narumi China Corp. 64
- T-2 High Dielectric Constant Ceramics for Microwave Resonators
H. Sato, K. Ayusawa, M. Saito and K. Kawamura, OKI Electric Industry CO. Ltd. 66
- T-3 High-Q Dielectric Resonator Material for Millimeters-Wave Frequencies
H. Tamura, D. A. Sagara, M. Murata and K. Wakino, Murata Manufacturing Co., Ltd. 69
- T-4 Dielectric Properties of BaO-TiO₂WO₃ System at Microwave Frequency
S. Nishigaki, S. Yano, H. Kato and T. Nonomura, Narumi China Corp. 73

Pyroelectrics

- T-5 Ferroelectric and Pyroelectric Properties of Sputter-deposited PZT and PT Films
M. Adachi, T. Shiosaki and A. Kawabata, Kyoto University 77
- T-6 Pyroelectric and Electrical Properties of Modified Lead Titanate Ceramics
N. Ichinose, Waseda University 79
- T-7 Properties of Hot-Pressed Lead Germanate Silicate Ceramics
K. Nagata and K. Okazaki, National Defense Academy 82

Mechanical Properties

- T-8 Comparison: Thermal and Mechanical Properties of Barium

- Titanate Versus Lead Perovskite Dielectrics
A. E. Brown and C. R. Koripella, Union Carbide Corp. 34
- T-9 Fracture Behavior of Capacitor Ceramics
S. W. Freiman and T. L. Baker, NBS 86
- T-10 Compositional Influences on PLZT Switching Properties
B. Koepke, F. Wallenhorst and J. Kyonka, Honeywell Inc. 88
- T-11 Electromechanical Failure Predictions
R. C. Pohanka, P. L. Smith and S. W. Freiman*, Office of Naval Research, *National Bureau of Standards 90
- T-12 The Relation of Anisotropy Between Crack Length and Fracture Toughness in Poled PLZT and Modified PbTiO_3 Ceramics
T. Yamamoto, H. Igarashi and K. Okazaki, National Defense Academy 93
- T-13 Mechanical and Dielectric Failure of BaTiO_3 Ceramics
A. Kishimoto, K. Koumoto and H. Yanagida, The University of Tokyo 96
- T-14 Ceramic Toughening by Crack-Stacking Faults Interactions
K. Niihara and T. Hirai*, National Defense Academy, Tohoku University 98

Electrooptics & PLZT

- T-15 Electrooptic Materials for Integrated Optic Device Applications
R. L. Holman, Battelle Columbus Laboratories 102
- T-16 Growth and Applications of Tungsten Bronze Family Crystals
R. R. Neurgaonkar, W. K. Cory, J. R. Oliver and W. F. Hall, Rockwell International Science Center 104
- T-17 Photoferroelectric Effect in PLZT Ceramics
G. Haertling, Motorola, Inc. 106
- T-18 Photodriven Relay Using PLZT Ceramics
K. Uchino, T. Sada and M. Inoue, Sophia University 108
- T-19 PLZT Thin Film on $\text{MgAl}_2\text{O}_3/\text{Si}$ Substrate
S. Matsubara, Y. Miyasaka, N. Shohata and M. Yonezawa, NEC Corp. 112
- T-20 Some Electrooptic Properties of PLZT Ceramics
K. Hikita, M. Hirama, Y. Tanaka and M. Ono, Mitsubishi Mining & Cement Co., Ltd. 114
- T-21 Dielectric Properties of Sputtered Polycrystalline $(\text{Pb},\text{La})(\text{Zr},\text{Ti})\text{O}_3$ Thin Films
K. Wasa, H. Adachi and T. Mitsuyu, Matsushita Electric Ind. Co., Ltd. 120

Poster Session III (Wednesday Morning)

Piezoelectrics

- W-1 Preparation and Performance of Ceramic-Air Composites for Hydrostatic Sensing
M. Kahn, A. Dalzell and B. Kovel, U. S. Naval Research Laboratory 122
- W-2 A Resonance Technique for Measuring the Complex Elastic, Dielectric and Piezoelectric Coefficients of Composite Materials
X. Q. Chang, A. R. Ramachandran and R. E. Newnham, Pennsylvania State University 124
- W-3 Ferroelectric Composite Transducers
B. A. Auld, Stanford University 129
- W-4 Piezoelectric Properties of Some New Hydrophone Materials

- W-5 R. Y. Ting, U. S. Naval Research Laboratory. 131
Dielectric and Piezoelectric Properties of
 PbZrO_3 - $\text{PZ}(\text{Zn}_{1-x}\text{Nb}_x)\text{O}_3$ Ceramics
K. Sakata and T. Takenaka, Science University of Tokyo 135
- W-6 Piezoelectric Properties of $(\text{Na}, \text{Li})\text{NbO}_3$ Ceramics
T. Honda, I. Kawamata, H. Watarai and T. Ido, Mitsubishi
Electric Corp. 137
- W-7 Electromechanical Properties of Planar Vibrational mode in
PZT/Polymer Piezoelectric Composites
H. Takeuchi and C. Nakaya, Hitachi Ltd. 141
- W-8 Anisotropic Piezoelectric Coupling Factor of
 $[\text{Pbx}(\text{Bi}_{1-x}\text{Na}_{1-x})_{1-y}\text{TiO}_3]$ Ceramics
S. Tashiro, Y. Oikawa, H. Igarashi and K. Okazaki,
National Defense Academy 142
- W-9 Effects of Shape and Volume Fraction of Closed Pore on
Dielectric Loss, Mechanical Quality Factor and
Electromechanical Coupling Factor of Dielectric and
Piezoelectric Ceramics-A Theoretical Approach-
H. Banno, NGK Spark Plug Co., Ltd. 145

Actuator

- W-10 Efficiency of Piezoelectric Ceramic Actuator
S. Takahashi, NEC Corp. 147
- W-11 Ceramic Green Sheet Puncher Using Piezoelectric Actuator
T. Yoshiura, K. Yoshida, I. Kagaya, Y. Shimada and S.
Takahashi, NEC Corp. 149
- W-12 Monomorph Actuators Using Semiconductive Piezoelectrics
K. Uchino, M. Yoshizaki, H. Yamamura*, K. Kasai*, N. Sakai*
and H. Asakura*, Sophia University, *Toyo Soda
Manufacturing Co., Ltd. 151
- W-13 Development of Electrostrictive Ceramics
S. Jomura and K. Maruta, Hitachi Metals Co., Ltd. 153
- W-14 Temperature Dependence of Electrostriction Under a High
Electric Field
K. Abe., O. Furukawa, M. Katura and K. Inagaki*
Toshiba Corp, *Marucon Electronics Co. Ltd. 155
- W-15 Preparation and Characteristics of New Monomorph Actuator
N. Sakai, K. Kasai and H. Yamamura, Toyo Soda Manufacturing
Co., Ltd. 157

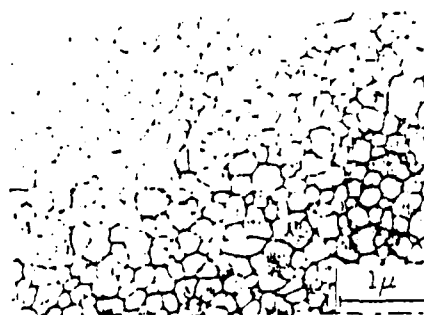
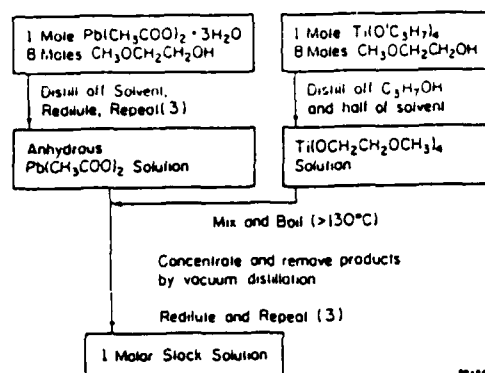
Miscellaneous

- W-16 Laser Patterning of Polymers for Electronic Packaging
H. S. Cole, Y. S. Liu, H. R. Philipp and L. M. Levinson,
General Electric Corporate Research and Development 160
- W-17 Characterization of the Role of Excess Magnesium Oxide and
Lead Oxide in Lead Magnesium Niobate
H. C. Wang and W. A. Schulze, Alfred University 162
- W-18 Trivalent Impurities in BaTiO_3
K. Takada, R. Y. Lee, S. R. Witek and D. M. Smyth, Lehigh
University 167
- W-19 Line-focus-beam Acoustic Microscope System for
Nondestructive Evaluation of Acoustic Inhomogeneity on PTZ
Wafer for SAW Devices
N. Chubachi and J. Kushibiki, Tohoku University 170
- W-20 Electrical Properties of $(\text{Sr}, \text{Ca})\text{TiO}_3$ Based Ceramic
Varistors
M. Masuyama, J. Funayama and N. Yamaoka, Taiyo Yuden Co.,
Ltd. 172

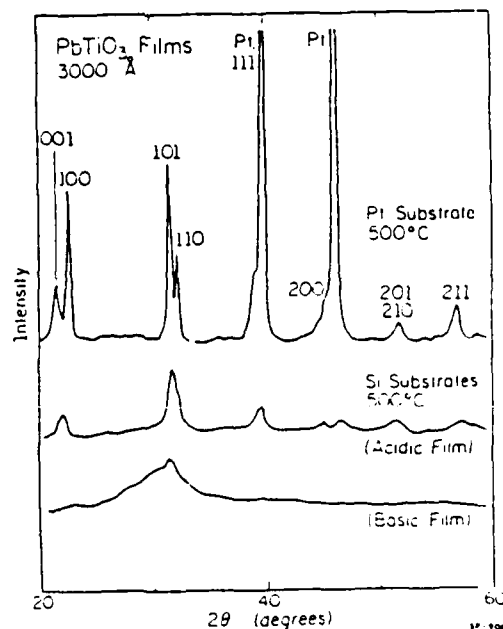
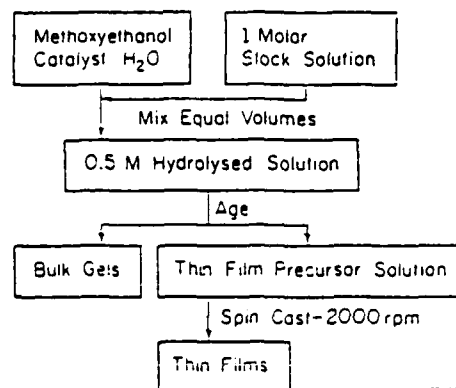
- W-21 Defect Structure and Electrical Property of La-Doped
Barium Titanate
S. Shirasaki, H. Haneda and M. Sugimoto*, National
Institute for Research in Inorganic Materials, *TDK Corp.
177
- W-22 Determination of a Compositional Fluctuation in Perovskite
Ternary Systems
K. Kakegawa and Y. Sasaki, Chiba University 179
- W-23 Properties of AlN Ceramics
T. Takahashi, K. Anzai, N. Takada and K. Shinozaki, New
Materials Department, Toshiba Corp. 181
- W-24 New Generation PZT-Polymer Composite Material For
Hydrophone Applications
I. Bedwell and Z. Jandera, Plessey Australia Pty. Ltd.,
Australia. 183

INTRODUCTION: An upset technology is in the making for the fabrication of dielectric thin-films by polymeric sol-gel processing. This novel processing route avoids powder (and attendant problems), and produces films of exceptional quality at relatively low temperatures. The present study reports on recent measurements on ferroelectric and dielectric properties.

Preparation of Precursor Solution



Preparation of Gels and Films



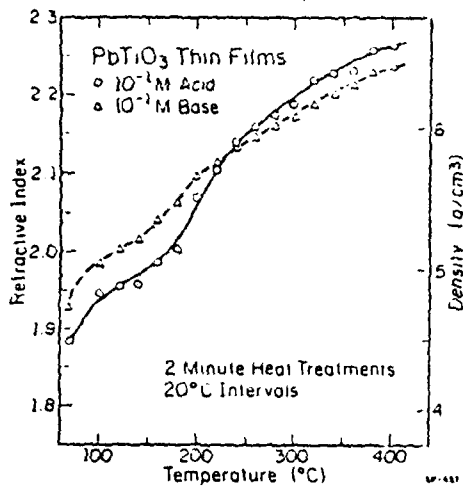
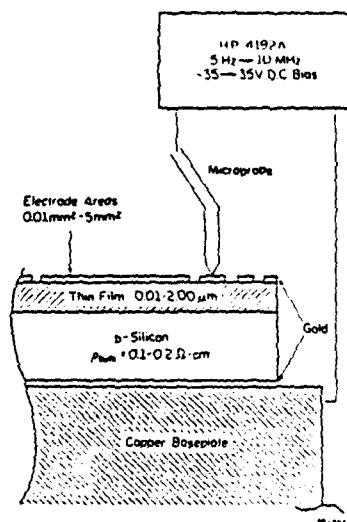
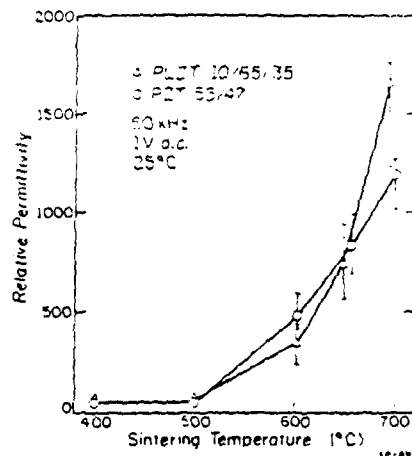
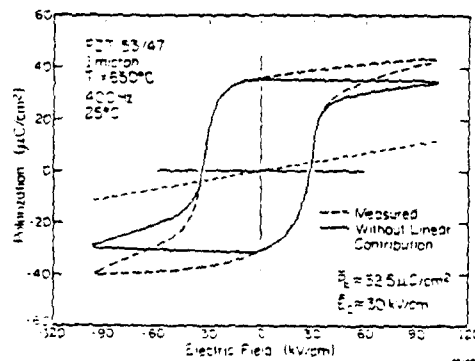
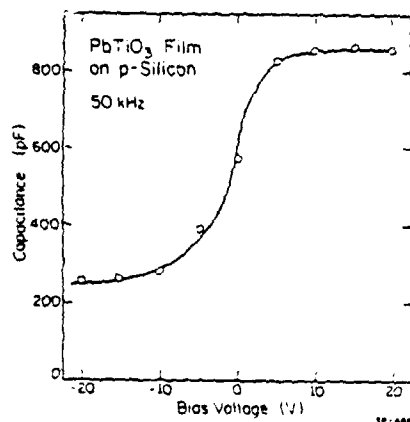


Table 1 Dielectric Properties of Sol Gel Derived Thin Films

Composition	Crystallinity	Permittivity	Dissipation Factor
PbTiO ₃	Amorphous	28 - 42	0.002 - 0.010
PbTiO ₃	Crystalline	155 - 185	0.006 - 0.020
PZT 53/47	Amorphous	35	0.005 - 0.010
PZT 53/47	Crystalline	300 - 1200	0.020 - 0.070
PLZT 10/65/35	Amorphous	35	0.005 - 0.010
PLZT 10/65/35	Crystalline	300 - 1700	0.020 - 0.030



SUMMARY: Dielectric thin-films of PbTiO₃ based materials were prepared by the spin-casting of a Pb, Ti-methoxyethoxide solution onto platinum, silicon and a variety of substrate materials. The resulting gel layers densified at relatively low temperatures (<350°C) with crystallization to the perovskite phase at 450-700°C, depending upon composition. The films were transparent and had electric strengths in excess of 100V/μm. Ferroelectric hysteresis loops were obtained for 1μm layers with grain sizes of 0.1μm. PZT 53/47 had P_R=32.5μC/cm², with E_C=30kV/cm; and the relative permittivity of PLZT 10/65/35 was 1700.

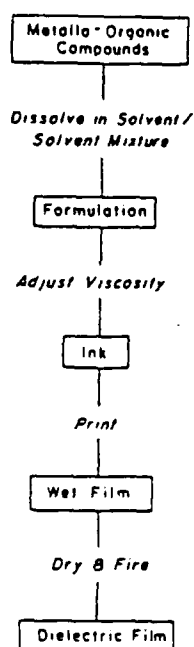


M2

PREPARATION AND PROPERTIES OF
FERROELECTRIC FILMS FROM
METALLO-ORGANIC PRECURSORS*

ROBERT W. VEST
PURDUE UNIVERSITY
W. LAFAYETTE, INDIANA

* SUPPORTED BY THE OFFICE OF NAVAL RESEARCH UNDER
CONTRACT No. N00014-83-K-0321



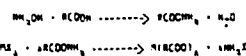
Flow chart of MOD process for dielectric films.

COMPOUND REQUIREMENTS

1. THERMALLY DECOMPOSE WITHOUT MELTING OR EVAPORATING TO GIVE THE METAL OR METAL OXIDE PLUS VOLATILE SPECIES
2. HIGH METAL CONTENT
3. HIGH SOLUBILITY IN COMMON SOLVENTS
4. STABLE UNDER AMBIENT CONDITIONS
5. COMPATIBLE WITH OTHER COMPOUNDS IN THE FORMULATION
6. COST EFFECTIVE TO PRODUCE AND HANDLE

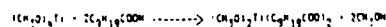
SYNTHESIS

Double Decomposition from Ammonium Salt

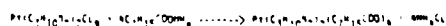
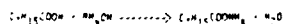
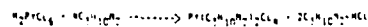


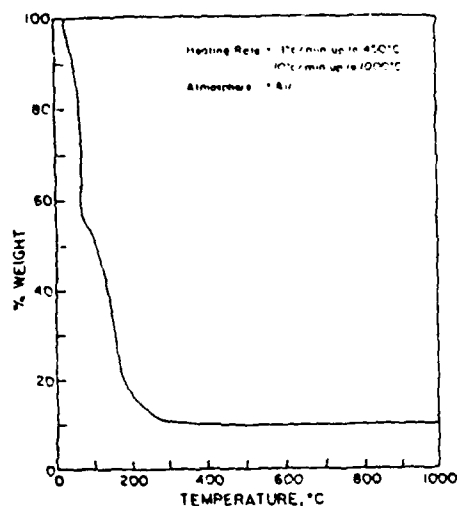
Metal	Acid	OS
Ba	NEODECANOIC	BaCl ₂
Pb	NEODECANOIC	Pb(HO ₂) ₂
Sn	NEODECANOIC	SnCl ₂
In	2-ETHYLBENZOIC	InCl ₃
Sb	2-ETHYLBENZOIC	SbCl ₃
Bi	2-ETHYLBENZOIC	Bi(HO ₂) ₃

Titanium Dioxide-Neodecanoic

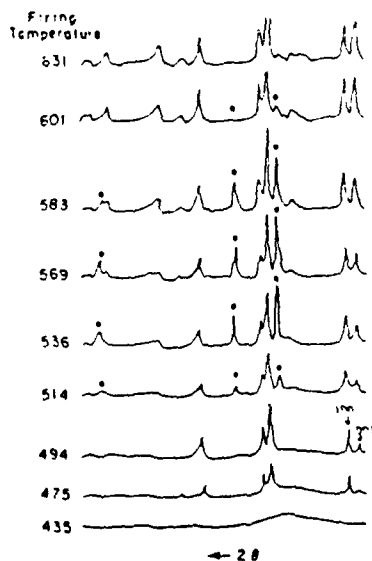


Platinum Oxide-2-Ethylbenzoic

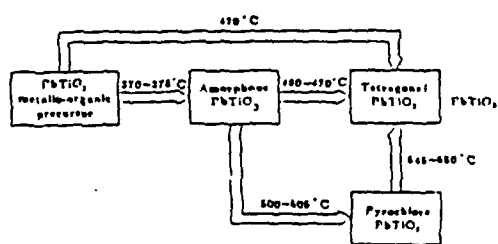




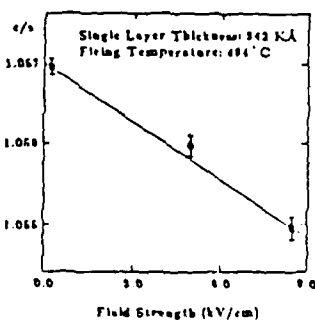
Thermogram of lead titanate formulation in air.



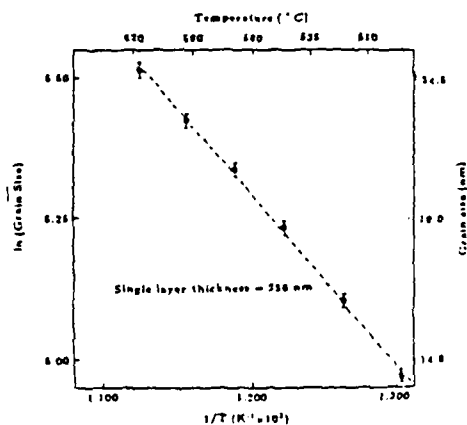
X-ray diffraction patterns (with CuK α for film) (1 μ) fired on Pt foil at various temperatures. The indicated peaks are not characteristic of tetragonal PbTiO $_3$.



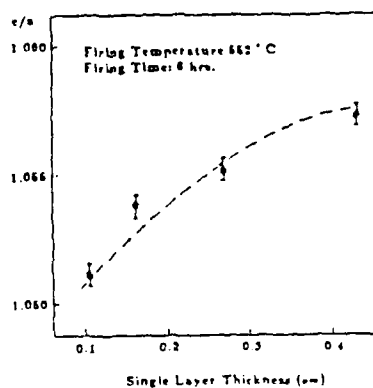
Phase transforming diagram for the PbTiO $_3$ system prepared by the MDS process



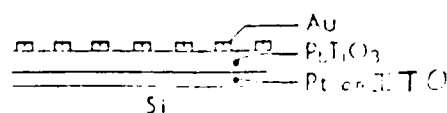
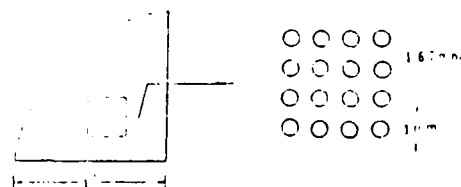
The dependence of c/a on D.C. electrical field strength during firing for the film with 2.42 μ m single layer thickness.



The grain size dependence of PbTiO $_3$ films on firing temperature.



The dependence of c/a on the single layer thickness



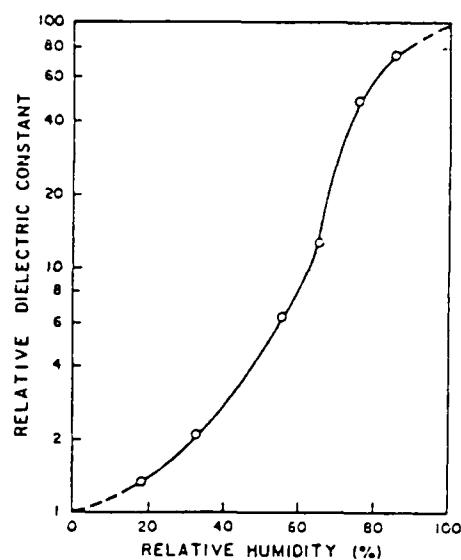
SEM illustration of planar capacitor made by Pt/PbTiO₃/Pt

After deposition of capacitor, all the capacitors in a 2 cm x 2 cm area were fired in air at 500°C for 8 hr.

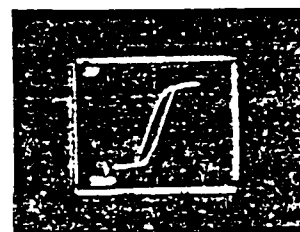


TEM X30,000 1 cm = 0.3 μm

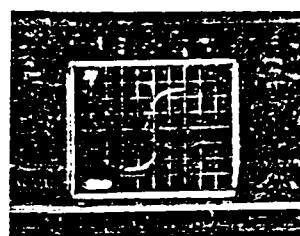
PbTiO₃ film deposited on one layer Pt (~10 nm) coated Si wafer fired at 500°C for 8 hr. in air.



The effect of relative humidity on the room temperature dielectric constant of PbTiO₃ films



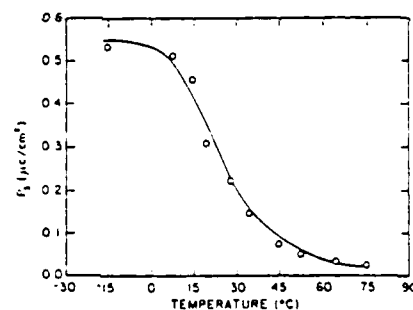
70°C



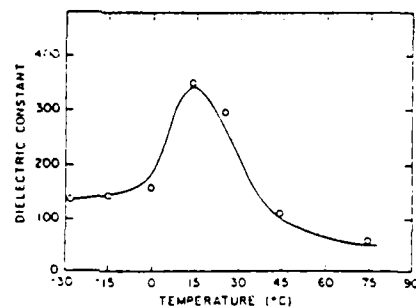
170°C

x: 85.0 kV/cm/div.
y: 0.254 μC/cm²/div.
f=50 Hz

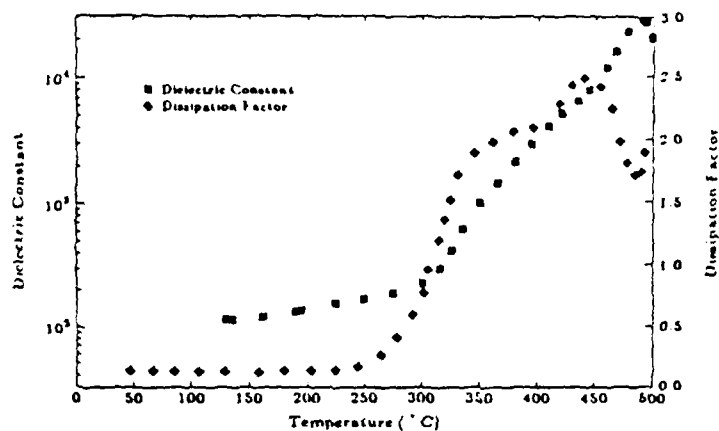
Ferroelectric Hysteresis Loop for Pb_{0.37}Sr_{0.63}TiO₃ Film of 26 nm Grain Size.



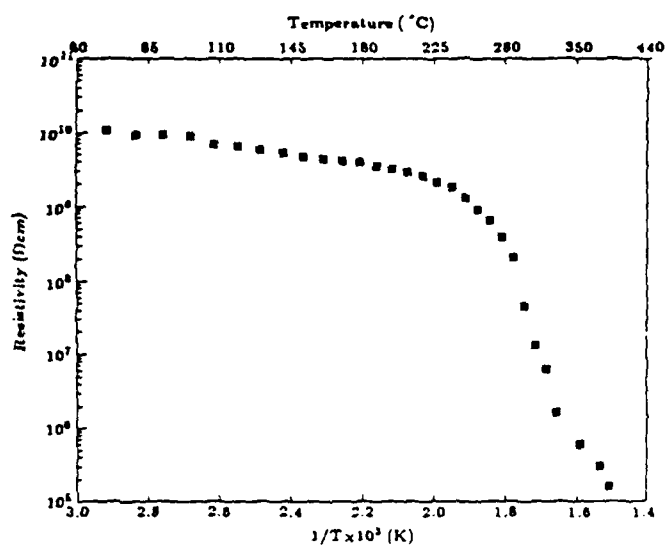
Temperature dependence of P_r for Pb_{0.37}Sr_{0.63}TiO₃ Film measured at 50 Hz (grain size = 26 nm)



Temperature dependence of Dielectric Constant for Pb_{0.37}Sr_{0.63}TiO₃ Film measured at 1 kHz (grain size = 26 nm)



The temperature dependence of dielectric constant and dissipation factor for a tetragonal PbTiO_3 film (1.8 μm thick).



The temperature dependence of D.C. resistivity of PbTiO_3 .

SUMMARY

1. DEFECT FREE FERROELECTRIC FILMS ($\geq 1\mu\text{m}$) OVER 2 CM. X 2 CM. AREA.
2. LOW TEMPERATURE PROCESSING (490°-700°C)
3. EASY CONTROL OF COMPOSITION (E.G., $\text{Pb}_x\text{Sr}_{1-x}\text{TiO}_3$).
4. CONTROL OF GRAIN SIZE AND ORIENTATION.
5. PbTiO_3 FILMS EXHIBIT BULK DIELECTRIC PROPERTIES.
6. $(\text{PbSr})\text{TiO}_3$ FILMS EXHIBIT RELAXOR BEHAVIOR.

Fabrication of Grain-Oriented $\text{KSr}_2\text{Nb}_5\text{O}_{15}$ Ceramics

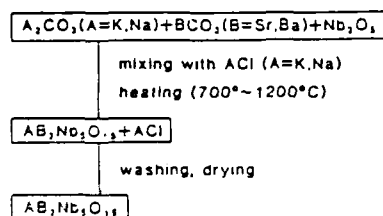
T. Kimura, Y. Ogino and
T. Yanaguchi

Keio University

Objectives

1. To prepare needle-like powder particles in alkali-alkaline earth niobate systems, $\text{AB}_2\text{Nb}_5\text{O}_{15}$.
2. To study the relation between direction of needle and crystal axis.
3. To prepare grain-oriented ceramics by normal sintering.

Powder Preparation



solid state reaction



with KCl



2μm

Fig. 1. Effect of molten salt on the particle shape of $\text{KSr}_2\text{Nb}_5\text{O}_{15}$. Molten KCl is necessary to prepare needle-like particles.

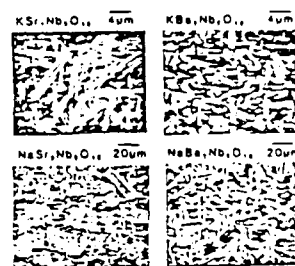


Fig. 2. Particle morphology depends on the chemical species of A and B. Small needle-like particles with large aspect ratio are obtained in the system $\text{KSr}_2\text{Nb}_5\text{O}_{15}$. 1200°C 1 h

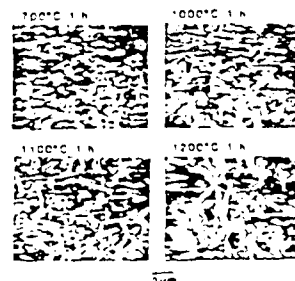


Fig. 3. Effect of preparation temperature on the particle morphology of $\text{KSr}_2\text{Nb}_5\text{O}_{15}$. Equiaxed particles formed at low temperature (700°C) grow to needle-like particles above 1100°C.

Forming and Sintering

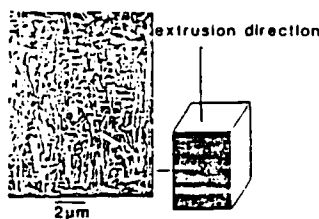
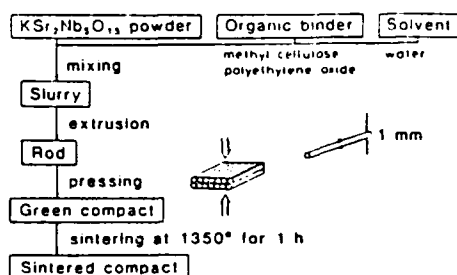


Fig. 4. SEM's of the surface of a green compact, indicating particle alignment.

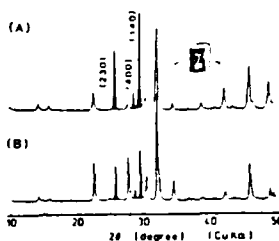


Fig. 5. X-ray diffraction patterns of (A) green compact and (B) sintered powder. The intensities of (hk0) lines are higher in the green compact, indicating orientation of crystal axis.

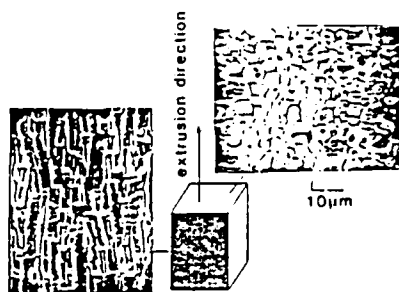


Fig. 6. SEM's of the sintered compact. Grains are rod-shaped and rod axes are aligned parallel to the extrusion direction.

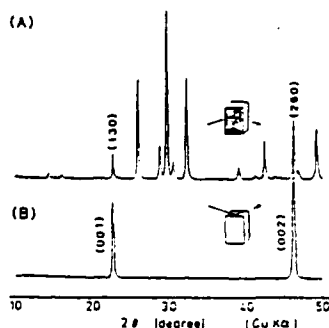


Fig. 7. X-ray diffraction patterns of a sintered compact. The intensities of (hk0) lines increase by sintering (A). Only (00l) lines are observed in the plane perpendicular to the extrusion direction (B).

These results indicate that c-axis (polar axis) is parallel to the needle axis.

Conclusions

1. Small needle-like particles with large aspect ratio are obtained in the system $\text{KSr}_2\text{Nb}_5\text{O}_{15}$.
2. The needle axis is parallel to c-axis, which is the polar axis.
3. Grain-oriented ceramics are obtained by extrusion forming and normal sintering.

Properties of Sub-micron BaTiO_3 with Additives
for Low Firing Temperature

Kazunobu Abe, Masashi Aoki, Kiyoshi Fukai
and Kazuhisa Hidaka

Research and Development Division, Sakai Chemical
Industry Co., Ltd., Sakai, Osaka Japan

We previously reported on the powder properties, sintering properties and electrical properties of Barium Titanate powder obtained by hydrothermal synthesis. This powder was easily sinterable; its particles are spherical in shape, uniform in size (0.1 μm) and sinterable at 1,200°C.

In this study, examined were the sintering and electrical properties of Barium Titanate powder with an additive for low firing temperature. Comparisons were made among three powder production methods, i.e. the hydrothermal synthesis method, the oxalate method and the calcination method, and among various additives for low firing temperature. As a result, it was found that the hydrothermal synthesis method provides the most excellent sintering and electrical properties for Barium Titanate powder with an additive for low firing temperature. The sample powder with one of the tested additives, in particular, was found to sinter at 1,000°C when added even in a very small amount (0.5 ~ 1.0 mole%) and therefore maintain an excellent electrical properties. It can be expected that the use of

Barium Titanate produced by the hydrothermal synthesis method and this additive in combination will contribute to the cost reduction for multilayer capacitors because it raises the ratio of Ag content of Pd-Ag alloy used in the internal electrode.

In addition, it was found that when some additives are used, an unique sintered product maintaining a cubic system is obtained.

1. Introduction

The authors previously suggested that Barium Titanate produced by the hydrothermal synthesis method not only satisfies the requirements of ceramic production, i.e. "fine", "spherical", "uniform", and "highly pure", but also possesses excellent packing property and low temperature sinterability.

It is already known well that sintering temperature of Barium Titanate can be reduced also by adding glassy materials having a low melting point. It is expected that sintering temperature will be further reduced by adding such an additive for low firing temperature to easily sinterable Barium Titanate obtained by the hydrothermal synthesis method. It is also expected that the amount of additives will decrease. Based on this expectation, the authors made measurements of the sintering and electrical properties of Barium Titanate powders produced by the hydrothermal synthesis method, the oxalate method, and the calcination method, respectively, with an additive for low firing temperature, after which they were compared with each other.

When mixed with 0.5 mole% of an Additive A, Barium Titanate produced by the hydrothermal synthesis method sintered at 1,000°C and exhibited sintering density of 5.81 g/ml; the sintered product from this mixture possessed excellent electrical properties, i.e. its relative permittivity (at 20°), dielectric loss, Curie temperature, and relative permittivity (at the Curie temperature) were 2817, 1.4%, 122°C, and 3783, respectively.

In addition, it was found that an unique sintered product having a cubic system which cannot be obtained from Barium Titanate produced by either the calcination method or the oxalate method, can be obtained by using another additive (Additive B, C, or D).

2. Experimental Methods and Materials

2.1 Samples

The following 3 Barium Titanate powders were used as samples:

- (a) Barium Titanate powder (Ba/Ti ratio = 1.01) produced by the hydrothermal synthesis method
- (b) Barium Titanate powder (1.1 μ m in mean particle size) produced by the calcination method
- (c) Commercially available Barium Titanate powder produced by the oxalate method

The Ba/Ti ratios and impurity contents of these powders were determined by fluorescent X-ray analysis and chemical analysis, respectively.

2.2 Additives

The 5 additives shown in Table 1 were each added to

each powder sample in a specified amount. Mixing was carried out in a polyethylene pot containing zirconia balls and acetone overnight.

2.3 Molding

PVA in an 8wt% aqueous solution was added in a 0.8wt% ratio to each powder sample supplemented with an additive and granulated in an agate mortar, after which the resulting granules were sieved through a 35-mesh sieve. 2.2g of the sieved granules were then placed in a die (20 mm ϕ) and pressed under 1T/cm² pressure for 1 minute, yielding a green mold. The resulting green mold, after drying at 110 ~ 120°C overnight, was subjected to measurements of weight and dimension to determine its green density.

2.4 Sintering

Each resulting green mold was heated at a temperature rise rate of 200°C/hr and maintained at a specified temperature for 3 hours. During the heating, the green mold was maintained at 400°C for 3 hours to burn out the PVA. After the completion of the firing, each fired product was cooled down to a temperature reducing rate of 200°C/hr, after which the sintering density of the resulting sintered pellet was determined by Archimedes's method.

2.5 Electrical properties

The both sides of each sintered pellet was polished to a thickness of approx. 1.0mm, after which they were coated with Ag using an ion coater for the determination of electrical properties. Curie temperature was determined as follows: Each sample was placed in a chamber

adjusted to a heating rate of 0.5°C/min and subjected to measurements of changes in capacitance at 1KHz using an LCR meter 4332A (HP). Both relative permittivity and dielectric loss at room temperature were determined at 1KHz using an LF impedance analyzer 4192A (HP). Resistivity was measured at 20°C after 1 minute of application at DC 25V using a PA meter/DC voltage source 4140B (HP).

2.6 X-ray diffraction analysis

Using an X-ray diffraction analyzer RAD-II (Rigaku Denki), measurements were made of the X-ray diffraction of each Barium Titanate powder and of each sintered pellet between 44° and 46° by CuK α radiation.

2.7 Grain size determination

The natural surface and if necessary, polished/thermal etched surface of each sintered pellet were observed by optical microscopy (magnification: $\times 1200$) and scanning electron microscopy to observe its grain.

3. Results and Discussion

3.1 Powder properties

Table 2 shows the powder properties of each Barium Titanate powder. Figure 1 shows the TEM micrographs of the powder samples.

As shown in Table 2 and Figure 1, Barium Titanate powder produced by the hydrothermal synthesis method is the most excellent among the three powder samples in particle shape (spherical), particle size (0.1 μ m), and particle size distribution (uniform). There is no significant

difference among the three in purity; because the hydrothermal synthesis method and the oxalate method are both wet reactions and the calcination method uses high-purity Barium Carbonate and high-purity Titanium Dioxide as the starting materials.

3.2 Sintering property

Figures 2 ~ 7 show the temperature dependence of sintered density for 3 kind of BaTiO_3 , either with or without an additive. As shown in these figures, the Barium Titanate powder produced by the hydrothermal synthesis method is the most easily sinterable independent of whether or not an additive is added; its sintering temperature is $100 \sim 150^\circ\text{C}$ and $150 \sim 200^\circ\text{C}$ lower than that of the Barium Titanate powder produced by the oxalate method and that of the powder produced by the calcination method, respectively. Based on this finding, it is thought that the low temperature sinterability of the main raw material rather than the effect of additives is an important factor for low temperature firing.

Additive E is the most effective additive for low firing temperature, but its requirement for significant amount of addition has an adverse effect on the electrical property of the sintered product. On the other hand, Additive A makes it possible to perform sintering at $1,000^\circ\text{C}$ even it is added in a small amount, thus having a less effect on the electrical property of the sintered product; it is thought of as the most excellent additive for low firing temperature.

3.3 X-ray diffraction analysis

Figures 8-11 show the typical X-ray diffraction patterns of various sintered pellets and powders. The Barium Titanate powder produced by the hydrothermal synthesis method is cubic, while the Barium Titanate powder produced either by the oxalate method or by the calcination method is tetragonal due to calcination in the production process. The X-ray diffraction pattern of the sintered pellet of Barium Titanate powder produced by either the oxalate method or the calcination method shows the presence of tetragonal system independent of additive type and sintering temperature. On the other hand, the Barium Titanate powder produced by the hydrothermal synthesis method exhibits a unique sintering behavior. That is, when it is sintered in the absence of an additive, it changes in crystal system to tetragonal at approx. 900°C; when it is sintered in the presence of an additive, its sintering behavior depends upon additive type, i.e., it changes in crystal system to tetragonal in the presence of Additive A or E, while it maintains a cubic system when sintered in the presence of Additive B, C or D.

3.4 Electrical properties

Figure 12 shows the typical temperature dependence of the relative permittivity of various sintered pellets. Table 3 shows the electrical properties of various sintered pellets at the minimum firing temperature for sintering. Based on the data shown in these figures and table, Additive A can be regarded as an excellent additive for low firing temperature. In addition, this additive produces

little shift in the Curie temperature of the sintering products; it is therefore conjectured that nearly all components of this additive are distributed in the grain boundary region.

4. Conclusions

Powder samples prepared by adding various additives for low firing temperature to Barium Titanate synthesized by various production methods were subjected to sinterability determination, crystal structure analysis for sintered pellet by X-ray diffraction, and electrical property determination, after which they were compared with each other. The results obtained are summarized as follows:

- (1) The Barium Titanate powder produced by the hydrothermal synthesis method was found to be more easily sinterable than that produced by oxalate method and calcination method even if additive were used.
- (2) It was found that the sinterability of Barium Titanate was the most important factor for low firing temperature even if additives were used.
- (3) Of the tested additives for low firing temperature, Additive A proved the most suitable to Barium Titanate sintering independent of production method type.
- (4) It was found that when some additives were used, a sintered pellet maintaining a cubic system can be obtained from Barium Titanate powder produced by the hydrothermal synthesis method.

Table 1. Additives

Additive	Content
A	1.0 wt%
B	1.0 wt%
C	1.0 wt%
D	5 wt%
E	5 wt%

Table 2. Preparation method of BaTiO_3 and its properties

Property	Preparation Method (Solid Phase Reaction)	Oxalate Method (Thermal decomposition of Barium Titanate Oxalate)	Hydrothermal Synthesis
Particle shape	like crush stone	like crush stone	spherical
Particle size	coarser than $3 \mu\text{m}$	about $0.5 \mu\text{m}$	about $0.1 \mu\text{m}$
Particle size distribution	very wide	wide	narrow
BET Surface Area (m^2/g)	1	2	12
Bulk density (g/cc)	0.83	0.72	0.59
Impurity (wt%)			
SiO_2	0.01	0.011	0.01
Al_2O_3	0.01	0.011	0.011
Fe_2O_3	0.02	0.011	0.011
Fe_2O_3	0.011	0.011	0.011



Calcination Method



Oxalate Method



Hydrothermal synthesis

Fig. 1. TEM photographs of BaTiO_3 powders ($\times 10000$)

Table 3. Properties of Sintered Products including an Additive

Preparation Method	Additive	Firing Temperature ($^{\circ}\text{C}$)	Sintered density (g/cc)	Grain size (μm)	Relative Permittivity		Curie Point ($^{\circ}\text{C}$)	Tan δ (%)	Resistivity (Ωcm)
					20 $^{\circ}\text{C}$	Max			
Hydrothermal Synthesis	H0	1200	5.83	0.1	2228	6430	125	0.01	1.9×10^{11}
	A	1000	5.82	0.8	2517	3763	122	1.40	2.4×10^{12}
	B	1100	5.78	0.48	1998	2597	127	3.10	6.0×10^{11}
	C	1100	5.53	0.34	1023	1023	112	1.25	5.7×10^9
	D	1100	5.53	0.34	1218	2095	110	3.27	3.8×10^{10}
	E	900	5.64	11.5	825	2223	120	1.70	1.0×10^{11}
Oxalate Method	H0	1200	5.83	4.3	2147	10189	120	3.28	8.7×10^{11}
	A	1100	5.78	2.8	2230	4845	123	2.84	1.5×10^9
	B	1300	5.27		cannot be sintered				
	C	1200	5.45	7.0	1110	6225	120	3.21	4.4×10^{10}
	D	1200	5.53	2.8	1712	6561	120	4.87	2.5×10^9
	E	1000	5.70	4.3	1874	4481	144	18.5	2.1×10^9
Calcination Method	H0	1250	5.84	7.7	2012	9023	124	1.54	1.0×10^{10}
	A	1100	5.85	12.0	2113	6210	116	1.12	2.0×10^{12}
	B	1200	5.80	2.0	1774	5229	120	2.86	4.0×10^{11}
	C	1200	5.53		cannot be sintered				
	D	1220	5.81	2.5	1477	5740	122	3.04	2.3×10^{11}
	E	1000	5.54	10.8	236	1031	144	5.17	8.0×10^9

F: cubic system at room temperature

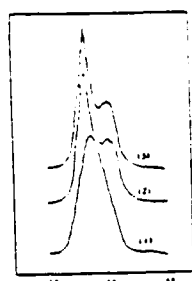


Fig. 8 X-ray diffraction patterns of BaTiO_3 prepared by hydrothermal synthesis (1) without additive (2) with additive A (3) with additive B.



Fig. 9 X-ray diffraction patterns of sintered BaTiO_3 prepared by hydrothermal synthesis (1) without additive (2) with additive A (3) with additive B.

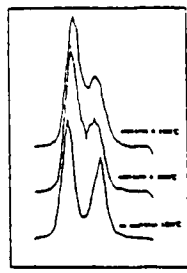


Fig. 10 X-ray diffraction patterns of sintered BaTiO_3 prepared by hydrothermal synthesis (1) without additive (2) with additive A (3) with additive B.

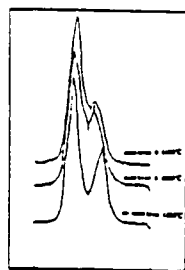


Fig. 11 X-ray diffraction patterns of sintered BaTiO_3 prepared by hydrothermal synthesis (1) without additive (2) with additive A (3) with additive B.

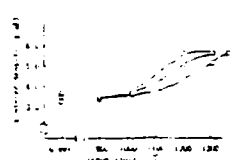


Fig. 2 Sintering density curves of BaTiO_3 prepared by hydrothermal synthesis (1) without additive (2) with additive A (3) with additive B.

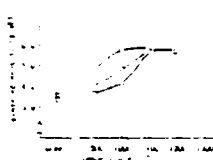


Fig. 3 Sintering density curves of BaTiO_3 prepared by hydrothermal synthesis (1) without additive (2) with additive A (3) with additive B.

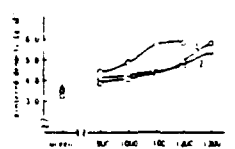


Fig. 4 Sintering density curves of BaTiO_3 prepared by hydrothermal synthesis (1) without additive (2) with additive A (3) with additive B.

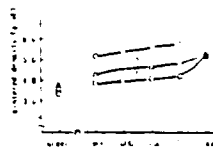


Fig. 5 Sintering density curves of BaTiO_3 prepared by hydrothermal synthesis (1) without additive (2) with additive A (3) with additive B.

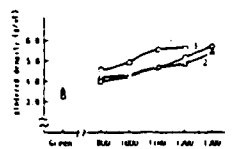


Fig. 6 Sintering density curves of BaTiO_3 prepared by hydrothermal synthesis (1) without additive (2) with additive A (3) with additive B.

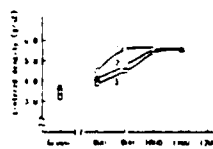


Fig. 7 Sintering density curves of BaTiO_3 prepared by hydrothermal synthesis (1) without additive (2) with additive A (3) with additive B.

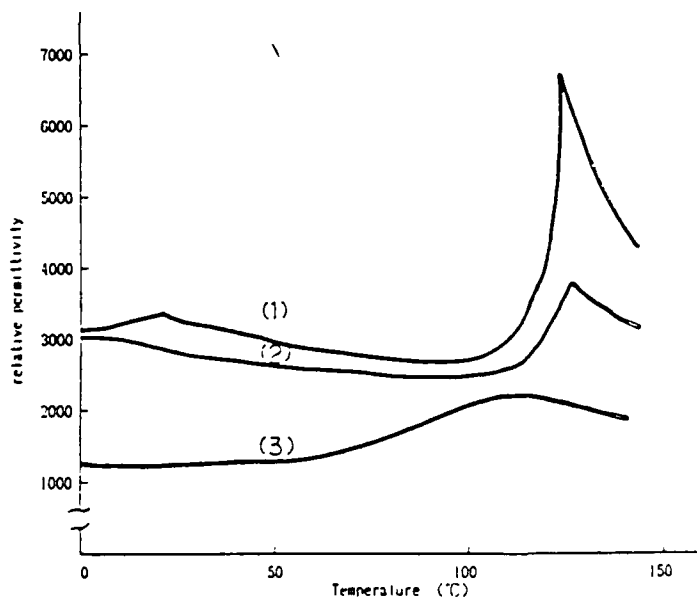


Fig. 12 Temperature dependence of relative permittivity for sintered BaTiO_3 products prepared by hydrothermal synthesis (1) without an additive (2) with an additive A (3) with an additive B.

EFFECT OF TREATMENT ON POLYMER GROWTH OF POLYMER-CLAY COMPOSITE

SHIROGUCHI, T. / SYOHEI, M. / OGATA, T. / OGATA, T. / OGATA, T.

CERAMIC COMPONENTS, R&D DIVISION
TOKYO CERAMIC CO.

Table 1. a) Composition of samples (wt.%)

Sample	BaCO ₃	TiO ₂	SiO ₂	Al ₂ O ₃
A	80	10	5	5
B	70	10	10	10
C	60	10	15	15

b) Preparation method of samples

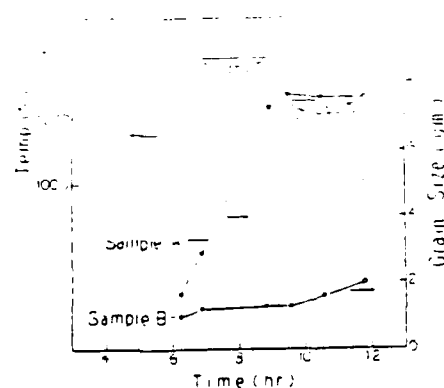
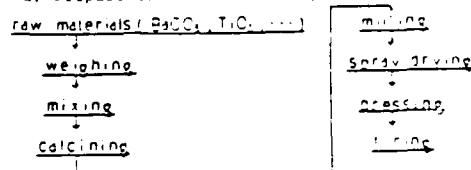


Fig. 1. Change of grain sizes of sample A and B by Rapid Cooling Experiment

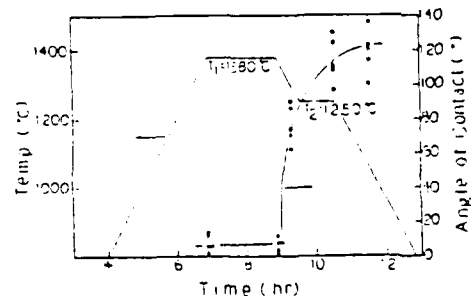


Fig. 2. Angle of contact by Rapid Cooling Experiment (sample B)

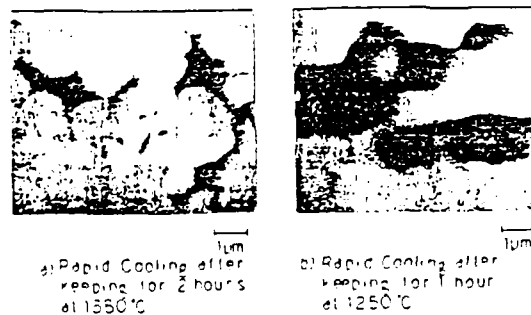


Photo 1. Microstructures of sample B observed by SEM (Composition Image)

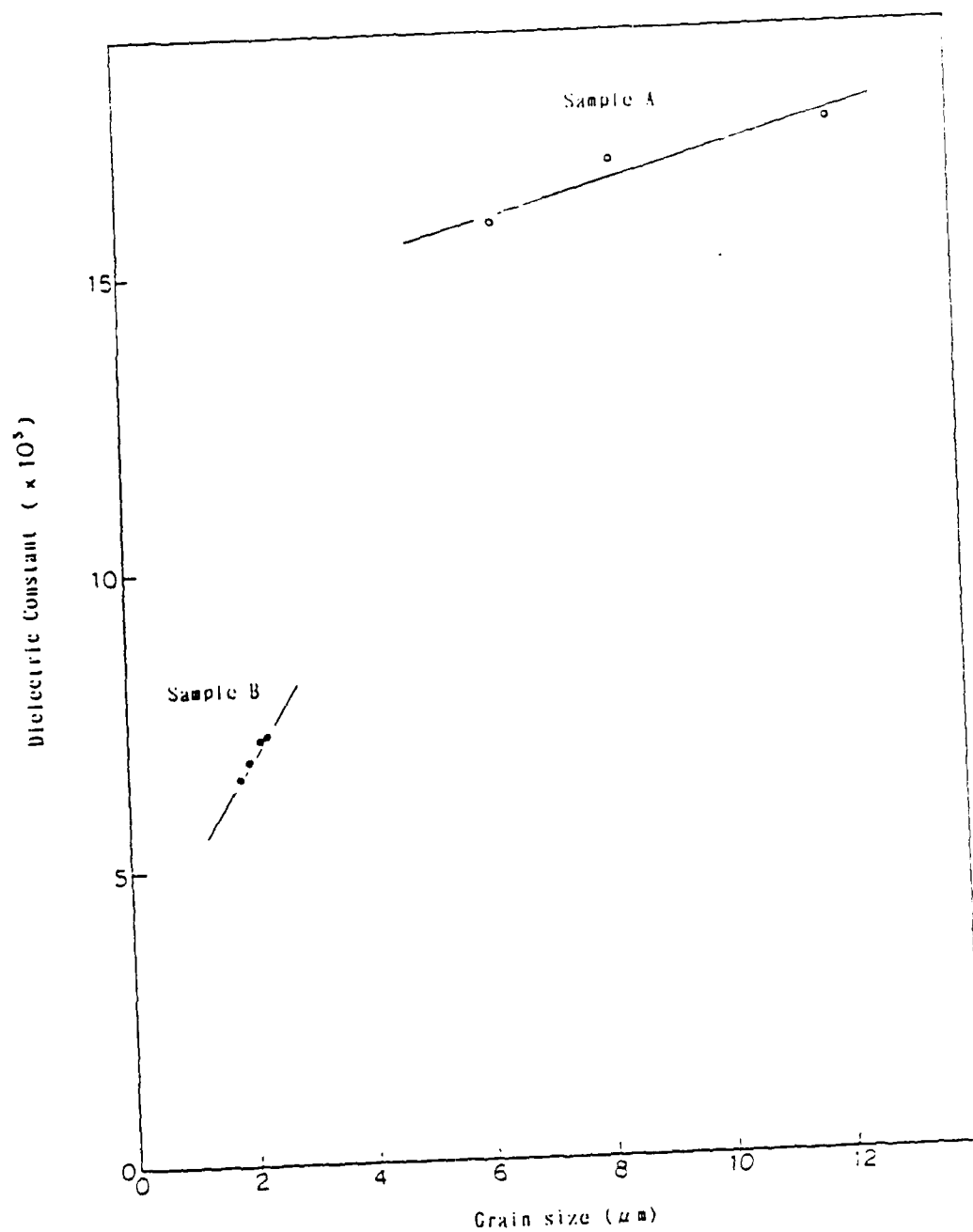


Fig.3. Relation between dielectric constant and grain size

MACHINING OF PZT, PT, AND (Mn, Zn)Fe₂O₄ CERAMICS

BY LASER-INDUCED CHEMICAL ETCHING

T. SHIOSAKI and A. YAWABAIA

Department of Electronics, Faculty of Engineering,

Kyoto University, Kyoto, 606, Japan

ABSTRACT: Laser-enhanced chemical etching of PbTiO₃, PZT and (Mn-Zn)-ferrite ceramics is reported. The KOH solution of 10 mol/l is suitable for the laser enhanced inter-granular etching of the PbTiO₃ and PZT with depth etching rate higher than 100 $\mu\text{m/s}$ in the initial laser irradiation period of Ar⁺ laser of 1W.

The KOH and NaOH solutions are also suitable for the inter-granular etching of (Mn-Zn)-ferrite. The H₃PO₄ solution of 6 mol/l is suitable for the laser enhanced trans-granular etching of (Mn-Zn)-ferrite with the depth etching rate of about 10 $\mu\text{m/s}$ in the initial irradiation period of an Ar⁺ laser of 1W.

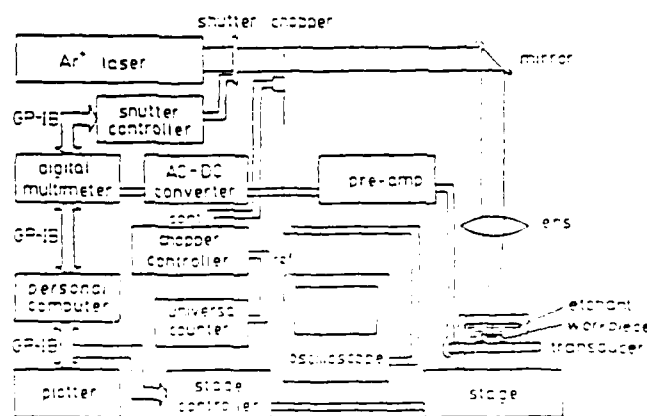


Fig. 1. Experimental setup for laser-induced chemical etching. The photo-adjustable armature detected by the transducer is used for the automatic focusing. The convex lens is of quartz with a focal length of 100 mm.

Table 1. Solubility of PZT and PbTiO₃ ceramics in various etchants

	PZT	PbTiO ₃	TiN AlN/AlN
HF(10wt%)	0.0108mg/10min	0.0122mg/10min	0.0078mg/10min
HCl(10wt%)	0.0091	0.0015	0
HNO ₃ (10wt%)	0.0081	0.0015	0.0025
H ₂ SO ₄ (10wt%)	0.0425	0.0011	0.0011
H ₂ SO ₄ (95%)	0.087	0.0178	0
HCl(35%)	0.68	0.058	0.003
HNO ₃ (40%)	0.15	0.047	0.007
(COOH) ₂ (4%)	0.014	0.0058	0.008

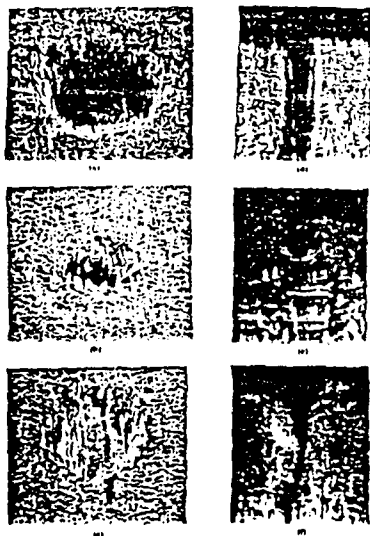


Fig. 2. SEM photographs of laser etched samples of modified PbTiO₃ ceramics using 1W incident Ar⁺ ion laser power. Holes produced with 5s exposure in (a) 10mol/l KOH, (b) air and (c) water. Slots in (d) 10mol/l KOH, (e) air and (f) water scanned at 8mm/min.

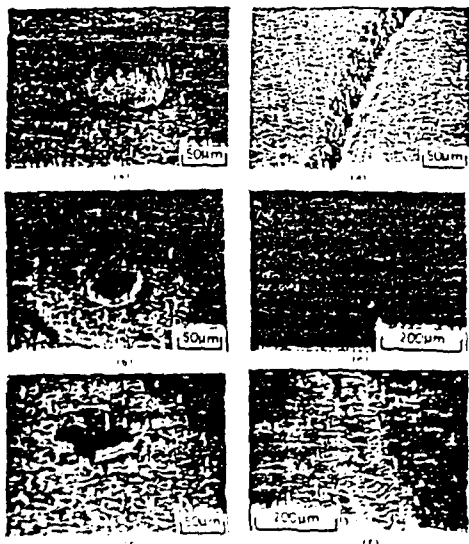


Fig. 3. SEM photographs of laser etched PbTiO₃ ceramics using 1W incident Ar⁺ ion laser power. Holes produced with 5s exposure in (a) 10mol/l KOH, (b) air and (c) water. Slots in (d) 10mol/l KOH, (e) air and (f) water scanned at 8mm/min.

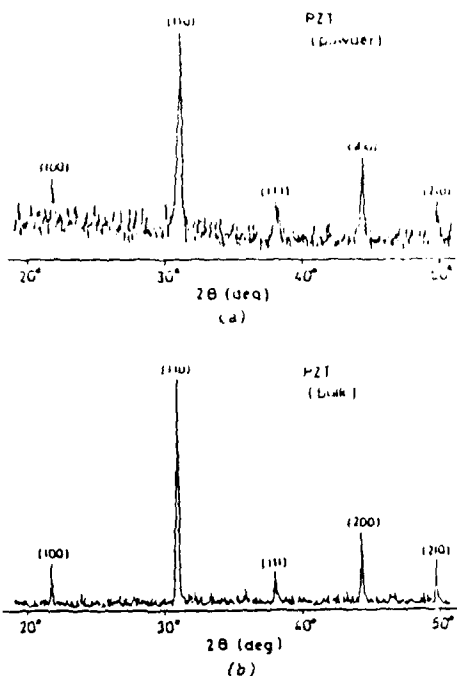


Fig. 4. The X-ray diffraction patterns of the powders (a) and bulk (b) of PZT. The PZT powders are collected from the etchant.

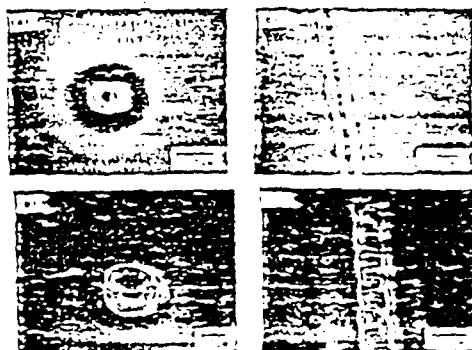


Fig. 5. SEM photographs of laser etched PbTiO₃ ceramics using 1W incident Ar⁺ ion laser power. Holes produced with 5s exposure in (a) 10mol/l KOH, (b) air and (c) water. Slots in (d) 10mol/l KOH, (e) air and (f) water scanned at 8mm/min.

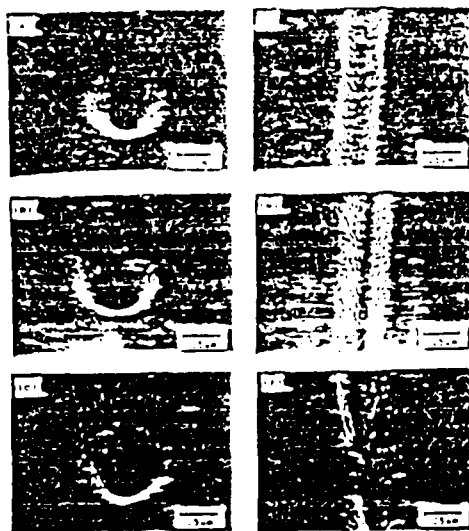


Fig. 8. SEM micrographs of laser etched $\text{Mn}_2\text{FeP}_2\text{O}_7$ processed using 35mm incident laser power. Notes made with 10 exposure in (a) 2mol/l NaOH, (b) 2mol/l NaOH and (c) 2mol/l H_2PO_4 . Slits in (d) 2mol/l NaOH, (e) 2mol/l NaOH and (f) 2mol/l H_2PO_4 scanned at 5mm/min.

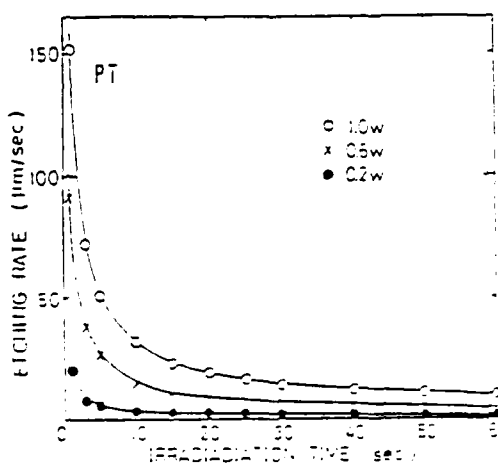


Fig. 9. Etching rate dependence of etching depth rate of PT. The etching rate is 10mm/min. The laser output is 1W and NaOH solution is 2mol/l.

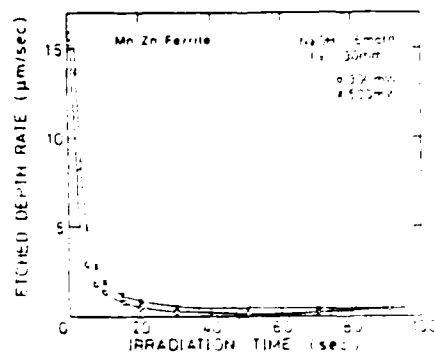


Fig. 10. Etching rate dependence of etching depth rate of Mn₂Zn Ferrite. The etching rate is 10mm/min. The laser output is 1W and NaOH solution is 2mol/l.

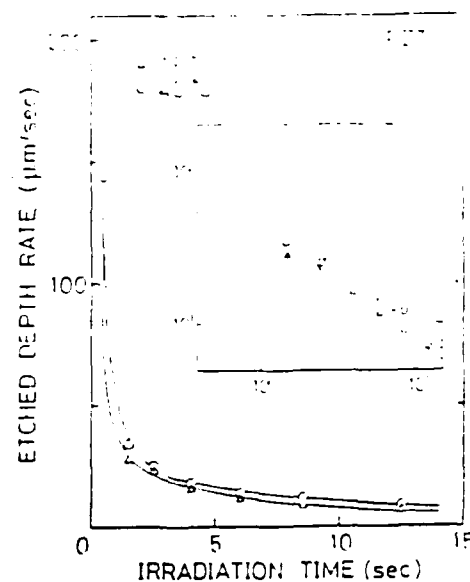


Fig. 11. The relation between the laser-induced etching rate and the laser irradiation time. The laser output is 1W and NaOH solution is 2mol/l.



Fig. 12. The appearance of holes on laser-etched surfaces of PT and PbTiO₃ on terrapins using 35mm incident laser power. Notes processed with 10mm/min exposure at 10mm/min.

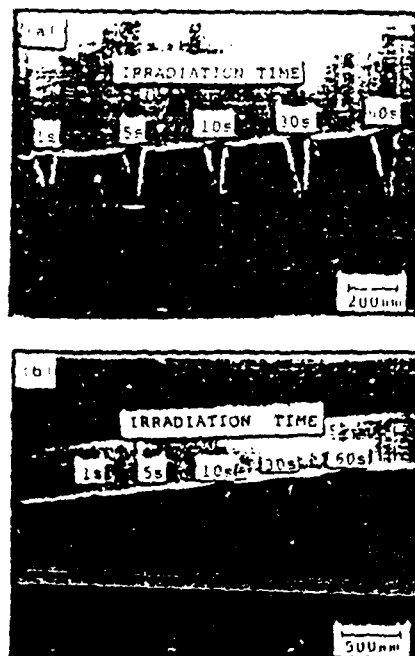


Fig.11. The appearances of holes of laser etched $\text{Mn, Zn/Fe}_2\text{O}_3$ ceramics using 1W incident laser power. Holes processed with 1 to 60s exposure in (a) 6mol/l NaOH and (b) 6mol/l H_3PO_4 .

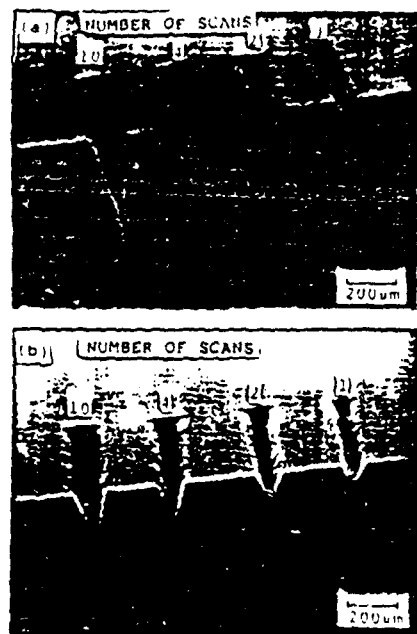


Fig.12. The appearances of slots of laser etched $\text{Mn, Zn/Fe}_2\text{O}_3$ ceramics. Slots made with 1 to 10 scannings using incident laser power of 1W in 6mol/l NaOH (a) and 0.5W in 6mol/l H_3PO_4 (b) scanned at 6mm/min.

SYNTHESIS AND PROPERTIES OF ALKOXY-DERIVED $Zr_xTi_ySn_{2-z}O_4$

S. HIRANO, T. HAYASHI and A. HATTORI

NAGOYA UNIV., JAPAN

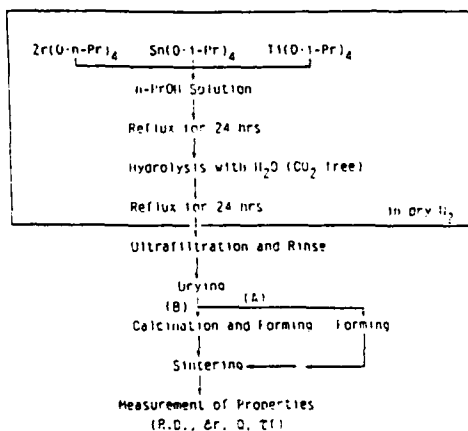
Introduction :

Many kinds of dielectric materials have been developed for microwave applications. Among them, the compound in the system $Zr-Ti-Sn-O$, $Zr_xTi_ySn_{2-z}O_4$ ($x+y+z=2$), is known to have a high dielectric constant, a low dielectric loss and a low temperature coefficient of resonance frequency. The compound has been sintered with the sintering aids like ZnO , NiO , Fe_2O_3 and La_2O_3 .

Objectives :

- 1) Preparation of monosized unagglomerated spherical particles by controlled hydrolysis of metal alkoxides
- 2) Sintering behaviors without additives
- 3) Dielectric properties (ϵ_r , Q , τ_f) of sintered bodies without additives

Experimental



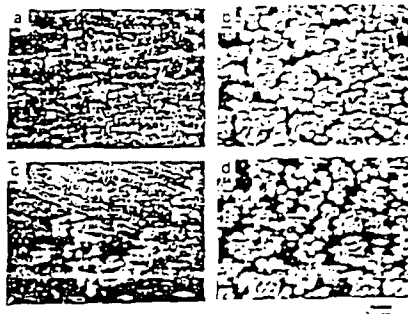
Results

Effect of Hydrolysis Conditions on Particle Size and Morphology of As-precipitates, $Zr_{0.30}Ti_{1.70}Sn_{0.20}O_4$

Conc. (mol/l)	Hydrolysis Temp.	Particle Size (μm)	Morphology
0.05	room temp.	< 0.1	Irregular
0.05	reflux	0.3-0.4	spherical
0.025	room temp.	0.1-0.2	spherical
0.025	reflux	0.3-0.4	spherical

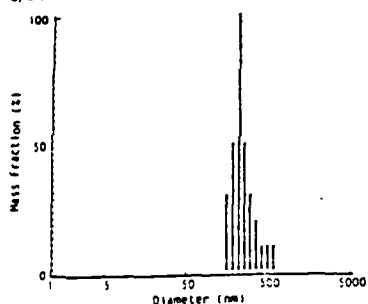
(As-precipitated powders were amorphous)

* Amount of water, 4 times the equivalent amount required for hydrolysis



SEM of as-precipitated powders

- a) 0.05 mol/l, room temp. b) 0.05 mol/l, reflux.
c) 0.025 mol/l, room temp. d) 0.025 mol/l, reflux

Particle Size Distribution of Alkoxy-derived $Zr_{0.30}Ti_{1.70}Sn_{0.20}O_4$ Effect of Processing on Sintering of $Zr_{0.30}Ti_{1.70}Sn_{0.20}O_4$

Particle Size (μm)	Process*	Relative Density (%)	
		Green Body	Sintered Body
0.1-0.2	A	49	96
0.3-0.4	A	55	92
0.3-0.4	B	55	80

*Process A: As-precipitates + Consolidation
+ Crystallization(650°C, 3hrs) + Sintering(1600°C, 2hrs)
Process B: As-precipitates + Calcination(650°C, 3hrs)
+ Forming + Sintering(1600°C, 3hrs)

Effect of Processing on Sintering of $Zr_{0.30}Ti_{1.70}Sn_{0.20}O_4$

Process*	Relative Density (%)		Shrinkage (%)
	Green Body	Sintered Body	
A	45	95	23.0
B	45	82	14.5

*Process A: As-precipitates + Consolidation
+ Crystallization(650°C, 3hrs) + Sintering(1600°C, 3hrs)
Process B: As-precipitates + Calcination(650°C, 3hrs)
+ Forming + Sintering(1600°C, 3hrs)

Densities and Phases of Sintered Bodies

Z	Bulk Density (g cm ⁻³)		Phases
	Green Body	Sintered Body	
0.20	2.92 (55)*	5.13 (98)*	Zr _{0.80} Ti _{0.20} Sn _{0.20} O ₄
0.30	2.85 (54)*	5.15 (98)*	Zr _{0.70} Ti _{0.30} Sn _{0.20} O ₄
0.40	2.99	5.10	Zr _{0.60} Ti _{0.40} Sn _{0.20} O ₄ , Ti ₂ SnO ₇

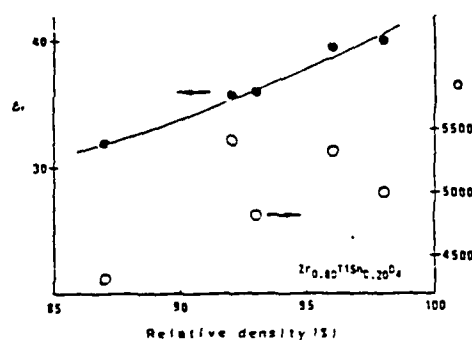
* Relative Density (%)

1600°C, 3hrs in O₂

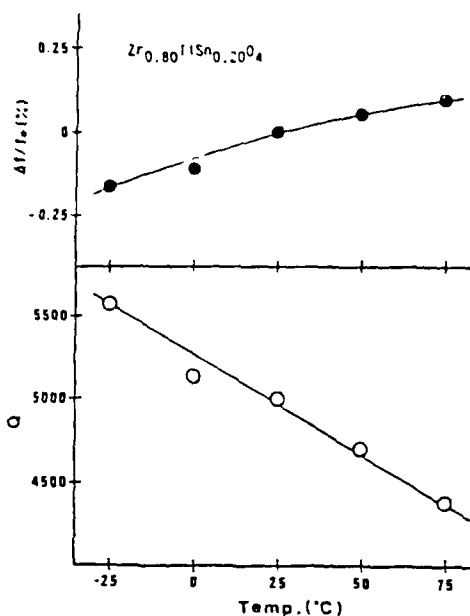
Properties of Bodies Sintered at 1600°C for 3 hrs

Z	R.D.(%)	Er	Q	Tf(ppm/°C)
0.00	100	46.2	2700	71.8
0.20	98	40.0	5000	2.6
0.30	98	37.7	5200	-10.6
0.40*	--	39.6	5000	45.2

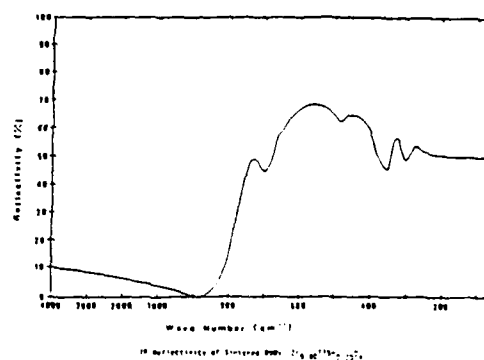
Zr_xTi_{1-x}Sn_{0.20}O₄, * not single phase at 10GHz



Changes of Er and Q with Relative Density of Sintered Body



Temperature dependences of Q and Δf/f



IR Spectroscopy of Sintered Body: Zr_{0.80}Ti_{0.20}Sn_{0.20}O₄

Conclusions

- 1) Monosized unagglomerated spherical particles of Zr_{0.80}Ti_{0.20}Sn_{0.20}O₄ were synthesized by controlled hydrolysis of metal alkoxides.
- 2) Dense sintered bodies of Zr_xTi_{1-x}Sn_{0.20}O₄ were prepared by sintering consolidated as-precipitated particles without sintering additives.
- 3) Dense sintered body of Zr_{0.80}Ti_{0.20}Sn_{0.20}O₄ showed good properties (Er=40.0, Q=5000 and Tf=3 ppm/°C) at 10 GHz.

EFFECT OF AGGLOMERATED PARTICLES ON PROPERTIES OF CERAMIC GREEN SHEETS.

Tamotsu Ueyama, Naoya Kaneko
and Yoichi Machii

Shinodate Research Laboratory,
Hitachi Chemical Co., Ltd.
1380-1 Tarazaki, Katsuta,
Ibaraki, 312 Japan.

Table 1 Typical composition of Al_2O_3 green sheets

Material	weight parts
Al_2O_3	100
Binder (Poly Vinyl Butyral)	6
Plasticizer (Butyl Benzil phthalate)	3
Solvent (Chlorinated Hydrocarbon & Alcohol Mixture)	Proper Quantity

Table 2 Typical composition of $BaTiO_3$ green sheets

Material	weight parts
$BaTiO_3$	100
Binder (Poly methyl methacrilat)	12.4
Plasticizer (Butyl Benzil phthalate)	1.4
Solvent (Chlorinated Hydrocarbon & Keton Mixture)	Proper Quantity

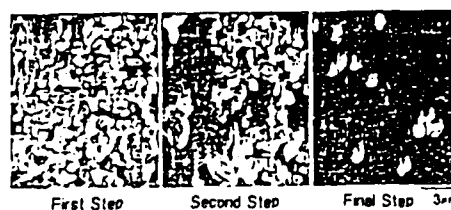


Fig.1 Agglomerated particle size of Al_2O_3 powder in slurry

Agglomerates size was measured by SEM on slurry sample diluted and dispersed with solvent and 28KHz ultrasonic wave treatment.

New advanced process: agglomerates Al_2O_3 powders were gradually pulverized during mixing, and the particle size was finally reduced to primary particles.

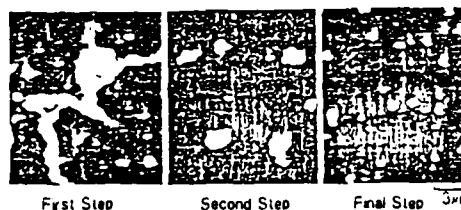


Fig 2 Agglomerated particle size of $BaTiO_3$ Powder in slurry

In conventional process, agglomerated particles of barium titanate were almost not pulverized, and agglomerated particle diameter was about $4.6\mu m$.

On the other hand, in the new advanced process, agglomerated particles were pulverized sufficiently, and the diameter became under $1.0\mu m$, which was nearly equal to primary particle diameter of $0.6\mu m$.

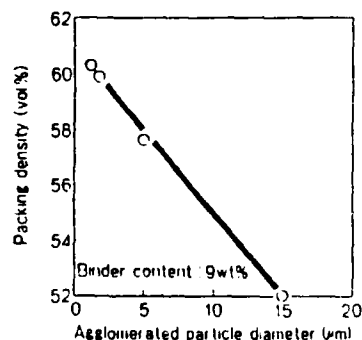


Fig. 4 Relationship between agglomerated particle diameter and packing density of Al_2O_3 green sheet

The smaller the agglomerates diameter, the higher the packing density of Al_2O_3 powders. Particularly, when agglomerates become the primary particle, packing density of Al_2O_3 powders reaches the maximum value of 60.3 vol%.

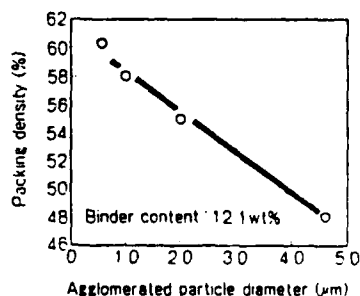


Fig. 7 Relationship between agglomerated particle diameter and packing density of BaTiO_3 green sheet

The packing density (P) in the green sheet is calculated in accordance with expression (1), when green sheet density (pg), dielectric powder density (pd) and weight component ratio Xd of dielectric powder in the green sheet are measured.

$$P = pg \cdot Xd / pg \quad (1)$$

When agglomerates are pulverized the packing density gradually increases, and reaches the saturation value of 60.4 vol% when the size of the primary particles is attained. This value is almost equal to the packing density of 60.45 vol% calculated with monosized powders cast without pressure.

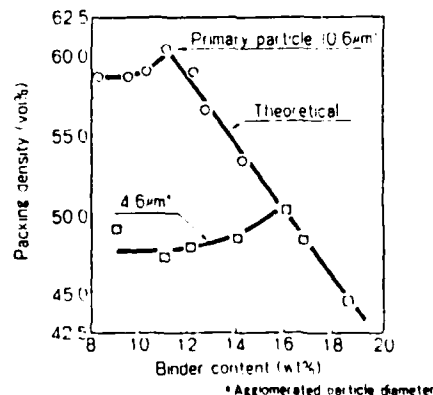


Fig. 9 Relationship between binder content and packing density of BaTiO_3 green sheet

The smaller agglomerated particle diameter and/or binder content was, the higher packing density of barium titanate powders became.

Particularly, when agglomerated particle diameter was below 1 μm, packing density reached the maximum value of 60.4 vol% at the binder content of 11.1 wt%.

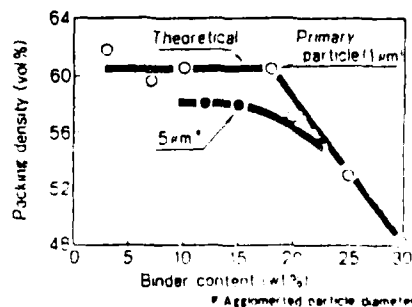


Fig. 10 Relationship between binder content and packing density of Al_2O_3 green sheet

The smaller the agglomerates diameter and/or binder contents, the higher the packing density of Al_2O_3 powders. Especially, when binder content was 18 weight%, packing density reaches the saturated value of 60.3 vol%.

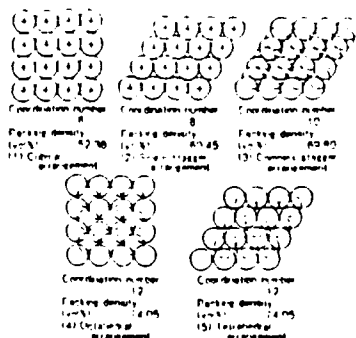


Fig 5 Packing forms of monosized balls

when monosized powders are packed without external force like doctor blading process, it can be presumed that the maximum coordination number is 8.

Therefore, theoretically, the maximum packing density of monosized powders in green sheets is 60.45 vol%.

The maximum packing density of barium titanate powders, which was obtained in this work, was nearly equal to this theoretical packing density of monosized powders.

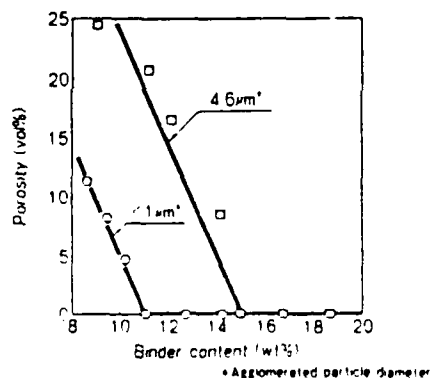


Fig 11 Relationship between binder content and porosity of green sheets

When binder content increased, porosity of green sheets decreased linearly.

The binder content at which porosity reached 0 vol% became smaller when agglomerated particle diameter became smaller.

This value was the same as the content at which green density reached the maximum value.

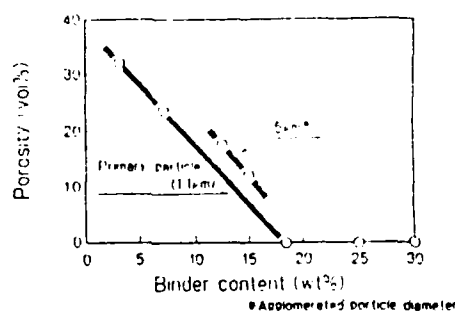


Fig.12 Relationship between Binder content and Porosity of Al_2O_3 Green Sheet

Conclusions

- 1 Green sheet density is largely affected by the agglomerate size.
- 2 Green sheet density increases with the decrease of the size of agglomerates, and reaches the saturation value when the agglomerate size equals the primary particle size.
- 3 Packing density in the green sheets increases at decreasing agglomerate size, and reaches the saturation value of 60.2 vol% of Al_2O_3 powder and 60.4 vol% of $BaTiO_3$ powder respectively, the size of agglomerates reaches the primary particle size.
- 4 The saturation value of 60.2 vol% of Al_2O_3 and 60.4 vol% of $BaTiO_3$ powder is well matched with the packing density of 60.45 vol% corresponding to a coordination number 8 for monosized particles in single stagger arrangement.
- 5 Especially, in case of $BaTiO_3$ green sheet, when agglomerates are pulverized packing density reaches a maximum at a definite binder content, and decreases when the binder content deviates from this level either downward or upward.
- 6 The packing density of $BaTiO_3$ decrease which occurs when the binder content in the green sheets is too small is assumed to derive from a weaker bonding force of the binder which incompletely fills interparticle voids.

Sinterability of High-Packing Density BaTiO₃ Green Sheet

Tamotsu Ueyama
* Shozo Yamana
&
Naoya Kaneko

Simodate Research Laboratory
Hitachi Chemical Co., Ltd.
1380-1 Tarazaki Katsuta.
Ibaraki, 312, Japan

Table 1 Characteristic of BaTiO₃ powder*

Item	density	specific surface area	Average particle Diameter
Unit	g/cm ³	m ² /g	μm
observation	6.01	2.52	0.6

Item	Chemical composition										
Unit	%										
observation	69.18	25.35	2.14	1.10	1.09	0.60	0.27	0.17	0.03	0.03	0.01

* TAMTRON CERAMICS

As dielectric material, BaTiO₃ was used in this work. Table 1 gives the chemical composition of BaTiO₃ powder. Dielectric green sheets were produced by the doctor blade process. Samples were sintered in the range 700–1300°C in atmosphere. The packing density (P₀) of the green sheets

was calculated by the equation (1):

$$P_0 = \frac{\rho_g \cdot x_d}{\rho_d} \quad (1)$$

ρ_g: Green sheet density

ρ_d: Density of dielectric powder

x_d: Weight component ratio of dielectric powder

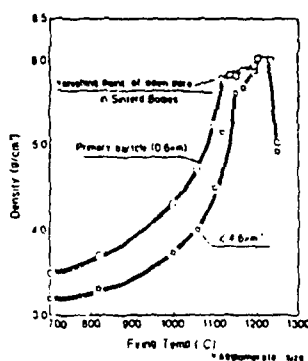


Fig. 1 Relationship between the firing temperature and fired density.

- 1) 700–1120°C: Density increases rapidly and exponentially. The open pores of a sintered body vanish at 1120°C in the green sheets is 60.4 vol%.
- 2) 1120–1200°C: Density slightly increases toward the saturated density.
- 3) 1200–1210°C: Increases discontinuously toward the saturated density.
- 4) 1210–1240°C: The density reaches the saturated value 6.0 g/cm³ at 1210°C and does not change up to 1240°C.
- 5) 1240°C: The density decreases rapidly and open pores increases.

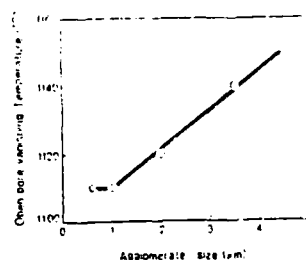


Fig. 2 Relationship between the agglomerate size of BaTiO_3 and vanishing temperature of the open pore in sintered body

The smaller the agglomerate size is, the lower the firing temperature is. This means that sinterability is improved when agglomerated particles are pulverized.

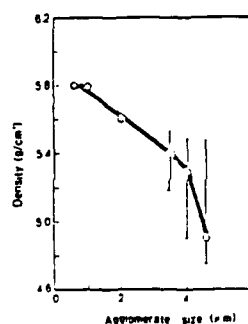


Fig. 4 Relationship between the agglomerate size and fired density which was fired at open pore vanishing temperature.

The density of a sintered body increases rapidly when agglomerated particles are pulverized in to small agglomerate size and at the primary particle diameter, saturation is carried out at the maximum value 5.8 g/cm^3 .

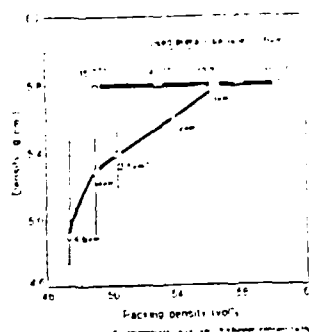


Fig. 3 Relationship between the packing density and fired density when was fired at open pore vanishing temperature

Circle marks in the figure shown the packing density changed by changing the amount of binder using green sheets which agglomerated particles are pulverized into primary particles. Suffix numbers shown the amount of binder. On the other hand, square marks shown the packing density changed by changing agglomerate size with the amount of binder fixed at the value 11 wt%. Suffix numbers shown agglomerate size.

CONCLUSIONS

1. The fired density of BaTiO_3 varies greatly within five temperature regions.
2. When the agglomerated size in a green sheet is small, the temperature at which open pores vanish is low.
3. When agglomerated particles are dispersed into primary particles, the fired density of BaTiO_3 at optimum temperature becomes a fixed value of 5.8 g/cm^3 .
4. This value does not change when the amount of binder in a green sheet varies and when the packing density changes from 40–60%. The reason is that the packing density becomes the same value of 60% after burning off its binder.
5. The fired density changes as agglomerate size changes. For instance, it becomes 4.8 g/cm^3 when the agglomerate size of BaTiO_3 is $4.8 \mu\text{m}$. This value becomes 5.4 g/cm^3 at $3.5 \mu\text{m}$ and 5.8 g/cm^3 at $2 \mu\text{m}$. The estimated reasons are as follows: pores caused by steric hindrance among agglomerated particles and pores in agglomerated particles are left in the sintered body at the temperature that open pores vanish.

AN INVESTIGATION OF THE LOW VOLTAGE FAILURE MECHANISM IN MULTILAYER CERAMIC CAPACITORS

C. JOHN BRANNON AND H. U. ANDERSON
DEPARTMENT OF CERAMIC ENGINEERING
UNIVERSITY OF MISSOURI-ROLLA
ROLLA, MO 65401

THIS WORK SPONSORED BY
THE OFFICE OF NAVAL RESEARCH

LOW-VOLTAGE FAILURE

LOW-VOLTAGE FAILURE IN MULTILAYER CERAMIC CAPACITORS IS DEFINED AS INSULATION RESISTANCE FAILURE OCCURRING WHEN THE CAPACITOR IS BIASED FAR BELOW ITS RATED VOLTAGE. TYPICAL BIAS VOLTAGES FOR LOW-VOLTAGE FAILURE ARE 1 OR 2 VOLTS. TWO CONDITIONS NECESSARY FOR LOW-VOLTAGE FAILURE ARE THE PRESENCE OF MOISTURE AND THE EXISTANCE OF STRUCTURAL DEFECTS SUCH AS CRACKS OR VOIDS EXTENDING FROM THE SURFACE OF THE CAPACITOR THROUGH AT LEAST TWO ELECTRODE LAYERS. WHEN EXPOSED TO A HIGH BIAS, CAPACITORS EXPERIENCING LOW-VOLTAGE FAILURE TEND TO RECOVER, OR REGAIN THEIR ORIGINAL HIGH INSULATION RESISTANCE LEVEL. CAPACITORS MAY ALSO RECOVER AFTER A MODERATE HEAT TREATMENT.

PROPOSED LOW-VOLTAGE FAILURE MECHANISMS

CURRENTLY, THE MOST POPULAR THEORY OF LOW-VOLTAGE FAILURE CONCERNS THE GROWTH OF METALLIC DENDRITES OF ELECTRODE MATERIAL THAT BRIDGE THE GAP BETWEEN THE ELECTRODES. THESE DENDRITES CREATE A CONDUCTION PATH BETWEEN TWO ELECTRODE LAYERS, THUS PRODUCING A SHORT AT LOW VOLTAGES. THE DENDRITE IS FORMED WHEN ELECTRODE MATERIAL IS DISSOLVED IN WATER WHICH HAS CONDENSED IN THE PRESENT DEFECTS. THE DENDRITE THEN GROWS ALONG THE DEFECT EITHER BY ELECTROCONDUCTION OR BY PRECIPITATION. WHEN EXPOSED TO A HIGH BIAS, THE ELECTRODE IS VAPORIZED AND THE FAILURE CEASES.

A SECOND PROPOSED MECHANISM OF LOW-VOLTAGE FAILURE HAS TO DO WITH ACCELERATED AGING OF THE DIELECTRIC LAYER BETWEEN THE ELECTRODES. CRYSTAL-PHASE TRANSFORMATIONS OCCUR IN THE DIELECTRIC CAUSING A DEGRADATION ACCOMPANIED BY A SUBSEQUENT INCREASE IN CONDUCTIVITY. APPLICATION OF A HIGH VOLTAGE PRODUCES A HEATING EFFECT WHICH ALLOWS THE DIELECTRIC TO RETRANSFORM TO ITS ORIGINAL STRUCTURE.

EXPERIMENTAL TECHNIQUE

1. ALL CAPACITORS WERE SUBJECTED TO THE METHANOL TEST. THE METHANOL TEST WAS PERFORMED AS FOLLOWS:
 1. 10 VDC WAS APPLIED TO THE CAPACITOR AND AFTER 15 SECONDS THE LEAKAGE CURRENT (I_1) WAS MEASURED.

2. THE CAPACITOR WAS THEN IMMERSSED IN METHANOL FOR 30 MINUTES ALLOWING THE METHANOL TO PENETRATE INTO CRACKS AND OPEN POROSITY.
3. THE CAPACITOR WAS REMOVED FROM THE METHANOL AND ALLOWED TO DRY ON A TISSUE TO MINIMIZE THE RESIDUAL METHANOL LEFT ON THE SURFACE.
4. STEP 1 WAS REPEATED IMMEDIATELY AFTER DRYING AND (I_2) WAS MEASURED.

A CAPACITOR WAS CONSIDERED TO HAVE FAILED THE METHANOL TEST IF I_2 WAS AN ORDER OF MAGNITUDE OR MORE GREATER THAN I_1 .

2. STRUCTURAL DEFECTS IN THE FORM OF CRACKS WERE INTRODUCED INTO THE CAPACITOR. THIS WAS ACCOMPLISHED BY THERMAL SHOCKING THE CAPACITORS. SPECIMENS WERE HEATED TO 575°C AND ALLOWED TO SOAK FOR 1 HOUR. SPECIMENS WERE THEN IMMEDIATELY QUENCHED IN LIQUID N₂ AT -196°C, ACHIEVING A THERMAL GRADIENT SUFFICIENT TO INDUCE CRACKS EXTENDING FROM THE SURFACE THROUGH THE ELECTRODE LAYERS, BUT INSUFFICIENT TO OTHERWISE DAMAGE THE CAPACITOR OR ITS ELECTRICAL PROPERTIES.

3. SPECIMENS WERE SUBJECTED TO A VARIATION OF THE STANDARD 85-85 TEST IN WHICH THE ATMOSPHERE WAS ALLOWED TO BE EITHER DRY OR TO CONTAIN 85% RH. THE ATMOSPHERE WAS VARIED AS 4 HOURS DRY, 4 HOURS WET, AND 4 HOURS DRY. SEVERAL TESTS WERE MADE WITH VOLTAGES SET AT 1.5, 1.0, 1.5, 2.0, 5.0, 10.0, 20.0, AND 70.0 VDC.

4. SPECIMENS SUBJECTED TO ANOTHER VARIATION OF THE STANDARD 85-85 TEST. VOLTAGE BIAS REMAINED AT 1.5 VDC WHILE THE ATMOSPHERE WAS VARIED 4 HOURS DRY FOLLOWED BY 4 HOURS WET. THE INITIAL TEMPERATURE WAS 35°C. AFTER 4 HOURS 4 HOURS OF WET ATMOSPHERE, THE TEMPERATURE WAS RAISED TO 115°C.

5. THE STANDARD 85-85 TEST WITH STANDARD 1.5 VDC BIAS WAS PERFORMED ON 20 SPECIMENS FOR A PERIOD OF 20 DAYS. OF THESE 15 WERE CRACKED AND 5 WERE UNCRACKED CONTROLS. THE ATMOSPHERE WAS DRY FOR THE FIRST AND LAST DAYS OF THE TEST AND WAS MAINTAINED AT 85% RH THE REST OF THE TIME.

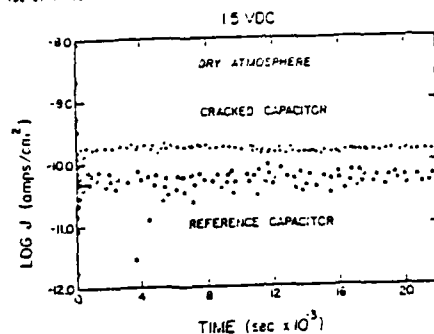
6. SPECIMENS FOUND TO EXHIBIT LOW-VOLTAGE FAILURE WERE MOUNTED IN PLASTIC AND SECTIONS. SECTIONING WAS ACCOMPLISHED BY VIBRATION WITH 500 GRIT ABRASIVE PAPER FOLLOWED BY A POLISHING WITH 1 MICRON PARTICLE SIZE DIAMOND PASTE. SPECIMENS WERE THEN EXAMINED AND PHOTOGRAPHED USING OPTICAL AND SCANNING ELECTRON MICROSCOPY. QUALITATIVE AND SEMI-QUANTITATIVE EXAMINATION OF THE CRACK AREAS WAS MADE USING THE ENERGY DISPERSIVE X-RAY SPECTROMETER OF THE SEM.

THE CRACKED CAPACITORS IN THIS STUDY SHOWED THE FOLLOWING FAILURE CHARACTERISTICS: (1) THE PRESENCE OF STRUCTURAL DEFECTS AND THE TENDENCY TO LEAKAGE UNDER BIAS; (2) IN SEVERAL NOTABLE INSTANCES, A LEAKAGE PATTERN OF FAILURE WAS SEEN TO OCCUR. THIS LEAKAGE PATTERN IS SIMILAR TO THIS STUDY AND HAS A PERIOD OF APPROXIMATELY 10 SECONDS.

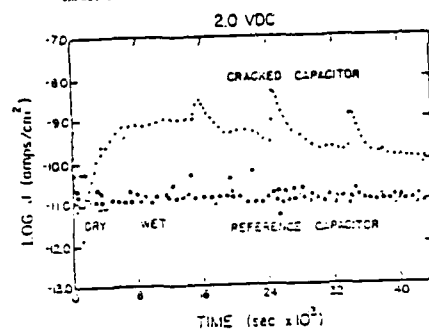
NO EXCESS ELECTRODE MATERIAL WAS FOUND ANYWHERE IN ANY OF THE CRACKS EXAMINED.

ANY TIME THE MOISTURE WAS REMOVED FROM THE CAPACITOR, EITHER BY MANIPULATION OF THE ATMOSPHERE OR BY HEATING THE CAPACITOR, FAILURE IMMEDIATELY CEASED.

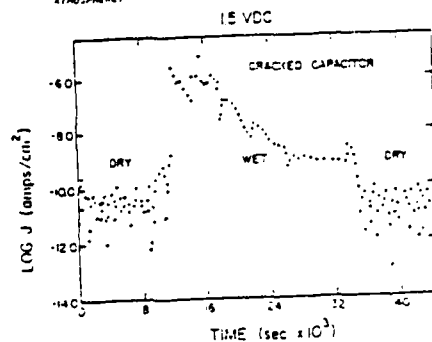
THE ELECTRODE MATERIAL, Pd, IS PRACTICALLY INSOLUBLE IN WATER. LOW VOLTAGE DID NOT OCCUR AT 0.5 VDC BIAS, BUT DID OCCUR AT 1.0 VDC BIAS, ESTABLISHING A FAILURE THRESHOLD BETWEEN THESE TWO VOLTAGES.



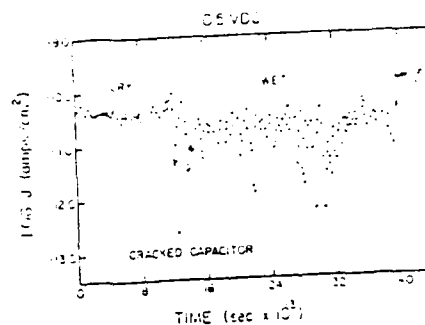
PLOT OF THE LOGARITHM OF THE LEAKAGE CURRENT DENSITY VS. TIME IN SECONDS FOR BOTH A CRACKED AND AN UNCRACKED CAPACITOR AT 0.5°C AND 1.5 VDC IN A DRY ATMOSPHERE.



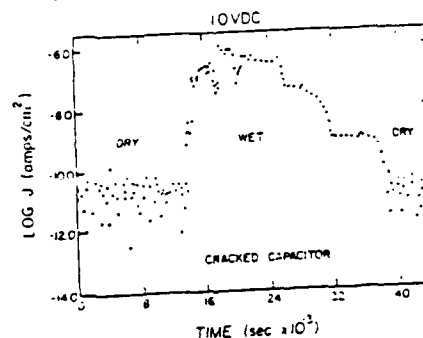
PLOT OF THE LOGARITHM OF THE LEAKAGE CURRENT DENSITY VS. TIME IN SECONDS FOR BOTH A CRACKED AND AN UNCRACKED CAPACITOR UNDERGOING THE 45/25 2.0 VDC TEST WITH VARYING ATMOSPHERE.



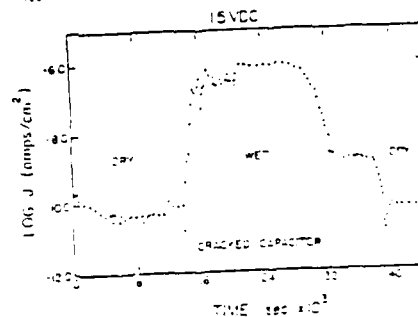
PLOT OF THE LOGARITHM OF THE LEAKAGE CURRENT DENSITY VS. TIME IN SECONDS FOR A CRACKED CAPACITOR UNDERGOING THE 45/25 1.5 VDC TEST WITH VARYING ATMOSPHERE.



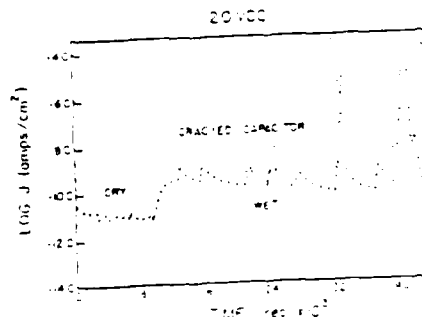
PLOT OF THE LOGARITHM OF THE LEAKAGE CURRENT DENSITY VS. TIME IN SECONDS FOR A CRACKED CAPACITOR UNDERGOING THE 45/25 0.5 VDC TEST WITH VARYING ATMOSPHERE.



PLOT OF THE LOGARITHM OF THE LEAKAGE CURRENT DENSITY VS. TIME IN SECONDS FOR A CRACKED CAPACITOR UNDERGOING THE 45/25 1.0 VDC TEST WITH VARYING ATMOSPHERE.



PLOT OF THE LOGARITHM OF THE LEAKAGE CURRENT DENSITY VS. TIME IN SECONDS FOR A CRACKED CAPACITOR UNDERGOING THE 45/25 1.5 VDC TEST WITH VARYING ATMOSPHERE.



PLOT OF THE LOGARITHM OF THE LEAKAGE CURRENT DENSITY VS. TIME IN SECONDS FOR A CRACKED CAPACITOR UNDERGOING THE 45/25 2.0 VDC TEST WITH VARYING ATMOSPHERE.

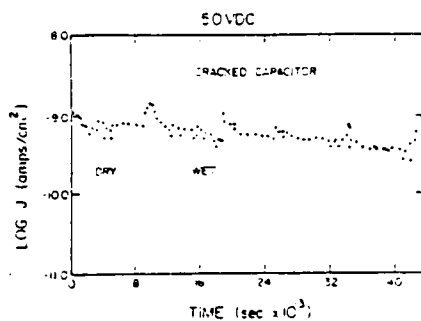


FIGURE 1
 PLOT OF THE LOGARITHM OF THE LEAKAGE CURRENT DENSITY VS. TIME IN SECONDS FOR A CRACKED CAPACITOR UNDERGOING THE 55 AN 50 VDC TEST WITH VARYING ATMOSPHERE

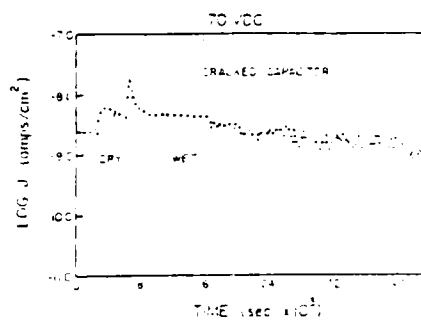


FIGURE 2
 PLOT OF THE LOGARITHM OF THE LEAKAGE CURRENT DENSITY VS. TIME IN SECONDS FOR A CRACKED CAPACITOR UNDERGOING THE 55 AN 70 VDC TEST WITH VARYING ATMOSPHERE

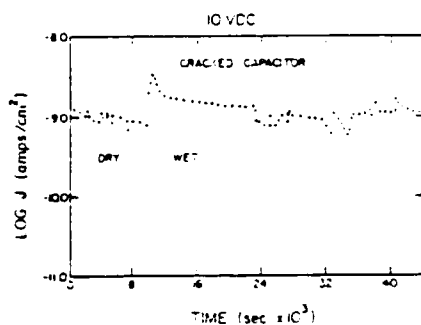


FIGURE 3
 PLOT OF THE LOGARITHM OF THE LEAKAGE CURRENT DENSITY VS. TIME IN SECONDS FOR A CRACKED CAPACITOR UNDERGOING THE 55 AN 10 VDC TEST WITH VARYING ATMOSPHERE

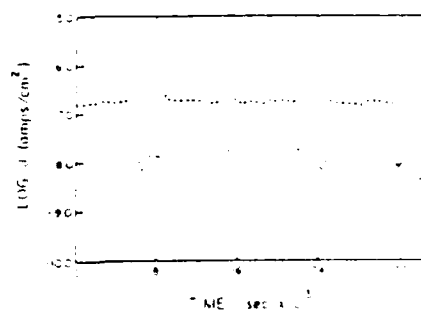


FIGURE 4
 PLOT OF THE LOGARITHM OF THE LEAKAGE CURRENT DENSITY VS. TIME IN SECONDS FOR A CRACKED CAPACITOR UNDERGOING THE 55 AN 10 VDC TEST WITH VARYING ATMOSPHERE

DISCUSSION

THE RESULTS INDICATE THAT THE LEAKAGE CURRENT IN A LOW VOLTAGE FAILURE (THE FAILURE OF THE CAPACITOR SHORTLY AFTER THE DESTRUCTION OF THE CAPACITOR BY A SUPERHEATING CAUSED BY WATER) IS A FUNCTION OF TEMPERATURE, BOTH IN THE WET AND DRY STATES. FAILURE BEGINS TO OCCUR IMMEDIATELY AFTER REMOVAL FROM THE SUPERHEATED STATE TO THE AMBIENT STATE, REMOVING THE PROPORTIONAL FACTOR OF THE SUPERHEATED CONDENSED.

TESTS WITH WATER INDICATE THAT THE LEAKAGE CURRENT IN A LOW VOLTAGE FAILURE (THE FAILURE OF THE CAPACITOR SHORTLY AFTER THE DESTRUCTION OF THE CAPACITOR BY A SUPERHEATING CAUSED BY WATER) IS A FUNCTION OF TEMPERATURE, BOTH IN THE WET AND DRY STATES. FAILURE BEGINS TO OCCUR IMMEDIATELY AFTER REMOVAL FROM THE SUPERHEATED STATE TO THE AMBIENT STATE, REMOVING THE PROPORTIONAL FACTOR OF THE SUPERHEATED CONDENSED.

[illegible]

Journal of Management Education

Table 4 identifies the factors such as temperature and time are normally the representative of the process. The other representative factors of the system are the material properties, identification and the extent of the process. The identification exists as a prior knowledge of the system. The representative process parameters are the process parameters, such as, pressure, temperature, and the factor below a percent.

Also, BaTiO_3 modified with flux additions to the system $[\text{Ca}]$ Al_2O_3 - BaTiO_3 - 5CaO was sintered at 1450°C and gave a similar result. The melting temperature of the eutectic is about 1250°C as calculated also. The solid phase is a mixture of high-purity flux components, defined as BaTiO_3 and a eutectic phase in the BaTiO_3 - CaO system, with a $2:1$ molar ratio.

The investigation of possible mechanisms of the pathogenesis necessary to guide the development of therapies is critical to the development of new therapies. In this regard, the following are the most important findings of the study:

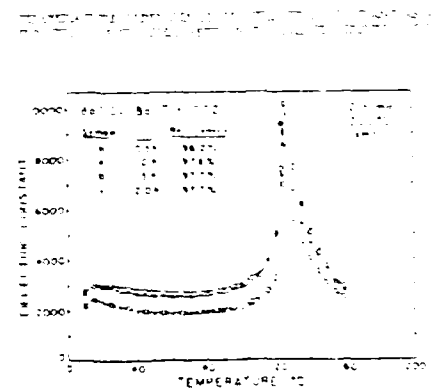
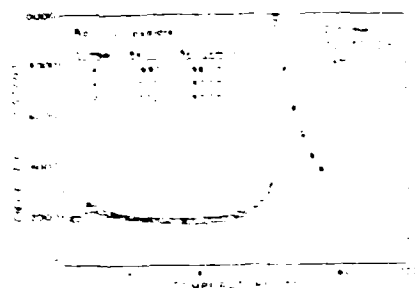
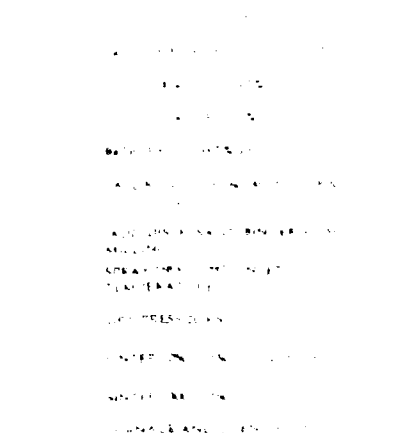
STATE OF TEXAS, COUNTY OF DALLAS, ss. I, the undersigned, a Notary Public in and for said State, do hereby certify that the foregoing is a true and correct copy of the original of the same as the same appears from the records of said County.

PRESENCE OF J. J.

- 1) PROMOTES RANDOMIZATION AT REQUIRED TEMPERATURES
- 2) DIFFUSES INTO GRAIN BOUNDARIES
- 3) APPARENT SUBSTITUTION OF Fe^{2+} INTO LATTICE
 - a) INDUCES STRAIN RESULTING IN REDUCTION OF TETRAGONAL DISTORTION
 - b) INCREASES THE DIELECTRIC CONSTANT AND DECREASES LOSSES

PRESNCE OF ZrO₂

- 1) RESIDES AT GRAIN BOUNDARY
 - 2) SUPPRESSES GRAIN GROWTH
 - 3) DEPRESSES TETRAGONAL DISTORTION
- RESULTING IN FLAT DIELECTRIC
CONSTANT RESPONSE WITH
TEMPERATURE AND LOW LOSSES



TEMPERATURE DEPENDENCE OF DIELECTRIC CONSTANT AS A
FUNCTION OF MOLECULAR ORIENTATION IN POLYMER FOR
POLARIZATION BY AC FIELD

NO-A185 113

UNITED STATES - JAPAN WORKSHOP ON DIELECTRIC AND
PIEZOELECTRIC CERAMICS ((3RD)) HELD IN TOYAMA JAPAN ON
NOVEMBER <9>-<12> <1986>(U) KEIO UNIV TOKYO (JAPAN)

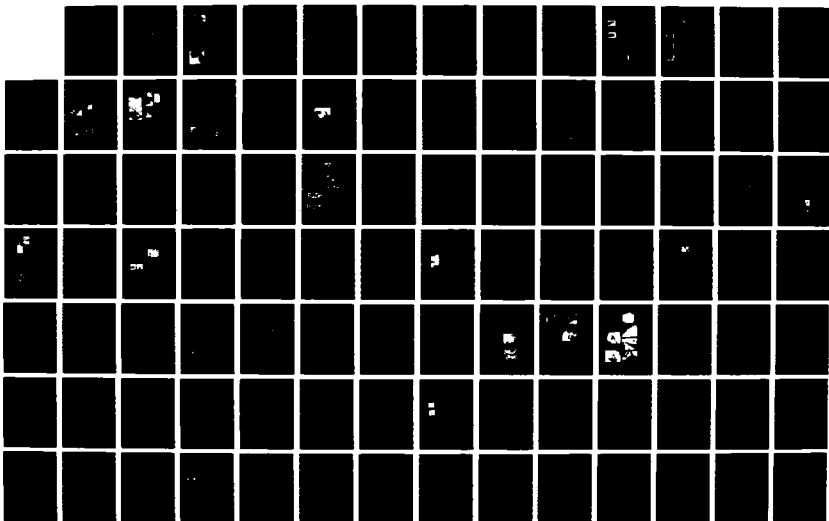
3/8

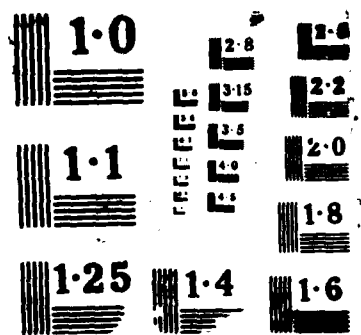
UNCLASSIFIED

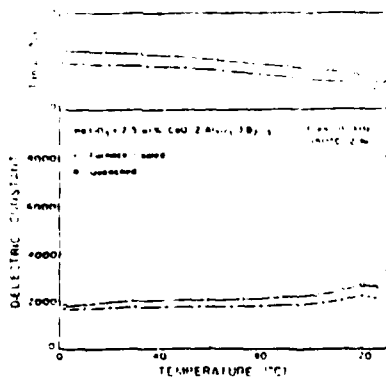
30 JUL 87

F/G 11/2

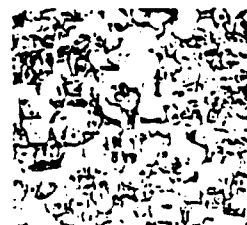
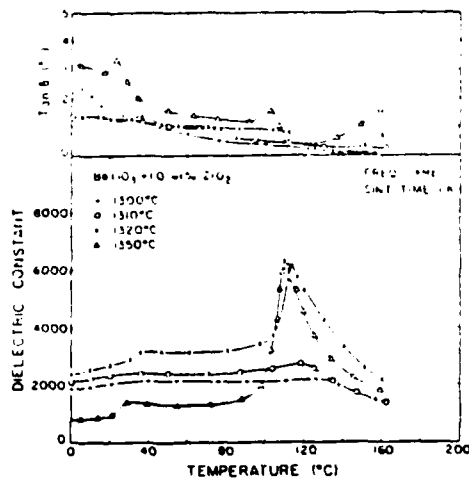
NL



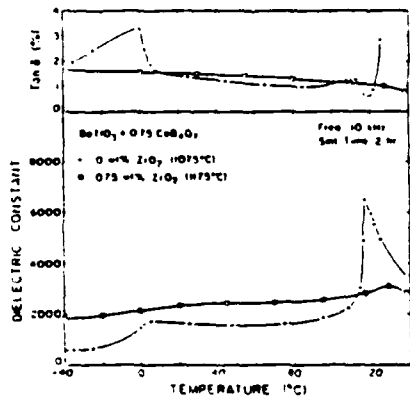




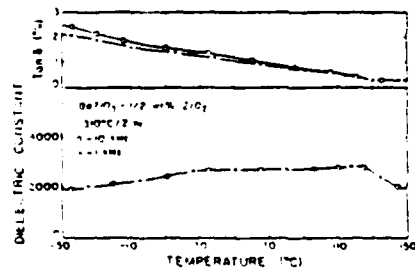
DIELECTRIC CONSTANT AND TAN δ PROFILE AS A FUNCTION OF TEMPERATURE FOR Ca ALUMINATE MODIFIED BaTiO_3 SAMPLE.



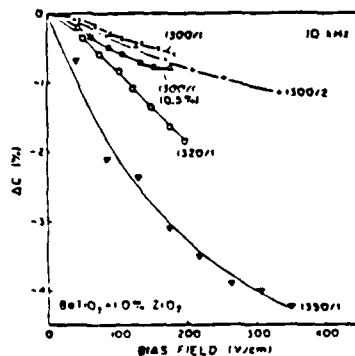
SEM PHOTOMICROGRAPH IS COMPARING MICROSTRUCTURES FOR BaTiO_3 AND MODIFIED WITH 1.0 WT% ZrO_2 (1300°C/2HR).



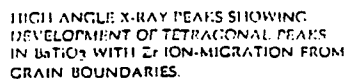
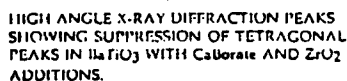
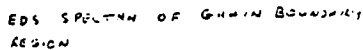
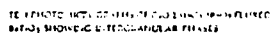
DIELECTRIC CONSTANT AND TAN δ PROFILE COMPARING Calcium and ZrO_2 MODIFIED BaTiO_3 .



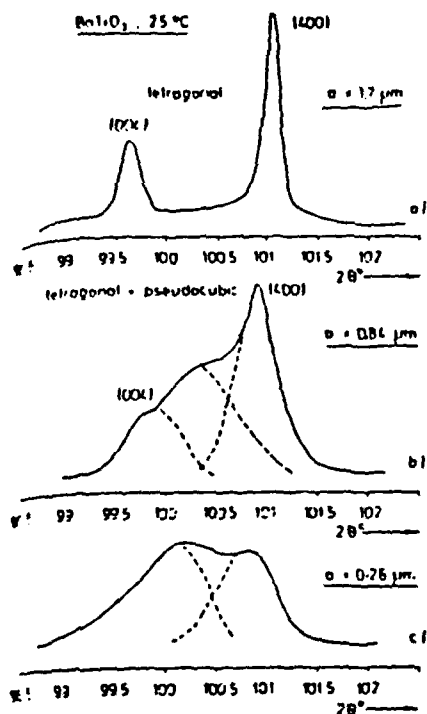
DIELECTRIC CONSTANT AND TAN δ CHANGES WITH TEMPERATURE FOR BaTiO_3 SAMPLE AND GRAIN BOUNDARY ZrO_2 PHASE.



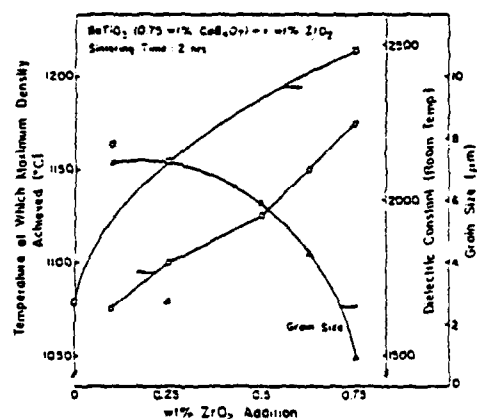
PERCENT CAPACITANCE CHANGE WITH DC BIAS FIELD FOR ZrO_2 MODIFIED BaTiO_3 AT DIFFERENT SINTERING TEMPERATURES.

Table 3. EFFECT OF FLUTES ON THE AXIAL RATIO OF u_{110} .

- 37 -



Change in BaTiO_3 structure with grain size (HRLT)



PLOT SHOWING VARIATION OF GRAIN SIZE, DIELECTRIC CONSTANT AND MAXIMUM DENSIFICATION TEMPERATURE WITH ZrO_2 CONTENT.

SUMMARY

ZrO_2 ADDED TO CaB_4O_7 FLUXED BaTiO_3 (< 1 WT%) PREFERENTIALLY RESIDES AT THE GRAIN BOUNDARIES. THIS CONSTRAINS DISCONTINUOUS GRAIN GROWTH, SO THAT POLARIZATION IS ESSENTIALLY CONTROLLED BY THE GRAIN SIZE.

$\text{CaO} \cdot 2\text{Al}_2\text{O}_3 \cdot 3\text{B}_2\text{O}_3$ ADDED TO BaTiO_3 SUPPRESSES GRAIN GROWTH AND THE TETRAGONAL TO CUBIC TRANSITION, GIVING A HIGH DIELECTRIC CONSTANT LOW LOSS, AND LOW D.C. SENSITIVITY. THIS MAY BE PARTIALLY ATTRIBUTED TO THE FINE GRAIN SIZE ($< 1\mu\text{m}$) PRESENCE OF Al^{3+} IONS IN THE LATTICE.

THE ABOVE GAVE A FLAT DIELECTRIC CONSTANT/TEMPERATURE PROFILE WITH YSR CHARACTERISTICS.

Barium Titanate-Based Dielectric For MLC's With High K and Low Firing Temperature

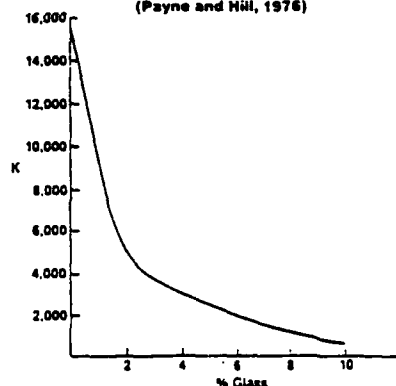
I. Burn & M. T. Secaur

E. I. Du Pont de Nemours & Co.
Photosystems and Electronic Products Department
Electronic Materials Division

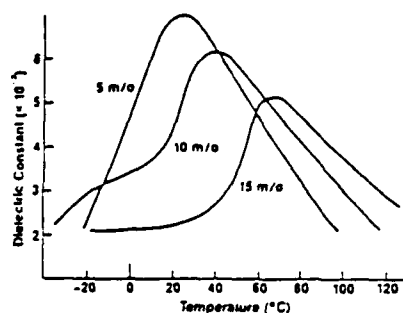
Low Cost Electrode Technologies For High K Dielectrics (Z5U)

	Electrode	K
• Low-fired BaTiO ₃	≥70% Ag	6000
• Pb Injection	Pb	8000-10,000
• Base Metal	Ni	8000-10,000
• PbO-based Relaxors	≥85% Ag	9000-15,000

Effect of Glass Addition on K
(Payne and Hill, 1976)



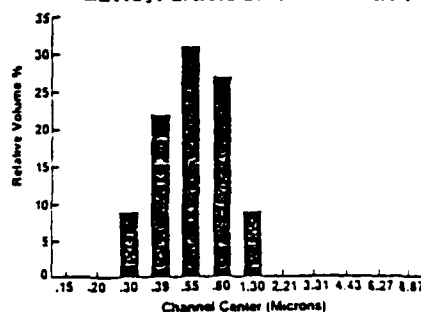
Influence of PbO on TCC (BaTiO₃)
(Sintering Temperature 1100°)



Low Fire BaTiO₃ Technology: Principles

- Small amount of glass-forming oxides (no fluorides)
- A/B Stoichiometry
 - System approach (ceramic + flux)
 - Grain growth control
- Fine particle size powders ($\leq 1 \mu\text{m}$)

BaTiO₃ Particle Size Distribution



Dielectric Tape Formulation

Binder Mix Formulation

	WT. %
Du Pont 5200 Binder Solution	28.3 (8.5% resin)
Monsanto Santicizer 160 (Butyl Benzyl Phthalate)	2.1 (2.1% resin)
1,1,1-Trichloroethane	66.1
10% Hercules Polypale Solution in Isopropanol	1.50 (0.15% resin)
Total	100.0 (10.75% resin)

Mill Batch

Ceramic Powder	100
Binder Mix	65

XL103 Firing

- Bakeout
 - 400°C (min)
 - 750°C (bisque)
- Sintering
 - 1100°C (2012°F): 2 hours
 - Sinters (optional)
 - Containers (no sand)

XL103 Z5U Dielectric Electrical Properties

Firing Temp. (°C)	Effective K	1 VRMS % DF	$\Delta C @ 85^\circ\text{C}$ (%)	RxC 25°	RxC 85°
----------------------	----------------	----------------	--------------------------------------	------------	------------

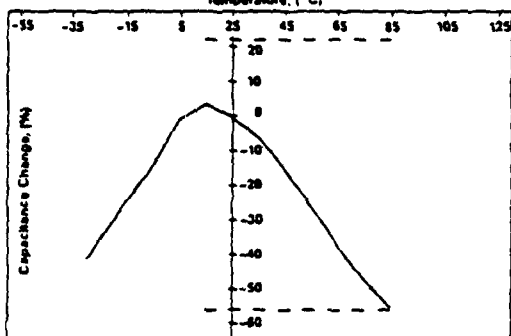
(0.5 μF 2225 Size 5 Active Layers)

1100	10,000	1.00%	-61.9	11500	2100
1080	9,700	1.20%	-55.9	10900	2000

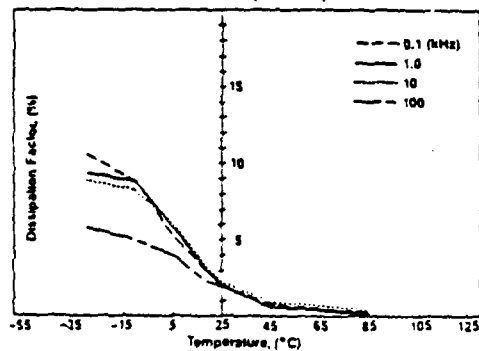
(0.17 μF 1209 Size 10 Active Layers)

1100	10,000	1.30%	-56.9	10000	1000
1080	9,300	1.40%	-54.5	10000	1000

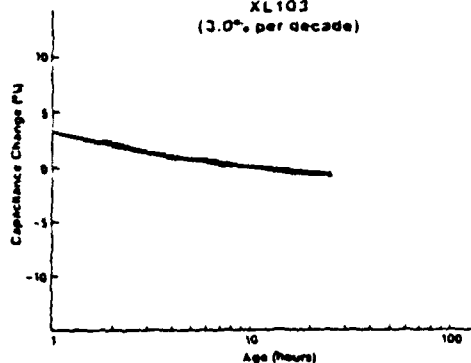
TCC XL103 K = 10,000 \pm 500 Temperature (°C)



DF vs. Frequency XL103 (1V/mil)



Aging Rate XL103 (3.0% per decade)



XL103 Reliability

DWV

>600 VDC/mil

Life Test

- 100 V/mil, 85°C, 1000 hours
 - OF/30 (5 layer 2225)
 - No degradation
- 200 V/mil, 125°C, 24 hours
 - OF/ca. 100 (5 layer 1209)
- 50 V/mil, 85°C/85% RH, 1000 hours
 - No degradation (5 layer 1209)

Fracture Toughness

- $K_{IC} = 0.9 \text{ MPa.m}^{1/2}$

Summary

Low Fire BaTiO₃-Based Dielectrics

- Low PbO content
(Safe and easy to process)
- Proven reliability
- Preferred for SMT
- Now available with Competitive K

ELECTRICAL CONDUCTION IN BaTiO₃-BASED CERAMIC

by

L.C. Burton and H.Y. Lee
Virginia Polytechnic Institute
& State University
Blacksburg, VA 24061 USA

CONTENTS

1. Electronic Current and Ionically Induced Current

a. Model

b. Experimental

Region 1: Stable electron current

Region 2: Ionically induced current

2. Role of Grain Boundaries

a. Evidence in I-V and u(T)?

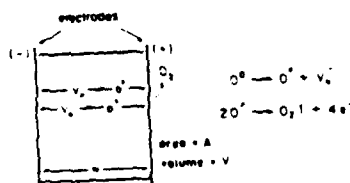
b. Voltage biased impedance

c. Significance of grain size

1a. Ionically Induced Electron Current Model

Electron density $n = n_0 + 2(V_0)$

background ionically induced



Q_{ox} = total O^{2-} charge arriving at anode per sec
 $= \int i_{ox} dt$

$$[V_0] = \frac{Q_{ox}}{2av} = \frac{1}{2av} \int i_{ox} dt = \frac{1}{2av} \int i_{ox} dt$$

But $i_{ox} = i_{V_0}$ if O^{2-} moves by hopping and V_0 sites

$$\therefore \frac{d[V_0]}{dt} = \frac{Q_{ox}}{2av} = \frac{J_0}{2av} \quad \therefore V_0 = 2av \frac{d[V_0]}{dt}$$

Also $J_{V_0} = i_{V_0} = 2q[V_0] \mu_{V_0} \frac{V}{w}$ (V = voltage)

This assumes ohmic behavior. At elevated voltages, this current will be superohmic

$$\therefore J_{V_0} = 2q[V_0] \mu_{V_0} \frac{V}{w} \quad n > 1$$

$$\text{Thus } 2av \frac{d[V_0]}{dt} = 2q \mu_{V_0} \frac{V}{w} [V_0]$$

This integrates to $[V_0] = [V_0]_0 \exp\left(\frac{\mu_{V_0} V}{w^2} t\right)$

Use $n = n_0 + 2[V_0]$ $n_0 = 2[V_0]_0$

$$n = n_0 \text{ at } t = t_0$$

$$\text{to obtain } n = \frac{n_0}{2} [1 + \exp B(t - t_0)] \quad B = \frac{\mu_{V_0} V}{w^2}$$

$$\text{Degradation rate} = B = \frac{\mu_{V_0} V}{w^2}$$

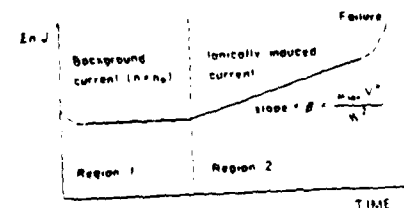
$$\text{Lifetime} = \tau = 1/B = \frac{w^2}{\mu_{V_0} V}$$

Dominated by ionic mobility μ_{V_0} at fixed w and V

Generic Electron Current Curve

$$J = an \mu_e \frac{V^m}{w} = a \mu_e \frac{V^m}{w} \left[\frac{n_0}{2} (1 + \exp B(t - t_0)) \right]$$

($m \geq 1$)



- Notes:
1. Currents expected to deviate at beginning and end (initial burn-in and final failure)
 2. V_0 may not equal V due to other transport mechanisms
 3. μ_{V_0} and w are also expected to change with time

Temperature dependence of μ_{on} is contained within

$$\mu_{on} = \mu_0 e^{-\frac{E_a}{kT}} \quad E_a = \text{activation energy}$$

$$\text{Lifetime} = \tau = \frac{w^2}{\mu_{on} V^n} = \frac{w^2 e^{E_a/kT}}{\mu_0 V^n}$$

For lifetimes τ_1, τ_2 at temperatures T_1, T_2 and voltages V_1, V_2

$$\tau_1 = \frac{w^2 e^{E_a/kT_1}}{\mu_0 V_1^n} \quad \tau_2 = \frac{w^2 e^{E_a/kT_2}}{\mu_0 V_2^n}$$

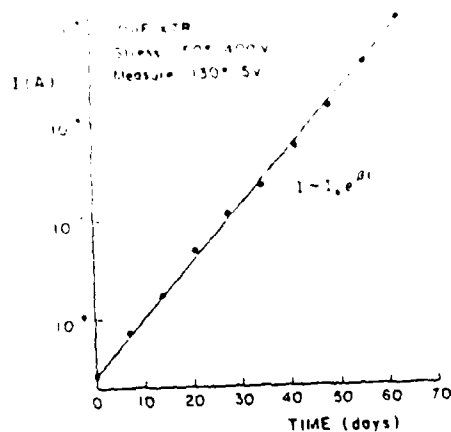
and

$$\frac{\tau_1}{\tau_2} = \left(\frac{V_2}{V_1} \right)^n \exp \left[\frac{E_a}{k} \left(\frac{1}{T_1} - \frac{1}{T_2} \right) \right]$$

This is the same as the empirical result reported by Minford (IEEE Transactions CHMT-5, 297, 1982)

Figure 2: Exponential increase in current and degradation as predicted by model

- Exponential increase with time to degradation as predicted by model

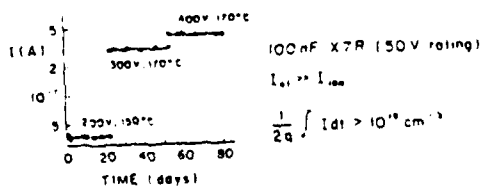


- Dark colors seen in reduced regions near cathode

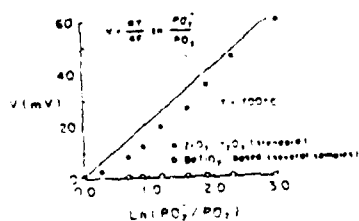
1b. Experimental

Region 1: Background current is electronic, as evidenced by -

- $I(t)$ stable over long time periods

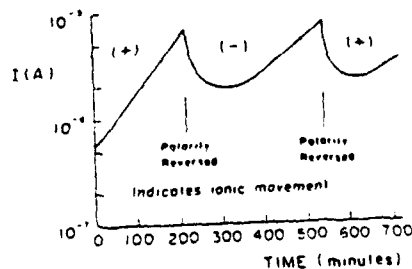


- Galvanic voltages are \approx zero

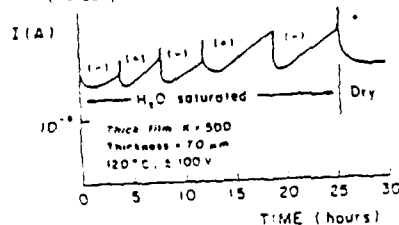


- Negative stable thermoelectric voltages
- Evidence of space charge limited currents

- Exponential increase: polarity reversal effect (100nF Z5U, 150°C, \approx 100V)



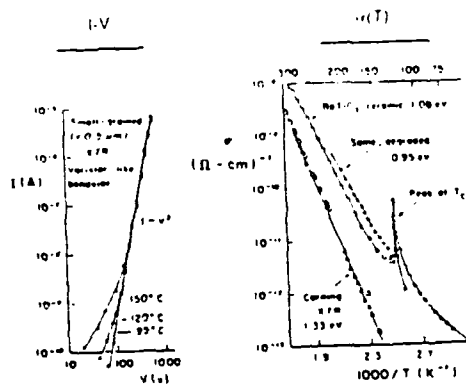
- More rapid degradation for porous thick film, even though 700μm thick. Accelerated by humidity (Porosity increases μ_{on})



2. Possible Effects of Grain Boundaries (GB):

2a. Evidence of GB controlled current

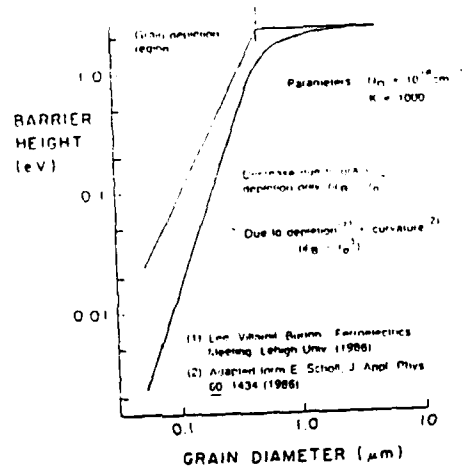
- Superohmic currents (i.e. $V^{1/2}$ to $V^{5/3}$) resemble varistor in some cases, do not show correct thickness dependence for SCLC
- Conductivity discontinuous at Curie temperature



2b. Impedance measurements under bias

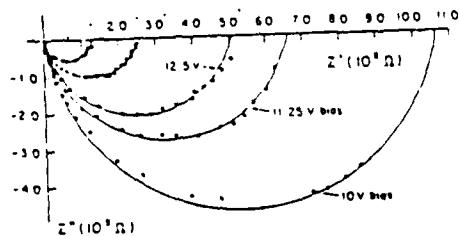
GB has an impact on the impedance response of the device because of:

- Grain depletion
- Grain curvature

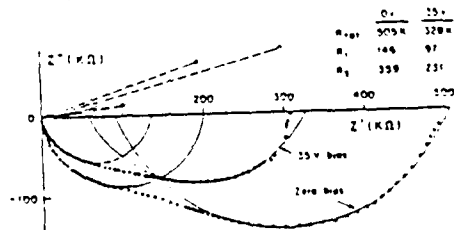


2b. Impedance measurements under bias

- Varistor is known GB controlled device.
($T = 125^\circ\text{C}$; biases 10, 11.25, 12.5, 13.75, 15V)

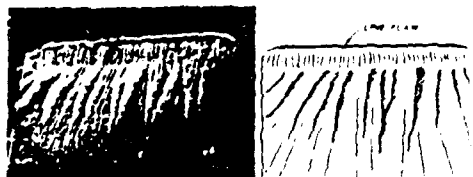


- BaTiO₃ ceramic shows similar reduction.
(Polished X7R disc; $t = 0.21 \text{ mm}$; $T = 150^\circ\text{C}$)



M14

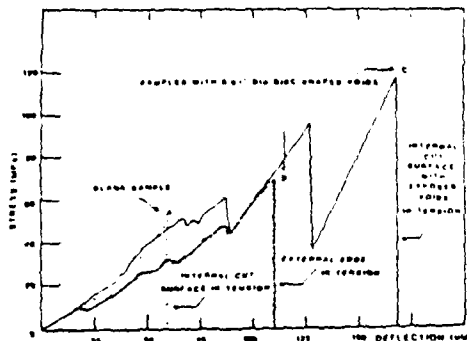
Line Fiaws



40 MPa, .7 J/m²
void free blank



76 MPa, 4.7 J/m²
highly ordered void array



STRESS VERSUS DEFLECTION OF POLED PZT IN THREE POINT BENDING

FRACTURE STRENGTHS AND ENERGIES

	BLANKS	DISC SHAPED VOIDS 0.010" DIAMETER	
VOID PLANE SPACING		1.9 mil	2.8 mil
FRACTURE STRENGTHS	68 MPa	91 MPa	117 MPa
FRACTURE ENERGIES	2.6 J/m ²	2.7 J/m ²	9.7 J/m ²

* Shear planes and cut internal surfaces with tapered ends under tension

Point

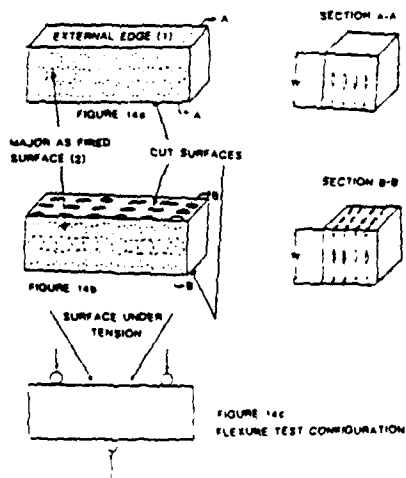
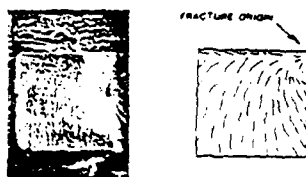
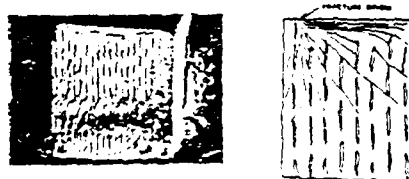


FIGURE 14
CONFIGURATIONS USED FOR 3 POINT FLEXURE TESTS

(1) surface edges held during bending
(2) surface edges released during bending



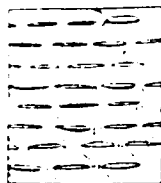
51 MPa, 2.2 J/m²
blank has some hackle curvature



70 MPa, 6.3 J/m²
some hackles parallel to and even towards
surface under tension



FIG. 10



121 MPa, 6.3 J/m²
some disorder in void array

Fast propagation parallel to voids
near tensile surface

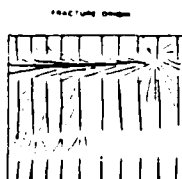
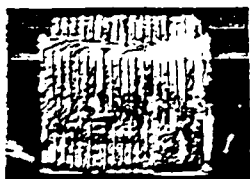
Fracture Origins



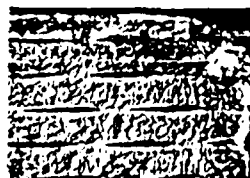
70 MPa, 6.3 J/m²

flaw near void tip, crack curves around void

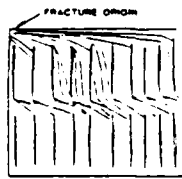
Flaws



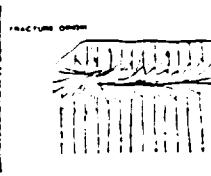
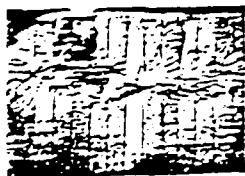
78 MPa, 3.14 J/m²
hackles primarily in void free column



117 MPa, 14.5 J/m²
origin in between void tips



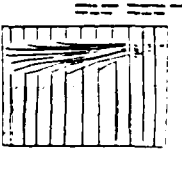
104 MPa, 6 J/m²
sidewise hackles in margin and in void
free column



78 MPa, 3.14 J/m²
flaw near void tip inside ceramic

All samples 0.09" x 0.09"
in cross-section

All voids 0.0005" thick



92 MPa, 11.5 J/m²
noncritical and critical crack propagation

Note: Upper surface of all samples
in tension

M15

OPERATIONALLY INDUCED
THERMAL STRESS GRADIENTS
IN
MULTILAYER CAPACITORS

JOSEPH F. DOUGHERTY

Advanced Materials Technologies

Niles, Michigan 49120

U.S.A.

AUTOMOTIVE APPLICATIONS
INVOLVING AMBIENT TEMPERATURE
CIRCUIT START-UP CONDITIONS
MAY BE A HIGH STRESS MODE
FOR MULTILAYER CAPACITORS
USED IN CERTAIN CIRCUIT DESIGNS

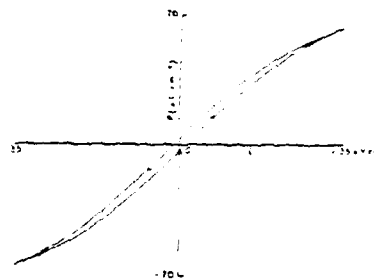
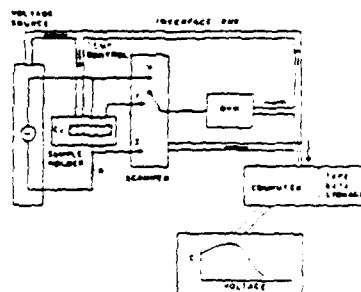
HIGH PERMITTIVITY
FERROELECTRIC MULTILAYER CAPACITORS
HAVE UNIQUE PROPERTIES
DUE TO POLARIZATION REVERSAL

OPERATIONAL FAILURES

A FERROELECTRIC MULTILAYER CAPACITOR MAY
BE UNDER MORE STRESS DURING TYPICAL
CIRCUIT OPERATION THAN DURING AN
ACCELERATED LIFE TEST.

LOW OR ROOM TEMPERATURE START-UP OF A
CIRCUIT, WHERE THE CAPACITORS HAVE A.C.
OR PULSE DRIVE, MAY BE THE WORST-CASE
TEST FOR AN MLC.

A FERROELECTRIC MLC MAY BE MORE LIKELY TO
FAIL IN OPERATION THAN DURING A LIFE
TEST.



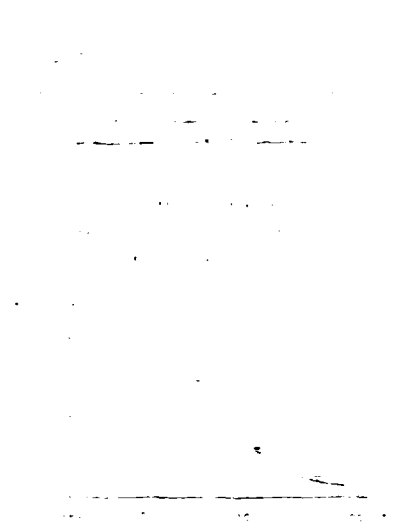
TYPICAL LOOP FOR DSU TYPE MATERIALS

EFFECTIVE DISSIPATION FACTOR

$$D_{eff} = \frac{W_2}{W_1}$$

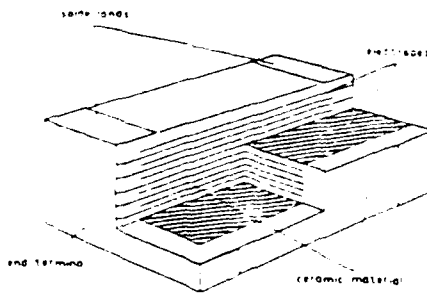
W_2 = Energy lost cycle
 W_1 = Area of hysteresis loop

W_1 = Energy stored cycle
 $W_1 = Q_{max} \times V_{max}$



TEMPERATURE DEPENDENCE
OF
HYSTERESIS LOSSES

QSL TYPE 84 (100% QSL)
SOURCE TEMPERATURE = 100°C



TYPICAL CHIP CAPACITORS

QSL TYPE 84 (100% QSL)

TYPE	ACTIVE VOLUME (mm ³)	CROSS SECTION (mm ²)
QSL	22.3	6.4
QSL	3.0	2.4
QSL	1.24	0.24

HEAT REMOVAL RATE = 0.12 W/°C
WHICH LOWERS THE ACTIVE VOL BY 0.12°C/sec

CHIP HEATING RATE FOR COLD START CONDITIONS
USE LOSS FACTORS FROM MANUFACTURERS' DATA

VOLTAGE = 5 V RMS
FREQUENCY = 1 MHz
CAPACITANCE = 0.1 μF

TYPE	LOSS (%)	TEMP RISE (°C/SEC)
QSL	7.0	8.26
QSL	0.0	2.54

FOR 1 = 12 V SQUARE WAVE (8.5 V RMS)
QSL = 22.8°C/sec.
QSL = 10.2°C/sec.

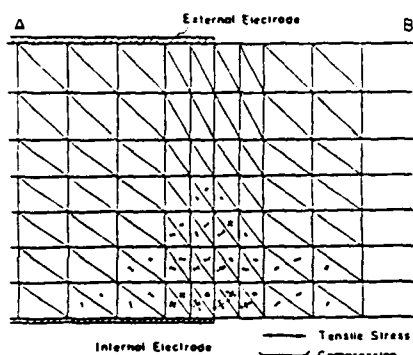
THERMAL EXPANSION

STRAIN RATE = THERM. EXPANSION COEFF. x HEAT RATE

FOR HEAT RATE = 22.8°C/sec.
THERM. EXP. COEFF. = $6 \times 10^{-6}/°C$

STRAIN RATE = 147×10^{-6} /sec

BUT A COMMERCIAL PEROVSKITE ONLY HAS A PEAK
STRAIN OF ABOUT 10^{-3}



Calculated internal stress distribution.

PEAK STRESS LIMITS

MULTILAYER ACTUATOR ANALYSIS (TAKAHASHI):

STRAIN = 1840 MICROSTRAIN

STRESS = 1000 KG/M²

AN MLC WITH A 120°C GRADIENT FROM
HYSTERETIC HEATING WILL REACH A

PEAK STRESS = 400 KG/M²,

AND MAY ATTAIN THIS LEVEL

IN LESS THAN 10 SECONDS.

S. TAKAHASHI et al.

THE THERMAL EXPANSION DIFFERENCE BETWEEN:

1. ELECTRICALLY HEATED BODY
2. INACTIVE ENDS

WILL CREATE STRESSES SIMILAR TO THOSE IN
PIEZOELECTRIC ACTUATORS.

SINCE THE HEATING MECHANISMS ARE THE DOMINANT
DRIVE, THE PEAK STRESSES WILL BE DETERMINED BY:

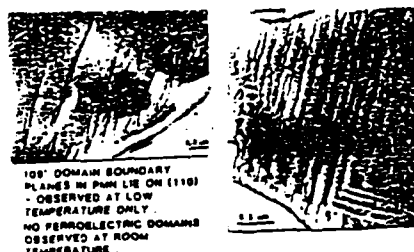
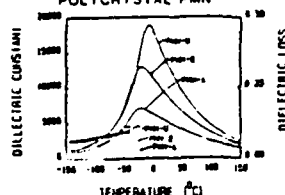
1. EQUILIBRIUM TEMPERATURE
(about 10-20° above Curie Point)
2. THE STARTING TEMPERATURE.

MIC

MATERIALS STUDIED

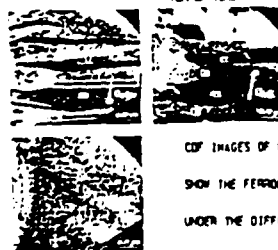
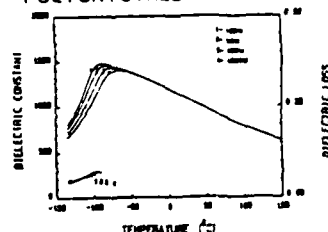
Dielectric
Behavior

H.M. CHAN, A.I. GORTON, J. CHEN AND

1. $\text{PB}(\text{MG}_{1/3}\text{NB}_{2/3})\text{O}_3$
POLYCRYSTAL PMN

NANOSTRUCTURES

M.P. HARMER, MATERIALS RESEAR

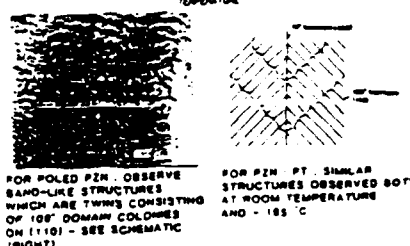
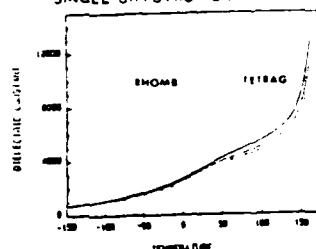
2. $\text{PB}_{0.9}\text{LA}_{0.1}(\text{MG}_{0.367}\text{NB}_{0.633})\text{O}_3$
POLYCRYSTALLINE PLMN

OF RELAXOR FERR

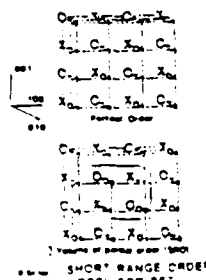
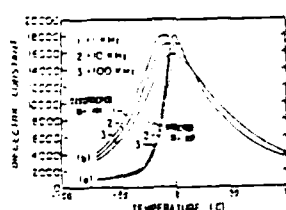
CENTER, LEHIGH UNIVERSITY, BETHLEHEM PA

3. $\text{PB}(\text{ZN}_{1/3}\text{NB}_{2/3})\text{O}_3$ 10 MOL% PbTiO_3

SINGLE CRYSTAL PZN-PT



OELECTRICS

ACKNOWLEDGMENTS
THIS WORK WAS SUPPORTED
BY NSF, ONR AND EIDUPONT
DE MEMOURS INC.4. $\text{PB}(\text{SC}_{1/2}\text{TA}_{1/2})\text{O}_3$
SINGLE CRYSTAL AND
POLYCRYSTAL PST

Ordering Microchemical Ordering



POLYCRYSTALLINE PMN
- CDF IMAGE SHOWS
ORDERED REGIONS AND APB'S

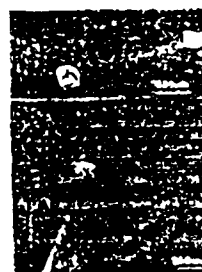
Second Phases



PYROCHLORE GRAIN IN PMN
THE COMPOSITION IS
 $Pb_{0.25}Mg_{0.25}Nb_{1.75}O_{8.62}$



INTERGRANULAR PHASE RICH
IN PHOSPHOROUS AND LEAD IN PMN-A



MAGNESIUM RICH
PRECIPITATES IN PMN-B
CONTAINING 2 MOL%
EXCESS MGO



POLYCRYSTALLINE PST
AFTER ANNEALING 30 HRS
AT 1000°C

CONCLUSIONS

1. AT ROOM TEMPERATURE
FERROELECTRIC DOMAINS OBSERVED
FOR PZN-PT BUT NOT PMN
2. AT -185°C, DOMAINS OBSERVED
FOR PZN-PT AND PMN-PT
3. ALL DOMAIN CONFIGURATIONS
CONSISTENT WITH RHOBOHEDRAL
STRUCTURE
4. IN PMN AND PMN- Mg^{+2} AND Nb^{+5}
IONS COULD EXHIBIT NAOL-TYPE
SHORT RANGE ORDER
5. INTERGRANULAR PHASES AND
LATTICE IMPURITIES DEGRADE THE
PROPERTIES OF PMN CERAMICS
SIGNIFICANTLY MORE THAN THE EFFECT
OF PYROCHLORE



FERROELECTRIC DOMAIN
BOUNDARY PLANES IN PMN
LIE ON (100) (100) DOMAINS
AND (110) (100) DOMAINS
- OBSERVED AT LOW
TEMPERATURE ONLY

SUGGESTED MODE OF
ORDERING IN PMN

CDF FROM SUPERLATTICE
REFLECTION (1/2, 1/2, 1/2)
BRIGHT
REGIONS ARE ORDERED
DOMAINS (40 Å)



OBSERVE SUPERLATTICE
REFLECTION (1/2, 1/2, 1/2)
TWO POSSIBLE TYPES OF
ORDERING OF Mg^{+2} AND Nb^{+5}
IONS: A NAOL TYPE WITH
REGIONS OF EXCESS Nb^{+5}
B. ALTERNATE (111) PLANES
OF 1:1 ALL Nb^{+5} (2) MIXED
 Nb^{+5} AND Mg^{+2}

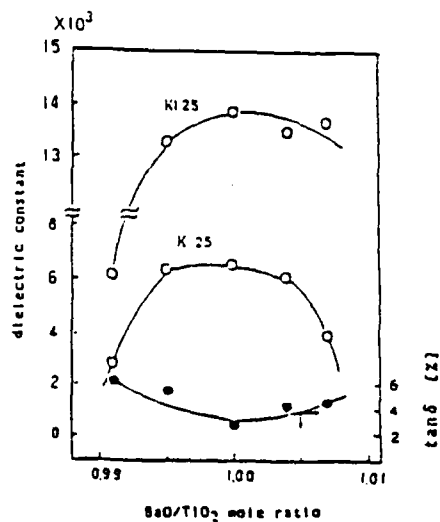


FIG. 1. Effect of BaO/TiO₂ mole ratio on dielectric properties at 1250°C

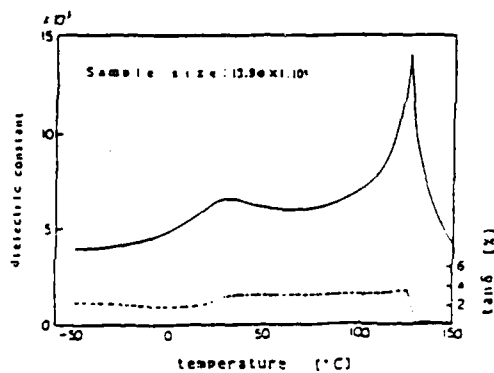


FIG. 2. Temperature dependence of the dielectric properties of BaTiO₃ ceramic with BaO/TiO₂ mole ratio = 1.000



Ratio of lead and lead oxide are very useful for electrical materials such as capacitors, piezoelectric and ferroelectric materials. The General Electric Co. Ltd. have developed a new process for making electrical materials and their products are named "Ceramic Series".

Characteristics Ceramic Series are noted for:
 1. Extremely high purity. Total impurities are less than 100 ppm.
 2. Fine size. Distribution properties are also available.
 3. High strength. Sintered products.
 4. Easily sinterable and attainable to high performance properties.

Chemical Analysis

C6-610-2 C6-610-3 C6-610-4			
Al ₂ O ₃ 50.0	50.0	50.0	50.0
SiO ₂ 30.0	30.0	30.0	30.0
Fe ₂ O ₃ 10.0	10.0	10.0	10.0
CaO 10.0	10.0	10.0	10.0
MgO 10.0	10.0	10.0	10.0
Na ₂ O 10.0	10.0	10.0	10.0
K ₂ O 10.0	10.0	10.0	10.0
Li ₂ O 10.0	10.0	10.0	10.0
Sum 100.0	100.0	100.0	100.0
Chemical Analysis			
Si	4.1	4.1	4.1
Al	4.0	4.0	4.0
Fe	1.0	1.0	1.0
Ca	1.0	1.0	1.0
Mg	1.0	1.0	1.0
Na	1.0	1.0	1.0
K	1.0	1.0	1.0
Li	1.0	1.0	1.0
Sum	10.0	10.0	10.0
Si	4.1	4.1	4.1
Al	4.0	4.0	4.0
Fe	1.0	1.0	1.0
Ca	1.0	1.0	1.0
Mg	1.0	1.0	1.0
Na	1.0	1.0	1.0
K	1.0	1.0	1.0
Li	1.0	1.0	1.0
Sum	10.0	10.0	10.0

LOW TEMPERATURE FIRED GLASS-CERAMIC DIELECTRIC MATERIAL

M. TAKABATAKE, E. SAWAKAMI, M. SASAKI

RESEARCH AND DEVELOPMENT DIVISION, ASahi GLASS COMPANY

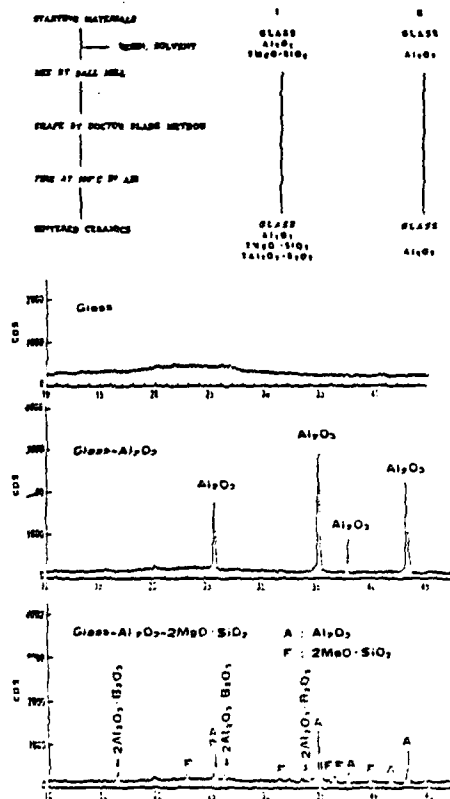
PURPOSE

1. Investigate reaction mechanism among borosilicate glass, $2\text{MgO} \cdot \text{SiO}_2$ and Al_2O_3 at high temperature. (below 900°C)
2. Features of borosilicate glass- $2\text{MgO} \cdot \text{SiO}_2$ - Al_2O_3 composite comparing with borosilicate- Al_2O_3 composite.

RESULTS

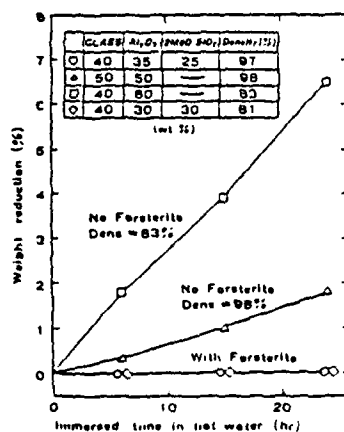
1. $2\text{MgO} \cdot \text{SiO}_2$ dissolves in the glass, and then B_2O_3 in the glass reacts with Al_2O_3 and $2\text{Al}_2\text{O}_3 \cdot \text{B}_2\text{O}_3$ crystal phase occurs.
2. (1) good sintered
(2) chemically stable
(3) good mechanical toughness

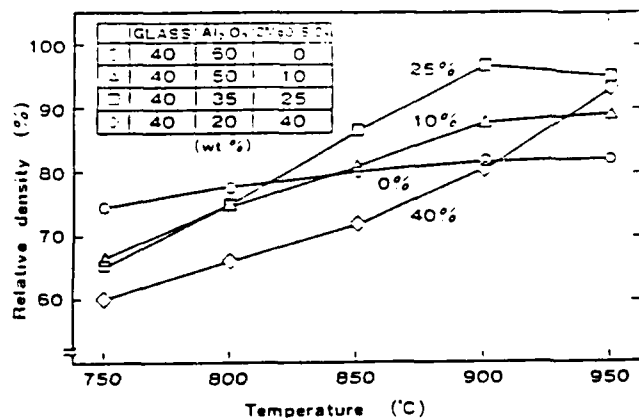
EXPERIMENTAL PROCEDURE

X-ray diffraction patterns of various compositions sintered at 900°C

	GLASS- Al_2O_3 - $2\text{MgO} \cdot \text{SiO}_2$	98% Al_2O_3
Sintering Temperature ($^\circ\text{C}$)	900	1550~1800
Flexural Strength (kg/cm^2)	2000	3500
Thermal conductivity ($\text{cal}/\text{cm} \cdot \text{sec} \cdot ^\circ\text{C}$)	0.007	0.05
Thermal Expansion Coefficient ($10^{-6}/^\circ\text{C}$)	80×10^{-7}	75×10^{-7}
Dielectric Constant (100kHz)	6.5	9.0
Dielectric Factor (100kHz)	1.5×10^{-2}	4.0×10^{-2}
Volume Resistivity ($\Omega \cdot \text{cm}$)	$> 10^{14}$	$> 10^{14}$
Surface Resistivity (Ω/\square)	0.5	1.0

Properties of the substrate

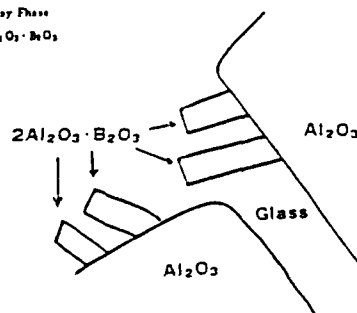
Corrosion resistance to hot water at 92°C
(sample dimension: $17 \times 17 \times 5 \text{ mm}$)



Relative density of various glass-Al₂O₃-2MgO·SiO₂ compositions with temperature.



A : α -Al₂O₃
 G : Glassy Phase
 AB : 2Al₂O₃·B₂O₃



Transmission Electron Microscope Observation

LOW TEMPERATURE FIRED MULTILAYER CERAMIC CAPACITORS WITH N_i ELECTRODES.

H. KISHI, T. WADA, S. MURAI,
H. CHAZONO and N. YAMAKA

TRIYO YUDEN CO., LTD.

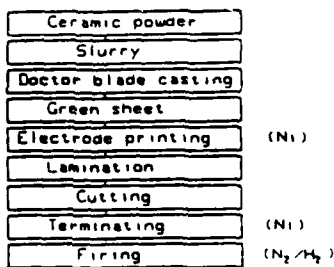
ABSTRACT: Dielectric materials based on barium titanate and glass components for multilayer ceramic capacitors with nickel electrodes have been developed. The ceramics could be fired at temperatures less than 1200°C in an atmosphere of low oxygen partial pressure, exhibited high dielectric constants (YSV: 10000-12000, X7R: 2700-3300) and high resistivity (above 10^{12} Ohm-cm).

The multilayer chip capacitors with nickel electrodes using these dielectric materials have good characteristics.

EXPERIMENTAL PROCEDURE

(b) Application to multilayer chip capacitors

Nickel metal powders were used as both of internal and terminal electrodes which were co-fired in the firing process of ceramic bodies.

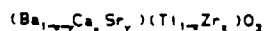


Fabrication process of the multilayer chip capacitors with Ni electrodes.

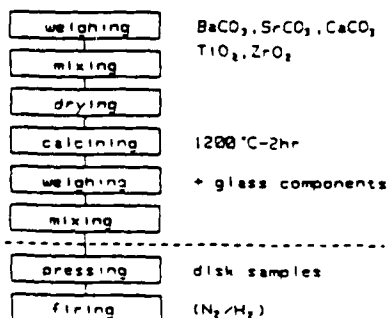
EXPERIMENTAL PROCEDURE

(a) Dielectric materials

Composition:



+ Li_2O-SiO_2-MeO glass system
(MeO: alkaline earth)



Flow chart of fabrication process of the dielectric materials.

RESULTS

(a) Dielectric materials

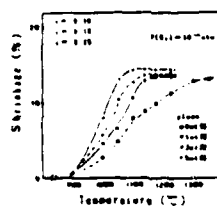


Fig. 1

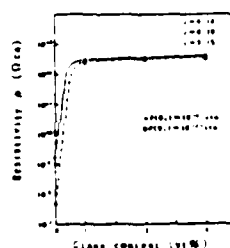


Fig. 2

The samples with glass components added are fired with full densification from 1100°C to 1200°C .

Insulation resistance increase markedly on addition of glass components.

The insulation resistance is higher than 10^{12} ohm-cm.

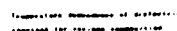
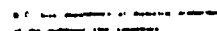


Fig. 3. a.



specification	dielectric constant
Y5V	10000-12000
X7R	2700-3300



F 18 5



FILE 6

ESR (equivalent series resistance) is small.

(1) Addition of glass components was found to markedly increase the resistivity when the ceramics were fired in a low oxygen atmosphere.

Q15V: 10000-12000 , X7R: 2700-3300)



FILE 4

	2010 (Millions)				2009 (Millions)				2008 (Millions)			
	1	2	3	4	5	6	7	8	9	10	11	12
157	1	2	3	4	5	6	7	8	9	10	11	12
158	1	2	3	4	5	6	7	8	9	10	11	12

• 1. Absence of distal air (a)

Table 1 Characteristics of the multilayer chip capacitors with Ni electrode

BARIUM TITANATE CERAMICS FOR BASE METAL MONOLITHIC CERAMIC CAPACITORS

Y. SAKABE, H. TAKAGI and K. WAKINO



Research and Development Department V,
Murata Manufacturing Co., Ltd.,
2-26-10 Tenjin, Nagaokakyo-shi, Kyoto 617, Japan

1. ABSTRACT

Barium titanate ceramics doped with SrO , CaO and ZrO_2 were fired under several low oxygen partial pressures, and their dielectric properties were measured. The dielectrics yielded a high dielectric constant ($\sim 14,000$) and high resistivity ($> 10^{11} \Omega \cdot \text{cm}$) when they were fired with a nickel electrode in a reducing atmosphere of $10^{-12} < \text{P}(\text{O}_2) < 10^{-11}$ MPa. The dielectrics are suitable for large capacitance monolithic ceramic capacitors with nickel electrodes.

2. EXPERIMENTAL

Two dielectric materials "A" and "B" were prepared by the conventional powder process. "A" is a new composition and "B" is a normal one.

A: $[(\text{Ba}_{0.97}\text{Sr}_{0.03}\text{Ca}_{0.10}\text{Ti}_{0.99}(\text{Ti}_{0.91}\text{Zr}_{0.09}\text{O}_2) + 0.1 \text{ at } \% \text{MnO}_2]$
B: $\text{Ba}(\text{Ti}_{0.91}\text{Zr}_{0.09}\text{O}_2)$

The test samples were prepared in disc form (14 mm in diameter by 1.0 mm thick). The discs, with and without Ni-paste on the surface, were sintered under $\text{P}(\text{O}_2)$ ranges of 10^{-12} to 10^{-11} MPa. An In-Ga alloy was applied as a conducting electrode on the sintered disc. Resistance was measured at room temperature on a megohmmeter at 500 V dc or on a resistance meter with low voltage. Capacitance was measured on an LF impedance analyzer at 1 V and 1 kHz.

3. RESULTS

Figure 1 shows the resistivity at room temperature vs sintering $\text{P}(\text{O}_2)$. The "A" dielectrics yielded high resistivity ($> 10^{11} \Omega \cdot \text{cm}$) when $\text{P}(\text{O}_2)$ was higher than 2×10^{-11} MPa. At $\text{P}(\text{O}_2)$ lower than 10^{-11} MPa, the samples were converted to dark-colored semiconductors. This marginal $\text{P}(\text{O}_2)$ was close to the equilibrium one for Ti_2O_3 , TiO , i.e., 5×10^{-11} MPa at 1300°C . The dielectrics "B" always showed low resistivity.

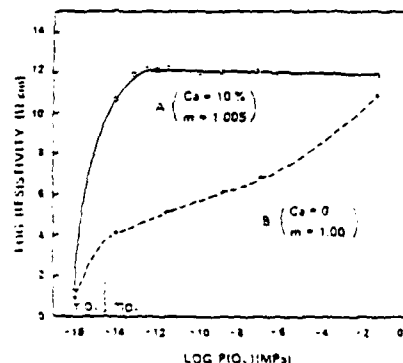


Fig. 1 Resistivity of the "A" and "B" dielectrics sintered under various $\text{P}(\text{O}_2)$ at 1300°C and 1400°C , respectively, for 2 h.

Figure 2 shows the dependence of the dielectric constant on the sintering atmosphere. The "A" dielectrics sintered in the $\text{P}(\text{O}_2)$ range of 10^{-12} to 10^{-11} MPa showed a very high dielectric constant (14,000) and low dissipation factor ($< 1.5\%$). At the $\text{P}(\text{O}_2)$ regions higher than 10^{-11} MPa, the dielectric constant of the Ni-electroded disc decreased with increasing $\text{P}(\text{O}_2)$.

The equilibrium $\text{P}(\text{O}_2)$ for Ni-NiO at 1300°C is 2×10^{-11} MPa. But even in the lower $\text{P}(\text{O}_2)$ regions ($< 10^{-11}$ MPa), nickel metal on the dielectric ceramics was partially oxidized and reacted with ceramics, resulting in a degradation of the dielectric properties. Firing atmosphere for the nickel electrode monolithic ceramic capacitors with "A" dielectrics has to be controlled accurately within the $\text{P}(\text{O}_2)$ ranges of 10^{-12} to 10^{-11} MPa.

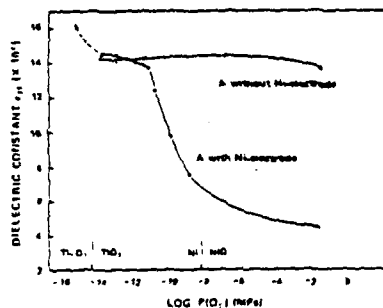


Fig. 2 Dielectric constant of the "A" dielectrics sintered with and without Ni-electrode under various $\text{P}(\text{O}_2)$ atmosphere at 1300°C for 2 h.

The dependence of the dielectric constant on temperature for the "A" dielectrics co-fired with the nickel electrode in various $\text{P}(\text{O}_2)$ atmosphere is shown in Fig. 3. The temperature which shows maximum dielectric constant was not affected by the sintering atmosphere.

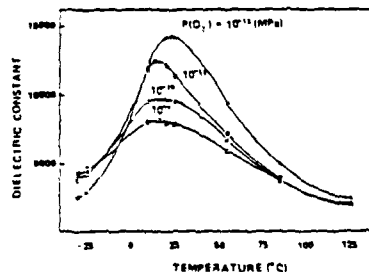


Fig. 3 Temperature dependence of dielectric constant of the "A" dielectrics sintered with Ni-electrode under low oxygen partial pressures at 1300°C for 2 h.

4. APPLICATION

The resultant material slightly modified from "A" composition was applied to the monolithic capacitor with nickel electrode. The capacitor was made into a large capacitance capacitor from 10 to 100 μ F for high frequency applications.

Impedance and ESR characteristics of 56 μ F multilayer capacitor are superior to the 3300 μ F aluminum electrolytic capacitor at frequencies more than 50 KHz. When 20 amperes of ripple current at 100 KHz are applied to the new capacitor, the surface temperature rise is only 5 C which is one-fifth of that of the aluminum electrolytic capacitor. The results of load life test are shown in Fig. 4, which shows that these base metal monolithic capacitor are as reliable as conventional monolithic capacitors. The failure rate of ZSU-56 μ F-25 Volt capacitor was estimated to be less than 0.025% per 1000 hrs at rated conditions.

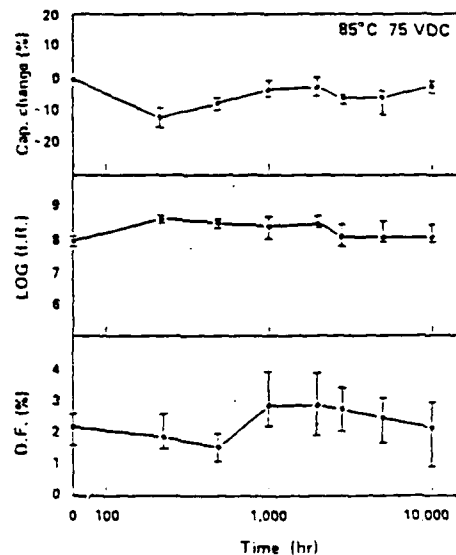


Fig. 4 Load life test results for nickel electrode monolithic capacitors, ZSU 56 μ F 25 volt. Sample volume was 40 pcs.

sumitomo

Nickel Electrode Monolithic Ceramic Capacitors

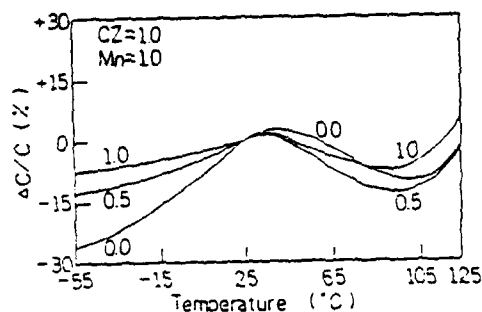
Type	ZSU			
	0.1 μ F	1.0 μ F	10 μ F	56 μ F
Chip type				
Dipped type				

M21

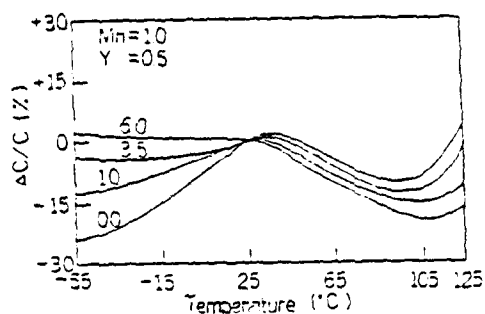
TEMPERATURE STABLE BARIUM TITANATE CERAMICS FOR BASE METAL MULTILAYER CAPACITORS

DIELECTRIC MATERIAL

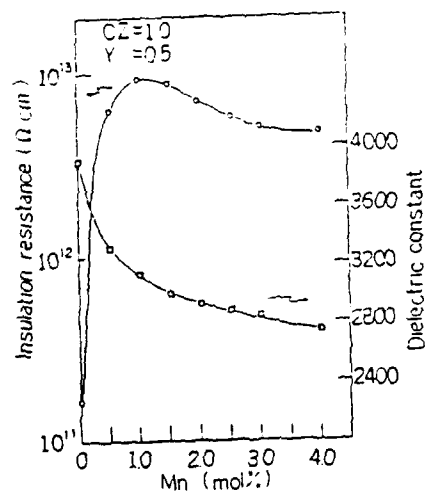
1. SYSTEM:
 $\text{BaTiO}_3 - \text{CaZrO}_3 - \text{MnO} - \text{Y}_2\text{O}_3$
2. FIRING TEMPERATURE:
1270-1350°C
3. FIRING ATMOSPHERE:
 $\text{PO}_2 = 3 \times 10^{-10} - 3 \times 10^{-5} \text{ atm.}$



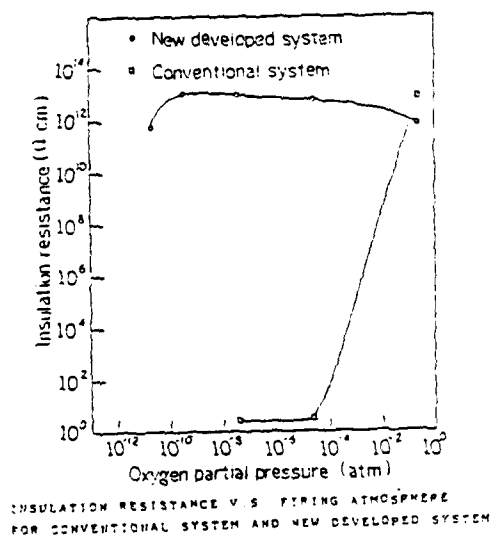
TEMPERATURE CHARACTERISTICS OF DIELECTRIC CONSTANT FOR VARIOUS Y_2O_3 CONTENT (MOL%)



TEMPERATURE CHARACTERISTICS OF DIELECTRIC CONSTANT FOR VARIOUS CaZrO_3 CONTENT (MOL%)



INSULATION RESISTANCE AND DIELECTRIC CONSTANT V. S. MNO CONTENT (MOL%)



INSULATION RESISTANCE V. S. FIRING ATMOSPHERE FOR CONVENTIONAL SYSTEM AND NEW DEVELOPED SYSTEM

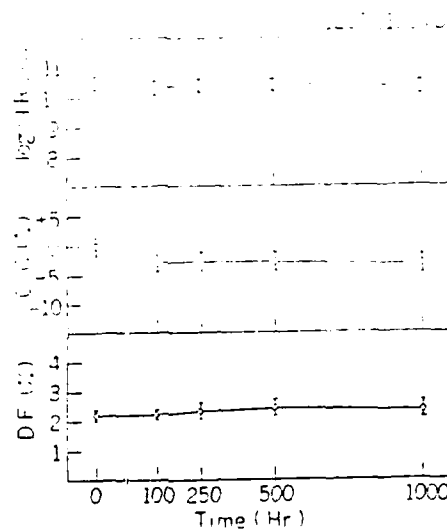
APPLICATION TO MLC WITH NICKEL ELECTRODES

CHIP SIZE 2.2 x 1.5 mm
 GREEN THICKNESS 45 μ m
 NUMBER OF LAYERS 20 OR 40
 ELECTRODES NICKEL

MLC CHIP CONSTRUCTION

CHARACTERISTICS	20LAYERS	40LAYERS
CAPACITANCE (nF)	53.4	110.5
D.F. (%)	2.2	2.0
IR (G Ω)	25	12
CR PRODUCT (nF)	1300	1300
BDV (VDC min.)	500	400
TCC (E1A)	X7R	X7R

ELECTRICAL CHARACTERISTICS OF MLC
WITH NEW DEVELOPED DIELECTRICS
AND NICKEL ELECTRODES.



LIFE TEST AT 125°C, 100VDC

BARIUM MODIFIED LEAD ZINC NIOBATE DIELECTRICS FOR MULTILAYER CERAMIC CAPACITOR

E. INAGAKI, Y. YAMASHITA and K. YUUKI

Engineering Department, Marcon Electronics Co., Ltd.,
1-1 Saiwai-cho, Nagai, Yamagata 993, Japan

ABSTRACT

Substitution effects for lead zinc niobate based ceramic by barium and titanium have been systematically investigated. It was found that the partially substituted lead zinc niobate dielectric by barium and titanium has shown to be a promising candidate for multilayer ceramic capacitor. This ceramic materials can be fired at 980 - 1,150°C, and exhibit high dielectric constant of 4,000 - 8,500, and high insulation resistance of $10^{12} - 10^{15} \Omega \text{cm}$. In this system, a $(\text{Pb}_{0.75}\text{Ba}_{0.25})_{1/3}(\text{Zn}_{1/3}\text{Nb}_{2/3})_{1/3}\text{Ti}_{1/3}\text{O}_3$ shows dielectric constant of 8,440, dissipation factor of 1.9%, insulation resistance (CR product) of 14,600 Ω at 25°C and 3,300 Ω at 125°C, respectively. This material offers superior performances and low cost to conventional barium titanate based ceramic.

INTRODUCTION

In order to improve disadvantages of barium titanate based dielectric material, studies of new high dielectric constant relaxor materials are widely carried out. The authors have succeeded in easily synthesizing perovskite type lead zinc niobate as a ceramic form. By means of partial substitution by strontium and titanium. In the present study, dielectric properties of the lead zinc niobate based compositions, in which the dielectric constant maxima show around the room temperature, has been investigated by the adjustment of the amount of barium and titanium substitution.

Basic compositions for the dielectrics (Table 1)

1) ELECTRICAL PROPERTIES	
• High resistivity	$> 10^{12} \Omega \text{cm}$
• High dielectric constant	$> 1,000$
• Small temperature coefficient of capacitance	$\pm 0.1\% / ^\circ\text{C}$
• Low dissipation factor	$D.F. < 2.5\%$
• High breakdown voltage	$> 10 \text{ kV/cm}$
• Small dielectric dependency	$< 10\% \text{ at } 100^\circ\text{C}$
2) PHYSICAL PROPERTIES	
• Homogeneous and small grain size	$< 0.5 \mu\text{m}$
• High mechanical strength	$> 10 \text{ kgf/cm}^2$
• Low water absorption	$< 0.1\%$
3) OTHER PROPERTIES	
• Broad sintering temperature	1000 - 1,150°C
• Good electrode compatibility	
• Reliability	
• Low cost	

Sample Preparation

- Composition
 $(\text{Pb}_{1-x}\text{Ba}_x)(\text{Zn}_{1/3}\text{Nb}_{2/3})_{1/3}\text{Ti}_{1/3}\text{O}_3$ $x=0-0.5$ $y=0.6-1.0$
- Raw Materials
 PbO , BaCO_3 , ZnO , Nb_2O_5 , TiO_2 $x=0-0.4$
- Calcining
750°C x 2H
- Sintering
980 - 1,150°C x 2H
- Specimen Size
12 x 10 mm
- Measurement
X-ray, Relative Permittivity, Dissipation Factor, Electrical Resistivity, Curie Temperature, Capacitance Temperature Change

CONCLUSION

Dielectric properties of $(\text{Pb}_{1-x}\text{Ba}_x)(\text{Zn}_{1/3}\text{Nb}_{2/3})_{1/3}\text{Ti}_{1/3}\text{O}_3$ ceramics were investigated from a viewpoint of application to multilayer ceramic capacitor (MLC). The ceramic materials can be fired 980 - 1,150°C and exhibit high dielectric constant of 4,000 - 8,500. Effects of Ba substitution for Pb is summarized as follows: stabilizes perovskite structure, improves sinterability, improves mechanical strength, increases electrical resistivity, increases breakdown voltage, shifts Curie temperature and increase sintering temperature.

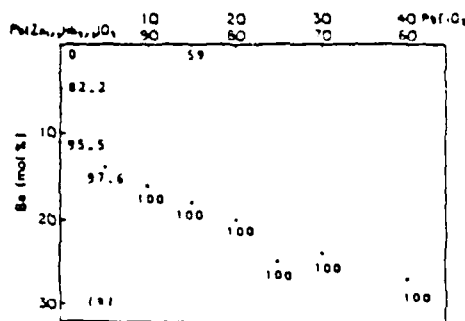


Fig. 1. Relative amount of perovskite phase for the PBZT system.

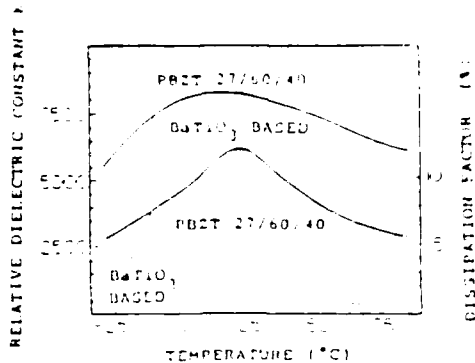
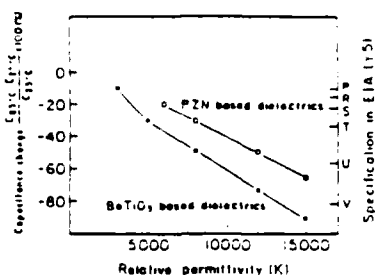
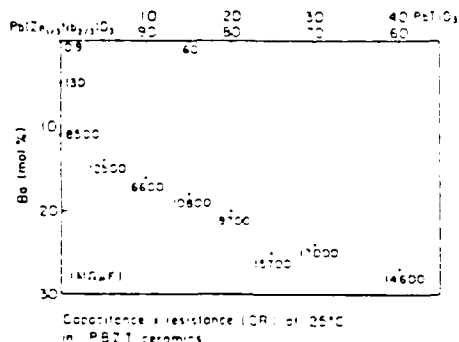


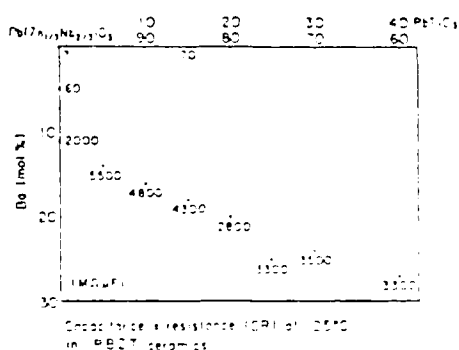
Fig. 2. Dielectric properties for the PBZT 27/60/40 and conventional YST characteristics BaTiO₃ based dielectric.



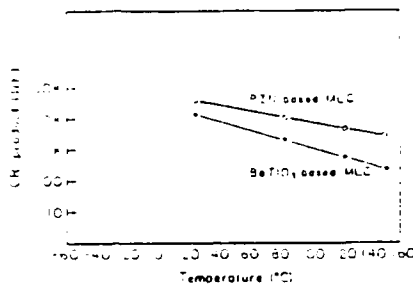
Temperature capacitance change vs. relative permittivity of PZN based MLC and BaTiO₃ based MLC.



Capacitance & resistance (CR) at 25°C in PBZT ceramics



Capacitance & resistance (CR) at 25°C in PBZT ceramics



CR product vs. temperature of PZN based MLC and BaTiO₃ based MLC.

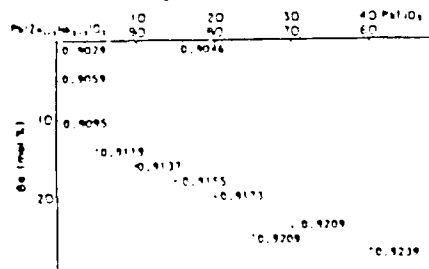


Fig. 3. Tolerance factor for the PBZT system.

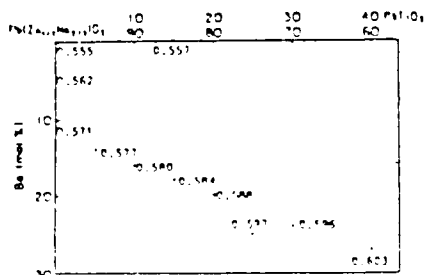


Fig. 4. Amount of ionic character for the PBZT system.

(BASIC REQUIREMENTS FOR PEROVSKITE STRUCTURE)

- 1) Tolerance Factor (1)

$$T = \frac{r_A + r_B}{\sqrt{2}(r_B + r_O)}$$

r_A - ionic radii for A ions
 r_B - " " " " for B ions
 r_O - " " " " for O ions
- 2) Ionic Character

$$P_{AB} = \frac{1}{2} \left(\frac{X_A - X_B}{X_A + X_B} \right)^2$$

P_{AB} - amount of ionic character
 X_A - electronegativity value for A ion
 X_B - " " " " for B ion

Effects of Ba substitution in PZN

1. Stabilizes perovskite structure
2. Improves mechanical strength
3. Increases electrical resistivity
4. Increases breakdown voltage
5. Improves sinterability
6. Shifts Curie temperature
7. Increases firing temperature

DIELECTRIC RELAXATION STUDIES IN SOME POLYMER - PET COMPOSITES

A. M. VARAPRASAD

Department of Physics, Sophia University, Kioi-cho, Chiyoda-ku, Tokyo 102, Japan

Due to the rapid increase in application of ferroelectricity in electronic industries, ferroelectric polymers and hybrid materials have been studied extensively [1,2] and composite materials made up of such ferroelectric particles dispersed in a polymer matrix have attracted the attention of materials technologists due to its use of preparation, lower sensitivities and favorable dielectric, ferroelectric and piezoelectric properties have been noticed [3] in composites. Basically due to the change in the molecular motion of the polymer. In the present study dielectric relaxation studies were therefore planned on composites between PET and certain mechanically sound polymeric materials to unfold the effect of composite formation.

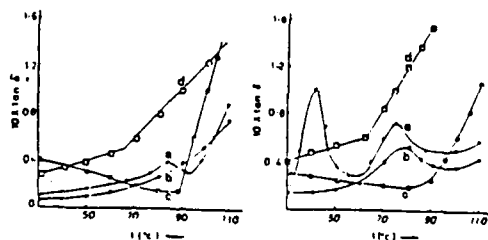
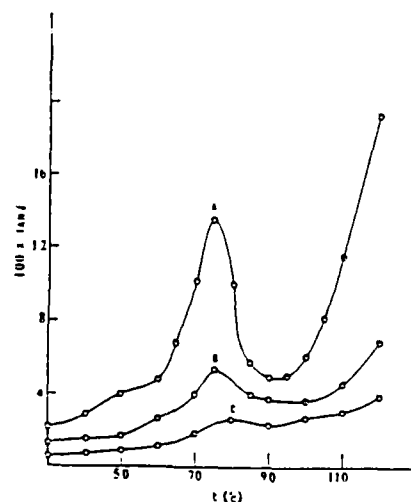
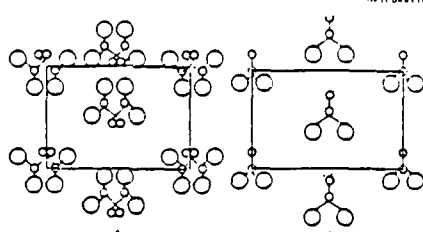


Fig.1. Dielectric relaxations in some polymers used for composite formation (a)VA-VC (b)PVDF (c)PET/VA-VC (d)PET/VA-VC/PVDF

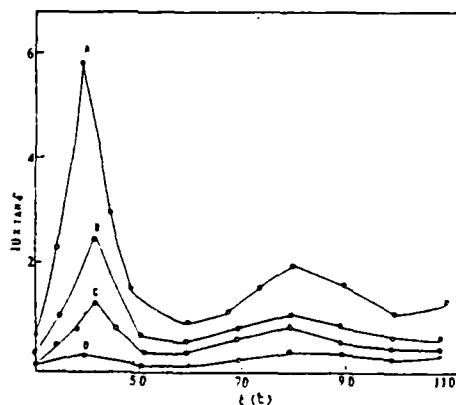
Fig.2. Dielectric relaxations in the composites (a)VA-VC (b)PVDF (c)PET/VA-VC (d)PET/VA-VC/PVDF



Temperature vs. $\tan \delta$ for PET/PVDF COMPOSITES (a) 100Hz (b) 500Hz (c) 1KHz (d) 10KHz.

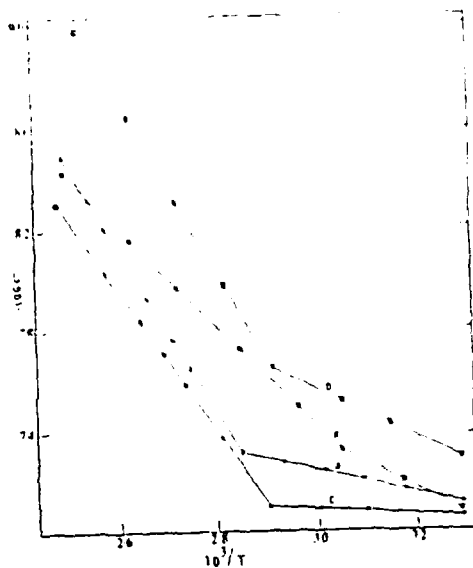


In the case of PVDF, a relaxation around 10°C was known to occur due to the segmental motion in the TGTG conformation. The new relaxation was however found for the all trans (TTTT) conformation. In fact the starting PVDF material (Fig.1b) shows no relaxation near around this temperature. The observation of new relaxation was in the composite at about 50°C (Fig.2b) was therefore ascribed to the effect of conformation of the PVDF to the TGTG conformation. Relaxation due to the segmental motion of VA-VC and PET composites were not observed in the experimental range of temperature viz 10 to 150°C. The high temperature β -relaxation due to the motion of the main polymer chain next glass transition was mostly unchanged in the composites.



Temperature vs. $\tan \delta$ for PET/VA-VC COMPOSITES (a) 100Hz (b) 500Hz (c) 1KHz (d) 10KHz.

IN VA-VC COMPOSITE THE OBSERVED NEW RELAXATION AT 40°C WAS ATTRIBUTED TO THE SEGMENTAL MOTION OF VA AND VC SEGMENTS. In the case of pure VA-VC the relaxation occurs at -20°C. Owing to the coupling of polymer segments with the polarisation charge of PET particles the relaxation has been shifted to higher temperatures.

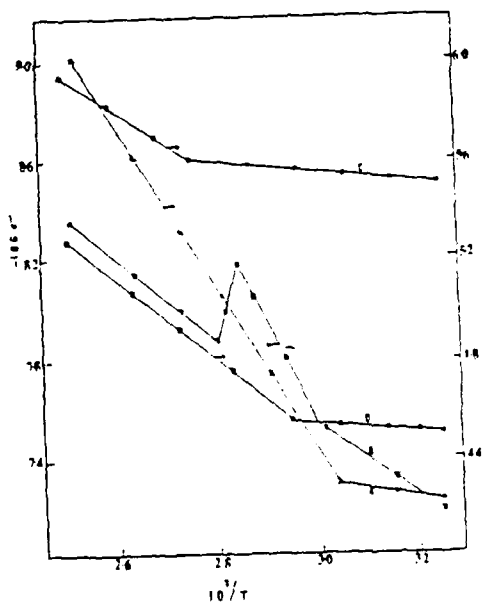


Electrical conductivity vs. temperature
inverse for different polymers.
(VA-VC) (PVCF) (EPOXY) (NR-PVC)

APPROXIMATE DATA FOR ELECTRICAL CONDUCTIVITY

POLYMER	TEMPERATURE (°C)		CONDUCTIVITY (Ω ⁻¹ CM ⁻¹)	
	25	100	25	100
VA-VC	1.25	1.22	1.25	1.22
PVCF	1.25	1.22	1.25	1.22
EPOXY	1.25	1.22	1.25	1.22
NR-PVC	1.25	1.22	1.25	1.22

- ΔE below and above glass transition temperature T_g
- Below T_g , ΔE decreases on composite formation due to the decrease in free volume available for electrical conduction.
 - Above T_g , similar behaviour is noticed for EPOXY and NR-PVC composites where there are no new dielectric relaxations on composite formation.
 - New dielectric relaxations in VA-VC and PVCF composites increase the ΔE as the trapped charge gets released due to the molecular motion of the polymer chains.



Electrical conductivity vs. temperature
inverse for different composites.
(VA-VC) (PVCF) (EPOXY) (NR-PVC)

T1

MICROWAVE DIELECTRIC PROPERTIES OF $Pb(Zr,Ce)O_3$ CERAMICS

K. MURANO, K. TATSUKI

Sony Development Center, Sony Corp. Tokyo, Japan

S. NISHIGAKI, S. YANO, H. KATO

Narumi Technical Lab. Narumi China Corp. Nagoya, Japan

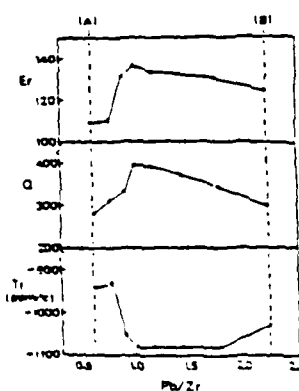
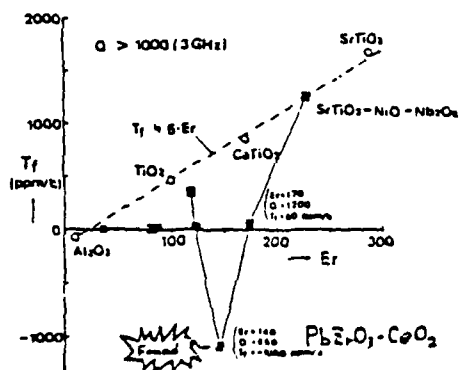
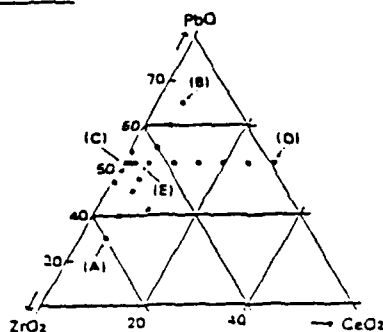
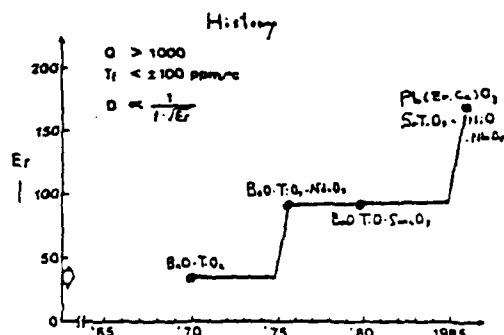
CERAMICS USED AT MICROWAVE FREQUENCIES

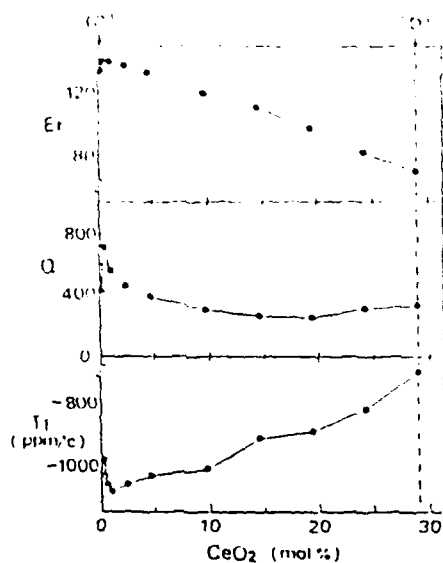
- (1) A HIGH DIELECTRIC CONSTANT (ϵ_r)
- (2) A HIGH Q FACTOR (Q)
- (3) A NEARLY ZERO TEMPERATURE COEFFICIENT (T_f)

$$\epsilon_r > 100 \quad Q > 1000 \quad T_f > 100 \text{ ppm}/^\circ\text{C}$$

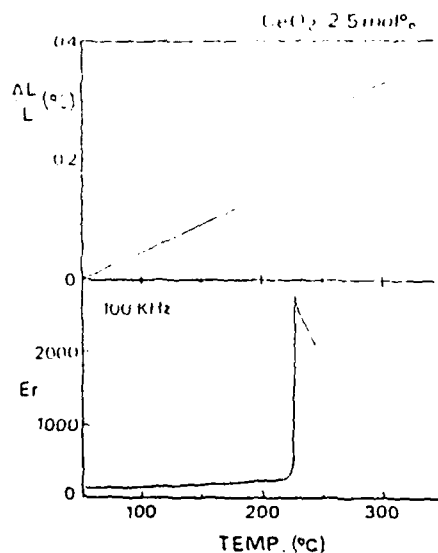
LARGE POSITIVE

IF T_f IS NEGATIVE:



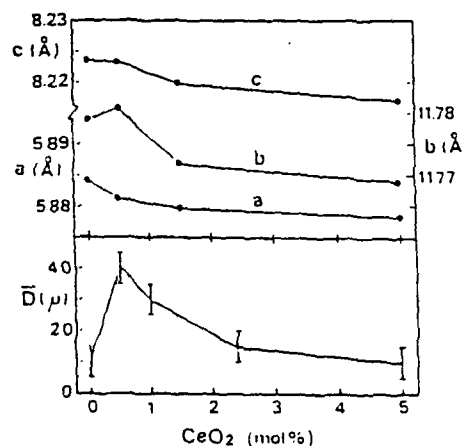


Dielectric properties of PbZrO_3 vs CeO_2 content at 3GHz

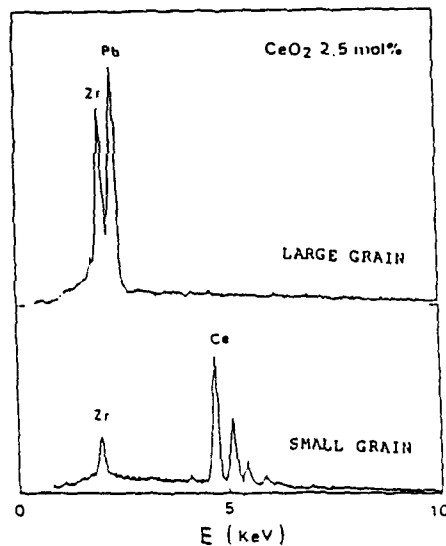


The thermal expansion and E_r vs. temperature.

EPMA (EDX)



The change of lattice constants and grain size vs. temperature.



The compositions of grains.

Dielectric properties of combined ceramics

Comp.	(1) $\text{PbZrO}_3\text{-CeO}_2$	(2) $\text{SrTiO}_3\text{-NiO-Nb}_2\text{O}_5$	(1)×(2)
E_r	140	230	170
Q	850	2300	1200
T_d (pK/m°C)	-1080	1250	80

H. SATO, K. AYUSAWA, M. SAITO, and K. KAWAMURA

Research Laboratory, Oki Electric Industry Co., Ltd. Tokyo, Japan.

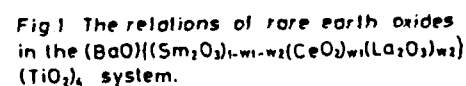


Fig 1 The relations of rare earth oxides in the $(\text{BaO})\{(\text{Sm}_2\text{O}_3)_{1-w_1-w_2}(\text{CeO}_2)_{w_1}(\text{La}_2\text{O}_3)_{w_2}\}(\text{TiO}_2)_4$ system.

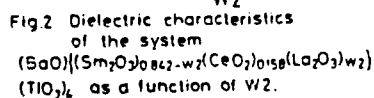


Fig.2 Dielectric characteristics of the system $(\text{BaO})\{(\text{Sm}_2\text{O}_3)_{0.842-w}(\text{CeO}_2)_{0.158}(\text{La}_2\text{O}_3)_w\}(\text{TiO}_2)_4$ as a function of $w/2$.

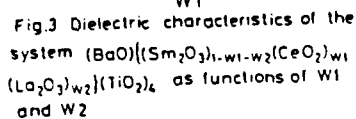


Fig.3 Dielectric characteristics of the system $(\text{BaO})\{(\text{Sm}_2\text{O}_3)_{1-w_1-w_2}(\text{CeO}_2)_{w_1}(\text{La}_2\text{O}_3)_{w_2}\}(\text{TiO}_2)_x$ as functions of w_1 and w_2

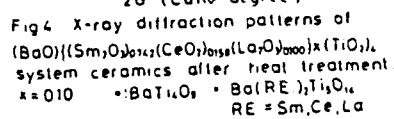


Fig. 4 X-ray diffraction patterns of
(BaO)_{1-x}(Sm₂O₃)_{0.1-0.2}(CeO₂)_{0.15-0.2}(La₂O₃)_{0.05-0.1}(TiO₂)_{0.1}
system ceramics after heat treatment
x = 0.10 • BaTi₄O₉ • Ba(RE)₂Ti₂O₁₀
RE = Sm, Ce, La

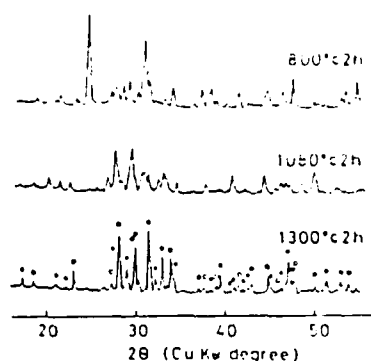


Fig 5 X-ray diffraction patterns of $(\text{BaO})((\text{Sm}_2\text{O}_3)_{0.5x2}(\text{CeO}_2)_{0.5x2}(\text{La}_2\text{O}_3)_{0.5x2})(\text{TiO}_2)_x$ system ceramics after heat treatment $x=0.50$ \bullet $\text{Ba}(\text{RE})_{1/3}\text{O}_{1/6}$ \bullet $\text{Ba}_{1/3}\text{O}_2$

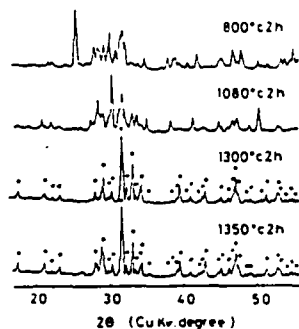


Fig 6 X-ray diffraction patterns of $(\text{BaO})((\text{Sm}_2\text{O}_3)_{0.5x2}(\text{CeO}_2)_{0.5x2}(\text{La}_2\text{O}_3)_{0.5x2})(\text{TiO}_2)_x$ system ceramics after heat treatment $x=1.0$ \bullet $\text{Ba}(\text{RE})_{1/3}\text{O}_{1/6}$ \bullet $\text{RE} = \text{Sm, Ce, La}$

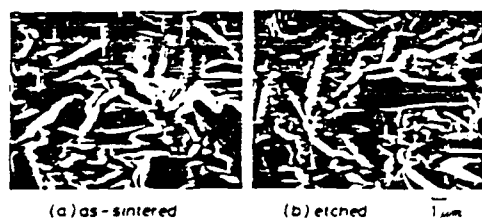


Fig 7 SEM photographs as-sintered and etched $(\text{BaO})((\text{Sm}_2\text{O}_3)_{0.5x2}(\text{CeO}_2)_{0.5x2}(\text{La}_2\text{O}_3)_{0.5x2})(\text{TiO}_2)_x$ ceramics in $(\text{HF}+\text{HNO}_3)$ acid

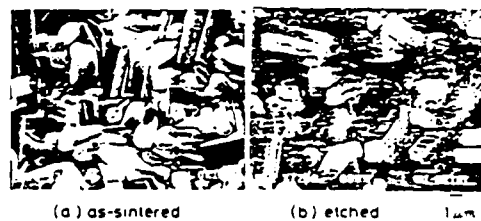


Fig 8 SEM photographs as-sintered and etched $(\text{BaO})((\text{Sm}_2\text{O}_3)_{0.5x2}(\text{CeO}_2)_{0.5x2}(\text{La}_2\text{O}_3)_{0.5x2})(\text{TiO}_2)_x$ ceramics in $(\text{HF}+\text{HNO}_3)$ acid



Fig 9 SEM photographs as-sintered and etched $(\text{BaO})((\text{Sm}_2\text{O}_3)_{0.5x2}(\text{CeO}_2)_{0.5x2}(\text{La}_2\text{O}_3)_{0.5x2})(\text{TiO}_2)_x$ ceramics in $(\text{HF}+\text{HNO}_3)$ acid

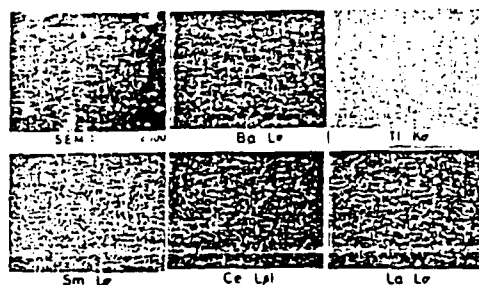


Fig 10 X-ray images of $\text{BaO-Sm}_2\text{O}_3\text{-CeO}_2\text{-La}_2\text{O}_3\text{-TiO}_2$ ceramics.

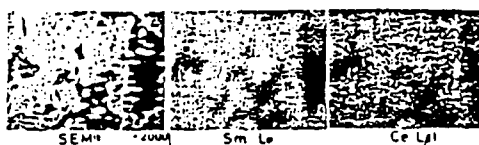


Fig 11 X-ray images of $\text{BaO-Sm}_2\text{O}_3\text{-CeO}_2\text{-TiO}_2$ ceramics.

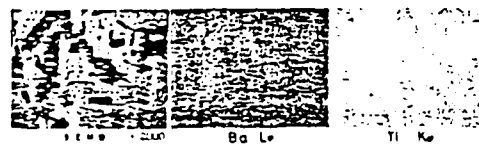


Fig 12 X-ray images of $\text{BaO-Sm}_2\text{O}_3\text{-CeO}_2\text{-TiO}_2$ ceramics

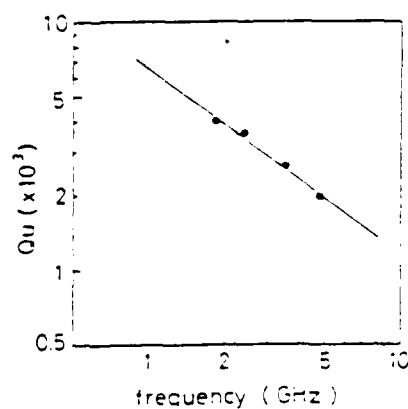


Fig 13 Q_u values vs frequency for $\text{BaO-Sm}_2\text{O}_3\text{-CeO}_2\text{-La}_2\text{O}_3\text{-TiO}_2$

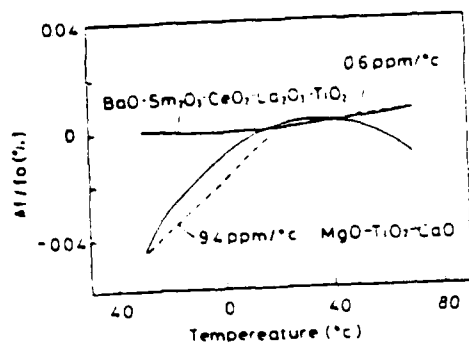


Fig 14 Resonant frequency vs temperature

Table 1 Properties of $\text{BaO-Sm}_2\text{O}_3\text{-CeO}_3\text{-La}_2\text{O}_3\text{-TiO}_2$ ceramics.

Dielectric constant ϵ_r	75.5
Unloaded Q	1870 (at 5 GHz)
Qu	6300 (at 1 GHz)
Temperature coefficient τ_f	0 ppm/ $^{\circ}\text{C}$
Metallization by chemical plating	Very easy (susceptible to HF-HNO_3 mixed acid)

HIGH-Q DIELECTRIC RESONATOR MATERIAL FOR MILLIMETER-WAVE FREQUENCIES

H. TAMURA, D. A. SAGALA, M. MURATA, and K. WAKINO
Research & Development Department W, Murata Manufacturing Co., Ltd., Kyoto,
Japan

INTRODUCTION AND RESULT

Dielectric resonator ceramics have gained an important position as a key element for microwave components. Among many materials developed for dielectric resonators, those with complex perovskite structure have very high Q values. Complex perovskite materials of the system $\text{Ba}(\text{Mg,Ta})\text{O}_3$ - BaSnO_3 are investigated here. This system presented a very high Q value and would be useful for applications of millimeter-wave frequency.

The addition of BaSnO_3 on $\text{Ba}(\text{Mg,Ta})\text{O}_3$ was effective both to obtain a 0 ppm/°C temperature coefficient of resonant frequency and to improve a Q value. Although $\text{Ba}(\text{Mg}_{1/3}\text{Ta}_{2/3})\text{O}_3$ had a perovskite pseudocell and hexagonal superstructure, the superstructure was not formed after the addition of BaSnO_3 of more than about 10 mol%. Sintering of solid solution $\text{Ba}(\text{Sn}_{0.1}\text{Mg}_{0.9}\text{Ta}_{0.6})\text{O}_3$ was accelerated compared to those of $\text{Ba}(\text{Mg,Ta})\text{O}_3$ alone, and the microwave Q value was also improved.

The resultant dielectric characteristics are as follows: $K=24.5$, $Q > 20,000$ at 10 GHz, and temperature coefficient of resonant frequency, $\tau_f=0$ ppm/°C.

In a study investigating the crystal structure of the complex perovskite material, Galasso and Pyle reported that complex perovskites containing Ta ions had pseudocubic unit cells with hexagonal superstructures because the two B-site ions were of ordered configuration.

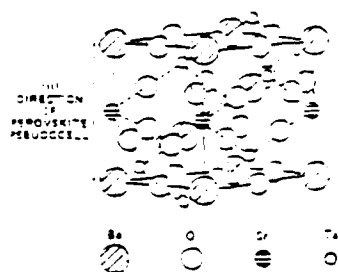


Fig. 1. $\text{Ba}(\text{Sr}_{0.25}\text{Ta}_{0.75})\text{O}_3$.

Fig. 1. P. Galasso and J. Pyle, "Ordering in Compounds of the $\text{AB}_{1/3}\text{Ta}_{2/3}\text{O}_3$ Type," *Inorganic Chemistry*, 3, 2482 (1963).

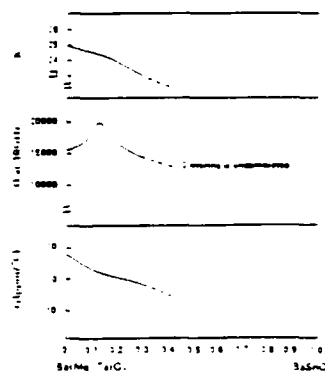
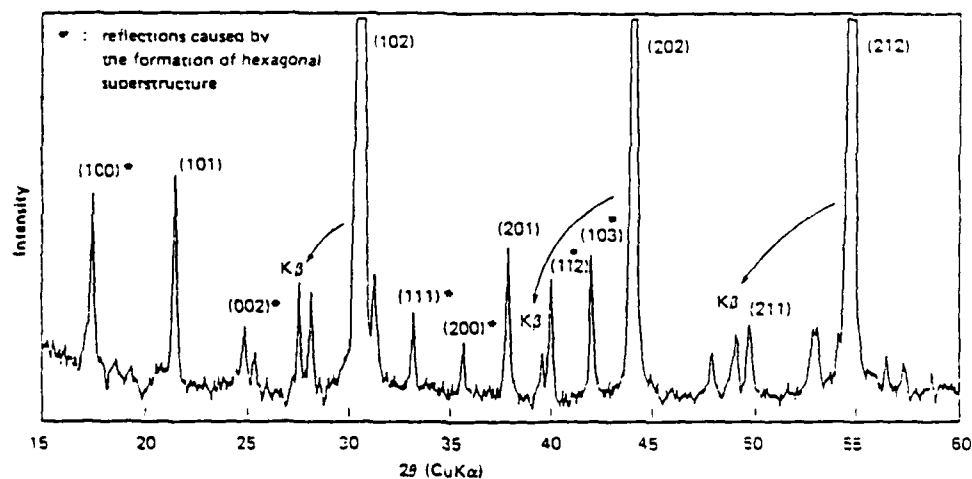


Fig. 2. Dielectric characteristics of $\text{Ba}(\text{Mg,Ta})\text{O}_3$ - BaSnO_3 ceramics.

$\text{Ba}(\text{Mg}_{1/3}\text{Ta}_{2/3})\text{O}_3$ has pseudocubic unit cells with hexagonal superstructures. Fig. 4 shows the X-ray powder diffraction patterns of this material. The Miller indices parameters in the figures are those of hexagonal superstructure, and the peaks marked by an asterisk are caused by the formation of superstructures.

The peaks of superstructure have disappeared in the X-ray diffraction patterns of $\text{Ba}(\text{Sn}_{0.1}\text{Mg}_{0.3}\text{Ta}_{0.6})\text{O}_3$.



X-ray powder diffraction pattern of $\text{Ba}(\text{Mg}_{1/3}\text{Ta}_{2/3})\text{O}_3$.

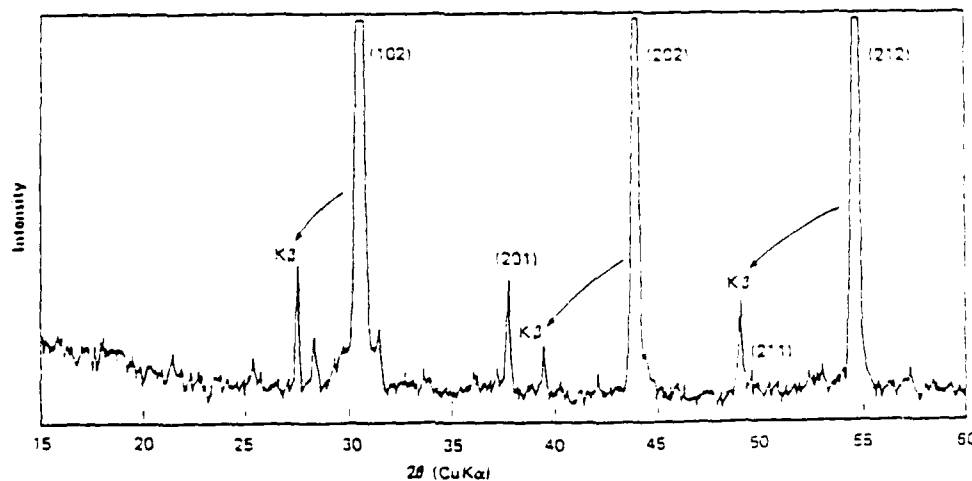


Fig. 4 . X-ray powder diffraction pattern of $\text{Ba}(\text{Sn}_{0.1}\text{Mg}_{0.3}\text{Ta}_{0.6})\text{O}_3$

Fig. 5 shows the frequency dependence of this $\text{Ba}(\text{Sn}, \text{Mg}, \text{Ta})\text{O}_3$ ceramic whose Q is optimized to 3 ppm $^\circ\text{C}$.

Dielectric characteristics at microwave frequency can be determined mainly to the ionic polarization which is strongly related to lattice vibrations at far infrared region. The dielectric constant given here is constant in the microwave region, and the dielectric loss increases proportionally to frequency.

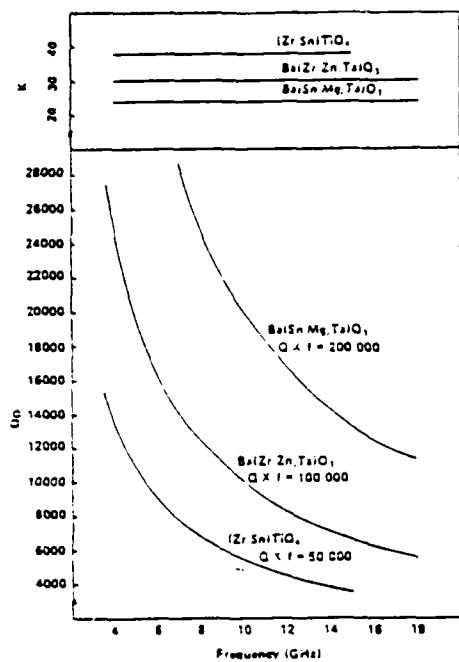
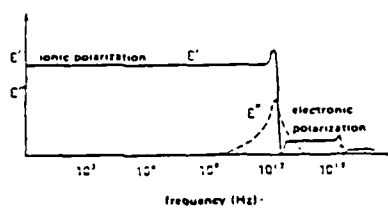


Fig. 5 Frequency vs. K and Q for $\text{Ba}(\text{Sn}, \text{Mg}, \text{Ta})\text{O}_3$ ceramic



$$E'(\omega) - E'(\infty) = \frac{\omega_{\tau}^2 \cdot (E'(0) - E'(\infty))}{\omega_{\tau}^2 - \omega^2 - j\gamma\omega}$$

under the condition of $\omega^2 \ll \omega_{\tau}^2$,

$$E'(\omega) - E'(\infty) = E'(0) - E'(\infty)$$

$$\tan \delta = \frac{E''(\omega)}{E'(\omega)} = \frac{\gamma}{\omega_{\tau}^2} \cdot \omega$$

Fig. 6 Dielectric Characteristics at microwave frequency

$$E'(\omega) = n^2 - \kappa^2 = E_{\infty} + \sum_i \frac{4\pi\omega_i^2 \cdot \omega_i^2 \cdot (\omega_i^2 - \omega^2)}{(\omega_i^2 - \omega^2)^2 + (\gamma_i\omega)^2} \quad (1)$$

$$E''(\omega) = 2n\kappa = \sum_i \frac{4\pi\omega_i^2 \cdot \omega_i^2 \cdot (\gamma_i\omega)}{(\omega_i^2 - \omega^2)^2 + (\gamma_i\omega)^2} \quad (2)$$

$$R = [(n-1)^2 + \kappa^2] / [(n+1)^2 + \kappa^2] \quad (3)$$

where, $4\pi\omega_i^2$: Strength
 γ_i : Width
 ω_i : Resonant frequency
 n : Refractive index
 κ : Extinction coefficient
 R : Reflectivity

Far infrared reflection spectra were taken in order to get the information of lattice vibrations.

Fig. 7 shows the measured and calculated reflection spectra of $\text{Ba}(\text{Mg}_{1/3}\text{Ta}_{2/3})\text{O}_3$ ceramics. The crystal structure of this material belongs to the space group D_{3d}^3 of a trigonal system. Taking Γ point or $K=0$ into consider, whose point group is D_{3d} , lattice vibrations can be written in terms of normal modes such as $4\text{A}_{1g} + \text{A}_{2g} + 5\text{E}_g + 2\text{A}_{1u} + 8\text{A}_{2u} + 10\text{E}_u$.

Among them, A_{2u} and E_u modes are infrared active. And as one of the A_{2u} and one of the E_u modes correspond to the uniform displacements of ions, the number of infrared-active modes to be observed is 16 at most.

The dispersion parameters used for analysing the reflection spectra are also shown in Fig. 7. Table 1 shows the measured and calculated dielectric characteristics at 10 GHz. They show preferable agreement.

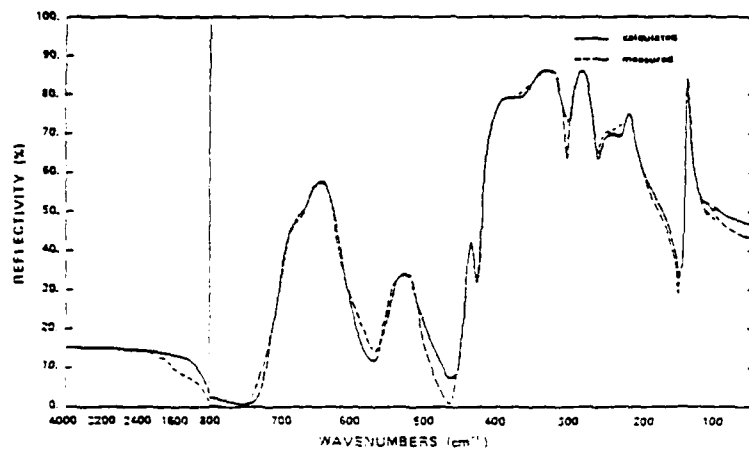


Fig. 7 Measured and calculated far infrared reflectivity of $\text{Ba}(\text{Mg}_{1/3}\text{Ta}_{2/3})\text{O}_3$ ceramic

i	ω_i	η_i/ω_i	γ_i/ω_i	$A\omega_i$
1	104.0	0.000	0.020	0.14
2	115.0	0.000	0.030	0.10
3	140.0	0.000	0.018	3.70
4	150.0	0.000	0.028	0.20
5	222.0	0.000	0.045	4.23
6	240.0	0.045	0.020	6.20
7	276.0	0.000	0.046	3.80
8	312.0	0.000	0.080	1.50
9	368.0	0.000	0.120	0.23
10	434.0	0.000	0.025	0.03
11	524.0	0.000	0.090	0.60
12	625.0	0.000	0.045	0.57
13	670.0	0.000	0.085	0.04
$\epsilon_\infty = 5.50$				

Table I Measured and calculated dielectric characteristics for $\text{Ba}(\text{Mg}_{1/3}\text{Ta}_{2/3})\text{O}_3$ ceramic at 10 GHz.

	ϵ	Q (at 10 GHz)	τ_i (ppm/°C)
Measured	24.8	16000	8.0
Calculated	25.7	24900	-

$$\epsilon = \epsilon_\infty + \sum_i \frac{A\omega_i^2}{\omega_i^2 - \omega^2 - j\gamma_i\omega}$$

$$\frac{1}{Q} = \tan \delta = \frac{\sum_i \frac{A\omega_i^2 \gamma_i \omega}{\omega_i^2 - \omega^2 - j\gamma_i\omega}}{\epsilon_\infty + \sum_i \frac{A\omega_i^2}{\omega_i^2 - \omega^2 - j\gamma_i\omega}}$$

DIELECTRIC PROPERTIES OF $\text{BaO-TiO}_2\text{-WO}_3$ SYSTEM AT MICROWAVE FREQUENCY

S. NISHIO, M. S. YANO, H. KATO and T. NONOMURA

Natumi Technical Laboratory, Natumi Chemical Corporation, Nagoya, Japan

ABSTRACT Microwave Properties of $\text{BaO-TiO}_2\text{-WO}_3$ ceramic system were investigated. Addition of a small amount of WO_3 to BaO-xTiO_2 leads to an explicit improvement of Q and τ_f (temperature coefficient of resonant frequency). Microwave properties of the compositions with $x=4$ to 4.5 and $y=0$ to 0.04 in the equation of $\text{BaO-xTiO}_2\cdot(1+x)y\text{WO}_3$ were observed. With the range of $x=4$ to 4.5 and $y=0.02$ to 0.035, higher Q values (4881~4981 at 4GHz) and lower τ_f values of nearly zero (-0.5 to 2.5 ppm/°C) with ϵ of 35~38 were obtained. These ceramics had three kinds of crystallines composed of $\text{BaTi}_4\text{O}_{10}$, $\text{Ba}_2\text{Ti}_2\text{O}_7$, and BaWO_4 . It was found that these improvements seem to be attributed to BaWO_4 crystallines with a negative τ_f , which is segregated as a secondary phase by WO_3 addition in the dielectrics.

1. INTRODUCTION

Ceramics of the TiO_2 rich region of BaO-TiO_2 system such as $\text{BaTi}_4\text{O}_{10}$ ¹⁾ and $\text{Ba}_2\text{Ti}_2\text{O}_7$ ^{2,3)} are well known to be good dielectric resonator materials at microwave frequency. In order to improve the Q values, such methods as chemical treatment^{4,5)} of calcined materials or addition of small amounts of Mn^{2+} were reported previously. There are, however, few data on the reduction of τ_f . The optimum of these published data for BaO-TiO_2 dielectrics are understood as following: $\text{BaTi}_4\text{O}_{10}$ (BaO-4TiO_2): $\epsilon=38$, $Q=4881$ at 4GHz, ($Q=4881$ at 6GHz), $\tau_f=15\sim20$ ppm/°C,¹⁾ $\text{Ba}_2\text{Ti}_2\text{O}_7$ (BaO-4.5TiO_2): $\epsilon=39\sim41$, $Q=4881\sim11,181$ at 4GHz, ($Q=5381\sim7381$ at 6GHz), $\tau_f=2$ ppm/°C.^{2,3)}

In our case, the segregated BaWO_4 crystallines formed by WO_3 addition have an advantage for both improvement of Q and τ_f . This paper is mainly concerned with the relation between the WO_3 amount, the microstructure and the microwave properties.

2. EXPERIMENTAL

2.1. Material and Procedure

The starting materials composed of BaCO_3 , TiO_2 , WO_3 and MnCO_3 powder with a purity of 99.7 to 99.9% were mixed to be the designated composition mentioned above, in which MnO was fixed to 0.1 mol%. The mixed powder was calcined at 1000°C in air for 4Hrs. Ball milled powder was cold pressed into disks and then sintered at a temperature ranging between 1300°C to 1420°C in O_2 for 2Hrs.

2.2. Measurement

The microwave properties of the dielectrics were measured by the resonant cavity method on the TE_{011} mode at 6GHz. XRD, SEM and EPMA analysis were used to examine the microstructure of the dielectrics.

3. RESULT AND DISCUSSION

In order to study microwave properties for our dielectrics, we selected several points of $x(4\sim4.5)$ in the composition written as $\text{BaO-xTiO}_2\cdot(1+x)y\text{WO}_3$.

The properties of BaO-4TiO_2 and BaO-4.5TiO_2 with a small amount of WO_3 ($y=0\sim0.04$) were represented typically in Fig. 1. In each case, the addition of WO_3 at $y=\frac{0.02}{0.04}$ shows a remarkable increase of Q (71181, 57181~4881~4981), which is however saturated with further addition. It is still difficult to explain this favorable Q behavior (at $y=\frac{0.02}{0.04}$).

On the other hand, it is well explained from Fig. 1 and the microstructure of these dielectrics (Fig. 2) that the change of ϵ and τ_f seems to depend on the segregation of BaWO_4 and $\text{Ba}_2\text{Ti}_2\text{O}_7$ in BaO-4TiO_2 or of BaWO_4 and TiO_2 in BaO-4.5TiO_2 . The increase of ϵ and τ_f is due to segregation of TiO_2 . The decrease of ϵ and τ_f is due to segregation of BaWO_4 . It is thought from the optimum data of τ_f , -0.5 ppm/°C for $\text{BaO-4TiO}_2\cdot0.1\text{WO}_3$ ($y=0.02$) that BaWO_4 must have negative τ_f with smaller ϵ than $\text{Ba}_2\text{Ti}_2\text{O}_7$ and $\text{BaTi}_4\text{O}_{10}$. The segregation of $\text{Ba}_2\text{Ti}_2\text{O}_7$ is effective for ϵ increase and τ_f decrease. Therefore in order to obtain a dielectric resonator with high Q and zero τ_f with relatively high ϵ , coexistence of three kinds of crystallines of $\text{BaTi}_4\text{O}_{10}$, $\text{Ba}_2\text{Ti}_2\text{O}_7$ and BaWO_4 is required. ($\epsilon=35\sim38$). The reaction equations with WO_3 , which was identified by EPMA quantitative analysis for the microstructures, would be interpreted as follows. Table 1 is the summary of our study.

- (1) $\text{BaO}(\text{TiO}_2 + \text{BaTi}_2\text{O}_7) + \text{WO}_3 \rightarrow \text{BaTi}_2\text{O}_7 + \text{Ba}_2\text{Ti}_2\text{O}_7 + \text{BaWO}_4$
 $\text{BaO}(\text{TiO}_2 + \text{BaTi}_2\text{O}_7) + \text{BaWO}_4 + \text{WO}_3 \rightarrow \text{Ba}_2\text{Ti}_2\text{O}_7 + 3\text{BaWO}_4 + \text{TiO}_2$
 (2) $\text{BaO} + 5\text{TiO}_2 + \text{BaTi}_2\text{O}_7 + \text{WO}_3 \rightarrow \text{Ba}_2\text{Ti}_2\text{O}_7 + \text{BaWO}_4 + \text{TiO}_2$

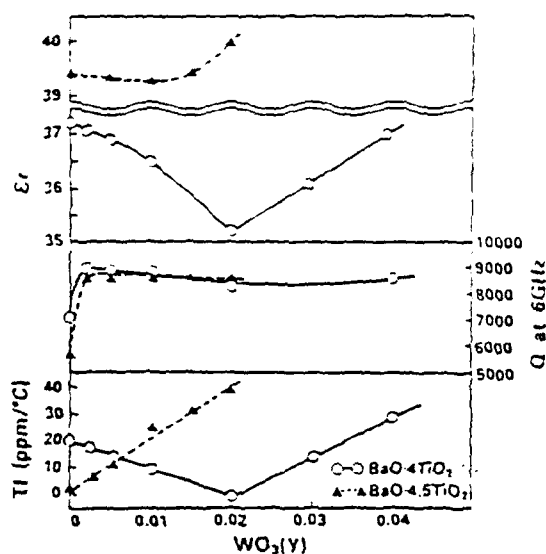
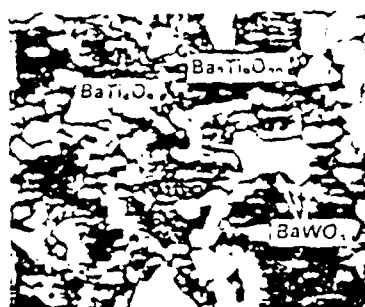


Fig. 1 Dielectric Properties of $\text{BaO} \cdot 4\text{TiO}_2 \cdot (1+4y)\text{WO}_3$ and $\text{BaO} \cdot 4.5\text{TiO}_2 \cdot (1+4.5y)\text{WO}_3$ at 6GHz

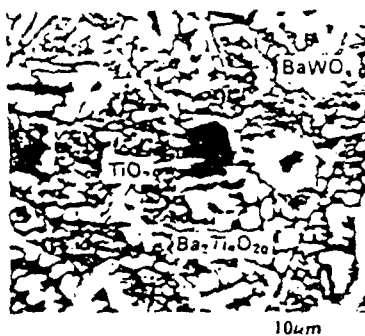
Table 1 Dielectric Properties of $\text{BaO} \cdot x\text{TiO}_2 \cdot (1+y)\text{WO}_3$

Composition	x	y	Properties at 6GHz			Phase
			ε	Q	Ti	
	4.0	—	37	7100	19	BT_4
	4.0	0.02	35	8400	-0.5	$\text{BT}_{4.5}\text{BT}_{4.5}\text{BW}$
	4.2	0.01	37	8800	1.6	$\text{BT}_4\text{BT}_{4.5}\text{BW}$
	4.3	0.005	38	8300	2.5	$\text{BT}_4\text{BT}_{4.5}\text{BW}$
	4.5	—	39	5700	1.4	$\text{BT}_{4.5}$
	4.5	0.002	39	8800	4.0	$\text{BT}_{4.5}\text{BW}$

BT_4 : $\text{BaTi}_4\text{O}_{13}$, $\text{BT}_{4.5}$: $\text{Ba}_7\text{Ti}_9\text{O}_{20}$, T: TiO_2 , BW: BaWO_4



$\text{BaO} \cdot 4\text{TiO}_2 \cdot 0.1\text{WO}_3$ ($y = 0.02$)



$\text{BaO} \cdot 4.5\text{TiO}_2 \cdot 0.01\text{WO}_3$ ($y = 0.002$)

Fig. 2 Microstructure of $\text{BaO} \cdot 4\text{TiO}_2 \cdot 0.1\text{WO}_3$ and $\text{BaO} \cdot 4.5\text{TiO}_2 \cdot 0.1\text{WO}_3$

REFERENCES

- D.J. Masse et al. "A New Low-Loss High-K Temperature-Compensated Dielectric for Microwave Applications", proceeding of the IEEE Nov. 1628-1629 (1971).
- H.M. O'Brien and J. Thummin, Jr. "Phase Equilibria in the TiO_2 -Rich Region of the System $\text{BaO}-\text{TiO}_2$ ", Jour. Am. Ceram. Soc., **57** (12) 522-526 (1974).
- H.M. O'Brien and J. Thummin, Jr. "A New $\text{BaO}-\text{TiO}_2$ Compound with Temperature-Stable High Permittivity and Low Microwave Loss", Jour. Am. Ceram. Soc., **57** (10) 450-453 (1974).
- H.M. O'Brien and J. Thummin, Jr. " $\text{Ba}_7\text{Ti}_9\text{O}_{20}$ as a Microwave Dielectric Resonator", Jour. Am. Ceram. Soc., **58** (9-10) 418-420 (1975).
- H.M. O'Brien, Jr. J. Thummin and J.K. Plourde, "Effect of Chemical Treatment on Loss Quality of Microwave Dielectric Ceramics", Ber. Dt. Keram. Ges., **55** (7) 348-351 (1978).
- H.M. O'Brien and J. Thummin, " $\text{Ba}_7\text{Ti}_9\text{O}_{20}$ with Improved Microwave Loss Quality" Am. Ceram. Soc. Annual Meeting, 121-E-46, May 1 (1986).
- S. Nomura, K. Tomiya and K. Kaneta, "Effect of Mn Doping on the Dielectric Properties of $\text{Ba}_7\text{Ti}_9\text{O}_{20}$ Ceramics at Microwave Frequency", Jap. Jour. Appl. Phys., **22** (7) 1125-1128 (1983).

Summary

- 1) High Q (around 8000 at 6GHz) was attained by adding a small amount of WO_3 to 0.01mol to $BaO \cdot 4TiO_2$, $(Ba_{1-x}Ti_xO_3)$ and $BaO \cdot 4.5TiO_2$, $(Ba_{1-x}Ti_{4.5}O_3)$.
- 2) Nearly zero T_f was attained by adding a small amount of WO_3 (0.1mol) to $BaO \cdot 4TiO_2$, $(Ba_{1-x}Ti_xO_3)$ resulting in ternary phases containing $BaTi_4O_{13}$, $Ba_{1-x}Ti_{4-x}O_{13}$ and $BaWO_4$.
- 3) Excellent dielectric resonator ($Q = 35$, $Q = 8400$ at 6GHz, $T_f = 0$) was obtained by a composition of $BaO \cdot 4TiO_2 \cdot 0.1WO_3$.
- 4) It was found that $BaWO_4$ compound has negative T_f .

Microstructure of $BaO \cdot 4TiO_2 \cdot 0.1WO_3$ and $BaO \cdot 4.5TiO_2 \cdot 0.01WO_3$

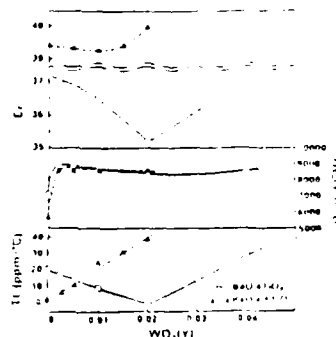


$BaO \cdot 4TiO_2 \cdot 0.1WO_3$



$BaO \cdot 4.5TiO_2 \cdot 0.01WO_3$

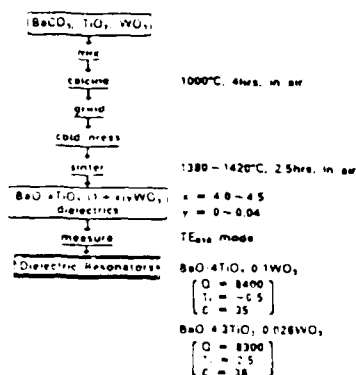
Dielectric Properties of $BaO \cdot 4TiO_2 \cdot (1-x)yWO_3$ and $BaO \cdot 4.5TiO_2 \cdot (1-x)yWO_3$ at 6GHz



DIELECTRIC PROPERTIES OF $BaO \cdot TiO_2 \cdot WO_3$ SYSTEM AT MICROWAVE FREQUENCY

Microstructure of $BaO \cdot xTiO_2 \cdot (1-x)yWO_3$ ($x=4-4.5$, $y=0-0.04$)
Ceramics by SEM and EPMA

Sample Preparation and Measurement



$x=4.0$

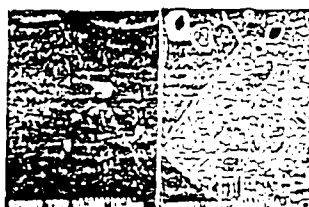
$x=4.2$

$x=4.5$

$y=0$



$y=0.002$



Dielectric Properties of $BaO \cdot xTiO_2 \cdot (1-x)yWO_3$

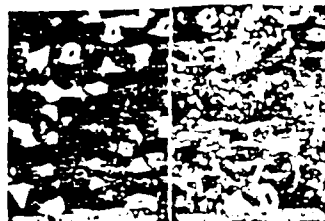
Composi-	Proper-				
x	y	z	Q	T _f	Phase
4.0	-	37	1100	19	BT ₁
4.0	0.02	35	8400	-0.5	BT ₁ ·BT ₂ ·BW
4.2	0.01	37	8900	1.6	BT ₁ ·BT ₂ ·BW
4.3	0.005	38	8300	2.9	BT ₁ ·BT ₂ ·BW
4.5	-	39	5100	1.6	BT ₁
4.5	0.002	38	8900	4.0	BT ₁ ·BT ₂ ·BW

BT₁: BaTi₄O₁₃, BT₂: Ba_{1-x}Ti_{4-x}O₁₃, * TiO₂, BW: BaWO₄

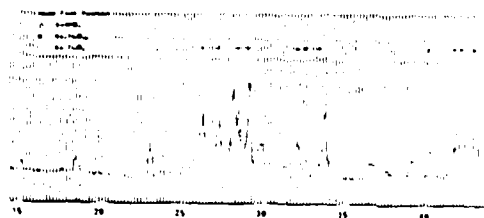
$y=0.01$



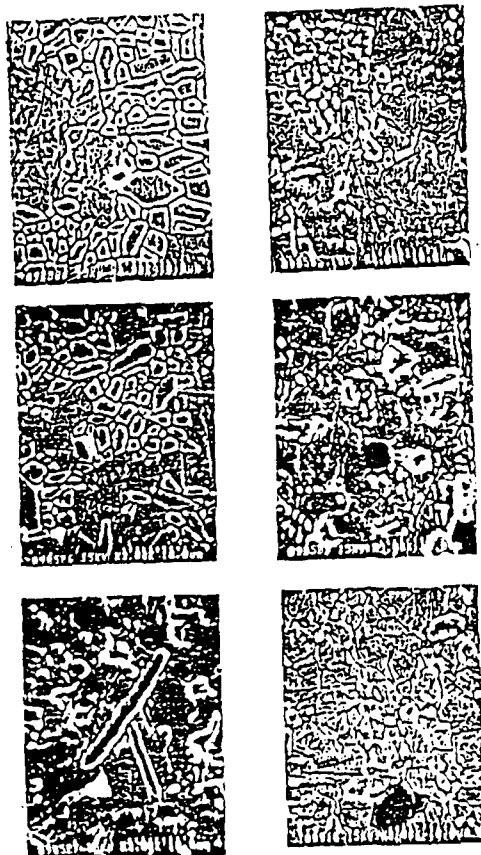
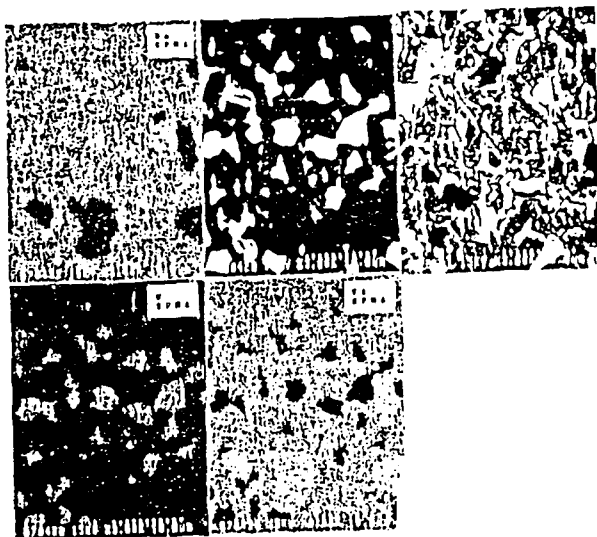
$y=0.02$



X-ray Diffraction Pattern of $BaO \cdot 4TiO_2 \cdot 0.1WO_3$ ($y=0.02$)



$\gamma = 0.04$



FERROELECTRIC AND PYROELECTRIC PROPERTIES OF SPUTTER-DEPOSITED PZT AND PT FILMS

H. ADACHI, T. SHIOSAKI, and A. KAWABATA

Department of Electronics, Faculty

of Engineering, Kyoto University,

Sakyoku, Kyoto 606, Japan

ABSTRACT: [111]-oriented PZT(90/10) films have been successfully grown with good epitaxy onto the c plane of sapphire and epitaxial Pt film substrates by the rf-magnetron sputtering method. The crystallographic identifications of these PZT and PT films are made by the X-ray and PHEED measurements. Dielectric, ferroelectric and pyroelectric properties of the films are measured. Pyroelectric coefficients at room temperature have been determined as 4.5 and $3.5 \times 10^{-8} \text{C/cm}^2\text{K}$ for epitaxial PZT and polycrystalline PT films, respectively. Epitaxial PZT(90/10) films on Pt/sapphire possess desirable properties for potential applications in pyroelectric devices.

Table I. Sputtering condition

Targets	PZT: A mixture of $\text{Pb}(\text{Zr}_{0.9}\text{Ti}_{0.1})\text{O}_3$ powder with excess PbO of 10wt%. PT: PbTiO_3 ceramics with excess PbO of 10 - 15wt%
Target-substrate distance	39 - 44mm
Input power	around 100W
Sputtering gas pressure	2×10^{-2} Torr
Sputtering gas conten	$\text{Ar}(\text{BO}_3) = \text{O}_2(20\%)$
Substrate temperature	550 - 650°C

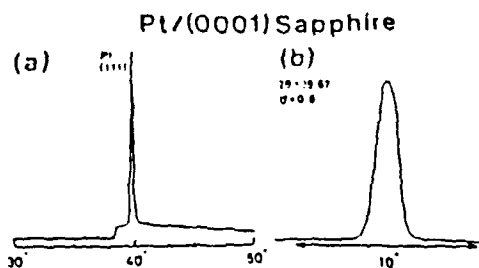


Fig. 1. X-ray diffraction patterns of a platinum (Pt) thin film on the c plane of sapphire.

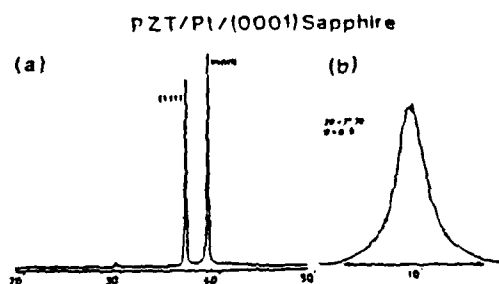


Fig. 2. X-ray diffraction patterns of a PZT(90/10) film on the epitaxial Pt/sapphire substrate.

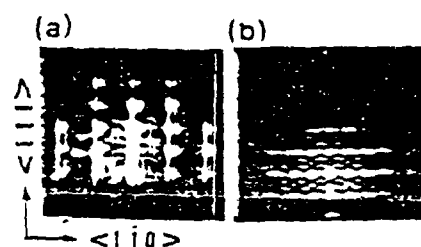


Fig. 3. RHEED patterns of epitaxial Pt (a) and PZT(90/10) (b) films on Pt/sapphire.

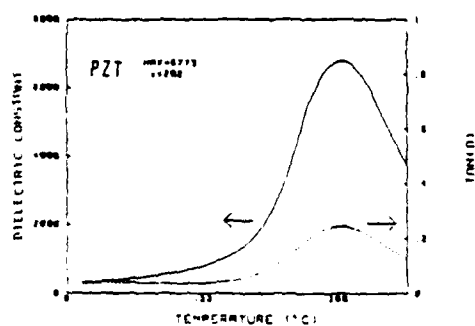


Fig. 4. Temperature dependence of the dielectric constant of a PZT(90/10) film on the Pt/sapphire.

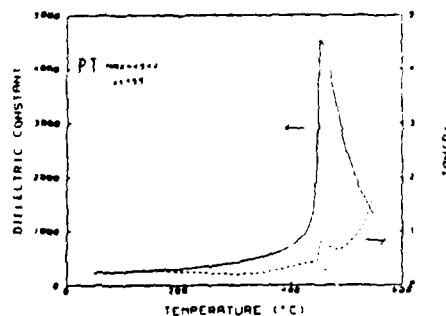


Fig. 5. Temperature dependence of the dielectric constant of a Pt(10) film on the Pt/sapphire.

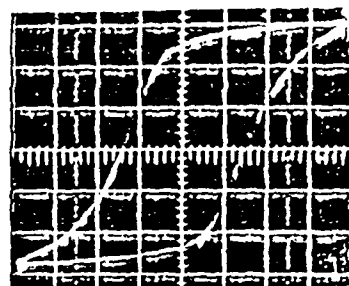


Fig. 6. D-E hysteresis loop of a PZT film with a thickness of 12 μm. P is 35 kV/cm and E is 35 nC/cm². Scale units: x axis: 35 kV/cm/div., y axis: 15 nC/cm²/div.

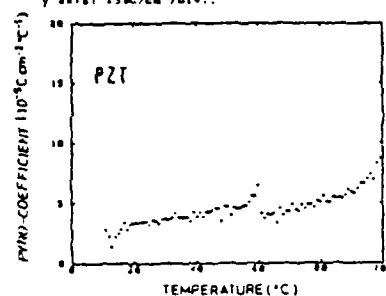


Fig. 7. Temperature dependence of the pyroelectric coefficient of an epitaxial PZT film without poling treatment.

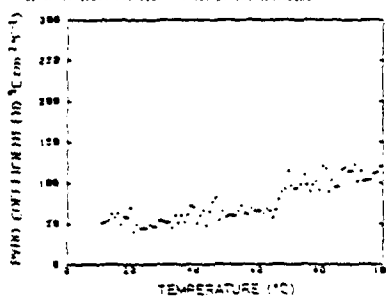


Fig. 8. Temperature dependence of the pyroelectric coefficient of a PZT film with poling treatment.

Table 1. Electrical and Pyroelectric Properties of PZT and Pt Films.

	PZT(90/10)	PZT(90/10)	PZT(90/10)	Pt(10)
Pyroelectric Coefficient (10⁻⁹ C/m²·°C)	100	100	100	100
Dielectric Constant	100	100	100	100
tan δ	0.5	0.5	0.5	0.5
Curie Temperature (°C)	100	100	100	100

PYROELECTRIC AND ELECTRICAL PROPERTIES OF MODIFIED LEAD TITANATE CERAMICS

N. ICHIMOSE

School of Science and Engineering,
Waseda University, Tokyo, Japan

ABSTRACT:

Pyroelectric and electrical properties of the modified $(\text{Pb, Me})[(\text{Co}_{1/3}\text{Ti}_{2/3}), \text{Ti}]\text{O}_3$ ceramics (Me=Ba, Sr or Ca) containing small amounts of BaO and NiO have been investigated. These ceramics are characterized by high apparent density, small dielectric constant (about 200) and facility in poling procedure. Among the ceramics substituted with the alkaline earth metals, the Ca-modified ceramics show markedly excellent pyroelectric and piezoelectric properties. Various kinds of pyroelectric detectors and ultrasonic transducers have been developed by employing these modified PbTiO_3 ceramics.

1. INTRODUCTION

Recently, pyroelectric infrared sensors have been widely used in consumer electric appliances and other electric equipments such as microwave ovens, automatic door systems, human body sensors and burglar alarm systems. Pyroelectric infrared sensors show good sensing characteristics. Differing from photon sensors, they can be used at room temperature and their infrared response does not depend on the wavelength of the infrared rays used. The pyroelectric materials performance is represented by the figure of merit F_v , defined as $P/\sqrt{\epsilon C_v}$, where, P , ϵ and C_v are pyroelectric coefficient, relative dielectric constant and volume specific heat, respectively. Nowadays, various kinds of pyroelectric materials, like LiTaO_3 single crystal, are commercially available and used. Among them, PbTiO_3 ceramics have been regarded as good

pyroelectric materials, because of their large pyroelectric coefficient P , small dielectric constant ϵ and high Curie temperature T_c . The present paper reports the pyroelectric and electrical properties of $(\text{Pb, Me})[(\text{Co}_{1/3}\text{Ti}_{2/3}), \text{Ti}]\text{O}_3$ ceramics (Me=Ba, Sr or Ca).

2. EXPERIMENTAL

Figure 1 shows the pyroelectric ceramics manufacturing process. Raw materials, PbO , TiO_2 , CoO , MeCO_3 , VO_3 , NiCO_3 , and NiO , were calcined at 900°C for 2 hours in air after weighing and mixing. The mixture were formed by die pressing and fired at $1100\sim 1180^\circ\text{C}$ for several hours. Because of the low firing temperature and small amount of PbO vaporization, in comparison with PZT ($\text{PbTiO}_3\text{-PbZrO}_3$) ceramic, the mixture was not fired in PbO atmosphere. Both surfaces of the fired samples were polished until the samples were 0.5 mm thick and their diameter was 20 mm.

Usually, PbTiO_3 ceramic polarization requires a markedly high voltage and high temperature, more than 60kV and 200°C , respectively. However, $(\text{Pb, Me})[(\text{Co}_{1/3}\text{Ti}_{2/3}), \text{Ti}]\text{O}_3$ ceramic can be polled at lower voltage and temperature, 40~50kV/cm, 100°C , respectively, in silicone oil. Aging tests were performed for each sample. Pyroelectric coefficient P values were measured by the conventional system. Relative dielectric constant ϵ values were measured by LCR meter (YHP-4261A) at 1kHz. Responsivity R_v and relative detectivity D^* were measured under chopped light irradiation from He-Ne laser (Hughes Aircraft Co. Model 33211H-PC) by signal analyzer (Ivatsu Sm-2100A) and a spectrum analyzer (Hewlett Packard 3582A).

The spontaneous polarization values were measured by the Sawyer-Tower method. Using the system in Fig. 2, we have measured pyroelectric coefficient values.

3. RESULTS

Figure 3 shows pyroelectric coefficient P , relative dielectric constant ϵ and figure of merit F_v for $(\text{Pb}_{1-x}\text{Ca}_x)((\text{Co}_{1/2}\text{V}_{1/2})_{0.9}\text{Ti}_{0.1})\text{O}_3$ as a function of Ca concentration. As Ca is introduced into PbTiO_3 ceramic, the pyroelectric coefficient increases to a great extent.

Curie temperatures and coupling factors for the $(\text{Pb}_{1-x}\text{Me}_x)((\text{Co}_{1/2}\text{V}_{1/2})_{0.9}\text{Ti}_{0.1})\text{O}_3$ system are shown in Fig. 4 and Fig. 5, respectively. From Fig. 5, it is found that these piezoelectric materials have an extremely anisotropic piezoelectric effect.

4. DISCUSSION

The improvement of pyroelectricity by the Ca introduction into PbTiO_3 host lattice may be attributed to the increase of the spontaneous polarization as shown in Fig. 6.

The large piezoelectric anisotropy of these ceramics may be understood when the piezoelectric properties are reduced from the electrostrictive coefficient and the piezoelectric constant d_{31} disappears for a particular ratio of the electrostrictive coefficients and a certain degree of polarization.

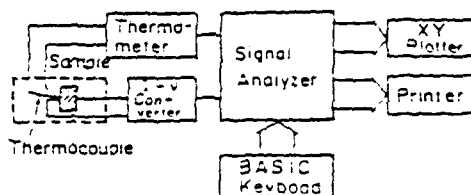


Fig. 2. Schematic diagram for measuring pyroelectric coefficient P .

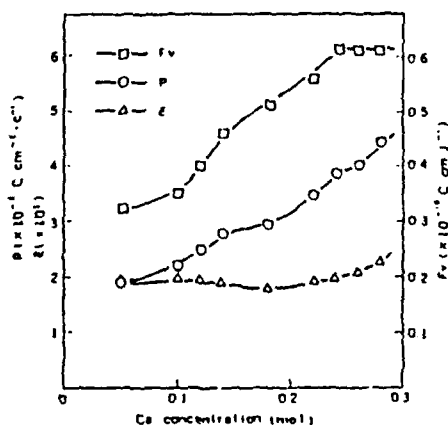


Fig. 3. Pyroelectric coefficient P , relative dielectric constant ϵ , and figure of merit F_v for $(\text{Pb}_{1-x}\text{Ca}_x)((\text{Co}_{1/2}\text{V}_{1/2})_{0.9}\text{Ti}_{0.1})\text{O}_3$ as a function of Ca concentration.

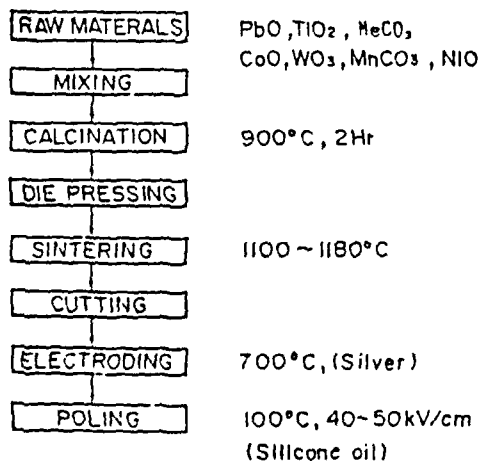


Fig. 1. Manufacturing process for $(\text{Pb}, \text{Me})((\text{Co}_{1/2}\text{V}_{1/2})_{0.9}\text{Ti}_{0.1})\text{O}_3$ Ceramics. (Me=Ba, Sr, or Ca)

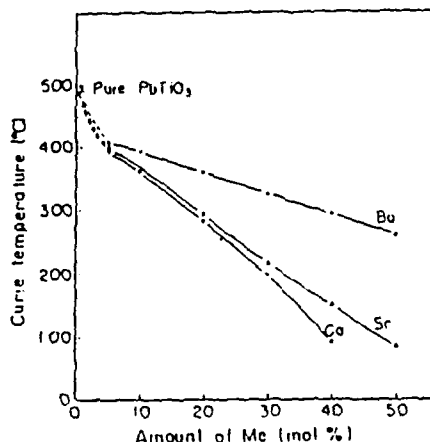


Fig. 4. Curie temperature vs amount of Me for $(\text{Pb}_{1-x}\text{Me}_x)((\text{Co}_{1/2}\text{V}_{1/2})_{0.9}\text{Ti}_{0.1})\text{O}_3$ system.

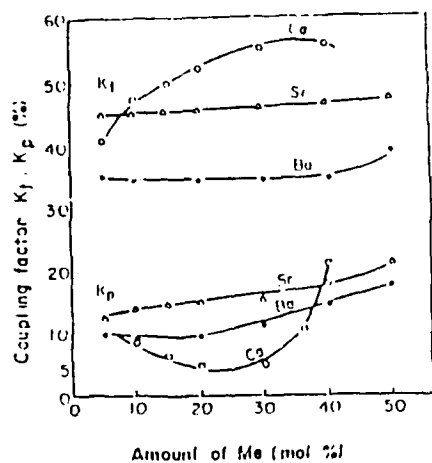


Fig. 5. Coupling factors vs amount of Me for $(Pb_{1-x}Me_x)(Co_{1/2}W_{1/2})_{1-x}Ti_{0.5x}O_3$ system.

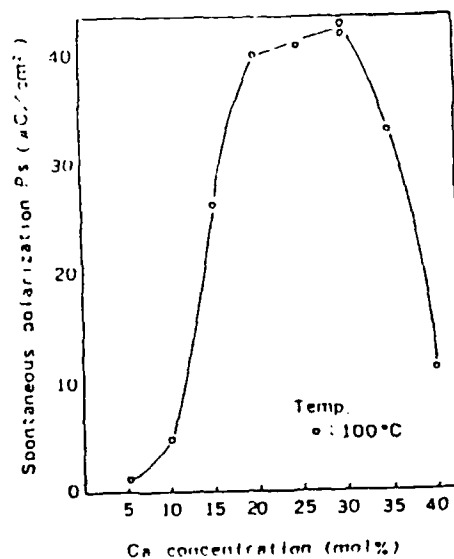


Fig. 6. Relation between spontaneous polarization P_s and Ca concentration of $(Pb_{1-x}, Ca_x)(Co_{1/2}W_{1/2})_{1-x}TiO_3$ ceramics.

ABSTRACT

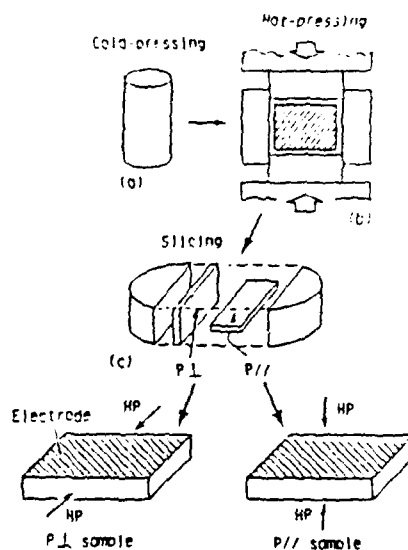
GRAIN-ORIENTED LEAD GERMANATE SILICATE CERAMICS WERE PREPARED BY HOT-PRESSING METHOD. THE MICROSTRUCTURE AND THE ELECTRICAL AND OPTICAL PROPERTIES OF GRAIN-ORIENTED SAMPLES WERE MEASURED.

THE ANISOTROPIES OF 2 TO 4 TIMES IN THE PERMITTIVITY AND PIEZOELECTRIC AND PYROELECTRIC COEFFICIENTS WERE FOUND BETWEEN THE PARALLEL AND PERPENDICULAR DIRECTION TO THE HOT-PRESSING DIRECTION.

IT WAS FOUND THAT GRAIN-ORIENTED LEAD GERMANATE SILICATE CERAMICS HAVE HIGHLY ACTIVE PYROELECTRIC EFFECT. THE COEFFICIENT IN THE ROOM TEMPERATURE WAS $2.5 \times 10^{-2} \mu\text{C}/\text{cm}^2 \text{ } ^\circ\text{C}$, WAS AS SAME AS THAT OF LiTaO_3 SINGLE CRYSTAL AND ABOUT 9 TIMES AS LARGE AS THAT OF LiNbO_3 SINGLE CRYSTAL.

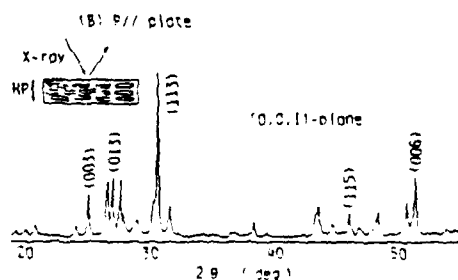
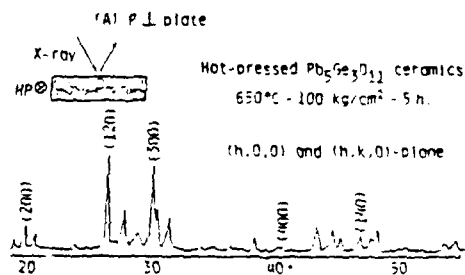
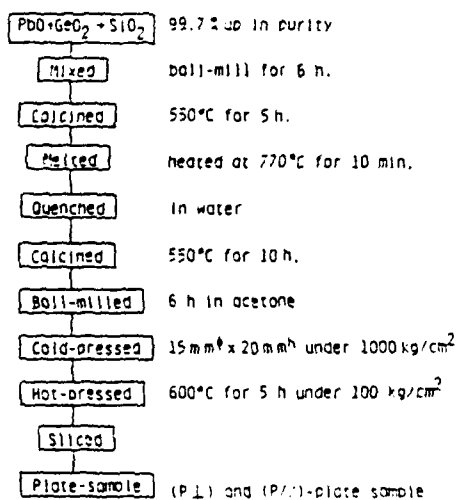
HOT-PRESSED LEAD GERMANATE SILICATE CERAMICS WITH A POROSITY OF LESS THAN 0.5 % SHOWED A TRANSMITTANCE OF ABOUT 60 % AT A WAVE-LENGTH OF $6 \mu\text{m}$.

Hot-pressed Lead Germanate Silicate Ceramic

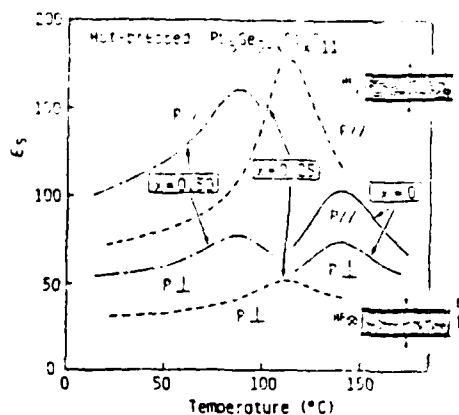


Preparation of Lead Germanate Silicate Ceramics

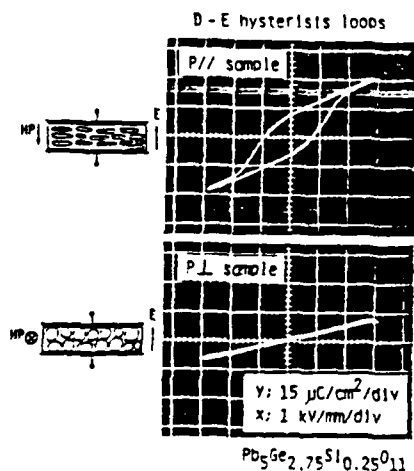
Composition: $\text{Pb}_{0.9}\text{Ge}_{0.1}\text{Si}_{0.1}\text{O}_{11} \rightarrow \text{PSSO} / x$



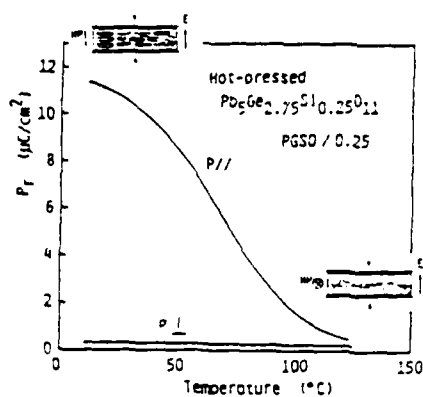
Typical X-ray diffraction patterns of hot-pressed lead germanate ceramics.



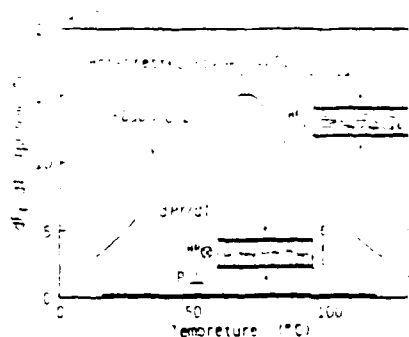
Temperature dependence of dielectric constant of hot-pressed lead germanate silicate ceramics.



D-E hysteresis loops for hot-pressed lead germanate silicate ceramics



Temperature dependence of remnant polarization of hot-pressed lead germanate silicate ceramics.



Pyroelectric coefficient as a function of temperature for hot-pressed lead germanate silicate ceramics.

Pyroelectric properties of hot-pressed $\text{Pb}_5\text{Ge}_{2.75}\text{Si}_{0.25}\text{O}_{11}$ and typical materials

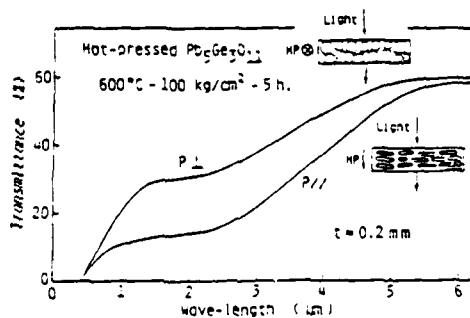
Materials	T_c (°C)	ϵ_s	dP/dT ($\mu\text{C}/\text{m}^2\text{°C}$) $\times 10^{-4}$	$dP/dT/\epsilon_s$ (A/mV) $\times 10^{-12}$
Hot-pressed $\text{Pb}_5\text{Ge}_{2.75}\text{Si}_{0.25}\text{O}_{11}$	112	71	3.9	2.2
$\text{Pb}_5\text{Ge}_{2.75}\text{Si}_{0.25}\text{O}_{11}$	177	40	0.5	0.22
$\text{Pb}(\text{Zr}_{0.7}\text{Ti}_{0.3})\text{O}_3$	300	450	3.1	0.24
PbTiO_3	470	200	6.0	0.94
Crystal				
TGS	49	35	4.0	4.6
LiTiO_3	660	54	2.3	2.3
LiNbO_3	1200	30	0.4	0.46
Film				
PVF_2	120	11	0.3	1.2

* This work $\text{Pb}_5\text{Ge}_{2.75}\text{Si}_{0.25}\text{O}_{11}$ ceramics

Piezoelectric properties of hot-pressed $\text{Pb}_5\text{Ge}_{2.75}\text{Si}_{0.25}\text{O}_{11}$

x (mol)	0.00		0.25		0.50	
Sample	P//	P⊥	P//	P⊥	P//	P⊥
Es	35	25	71	28	105	53
kD	0.05		0.10		0.04	
G _R	1020		950		1450	
λ ₁₁	0.03		0.06		0.02	
g ₁₁ (10 ⁻¹² V/V)	2.12		7.02		2.98	
g ₃₁ (10 ⁻³ V/m/V)	6.84		11.33		3.21	
S ₁₁ (10 ⁻¹² m ² /V)	17.3		17.7		18.1	
ε	0.32		0.32		0.32	
T _C (°C)	142		122		88	

Poled, 20°C-30kV/cm-1 h.



Optical transmittance as a function of wave-length for grain-oriented lead germanate ceramics.

T8

T9

FRACTURE BEHAVIOR OF CERAMICS USED IN MULTILAYER CAPACITORS

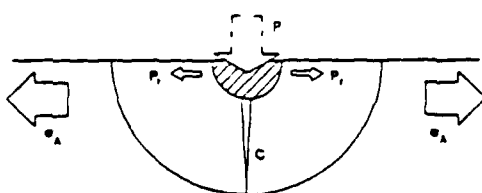
Theresa L. Baker and Stephen W. Freiman
National Bureau of Standards Gaithersburg, MD

EXPERIMENTAL PROCEDURE

Material- Various capacitor compositions
(No electrodes)(AVX)

Form- 25mm squares, 1-2mm thick, as-fired

Test- indentation fracture (biaxial flexure)



DYNAMIC FATIGUE

Assume $V = V_0 (K_I / K_C)^N$

then: $\sigma_f = (\lambda' \dot{\sigma})^{(1/N'+1)}$

where $N = 4N'/3 - 2/3$

For isotropic, homogeneous material, e.g. glass:

$$K = \chi PC^{-3/2} + \psi \sigma C^{1/2}$$

obtain:

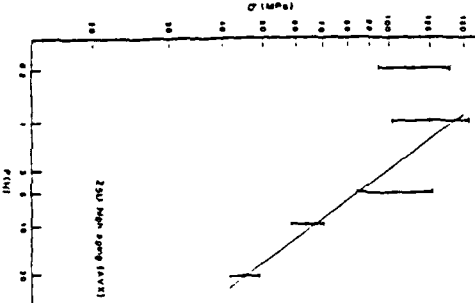
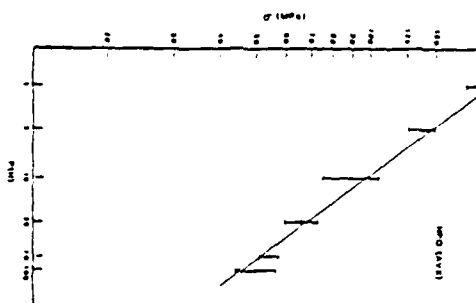
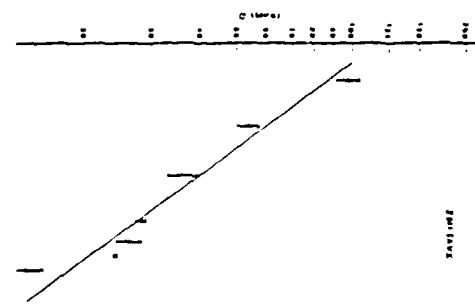
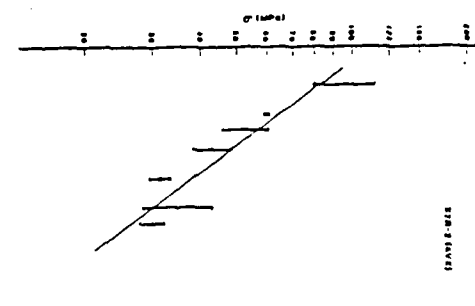
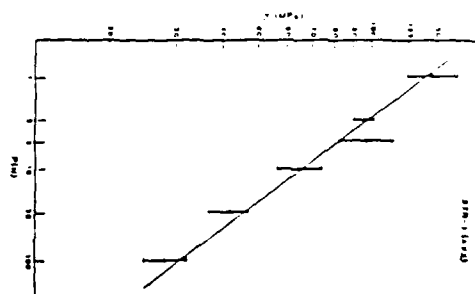
$$K_C = \eta (E/H)^{1/2} (\sigma_f P^{1/2})^{3/2}$$

For polycrystalline ceramics:

$$K = K_{\text{isotropic}} + K_{\text{microstructure}}$$

where

$$K_{\text{microstructure}} = f(C/G)$$



FRACTURE BEHAVIOR OF CERAMICS USED IN MULTILAYER CAPACITORS

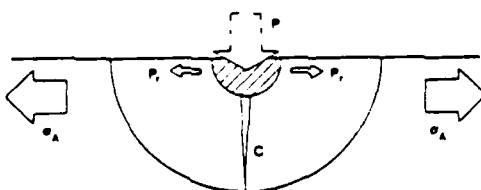
Theresa L. Baker and Stephen W. Freiman
National Bureau of Standards Gaithersburg, MD

EXPERIMENTAL PROCEDURE

Material - Various capacitor compositions
(No electrodes)(AVX)

Form - 25mm squares, 1-2mm thick, as-fired

Test - Indentation fracture (biaxial flexure)



DYNAMIC FATIGUE

$$\text{Assume } V = V_0 (K_I / K_C)^N$$

$$\text{then: } \sigma_f = (\lambda' \dot{\sigma})^{(1/(N+1))}$$

$$\text{where } N = 4N'/3 - 2/3$$

For isotropic, homogeneous material, e.g. glass:

$$K = \chi P C^{-3/2} + \psi \sigma C^{1/2}$$

obtain:

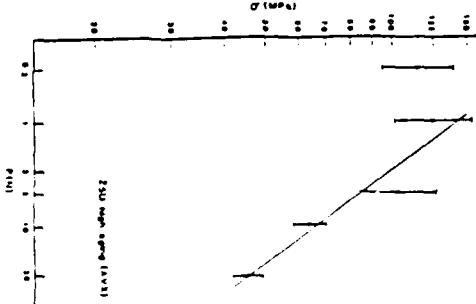
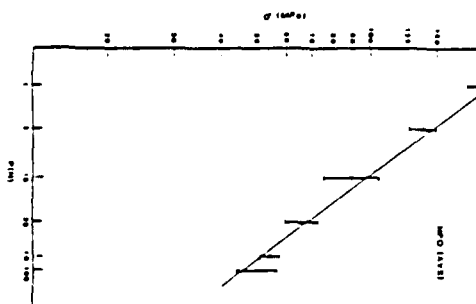
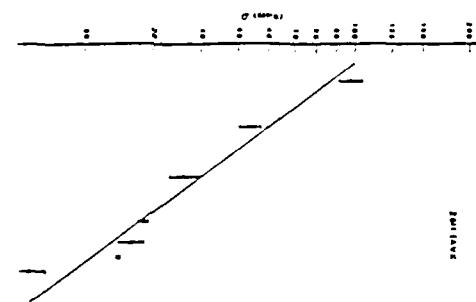
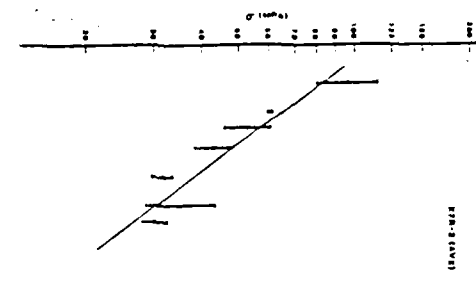
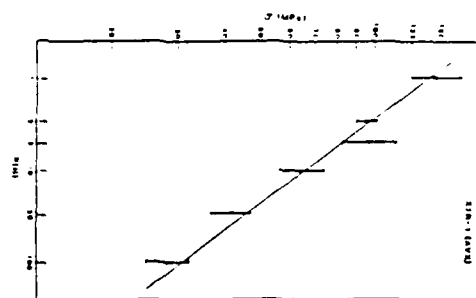
$$K_C = \eta (E/H)^{1/2} (\sigma_f P^{1/3})^{3/2}$$

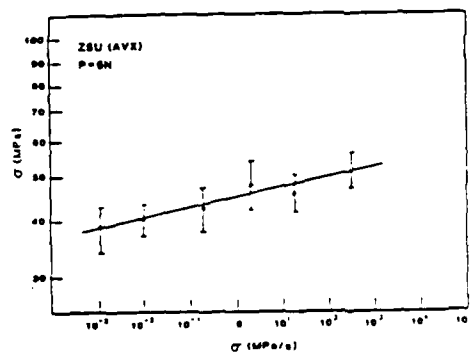
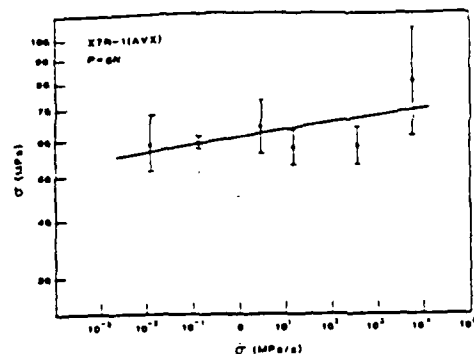
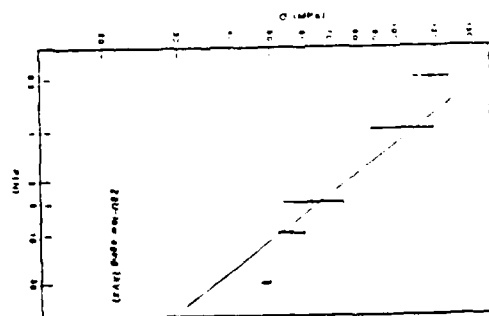
For polycrystalline ceramics:

$$K = K_{\text{isotropic}} + K_{\text{microstructure}}$$

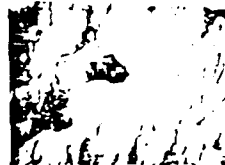
where

$$K_{\text{microstructure}} = f(C/G)$$





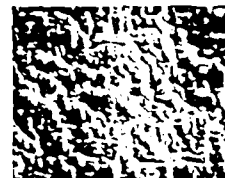
X7R $K_{IC} = 0.67$



ZSU $K_{IC} = 0.75$



X7R $K_{IC} = 1.0$



NPO $K_{IC} = 1.4$

CONCLUSIONS

- K_{IC} and N depend on composition and microstructure
- K_{IC} correlates with degree of crack deflection
- Preliminary data indicates correlation between dielectric aging and internal stresses

Compositions and Properties of Capacitor Ceramics

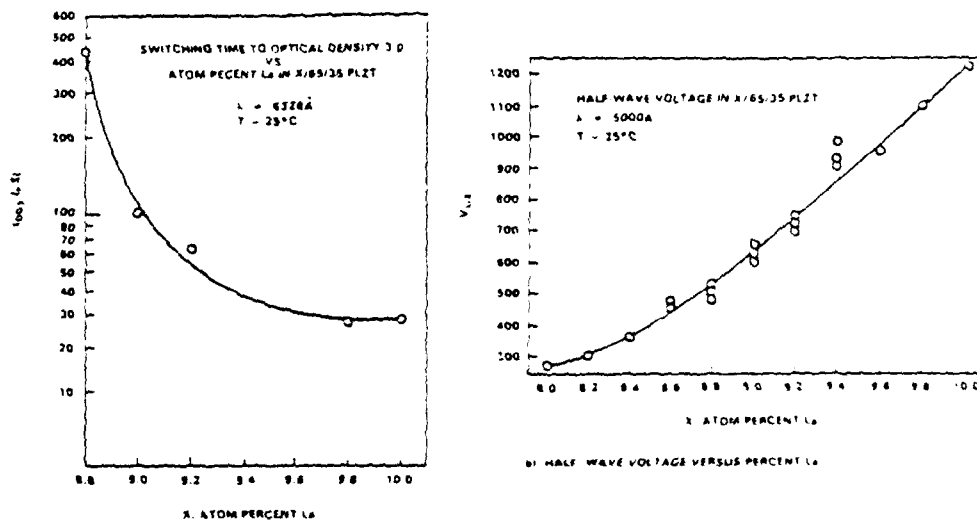
Designation	Composition ¹	Grain Size (μm)	K_{IC} (MPa $m^{1/2}$)	N
NPO	Rare Earth Oxides	1-3	1.4	99 ± 49
X7R-1	BaTiO ₃ (B1)	s1	1.0	85 ± 60
X7R-2	BaTiO ₃	s1	0.7	158 ± 212
ZSU	BaTiO ₃	3-7	0.8	58 ± 10
ZSU "high" aging	BaTiO ₃	3-7	1.1	
ZSU "low" aging	BaTiO ₃	3-7	0.9	

¹ Major constituent

Compositional Influences on PLZT Switching Properties

B. KOEPKE, F. WALLENIORST and J. KYONKA
Honeywell Inc., Minneapolis, MN

ABSTRACT: Half-wave voltages, polarization and capacitance were measured for a series of PLZT samples with varying La contents and Zr/Ti ratios. These parameters, particularly half-wave voltage, are critical in the design of active PLZT optical components. Lower values of half-wave voltage are highly desirable. This work establishes that as the La content exceeds 9.4 atom % and as the Zr/Ti ratio exceeds 65/35, undesirable increases in half-wave voltage will result.



(a) SWITCHING TIME TO OPTICAL 3.0 VERSUS ATOM PERCENT LA

FIGURE 1

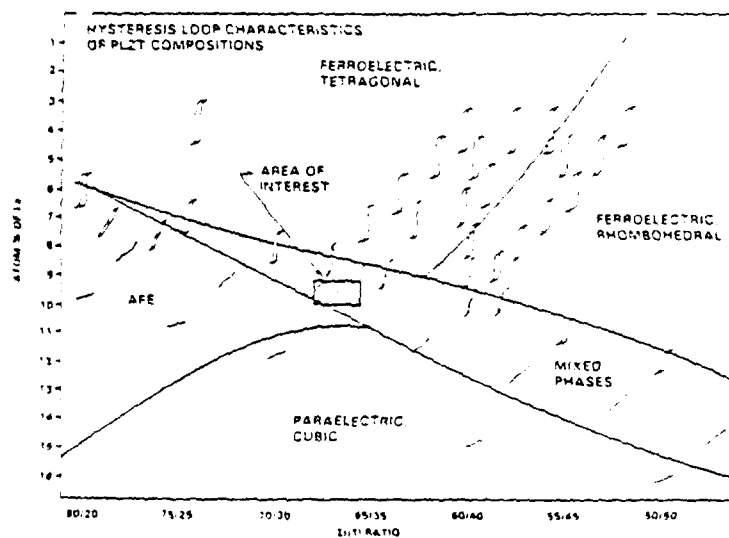


FIGURE 2. PARTIAL PLZT PHASE DIAGRAM SHOWING COMPOSITIONAL AREA OF INTEREST

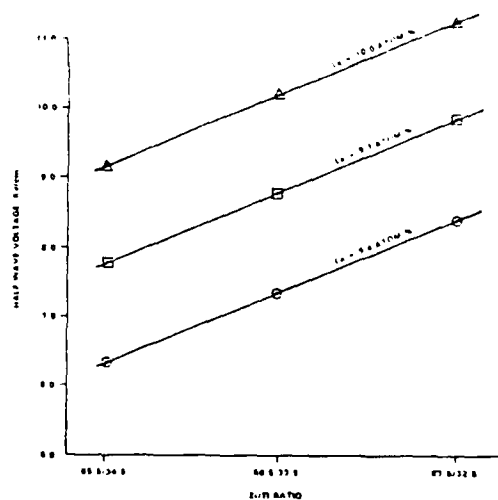


FIGURE 3. HALF-WAVE VOLTAGE DEPENDENCE ON LA CONTENT & Zr/Ti RATIO

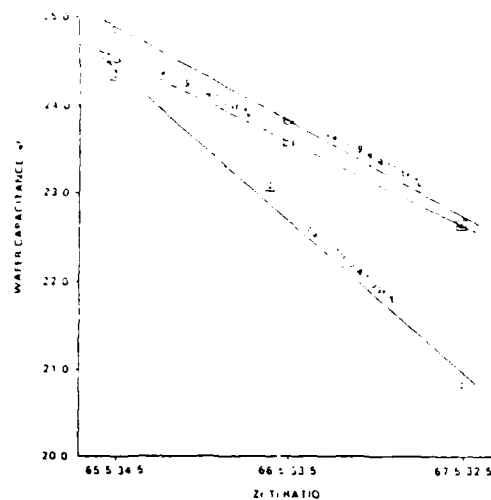


FIGURE 5. WATER CAPACITANCE DEPENDENCE ON LA CONTENT & Zr/Ti RATIO

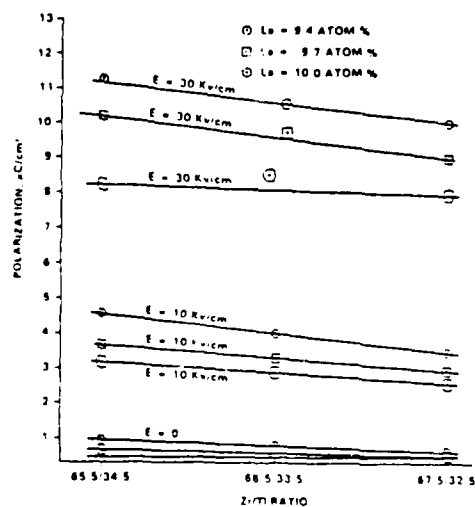


FIGURE 4. POLARIZATION DEPENDENCE ON Zr/Ti RATIO

Discussion

This work shows that, as the Zr/Ti ratio is raised above the 65/35 level, the half-wave voltage raises for 9.4 atom percent and higher La contents. Switching time measurement scatter was such that differences between samples were not detectable. The data did not, however, suggest a significant trend over the compositional range tested. Figure 3 shows that the water capacitance and therefore dielectric constant is inversely related to both the La content and the Zr/Ti ratio. Polarization is shown in Figure 4 to be inversely related to both La content and Zr/Ti ratio. The results of this work indicate that Zr/Ti ratios of less than 65/35 along with La contents of less than 9.4 atom % should be explored. It appears that lower half-wave voltages can be achieved with probable minor impact on switching time but at some cost in higher dielectric constants and polarization values.

Electromechanical Failure Predictions

R. C. Ponanke and P. L. Smith

Office of Naval Research

and

S. W. Freiman

National Bureau of Standards

Table 1

Electromechanical Conditions

<u>Device</u>	<u>Electrical Field</u>	<u>Strain Condition</u>	<u>Stress</u>
Capacitors Microdispersive Devices	Static	Static	Stresses at Flaws Increased by Electric Field Concentrations
Piezoelectric Transducers	Cyclic	Cyclic	Uniform at Cross Section
Electrostrictive Transducers			Uniform at Cross Section
a) biased	Static + Cyclic	Cyclic + Static	
b) non-biased	Cyclic	Cyclic	

For Subcritical Crack Growth

$$\text{Crack Velocity, } V = V_0 (K_I / K_{IC})^N$$

$$\text{then } \frac{da}{dt} = (V_0 / K_{IC}) K_I^N$$

where a is crack length

Re-arranging

$$dt = (K_{IC}^N / V_0) K_I^{-N} da$$

Integrating

$$t_f = \int_0^{t_f} dt = (K_{IC}^N / V_0) \int_{a_i}^{a_f} K_I^{-N} da$$

where $K_I = f(a)$ Estimation of electrical field
and strain field in ceramic
capacitors

With solution of the spatial potentials within the dielectric the electrostrictive strain may be calculated via:

$$(s) = (0) (E, k_0 E - k_0 E^2)$$

$$s = -\nabla V$$

The local enhancements of the electrical field within a parallel plate capacitor are summarized below

inside of flaw exterior of flaw

Spherical voids

• closed-form

1.5

1.5

• roughened

2.3

2.7

• roughened

5.1

2.6

w/protruding

voids

3.2

2.9

Diamond void

2.7

1.9

Square void

1.3

3.6

Delamination

1.2

2.8

50 thickness

End of conductors

9.2

2.8

Delamination on

conductor

10% delam

thickness

thickness

Electric Field Enhanced Stress at Crack Tips

Electrostriction Calculations

- Polarization and Electrostrictive strain

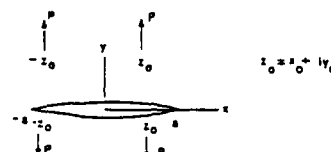
$$P_i = \epsilon_0 \chi_{ij} E_j \quad \text{and} \quad \epsilon_{ijk} = Q_{ijkl} P_k P_l$$

- For BaTiO_3 in isotropic form the above relations reduce to

$$\begin{bmatrix} \epsilon_1 \\ \epsilon_2 \\ \epsilon_3 \\ \epsilon_4 \\ \epsilon_5 \\ \epsilon_6 \end{bmatrix} = \begin{bmatrix} Q_{11} & Q_{12} & Q_{12} & 0 & 0 & 0 \\ Q_{12} & Q_{11} & Q_{12} & 0 & 0 & 0 \\ Q_{12} & Q_{12} & Q_{11} & 0 & 0 & 0 \\ 0 & 0 & 0 & Q_{44} & 0 & 0 \\ 0 & 0 & 0 & 0 & Q_{44} & 0 \\ 0 & 0 & 0 & 0 & 0 & Q_{44} \end{bmatrix} \begin{bmatrix} (\epsilon_1 X \epsilon_1)^2 \\ (\epsilon_2 X \epsilon_2)^2 \\ (\epsilon_3 X \epsilon_3)^2 \\ (\epsilon_4 X \epsilon_1)^2 \\ (\epsilon_5 X \epsilon_1)^2 \\ (\epsilon_6 X \epsilon_1)^2 \end{bmatrix}$$

$$\text{where } Q_{44} = 2(Q_{11} - Q_{12})$$

Courtesy: W. B. Carlson
The Pennsylvania State University



From Tada: the Stress Analysis of Cracks Handbook

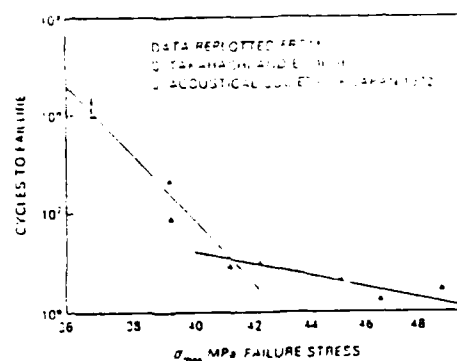
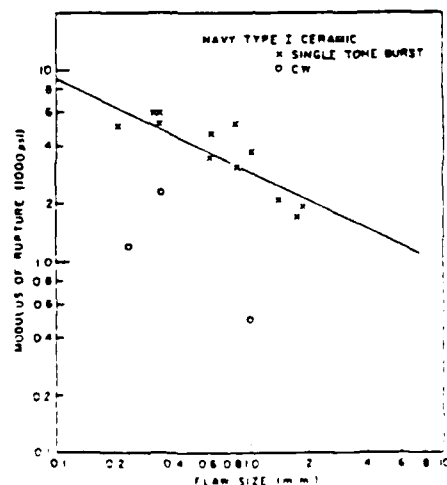
$$K_I = \frac{\sigma}{\sqrt{\pi a}} \left[1 + \alpha \frac{y_0}{a} \frac{\partial}{\partial y_0} \right] \left[\frac{a}{\sqrt{a^2 - z_0^2}} + \frac{a}{\sqrt{a^2 - z_0^2}} \right]$$

$$\text{where } \alpha = \begin{cases} 1/2(1+U) & \text{Plane stress} \\ 1/2(1-U) & \text{Plane strain} \end{cases}$$

Cyclic Strength Behavior Dynamic Strength Equations

$$\text{Bar} \quad \sigma_{\text{Peak}} = \frac{I_P}{4 f A d_{51}}$$

$$\text{Ring} \quad \sigma_{\text{Peak}} = \frac{I_P}{2 \pi f d_{51} h}$$



STRESS CORROSION EXponents

for

DIELECTRIC and PIEZOELECTRIC
CERAMICS

Material	n
BaTiO ₃	60-70
Ba _x Ca _{1-x} Ti _{1.03} O ₃	23-38
PZT	40-60

Capacitors

ZSU	40-60
NFO	100
XTR	80-150

First Approximation to Predicting
Dynamic Lifetime

All Crack Growth Takes Place
Under Tensile Stress

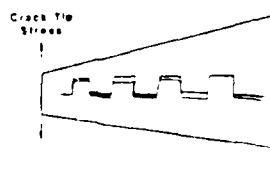
Time to Failure

$$\frac{t_{\text{cyclic}}}{t_{\text{static}}} \approx \left(\frac{\sigma_{\text{static}}}{\sigma_{\text{cyclic}}} \right)^{1/n}$$

σ_{cyclic} = Amplitude of Cyclic Stress

$$\sigma_{\text{cyclic}} = (\sigma_{\text{static}})^{1/n} \left[1 + \frac{1}{4n} + \frac{1}{32n^2} + \dots \right]$$

Compressive Load



GRAIN WEDGING PRODUCES TENSILE STRESS
AT CRACK TIP

Cyclic Electrostrictive Strength

Electric Field Biased Electrostriction

Experimentally Determine Effective d Constant

$$d = k(\epsilon S_0)^{1/2}$$

k Determined Experimentally from Resonance
and Antiresonance Frequencies

Calculations Are Made Similar to Piezoelectric Case

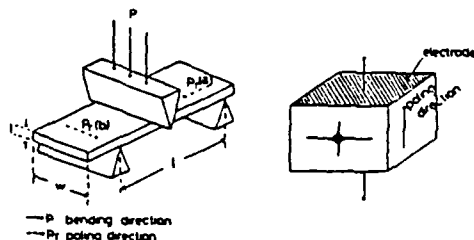
Non Biased Electrostriction Is Highly Nonlinear
and Needs Further Analysis

Combined Effects Due to Mechanical and Electrical
Loads and Internal Microstructural Stresses
Must be Considered

The relation of anisotropy
between crack length and
fracture toughness in poled
PLZT and modified PbTiO₃

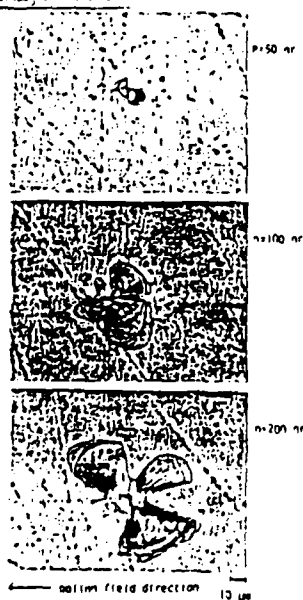
T. Taniamoto et. al.
National Defense Academy

three point bending test and microindentation test



Experimental configuration

poled LiNbO₃ single crystal



Crack and indent of poled LiNbO₃ single crystal



Crack and indent of poled modified PbTiO₃ ceramics

Calculation equations of K_{Ic}

$$K_{Ic} = 0.073PC^{-1/2} \quad \text{Evans et. al.}$$

$$K_{Ic} = 0.036C^{0.4}P^{0.5}a^{-0.7}(C/a)^{-1.5} \quad \text{Marshall et. al.}$$

$$K_{Ic} = 0.030C^{0.3}P^{0.5}a^{-0.5}(C/a)^{-1.5} \quad \text{Leah et. al.}$$

E: Young modulus
P: indented load

$$\sigma_1 = \sigma_{ex} - \sigma_1$$

$$K_{Ic} = \frac{3}{2} \pi \sigma_1 \sqrt{a}$$

$$K_{Ic} = \frac{3}{2} \pi (\sigma_{ex} - \sigma_1) \sqrt{a} = K_{Ic}^{eff} = \frac{3}{2} \pi \sigma_1 \sqrt{a}$$

$$K_{Ic}^{eff} = K_{Ic} + \frac{3}{2} \pi \sigma_1 \sqrt{a}$$

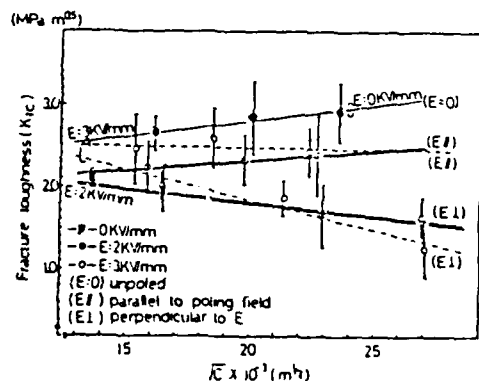
If the sample has an internal stress σ_1 , K_{Ic} change by the square root of crack length, \sqrt{a} .

(Pb,Ca)TiO₃ ceramics

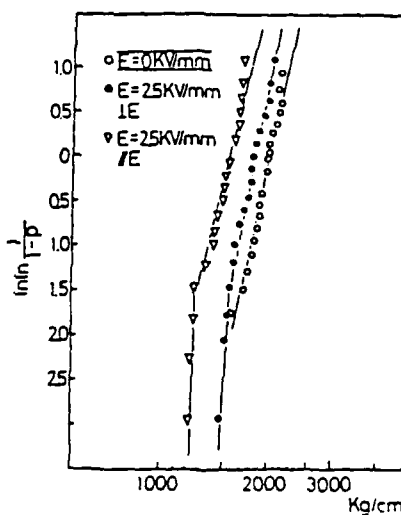
coupling factor	elastic constants ($\times 10^{12}$ dyn/cm ²)	poisson's ratio
$\nu_{12} = 0.043$	$\epsilon_{11}^0 = 7.35$ $\epsilon_{12}^0 = 7.34$	$\sigma^* = 0.205$
$\nu_{21} = 0.037$	$\epsilon_{12}^0 = -1.50$ $\epsilon_{13}^0 = -1.51$	
$\nu_{31} = 0.034$	$\epsilon_{13}^0 = -1.46$ $\epsilon_{23}^0 = -1.34$	
$\nu_{22} = 0.361$	$\epsilon_{23}^0 = 0.59$ $\epsilon_{33}^0 = 0.09$	
$\nu_{32} = 0.361$	$\epsilon_{33}^0 = 10.11$ $\epsilon_{44}^0 = 15.75$	
	$\epsilon_{44}^0 = 17.78$	

PLZT 2/50/50

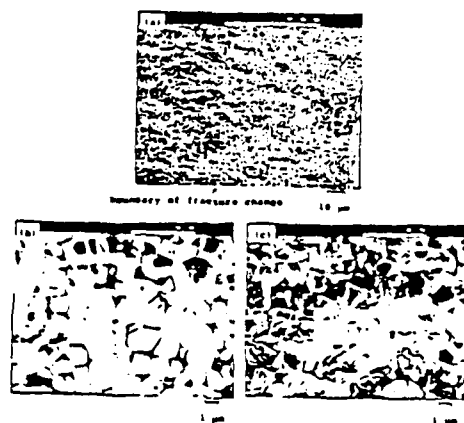
coupling factor	elastic constants ($\times 10^{12}$ dyn/cm ²)	poisson's ratio
$\nu_{12} = 0.34$	$\epsilon_{11}^0 = 12.5$	$\sigma^* = 0.373$
$\nu_{21} = 0.3$	$\epsilon_{22}^0 = 15.4$	



Fracture toughness as a function of square root of crack length in poled modified $PbTiO_3$ ceramics



Weibull plots of failure stress of unpoled and poled modified $PbTiO_3$ ceramics



Fracture surface of poled modified $PbTiO_3$



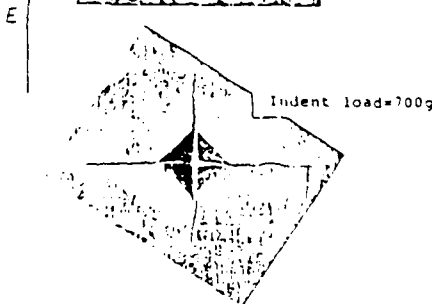
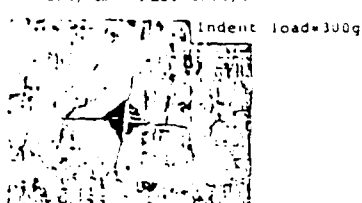
Fracture surface of (a) and (b) regions

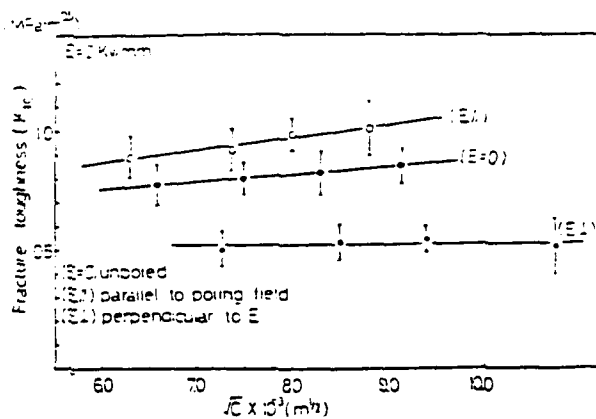
Poled $(Pb,Ca)TiO_3$ ceramics

$E=6 KV/mm$

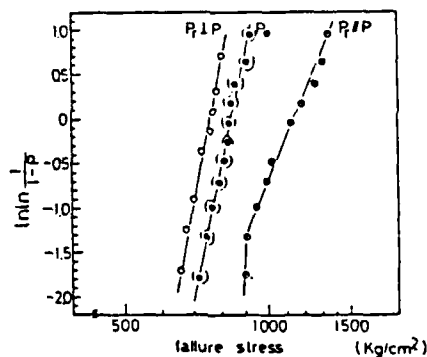


$E=2KV/mm$ PLZT 2-50/50





Fracture toughness as a function of square root of crack length for PLZT (2/50/50) ceramics



Weibull plots of failure stress of poled and unpoled PLZT (2/50/50) ceramics

Fracture surface of PLZT (2/50/50)



P (%)	$K_{Ic}(E)$ $\text{MN/m}^{3/2}$	$K_{Ic}(E\perp)$ $\text{MN/m}^{3/2}$	$c(E)$ mm	$c(E\perp)$ mm	$c(E)/c(E\perp)$	$c(E)$ mm	$c(E\perp)$ mm	$c(E)^2/c(E\perp)^2$
10	2.361	1.640	0.541	0.728	1.4	0.527	0.610	1.18
20	2.382	1.658	0.381	0.526	1.4	0.400	0.439	1.11
50	2.272	1.640	0.253	0.273	1.1	0.264	0.276	1.05

P: indented load, $K_{Ic}(E||)$: K_{Ic} parallel to the poling field

$K_{Ic}(E\perp)$: K_{Ic} perpendicular to the poling field

$c(E||)$: crack length parallel to the poling field $c(E||)/c(E\perp)$: the ratio of $c(E||)$ and $c(E\perp)$

$c(E\perp)$: crack length perpendicular to the poling field

Internal stress = zero

Anisotropy of crack length \Rightarrow Internal stress

Mechanical and Dielectric Failure of BaTiO_3 Ceramics

A. KISHIMOTO, K. KOUMOTO, and H. YANAGIDA

Department of Industrial Chemistry,

Faculty of Engineering, The University of Tokyo,

7-3-1 Hongo, Bunkyo-Ku, Tokyo 113

ABSTRACT A usual method for mechanical strength measurement requires a lot of test pieces and time, which should be inconvenient from the technological point of view.

The present paper reports the alternative method to predict the mechanical failure probability, utilizing the analogy between mechanical and dielectric strength distributions, without spending a lot of test pieces.

Sample preparation

Grain size distributions

Measuring Apparatus

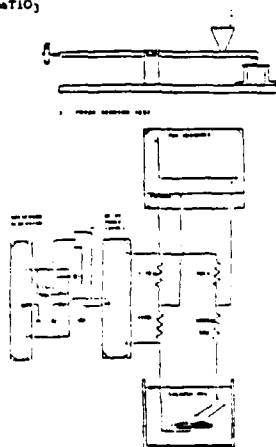
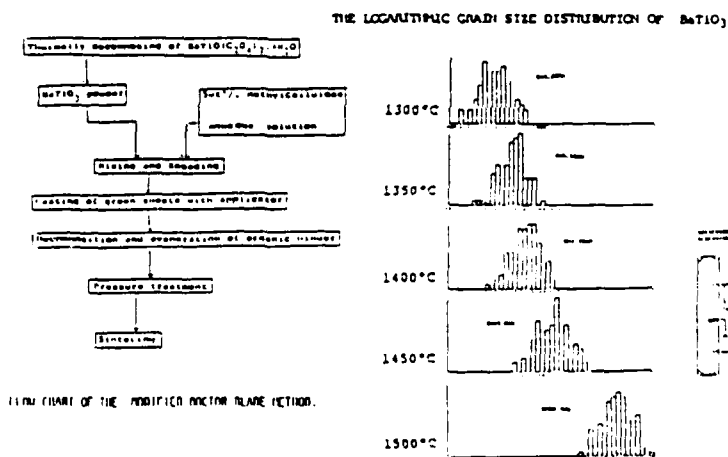
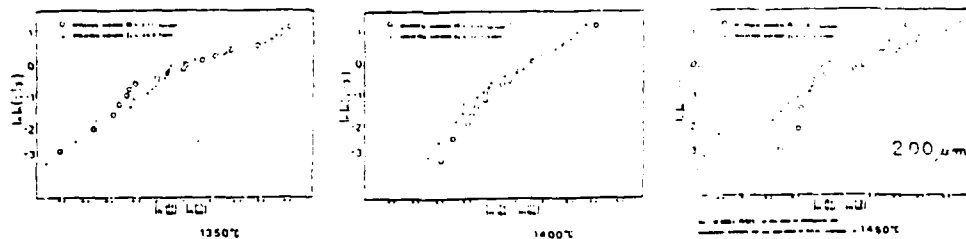


FIG. THE APPARATUS FOR DIELECTRIC STRENGTH MEASUREMENT.

1. Low grain strength measurements, the effect of grain size on strength reliability.

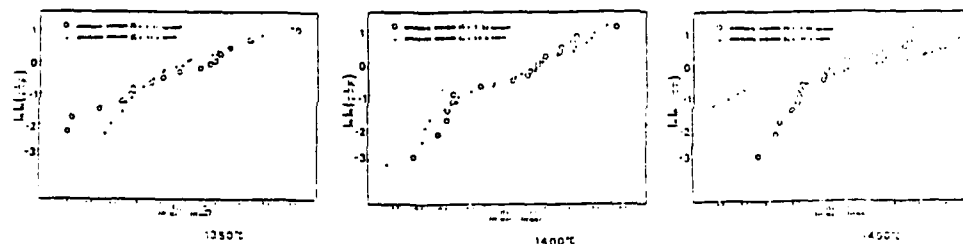
Measured at room temp.



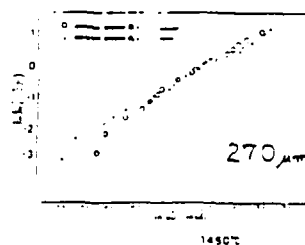
2. Correlation between both failures depends on weak spot distribution.

K_{IC} changes above and below Curie temp.
while crack size remains the same.

Measured at 145°C



3. Effects of thickness on Weibull plots.



DISCUSSION: The fracture origins in both failures are the same. (?)

Crack stress concentrator
 field concentrator

Toughening of Ceramics by Crack Tip /Stacking Faults Interaction

K. Niihara, The National Defense Academy

T. Hirai, RIISOM, Tohoku University

1. Introduction

The intent of this work is to clarify the microstructure characteristics of CVD-SiC ceramics and to examine their mechanical properties such as fracture strength and toughness up to 1500°C. Particular emphasis is placed on the understanding of characteristic superfine structure effects on mechanical properties, i.e. fracture toughness.

2. Preparation of CVD-SiC

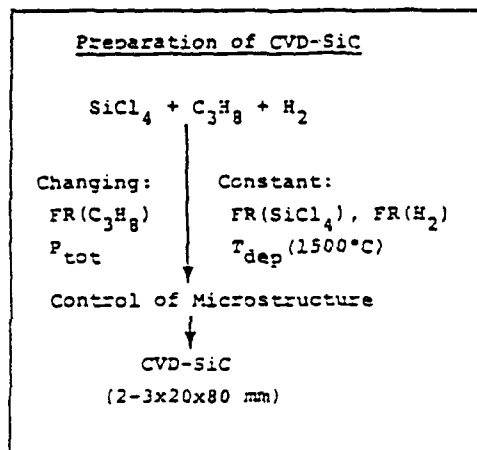


Fig. 2 Typical microstructure of CVD-SiC

3. Superfine Structure

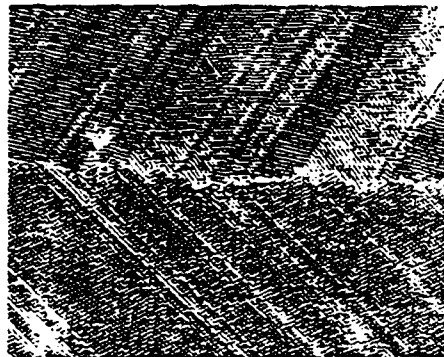
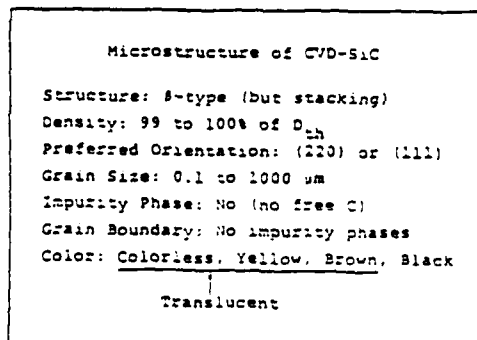


Fig. 3 High resolution lattice image of grain

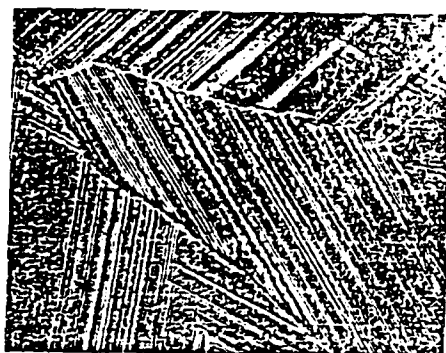


Fig. 4 High resolutional lattice image of multiple



Fig. 7 Small plastic deformation at crack tip for CVD-SiC.

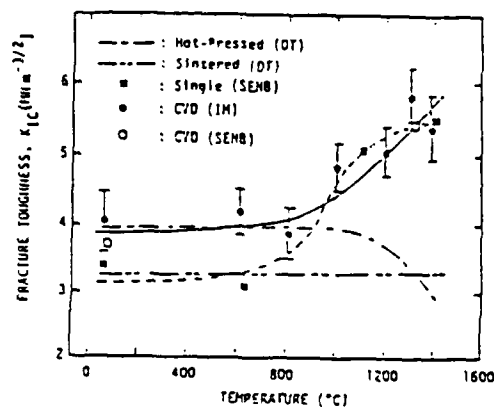


Fig. 5 Temperature dependence of fracture toughness for CVD-SiC.



Fig. 8 Small plastic deformation at crack tip for CVD-SiC.

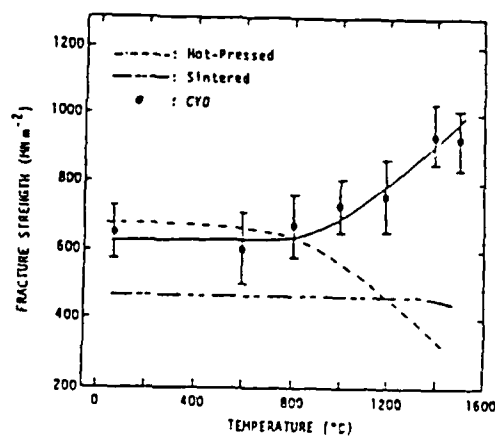


Fig. 6 Temperature dependence of fracture strength of CVD-SiC.

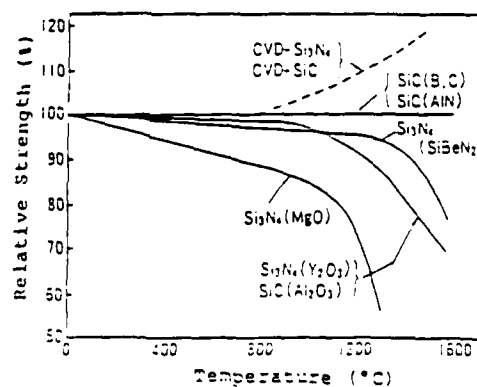


Fig. 9 Temperature dependence of fracture strength for various SiC ceramics.

Grain-Boundary Control and Toughness of Si_3N_4 & SiC

Ceramics	Toughness ($\text{MN}/\text{m}^{3/2}$)
(a) Grain-Boundary Control	
GP- $\text{Si}_3\text{N}_4(\text{SiBeH}_2, \text{SiO}_2)$	2.9
HP- $\text{Si}_2.9\text{BeO}_{0.1}\text{H}_{3.8}\text{O}_{0.2}$	3.3
Sialon	3.1
CVD- Si_3N_4	3.2
PS-SiC(B, C)	3.5
HP-SiC(AlN)	3.5
CVD-SiC	3 ~ 3.5
(b) No Grain-Boundary Control	
HP- $\text{Si}_3\text{N}_4(\text{MgO})$	5 ~ 6.8
HP-SiC(Al_2O_3)	4 ~ 6.0

GP: gas pressure sintering, HP: hot-pressing
PS: pressureless sintering, (): sintering aids

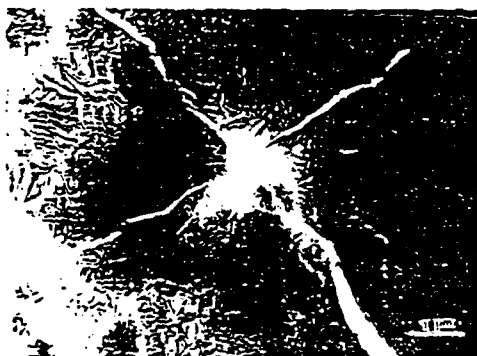


Fig. 10 TEM observation around indentation for CVD-SiC.

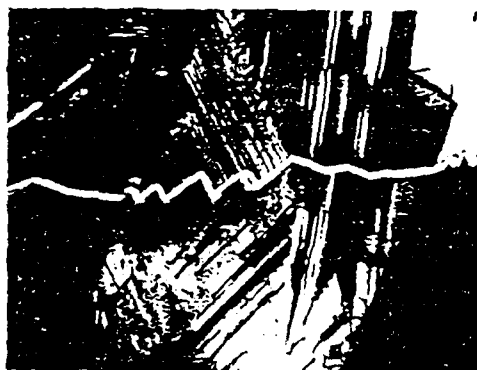


Fig. 13 High resolution lattice image of SiC for CVD-SiC.

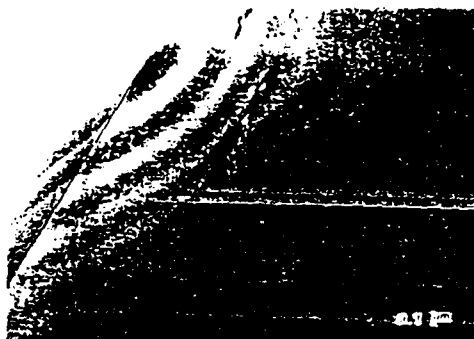


Fig. 15 TEM micrograph for CVD-SiC with low density.



Fig. 16 TEM micrograph for CVD-SiC with low density.

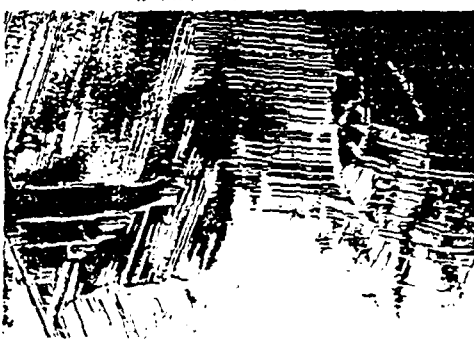


Fig. 17 TEM micrograph for CVD-SiC with high density.

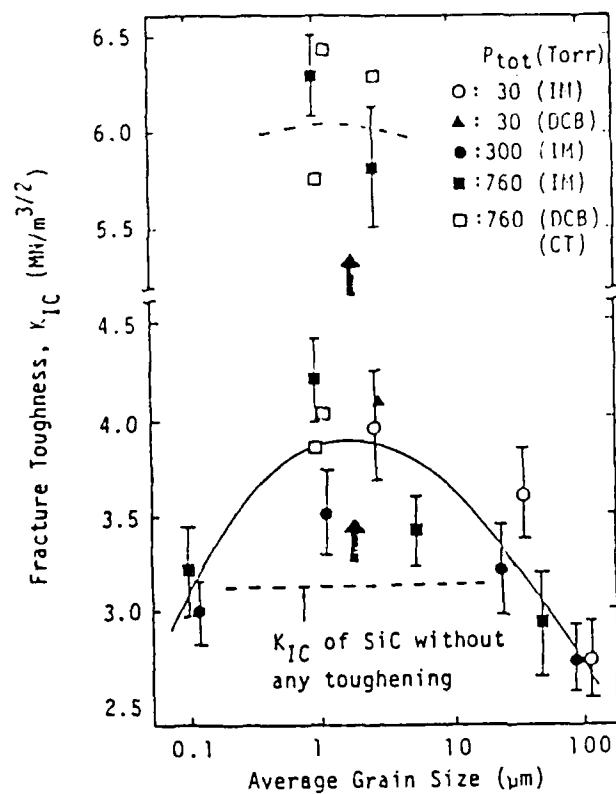


Fig. 18 Fracture toughness for CVD-SiC.

6. Conclusions

- (1) Highly pure and Dense SiC without any impurity phases at grain boundaries were prepared by CVD.
- (2) Toughness and strength of CVD-SiC increased above about 1000°C due to small plastic deformation at crack tip.
- (3) Toughness of CVD-SiC was extremely improved by introducing stacking faults into grains.

New toughening mechanism: stacking faults-crack tip interaction

T16

PHOTOELECTRIC EFFECTS IN PLT CERAMICS

GENE HARRINGTON

MOTOROLA, INC., ALBUQUERQUE, NEW MEXICO, U.S.A.

ABSTRACT

Several non-memory PLT compositions were evaluated for their resistance to the combined effects of high electric field, elevated temperature and high intensity light exposure. All materials exhibited behavior which limit their performance under these conditions. It was found that complete cancellation of the electrooptic effect (an activated shutter degrading to an off condition) could be obtained under certain conditions. This was believed to be due to either anode or thermally excited space charge screening out the applied field. The photoexcited space charge effects could be essentially eliminated by means of ac rather than dc voltage operation.

INTRODUCTION

Since the early 1970's when the transparent, solid-state ferroelectric PLT materials were first utilized in shutter devices, it was noted that these materials were limited on their performance by residual memory phenomena manifested in a time-dependent deterioration of the OFF condition. Subsequent research investigations have contributed greatly to an understanding of these phenomena which are generally classified as (1) residual memory effects resulting from a field-induced ferroelectric state and (2) space charge effects produced by the photoexcitation of charge carriers and their movement under the influence of an electric field. The present study reports on some observed effects in the latter category as they relate to SPE (pseudoferroelectric) materials in transverse-mode, shutter devices.

EXPERIMENTAL

Not pressed, polished and electrodeposited samples of PLT compositions 9/65/35, 8/65/35, 7/65/35, 8/70/30 and 15/40/45 were selected for study. The vacuum deposited, Cr-Au, single-sided, surface electrodes consisted of an interdigital array of electrode widths and gaps ranging from 0.05 μ m to 0.25 μ m. Electrical and electrooptic measurements were made on the samples as a function of electric field, temperature, time and light exposure. A high intensity mercury arc lamp (15 mW/cm²) was used as the light source in conjunction with various filters ranging from 300 nm to several microns.

Space charge and photoconductivity measurements were conducted on the setup shown in Figure 1. These measurements were taken and recorded while under visual observation at a magnification of $\times 200$.

RESULTS

It was found that (1) the PLT materials evaluated in this study were highly susceptible to the combined effects of high intensity light exposure and high electric fields; (2) the effects are more pronounced at temperatures near or above T_c (maximum dielectric constant, 65°C for 9/65/35) and (3) the effects are time dependent and will always anneal out at a rate which is dependent on temperature and light exposure. A typical set of curves are shown in Figures 2, 3 and 4. As noted, the virgin material is symmetric about the zero E axis, whereas the materials subjected to either a positive or negative bias while illuminated (the usual situation in a shutter device) exhibit varying degrees of light intensity asymmetry. The relaxation time for this effect at 100°C for PLT 9/65/35 was found to be approximately 5 seconds (UV light on) and consequently, an activated shutter would be totally compensated (turned off) by the photoexcited space charge field in this time frame. This deleterious effect was essentially eliminated by driving the shutter with an ac voltage at 30 Hz as can be seen in Table 1. Figure 5 summarizes these results in a plot of contrast ratio (CR) vs. temperature

Photoconductive effects in these materials were also studied by monitoring the voltage across a 22 M Ω resistor connected in series with the shutter and the power supply. Hysteresis loops, when a bias voltage was applied to the shutter without illumination, occur or no steady state voltage was developed across the resistor. However, when the light source was turned on, several millivolts (depending on temperature) would develop across the resistor as a result of the conduction of photoexcited space charge across the gaps of the interdigital electrodes. The voltage trace shown in Figure 6 was thus generated by mechanically shuttering the light source at the various rates indicated. This effect was found to be the predominant one associated with the short wavelength region from 320-380 nm through the use of various narrow band optical filters as well as broad band practical materials such as plain glass, UV blue filter, G-5 glass, ruby fiber and PLT.

CONCLUSIONS

1. The PLT materials are highly complex in nature and exhibit a wide variety of electrical, optical and thermally activated effects such as the photovoltaic effect, photoconduction, pyroelectricity, photo-induced space charge, photochromic behavior and a photo-induced change in index of refraction (PIL). Some of these effects are due directly to the chemical stoichiometry and defect concentration vacancies of the materials.
2. Residual memory effects in the solid-state non-memory PLT's are predominant at room temperature whereas the photoexcited space charge effect is significant at elevated (100-150°C) temperatures.
3. A maximum in contrast ratio for shutter devices exists in the temperature range from 40-60°C.
4. Photoconduction in the PLT's is most sensitive to UV wave lengths in the range of 320-380 nm.
5. Many of the degradation effects in the PLT materials can be essentially eliminated by means of ac rather than dc operation.

TABLE 1

CONTRAST RATIO VALUES OF 4.3-6.5 μ m SHUTTER

ADDRESSING CONDITIONS	1 MINUTE		30 MINUTES		DAY		WEEK	
	25°C	100°C	25°C	100°C	25°C	100°C	25°C	100°C
UV LIGHT ON	94	32	21	25	—	—	—	—
UV LIGHT OFF	32	208	25	67	28	75	20	61
UV LIGHT ON	93	63	32	—	—	—	—	—
UV LIGHT OFF	32	232	25	92	30	85	87	97

NOTE: ELECTRODES = 0.5MM WIDE \times 0.5MM GAP
OPERATING VOLTAGE = 200V

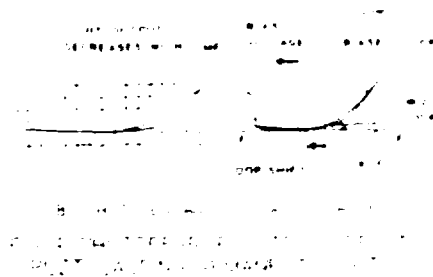
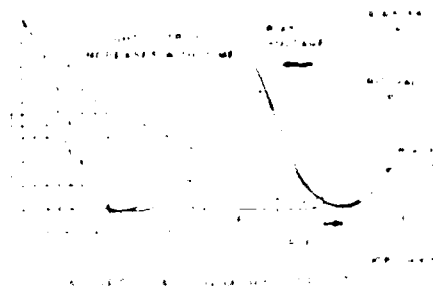


TABLE 1

SAMPLE	Preparation	Grain size, μm	Grain volume, μm^3
N-O	HP-0	13.5	2.01
HP-O	HP-0	20.8	1.60
N-CP	HP-0	17.8	2.40

PHOTOVOLTAIC CHARACTERISTICS

of Three Samples

$$J_{ph} = K \cdot I$$

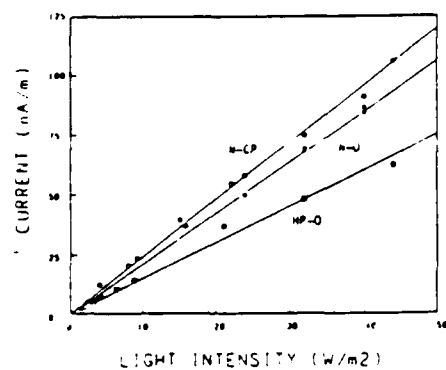
$$J = j_0 (1 + \beta I)$$

$$E_{oc} = 1.22 \cdot J$$

$$= (K/\beta) (1/(1 + \beta I))$$

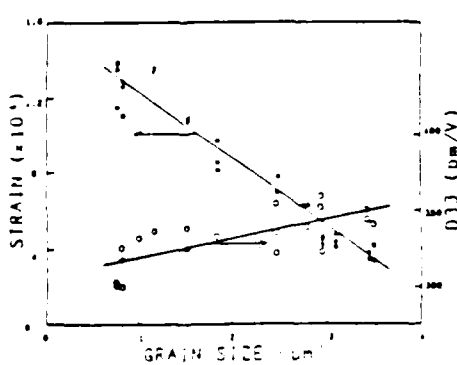
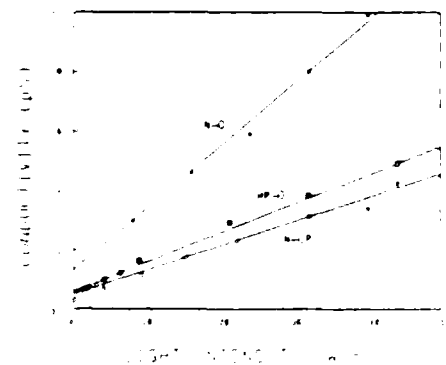
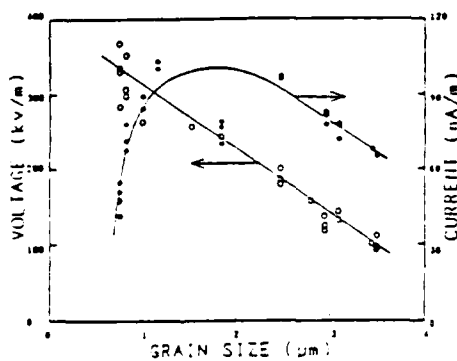
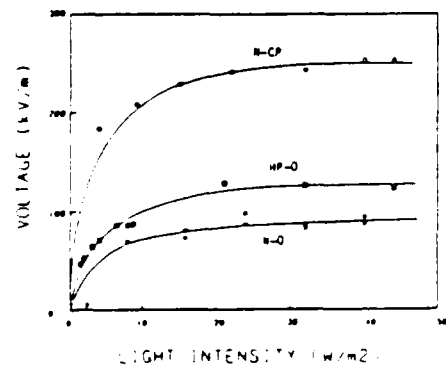
Photovoltaic Effect

in Three Samples, N-O, HP-O and N-CP

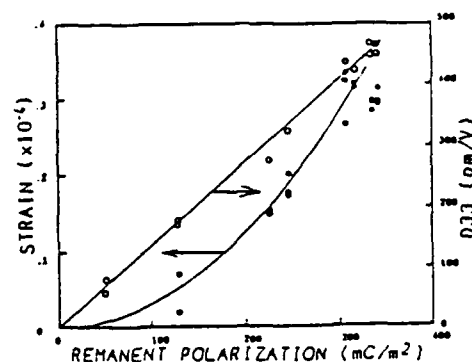
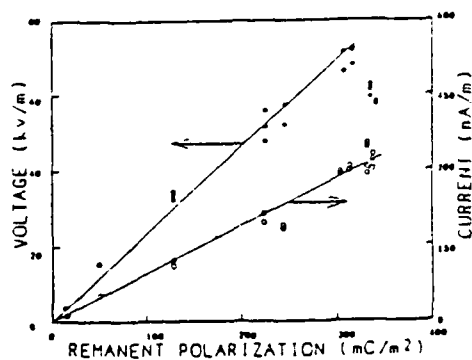


SAMPLE	$G_s (\mu\text{S}/\text{cm})$	$\beta (10^{-4} \text{ m}^2/\text{W})$	$K (\text{nA}/\text{W})$
N-O	46.4	4.68	2.12
HP-O	20.8	4.66	1.60
N-CP	17.8	4.60	2.40

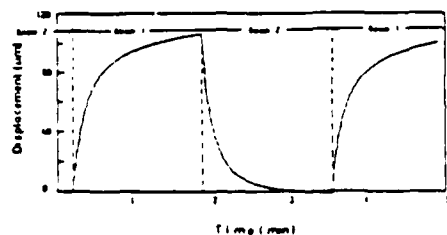
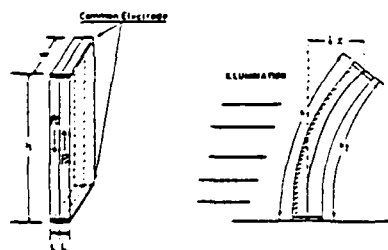
Grain Size Dependence of Photostriction



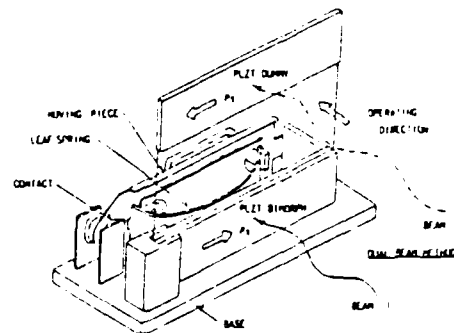
Remanent Polarization Dependence of Photostriction



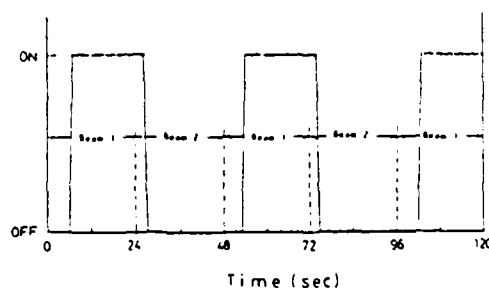
Bimorph Structure and Its Tip-End Deflection



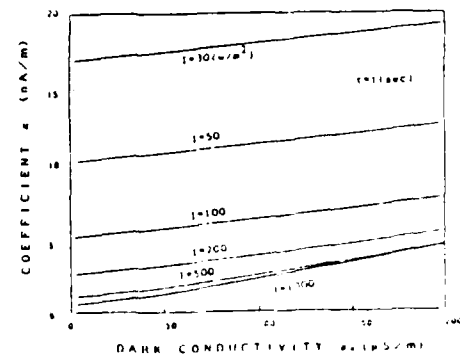
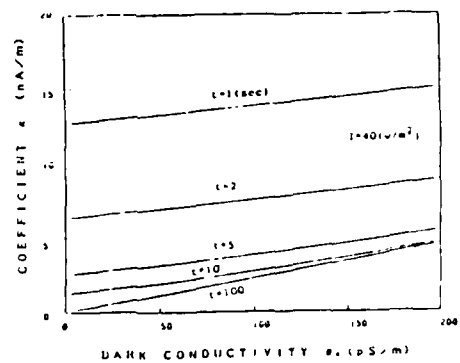
Structure of Photodrive Relay



ON/OFF Response of the Newly Developed Relay



Calculation of Photodrive Relay Response



Analysis of Photodriven Delay

Tip-end Deflection of Bimorph

$$\Delta X = \frac{3}{4} \cdot \frac{h^2 \kappa d_{33}}{L} \cdot t \quad (1)$$

Longitudinal Electric Field
generated by the charge on the Electrode

$$E(t) = (J_{ph} R/h) \cdot (1 - \exp(-t/CR)) \quad (2)$$

Photocurrent and Photoconductivity

$$J_{ph} = h \cdot I \quad (3)$$

$$\sigma = \sigma_0 (1 + \beta \cdot I) \quad (4)$$

Tip-end Deflection as a Function of
Light Intensity and Time (from (1)-(4))

$$\Delta X(t) = \frac{3}{4} \cdot \frac{h^2 \kappa d_{33}}{L \cdot \sigma_0 (3L + \beta I)} \left\{ 1 - \exp\left(\frac{-\sigma_0 (3L + \beta I)}{3L C h R} \cdot t \right) \right\} \quad (5)$$

Parameters

$$h = 0.02 \text{ (cm)}, L = 2 \times 10^{-3} \text{ (cm)}, \kappa = 40 \text{ (V/m)}$$

$$\sigma_0 = 3.50 \times 10^{-7} \text{ (S/cm)}, \beta = 2000$$

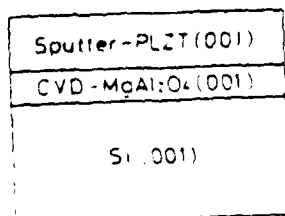
$$\beta = 2.6 \times 10^{-4} \text{ (cm}^2/\text{V)}, \beta \cdot I = 2.5 \times 10^{-3}$$

PLZT THIN FILMS ON $\text{MgAl}_2\text{O}_4/\text{Si}$ SUBSTRATE

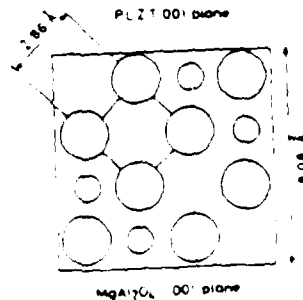
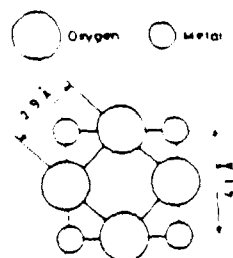
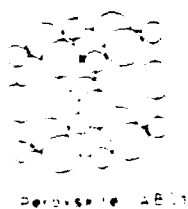
S. MATSUBARA, Y. MIYASAKA, N. SHOHATA and M. YONEZAWA
NEC Corporation, Kawasaki, JAPAN

SUMMARY

- PLZT FILMS WERE SPUTTER DEPOSITED ONTO $(001)\text{MgAl}_2\text{O}_4/\text{Si}$ SUBSTRATE
- EPITAXIAL GROWTH OF PLZT FILMS ALONG THE $\langle 001 \rangle$ AXIS OF THE MgAl_2O_4 FILMS WAS OBSERVED
- THE CRYSTALLINITY AND THE LATTICE CONSTANT DEPENDED ON THE La CONTENT OF THE TARGET
- DIELECTRIC CONSTANT WAS MEASURED WITH A MIS STRUCTURE $\epsilon = 488$ AT 100 KHz

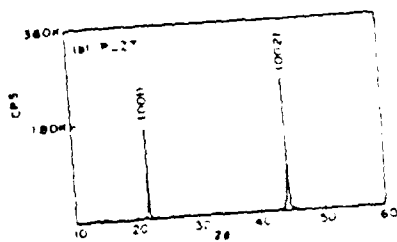


PLZT $\text{MgAl}_2\text{O}_4/\text{Si}$ STRUCTURE

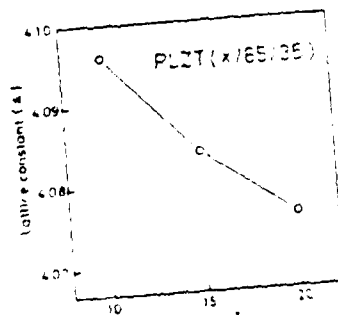


001 PLANES OF PLZT AND MgAl_2O_4

Sputtering system	RF Magnetron
Substrate	$(001)\text{MgAl}_2\text{O}_4/\text{Si}$
Target	PLZT = 45.35 g. sintered powder
Substrate temperature	500°C
Sputtering gas	$\text{Ar} + \text{O}_2$
Pressure	$0.01 \sim 0.05$ Torr
RF power	50 W
RF frequency	13.56 MHz
Deposition rate	10 nm/min



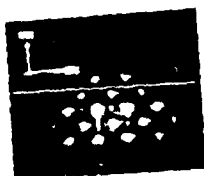
X-RAY DIFFRACTION PATTERN FOR PLZT MgAl_2O_4



La CONTENT DEPENDENCE OF LATTICE CONSTANT

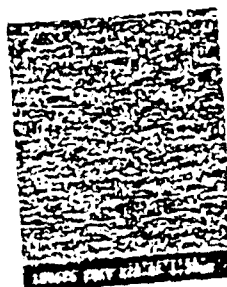


PLZT

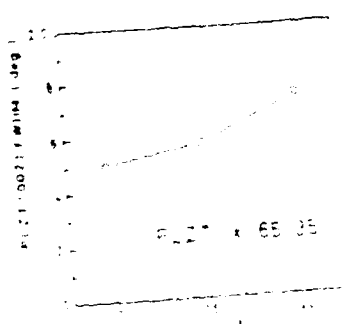


MgAl_2O_4

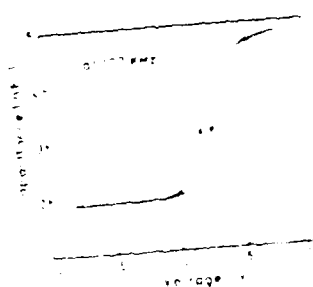
RHEED PATTERN FOR PLZT MgAl_2O_4



SURFACE MORPHOLOGY OF PLZT FILM



La CONTENT DEPENDENCE OF PIEZOELECTRICITY



CHARACTERISTICS WITH A MICROSTRUCTURE

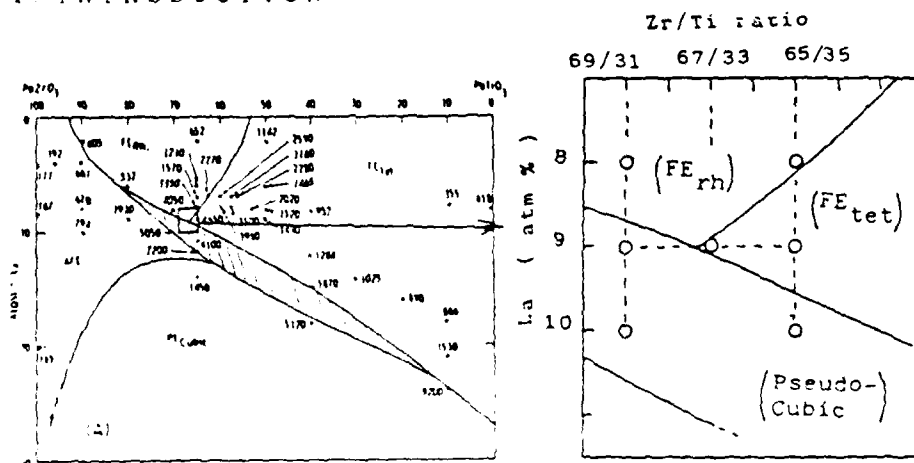
T20

SOME ELECTROOPTIC PROPERTIES OF PLZT CERAMICS

K. Hikita, M. Hiramatsu, Y. Tanaka
and M. Ono

R&D Center, Ceramics
Mitsubishi Mining & Cement
CO., LTD.

1. INTRODUCTION



According to the phase diagram of PLZT, phase boundaries among two ferroelectric phases and a pseudo-cubic phase are crossed near the composition of (9/67/33), and near where the composition of (9/65/35), which is suitable for optical shutter applications, locates.

However, the electrooptic properties have been scarcely studied around the crossed point. Then the present study reports the dielectric and electro-optic properties in this region.

2. EXPERIMENTAL PROCEDURES

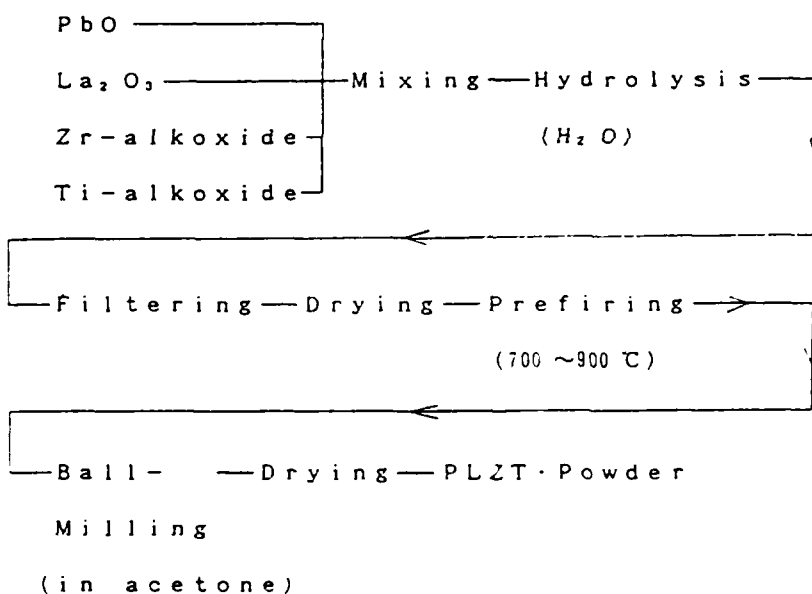
1) Sample Preparation

*Composition: $\text{Pb}_{1-x}\text{La}_x(\text{Zr}_y\text{Ti}_{1-y})_{1-x/4}\text{O}_3$

$x = 0.08, 0.09, 0.10$

$y = 0.65, 0.67, 0.69$

*Processing of PLZT powder



*Hot Pressing and Annealing

(Two-Stage Method)

Hot Pressing: 1200°C, 5Hr, $P = 100 \text{ kg. cm}^{-2}$

Annealing: 1200°C, 20Hr.

2) Measurement

*XRD

Crystal phase

*D-E Hysteresis Loop

AC electric field: 2kV/mm, 50Hz.

Sample: 5x5 mm², thickness 0.25 mm

*Birefringence (Δn)

Polarizing Microscope, Senarmon
Compensator

Sample: Mirror-polished PLZT

thickness 0.5 mm

gap between electrodes 0.5 mm

Determining the rotating angle of
Analyzer \rightarrow Retardation ($P = \Delta n \cdot l$)

Quadratic electrooptic coefficient

, R, was determined by following eq.

$$R = -2\Delta n / n_1^3 E_s^2$$

where, n_1 : refractive index

E_s : electric field

3. RESULTS and DISCUSSION

1) D-E Hysteresis

(X/69.31). The loop changed to slim
with increasing in La
ratio

(X/65/35) : The same tendency.

(9/Y/Z) : The loop changed to slim
with increasing in Zr/Ti
ratio.

*Ec and Pr decreased with increasing
in both La ratio and Zr ratio.

*D-E hysteresis loop also became
slim with increasing temperature.

2) Birefringence and Quadratic electro- optic coefficient (R)

(X/69/31) : Memory effect was observ-
ed for La 8 atm%.

Quadratic electrooptic
effect was shown for La
9 and 10 atm%.

(X/65/35) : the same tendency.

(9/Y/Z) : quadratic curves changed
to flat as Zr ratio inc-
reased.

Quadratic electrooptic
coefficient increased
with decreasing in Zr
ratio.

*A little hysteresis was observed in
the quadratic curves, which decrea-
sed with increasing in both La
ratio and Zr ratio.

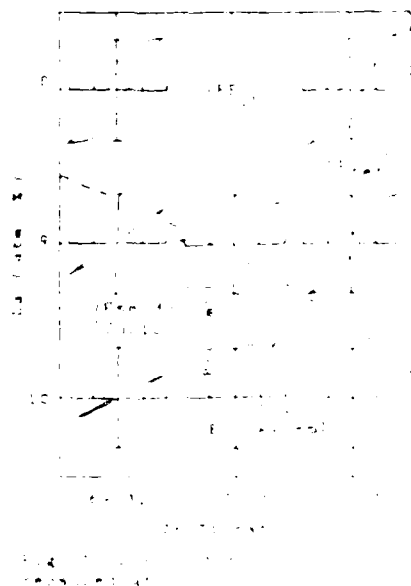
*The difference between the experimental results and reference data of quadratic electrooptic coefficient was considered due to thickness of the samples.

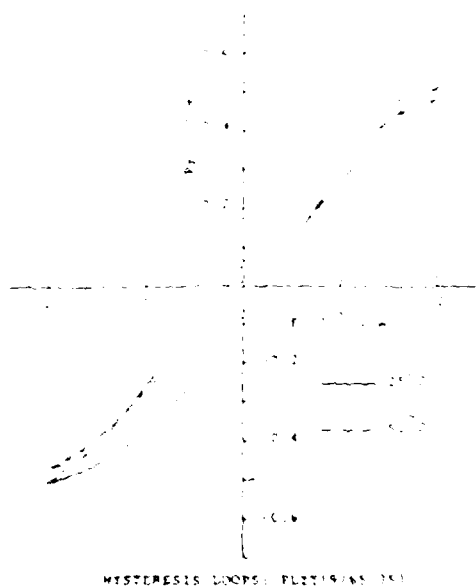
3) X-Ray Diffraction

Crystal phases were examined by means of XRD. However, apparent difference was not observed on the XRD patterns, therefore it was so hard to determine the crystal phase only by means of XRD.

RESULTS

1) THE HYSTERESIS LOOP





HYSTERESIS LOOPS: PZT/95/5

2. BIREFRINGENCE

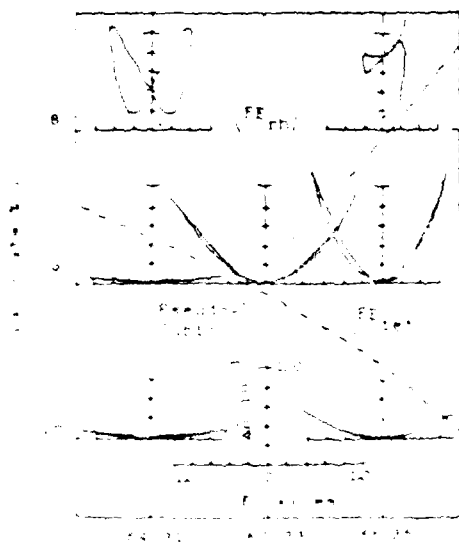
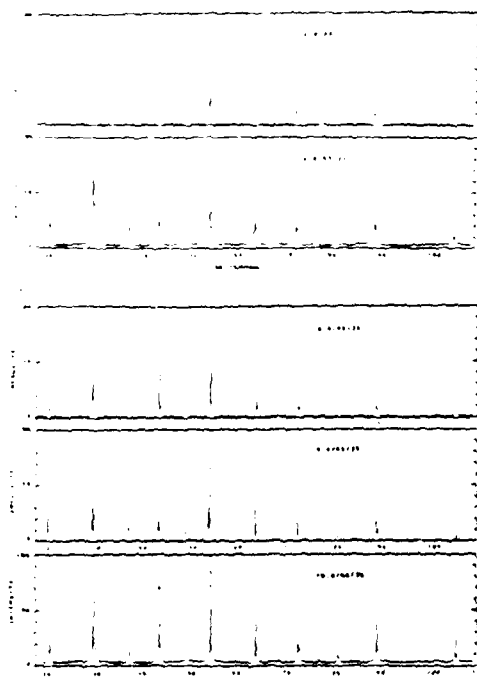


Fig. 2. Birefringence vs. electric field for PZT/95/5.

TABLE I. Birefringence vs. electric field for PZT/95/5.

A. Birefringence vs. electric field for PZT/95/5.

B. Birefringence vs. electric field for PZT/95/5.



4. SUMMARY

Dielectric and electrooptic properties were studied for the both-doped lanthanum-modified lead zirconate titanate (PZT) ceramics near the composition of (95/5) where three phase boundaries were crossed.

1. The hysteresis loop became slim with increasing in Zr/Ti ratio. For the composition of (95/5) the hysteresis loop also changed to slim with increasing in LA ratio for both series of (A 65/35) and (A 45/55).

2. The quadratic electrooptic coefficient were decreased with increasing in both LA ratio and Zr/Ti ratio. The hysteresis were also decreased with increasing in both LA ratio and Zr/Ti ratio.

3. The ferroelectric phase was not observed in XRD means of XRD. However, the results of D-E hysteresis loops and birefringence were in accord with the phase diagram given by the XRD data.

DIELECTRIC PROPERTIES OF SPUTTERED POLYCRYSTALLINE $(\text{Pb}, \text{La})(\text{Zr}, \text{Ti})\text{O}_3$ THIN FILMS

K. WASA, H. ADACHI, and T. MITSUYU

Central Research Laboratories, Matsushita Electric Ind. Co., Ltd.

Yagumo-Nakamachi 3-15, Moriguchi 570, Japan

ABSTRACT: Thin films of polycrystalline $\text{Pb}_{1-x/100}\text{La}_{x/100}(\text{Zr}_y/100\text{Ti}_{1-y}/100)_{1-x/400}\text{O}_3$, PLZT, were prepared on a sapphire substrate by rf-magnetron sputtering from the PLZT sintered powder target. The sputtered films show a perovskite structure and exhibit a dielectric anomaly. Dielectric properties were discussed in comparison with bulk ceramics.

1. INTRODUCTION

Thin films of ferroelectric materials are of much interest for a fabrication of novel functional devices. The single crystal films of the quaternary solid solution of $\text{Pb}_{1-x/100}\text{La}_{x/100}(\text{Zr}_y/100\text{Ti}_{1-y}/100)_{1-x/400}\text{O}_3$, PLZT(x,y,z), were extensively studied for making an electro-optic devices. Recently we have prepared polycrystalline thin films of the PLZT(x/y/z) by rf-magnetron sputtering and evaluated their dielectric properties.

2. PREPARATIONS AND MEASUREMENTS

The PLZT thin films were deposited by the sputtering from sintered PLZT powder target. The sputtering conditions are shown in TABLE 1. Sapphire wafers were used as the substrates. The substrate temperature was kept at 500 to 700°C. The dielectric properties of the sputtered PLZT films were evaluated in a sandwich structure, Au thin film top electrode/sputtered PLZT films/TiN thin film base electrode, prepared on the sapphire wafers. The TiN base electrode was sputtered onto the sapphire wafer prior to the sputtering deposition of the PLZT films. The Au top electrode was deposited by a conventional vacuum deposition after the deposition of the PLZT films.

3. RESULTS AND DISCUSSIONS

The sputtered PLZT films showed a polycrystalline form with the perovskite structure. Their room temperature permittivity was ranged from 100 to 700 depending on their composition, and dielectric loss, $\tan \delta$ 0.01 to 0.1. The frequency dispersion of the permittivity was 5 to 15 % from the frequency range of 10 kHz to 1 MHz. These sputtered films exhibited a dielectric anomaly. Typical results for the PLZT films sputtered from PLZT(9/65/35) target are shown in Fig. 1.

Figure 2 shows a variation of the dielectric properties with the La concentration in the target of PLZT(x/65/35). It is seen that the permittivity shows a maximum at the La concentration of about 10 %. This may suggest that there appears a phase change from rhombohedral/tetragonal/cubic by the increase of the La concentration similar to the case of bulk ceramics. The dielectric anomaly temperature observed in the sputtered films was 220 to 280°C which is lower than the dielectric-anomaly temperature for bulk ceramics. This may be due to the difference of the net composition between bulk ceramics and sputtered films.

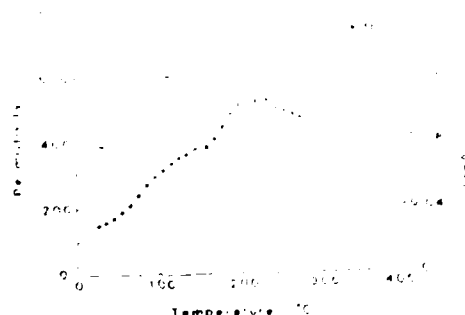
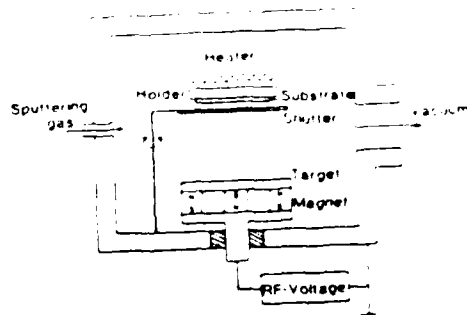
1. *Chlorophyll a* (Chl *a*)

1000

THE UNIVERSITY OF CHICAGO

GALES IN THE WINTER OF 1851-52

6.50.88. 19

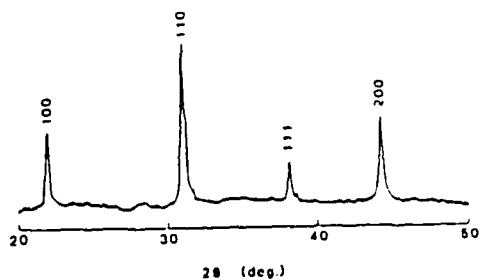


7. Temperature of the water is 10°C.

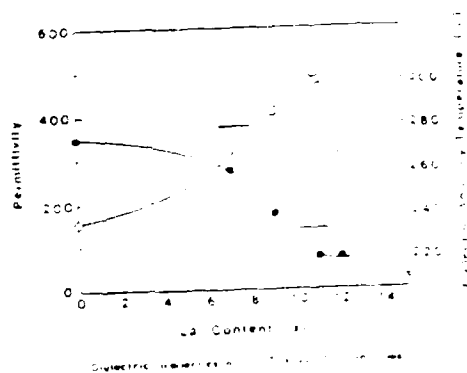
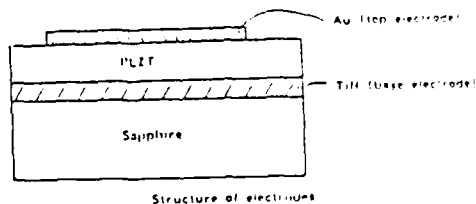
Rf-planar Magnetron Sputtering System

TABLE 1. Sputtering conditions.

Target	PLZT powder, 100%
Substrate	Sapphire
Substrate temperature	500~700 °C
Sputtering gas	Ar(60%)+O ₂ (40%)
Gas pressure	6.3×10^{-2} Torr
Rf power	160 W
Deposition rate	70~100 Å/min

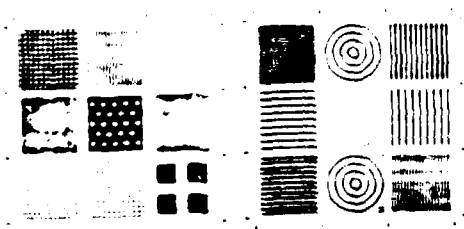
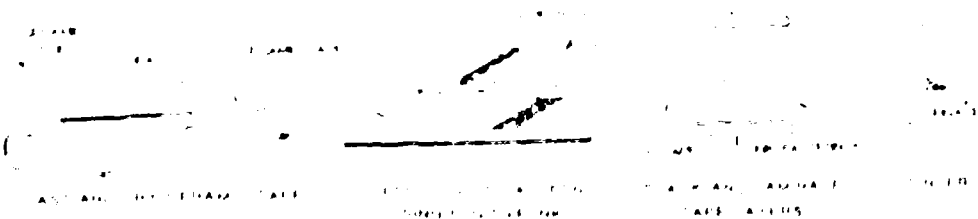


X-ray diffraction patterns of PLZT11/65/35 thin film

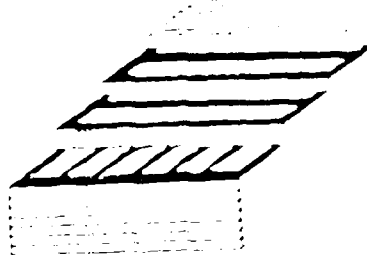


W1

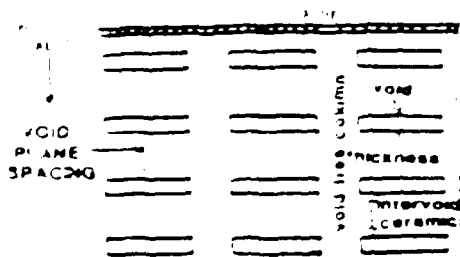
PREPARATION OF CERAMICS WITH ORDERED VOID ARRAYS



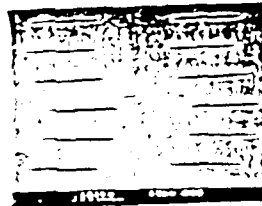
VOID PATTERNS FOR DEPOSITION OF FUGITIVE INK



SCHEMATIC OF CERAMIC WITH CROSSED BAR SHAPED VOIDS MADE BY ROTATING PARALLEL BAR PATTERN BY 90° IN ALTERNATE LAYERS

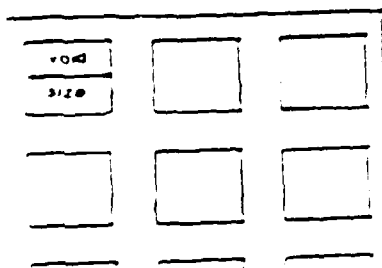


EDGE VIEW



CROSSSECTION OF CERAMIC WITH CORNER CONNECTED SQUARE SHAPED VOIDS

VOID THICKNESS 0.54×10^{-3} in.
VOID PLANE SPACING 3.7×10^{-3} in.



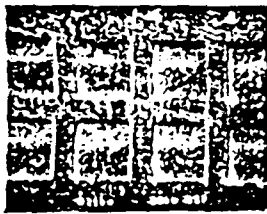
TOP VIEW

MODEL OF CERAMIC WITH SQUARE SHAPED VOIDS



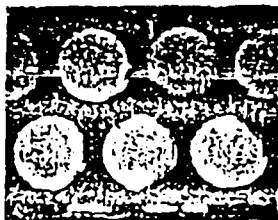
TOP VIEW OF CERAMIC HAVING CORNER CONNECTED SQUARE SHAPED VOIDS

VOID LENGTH AND WIDTH 1.5×10^{-3} in.



TOP VIEW OF CERAMIC HAVING
UNCONNECTED SQUARE SHAPED VOIDS

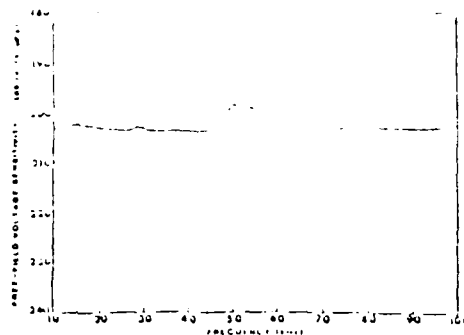
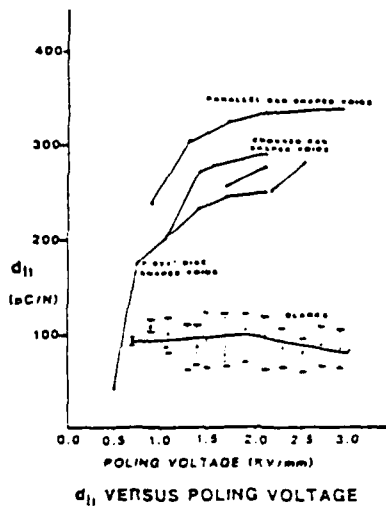
VOID LENGTH AND WIDTH 22×10^{-3} in.



TOP VIEW OF CERAMIC HAVING
DISC SHAPED VOIDS

VOID DIAMETER 24×10^{-3} in.

OPTIMUM POLING VOLTAGE IS 2.1 KV/mm
AVERAGE d_{33} IS 353 pC/N.



FREE FIELD OPEN CIRCUIT VOLTAGE SENSITIVITY OF
1.25\"/>

PIEZOELECTRIC AND HYDROSTATIC PRESSURE RESPONSE OF PZT WITH VARIOUS VOIDS

VOID CONFIGURATION	d_{33} pC/N	d_{31} pC/N	d_{32} pC/N	d_{33} pC/N	d_{31} pC/N	d_{32} pC/N
Crossed Bars 0.076" void 0.076" void	710	1.22	-0.05	110	700	150
0.076" void 0.076" void	100	1.10	-0.11	100	222	80
0.076" void 0.076" void	900	1.00	-0.00	151	700	12
0.076" void 0.076" void	N/A	1.00	-0.10	0.00	151	70
0.076" Box Bevel 1.25" top flange 0.076" top flange	000	1.25	-0.15	150	700	52
	000	1.10	-0.20	000	700	00

1) $d_{33} = \frac{d_{33} + d_{31} + d_{32}}{3}$ 2) Calculated d_{31} 3) Calculated d_{32}

THE CROSSED BAR PATTERN HAS THE
HIGHEST PIEZOELECTRIC SENSITIVITY

FREE FIELD HYDROSTATIC RESPONSE OF PZT WITH VARIOUS VOIDS

VOID CONFIGURATION	d_{31}	d_{32}	d_{33} $\frac{d_{31} + d_{32} + d_{33}}{3}$	d_{31} d_{32}
	(mm/ft)	(in./ft)		(mm/ft)
Crossed Bars				
0.076" wide 0.010" spaced	170	275	0.80	21000
0.076" wide 0.020" spaced	66	270	0.81	10000
0.010" wide 0.010" spaced	58	251	0.80	15100
Parallel Bars				
0.076" wide 0.010" spaced	61	195	0.58	8100
0.076" Dia. Bars 1.75" sq. plate	60	197	0.76	7880

SAMPLES EXHIBIT NO IRREVERSIBLE PROPERTY
CHANGES UP TO AT LEAST 1000 psi.

RESONANCE MEASURING TECHNIQUE FOR COMPLEX COEFFICIENTS OF PIEZOELECTRIC COMPOSITES

BY

Q.C. XU, A.R. RAMACHANDRAN AND R.E. NEWNHAM

MATERIALS RESEARCH LABORATORY,
THE PENNSYLVANIA STATE UNIVERSITY,
UNIVERSITY PARK, PA 16802.

INTRODUCTION

Two measurement techniques for piezoelectric composites based on resonance methods are described. One is used for estimating the real coefficients and is based on a lumped equivalent circuit model. The other involves the complex coefficients derived from an analytical solution of a single mode vibration. Representative plots of conductance-vs-frequency, capacitance-vs-frequency and the mechanical quality factor, Q_m , are presented along with the real and imaginary parts of the dielectric, elastic and piezoelectric coefficients of 0-3 composites (NTK), 0-3 fired composites (PZT), Lead titanate-Bismuth ferrite composites, PVDF voided thick films and PVDF nonvoided thin films.

Resonance Technique for Measuring the Complex Coefficients of Piezoelectric Composites

TE (Thickness Mode)

$$C_{11}^* = C_0(1 - jD), \quad D = \tan \delta_e$$

$$C_{33}^* = C_{33}(1 + jJ), \quad J = \tan \delta_m$$

$$k_{31}^* = k_{31}(1 + jPK)$$

(Assume $\rho^2 \ll 2^2$ (PM) $2 \ll 1$)

The impedance of the thickness mode is

$$Z = \frac{1}{j\omega C_0} \left(1 - \frac{\rho^2 \tan b^*}{b^*} \right)$$

where

$$b^* = \frac{\sqrt{C_0}}{2V} = \frac{\sqrt{C_0}}{2V} \left(1 - \frac{\rho^2}{2} \right)$$

$$V^* = \sqrt{\frac{C_0}{\rho^2}} = \sqrt{\frac{C_0}{\rho^2}} + j\frac{\rho^2}{2}$$

If $\rho^2 \ll 1$ PM = 0.4
then error $\approx 10\%$

$$V_{31}^{*2} = V_{31}^2 (1 + jPK)$$

$$Z = R + jX$$

$$R = \frac{1}{\omega C_0} \left(\rho + \frac{\rho^2}{b} \frac{[\tanh^2(b) + \tanh^2(b^*) + 10 + \frac{1}{2} + 2\rho \tanh(b) \tanh(b^*)]}{(1 + \tanh^2(b) \tanh^2(b^*))} \right)$$

$$X = \frac{1}{\omega C_0} \left(-1 + \frac{\rho^2}{b} \frac{[\tanh(b) + \tanh^2(b^*) + 10 + \frac{1}{2} + 2\rho \tanh(b) \tanh(b^*)]}{(1 + \tanh^2(b) \tanh^2(b^*))} \right)$$

Therefore

$$\frac{C_1 - C_2}{A_1} = 20 = \frac{C_1 - 30}{A_1}$$

WHEAT

$$U_1 = \tan^{-1} \frac{b}{a} = \tan^{-1} \frac{5}{12}$$

$$A_1 = b_1 - 1 = \tan^2 b_1 \quad \tan^2 \frac{b_1}{2}$$

$$Q_1 = \csc \theta \cdot \frac{b \cdot \sin \theta}{2} \cdot (2 + \tan^2 \theta_1)$$

B - 3 - 4 - 2 PM

$$b_1 = w_1 T / 2V$$

$$K = K_1^2$$

1 = 1, 2, 3 corresponding to f_1 , f_2 and f_3 .

Using an iterative method, the values of κ , μ and λ are calculated

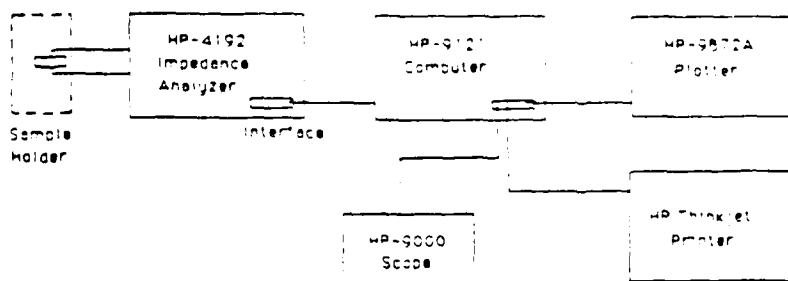
Furber

$$n_{11} = \frac{C_{11}}{C_{11} + C_{12}} (1 - 0.99) = \frac{1}{1 + 1} (1 - 0.99) = \frac{1}{2} (1 - 0.99)$$

$$33 = \sqrt{33 \cdot 33} \quad 34 = 2 \cdot 17 \quad 35 = 5 \cdot 7$$

$$v^* = v(x) + y \frac{dv}{dx}$$

A similar procedure was followed for the other nodes



SCHEMATIC DIAGRAM OF THE MEASURING TECHNIQUE

... ..

... ..

... ..

... ..

The

... ..

... ..

$$\frac{1}{\omega} = \frac{1}{\omega_0} \left(1 - \frac{\omega^2}{\omega_0^2} \right)^{-1/2}$$

Static current Dynamic current

$$\begin{pmatrix} U_1 \\ U_2 \end{pmatrix} = \begin{pmatrix} U_1 \\ U_2 \end{pmatrix}$$

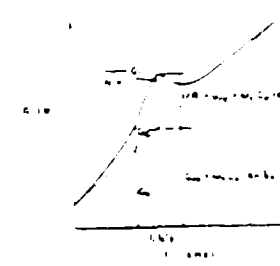
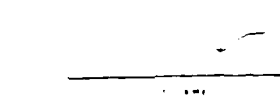
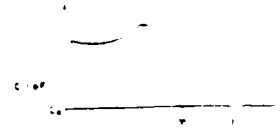
$$\frac{1}{\omega} = \frac{1}{\omega_0} \left(1 - \frac{\omega^2}{\omega_0^2} \right)^{-1/2}$$

... ..

... ..

$$\frac{1}{\omega} = \frac{1}{\omega_0} \left(1 - \frac{\omega^2}{\omega_0^2} \right)^{-1/2}$$

Equivalent circuit of a single mode piezoelectric resonator



$$\frac{1}{\omega} = \frac{1}{\omega_0} \left(1 - \frac{\omega^2}{\omega_0^2} \right)^{-1/2}$$

$$\frac{1}{\omega} = \frac{1}{\omega_0} \left(1 - \frac{\omega^2}{\omega_0^2} \right)^{-1/2}$$

$$\frac{1}{\omega} = \frac{1}{\omega_0} \left(1 - \frac{\omega^2}{\omega_0^2} \right)^{-1/2}$$

$$\frac{1}{\omega} = \frac{1}{\omega_0} \left(1 - \frac{\omega^2}{\omega_0^2} \right)^{-1/2}$$

$$r_{12} = r_{21}$$

and

$$r_{13} = r_{31}$$

$$r_{14} = r_{41} = \frac{1}{2} \left(\frac{r_{12} + r_{23}}{r_{12} + r_{23} + r_{24}} \right)$$

$$r_{15} = r_{51} = \frac{1}{2} \left(\frac{r_{12} + r_{23}}{r_{12} + r_{23} + r_{24}} \right)$$

$$r_{16} = r_{61} = \frac{1}{2} \left(\frac{r_{12} + r_{23}}{r_{12} + r_{23} + r_{24}} \right)$$

$$r_{17} = r_{71} = \frac{1}{2} \left(\frac{r_{12} + r_{23}}{r_{12} + r_{23} + r_{24}} \right)$$

$$r_{18} = r_{81} = \frac{1}{2} \left(\frac{r_{12} + r_{23}}{r_{12} + r_{23} + r_{24}} \right)$$

$$r_{19} = r_{91} = \frac{1}{2} \left(\frac{r_{12} + r_{23}}{r_{12} + r_{23} + r_{24}} \right)$$

$$r_{20} = r_{21} = r_{22}$$

$$r_{21} = r_{12} = r_{22} = \frac{1}{2} \left(\frac{r_{12} + r_{23}}{r_{12} + r_{23} + r_{24}} \right)$$

$$r_{22} = r_{21} = r_{22} = \frac{1}{2} \left(\frac{r_{12} + r_{23}}{r_{12} + r_{23} + r_{24}} \right)$$

$$r_{23} = r_{32} = \frac{1}{2} \left(\frac{r_{12} + r_{23}}{r_{12} + r_{23} + r_{24}} \right)$$

$$r_{24} = r_{42} = \frac{1}{2} \left(\frac{r_{12} + r_{23}}{r_{12} + r_{23} + r_{24}} \right)$$

$$r_{25} = r_{52} = \frac{1}{2} \left(\frac{r_{12} + r_{23}}{r_{12} + r_{23} + r_{24}} \right)$$

$$r_{26} = r_{62} = \frac{1}{2} \left(\frac{r_{12} + r_{23}}{r_{12} + r_{23} + r_{24}} \right)$$

$$r_{27} = r_{72} = \frac{1}{2} \left(\frac{r_{12} + r_{23}}{r_{12} + r_{23} + r_{24}} \right)$$

$$r_{28} = r_{82} = \frac{1}{2} \left(\frac{r_{12} + r_{23}}{r_{12} + r_{23} + r_{24}} \right)$$

$$r_{29} = r_{92} = \frac{1}{2} \left(\frac{r_{12} + r_{23}}{r_{12} + r_{23} + r_{24}} \right)$$

and

$$r_{31} = r_{13}$$

$$r_{32} = r_{23}$$

$$r_{33} = \frac{1}{2} \left(\frac{r_{12} + r_{23}}{r_{12} + r_{23} + r_{24}} \right)$$

$$r_{34} = \frac{1}{2} \left(\frac{r_{12} + r_{23}}{r_{12} + r_{23} + r_{24}} \right)$$

$$r_{35} = \frac{1}{2} \left(\frac{r_{12} + r_{23}}{r_{12} + r_{23} + r_{24}} \right)$$

$$r_{36} = \frac{1}{2} \left(\frac{r_{12} + r_{23}}{r_{12} + r_{23} + r_{24}} \right)$$

$$r_{37} = \frac{1}{2} \left(\frac{r_{12} + r_{23}}{r_{12} + r_{23} + r_{24}} \right)$$

Table 2. Property Coefficients Measured Using the Test Cell

Parameter	HTS	HTS-2	HTS-3	HTS-4	HTS-5
Complex dielectric coefficients	$11.4(1 \pm 0.27)j$ (100 kHz)	$10.1(0.058 \pm 0.004)j$ (100 kHz)	$41.2(1 \pm 0.012)j$ (100 kHz)	$7.5(1 \pm 0.022)j$ (100 kHz)	$11.1(0.016 \pm 0.001)j$ (100 kHz)
k_{11}^*	$1.1(1 \pm 0.037)j$ (100 kHz)	$1.04(0.0058 \pm 0.0004)j$ (100 kHz)	$3.6(1 \pm 0.012)j$ (100 kHz)	$0.6(1 \pm 0.020)j$ (100 kHz)	$1.0(0.0016 \pm 0.0001)j$ (100 kHz)
Complex elastic coefficients	$8.1(10^8 \pm 1.0 \times 10^8)j$ (100 kHz)	$1.1(10^8 \pm 1.0 \times 10^8)j$ (100 kHz)	$1.1(10^8 \pm 1.0 \times 10^8)j$ (100 kHz)	$1.1(10^8 \pm 1.0 \times 10^8)j$ (100 kHz)	$1.1(10^8 \pm 1.0 \times 10^8)j$ (100 kHz)
CD_{11}^* (N/m ²)					
Complex piezoelectric coefficient	$0.1(1 \pm 0.001)j$ (100 kHz)	$0.1(1 \pm 0.016)j$ (100 kHz)	$1.1(1 \pm 0.010)j$ (100 kHz)	$0.1(1 \pm 0.010)j$ (100 kHz)	
h_{11}^* (V/m)	$6.1(10^8 \pm 1.0 \times 10^8)j$ (100 kHz)	$1.1(10^8 \pm 1.0 \times 10^8)j$ (100 kHz)	$1.1(10^8 \pm 1.0 \times 10^8)j$ (100 kHz)	$6.1(10^8 \pm 1.0 \times 10^8)j$ (100 kHz)	
Electromechanical Coupling Coefficients k					
k_{11}^*	$0.13(1 \pm 0.12)j$	$0.092(1 \pm 0.1)j$	$0.07(1 \pm 0.06)j$	$0.13(1 \pm 0.14)j$	
k_{31}	≈ 0.01	0.017	≈ 0.01	$k_{31}^* = -0.0094$ (1.0 ± 0.008)j	$k_{31}^* = -0.009$ (1.0 ± 0.011)j
k_p	≈ 0.03	0.044	≈ 0.02	$k_{32} = 0.01$	
k_{33}	0.13	0.091	0.077		
k_h	0.17	0.030	≈ 0.47		
Piezoelectric Coefficients (pC/m)					
d_{33}	39	20*	45	-17	-16
d_{31}	-3.8	-5.8	-7	$d_{31}^* = 15(1 \pm 0.093)j$	$d_{31}^* = 15(1 \pm 0.088)j$
d_h	31	8.1	30		
Density (kg/m ³)	4.25×10^3	4.19×10^3	4.3×10^3	4.46×10^3	4.78×10^3
Compliance (m²/N)					
S_{11}^E	3.64×10^{-10}	0.76×10^{-10}	9.22×10^{-10}	3.73×10^{-10}	2.9×10^{-10} (1.0 ± 1.5)
S_{12}^E	1.64×10^{-10}	0.19×10^{-10}	2.67×10^{-10}		

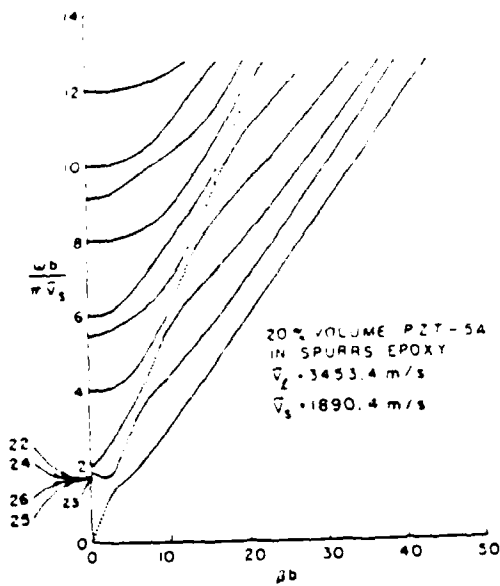
1) Voided uni-stretched thick film

2) Non-voided bi-stretched thin film

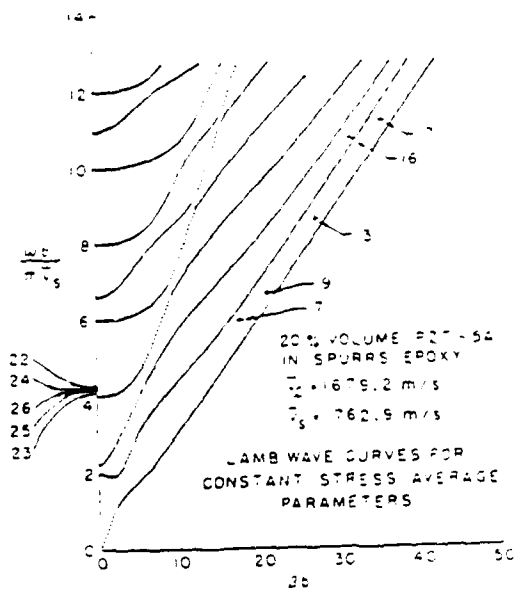
*Varies obviously with frequency

SUMMARY

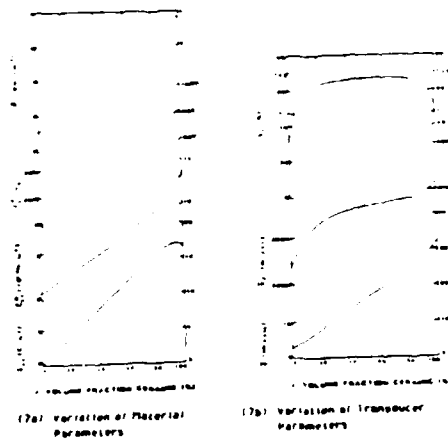
- 1) Regarding the complex coefficients, the measurement techniques are effective even for samples with $Q_{11} < 10$ and a figure of merit $|M| = kQ_{11} > 100$. When $Q_{11} > 10$ and $kQ_{11} > 1000$, the measuring technique for real coefficients can still be applied for estimating approximate magnitudes.
- 2) The experimental results indicate that the piezoelectric coefficient k_{31} is complex, violating the usual assumption that it is real.
- 3) Using just one disk composite sample, it is possible to estimate all of the real coefficients for the LE, TE, PE and Hydrostatic modes.
- 4) Because experimental data for Q_{11} , Q_{33} are very accurate, the error in the coefficients can be reduced to less than 5% when the vibration mode is pure.
- 5) For the iterative method, we recommend choices for the three measurement frequencies which lead to rapid convergence.
- 6) The technique for measuring real coefficients can be applied to single mode vibrations of low Q_{11} transducers vibrating in a liquid or attached to a solid. The effective electromechanical coupling coefficient, the conversion efficiency and the bandwidth can be estimated in this manner.
- 7) In principle, these techniques can be used for measuring the property coefficients as a function of frequency if the sample's size is changed.
- 8) These techniques are not suitable for high Q_{11} piezoelectric ceramics but are useful for measuring composites and PZT film properties.



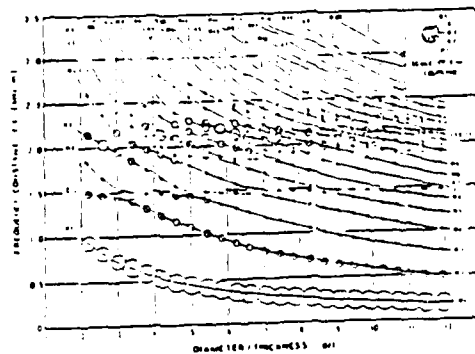
(5) Constant Strain Modeling of a One-Dimensional Composite Plate. Thickness Resonance is Accurately Predicted



(6) Constant Stress Modeling of a One-Dimensional Composite Plate. Stopband Resonances are Accurately Predicted

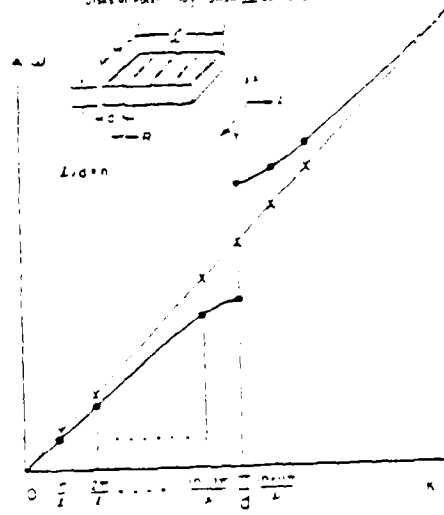


(7a) Variation of Material Parameters (7b) Variation of Transducer Parameters



(8) Lateral and Thickness Mode Interactions in a Noncomposite Disk Transducer

From S. J. D'Amico and E. P. E. The Measurement of Vibration Amplitude Distributions and Mode Analysis of Thick Disks of Polyimide, NASA 22-30214-2



(9) "Window" Induced in the Lateral Model Spectrum by the n Mode Stopband of a One-Dimensional Composite

PIEZOELECTRIC PROPERTIES OF SOME NEW HYDROPHONE MATERIALS

Robert Y. Ting

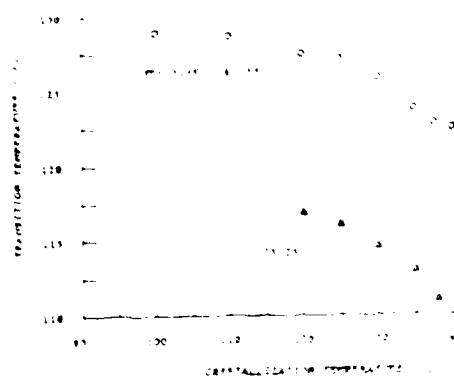
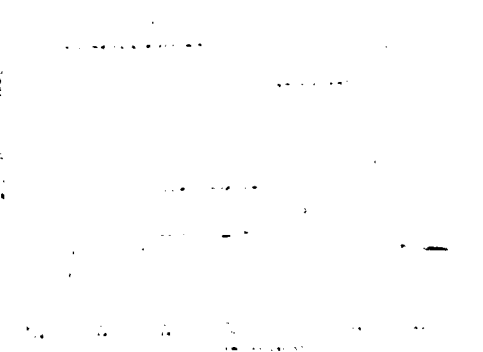
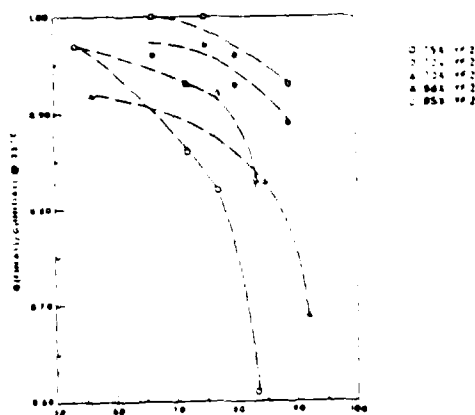
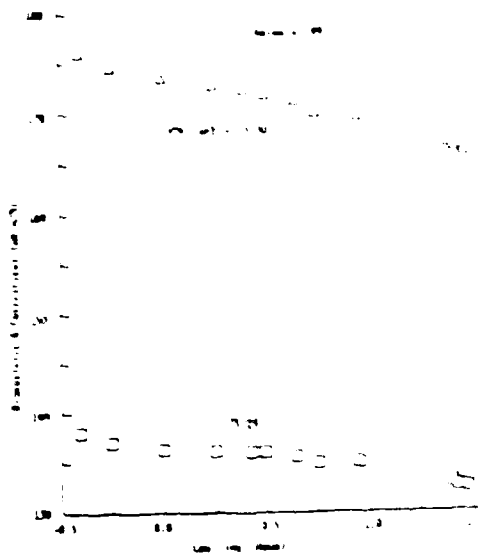
Underwater Sound Reference Detachment
U. S. Naval Research Laboratory
Orlando, FL 32856-8337, U.S.A.

New piezoelectric materials are constantly sought for sonar transducer applications in order to improve performance and reliability. We have a continuing effort in this endeavor under the support of the Office of Naval Research. Recent interest has been in the materials for large-area hydrophones. Polyvinylidene fluoride is now known to be inadequate as a large-area hydrophone material because of its poor thermal stability, low dielectric constant and planar anisotropy. Alternative materials are therefore being sought in the research program at the Underwater Sound Reference Detachment, Naval Research Laboratory (NRL-USRD). Recent studies have been concentrated on three material systems:

- (1) Piezoelectric copolymers of vinylidene fluoride and trifluoroethylene.
- (2) A "1-3" type piezoceramic composite developed by Plessey Australia Ltd., and
- (3) New lead titanate ceramics available from both Japanese and U. S. sources.

(1) Temperature Effects in VDF/TrFE Copolymers

- * High temperature exposure leads to greater losses in sample's piezoelectric activity if VDF content is lower.
- * The degradation is related to a solid-state transition characterized by changing from a well ordered, ferroelectric, all-trans configuration to a paraelectric phase of disordered pseudo-hexagonal lattice structure in the crystalline region.
- * This transition is found to be affected by both thermal treatment and the crystallization temperature the sample was exposed to, as evidenced by differential scanning calorimetry (DSC) results. Further wide-angle X-ray investigations are being carried out to further characterize the crystalline phase.



(2) Plessey Australia "1-3" Piezoelectric Composite

Reference: M. Baker and I. Bakervall, "Acoustical Sensitivity of PZT Polymer Composites As A Function of Fabrication Parameters", Presented at the Amer. Ceram. Soc. Meet., Pittsburgh, PA April 1984.

Samples evaluated are described in the manufacturer publication as shown below. The complete specifications are given. The samples were tested for their capacitance, dissipation and sensitivity as functions of pressure, temperature and frequency. Data are tabulated as shown in Table 1.

NO-A105 113

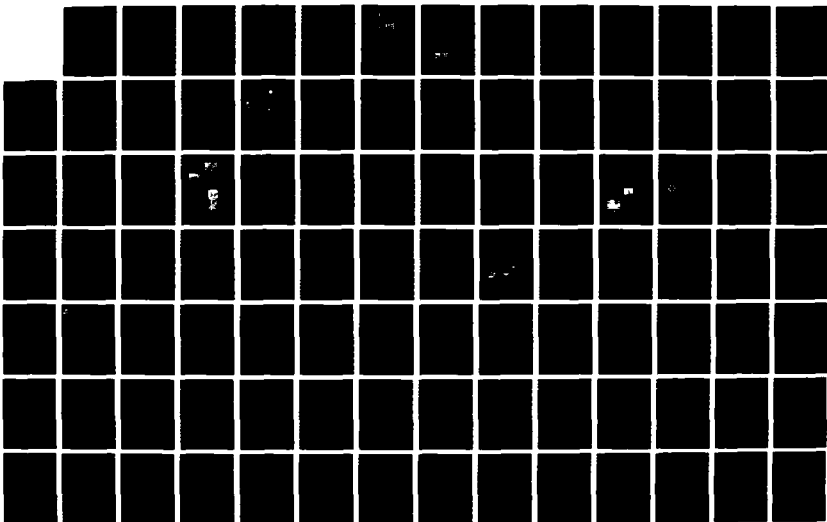
UNITED STATES - JAPAN WORKSHOP ON DIELECTRIC AND
PIEZOELECTRIC CERAMICS ((3RD)) HELD IN TOYAMA JAPAN ON
NOVEMBER (9)-(12) (1986)(U) KEIO UNIV TOKYO (JAPAN)
30 JUL 87

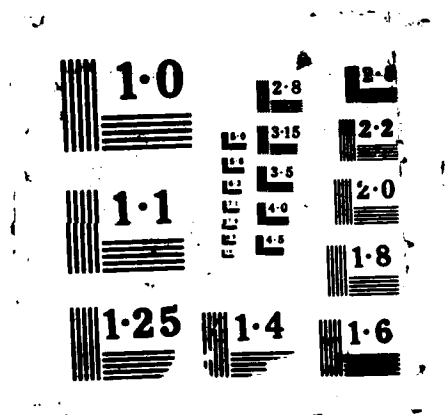
4/3

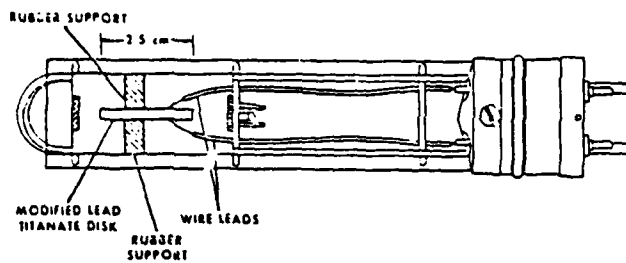
UNCLASSIFIED

F/G 11/2

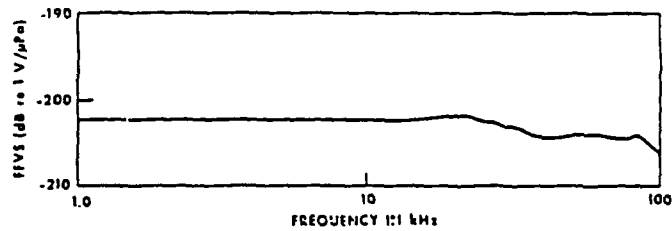
NL





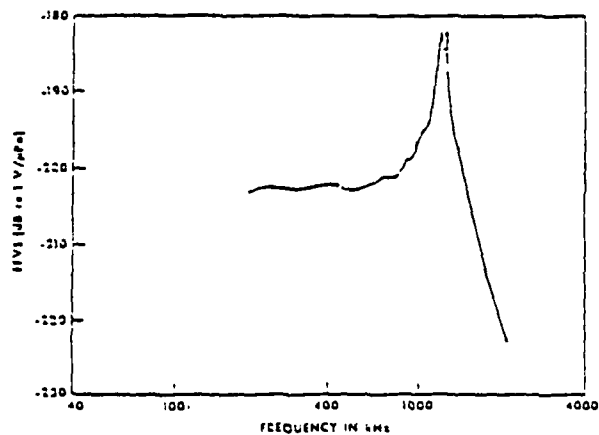
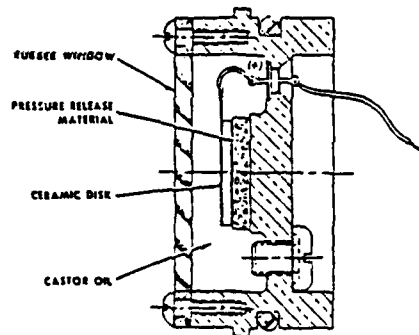


SECTIONAL VIEW OF THE 15P1-TYPE U23 STANDARD HYDROPHONE HOUSING, USED FOR LOW-FREQUENCY EVALUATION OF LEAD TITANATE CERAMICS.



FREE FIELD VOLTAGE SENSITIVITY OF LEAD TITANATE SAMPLE IN U23 HYDROPHONE.

SECTIONAL VIEW OF THE 15P1-TYPE 22 TRANSDUCER HOUSING, USED FOR HIGH-FREQUENCY TESTS.



FREE FIELD VOLTAGE SENSITIVITY OF LEAD TITANATE CERAMIC SAMPLE IN 22 TRANSDUCER.

DIELECTRIC AND PIEZOELECTRIC PROPERTIES OF $\text{PbZrO}_3\text{-Pb}(\text{Zn}_{1/3}\text{Nb}_{2/3})\text{O}_3$ CERAMICS

K. SAKATA and T. TAKENAKA

Faculty of Science and Technology, Science University of Tokyo, Noda-shi, 278 Japan

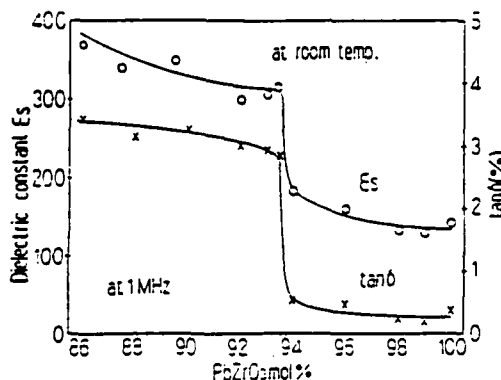
Introduction

Lead zirconate PbZrO_3 is a typical example of an antiferroelectric, and has been the most widely studied of the antiferroelectrics. Its solid solution system with PbTiO_3 (namely, PZT) has been investigated in detail, because the PZT system has a morphotropic phase boundary (MPB) whose components give superior piezoelectric activity.

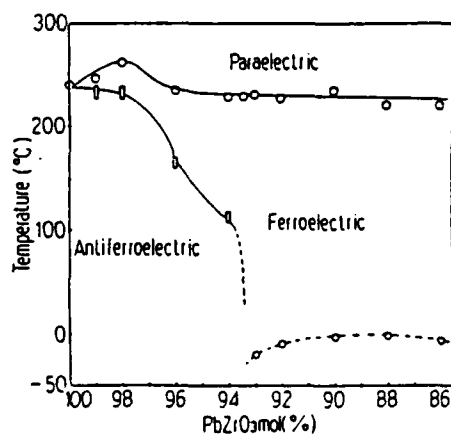
Application of an electric field to PbZrO_3 can induce a ferroelectric phase in the puckered structure in a certain temperature range, because the free energy of the puckered structure of PbZrO_3 seems to be very close to that of the ferroelectric phase.

Small additions of Ba or Ti to PbZrO_3 remarkably lower the free energy of the ferroelectric phase. For example, if 5% of the Pb ions are substituted by Ba, or about 1% of the Zr ions by Ti, a ferroelectric phase shows up even if no dc field is applied. Extensive research of PbZrO_3 -based compounds has been made from the standpoint of phase transitions. Recently, Takeuchi et al. found a large anisotropy in the electromechanical coupling factor of one PbZrO_3 -based ceramic.

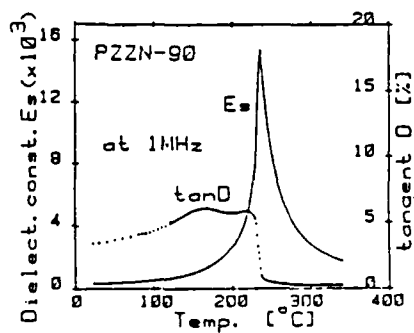
In this work, we have attempted to obtain basic information regarding a new piezoceramic group, from an applicational viewpoint of electronic device material. The dielectric, piezoelectric and pyroelectric properties of the $\text{PbZr}_x(\text{Zn}_{1/3}\text{Nb}_{2/3})_{1-x}\text{O}_3$ solid solution (abbreviated to "PZZN-100x") with up to 20 mol % ($\text{Zn}_{1/3}\text{Nb}_{2/3}$) were investigated.



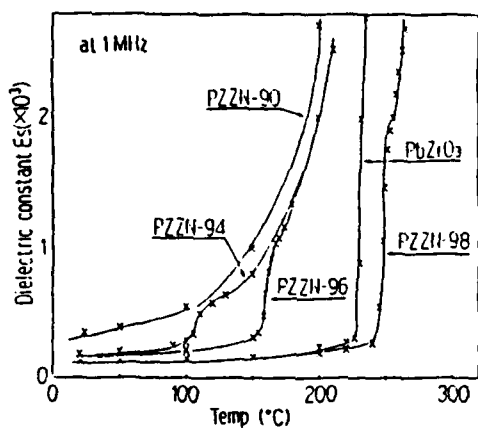
Dielectric constant ϵ_s and loss tangent $\tan\delta$ at room temperature of the PZZN system as a function of PbZrO_3 mol % (x).



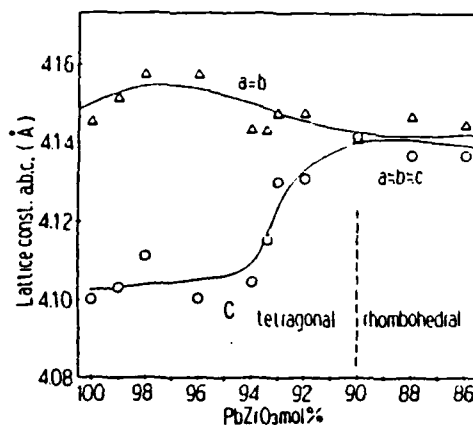
The phase relation of the $\text{PbZr}_x(\text{Zn}_{1/3}\text{Nb}_{2/3})_{1-x}\text{O}_3$ (PZZN) system.



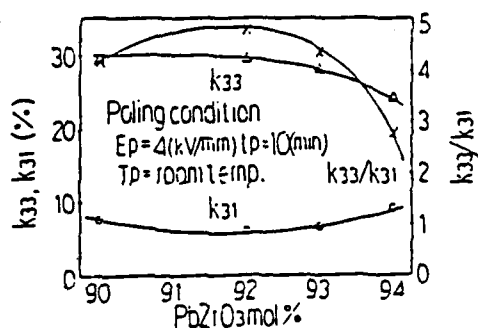
Temperature dependence of dielectric constant ϵ_s and loss tangent $\tan\delta$ of PZZN-90 (x=0.9).



Temperature dependence of dielectric constant ϵ' of the $\text{PbZr}_{1-x}(\text{Zn}_{10}\text{Nb}_{90})_x\text{O}_3$ (PZZN) system.



Unit cell parameters of the $\text{PbZr}_{1-x}(\text{Zn}_{10}\text{Nb}_{90})_x\text{O}_3$ (PZZN) system.



Coexisting factor k_{33} and k_{31} and the ratio k_{33}/k_{31} of the PZZN system, as a function of PbZrO_3 mol %.

Piezoelectric properties of the PZZN-90 and PZZN-92.

	Dielectric const.		-ent	Coupling factor		Frequency const.		Elastic compliance		Piezoelectric constant						
	ϵ'	ϵ''		k_{33}	k_{31}	N_{33}	N_{31}	S_{11}	S_{33}	d_{33}	d_{31}					
	10kHz	(%)		(%)	(Hz·m)	(10^{-12} m/N)	(10^{-12} C/N)	(10^{-12} V/m)								
FZZH-90	300	355	203	279	251	603	535	2090	2610	1520	743	155	741	1427	139	359
					133	841		2040	2710		810	740	141	862	161	408
PZZN-92	262	355	249	350	252	429	535	2090	2350	1550	773	205	745	402	157	349
					603	757		2050	2760		815	770	133	809	173	455

Piezoelectric Properties of $(\text{Na,Li})\text{NbO}_3$ Ceramics

T.HONDA
I.KAWAMATA
H.WATARAI
T.IDO

Materials and Electronic Device Laboratory,
Mitsubishi Electric Corporation
Sagamihara-city Miyashimo 1-1-57, Kanagawa 229, Japan

The PZT family of ceramics is currently being used in most applications utilizing piezoelectric polycrystalline materials. For the application to high frequency ultrasonic transducers for non-destructive testing, PZT ceramics present technological difficulties.

New materials with
(1) higher frequency constant,
(2) lower dielectric constant
are required

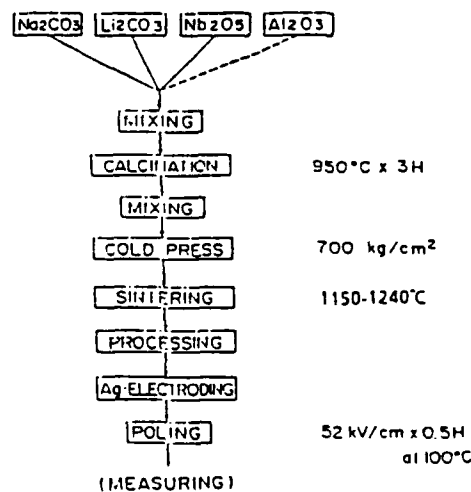
$(\text{Na,Li})\text{NbO}_3$ family of ceramics is one of the desirable materials.

The purpose of this work is:

- (1) to improve the sinterability of $(\text{Na,Li})\text{NbO}_3$ ceramics, and
- (2) to measure the piezoelectric properties for the high-frequency ultrasonic transducers.

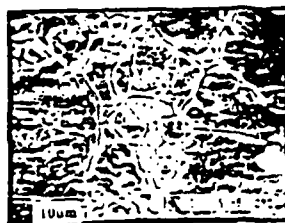
Experimental

1. Sample preparation

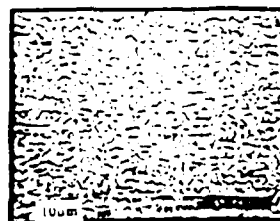


2. Measurements

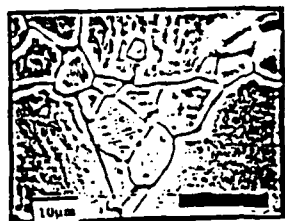
- (1) Microstructures
Density, SEM, XMA
- (2) Piezoelectric and dielectric properties
Coupling factor, Dielectric constant (3)



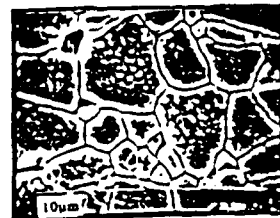
non additives



0.5 wt. % Al_2O_3

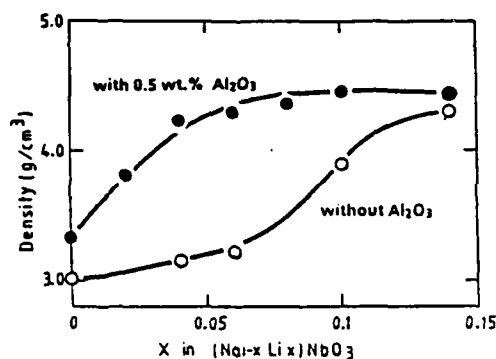


0.5 wt. % MgO

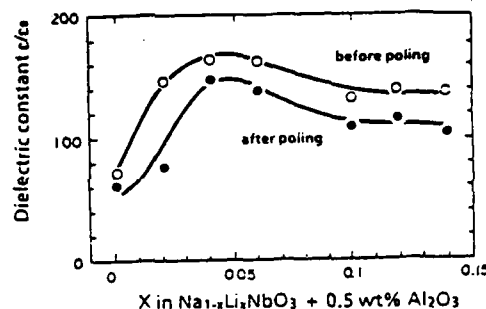


0.5 wt. % MnO

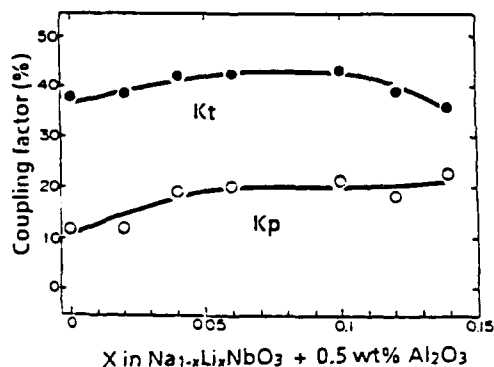
SEM photographs of the $\text{Na}_{0.9}\text{Li}_{0.1}\text{NbO}_3$ systems with additives. ($1100^\circ\text{C} \times 3 \text{ hrs}$)



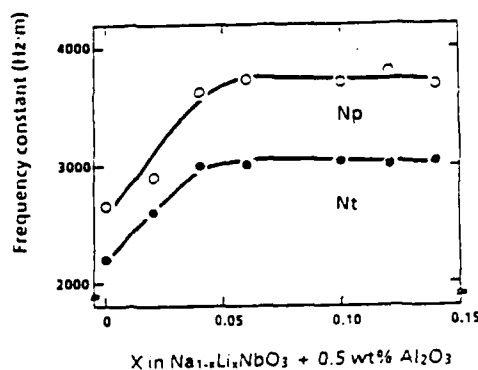
Densities of $\text{Na}_{1-x}\text{Li}_x\text{NbO}_3$ systems as a function of lithium concentration.



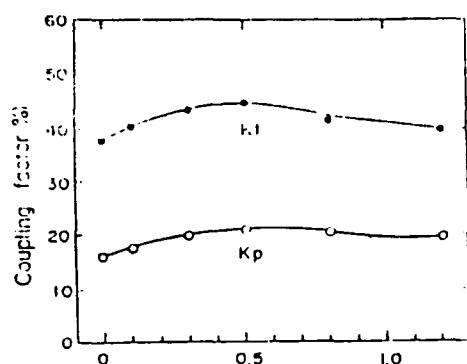
Dielectric constant (before and after poling) as a function of lithium concentration in the $\text{Na}_{1-x}\text{Li}_x\text{NbO}_3 + 0.5 \text{ wt. } \text{Al}_2\text{O}_3$ system.



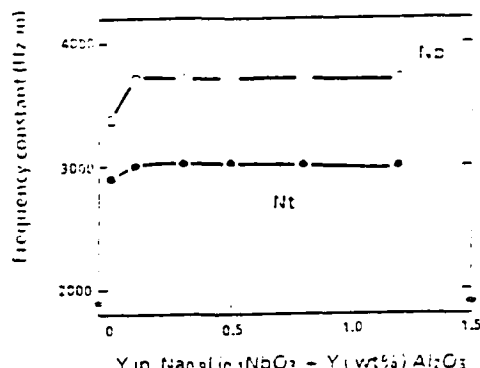
Thickness and planar mode coupling factors as a function of lithium concentration in the $\text{Na}_{1-x}\text{Li}_x\text{NbO}_3 + 0.5 \text{ wt. } \text{Al}_2\text{O}_3$ system. (7)



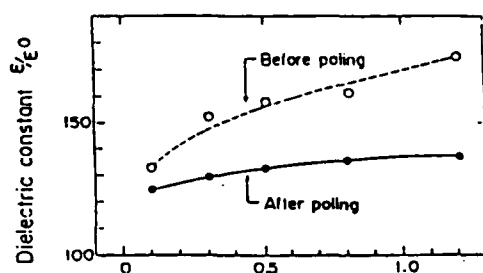
Thickness and radial frequency constants as a function of lithium concentration in the $\text{Na}_{1-x}\text{Li}_x\text{NbO}_3 + 0.5 \text{ wt. } \text{Al}_2\text{O}_3$ system



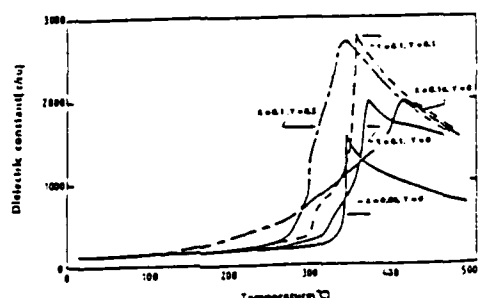
Y in $(\text{Na}_{0.9}\text{Li}_{0.1})\text{NbO}_3 + Y(\text{wt}\%)\text{Al}_2\text{O}_3$
Planar and thickness mode coupling factors as a function of alumina concentration (wt.%). (10)



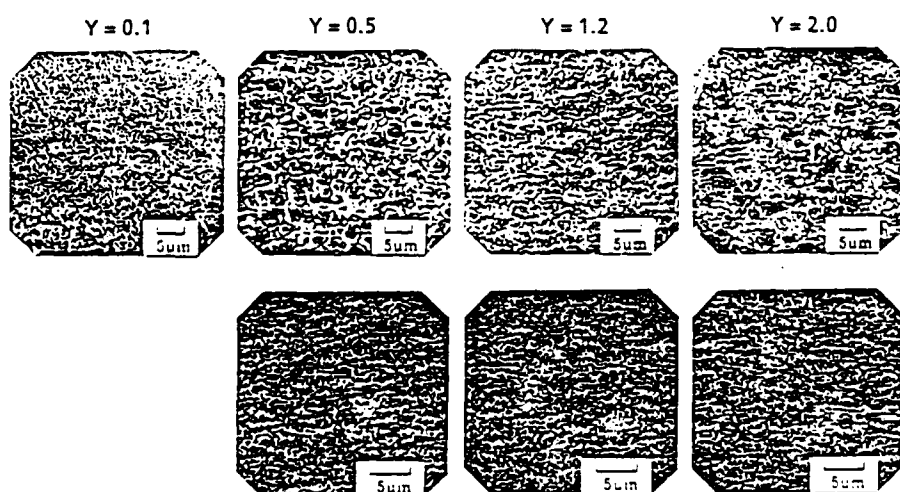
Y in $\text{Na}_{0.9}\text{Li}_{0.1}\text{NbO}_3 + Y(\text{wt}\%)\text{Al}_2\text{O}_3$
Thickness and radial frequency constants as a function of alumina concentration in the $\text{Na}_{0.9}\text{Li}_{0.1}\text{NbO}_3 + Y(\text{wt}\%)\text{Al}_2\text{O}_3$ system



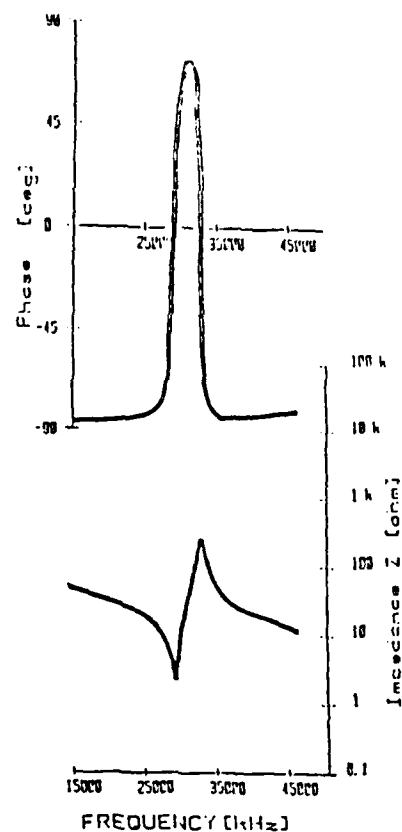
Y in $(\text{Na}_{0.9}\text{Li}_{0.1})\text{NbO}_3 + Y(\text{wt}\%)\text{Al}_2\text{O}_3$
Dielectric constant (at 1kHz) as a function of alumina concentration (wt.%).



Dielectric constant (at 1kHz) as a function of temperature for the $\text{Na}_{0.9}\text{Li}_{0.1}\text{NbO}_3 + Y(\text{wt}\%)\text{Al}_2\text{O}_3$ (10)



SEM micrographs (upper) and Al-K α X-ray image (lower) of $\text{Na}_{0.9}\text{Li}_{0.1}\text{NbO}_3 + Y(\text{wt}\%)\text{Al}_2\text{O}_3$.



Thickness-mode resonance of $\text{Na}_{0.9}\text{Li}_{0.1}\text{NbO}_3 + 0.5\text{wt.}\% \text{Al}_2\text{O}_3$ for vibrating element. (17)

Summary

Sodium-Lithium niobate systems have higher frequency constant and lower dielectric constant than those known for PZT piezoelectric ceramics.

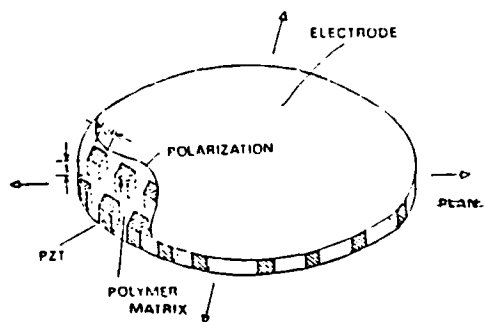
In order to improve the sinterability of the sodium-lithium niobate systems, the effect of alumina addition has been investigated.

It was found that alumina addition enhanced the density of the sintered body and improved the microstructure and piezoelectric properties for the sodium-lithium niobate system.

$(\text{Na,Li})\text{NbO}_3$ with a small amount of alumina is desirable material for the fabrication of high frequency ultrasonic transducers for non-destructive testing.

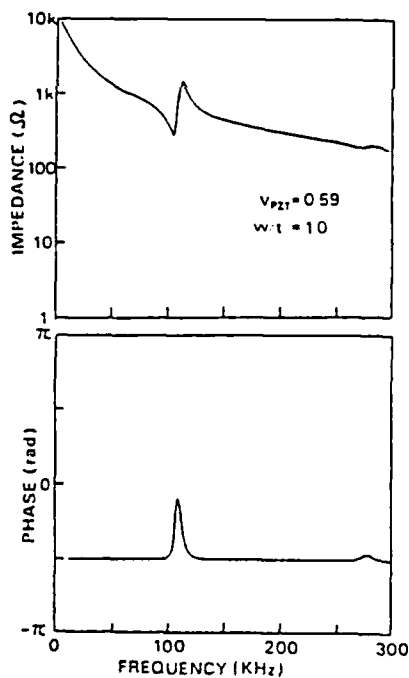
W7

~ Tufendi & C. Nakay

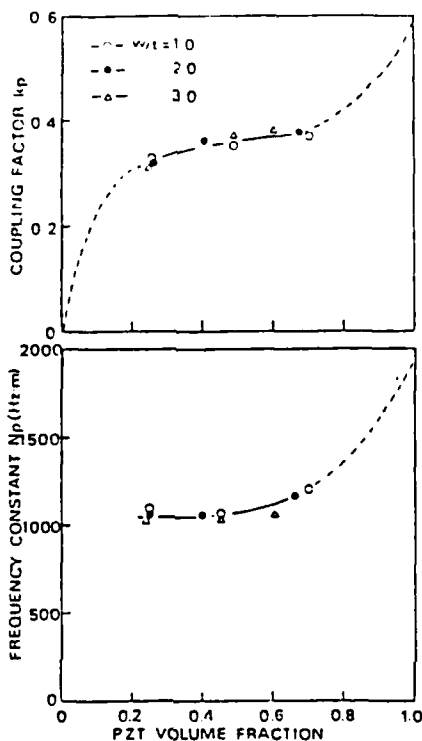


STRUCTURE PARAMETER : PZT VOLUME FRACTION v_{PZT}
PZT ROD SHAPE w/t

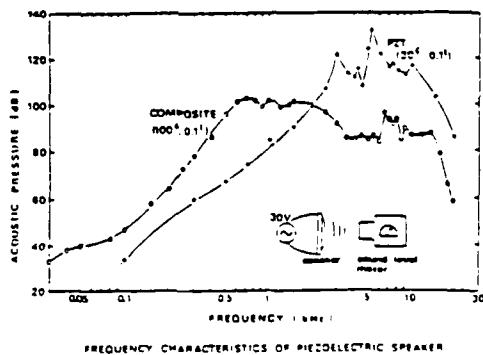
PIEZOELECTRIC COMPOSITE DISK VIBRATOR



IMPEDANCE AND PHASE CHARACTERISTICS OF PZT/EPOXY COMPOSITE DISK (diameter:11mm thickness:0.4mm)



FREQUENCY CONSTANT AND ELECTROMECHANICAL COUPLING FACTOR OF PLANAR VIBRATIONAL MODE IN COMPOSITE DISK AS A FUNCTION OF PZT VOLUME FRACTION (sample thickness:0.1mm)



FREQUENCY CHARACTERISTICS OF PIEZOELECTRIC SPEAKER

Anisotropic Piezoelectric Coupling Factor of $[\text{Pb}_x(\text{Bi}_{0.5}\text{Na}_{0.5})_{1-x}]\text{TiO}_3$ Ceramics

S.Tashiro, Y.Oikawa, H.Igarashi and K.Okazaki
 The National Defense Academy

1. Dielectric and Piezoelectric Properties of PbTiO_3 -($\text{Bi}_{0.5}\text{Na}_{0.5}$) TiO_3 system.
2. Effect of third components on piezoelectric coupling factor in PbTiO_3 -($\text{Bi}_{0.5}\text{Na}_{0.5}$) TiO_3 - $\text{Pb}(\text{B1}\cdot\text{B2})\text{O}_3$ system.

$(\text{Bi}_{0.5}\text{Na}_{0.5})\text{TiO}_3$ ceramics

By Smolenskii et al of USSR in 1960

Crystal structure : Perovskite
 Rhombohedral

Curie Temp. : 320° C

Ferroelectric

$x \cdot \text{PbTiO}_3$ - $y \cdot (\text{Bi}_{0.5}\text{Na}_{0.5})\text{TiO}_3$ system

By Sakata et al of Japan in 1967

M.P.B. : $x = 12.5 \text{ mol\%}$

$k_p = 0.28$ and $P_r = 33 [\mu\text{C}/\text{cm}^2]$ at M.P.B.

No Piezoelectric data in the tetragonal region with large c/a .

Comparison of ionic radii

[Source: 'Physical Constants Table' by Iida et al, Asakura Press, Tokyo, Japan, (1969)
 56-57, in Japanese.]

$\text{Ba}^{2+} = 1.43 [\text{\AA}]$	
$\text{Pb}^{2+} = 1.32 [\text{\AA}]$	
$\text{Sr}^{2+} = 1.27 [\text{\AA}]$	
$\text{La}^{3+} = 1.22 [\text{\AA}]$	
$\text{Nd}^{3+} = 1.15 [\text{\AA}]$	
$\text{Sm}^{3+} = 1.13 [\text{\AA}]$	
$\text{Ca}^{2+} = 1.06 [\text{\AA}]$	
$\text{Bi}^{3+} = 1.20 [\text{\AA}]$	
$\text{Na}^{+} = 0.98 [\text{\AA}]$	
	$\text{Av.} = 1.09 [\text{\AA}]$

Substituting elements of A-site in PbTiO_3 ceramics

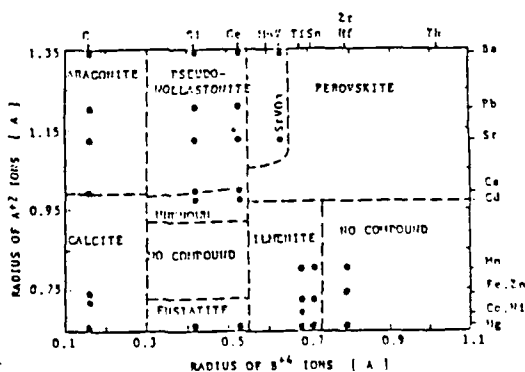
La : Matsushita

Ba, Sr, Ca : Toshiba

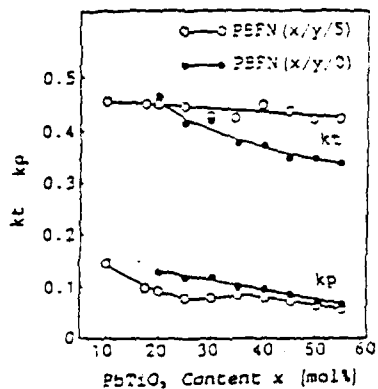
La, Pr, Nd, Sm, Gd : Hitachi

Ca and Sm—Large piezoelectric Anisotropy

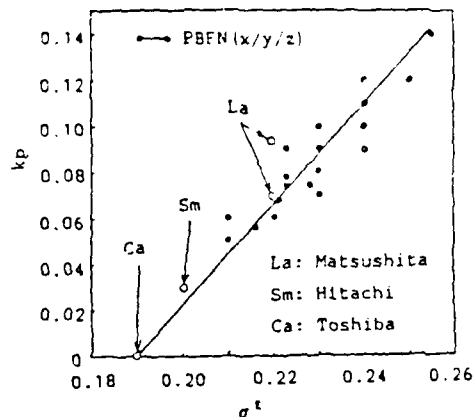
Ionic radius of Ca or Sm is smaller compared with Pb, Ba, Sr and La ions.



Classification of the A_2ZrO_6 -type compounds according to constituent ionic radii. From R.S.Poth, Journal of Research of The National Bureau of Standards, vol.58, No.2 (1957)



Effect of substitution of 5 mol% $\text{Pb}(\text{Fe}_{0.5}\text{Nb}_{0.5})\text{O}_3$ on coupling factors k_p, k_t of $\text{PBFN}(x/y/5)$.



Correlation between Poisson's ratio σ^t and coupling factor k_p in PbTiO_3 ceramics modified with various substituting elements.

Summary

Dielectric and piezoelectric properties of the $x \text{ PbTiO}_3$, $-y (\text{Bi}_{0.5}\text{Na}_{0.5})\text{TiO}_3$, $-z \text{ Pb}(\text{B} \mid \text{B} \mid \text{O})$, system with 1 mol% MnCO_3 were experimentally investigated.

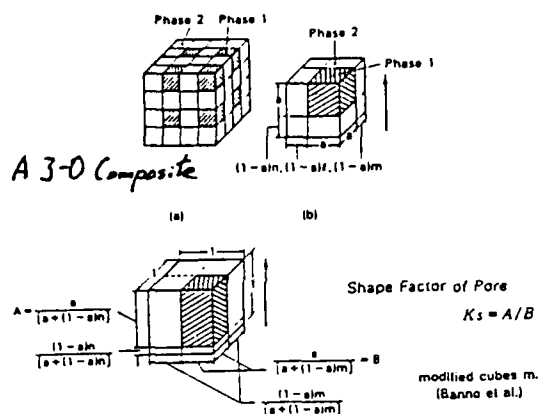
- 1) In the $x \text{ PbTiO}_3$, $-y (\text{Bi}_{0.5}\text{Na}_{0.5})\text{O}_3$ system, the dielectric constant was smaller than 200 and the Curie point T_c was higher than 380°C in the compositions above $x = 0.35$.
- 2) Substituting with 5 mol% $\text{Pb}(\text{Fe}_{0.5}\text{Nb}_{0.5})\text{O}_3$ was available in enhancement of the piezoelectric anisotropy, $K_p = 0.077$ and $k_t = 0.457$ were obtained in $\text{PBFN}(30/65/5)$.
- 3) More improvement of the properties such as small dielectric constant, high Curie point and large piezoelectric anisotropy can be expected by adjusting amount of $\text{Pb}(\text{Fe}_{0.5}\text{Nb}_{0.5})\text{O}_3$ and MnCO_3 additive.

Hisao BANNO

NTK Ceramic Div. NGK Sparkplug. Japan

Effects of Shape and Volume Fraction of
Closed Pores
on
Dielectric Loss Tangent, Mechanical Quality
Factor and Electromechanical Coupling Factor
of
Dielectric and Piezoelectric Ceramics

- A Theoretical Approach -



2nd US-Japan Seminar(1984) at Williamsburg

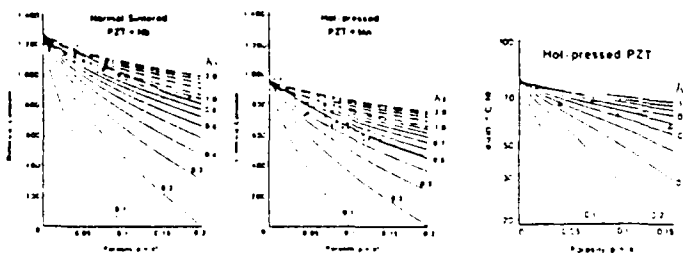
Theoretical Equations based on modified cubes model:

$$^1 X/X_0(\bar{\epsilon}_{11}) = 1 + \frac{1}{p^{1/2}(\epsilon_{22}/\epsilon_0 - 1) + 1} \cdot \left(\frac{p}{K_s}\right)^{1/2} - \left(\frac{p}{K_s}\right)^{1/2} \quad (1)$$

$$^2 X/X_0(\bar{\epsilon}_{11}) = 1 - \left(\frac{p}{K_s}\right)^{1/2} + \frac{\left(\frac{p}{K_s}\right)^{1/2} \left[1 - \left(\frac{p}{K_s}\right)^{1/2}\right]}{1 - p^{1/2} \cdot K_s^{1/2}} \quad (2)$$

$$^3 X/X_0(\bar{\epsilon}_{11} = 1/\sqrt{\epsilon_{11}}) = 1 - p^{1/2} \cdot K_s^{1/2} \quad (3)$$

Okazaki's Experimental Results

for normal sintered: $K_s \approx 1$ for hot-pressed: $K_s \approx 0.5$

THEORY See "ABSTRACT".

Eq.(20) should be read

$$\bar{\sigma}_{11} = \sigma_{11} (1 - P^{1/3} \cdot K_s^{1/3})$$

Electromechanical Coupling Factor kp
and

Resonant Impedance Z_r

Assuming that



$$\epsilon_{11} = 0 \quad (44)$$

$$\sigma_{12} = 0 \quad (45)$$

$$\epsilon_{12}/\epsilon_0 = 1 \quad (46)$$

$$\text{and } \tan \delta_{11} = 0 \quad (47)$$

$$k_s^2 = \frac{2d^2}{\epsilon_{11} \cdot 1 \cdot (1 - \epsilon_{11})} \quad (50)$$

$$\tan \delta_{11} = 2\pi f_r \cdot C \cdot Z_r (1 - (f_r/f_0)^2) \quad (51)$$

$$f_r = 1/\sqrt{\rho(1 - (\epsilon_{11}/\epsilon_0) \cdot 1)} \quad (52)$$

$$C = \epsilon_{11} \quad (53)$$

$$1/k_s^2 = 0.395 (f_r/f_0) / (1 - (f_r/f_0)^2) + 0.575 \quad (54)$$

$$\bar{\rho} = \rho(1 - \epsilon_{11}) = \rho(1 - P) \quad (55)$$

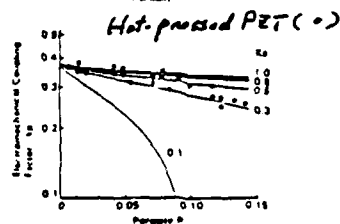
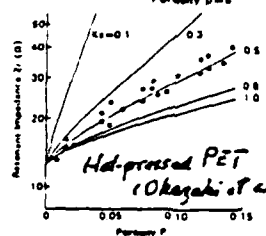
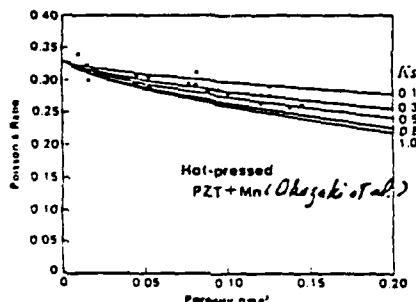
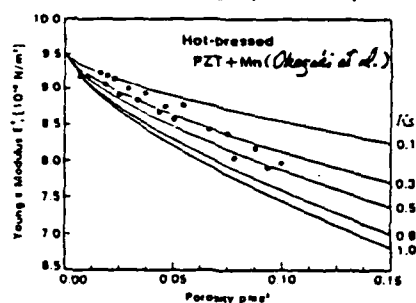
$$\bar{Q}_{11} = 1/(\tan \delta_{11}) = 1/(\tan \delta_{11}) = Q_{11} \quad (48)$$

$$\tan \delta_{11} = 1/\bar{Q}_{11} = \tan \delta_{11} = 1/Q_{11} \quad (49)$$

$$\therefore kp = f(P, K_s) \quad (56)$$

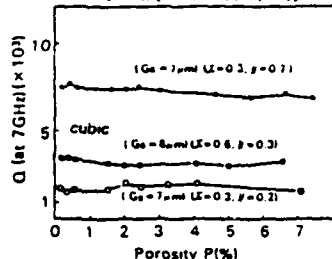
$$\bar{Z}_r = F(P, K_s) \quad (57)$$

No porosity dependence of Q_m and $\tan \delta$.



H. Banno et al. (1986)

(Sr_{1-x}Ba_x)[(Ni_{0.5}Nb_{0.5})_{1-y}Zr_y]O₃



Shape Factor of Pore K_s

	$\bar{\epsilon}_{11}$	$\bar{\sigma}_{11}$	$1/\bar{\rho}$	$\bar{\sigma}_{12}$	$\bar{\epsilon}_{12}$	\bar{Z}_r
Normal Sintered TiO ₂	$K_s=1$					
Normal Sintered PZT+Nb	$K_s=1$		$K_s=1$			
Hot-Pressed PZT+Mn	$K_s=0.5$	$K_s=0.5$	$K_s=0.5$	$K_s=0.5$	$K_s=0.5$	$K_s=0.5$
Hot-Pressed PLZT		$K_s=0.5$			$K_s=0.5$	$K_s=0.5$
(Sr _{1-x} Ba _x)[(Ni _{0.5} Nb _{0.5}) _{1-y} Zr _y]O ₃	* no porosity dependence of Q_m no porosity dependence of Q					

Conclusion

1. Theoretical equations for dielectric (ϵ , $\tan \delta$), elastic (s , c , Q_m) and electro-mechanical (d , k) properties : a function of shape factor (K_s) and porosity (P)
2. This theory is applied to the experimental results obtained by Okazaki et al. with good agreement between theory and experiments.
3. ϵ_{11} , σ_{11} , σ_{12} , d_{31} , and kp : dependent on not only volume fraction but also shape and distribution of pores, whereas Q_m and $Q (= 1/\tan \delta)$: of no porosity dependence
4. This theory predicts no effect of size of pores on the above-mentioned properties

EFFICIENCY OF PIEZOELECTRIC CERAMIC ACTUATOR

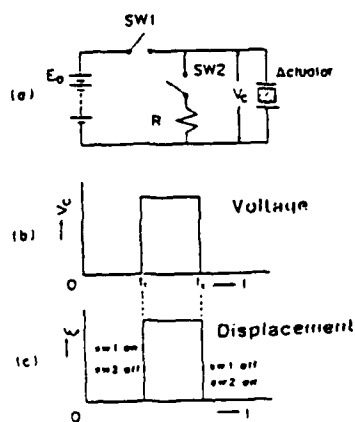
Sadayuki TAKAHASHI
NEC Corp.

Introduction

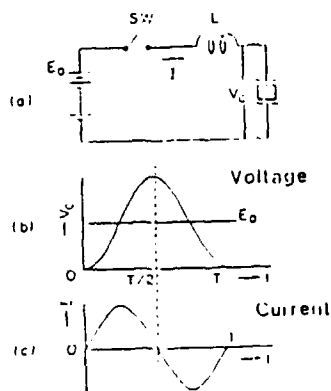
In order to operate the piezoelectric ceramic actuator in a pulse mode, a charge discharge circuit is required. A conventional circuit, however, wastes unused stored energy in the actuator in every discharge cycle.

The present study reports a new driving circuit which can recover unused stored energy.

Conventional Driving Circuit

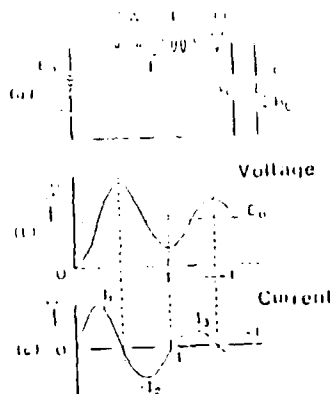


New Driving Circuit



During discharging cycle current I goes back to the source so that unused stored energy in the actuator is recovered.

Actual Equivalent Circuit



In the actual case a part of energy is lost as heat. The recovered energy is less than the supplied energy.

For $W = 0$

$$E_s = E_0 \int_0^{T/2} I dt$$

$$E_r = E_0 \int_{T/2}^T I dt$$

$$L_1 = \int_0^{T/2} (R_L + R_C) I^2 dt$$

$$L_2 = \int_{T/2}^T (R_L + R_C) I^2 dt$$

$$M_{s1} = k^2 E_s$$

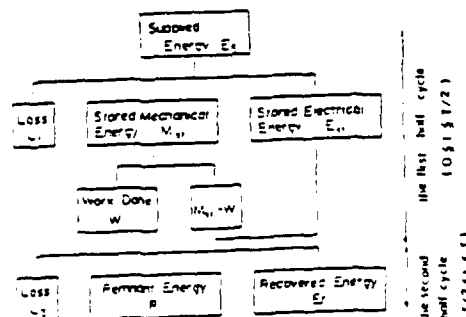
k^2 : coupling const.

$$E_{s1} = E_s - (M_{s1} + L_1)$$

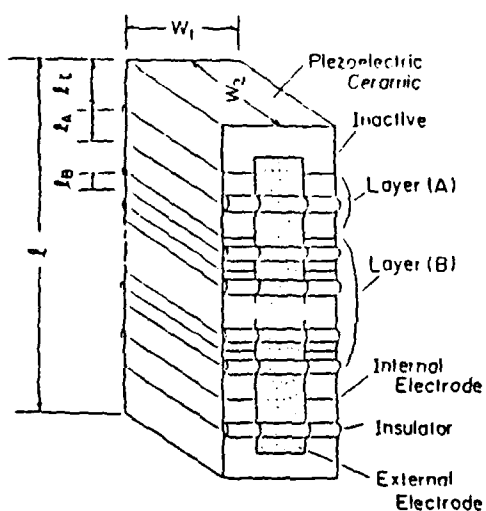
$$R = (E_{s1} + (M_{s1} - W)) - (E_r + L_2)$$

$$R_L + R_C = \frac{2L}{T} \log_e \frac{I_1}{I_3}$$

Energy Flow Chart

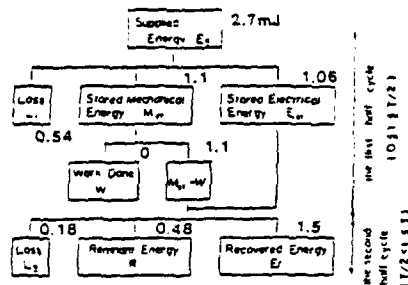


Specimen

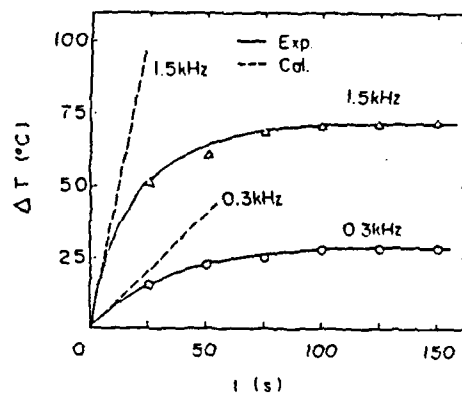


$l \times W_1 \times W_2 : 9 \times 2 \times 3 \text{ mm}$
 $l_1 : 0.59$ (2 layers)
 $l_A : 0.23$ (4 . .)
 $l_B : 0.115159$. .)

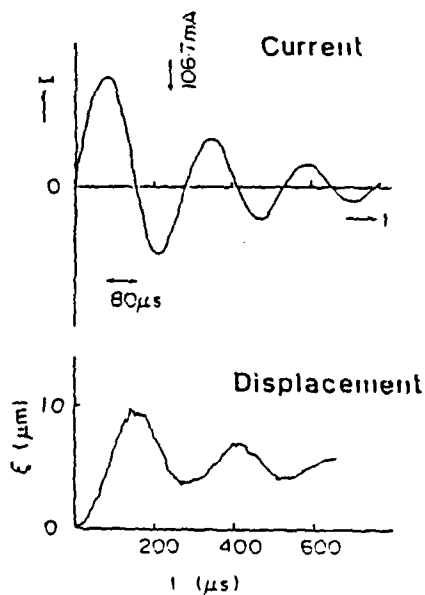
Energy Flow without Mechanical Loading



Actuator Temperature Rise during Pulse Mode Operation



Experimental Results



$E : 78 \text{ V}, L : 10 \text{ mH}, R_c : 10 \Omega$

Summary

For pulse mode operation without mechanical loading, 56 percent of the supplied energy can be recovered using a new circuit.

21 percent of the supplied energy is lost as heat in the actuator.

W11

CERAMIC GREEN SHEET PUNCHER USING PIEZOELECTRIC ACTUATOR

Tadashi YOSHIURA
NEC Corp.

Introduction

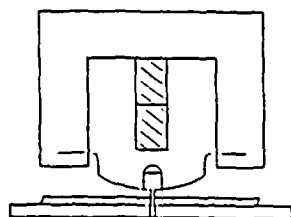
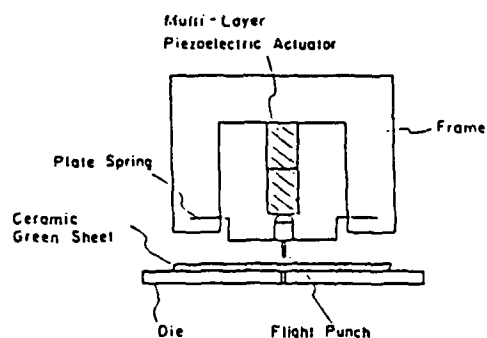
Multilayer ceramic wiring substrates which are used for high-speed large computers, are usually produced by ceramic green sheet technologies.

Individual ceramic green sheets used here have many tiny via holes to achieve a three dimensional wiring.

This report deals with a high precision and high speed green sheet puncher for via holes.

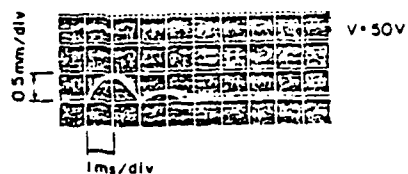
The puncher is basically driven by piezoelectric ceramic actuators.

Basic Structure



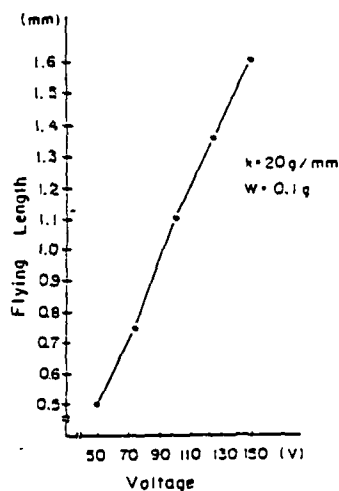
Punching by Flight Punch

Punch Flying Length



V: Voltage Impressed on Piezoelectric Actuator

Punch Flying Length

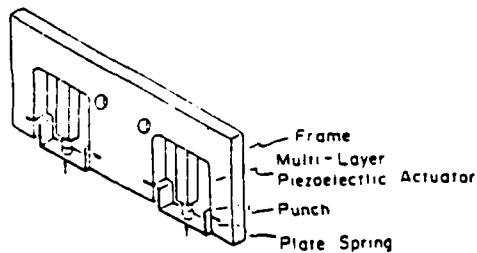


k: Spring Constant

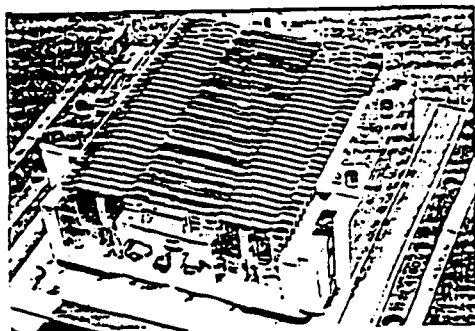
W: Punch Weight

Punch is fastened to plate spring

Punch Head

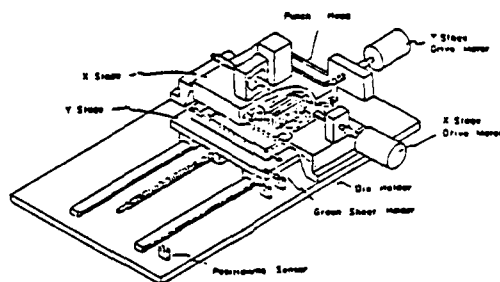


Punch Head Structure

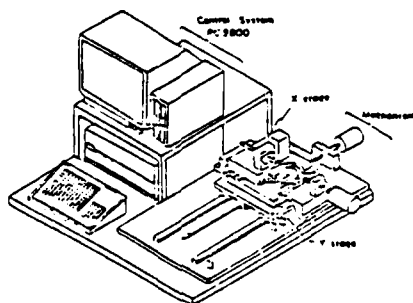


Punch Head has 60 punches

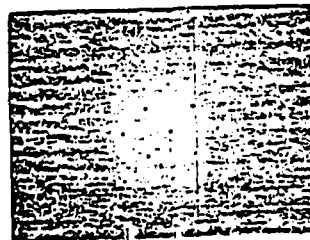
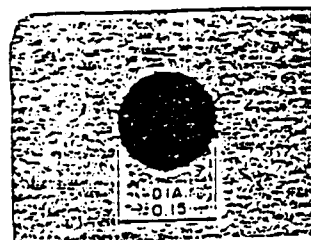
Mechanism



Punch System



Through Hole



2.592

Punch System



Punch System Specifications

X Y Stage	4.2 mm/sec
Max. Velocity	60 mm/sec
Punch	101.2 mm
Flying Length	1 mm
Punch Spring	100 mm
Response Frequency	(1000 cps)
Through Hole Diameter	0.15 mm
Through Hole Pitch	1.293 mm
Through Hole Pitch Error	±0.02 mm
Through Hole Number	About 2400/Sheet
Punch Ability	80 sec/2400 Holes
Green Sheet Thickness	100 μm
Green Sheet Size	100 mm x 100 mm

Conclusion

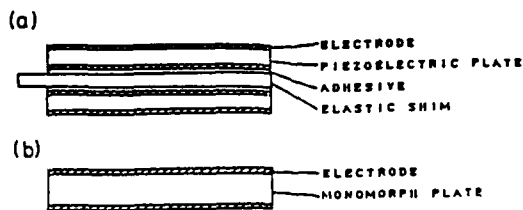
Piezoelectric Actuator

- Compact Punch Head
- High Speed Punch System
- High Precision Punch System
- Silent Punch System
- Low Energy Using Punch System

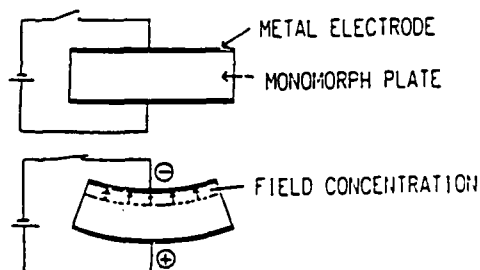
MONOMORPH ACTUATORS USING SEMICONDUCTIVE FERROELECTRICS

Kenji Uchino and Mikihiro Yoshizaki
Department of Physics, Sophia University
Kioi-cho 7-1, Chiyoda-ku, Tokyo 102

Hiroshi Yamamura, Kiyoshi Kasai, Naomichi Sakai
and Hiroshi Asakura
Advanced Materials Research Laboratory
Toyo Soda Manufacturing Co.:Ltd.
Hayakawa 2743-1, Ayase-shi 252

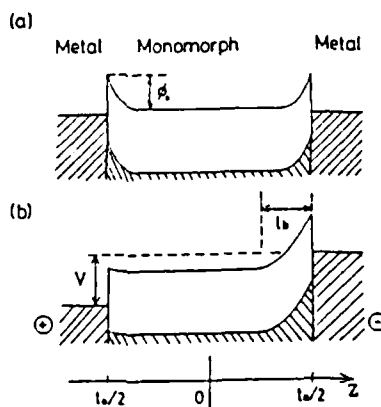


STRUCTURES OF A BIMORPH (A) AND A MONOMORPH ACTUATOR (B).



PRINCIPLE OF MONOMORPH BENDING.

ENERGY BARRIER MODEL FOR A MONOMORPH DEVICE.



$$E(z) = \frac{qN_A}{2\epsilon} \left[z - \frac{l_0}{2} + l_0 \right] \quad (1)$$

$$\left(\frac{l_0}{2} - l_0 < z < \frac{l_0}{2} \right)$$

$$l_0 = \left[\frac{2\epsilon}{qN_A} (\phi_0 + V) \right]^{1/2} \quad (2)$$

$$D = \frac{qN_A}{\epsilon\epsilon_0}$$

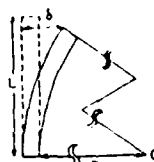
$$\delta = \frac{1}{2\pi} \quad (3)$$

$$\frac{1}{R} = \frac{1}{L} \int_0^L d_{31}(Z) E_1(Z) dZ \quad (4)$$

$$\text{for completely polarized: } d_{31}(Z) = d_{31} \text{ (constant)} \quad (5a)$$

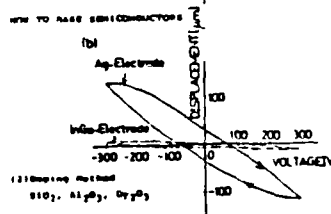
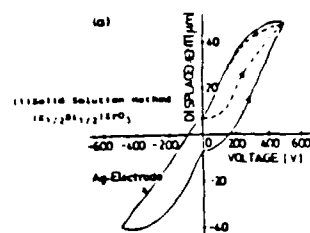
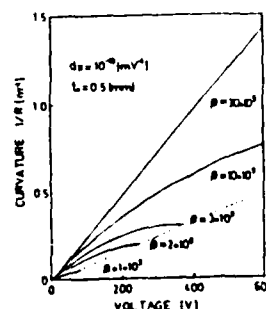
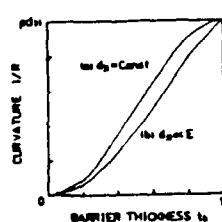
$$\text{for gradually polarized: } d_{31}(Z) = d_{31} (Z - \frac{1}{2}L + 1) / L \quad (5b)$$

(note $L_2 = L, < Z < \frac{1}{2}L$)

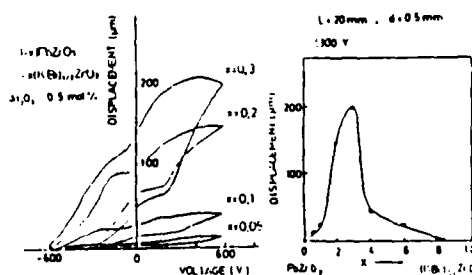


$$\frac{1}{R} = -\beta d_{31} \frac{L^2}{2} \left(\frac{1}{L} - \frac{1}{2} \right) \quad (6a)$$

$$\frac{1}{R} = -\beta d_{31} \frac{L^2}{2} \left(\frac{1}{L} - \frac{1}{2} \right) \quad (6b)$$

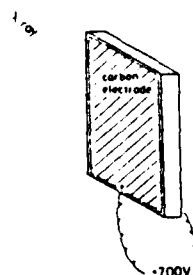


MONOPHASE CHARACTERISTICS IN
(a) LEAD ZIRCONATE BASED AND
(b) BARIUM TITANATE BASED CERAMICS.

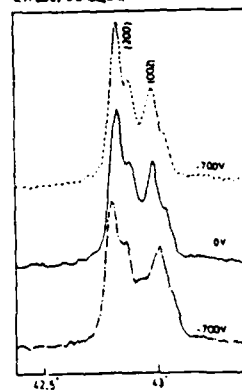


DISPOSITION DEPENDENCE OF MONOPHASE CHARACTERISTICS IN
THE $(\text{Pb}_{1-x}\text{Zr}_x)_2(\text{Ti}_{1-x}\text{Nb}_x)\text{O}_{12}$ CERAMICS

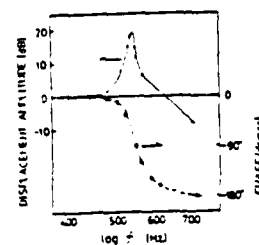
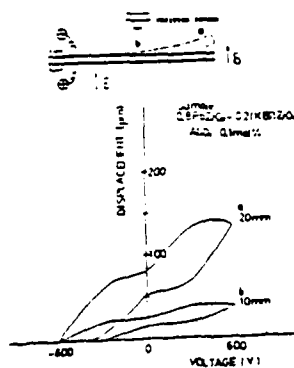
0.7PbZr_{0.3}0.2Nb_{0.5}Zr_{0.4}



X-RAY DIFFRACTION
0.7PbZr_{0.3}0.2Nb_{0.5}Zr_{0.4}



測定電圧 (V)	Lattice a		Lattice c	
	2θ (°)	a (Å)	2θ (°)	c (Å)
0	43.88	4.144	43.96	4.116
+700	43.88	4.144	43.98	4.118
-700	43.81	4.148	44.01	4.112



ELECTROMECHANICAL RESONANCE IN A PbZrO₃-BASED
MONOPHASE ACTUATOR.

Development of Electrostrictive Ceramics

S. Jomura, K. Maruta and J. Watanabe
Hitachi Metals Ltd.

Object:

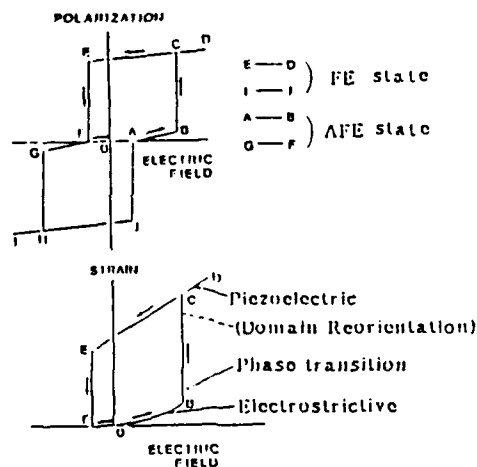
To obtain PZT ceramics with large strain for piezoelectric actuator.

Mechanism for the piezoelectric strains:

- (1) usual piezoelectric strain
- (2) domain reorientation
- (3) volume change of upl cell accompanying with phase transition (ex. AFE \rightarrow FE)
- (4) electrostrictive strain

Antiferroelectric (AFE) - Ferroelectric (FE)

Phases Coexisting PZT Ceramic:



Composition:

$(1-x)\text{Pb}(\text{Zr}_{1-x}\text{Ti}_x)\text{O}_3 - x\text{Sr}(\text{Ni}_{1-x}\text{Zn}_x)\text{Nb}_2\text{O}_7$
 $x=0.15$ $\text{Zr} \sim 0.25$

Ferroelectric Hysteresis Loop (D-E Loop):

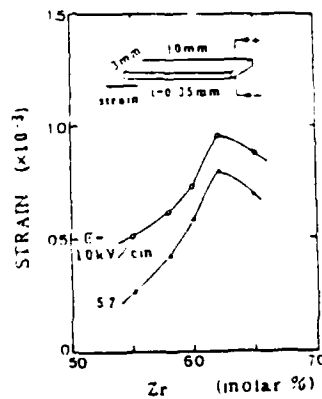
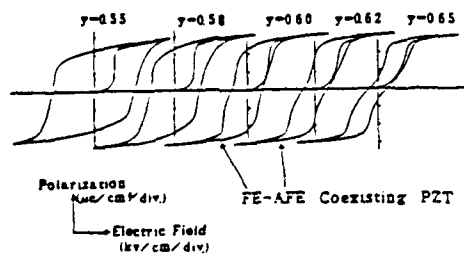


Fig. 1 Composition dependence of strain after poling

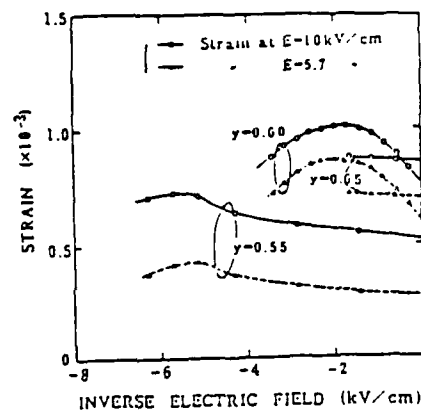


Fig. 2 Inverse electric field dependence of strain at E=10 kV/cm and 5.7 kV/cm

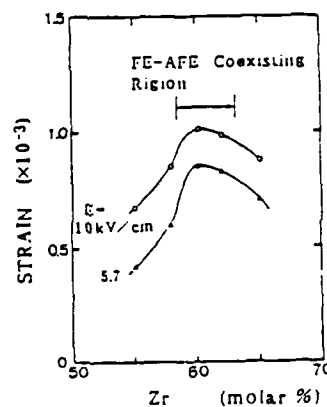
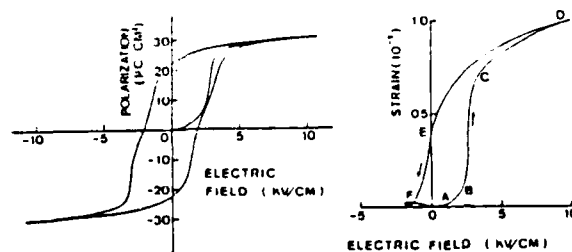


Fig. 3 Composition dependence of strain after inverse electric field are applied.

Summary :

1. It was found that a large strain can be obtained using electrically induced phase transition in the FE-AFE phases coexisting ceramics.
2. The typical value of the transverse strain of this material is 1×10^{-3} at 10 kV/cm .



TEMPERATURE DEPENDENCE OF ELECTROSTRICTION UNDER HIGH ELECTRIC FIELD

K ASE, O FURUKAWA, M KATSURA
and K INAGAKI*

Toshiba Corp. *Marcon Electronics Co. Ltd.

TEMPERATURE COEFFICIENT OF ELECTROSTRICTION

$$\left(\frac{1}{S} \frac{dS}{dT} \right)$$

$$\begin{aligned} E &= \alpha P + \beta P^3 + \gamma P^5 \\ S &= QP^2 \end{aligned} \quad \begin{array}{l} E: \text{electric field} \\ P: \text{polarization} \\ S: \text{electrostriction} \end{array}$$

$$\frac{1}{S} \frac{dS}{dT} = \frac{1}{Q} \frac{dQ}{dT} - \frac{2}{\alpha + 3\beta P^2 + 5\gamma P^4} \left(\frac{d\alpha}{dT} + P^2 \frac{d\beta}{dT} + P^4 \frac{d\gamma}{dT} \right)$$

$$\left| \frac{1}{Q} \frac{dQ}{dT} \right| \ll \left| \frac{2}{\alpha + 3\beta P^2 + 5\gamma P^4} \left(\frac{d\alpha}{dT} + P^2 \frac{d\beta}{dT} + P^4 \frac{d\gamma}{dT} \right) \right|$$

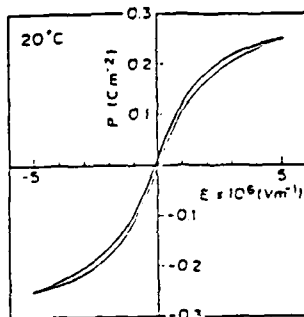


Figure 1 Electric field vs polarization
for modified $\text{Pb}(\text{Zn}_{1/3}\text{Nb}_{2/3})\text{O}_3$.

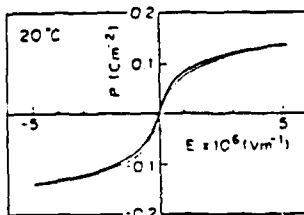


Figure 2 Electric field vs polarization
for modified BaTiO_3 .

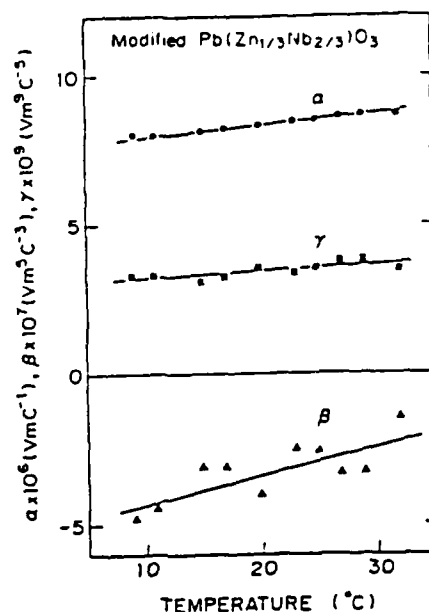


Figure 3 Temperature dependence of α , β
and γ in $E = \alpha P + \beta P^3 + \gamma P^5$.

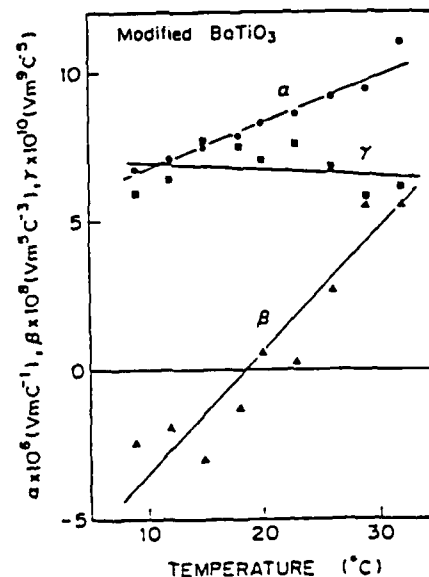


Figure 4 Temperature dependence of α , β
and γ in $E = \alpha P + \beta P^3 + \gamma P^5$.

Table 1. Values of α , β and γ in $E = \alpha P + \beta F^3 + \gamma F^5$ at 20°C and their temperature coefficients

Sample	Modified $\text{Pb}(\text{Zn}_{1/3}\text{Nb}_{2/3})\text{O}_3$	Modified BaTiO_3
$\alpha \times 10^6 (\text{VmC}^{-1})$	8.38	8.31
$\beta \times 10^7 (\text{Vm}^3\text{C}^{-3})$	-3.39	5.81
$\gamma \times 10^9 (\text{Vm}^5\text{C}^{-5})$	3.46	67.4
$\partial\alpha/\partial T \times 10^6 (\text{VmC}^{-1}\text{K}^{-1})$	0.042	0.157
$\partial\beta/\partial T \times 10^7 (\text{Vm}^3\text{C}^{-3}\text{K}^{-1})$	0.095	4.154
$\partial\gamma/\partial T \times 10^9 (\text{Vm}^5\text{C}^{-5}\text{K}^{-1})$	0.0024	-0.18

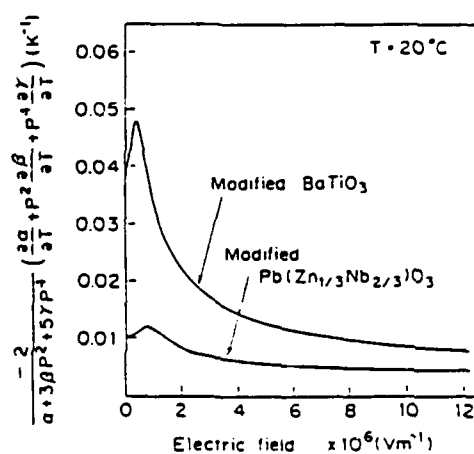


Figure 5. Calculated curves of

$$\frac{-2}{\alpha + 3\beta P^2 + 5\gamma P^4} \left(\frac{\partial\alpha}{\partial T} + P^2 \frac{\partial\beta}{\partial T} + P^4 \frac{\partial\gamma}{\partial T} \right)$$

as a function of electric field.

CONCLUSION

For a multilayer electrostrictor using modified lead zinc niobate

- 1 Temperature coefficient of electrostriction
< 12% / °C at 20°C
- 2 Utilization under high electric field
favorable for temperature stability

PREPARATION AND CHARACTERISTICS OF NEW MONOMORPH ACTUATOR

N. SAKAI, K. KASAI, YAMAMURA and K. UCHINO
Advanced Material Research Laboratory,
Toyo Soda Manufacturing Co., LTD
and Sophia University

ABSTRACT

Bending phenomenon was newly observed in a single ceramic plate of BaTiO_3 which was doped by small amount of SiO_2 and Al_2O_3 or Nb_2O_5 . The bending mode may occur by the presence of potential barrier between silver electrode and ceramic semiconductor, as a result of inhomogeneous distribution of an electric field and also by inhomogeneous polarization in oxidized surface layer.

Introduction

There are two modes of ceramic actuator, that is, longitudinal and bending modes. The bending mode can be realized in the *bi-morph* or *uni-morph*-type elements. Fig. 1 shows a schematic diagram of the uni-morph-type element. On the other hand, in the present study, it was found that the ceramic single plate of BaTiO_3 which was doped by small amount of SiO_2 and Al_2O_3 or Nb_2O_5 showed the bending effect by applying external field. (Fig. 2)

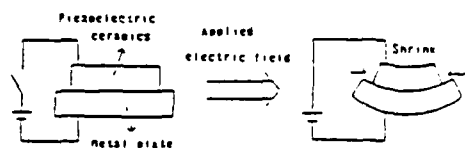


Fig. 1. A schematic diagram of the uni-morph-type element.

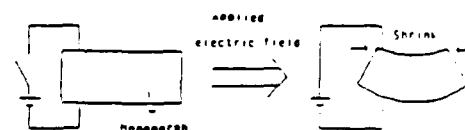


Fig. 2. A schematic diagram of the monomorph-type element.

EXPERIMENTAL

After BaTiO_3 was ball-milled with 5 mol% SiO_2 and 2.5 mol% Al_2O_3 , the powder was rubber-pressed to compacts. Sintering was performed at 1250°C for various periods, 1 to 15 hrs. in air. BaTiO_3 doped by Nb_2O_5 (0.1 to 1 at%) was also prepared in the similar procedure above-mentioned. Sintering was performed at 1300°C for 1 hr. Metal electrodes such as Ag, Au, Ga-In were used to check the electrode effect. Bending effect was measured by non-contact sensor method. The sample size measured was 40 mm length, 15 mm width, and 0.5 mm thickness. The measurement was proceeded at the position of 28 mm far from the fixed end.

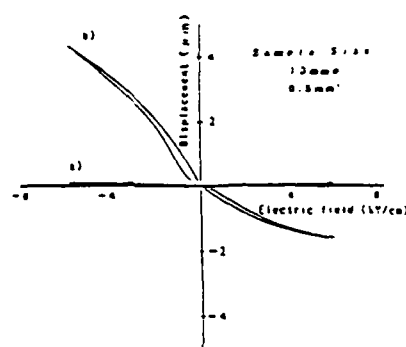


Fig. 3. Displacement versus applied electric field for the sample with Ag electrode.

Displacement was measured by contact method using potentiometer.

a) Non-doped BaTiO_3 .

b) 5 mol% SiO_2 and 2 mol% Al_2O_3 doped BaTiO_3 .

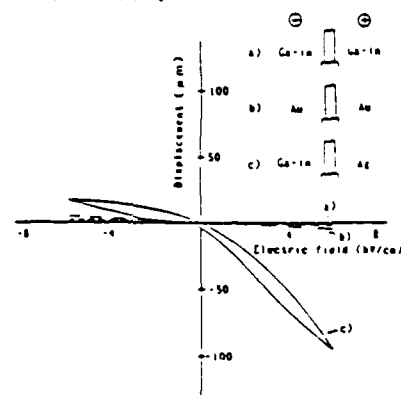


Fig. 4. Electrode dependence of displacement-applied electric field characteristics for the SiO_2 - Al_2O_3 doped BaTiO_3 .

a) Ga-In, Ga-In.

b) Au, Au.

c) Ga-In, Ag (Ag paste was fired at 750°C).

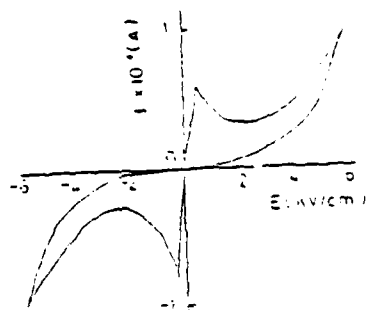


Fig. 5. Current-electric field characteristics for the $\text{SiO}_2\text{-Al}_2\text{O}_3$ doped BaTiO_3 with Ag electrodes.

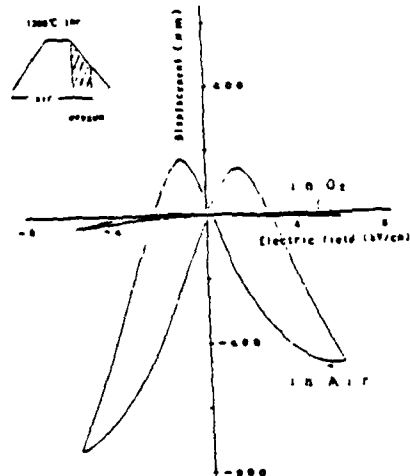


Fig. 6. Displacement versus applied electric field for the sample fired at 1200°C for 1 hr in different atmosphere and cut to the plate of 0.5 mm thickness from the surface.

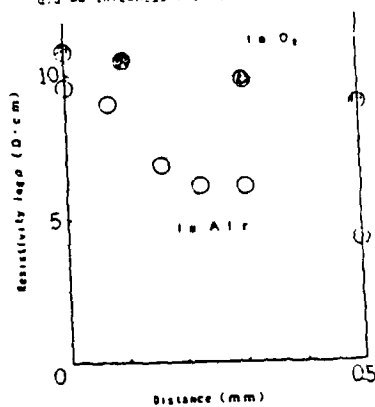


Fig. 7. Resistivity as a function of distance from surface to inside. The resistivity was measured after the oxidized surface was sliced. This procedure was repeatedly done many times.

- fired in air and then in oxygen gas on final stage;
- fired in air.

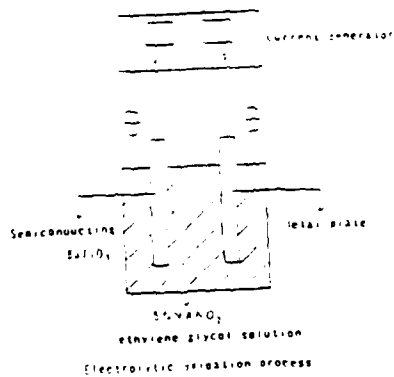


Fig. 8. Diagram of electrolytic oxidation process.

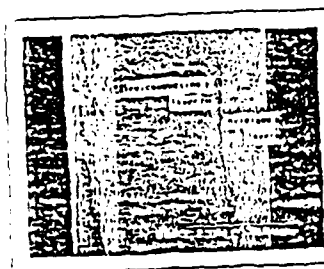


Fig. 9. SEM micrograph of electrolytically oxidized layer, which was oxidized at the current density of 2 mA/cm^2 for 1 hr. The $0.1 \text{ at}\%$ Nb -doped BaTiO_3 sintered at 1200°C for 1 hr was used.

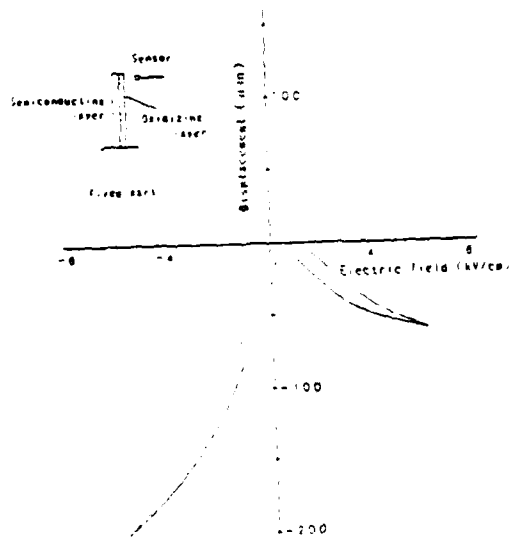


Fig. 10. Displacement versus applied electric field for the surface-oxidized plate which was horizontally cut in half and then fired at 1000°C for 1 hr in air.

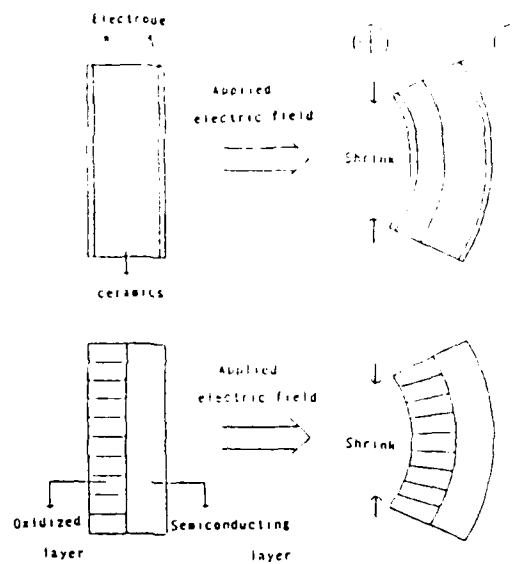


Fig.11. Diagrams of two different types of bending mechanism.

Summary

1. We got a new type's actuator of bending mode, which could occur bending phenomenon in a single plate of ceramics. We named it "MONOMORPH".
2. We can guess that it may occur by two major mechanisms as follows,
 - a) Presence of potential barrier between silver electrode and ceramic semiconductor.
 - b) Presence of resistivity distribution as a result of inhomogeneous oxidation.

W16

APPLICATIONS OF POLYMERS TO VLSI PACKAGING

- INEXPENSIVE
- EASILY FORMED
- SOLDERABLE
- HIGH DIELECTRIC STRENGTH
- LOW DIELECTRIC CONSTANT

Lionel M. Levinson
General Electric Company
Schenectady, NY

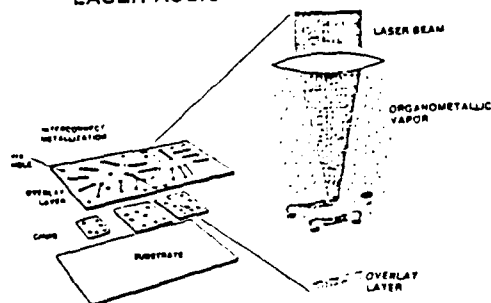
LASER PROCESSING OF POLYMERS FOR PACKAGING

- METALLIZATION BY LASER DEPOSITION
 - NON-CONTACT
 - MASKLESS
 - LOW TEMPERATURE
 - SELECTIVE
 - GOOD STEP COVERAGE
- POLYMER MACHINING BY LASER PHOTOETCHING
 - SELECTIVE
 - MASKLESS
 - LOW TEMPERATURE
 - NON-CONTACT
 - HIGH RESOLUTION

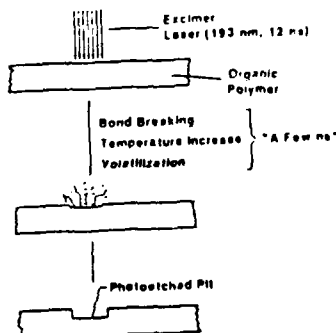
REQUIREMENTS OF POLYMERS FOR ELECTRONIC PACKAGES

- PROCESSABILITY
- ADHESION
- HIGH DIELECTRIC STRENGTH
- MOISTURE/SOLVENT RESISTANCE
- THERMAL STABILITY
- PATTERNABLE
- REWORKABLE

LASER ASSISTED PROCESSING



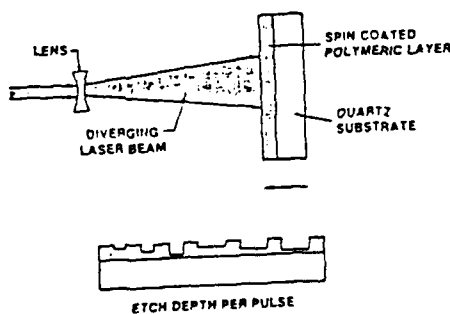
EXCIMER LASER PHOTOETCHING OF POLYMERS



FACTORS AFFECTING PHOTOETCH RATE

- LASER FLUENCE
- ABSORPTION COEFFICIENT
- POLYMER STRUCTURE
- LASER WAVELENGTH

EXPERIMENTAL DETERMINATION OF PHOTOETCHING RATE

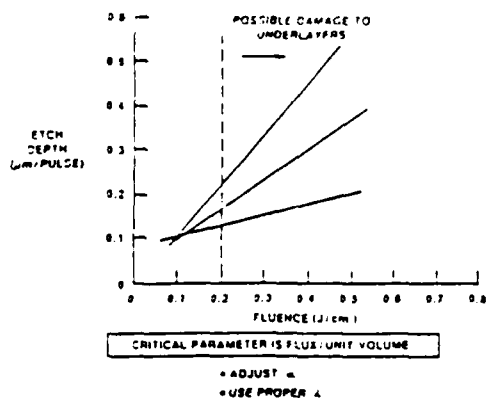


THRESHOLD DAMAGE LEVELS FOR VARIOUS FILM-SUBSTRATE COMBINATIONS

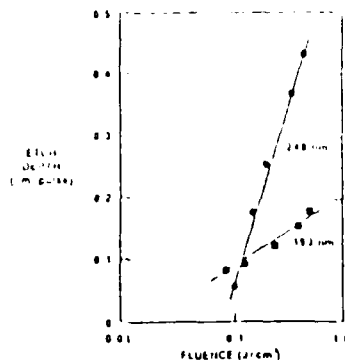
SAMPLE	λ	FLUENCE (mJ/cm ²)
Al ON POLYIMIDE	193 nm	200
Si, SiO ₂	193 nm	>400
Al on Si	193 nm	>400
Al ON MYLAR*	308 nm	140
Cr ON QUARTZ*	308 nm	240

* ANDREW, ET AL, APPL. PHYS. LETT. 43, 1076 (1983)

EXCIMER LASER PHOTOETCHING OF POLYMERIC MATERIALS

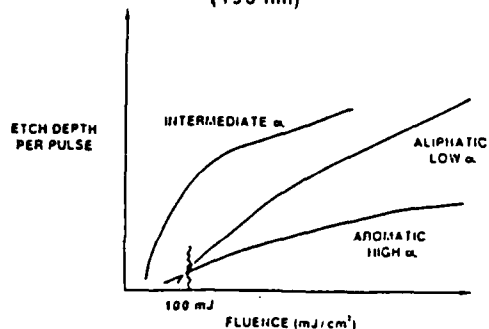


PHOTOETCHING OF POLY (p-METHYL) STYRENE



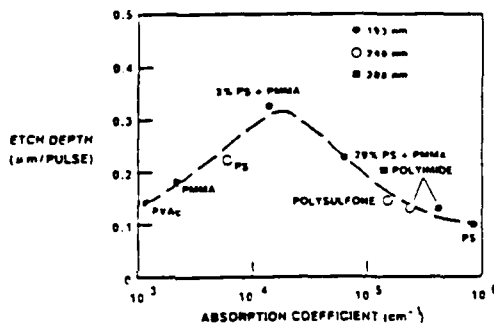
DIFFERENT ETCH WAVELENGTHS HAVE DIFFERING ETCH RATES

PHOTOETCHING STUDIES (193 nm)



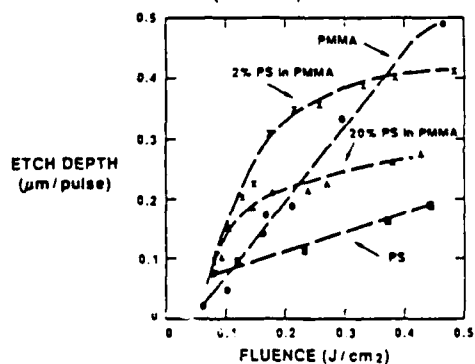
INTERMEDIATE ABSORPTION COEFFICIENT α (CAT) GIVE THE HIGHEST ETCH RATE

PHOTOETCHING OF VARIOUS POLYMERS (200 mJ/cm², 12 ns PULSE)



THERE EXISTS A GENERAL POLYMER ETCH RATE VERSUS ABSORPTION COEFFICIENT CURVE FOR MANY POLYMERS

PHOTOETCHING OF POLYMER BLENDS (193 nm)



SMALL AMOUNTS OF POLYSTYRENE (PS) IN POLYMETHACRYLATE (PMMA) DRAMATICALLY ENHANCES THE ETCH RATE OF PMMA

CHARACTERISTICS OF LASER PHOTOETCHING

- A FLUENCE THRESHOLD EXISTS FOR PHOTOABLATION
- AT LOW ABSORPTION COEFFICIENTS, LITTLE ETCHING OCCURS SINCE ABSORBED ENERGY PER UNIT VOLUME IS TOO SMALL
- AT VERY HIGH ABSORPTION COEFFICIENTS, PHOTONS DO NOT PENETRATE THE POLYMER AND LITTLE PHOTOETCHING OCCURS
- THE MAXIMUM POLYMER ETCH RATE OCCURS AT INTERMEDIATE ABSORPTION COEFFICIENTS
- FOR PRACTICAL APPLICATIONS, THE POLYMER ETCH FLUENCE MUST BE LIMITED TO AVOID DAMAGING UNDERLYING COMPONENT METALLIZATION

CONCLUSIONS

- EXCIMER LASER RADIATION CAN BE USED TO PHOTOETCH WITHOUT DAMAGE TO VLSI CIRCUITS
- POLYMER ETCH RATE CAN BE OPTIMIZED BY
 - ADJUSTING POLYMER ABSORPTION COEFFICIENT
 - ADJUSTING IRRADIATION WAVELENGTH

CHARACTERIZATION OF THE ROLE OF EXCESS MgO AND PbO IN LEAD MAGNESIUM NIOBATE

by

HUI-CHIEH WANG

ADVISOR: DR. WALTER A. SCHULZE

NEW YORK STATE COLLEGE OF CERAMICS

AT ALFRED UNIVERSITY

ALFRED UNIVERSITY

ABSTRACT

Near phase pure perovskite Lead Magnesium Niobate (PMN) was produced by reacting PbO with MgNb_2O_6 at 800°C. Powder x-ray diffraction studies support the conclusion of an earlier study that excess MgO produces the highest percentage perovskite phase PMN. Dense ceramic was prepared for characterization by sintering at 1200°C. Scanning electron spectroscopy combined with energy dispersive spectroscopy were conducted on both fractured and polished cross sections in an attempt to confirm the observations of Goo. Depth profiling on intergranular fracture cross sections was used to determine the average level of excess PbO and MgO in the grain boundary region as characterized by secondary ion mass spectroscopy. Microstructural and dielectric constant information is discussed as to the effect of excess PbO and MgO on PMN ceramic.

CHEMICAL COMPOSITIONS:

FABRICATION:

PMN-STD ($\text{PbMg}_{1/2}\text{Nb}_{3/2}\text{O}_6$)

PMN-2 Mol % MgO

PMN-2 Mol % PbO

PMN-5 Mol % MgO

PMN-5 Mol % PbO

PMN-10 Mol % MgO

Bulk properties of lead magnesium niobate

Composition	Green density	Fired density	Imp. partially	Imp. 3000	Green size
PMN-STD	4.7410 01	7.8210 02	0.20 15	1010 00	2.131 0
PMN-2% MgO	4.7510 13	7.8510 02	0.10 0	2020 05	2.150 0
PMN-5% MgO	4.8310 01	7.8720 02	0.15 9	3420 04	2.211 2
PMN-10% MgO	4.8410 05	7.8510 02	1010 15	5910 48	2.731 4
PMN-2% PbO	4.8910 23	7.8310 02	0.10 0	4020 05	1.810 7
PMN-5% PbO	4.8110 05	7.8210 04	2.7020 01	1.8110 22	1.810 0

Units:

Density: g/cm³
Grain size: μm

MgNb_2O_6 FORMATION

-- $\text{MgO} \cdot \text{Nb}_2\text{O}_5$, EXCESS MgO
--BALL MILL
--CALCINE 1000°C
8 hrs
--XRD

$\text{PbMg}_{1/2}\text{Nb}_{3/2}\text{O}_6$ FORMATION

-- MgNb_2O_6 / PbO, EXCESS Pb
--BALL MILL
--CALCINE 800°C, 4 hrs
--XRD
--PVA, PRESS
--SINTER 1200°C, 1 hr
--XRD SINTERED PELLETS

XRD PHASES IDENTIFICATION

% COLUMBITE MgNb_2O_6
AFTER 20 MIN. CALCINATION 80-100

% PEROVSKITE $\text{PbMg}_{1/2}\text{Nb}_{3/2}\text{O}_6$
1ST CALCINE

SINTERED PELLETS

	PMN-STD	PMN-2% MgO	PMN-5% MgO	PMN-10% MgO	PMN-2% PbO	PMN-5% PbO
% COLUMBITE	00.3	07.3	07.8	07.9	04.5	07.8
% PEROVSKITE	07.4	100	90.7	100	90.0	97.9

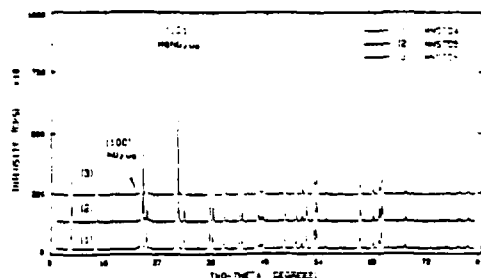


Figure 9. XRD for the second calcines of stoichiometric PMN-5%PbO.



Figure 8. BSE image of the polished and etched surface for an over-fired PMN-5%PbO sample. (Magnification=1000X.)

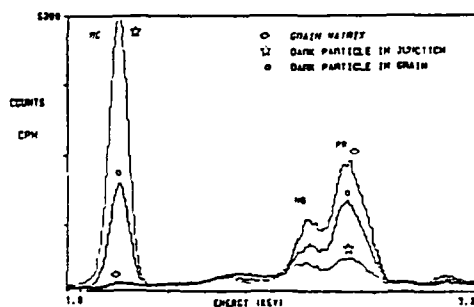


Figure 10. EDS spectra on the polished and etched surface for an over-fired PMN-5%PbO.

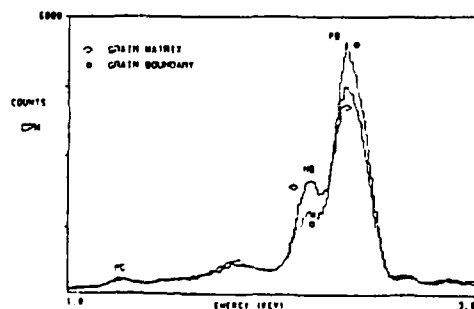


Figure 11. EDS spectra on the fracture surface for PMN-25%PbO.



Figure 10. BSE image of the fracture surface for PMN-25%PbO. (Magnification=6000X.)

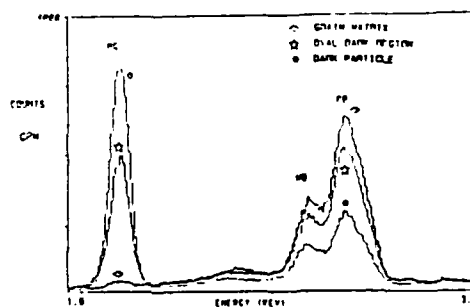


Figure 15. EDS spectra of sintered PMN-10%PbO. The sintered surface was polished with diamond to inspection surface of 10 μm. This shows the EDS spectra on the sintered surface after 250 minutes sintering.

(a)



(b)

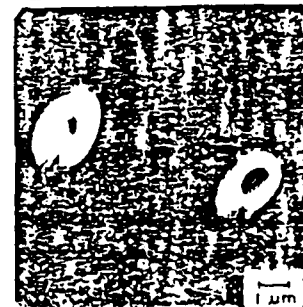


Figure 17. A polished surface of doubly sintered PMN-10%PbO was sputtered with argon at an emission current of 10 mA for 250 minutes. These show the images of the sputtered surface at the magnifications of (a) 2000X, SE mode and (b) 8000X, BSE mode.

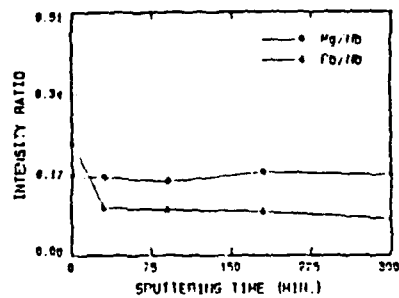


Figure 21. The SIMS depth profile on the PMN-5SPbO as-fired surface sputtered with argon for 300 minutes at an emission current of 10 mA.

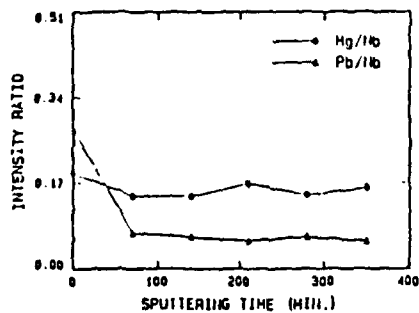


Figure 20. The SIMS depth profile on the PMN-5TbO as-fired surface sputtered with argon for 7 hours at an emission current of 10 mA.

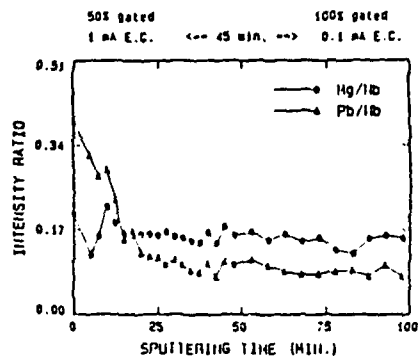


Figure 13. The SIMS depth profiles of (a) PMN-5TbO.

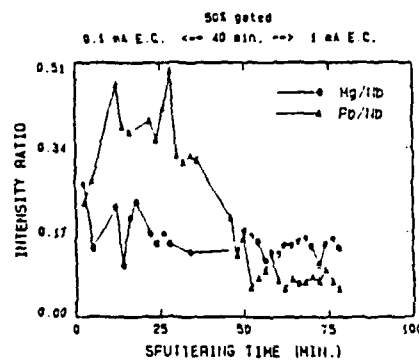


Figure 13. The SIMS depth profile of (b) PMN-25MgO.

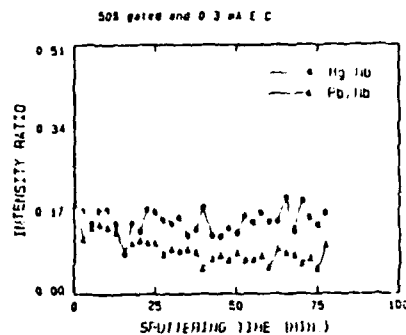


Figure 13. The SIMS depth profile of (c) PMN-21PbO.

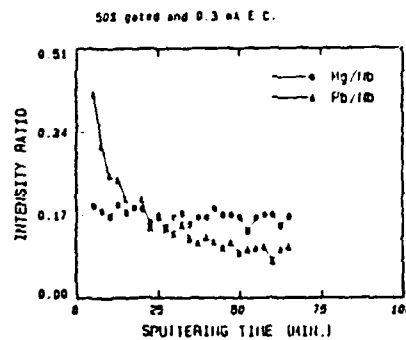


Figure 13. The SIMS depth profile of (f) PMN-21PbO.

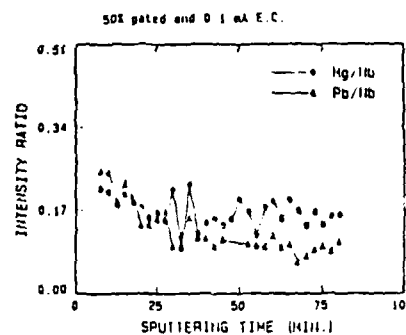


Figure 13. The SIMS depth profile of (c) PMN-51MgO.

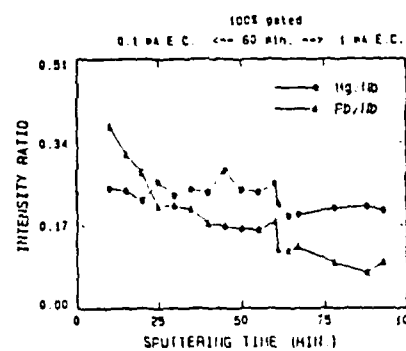


Figure 13. The SIMS depth profile of (d) PMN-10MgO.

DIELECTRIC PROPERTIES OF PMN

	0.1 KHz		1 KHz		10 KHz		100 KHz		1000 KHz	
Composition	ϵ_{max}	T_c	ϵ_{max}	T_c	ϵ_{max}	T_c	ϵ_{max}	T_c	ϵ_{max}	T_c
Pb0.975Sn0.025	14300	-14	13700	-10	13000	-5	12100	1	11300	8
Pb0.975Sn0.025	16400	-16	15800	-12	14700	-7	13700	-1	12700	6
Pb0.95Sn0.05	16400	-16	16400	-12	17200	-7	15800	-1	14800	7
Pb0.95Sn0.05	24800	-16	23400	-12	21800	-7	20200	-1	18800	7
Pb0.975Sn0.025	12100	-14	9800	-10	9400	-5	8000	1	6500	8
Pb0.95Sn0.05	8400	-14	8300	-10	8100	-5	5800	0	5700	7

NOTE: T_c - maximum dielectric constant temperature in $^{\circ}\text{C}$.

T_c - $^{\circ}\text{C}$
 ϵ_{max} - $\times 10^4$

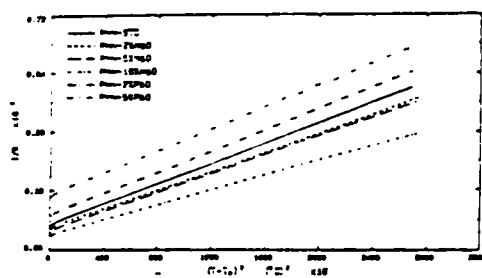


Figure 28. Plot of $1/K$ vs. $(T-T_c)^2$ for all compositions of PMN

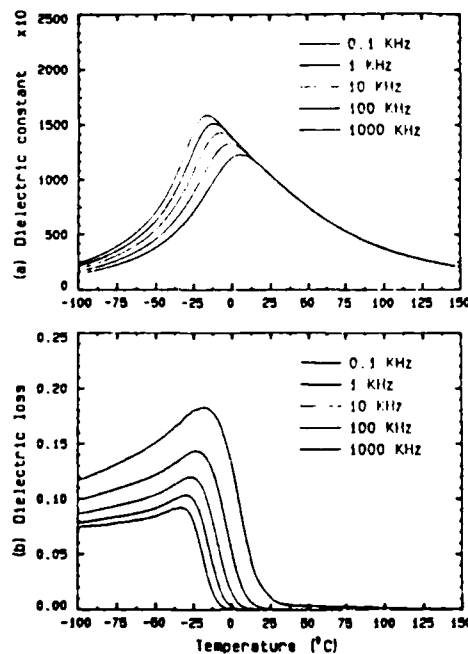
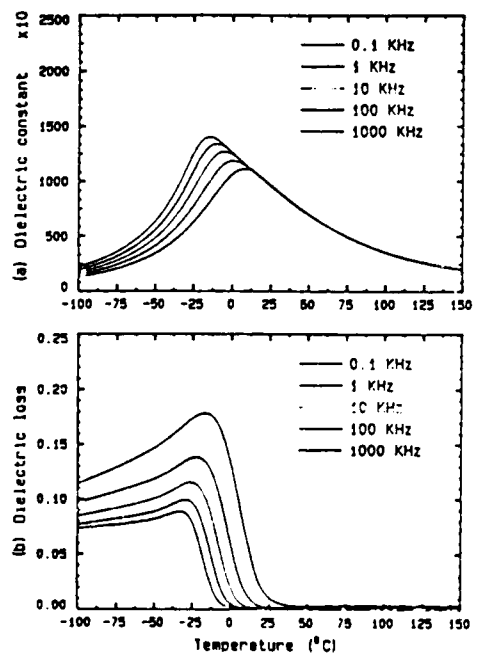
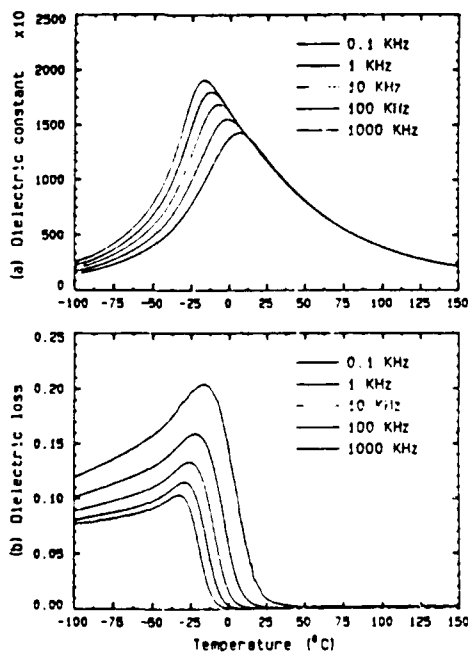


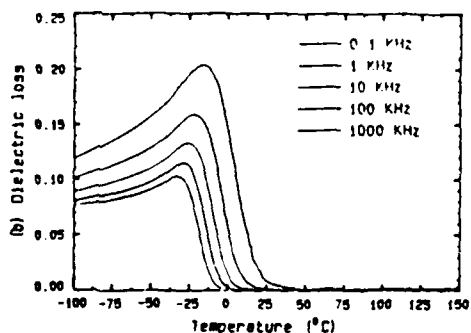
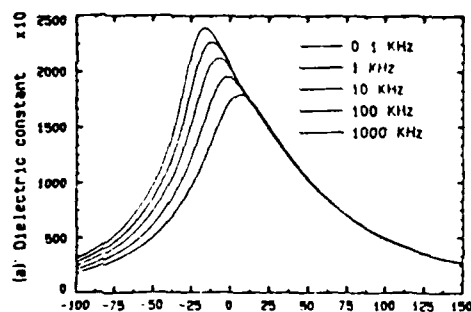
Figure 23. Temperature dependence of (a) dielectric constant and (b) dielectric loss for PMN-25MgO



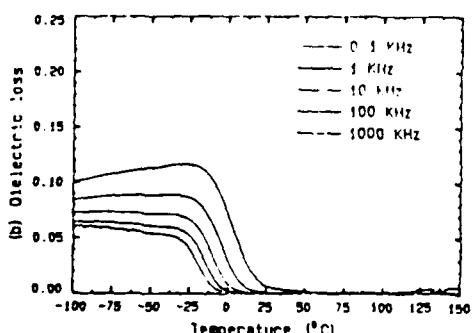
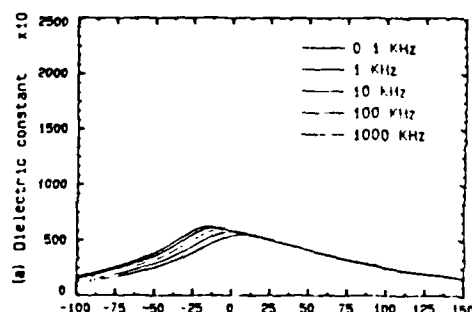
Temperature dependence of (a) dielectric constant and (b) dielectric loss for PMN-5TD



Temperature dependence of (a) dielectric constant and (b) dielectric loss for PMN-53MgO

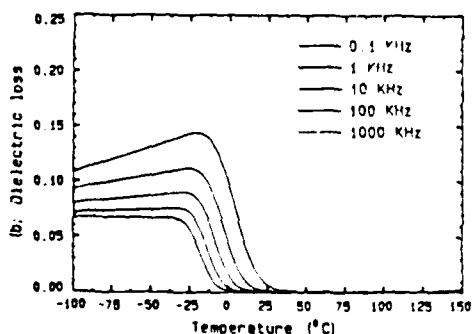
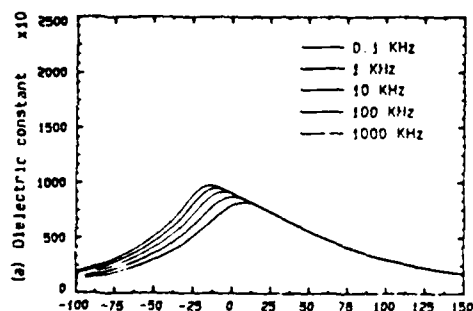


Temperature dependence of (a) dielectric constant and (b) dielectric loss for Pw1-103MgO



Temperature dependence of (a) dielectric constant and (b) dielectric loss for Pw1-52PbO

MODELLING



Temperature dependence of (a) dielectric constant and (b) dielectric loss for Pw1-23PbO

Ar ION BEAM

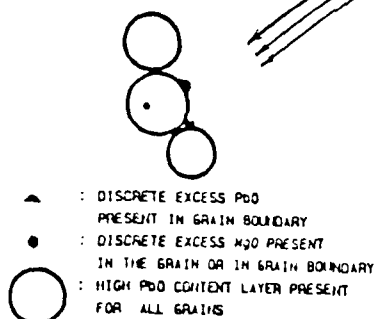


Figure 29. A modelling for the microstructure of lead magnesium niobate.

SUMMARY

- COMPOSITIONS CONTAINING EXCESS MgO . MgO IS PRESENT EITHER AS SUBMICRON SPHERICAL INCLUSIONS IN PEROVSKITE GRAINS, OR AS DISCRETE ISOLATED GRAINS
- COMPOSITIONS CONTAINING EXCESS PbO . PbO IS PRESENT AT TRIPLE POINT IN GRAIN BOUNDARY REGION
- XPS OBSERVES PbO -RICH LAYER ON THE SURFACE OF THE GRAINS FOR ALL COMPOSITIONS
- EXCESS PbO DECREASES DIELECTRIC CONSTANT BY INCREASING THE THICKNESS OF LOW K GRAIN BOUNDARY LAYER
- EXCESS MgO ENHANCES DIELECTRIC CONSTANT BY INCREASING THE GRAIN DIAMETER AND/OR CHANGING THE INTRINSIC DIELECTRIC CONSTANT OF THE GRAINS

TRIVALENT IMPURITIES IN BaTiO_3

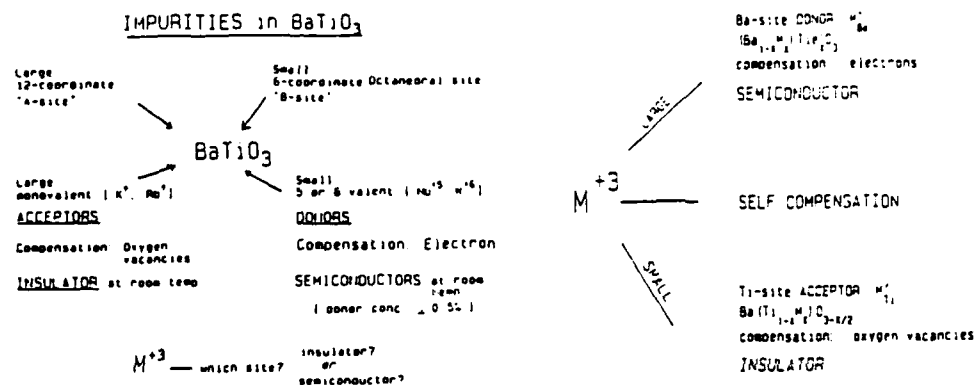
K. TAKADA*, R. Y. LEE, S. R. WITEK, and D. M. SMYTH

Materials Research Center, No. 32

* Sumitomo Metal Mining Co., Ltd.

Lehigh University
Bethlehem, PA 18015 U. S. A.Central Research Laboratory
3-18-5, Nakagokubun
Ichikawa, Chiba, JAPAN

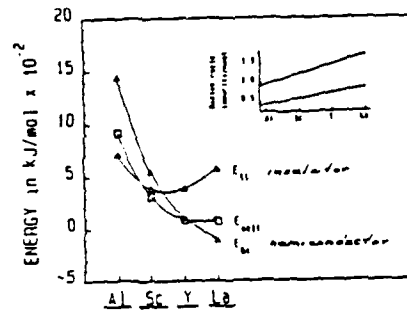
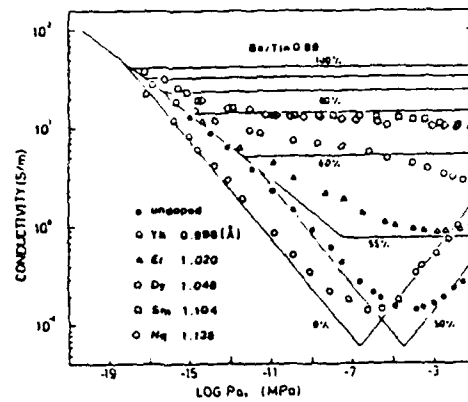
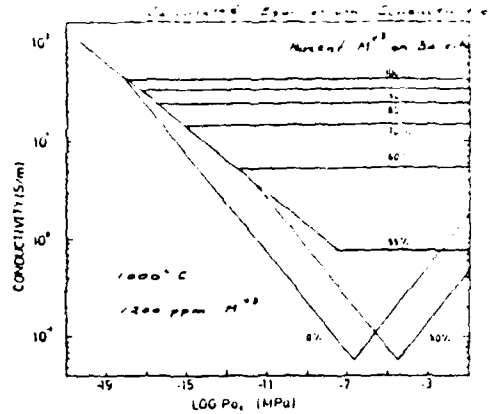
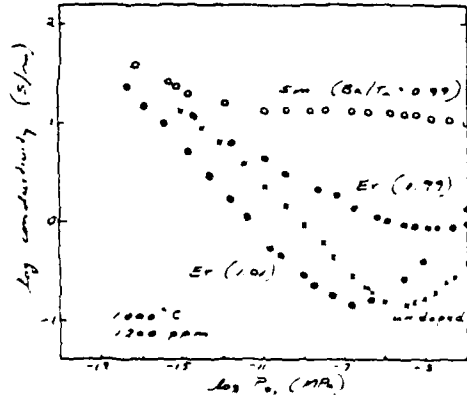
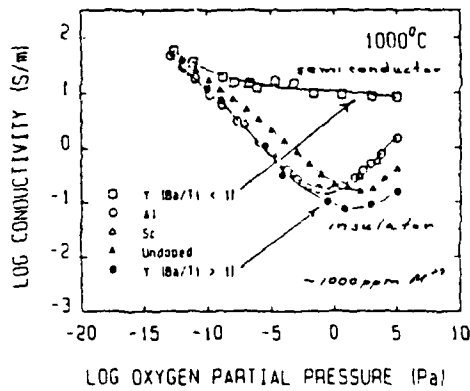
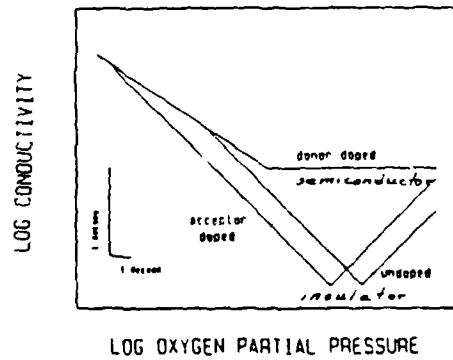
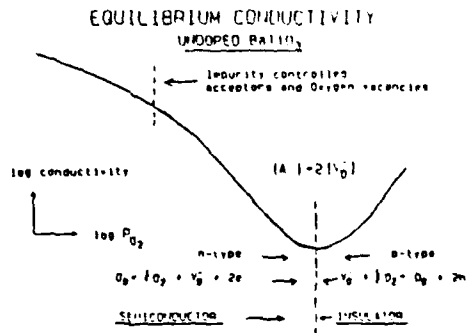
ABSTRACT: The effect of small additions of trivalent metallic impurities on the electrical conductivity of BaTiO_3 has been studied for samples having an excess of either BaO or TiO_2 . The properties change gradually with the ionic radius of the impurities, indicating that those of intermediate size occupy both Ba and Ti sites in varying amounts that depend on the Ba/Ti ratio.



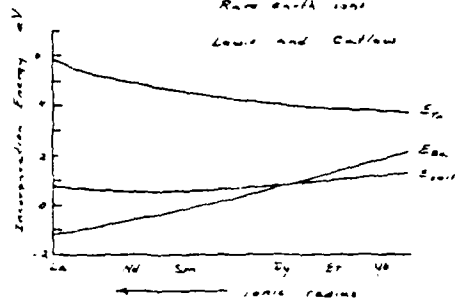
1 H 1.008																	2 He 4.003	
3 Li 0.681	4 Be 0.412																	10 Ne 0.719
11 Na 1.02	12 Mg 0.72																	18 Ar 0.94
19 K 1.38	20 Ca 0.99	21 Sc 0.87	22 Ti 0.76	23 V 0.63	24 Cr 0.72	25 Mn 0.81	26 Fe 0.74	27 Co 0.65	28 Ni 0.63	29 Cu 0.71	30 Zn 0.74	31 Ga 0.76	32 Ge 0.72	33 As 0.73	34 Se 0.71	35 Br 0.73	36 Kr 0.88	
37 Rb 1.47	38 Sr 1.12	39 Y 0.90	40 Zr 0.84	41 Nb 0.71	42 Mo 0.71	43 Tc 0.69	44 Ru 0.68	45 Rh 0.67	46 Pd 0.68	47 Ag 0.74	48 Cd 0.75	49 In 0.76	50 Sn 0.74	51 Sb 0.75	52 Te 0.76	53 I 0.78	54 Xe 1.08	
55 Cs 1.67	56 Ba 1.35	57-71 La-Lu 1.03-0.85	72 Hf 0.71	73 Ta 0.70	74 W 0.69	75 Re 0.68	76 Os 0.68	77 Ir 0.67	78 Pt 0.67	79 Au 0.68	80 Hg 0.71	81 Tl 0.72	82 Pb 0.74	83 Bi 0.75	84 Po 0.76	85 At 0.77	86 Rn 1.12	
87 Fr 1.80	88 Ra 1.48	89-103 Ac-Lr 1.10-0.85	104 Rf 0.71	105 Db 0.70	106 Sg 0.69	107 Bh 0.68	108 Hs 0.68	109 Mt 0.67	110 Ds 0.67	111 Rg 0.68	112 Uub 0.71	113 Uut 0.72	114 Uuq 0.74	115 Uup 0.75	116 Uuh 0.76	117 Uus 0.77	118 Uuo 1.15	

— acceptor
— intermediate
— donor

57 La 1.03	58 Ce 0.95	59 Pr 0.89	60 Nd 0.85	61 Pm 0.81	62 Sm 0.76	63 Eu 0.72	64 Gd 0.69	65 Tb 0.67	66 Dy 0.65	67 Ho 0.64	68 Er 0.62	69 Tm 0.61	70 Yb 0.60	71 Lu 0.59
89 Ac 1.10	90 Th 1.03	91 Pa 0.95	92 U 0.89	93 Np 0.85	94 Pu 0.81	95 Am 0.76	96 Cm 0.72	97 Bk 0.69	98 Cf 0.67	99 Es 0.65	100 Fm 0.64	101 Md 0.62	102 No 0.61	103 Lr 0.59

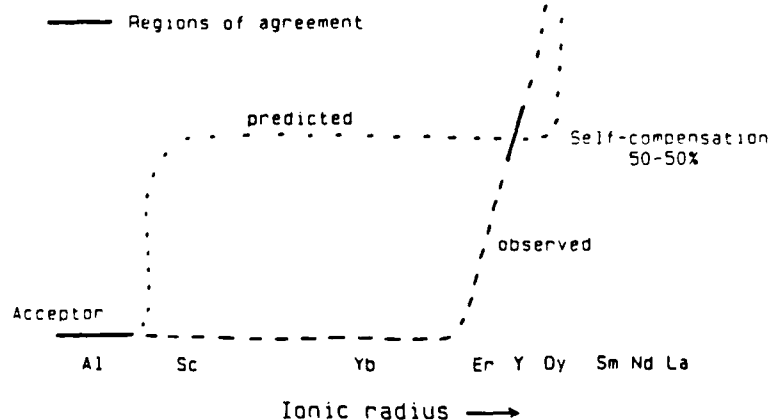


Calculated H^{+} incorporation energies
Lowe and Callow
Calculated H^{+} Incorporation Energies
Rane and Callow
Lowe and Callow



OBSERVED RESULTS vs PREDICTED BEHAVIOR

[LEWIS & CATLOW]



SUMMARY

1. LARGE M^{+3} : La^{+3} , Nd^{+3} , Sm^{+3}
Occupy Ba-sites
Donors - semiconductors
2. SMALL M^{+3} : Al^{+3} , Sc^{+3} , Yb^{+3}
Occupy Ti-sites
Acceptors - Insulators
3. INTERMEDIATE size : Y^{+3} , Er^{+3}
Can occupy either site
Division depends on:
size
Ba/Ti ratio
Can be insulator or semiconductor
4. Less self-compensation than predicted by theoretical calculations

ACKNOWLEDGEMENT: This research was supported by the Office of Naval Research,
the National Science Foundation, and Sumitomo Metal Mining Co., Ltd.

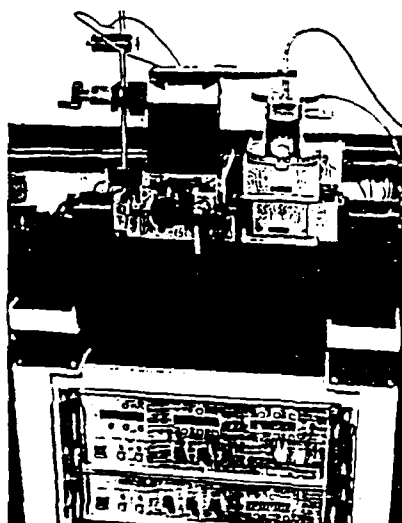
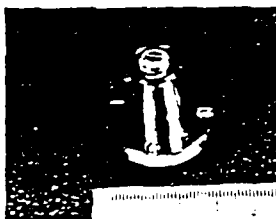
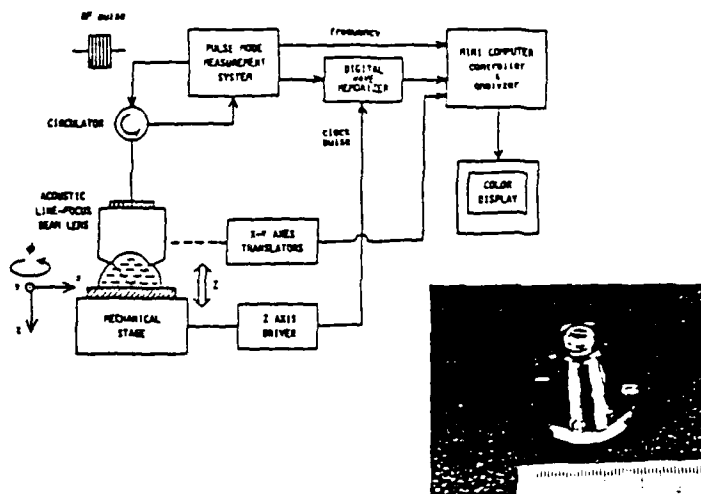
LINE-FOCUS-BEAM ACOUSTIC MICROSCOPE SYSTEM FOR NONDESTRUCTIVE EVALUATION OF ACOUSTIC INHOMOGENEITY ON PZT WAFERS FOR SAW DEVICES

N. CHUBACHI and J. KUSHIBIKI

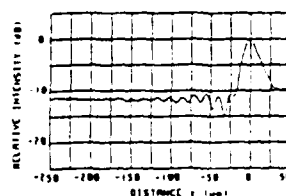
Department of Electrical Engineering, Faculty of Engineering,
Tohoku University, Sendai 980, Japan

The line-focus-beam acoustic microscope system has been developed which can inspect elastic properties of materials over an area of 55mm X 55mm with a measurement accuracy better than $\pm 0.02\%$ in velocity measurements. The evaluation of acoustic inhomogeneity on PZT ceramic wafers for SAW devices has been made successfully with this system. Large variations in SAW velocity have been detected on a wafer sample and also among wafers.

LINE-FOCUS-BEAM ACOUSTIC MICROSCOPE SYSTEM



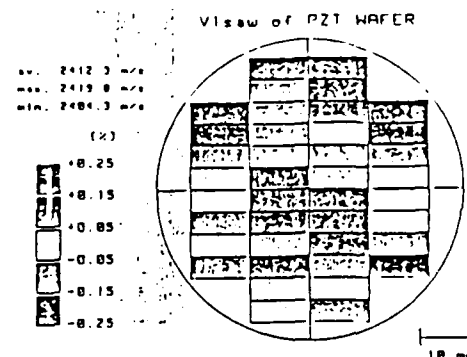
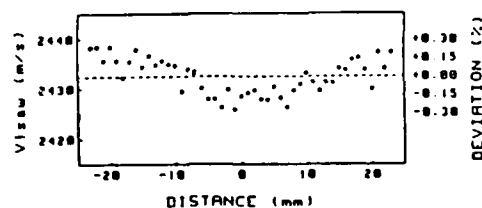
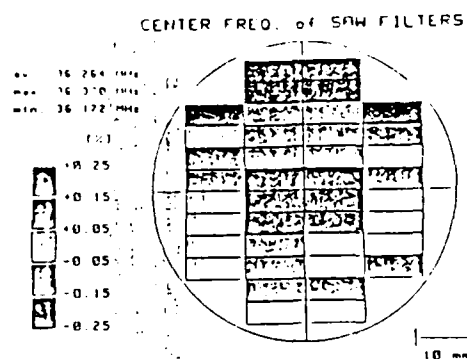
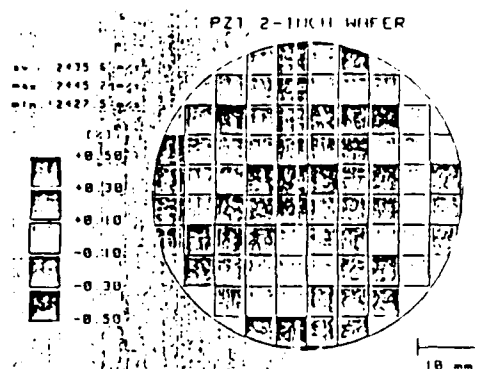
VARIATION OF ACOUSTIC PROPERTY



Typical A12 curve on water/PZT-ceramic measured with acoustic line-focus beam at 225MHz

Table 1 Average velocities of tested SAWs at the center of nine PZT ceramic wafers

Wafer No.	Average Velocity (m/s)
1	2627
2	2625
3	2625
4	2631
5	2628
6	2631
8	2623
9	2622



COMPARISON WITH SAW FILTER CHARACTERISTICS

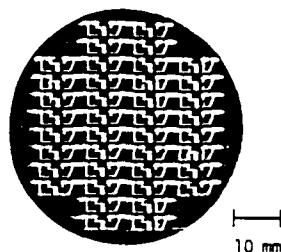
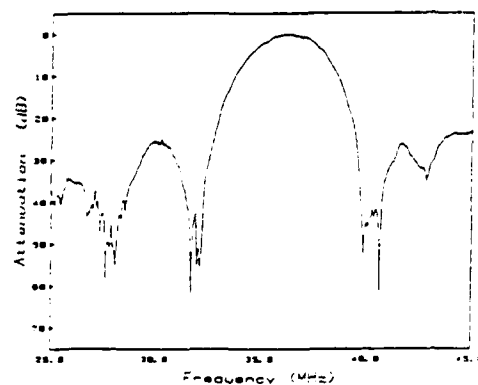


Table 2 Parameters of normal IDTs of SAW filters.

Electrode width (μm)	Gap width (μm)	Number of Electrode Pairs	Aperture width (mm)	Propagation Distance (mm)
16.68	16.69	3.5	1.42	3.09



Frequency response of SAW filter.

W20

ELECTRICAL PROPERTIES OF $(\text{Sr,Ca})\text{TiO}_3$ BASED
CERAMIC VARISTORS

N. YAMAOKA, M. MASUYAMA, AND J. FUNAYAMA
Central Research Institute, TAIYO YUDEN CO., Ltd.
1660 Kamisatomi, Haruna-machi, Gunma-ken, Japan.

ABSTRACT

Electrical properties of $(\text{Sr,Ca})\text{TiO}_3$ based ceramic varistors were investigated. Surge absorption characteristics of samples of which the basic semiconductive ceramics were fired in two reducing atmosphere were examined in relation of to the resistivities of the semiconductive ceramics, the impedance of the ceramic varistors and so on. The resistivity was $0.14\Omega\text{cm}$ at sample(A) or $0.09\Omega\text{cm}$ at sample(B), respectively. The resistivity was decreasing with increasing of H_2 concentration in the firing process. The surface resistance of the semiconductive grain after a diffusion process was $5.5\text{K}\Omega$ at sample(A) or $2.1\Omega\text{cm}$ at sample(B), respectively. Sample(B) indicated an excellent surge absorption characteristics in the region of high impulse surge voltages compared with that of sample(A). The depressed voltage was 280V at sample(B) or 340V at sample(A), respectively, when a high impulse surge of $5000\text{V}(3/20\mu\text{s})$ was supplied to samples. The difference of this depressed voltage is originated from the resistance of the semiconductive grains.

INTRODUCTION

Microstructures and some electrical properties of SrTiO_3 or $(\text{Sr,Ca})\text{TiO}_3$ based ceramic varistors were reported by our previous papers. It is well known that $(\text{Sr,Ca})\text{TiO}_3$ based ceramic varistors have a high apparent permittivity and a high surge capability. The these varistor characteristics are well unknown in the region of a high current or a high voltage surge.

In this work, we present the varistor characteristics in a high impulse surge region in the relation to the resistivity of the based semiconductive ceramics, the impedance of the varistors and so on.

EXPERIMENTAL

The starting materials used in this study were high purity materials of SrCO_3 , TiO_2 , CaCO_3 , Nb_2O_5 and small amount of additives. The basic components were weighed respectively and the powder mixtures were ballmilled. The mixed powders, with an appropriate organic binder, were pressed into tablets under a pressure of 10^4 Pa . After burning the binder, the tablets were fired at a temperature of 1380°C - 1420°C in $98\% \text{ N}_2$ - $2\% \text{ H}_2$ or $90\% \text{ N}_2$ - $10\% \text{ H}_2$ atmosphere, respectively. In order to make BL structure, a paste including Na_2O was printed on the surface of the based semiconductive ceramics. The printed specimen were heat treated at 1150°C - 1250°C in air for the grain boundary diffusion of the printed materials. In-Ga alloy were attached to the surfaces of the semiconductive ceramics, for the measurement of the resistivities. The surface resistance of the based semiconductive grains were measured using a micro manipulator after the metaloxide diffusion. Silver electrodes were fired on the surfaces of the ceramics. The capacitances were measured by a capacitance bridge. The impedance at various frequency was measured using an impedance analyzer (YHP: model - 4191). The current was measured by an amphere meter. A standard impulse wave of $8/20 \mu\text{s}$ in width was used to examine the surge capabilities of $(\text{Sr}, \text{Ca})\text{TiO}_3$ based ceramic varistors. Production flow chart is shown in fig. -1.

Figure-1 Production flow chart

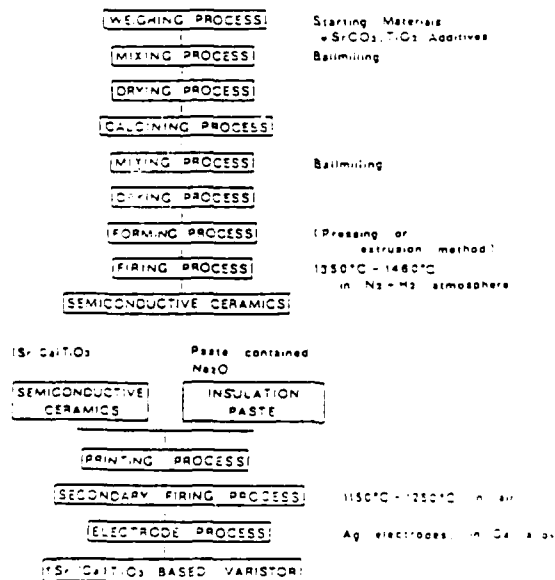


Table-1

Electrical Properties of (Sr,Ca)TiO₃ Varistors (Alor(B)).

Sample No.	P_n	$[C_{av}(cm^2)]$	$[Z_{01}]$	$[Q_{100-1000}]$	$[V_{10A}]$
A	0.11($\Omega \cdot cm$)	[19700(μF)]	[20(Ω)]	17.2	5.0(V)
B	0.09($\Omega \cdot cm$)	[20100(μF)]	60(Ω)	17.5	81.5(V)

Electrical properties of (Sr,Ca)TiO₃ based varistors and the based semiconductive grains were measured. The typical values are shown in Table-1. The basic semiconduction character of samples were found at 1450°C in 90%N₂-10%O₂ atmosphere at sample(A) and in 90%N₂-10%O₂ atmosphere at sample(B) respectively. As can be seen in Table-1, the resistivity of the based semiconduction ceramic was 0.11 $\Omega \cdot cm$ at sample(A) or 0.09 $\Omega \cdot cm$ at sample(B) respectively.

The grain size of the based ceramic found at 1450°C was 18-25 μm in average and was almost the same to that of sample(A).

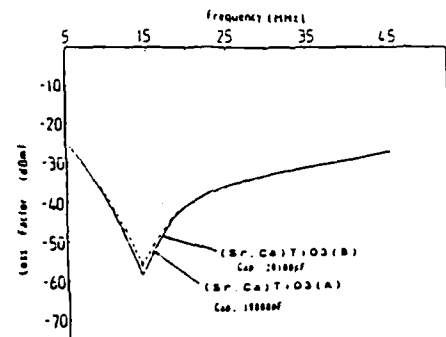


Figure-2 Frequency dependence of (Sr,Ca)TiO₃ Ceramic Varistors

The impedance at the resonant frequency of samples were 120 Ω at sample(A) and 85 Ω at sample(B), respectively as shown in fig -2. These results seem to indicate that the resistivity of the based semiconductive grains of sample(B) is evidently lower than that of sample(A).

Figure-3 I-V curve of the based semiconductive grains.

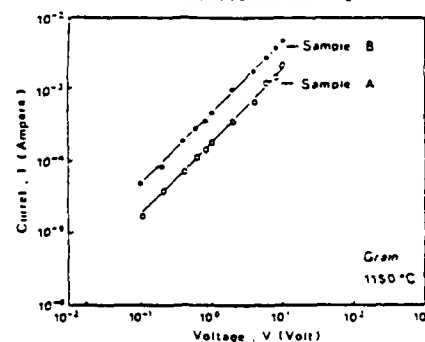


Figure-3 shows a I-V characteristics of the based semiconductive grains of sample(A) and (B). Au pattern was sputtered on the polished surface of a (Sr,Ca)TiO₃ based varistors for the measurement of the I-V curve using a micro manipulator method as shown in Figure-4. The surface resistance of the grain measured at 1Vdc were 1 k Ω at sample(B) or 5.5 k Ω at sample(A) respectively. If let us suppose the measured surface area (20 \times 10 μm^2) as a volume (20 \times 10 μm^3) approximately the resistivity of the grain is calculated. These are 0.42 $\Omega \cdot cm$ at sample(B), or 1.10 $\Omega \cdot cm$ at sample(A), respectively.

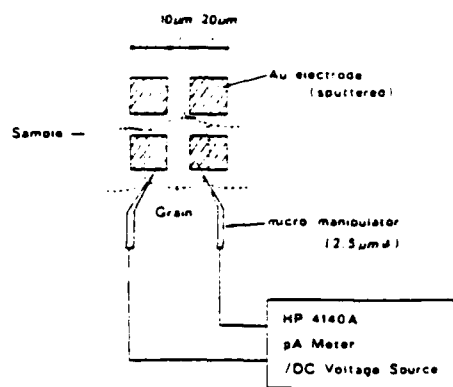


Figure-4 Micro-manipulator method for measurement of I-V curve of the grain.

Figure-5 V-I characteristics

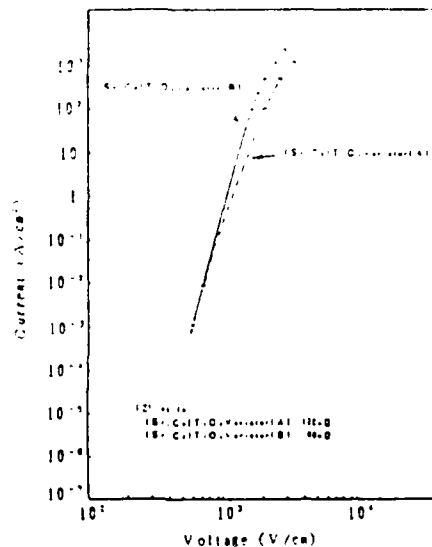
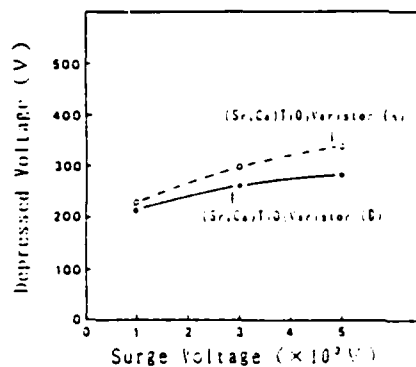


Figure-5 shows a I-V characteristics of sample (A) and sample(B). The I-V curve of both samples is almost the same line in a current region below 1000mA. However the I-V curve of sample(B) showed a more upright line as can be seen in fig. 5. This varistor can flow a current of 230A/cm² through the ceramics when the biasing of 2000 V/cm was supplied to a varistor. While, a calculated flowing current through a grain was as 230A/cm² as a supposition of a column grain roughly. This value seems to be corresponding to that in I-V curve of sample(B).

Figure-6 Supplied Surge Voltage vs. the depressed Voltage



Surge absorption capabilities of these samples were examined when various high impulse voltage (8/20 μs) were supplied to the samples. The results are shown in figure-6 when the impulse voltage of 5000V was supplied to samples. The depressed voltage was 340V at sample(A) or 230V at sample(B), respectively. The surge absorption capability of sample(B) was higher than that of sample(A) in a high surge region above 1000.

As a consequent, this difference of surge absorption capabilities between sample(A) and sample(B) is originated from the resistance of the semiconductive ceramic grains.

CONCLUSION

The impulse surge absorption capabilities of (Sr,Ca)TiO₃ based varistors were examined in the relation of other electrical characteristics. As the two samples were fabricated by the difference of the reducing atmosphere in the firing process of semiconductive ceramics.

As the results,

1. The resistivity of the basic semiconductive ceramics was $0.14 \Omega \text{ cm}$ at sample(A) or $0.09 \Omega \text{ cm}$ at sample(B), respectively.
2. The impedance at the resonant frequency of the ceramic varistors were $120 \text{ m}\Omega$ at sample(A) and $65 \text{ m}\Omega$ at sample(B), respectively.
3. I-V curve of sample(B) showed a more abrupt uprised line in a high current region compared with another one. Whereas, it was almost the same in the lower region below 1000V.
4. The surface resistance of the semiconductive grain was $2.1 \text{ K}\Omega$ at sample(B) or $5.5 \text{ K}\Omega$ at sample(A), respectively. It is supposed that a flowing current through the grain of sample(B) is ab. 250 A/cm^2 at 2000V roughly. This value seems to be corresponding to that in the I-V curve of the varistor.
5. When the impulse voltage of 5000V was supplied to samples, the depressed voltage was 340V at sample(A) or 230V at sample(B), respectively.

As a conclusion, it is considered that the difference of surge absorption capabilities between sample(A) and (B) is originated from the resistance of the based semiconductive ceramic grains.

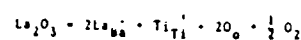
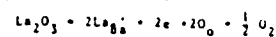
Defect Structure and Electrical Properties of La-Doped Barium Titanate

S. Shirasaki, H. Haneda and M. Sugimoto

National Institute For Research in Inorganic Materials, Tsukuba Science City

*T.D.K. Co., Ichikawa, Chiba

Reported Two Models



Our model

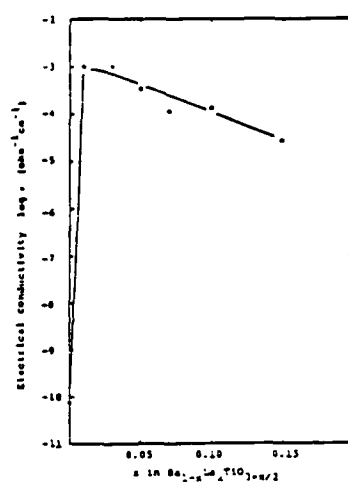
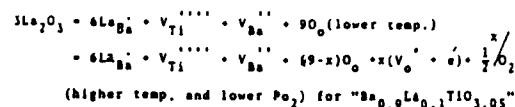


Fig. 1 Electrical conductivity as a function of x in composition $\text{Ba}_{1-x}\text{La}_x\text{TiO}_{3-x/2}$ sintered at 1350°C and quenched down to room temperature.

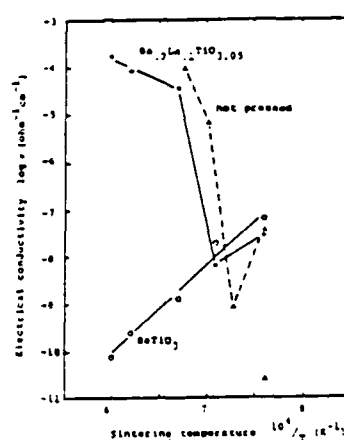


Fig. 2 Electrical conductivity as a function of sintering temperature ($1/T$) for quenched and hot pressed-quenched $\text{Ba}_{0.9}\text{La}_{0.1}\text{TiO}_{3.05}$ and quenched pure barium titanate.

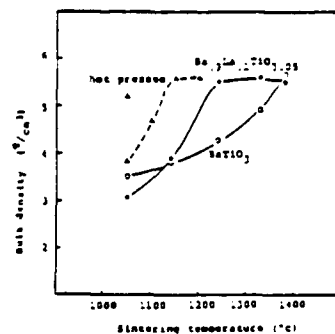


Fig. 3 Bulk density as a function of sintering temperature for quenched and hot pressed-quenched $\text{Ba}_{0.9}\text{La}_{0.1}\text{TiO}_{3.05}$ and quenched pure barium titanate.

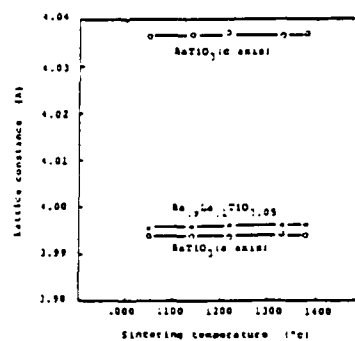


Fig. 4 Lattice constant as a function of sintering temperature for quenched $\text{Ba}_{0.9}\text{La}_{0.1}\text{TiO}_{3.05}$ and pure barium titanate.

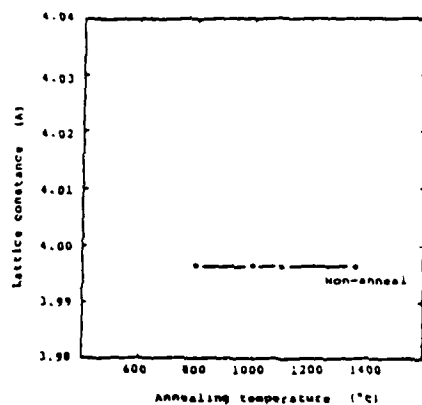


Fig. 1. Lattice constant as a function of annealing temperature for $\text{Ba}_{0.9}\text{La}_{0.1}\text{TiO}_{3.05}$ sintered at 1380°C . Annealing period is one year respectively.

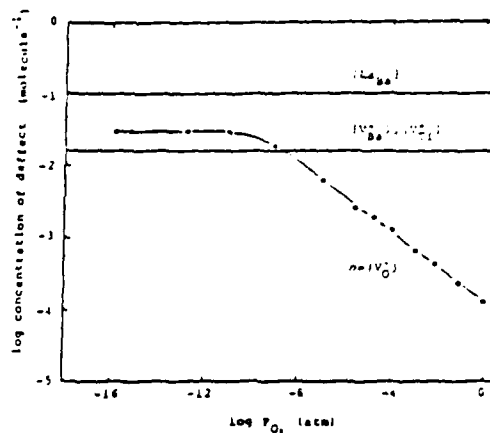


Fig. 12. Calculated concentrations of point defects as a function of P_{O_2} of La-doped material. The level of V_{O} was calculated from measurements and assuming $n = [V_{\text{O}}]$ and $\mu = 0.3 \text{ eV/sec}$.

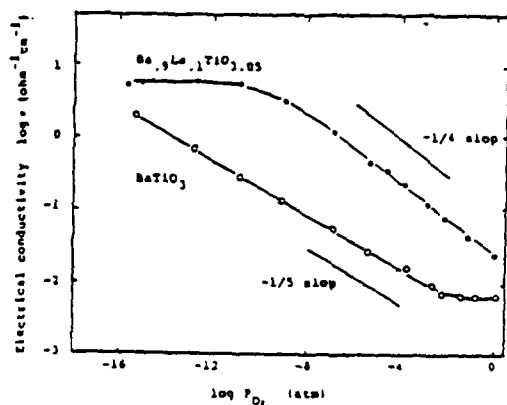


Fig. 11. Electrical conductivity as a function of P_{O_2} for $\text{Ba}_{0.9}\text{La}_{0.1}\text{TiO}_{3.05}$ and pure barium titanate at 1200°C .

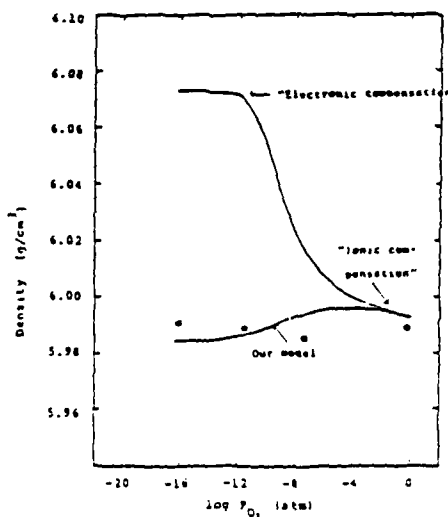


Fig. 13. Calculated densities as a function of P_{O_2} for $\text{Ba}_{0.9}\text{La}_{0.1}\text{TiO}_{3.05}$ on a basis of two models. One is based on a preferential occurrence of "electronic compensation" at lower P_{O_2} and ionic compensation at higher P_{O_2} and another, our model. Closed points are observed densities.

W22

DETERMINATION OF A COMPOSITIONAL FLUCTUATION IN PEROVSKITE TERNARY SYSTEMS

Chiba University

K.KAKEGAWA and Y.SASAKI

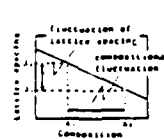
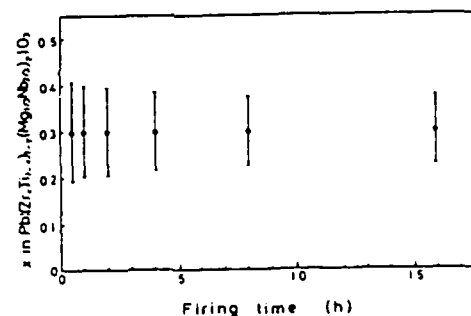
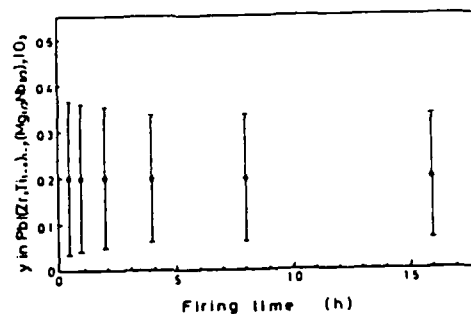
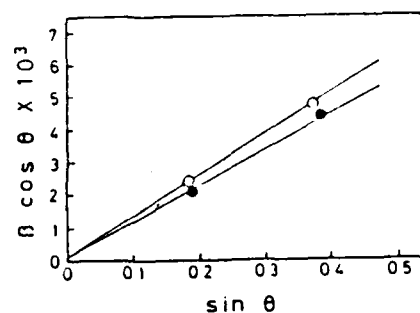
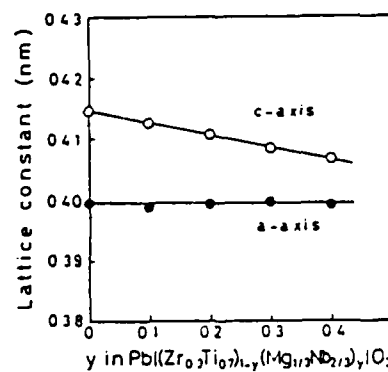
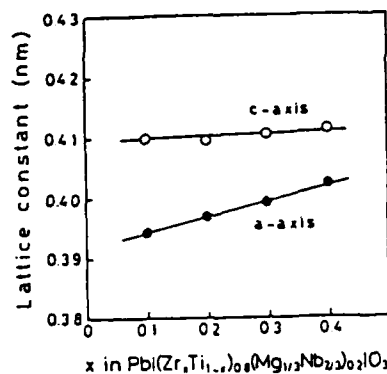
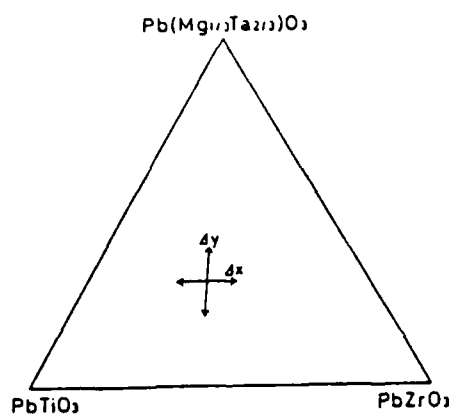


Fig. 1 Relation between fluctuation of lattice spacing and that of composition

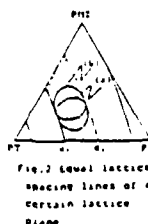


Fig. 2 Equal lattice spacing lines of a lattice plane

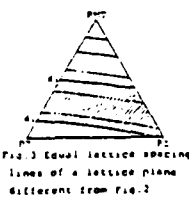


Fig. 3 Equal lattice spacing lines of a lattice plane different from Fig. 2



Fig. 4 Isothermal curves of a-spacing

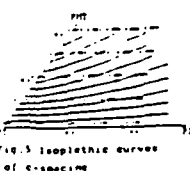
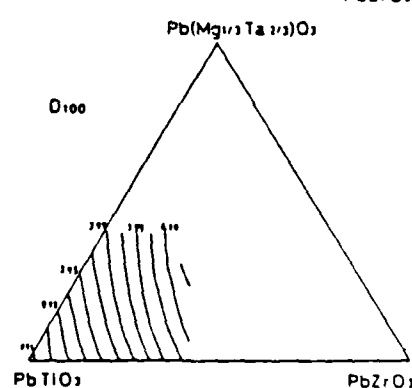
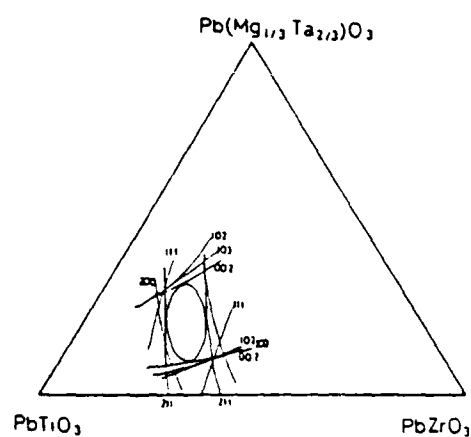
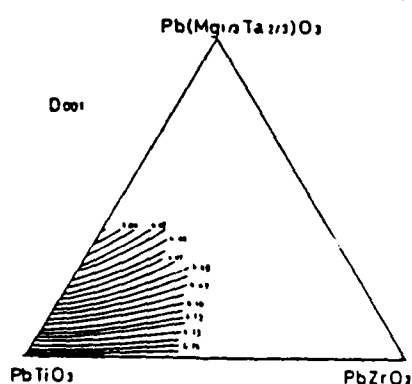
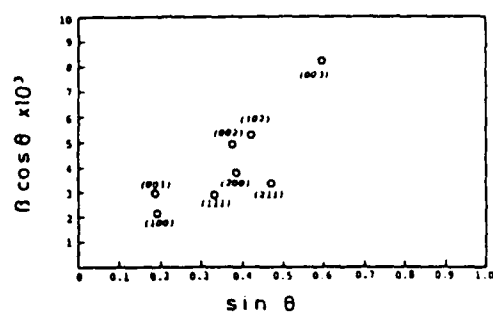
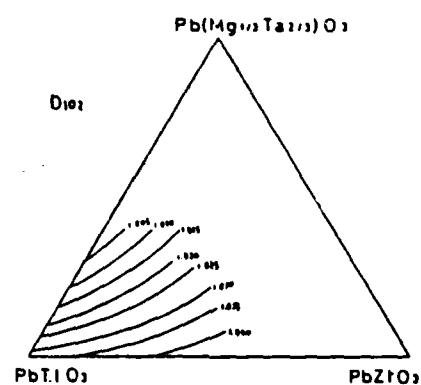
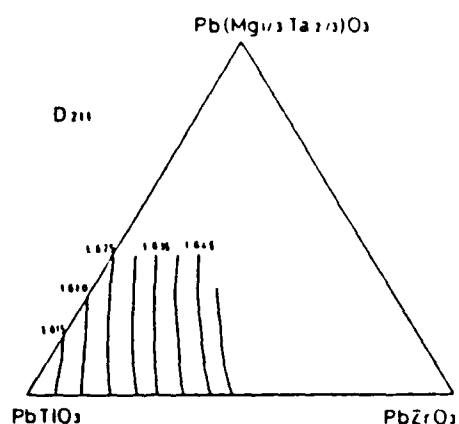
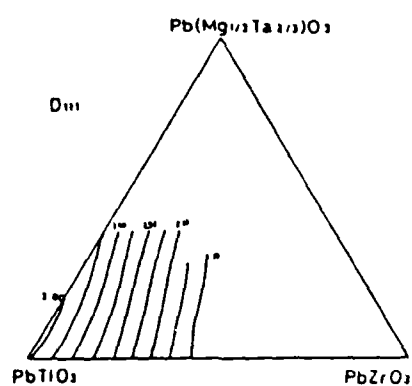


Fig. 5 Isothermal curves of c-spacing



Fig. 6 Compositional fluctuation region estimated for PTTT (1200°C, 3h)



PROPERTIES OF THE AlN CERAMICS

T. TAKAHASHI, K. ANZAI AND N. TAKADA

New Materials Department, Toshiba Corp. Tokyo, Japan

K. SHINOZAKI

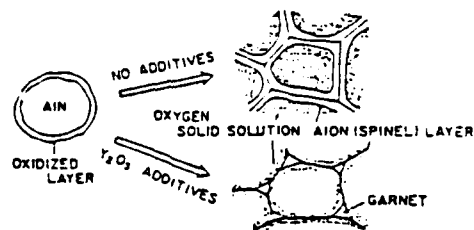
Metals & Ceramics Laboratory, R & D Center, Toshiba Corp. Kawasaki, Japan

Trends of Ceramic Substrates and Packages

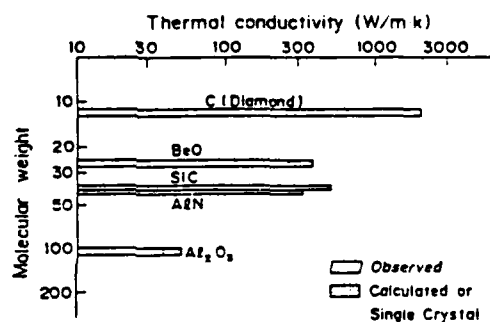
Trends of electronic equipments	Requirements to Substrate & Packages	Examples
High power	High thermal conductivity	AlN, DBC, BeO
Miniaturization	High density	Multi layered
High speed	Low dielectric constant	Glass/ceramics composite

RAW MATERIAL

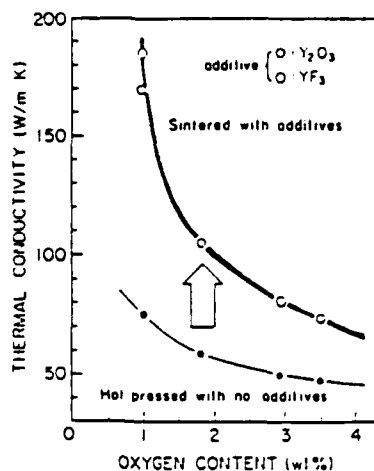
SINTERED BODY



HIGH THERMAL CONDUCTIVITY MECHANISM



Thermal Conductivity for Various Ceramic Materials



RELATION BETWEEN OXYGEN CONTENT OF ALN RAW POWDER AND THERMAL CONDUCTIVITY.

TOSHIBA

PROPERTIES OF CERAMICS FOR SEMICONDUCTOR SUBSTRATES

Item	Unit	AlN (Toshiba)	Al ₂ O ₃	BeO	SiC
Thermal conductivity	W/m K (RT)	170	20	250	270
Volume resistivity	Ω·cm (RT)	>10 ¹⁴	>10 ¹⁴	>10 ¹⁴	>10 ¹⁴
Dielectric strength	kV/cm (RT)	140~170	100	100	0.7
Dielectric constant	ε (RT, 1MHz)	8.8	8.8	6.5	4.0
Dielectric loss	10 ⁻⁴ tan δ (1MHz)	5~10	3	5	500
Thermal expansion coefficient	10 ⁻⁶ /°C (RT~400°C)	4.5	7.3	8	3.7
Density	g/cm ³	3.3	3.9	2.9	3.2
Young's modulus	10 ⁴ kg/mm ²	2.8	3.7	3.2	>4.8
Flexural strength	kg/mm ²	40~50	124~261	17~23	45

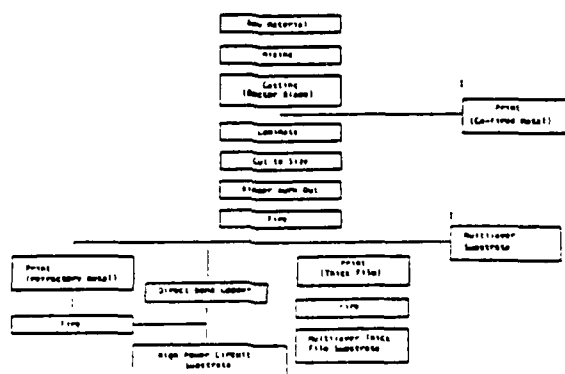
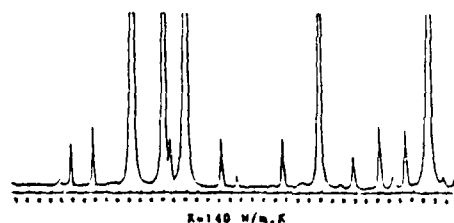
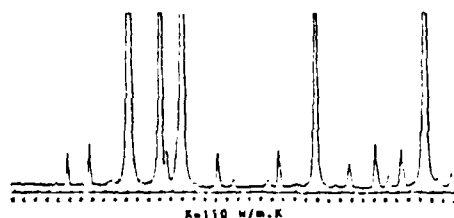
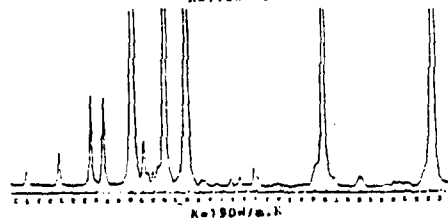
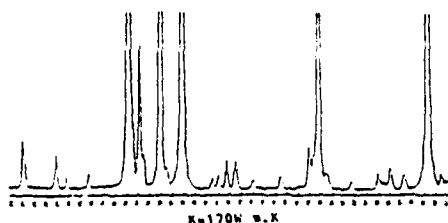


Fig. 2 Flow Chart for AlN Substrate

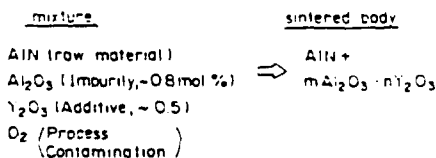


X-ray diffraction pattern



Microstructure of the AlN ceramics

(Reaction)



Thermal conductivities and compounds in the AlN ceramics

K - value	Compounds
110 W/m \cdot K	YAG \rightarrow AlON
140	YAG
170	YAL \rightarrow YAG
190	YAM \rightarrow YAL \rightarrow YAG
235	Y ₂ O ₃ \rightarrow YAM

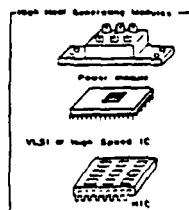
YAG : 3Y₂O₃ : 5Al₂O₃

YAG : Y₂O₃ : Al₂O₃

YAM : 2Y₂O₃ : Al₂O₃

- Molar fraction, Y₂O₃/Al₂O₃ has the probability to be a good index to estimate thermal conductivity and to judge the whether the manufacturing process is appropriate or not

Suggested applications

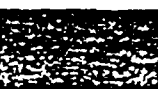


- Power transistor module
- Laser diode heat spreader
- Power hybrid IC substrate
- LSI, VLSI package
- Electrical insulator with high thermal conductivity

AlN Substrates and Applications



(K ~ 180)



(K ~ 70)

Bare substrates



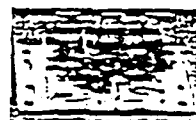
Mo metalized



Au thick film



DBC
(Direct Bonded Copper)



Giant transistor



Power amplifier



Chip carrier

W24

NEW GENERATION PZT - POLYMER COMPOSITE MATERIAL FOR HYDROPHONE APPLICATIONS

IAN BEDWELL AND EDENER JANDERA

Plessey Australia Pty. Ltd., Electronic Systems Division, Meadowbank, NSW,
2114, Australia.

GEOFF GILLMAN

Weapons Systems Research Laboratory, Defence Science and Technology
Organization, Defence Research Center, Salisbury

ABSTRACT: A PZT Polymer Composite Hydrophone Matrix has been developed. In comparison to other new generation materials, it has the highest acoustic performance. External tests have been performed by N.R.L., Orlando, U.S.A. and Plessey Naval Systems (P.N.S.), U.K. to assess the materials for Navy Hydrophone Applications. The Data as presented here show promising performance.

1. INTRODUCTION

Traditional Lead Zirconate Titanate (PZT) Hydrophones and Sensors utilize geometry and specialized designs to obtain their acoustic performance. However, they have drawbacks of fairly high density, rigid and somewhat brittle in nature, even though they are very well understood and are produced in enormous quantities. Lately there have been several new generation materials available, which have made the concept of Isotropic large area Hydrophones, feasible at a realistic cost. In addition flexible hydrophones for specialised application in towed arrays are also possible. The "New Generation" materials have been thoroughly studied in the literature and cover materials such as :

- Piezoelectric Polymers (PVDF, etc.)
- Piezoelectric Ceramics (Lead Titanate, Lead Meta-niobate, Crystallised Glasses, etc)
- Polymer/Piezoelectric Ceramic Composites.

The initial composite work was initiated and recently reviewed by R.E. Newnham at the Pennsylvania State University, P.A. ¹, where a thorough fundamental investigation is continuing. Different geometric combination of Ceramic/Polymer have been tried by various groups around the world, these are termed connectivities by the Pennsylvania State Workers who pioneered the concept. For a two phase system of Ceramic PZT and Polymer, there are ten different connectivities. Evaluation of some new Piezoelectric Composite materials for hydrophone applications have been published by R. Y. Ting ², in

which five of the ten types of Piezoelectric Polymer Ceramic Composites out of the ten are assessed. Properties are presented in Table 1.

2. PLESSEY AUSTRALIA COMPOSITE

Plessey became active in the manufacture of large components where our expertise in the formulation and fabrication of PZT Ceramics could be utilized. The combination adopted by us is the 1-3 connectivity with ceramic pegs embedded in polymeric phase. In house formulated piezoelectric ceramic and a modified polymer were used to produce the Composite. Volume fraction of PZT ranged from 16-20% with a nominal peg size of 1mm³ cross sections.

Comparison of Plessey Composite with other types of composites is shown in Table Two (Private correspondence with N.U.S.C.).

Three Hydrophones designated as P1, P2, & P3 were sent overseas to gain an unbiased evaluation of the performance of these Hydrophones. A schematic outline of the Hydrophone is shown in Figure 1.

Two Composite Hydrophones, P1 and P2 were sent to the Naval Research Laboratory, (N.R.L) Underwater Sound Reference Detachment, Orlando, Florida, U.S.A. for testing. Then P2 and P3 were sent to Plessey Marine, Templecombe, (PMT) U.K. who internally arranged for testing with Test Results on P1, P2 and P3, the Admiralty Research Establishment, Portland, U.K.

3. BEAMPATTERNS

Beampatterns were performed at 10 and 11.6 kHz which is near the first null of the edgefire response. Samples P1 and P2 were tested at N.R.L., Orlando, at 30°C whilst P3 was measured at Plessey Marine (P.M.T.) at about 18°C. These results are shown in Figures 2 & 3. As well P.M.T. measured P3 at 5, 7.5, 9, 15, 20, and 100 kHz. These results are shown in Figure 4.

4. RECEIVER SENSITIVITIES

The open-circuit receiver sensitivities of P1 and P2 were measured at 30°C at N.R.L., with the Hydrophones oriented at 0° (broadside) and 90° and 270° (edgefire).

The results for P1 are shown in Figure 5. P2 and P3 were also tested at P.M.S. and the results are as shown in Figure 5.

5. TEMPERATURE AND PRESSURE DEPENDENCE OF SENSITIVITIES AND CAPACITANCE

The receiver sensitivities and capacitances of the Hydrophones P1 and P2 were measured at N.R.L. at 4°C and 29°C with pressures of 35 kPa, 3.5MPa and 13.8MPa. The results of P1 are shown in Figure 6&7

6. ACCELERATION SENSITIVITY

Acceleration sensitivity has been measured at P.M.D. on P1 and P3 and typical result is shown in Fig. 6.

EXPLOSIVE SHOCK

Hydrophone P1 has undergone explosive shock testing at N.R.L.

7. DISCUSSION

The beampattern results show that the Hydrophones act as a theoretical aperture of their major dimension, as the beampatterns show good cartoid shape near the first null. Hydrophone P1 had a fault which manifested itself as a higher dissipation factor and an asymmetric extra lobe on the beampattern at 170° in Figure 3.

The sensitivity results show that at low frequencies the Hydrophones have a flat response. There was a resonance problem with these early Hydrophones that manifested itself as a very well defined resonance at about 6.5 kHz. This problem has since been resolved. The high frequency response is a good approach to the theoretical $\sin x/x$ behaviour of an aperture as the edgefire response indicates.

The temperature and pressure dependance of the Hydrophones indicates that the design will need some modification if the response is to be unaffected by extreme pressures. The ceramic used is relatively soft Type 2 which could be replaced by the harder types 1 or 3 which would then reduce both the pressure and temperature variations. The fact that the results were reproducible, and that the sample which underwent explosive shock testing survived with no apparent change in performance indicates the physical integrity of the design.

The acceleration sensitivity of the Hydrophone shows strong structural resonance of the mounting plate, however at low frequency it is at least 13 dB and probably >20 dB less than the output level due to fluid loading on the transducer. No special acceleration cancelling features were incorporated into this design. Although the work presented here refers to large hydrophones, development is continuing into the production of alternative configurations. Plessey Australia is associated with W.S.R.L. in the co-operative development of a small diameter towed array which incorporates flexible hydrophones. Projected performance indicate that the composite may be ideally suited for the towed array in that it may be possible to tailor over a wide range many performance criteria such as sensitivity, acoustic impedance and flexibility.

8. ACKNOWLEDGEMENT

The authors would like to thank Dr. R. Ting of N.R.L. Orlando for testing of P1 and P2 hydrophones. The authors would also like to thank A. Curtis of Plessey Marine U.K. for tests on P2 and P3 hydrophones. The effort by Mr. R. Roberts of A.R.E. is also appreciated.

9. REFERENCES

1. R. E. Newnham, Ferroelectrics 68, 1 (1986)
2. R. Y. Ting, Ferroelectrics 67, 143 (1986)
3. R. Y. Ting, A. Halliyal and A. S. Shalla, Appl. Phys. Lett., 44, 952 (1984)

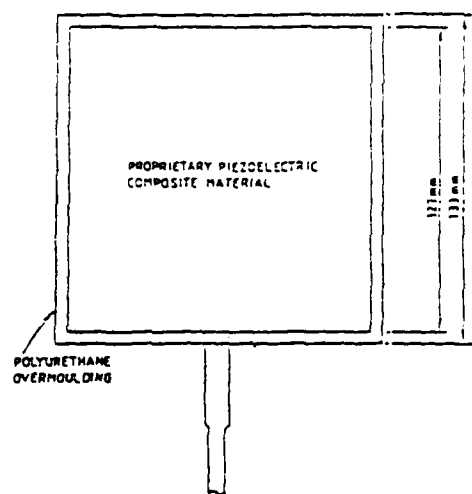


FIGURE 1 - PLESSEY AUSTRALIA COMPOSITE HYDROPHONE OUTLINE

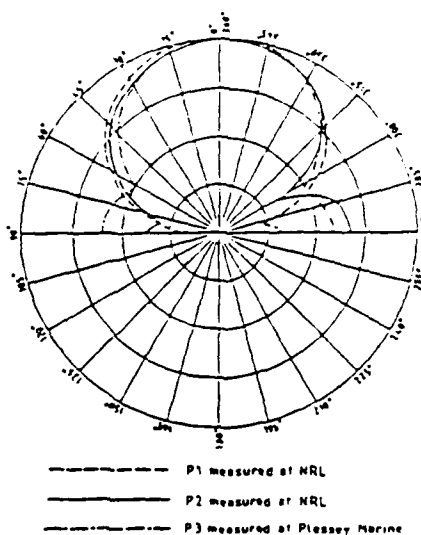


FIGURE 1 - BEAMPATTERNS AT 11.6 KHZ

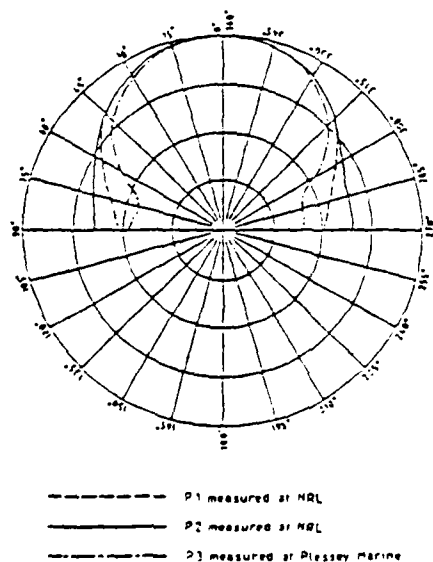


FIGURE 2 - BEAMPATTERNS AT 10 KHZ

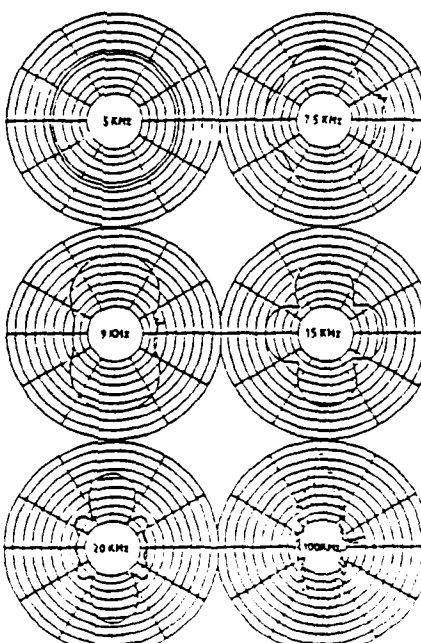


FIGURE 3 - BEAMPATTERNS FOR HYDROPHONE P1 MEASURED AT PLESSEY MARINE

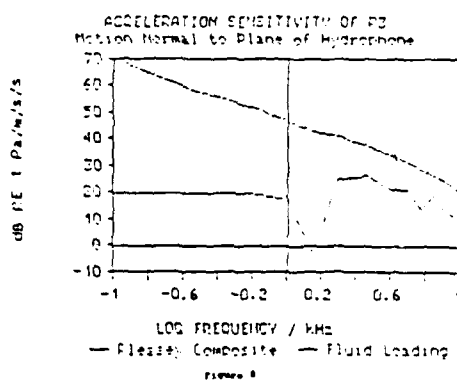
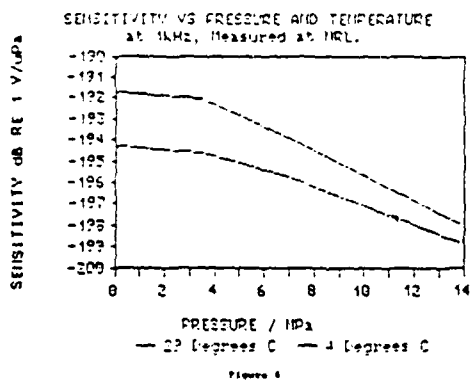
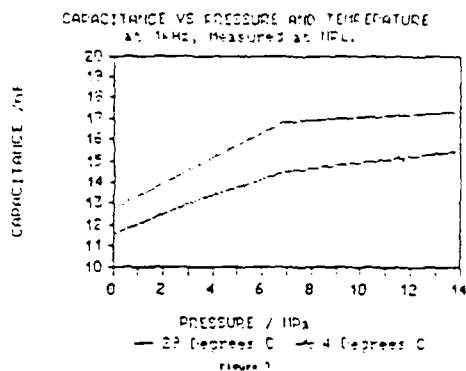
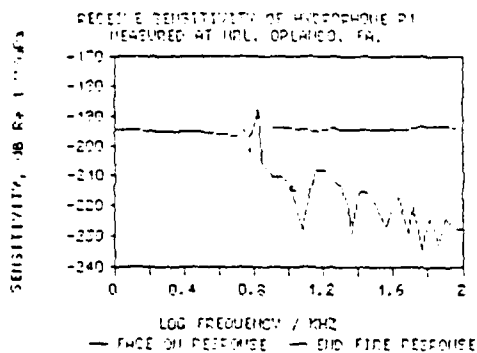


TABLE 1

(TABLE 11 IN REFERENCE 2)

Piezoelectric and Dielectric Properties of
Polymer-Ceramic Composites

Sample	d_{33} (pC/N)	d_{31} (pC/V)	d_{32} (pC/V)	K	Dissipation
P27-4	43	4	172	1300	0.02
P27-5	21	2	42	1690	0.02
3-1 Element	220	72	15,840	356	0.05
3-1 Composite	176	21	3,596	965	0.03
3-3 Composite	13	25	325	69	0.03
3-2 Composite	123	52	7,965	360	0.02
3-3 Composite a	32	50	1,600	200	0.02
3-3 Composite b	22	47	1,034	34	0.06
PVDF ^a	10	112	1,120	10	0.01
3-3 Composite d	100	100	20,000	226	0.015

a) Porous P27 from the Mitsubishi Mining & Cement Corporation, Japan.

b) NTK Plasto-Rubber.

c) Data from Reference 3.

d) Plessey Australia Pty., Ltd.

TABLE 2
HYDROSTATIC MODE PROPERTIES

Property/ Sample	(1)		t um	tan	g _h (mVm /N)	d _h g _{b2} 10 ⁻²² (M ² /N ⁻¹)	Comments
	K _T 33	Mv dB re V/upa					
EMI	8.5	- 198.6	600	.02	195.0	2.90	PVDF
PENNWALT	11.0	- 202.5	750	.02	100.0	1.00	PVDF
EDO	205.0	- 198.0	5000	.007	25.0	1.10	PBTiO ₃
NGK	38.0	- 197.0	3000	.03	58.0	1.10	Composite
PLESSEY	232.0	- 191.0	3000	.02	94.0	18.00	Composite
BELL LAB	4.3	- 199.0	3000	-	35.0	0.05	Tartaric Acid
BERLINCOURT	295.0	- 194.0	3000	.005	66.0	11.40	Sponge * Ceramic
PSU	98.0	- 194.0	3000	-	69.0	4.10	PZT/Epoxy.
PSU	44.0	- 181.0	3000	-	314.0	38.00	PZT/Foam + Urethane.
JAPAN	183.0	- 181.0	9800	.02	91.0	13.40	Porous Ceramic.
33082A	386.0	- 195.0	2800	.02	64.5	14.20	NRL Porous.
TYPE I	1300.0	- 218.0	3000	.004	4.0	0.20	MIL-STD 1376.
PbNb ₂ O ₆	225.0	- 200.0	3000	.006	34.0	2.30	Lead Meta Niobate.

- (1) Mv = g_h.²
- * Calculated.
- + Highly pressure dependent.
- ** Values for STP.



UNIVERSITY OF MISSOURI-ROLLA

School of Mines and Metallurgy

Department of Ceramic Engineering

January 14, 1987

Rolla, Missouri 65401
Telephone (314) 344-3400

TO: R. C. Pohanka
Office of Naval Research
and
S. Freiman
National Bureau of Standards

FROM: H. U. Anderson
University of Missouri-Rolla

SUBJECT: Report on Trip to Japan to Attend U.S.-Japan Seminar on
Dielectric and Piezoelectric Ceramics

I arrived at Narita at 5:00 p.m. on November 2, 1986 and was met by T. Tsukamoto who escorted me to Yokohama. On Tuesday, November 4, I spent the day at TechnoPatent Services where I presented a lecture and discussed U.S.-Japan patents. These discussions were directed at learning the patent procedures in Japan and how they differed from the U.S. It is apparent that the requirement of the U.S. patent office that the patent must be sufficiently detailed so that someone versed in the field can reproduce the patent is not true for the Japanese patent office. I also learned that a literal translation of a Japanese patent into English loses so much that the important teachings of the patent can be easily lost. In order to make a meaningful translation, the translator must understand the patent so that the correct meaning can be conveyed into English. These are probably the primary reasons that it is so difficult to reproduce the results quoted in Japanese patents.

On the morning of November 5 I traveled to Tsukuba City to visit the Applied Physics Department at Tsukuba University. I presented a lecture there and discussed order-disorder phenomena with Professor Tetsuro Suzuki. Our thermally stimulated current work which was previously sponsored by ONR and some of our subsequent automodulation work on PLZT, BaTiO_3 , and PMN was of great interest to Professor Suzuki because it indicates that the theories which he and Dr. Wuttig have on the martensitic type transformations may be applicable to nonmetallic solids. We are planning to initiate an interaction between my research group and Suzuki's group in order to further explore this effect. The initial interaction will be to share samples and data.

On November 6 I visited NIRIM in Tsukuba City. My host there was Dr. S. Shirasaki. I presented a seminar there and discussed defect chemistry with Dr. Shirasaki. This was my first visit to NIRIM and I came away very impressed by both the facilities and the personnel. They discussed with me a number of studies that they are doing. In particular, their work on oxygen diffusion in MgO and Al_2O_3 were of interest. There is a fundamental study in ZnO varistors in which an attempt to understand the grain boundary

structure is being made. The 10th group is working on optical waveguide materials. They had previously worked mainly on LiNbO_3 and LiTaO_3 , but are concentrating on $\text{Ba}_2\text{NaNb}_5\text{O}_{15}$ crystals both as films and bulk crystals. The BNN crystals are of interest because they have high transmission efficiency (~75%) and may be useable for pattern drawing in VLSI since they transmit green light well.

I was told that some perovskite oxide preparation techniques which have been developed at NIRIM are currently being exploited by Japanese industry to make theoretically dense perovskites, but no further information was offered due to secrecy restraints.

I was shown a number of AIN parts which had been made as a result of work at NIRIM. The substrates were translucent. NIRIM is no longer doing work on AIN, but did the initial studies which have lead to important AIN products.

On the evening of November 6 I traveled to Kyoto to visit Murata Manufacturing Co. Dr. Wakino served as an excellent host. I spent November 7 at the Central Research Laboratory of Murata. During my visit I presented a lecture and participated in general discussions on dielectrics. There was particular interest in thin film dielectrics. Y. Sakabe took me on a tour through their research facilities and showed me nearly everything they were doing. There was nothing particularly extraordinary in their facilities, but it was obvious that they are committed to product development and control. The work that Murata is doing in the area of microwave dielectrics is probably their most significant research area. They certainly appear to be the leader in this area.

From November 9 to the 12th I participated in the U.S.:Japan Seminar. I think that Drs. Yamaguchi and Freiman need special commendation for the outstanding facilities and the program format. This was our 3rd seminar and the format of each program has been different. The format of this program was superior to the previous endeavours. I suggest that it be retained. However, some attention must be put to the "roundtable discussions" since improvements are needed there.

The facilities that were provided by YKK were by far the best we have had. I want to express my personal thanks to YKK for the facilities and the hospitality.

I thought the papers presented at the conference were good and probably represented much of the current Japanese activity. The efforts in sputtering and actuators were of particular interest. From my viewpoint Japan definitely leads in these areas.

What did I learn at this meeting?

- 1) The Japanese have made tremendous strides towards component integration and in the development of sensors and actuators. In my discussions with individuals regarding these activities it is evident that many research organizations are devoting considerable resources to these areas. Japan is the clear leader in these areas. If we are to have any hope of keeping up in these areas our research and development activities must be expanded.

2) The AIN substrate work which is being done in Japan is first rate and certainly is showing the feasibility of this material for use as a substrate where high heat dissipation is required.

3) The Japanese are very interested in all methods for making oxide films. This apparently is a high priority research area since it is important to component integration. The U.S. is still competitive in this area, however we need to expand our efforts if we expect to remain a leader.

4) In the area of oxide synthesis, I think that the U.S. is still very competitive. I had several discussions regarding perovskite oxide synthesis which is an area where my research spends considerable time and learned that my knowledge in the field is as good as my Japanese counterparts. However, I must emphasize that the Japanese are moving fast and we will have to expand our efforts and knowledge both in the science of organic-metallic synthesis of oxides and in the implementation of our laboratory knowledge to production if we are to remain a leader.

5) In the area of dielectric materials the level of knowledge of the Japanese and U.S. participants was quite comparable except in the area of microwave dielectrics where Murata is the clear leader. I think the knowledge of the science of dielectric materials in the U.S. is superior to that in Japan, but Japan clearly leads in the area of implementation.

On November 12 I traveled from Toyama to Tokyo. On November 13 I visited with Toshiba Ceramics in Hanada City. There I presented a seminar and toured the research facilities. At this facility I saw the first 8" dia. Si single crystal boule that I have seen. It was very impressive since the puller has incorporated with it a super conducting magnet which provides the field to homogenize the melt. I also saw some very dense AIN substrates and AIN powder. Evidently Toshiba Ceramics is spending considerable effort to produce low oxygen content and sinterable AIN powders.

On November 14 I presented a seminar at Nihon Seiji Keizai Chosakai in Tokyo which is an organization of Japanese businessmen sponsored by the Japan Ministry of Education. In this presentation I discussed the status of high technology ceramics in the U.S.

On November 15 I left Japan and returned home.

I came away from Japan with the same opinion that I had four years ago. We are technically equal or superior to the Japanese, however we fall short in the area of implementing a laboratory concept into a product. I feel that this difference is due to a basic difference in the middle management of companies in the two countries. In the U.S. our managers have to have a product line profitable (<10%) in time periods anywhere from 6 months to 3 years. In Japan they think of product profitability in the 5 to 10 year range. They appear to worry more about market position rather than profits.

I found the Japanese to be much more relaxed than they were four years ago. This was especially true at Murata Manufacturing who were very quick to announce that they were now the number one MLC manufacturer in the U.S.

It is apparent that they feel now that they have won the battle in the U.S. and view their major competition as being Japanese.

I feel that the Japanese have progressed well in the area of component integration, actuators, and sensors. They certainly are the leaders in these areas. We are going to have to hustle in these areas to even keep them in sight.

Thank you very much for the chance to visit Japan. I found it very worthwhile.

Yours truly,



Harlan U. Anderson

HUA/lp

TRIP REPORT: U.S.-Japan Seminar on Dielectric
and Piezoelectric Ceramics
November 9-12, 1986, Toyama, Japan

B. A. Auld
Edward L. Ginzton Laboratory
Stanford University
Stanford, California 94305

I. Purpose

These U.S.-Japan seminars are biannual meetings between U.S. and Japanese materials and applications scientists and technologists, held alternately in the U.S. and Japan. The 1986 seminar was the third in the series. My responsibilities were to participate in the presentations as an invited speaker, to be present in discussion groups as a lead and panelist, and to be briefed on the research programs at selected Japanese laboratories (in my case, NEC and Hitachi—both in Tokyo).

II. Seminar (November 9-12)

(a) Presentations

The talks and poster sessions were held in the magnificent Conference Center of YKK Company in Korubu City. In the main lecture hall the technological level of the audio-visual facilities was truly awesome, as was the esthetic level of the decor. The organizational structure of the presentations was innovative and efficient.

Two general papers (one American and one Japanese) were given in the first session. These clearly reflected the general tone of the meeting and the distribution of the attendees. The American paper, presented by a professor, was very physics-oriented; the Japanese paper, presented by an industrial technologist, was at a very practical manufacturing level. Most of the members of the U.S. delegation were from universities, with only a few from industry; in the Japanese delegation the contrary was true. One Australian scientist, with an interest in composites for sensors, was present.

The poster session organization was very original in that each author gave a five minute slide summary of his poster in a joint session, held before each poster display presented in the corridors of the building. This was an excellent idea, but the short verbal presentations were very

mixed in quality. Many of the Japanese presentations were of poor quality, even allowing for the difficulty of speaking in a foreign language. I had the impression that a number of the Japanese authors were there to practice giving talks at an international meeting. The American speakers were generally older and more experienced.

The posters themselves were mainly oriented toward material science (fabrication and characterization of ceramics, where the Japanese excel). At the seminar itself the Japanese attendees appeared to be very open about giving details of their work (processing, etc.). This was also the opinion of my ceramicist colleagues. The same was, however, not the case for one of the subsequent industrial visits. I am not qualified to judge materials-oriented posters; but I gave careful study to those posters dealing with applications. These dealt almost exclusively with simple mechanical devices—actuators, punches, etc. One or two (both U.S. and Japanese) had to do with acoustic transducers. For me, the most useful exposure was to the work on ferroelectric thick film technology by both Japanese and American scientists. I saw several posters dealing with this subject and listened to some lively discussions on the merits of the techniques currently used (sputtering (NEC and Kyoto), sol-gel (U. of Illinois), precursors (Purdue University)). This appears to be a technology that will have an impact on acoustic transducers (both conventional and programmably-biased electrostrictors) for signal processing applications.

A striking feature of the attendance list was the absence of scientists and engineers concerned with high-tech device applications (signal processing, imaging, etc.), and this was most pronounced in the American delegation. This question was discussed by the U.S. group at an evaluation meeting at the end of the last day. Attempts had been made to invite scientists from U.S. industry, but most were unsuccessful. The conclusion was that industry felt they would give more information than they received. However, it was very clear from the Japanese presentations that they are very busy developing and commercializing products based on ideas originating in the U.S. and not being developed here. It was the sense of the group that U.S. industry could profit from observing first-hand what is going on in Japan and should be encouraged to send delegates to the next seminar (1988), to be held in the U.S.

(b) Discussion Groups

I was one of the panel members at the evening roundtable discussion on piezoelectrics. This began with Professor Cross first asking the members of the group to state the topics they wished to see discussed. Consistent with my above comments, most of the Japanese proposed very practical questions about the engineering properties of materials and their applications for very well-defined purposes, such as electrostrictors for actuators. There was a very strong interest in composites and ceramics.

with anisotropic coupling. A very lively discussion took place on the mechanism for variations in d_{31} and their relation to Poisson's ratio. This was at quite a basic level and involved both the U.S. representatives and the few Japanese representatives from the universities.

III. Industrial Visits (November 13 and 14)

(a) NEC

We were received with great hospitality, but the technical information provided about the company's activities was somewhat less detailed than at Hitachi, where we actually visited the laboratories.

In the morning we were given presentations about the organizational structure, were taken to the showroom for a short video presentation and a tour of the product display. We then heard talks on AlN ceramics for cooling chips, multilayer glass ceramics and monolithic multicomponent ceramics, and the ceramic ink-jet head; and, after lunch, talks on diamond-like thin films and low-firing dielectrics. We were able to examine material samples and were given reprints of papers related to the talks, as well as reprints concerning other activities of the company (underwater transducer arrays, ceramic filters, etc.). The day concluded with a presentation by each U.S. visitor of his Toyama Seminar paper.

(b) Hitachi

As at NEC, the day began with a general briefing on the laboratory activities and a tour of the exhibition room. This was followed by a series of laboratory presentations by members of Dr. H. Takeuchi's ultrasonics group. These covered the following topics: piezoelectric composites, covering their flexible composites and demonstrating their use in loudspeakers, piezoelectric crystal growth, growth of $PbTiO_3$ thin films, covering the details and effects of growth over metal electrodes, ultrasonic microscopy, and sound velocity measurement in biosystems, an ingenious signal processing technique. For the remainder of the afternoon I discussed acoustic waves in solids with a group of engineers, while the rest of the U.S. visitors visited groups doing materials research on LaB_6 and $TiSi_2$.

IV. Visit to Sophia University (November 15)

On Saturday, before returning to the U.S., a number of us paid a brief visit to Professor Kenji Uchino to see his research on ceramic electrostrictors and their use in actuators. This was very impressive. First, we had lunch with Uchino, his students and industrial visitors (about 30 people in all). This group spends every Saturday morning

attending a seminar by someone from industry and having technical discussions—an indication of the serious effort the Japanese put into their work. After lunch we visited Uchino's laboratories and collected reprints of his work. Uchino predicts that the electrostrictive actuators will eventually replace solenoids in many industrial applications. This is a prime example of where Japan is developing commercial outlets for materials first researched in the U.S. Uchino gave me a copy of his new book on materials and actuators (in Japanese), a book that sold out its first edition of, possibly, a few thousand copies in three months. It is now in its second edition and he has plans to come out with an English translation. This would be extremely valuable for U.S. industry and should be encouraged.

Third US-Japan Conference on Dielectric and Piezoelectric Materials

Toyama, Japan

November 9-12, 1986

Trip Report

R. C. Buchanan

University of Illinois

Dept. of Ceramic Engineering

Urbana, IL 61801

I. Introduction

Purpose of the trip was to participate in the technical presentations and discussions with the US and Japanese Ceramic scientists, which constituted the Third US-Japan Seminar on Dielectric and Piezoelectric Materials. It was hoped from this close interaction to make a critical evaluation of important trends in the development of these materials. A somewhat more pragmatic objective was to assess the advances in development and manufacturing of "Fine Ceramics" components in Japan.

The meeting was held in Toyama, which was not home to any of the Japanese participants, so that the closer interaction sought was indeed successfully accomplished. Regrettably, it also confirmed that most of the advances in manufacturing and utilization of ceramic dielectric and other state of the art

ceramic components was taking place in Japan.

Locations visited on the trip included Tokyo (4 days; Hitachi Corp., Science and Technology Agency), Toyama (4 days; site of the US-Japan Conference) and Nagoya (2 days; Narumi China, Japan Fine Ceramics Center and NTK-NGK Spark Plug Co., Ltd.). Assessments of these visits are included in this report. A side visit was subsequently made to China and is reported on in an addendum to this report.

II. Comments/Ohservations

1. Toyama Conference

The conference presentations were divided into sessions dealing roughly with Dielectric Processing (Session I), Dielectric Properties related to microwave, pyroelectric, mechanical and electrooptic applications (Session II) and Piezoelectric properties and applications (including miscellaneous topics (Session III)).

a) Processing

Emphasis in the processing session was primarily on chemical methods for the preparation and characterization of (mainly) BaTiO_3 type perovskite powders. Modifications in composition and processing to permit use of base metal electrodes (primarily Ni) in multilayer ceramic capacitors is now at the commercial stage. Both Murata and Taiyo Yuden offer these products. Likewise, studies on modification and processing of relaxor type formulations were very much in evidence. Glass-ceramic formulations for use as Cu-cofired substrates for MLC packaging was also a hot topic. This reflects the push for a more integrated packaging concept to achieve higher circuit density and

speed. Asahi glass, Central glass Co., Narumi China; Kyocera, NTK Ceramics and especially NEC are all active in this area.

b. Components

Microwave formulations for resonator and filter applications in the 1-20 GHz range were also featured by Sony, Murata and other companies. Development of microwave ceramic components is an area in which the Japanese have made significant strides, benefiting in many cases from vertical integration with their electronic consumer product lines. Emphasis in the development of the microwave formulations was on high dielectric constant (40-50), high Q and low temperature coefficient materials. Impressive Q values in the range of 8000-20,000 were reported.

Significant emphasis on the preparation of thin film PZT, PLZT and PbTiO_3 components was also noted. Deposition was mainly by magnetron sputtering using various control parameters. For PbTiO_3 this represents a significant advance, in view of the difficulty in preparing PbTiO_3 in any form without cracking. Projected uses for these films are as pyroelectric, piezoelectric or optical sensors and for device applications. Chemical (sol-gel) preparation of these films as is now common in the US (research), was not reported. Incidentally, Ca modified PbTiO_3 formulation (Ichinose-Waseda University) reportedly shows excellent potential for competing with or perhaps replacing LiNbO_3 for sensor applications. Even in the polycrystalline form, its large spontaneous polarization and coupling coefficients make PbTiO_3 an excellent piezo and pyroelectric sensor material. Overall, significant electrooptic use was envisaged for these sputtered films.

c) Piezoelectric Components

Significant activity in polymer PZT composites was reported. This now is

becoming a commercial product in Japan (Hitachi). Most important, is the recent and widespread development of PZT ceramic actuators. NGK and NEC (as well as others) now offer commercial PZT actuators for a wide range of motor applications. Much of this effort has developed from the pioneering work of Professor Uchino at Tokyo and now Sophia University. He presented a most innovative monomorph actuator based on charge coupled principles. Some interest in actuators based on electrostrictive ceramics was also in evidence as were formulations based on doped BaTiO_3 . This emphasis on ceramic actuators and its rapid commercialization surprised the US participants. We have no comparable effort in the US although the technology is well known.

Overall, the quality of the presentations and the technical interactions were excellent. It was noteworthy, however, that the emphasis in the presentations was quite different between the two sides. For the US participants, science and technological developments were the themes, compared to the decidedly product orientation of the Japanese participants. Our net gain, therefore was in seeing how many of the ideas developed in the US (polymer composites, relaxor formulations, thin film dielectrics etc) were being usefully applied in Japan. A topic worth pondering.

Plant Tours

1. Visit to Narumi China, Nagoya Japan

Narumi China is the largest manufacturer of fine china in Japan. This is carried out mainly at their factory in Nagoya. They also have a substantial position in the manufacture of thick film ceramic packages, although only the research and development facilities are located in Nagoya. I was given a tour of the china manufacturing line, which was mainly tableware. The process was substantially automated, but a significant amount of hand labor was required for such operations as attachment of handles and feet (cups, jugs etc.), decorating, inspectin, quality control and shipping. The equipment I saw was impressive and innovative, much of it being produced in the plant. Quality control, at all phases of manufacturing seemed to be a dominant emphasis.

The packaging effort was concentrated in three areas. First the development of screened Al_2O_3 substrates, some multilayer, for routine packaging applications. There did not appear to be any novelty about the materials used, but all operations - screening, firing, trimming, bonding, etc., were carried out in a clean room (Class II) environment and were significantly automated. Most effort was concentrated in this product area. Second, there was a strong effort in the manufacture of multilayer copper cofired packages. Dr. Nishigaki, research manager, was instrumental in this development, which is just now being marketed. The substrate composition is a glass ceramic (Al_2O_3 -glass-mullite) which sinters below $1000^\circ C$ in N_2 atmosphere. All processing operations were being carried out in a Class I clean environment. I would guess from the eager questions of the engineers that powder dispersion, binder burnout as well as tape casting were operations not fully under control. Finally, some development emphasis in producing AlN ,

SiC and Si_3N_3 substrates was clearly evident. AlN samples were being hot pressed above 1800°C using in house designed equipment. Most powders were commercially obtained. One gratifying note was that most test equipment used was supplied by Hewlett Packard.

2. NTK Technical Ceramics (NGK Spark Plug Co.) - Nagoya Japan

I did not actually tour this plant since the piezoelectric facility, which I wanted to see, was considered to be "in a very competitive position." I had previously toured the spark plug manufacturing plant in 1982. The sensitivity about the piezoelectric products derive from the fact that NTK is trying to establish a dominant position in piezoelectric stacks for actuators and linear motors, in composites, ultrasonic transducers, knock sensors and a wide range of sensor products. Many of these products require aggressive marketing development. NTK manufacture also a wide range of technical ceramic products including a turbocharger rotor (which is now being marketed) as well as other engine parts from SiC and Si_3N_4 . They have a very strong ceramic packaging effort with NEC as a major customer. I also noted a wide range of bioceramics products for use as implants and in prosthetic devices. Dr. Hisao Banno is in charge of the research and technical development effort.

3. Japan Fine Ceramics Center - Nagoya, Japan

Dr. Yoko Suyama (who was trained at MIT) was my host for the visit to the Center. I also met with the Executive Director and the Managing Directors for the Operating Divisions, namely: Administrative Affairs, Information and Public Relations, Education and Consultation as well as for Research, Testing and Development. The Fine Ceramics Center is an ambitious concept which is new even to Japan. The Center as a physical entity is just being completed

(due for occupancy in March, 1987). It consists of a brand new five story edifice which will house well equipped research laboratories, administrative offices, educational and display rooms. Some 50-70 scientists and technical personal will operate the center. Sponsorship is by the central government, local government and well over 200 companies. (I have in my possession a copy of their foundation publication which lists all the sponsors and also contains a first rate write-up on bioceramics development in Japan).

Among the objectives of the Center are: Establishment of a technical data bank with on-line retrieval service; development of procedures for testing and evaluation, leading to standardization; sponsoring of research conferences and seminars, including international cooperation; and, basic research and development in fine ceramic systems. This last function in my view, is an attempt to address the question of the perceived lack of basic research and innovation in the Japanese Ceramic Industry, but in any event there seems to be a serious committment by all parties to the success of the Center. Fine Ceramics has thus been targeted as a major thrust area going into the 21st century.

4. Hitachi Corp. - Tokyo

Hitachi is a very large and diverse corporation, hence our visit was fairly narrowly focussed to microelectronics concerns. Dr. Takeuchi was our host. Much of his previous work has been in piezoelectric materials and it is of significance that he has recently been shifted to the 9th Department, Medical Electronics. There was in fact a strong emphasis on use of ultrasonic techniques for medical diagnosis, using piezoelectric composites (3-1 in a planar mode) as transducers. Other piezoelectric materials, including sputtered (and epitaxial) PbTiO_3 films were also being used. The medical diagnostic effort seem well advanced and we were shown a number of prototype

machines. Deposition of ceramic films by sputtering or CVD processes seem to be a major effort of this group. We were told that there was a serious development effort on diamond films (different group) as a potential device and/or packaging material. Plasma CVD TiS_2 films were being deposited (with CdI_2 structure) for use as electrolyte films in solid state lithium batteries ($\text{Li}/\text{Li}_{3.6}\text{Si}_{0.6}\text{P}_{0.4}\text{O}_4/\text{TiS}_2$). Stoichiometric films with preferred orientation and desirable electrochemical properties were reportedly obtained. Other film work included ZnO sputtered films for transducer application: $\text{Au}/\text{ZnO}/\text{Au}/\text{fused quartz}$ which was said to have a very high efficiency. We were also shown LaB_6 crystals produced for electron emitter tip elements. Hitachi has substantial market in this product. As an aside, we were told that a fairly constant 8.1% of sales was ploughed back into research. Again much test vacuum and sputtering equipment, which we saw in the laboratories, was supplied by US companies.

5. Science and Technology Agency - Tokyo

My visit was to the Science and Technology Promotion Bureau (Policy Division) of the Ministry of Science and Technology: my host was Mr. Soichiro Katayama who did his graduate work (Nuclear Materials) at Illinois. In the materials area, the agency is charged with promoting research and development activities in a broad range of materials technologies (high strength, high temperatures, cryogenic, electronic materials etc). It funds ceramics research through the "National Institute for Research in Inorganic Materials" which is concerned with: materials for VLSI fabrication, optoelectronic materials of transparent ceramics, bioceramic materials and synthesis of new inorganic materials. The broad concern of the agency is that basic research be fostered and developed. There was again a concern that Japan is lagging in this area. I could not obtain a budget figure for these activities. A brochure detailing the agency operations is in my possession.

Travel Report of L. C. Burton (EE Dept., VPI&SU) for the 3rd. U.S.-Japan Seminar on Dielectric and Piezoelectric Materials, Toyama, Japan, Nov. 9-14, 1986. (Technical comments only)

Overview Session (Monday morning)

Talks were given by representatives from the U.S. and Japan. Eric Cross first reviewed the history of dielectrics and piezoelectrics. He pointed out the increasing activity in multicomponent structures, multilayer ceramic circuits being an example. I felt that his most important remarks were related to where emphasis should lie in the future. Basically, the pathways of semiconductors should be followed. Much of what has been learned in this field during its extensive development over the past 35 years could be applied to dielectric related systems. This applies across the board: examples pertaining to both semiconductors and dielectrics are single crystal and epitaxial layer growth; precise control of multilayer structures, especially as layers become thinner, with special emphasis on interfaces; definition of small structures; an understanding of the behavior of materials systems, with input from chemistry, materials science, solid state physics and ceramics. Dr. Cross emphasized the future necessity for smaller size, which includes patterning techniques and superlattices. Another example is the epitaxial growth of thin ferroelectric layers. Such layers could potentially be used directly on IC and other chips, removing the necessity for external bypass capacitors.

Dr. Ichinose reviewed the situation in Japan, discussing new ceramic substrate materials, piezoelectric materials, and dielectric materials (capacitors), the latter being subsequently discussed in more detail by Dr. Sakabe. Low firing temperature materials are necessary in order to reduce the need for noble metal electrodes and for compatibility with thick film processing, which occurs at $<1000^{\circ}\text{C}$. High thermal conductivity materials are necessary, especially in the

future as multilayer component densities increase, for increased power hybrid applications, for laser heat sinking, and for microwave applications since power generation increases with frequency. Dr. Ichinose made reference to the following materials which could satisfy some of those needs: SiC-BeO, AlN and CVD diamond films.

Dr. Sakabe then discussed new capacitor materials. They have a Pb-based Y5V type with $K=24,000$ (I assume this is at Murata). He also emphasized the need for thinner layers (to below $10\mu\text{m}$?) and the need for lower firing temperature materials.

Poster Sessions

I felt that the four minute summary presentations that preceeded the poster sessions were on the whole, very good, and recommend this format in the future. (It would be an improvement if only a summary of objectives and results were given; some speakers tried to present their entire papers.)

Of particular interest in Monday's session was some of the new fabrication work. An example is the sol-gel processing of PLZT dielectrics reported by D. Payne, with K up to around 2000. This is certainly an attractive technique (spin coating) for forming thin dielectric layers, with firing temperatures ($<700^\circ\text{C}$) that are compatible with ceramic, thick film, Si and GaAs technologies.

Base metal electrode work was reported by Murata, Kyocera and Taiyo-Yuden. The Japanese seem to be working more heavily in this area than the U.S. This could be important in development of lower cost electrodes compatible with lower firing temperature dielectrics.

Our paper "Conduction Mechanisms in BaTiO_3 Based Ceramic" was summarized in a four minute presentation and presented at the poster session.

I had several discussions with Y. Sakabe of Murata concerning capacitor degradation mechanisms. They have been doing some work that parallels our own. We discussed the concept of a "virtual cathode", which could potentially exist in

any n-type oxygen deficient oxide dielectric. Oxygen diffuses away from the cathode resulting in an adjacent lower resistance layer. This process can be apparently reversed, by reversing polarity, as we have shown. He agreed that this was a likely mechanism, but details still have to be worked out. Is the oxygen ion motion mainly through grain boundaries or bulk? How uniform is the thickness of the reduced layer? What changes are occurring in the rest of the dielectric? We agreed to continue discussing these questions, and he plans to send over samples for us to measure.

During Tuesday's poster session, it was obvious that the Japanese are doing alot of work in the microwave dielectric area. The U.S. had no papers in this area. The Japanese also reported work in an area where we do not seem to have alot of activity, that of sputtered dielectrics. The work reported by Kyoto University and Waseda University shows good progress toward deposition of thin films (<1um thickness) of PZT and PT.

On Wednesday, the work reported by Kahn of MRL and Banno of NGK Spark Plug Co. both dealt with the effects of controlled pores on piezoelectric and other properties. This is of interest not only in the context of piezoelectrics, but more generally, relative to porosity in dielectrics, including intentionally porous materials for low K, low firing temperature tape, and thick films. An interesting question is whether or not electrical reliability is inherently degraded by pores, or if it is determined more by ambient. It seems reasonable that high voltage material would be degraded due to electric field enhancement and partial breakdown, but the issue is not as clear for low voltage applications (<1V/um).

At the wrapup session on Wed. afternoon, it was agreed that the Seminar was useful and should be continued. However, there was some concern expressed about the small number of U.S. companies participating in the meeting.

Industrial Tours - NEC

On Thursday, six of us visited NEC (Nippon Electric Co.) NEC is doing alot in

semiconductor devices, VLSI, electronic materials and ceramic, including III-IV compounds, ultra-fine line generation and thin films.

Four areas of work were noted in their Materials Research Lab: Electronic Ceramics (including dielectric ceramics, low fire MLC, peizoelectrics, ML actuator, semiconducting ceramic and MLC varistor); Ultra-fine powders; Thin films (mainly carbon-like and ferroelectric); Metals (rapid-quenched, superconducting).

We then heard several seminars from NEC staff. Y. Kurokawa discussed AlN ceramics. This is being studied as a high thermal conductivity substrate. They have a huge MBE system, custom built (estimated cost \$1M), and a similar sputtering system. They can grow multilayer AlN substrates resulting from the reaction $2Al + 2NH_3 \longrightarrow 2AlN + 3H_2$. Thermograms were shown for a Si chip on an AlN substrate, and compared to a similar chip on Al_2O_3 . The former indicated a maximum temperature of 43°C, the latter 65°C. They also plan to use the AlN as a substrate for LED and laser diode chips.

K. Utsumi then discussed MGC (multilayer glass-ceramic) and MMC (monolithic multicomponent ceramic) substrate work. The MGC is composed of 55 wt. % Al_2O_3 and 45% Pb borosilicate glass) fired at 850-950°C. They use Au or Ag/Pd as the conductor. They obtain high insulation resistance ($\sim 3 \times 10^{14} \Omega\text{-cm}$) and current less than 1 μ A at 50V bias. (This material appears somewhat similar to DuPonts' low temperature green tape).

Their via capability is impressive: 110,000 vias 80 μ m dia. on several cm² of sheet. They use RuO₂ resistors for hybrids, sintered at 900°C, and have buried MLC capacitors, using both low K and high K layers, all with a single firing. So the result is an MLC system used as a substrate for a hybrid circuit, which contains the resistors, capacitors and conductors. I was very much impressed by this presentation. They appear to be substantially ahead of us in multi-component MLC technology.

Next Dr. Suga discussed the ceramic ink jet head. Ink jet nozzles are formed in a multi-layer structure using patterns formed photolithographically. The ink

ejection from the nozzles is controlled by actuating piezoelectric drivers, whose electrodes are buried in the multilayer.

Dr. Showata discussed diamond-like thin films. He reviewed methods used for forming such films (thermal decomposition, ion beam, direct sputtering, and CVD using DC, RF or microwave power). They use the DC approach in a rather simple diffusion pumped system. Films are amorphous when deposited at room temperature, on a Si substrate. Their thermal conductivity increases to about 400 when annealed at 400°C (compared to the diamond literature value of 2000 W/mK).

M. Yonezawa then discussed low firing temp. dielectrics, specifically a Pb-based ($\text{PbTiO}_3 + \text{PbZrO}_3$) composition used for X7R type MLC capacitors.

Each of the U.S. people then presented seminars on their own work. We then saw their "Show Room" exhibit, a very well put together exhibit of R&D areas on posters and in glass cases.

One apparent advantage of the overall organization of NEC (and of Hitachi, which we visited on Fri.) is that their dielectric and ceramic related work can draw from, and even work jointly with, the semiconductor related groups at the same company. Work on development of say new substrates for high power chips or multilayer substrates for active hybrid circuits can be coordinated between the chip people and the substrate people, in a more efficient fashion than if chips and substrates are made by different companies.

Hitachi

On Friday five of us took a tour of Hitachi's Central Research Lab. Here we visited several labs and heard the technical presentations in those labs.

C. Nakaya and Y. Ito discussed their work on piezoelectric composites and crystals. K. Kushida discussed the growth of PbTiO_3 thin films, by sputtering, onto a single crystal which had been previously covered with metal contact fingers. As the films grow, they cover over the contacts and coalesce into quite large crystallites.

H. Kanda discussed his ultrasonic microscope which has a depth damage resolution of about 5 μ m. T. Ogawa discussed sound velocity measurements in bio-systems. He indicated a 2-dimensional capability at present, with plans to expand to 3-dimensions. This system has been used to map sound velocity in biological tissue, and has demonstrated success at locating damaged regions in human organs.

The growth of LaB₆ single crystals was discussed in the lab of T. Aida. (LaB₆ is used as electron emitter in SEM machines because of its low work function.) We saw the molten zone facility where crystals are grown at 2700°C.

The final presentation was by K. Kanehori who discussed the growth of TiS₂ films for thin film batteries. These are quite thick films (30-60 μ m) deposited by CVD following the reaction $x \text{ Li} + \text{TiS}_2 \rightleftharpoons \text{Li}_x\text{TiS}_2$

Again, Hitachi is obviously a very diversified company. In such a situation, semiconductor and dielectric (and other) groups can interact when necessary if a product involving both disciplines is to be developed. It would be interesting to know how many US companies are diversified to the point, and have internal communications that are good enough, for such coordinated product development to occur. NEC and Hitachi both appeared impressive in this regard.

L. C. Burton

L. C. Burton

TRIP REPORT
TOYAMA, JAPAN
November 9-12, 1986

Stephen W. Freiman
Ceramics Division
National Bureau of Standards
Gaithersburg, MD

The purpose of this trip was to act as the U.S. chairman and to participate as a speaker in the Third U.S.-Japan Seminar on Dielectric and Piezoelectric Materials. The seminar was held in a hotel near Toyama, Japan. In arranging this meeting, it was agreed between professor Takashi Yamaguchi, the Japanese chairman, myself and other members of the U.S. organizing committee, Dr. Robert Pohanka and Dr. David Payne, that in order to maximize real communications between participants, it would be best if almost all of the papers were presented in poster form. In addition, each speaker was given four minutes to summarize his presentation at a session held before the posters were viewed. This arrangement turned out to be an excellent format and gave rise to extensive individual discussions.

There were approximately 25 U.S. participants and 60 Japanese. This ratio is reasonable considering that Japan was the host country. What is of concern, however, is the fact that about three quarters of the Japanese participants were from industry, as opposed to universities or government laboratories, compared to only one quarter from U.S. industry. For instance, there were no U.S. capacitor manufacturers represented at the seminar even though invitations had been issued to them. Other companies turned down invitations as well, a number citing financial reasons for not attending.

Since the first U.S.-Japan Seminar, held four years ago in Tokyo, the discussions between the U.S. and Japanese participants have become more open. I believe that this openness is a direct result of the fact that essentially the same core of people have been attending these meetings. We have gotten to know our counterparts in the other country, and feel more comfortable in discussing the details of our research. Much of what was learned came about during more informal talks rather than at the sessions.

From a technical point of view, the Japanese appear to be taking an increasing interest in mechanical properties, not just of structural ceramics, but of dielectric and piezoelectric materials as well. I see an expanding effort in relating the fracture behavior of these materials to chemistry and microstructure. They have recognized the need to be able to predict the reliability of ceramic devices such as switches and motors based upon fracture mechanics concepts. At present the Japanese rely heavily on work performed in the U.S., but their efforts in fracture mechanics research is increasing. There are

programs at Sophia University, the University of Tokyo, and the Japanese National Defense Academy directed at understanding the mechanical properties of piezoelectric ceramics.

In particular, a number of the Japanese participants were concerned about the selection of an optimum technique which can be used to determine the critical fracture toughness, K_{IC} , of dielectric or piezoelectric materials. There was discussion on a number of topics involving specific aspects of the use of these ceramics. For instance, it appears that the alignment of the domains in a piezoelectric ceramic in the process known as poling, has a measurable effect on crack propagation. In a study at the University of Tokyo, cracks were observed to propagate more readily in the direction of poling than in the perpendicular direction. Another area of discussion involved the possible effects of cyclic, as opposed to static, loading on crack growth in components such as electrostrictive and photostrictive actuators for servovalves and photostrictive relays. Professor Uchino at Sophia University is currently investigating the mechanical reliability of electro-optic devices which undergo complex stress states in service. Although there is some work going on in the fracture of multilayer capacitors in Japan, it seems confined to the determination of fracture mechanics parameters, rather than being a research effort. There was one paper presented at the meeting, however, discussing the relationship between mechanical and dielectric failure of barium titanate ceramics.

A meeting of the U.S. participants was held at the close of the Seminar in which our views of various aspects of the technology could be summarized. Based upon these discussions, it was decided that the Japanese are clearly ahead of us in the areas of microwave dielectrics, actuators and motors, thin film ferroelectrics, and low fire dielectrics. While the U.S. has a greater knowledge of materials such as relaxor ferroelectrics, we are not making commercial use of this knowledge. In general the work discussed by the Japanese was of a more practical nature than the U.S. work. One participant was of the opinion that they were more open in their discussions than the U.S. One of the major topics of discussion at this meeting was how to generate more participation by U.S. industry. One way in which we will attempt to do this is to eliminate the series of post-seminar tours. It was thought that many companies did not come to Japan because of the possible obligation of hosting the Japanese in their plant at the next Seminar to be held in the U.S. in 1988. The preliminary plan is that I will be U.S. Chairman of the Seminar again in 1988, and that the meeting site will be the National Bureau of Standards. The format for the Seminar will remain essentially the same, with most presentations being given in the form of posters. These plans will be discussed with the incoming Japanese Chairman in the next couple of months.

THE THIRD U.S.:JAPAN SEMINAR ON DIELECTRIC AND
PIEZOELECTRIC CERAMICS, AND RELATED LABORATORY VISITS

NOVEMBER 8-17, 1986

Martin P. Harmer
Department of Materials Science and Engineering
Lehigh University
Bethlehem, PA 18015

THE THIRD U.S.:JAPAN SEMINAR ON DIELECTRIC AND
PIEZOELECTRIC CERAMICS, AND RELATED LABORATORY VISITS

NOVEMBER 8-17, 1986

The workshop provided an excellent forum for updating the U.S. and Japanese participants on recent developments and trends in the field of dielectric and piezoelectric ceramics. The laboratory visits provided an excellent opportunity to witness the workings of the Japanese electronic ceramics industry first hand. I visited the capacitor manufacturing division of Murata and the research laboratory of NEC. Frankly, I found the Japanese industrial participants to be more open about their research and manufacturing technology than I had expected. Murata showed us every aspect of their capacitor manufacturing process. NEC presented us with a detailed summary of their current research and development activities. The representation from industry and academia was significantly imbalanced amongst the two U.S. and Japanese delegations. The great majority of the U.S. delegates were from universities whereas the Japanese delegates were overwhelmingly from industry.

I list the following areas that I sensed the Japanese have developed an edge over the U.S. These are areas where the U.S. may need to catch up:

- (1) actuators and piezoelectric motors

A Japanese authority in this field is Dr. Kenji Uchino in the Department of Physics, Sophia University, Kioi-cho 7-1, Chiyoda-ku, Tokyo

102. NEC is working very actively in this area developing multilayer piezoelectric actuators to be used in ink jet printing heads. Relaxor materials (lead magnesium niobate $\text{Pb}(\text{Mg}_{1/3}\text{Nb}_{2/3})\text{O}_3$ in particular) are strong candidates for electrostrictive actuator applications. For a good review on actuators see the article by Kenji Uchino entitled "Electrostrictive Actuators: Materials and Applications" pp647-652 in Bull. Am. Ceram. Soc., Vol 65, No 4 (1986).

(2) thin film sputtering

Several of the Japanese papers presented at the workshop demonstrated the feasibility of sputter depositing epitaxial thin films of PLZT, PZT and PT onto a variety of substrates including silicon, platinum, sapphire and magnesium aluminate spinel. The ferroelectric and pyroelectric properties of the thin films look very promising. NEC has a group studying thin film sputtering of barium titanate and lead-based dielectrics as well as metals. NEC has been successful in producing sputter deposited artificial superstructures of Mo and Ni (5 monolayers of Mo codeposited with 5 atomic layers of Ni). An exciting area that this suggests for future research is the development of artificial superstructures of ceramic dielectrics/ferroelectrics.

(3) microwave dielectrics and pyroelectrics

It was noticable that only Japanese delegates and no U.S. representatives contributed papers on either of these topics at the seminar. Complex perovskites such as $\text{Ba}(\text{Mg}_{1/3}\text{Ta}_{2/3})\text{O}_3$ are being actively developed as microwave resonators at the Murata Manufacturing Co., Ltd. in

Japan. Dr's. Wakino, Tamura and coworkers at Murata are working in this area. They have been very successful in using far infrared spectroscopy for correlating lattice vibrational modes with crystal structure and B-site cation ordering. We plan to collaborate with Dr. Wakino in this area since their infrared techniques are very complimentary to our microstructural and defect chemistry work on relaxor type dielectrics for microwave applications. Nishigaki et al. (Naruma Technical Laboratory, Nagoya) presented an interesting paper on the microwave properties of BaO-TiO₂-WO₃ ceramics. A second phase (BaWO₄) with a negative T_f was used to produce microwave ceramics with a near zero T_f.

(4) thermally conducting substrates and integrated packages

Japan seems to be quite far ahead in the development of thermally conducting substrates, especially of aluminum nitride. NEC showed us translucent aluminum nitride substrates that were reported to have a thermal conductivity as high as 240-260 Wm⁻¹K⁻¹ which is very close to the theoretical maximum of 320 Wm⁻¹K⁻¹. NEC uses powders made by Tokuyama Soda and sinters or hot presses at 2000°C using CaC₂ as a sintering aid. NEC has also been the first to develop integrated cofired multilayer packages containing mixed layers of capacitors (lead-based relaxors) and resistors in with the conventional insulation/conduction layers. NEC has made structures with 41 layers cofirable in air for modules containing 36 chips. NEC is also working on producing amorphous carbon films with diamond like properties using CVD technology (CH₄-H₂) depositing on silicon.

(5) clean room manufacturing

It was very impressive at Murata to see capacitor mass production carried out under Class 10,000 clean room conditions. Murata claimed to see a dramatic improvement in product reliability and reject losses after converting to clean room manufacturing.

In summary, this meeting was an outstanding opportunity to become acquainted and exchange ideas with our Japanese counterparts. I found it to be very rewarding. It was very well organized and special commendations go to the cochairmen, Dr. Freiman and Professor Yamaguchi for their outstanding organization and to Dr. Pohanka and the Office of Naval Research for their support in making these seminars possible.

REPORT ON TRIP TO JAPAN
November 6 - November 18, 1986¹

M. Kahn
Naval Research Laboratory
Code 6363

The following report contains the Publication Release Request copy of:

- 1) Reviews of many of the papers presented at the Third, ONR sponsored U.S.-Japan Seminar on Dielectrics and on Piezoelectric Ceramics in Toyama, Japan, Nov. 9-12, 1986 as well as some information presented during laboratory visits.
- 2) Some notes from the panel meeting on piezoelectrics at the same seminar.
- 3) Some discussion of Dr. Yamagida's programs at the University of Tokyo.
- 4) My impressions from visits at the Sony Central Laboratories, at NGK and at some of the TDK ceramic capacitor operations in Akita.

Index

- I. Introductory remarks
- II. Contributed papers
 - A. Electronic Films
 - B. Processing
 - C. Barium Titanate Analysis and Dielectric Compositions
 - D. Dielectrics for Nickel Electrode Capacitors
 - E. Capacitor Reliability
 - F. Microwave Materials
 - G. Anisotropic Materials
 - H. Relaxors and Piezoelectric Materials
 - I. Piezoelectric Transducers
 - J. Piezoelectric Applications
 - K. Varistors
 - L. Photovoltaics
 - M. Modelling
- III. Panel Meeting on Piezoelectrics
- IV. Visit to Tokyo University
- V. Plant Visits
- VI. Summary
- VII. Art Buchwald's comments on the subject

1. Introductory Remarks

1) In his keynote address E. Cross proposed that unique and useful phenomena will be derived through investigating and optimizing ferroelectric behavior in extremely thin and small regions, following the example of semiconductor technology. Scaling down to "micro" and "nano" subdomain microstructures is presently not adequately understood but contrary to present interpretations, polar micro regions may well be possible. "Normal" ceramic surfaces are thought to be highly disordered, but with the advent of technologies such as vapor phase CVD, the implementation of atomic order on surfaces can well lead to the verification of very short range ferroelectric phenomena. 200-1000 Angstrom ferroelectric nanocomposites may then become feasible. Artificial super-lattice structures could then stabilize metastable configurations with shallow potential atomic energy wells. This could give large atomic displacements, providing high pyro and piezoelectric sensitivities and even positioners with atomic accuracy.

2) Ichenosi from Waseda University discussed the efforts of four manufacturers to develop and market lead silicate borate glass, filled with 30-60% of alumina as thermal substrate material, similar to what is being worked on by Dupont in the United States. Maximum density is attained between 800 and 900°C. He also described the well-known silicon carbide beryllium oxide doped substrate material (pioneered and publicized by Hitachi at least 2 years ago) as well a pressureless sintered, aluminum nitride composition, marketed under the name of Super Shapal by Toyo soda. This material is almost 85% translucent to visible light and transparent to infrared. Reduction of the oxygen content of both silicon carbide and aluminum nitride powders to significantly below 1% is thought to be the cause for significantly enhanced thermal conductances.

He mentioned work on diamond CVD coating and also showed a number of schematics of piezoelectric ultrasonic motors, both utilizing stationary as well as propagating waves. He also showed a design that used a magnet to couple piezoelectric motion into a rotor. Efficiencies of 80% were quoted.

3) Sakabe (Murata) presented a review of the properties of low fired, stable K materials and of relaxor based dielectrics that contain ZnO. The materials he discussed are utilized in Japan in large scale production, including in multilayer capacitors with nickel electrodes having capacities up to 400 micro farads, that are made at a rate of up to 20 million capacitors per week.

Murata are also making strontium titanate internal boundary layer capacitors and are reporting effective dielectric constants to 200,000. This is attained by making an ohmic, rather than a junction contact to the ceramic. This is implemented by indiffusion of aluminum. No advanced techniques to analyze the behavior of such devices (as for instance cole-cole plots) were shown. In closing he mentioned that they are conducting a substantial effort in 10 GHz dielectric resonators for applications in direct broadcast satellite receivers. Q's above 8,000 at 10 GHz with very low temperature coefficients are attained. Results giving even higher experimental Q values are discussed below. Their basic thrust is to obtain higher dielectric constants to lower resonator size without a significant reduction in the high frequency Q.

II. Contributed Papers (both at the symposium as well as presented during laboratory visits).

A. Electronic Films

It appears that the preparation of single crystal or of ferroelectric thin films is presently one of the most advanced areas of electronic materials research. Japanese researchers reported primarily on the utilization of sophisticated instrumental film forming methods, whereas applications of

chemistry (i.e. sol gel and organometallics) were reported on by U.S. workers.

1) Matsubara (NEC) reported on the CVD deposition of $MgAl_2O_4$ epitaxial films on top of N type single xtal silicon wafers. Onto these they R.F. magnetron sputtered PLZT films which again grew epitaxially on top of the $MgAl_2O_4$ substrate layer. The films showed single crystal structure, using Reflection High Energy Electron Diffraction (Rheed). The lattice constants varied with the lanthanum content. The sophistication of this work is substantial.

2) Wasa (Matsuchita) discusses results from magnetron sputtering of PLZT onto sapphire substrates. His films were polycrystalline and showed a maximum dielectric constant of about 500 with 10% lanthanum. Changes in deposited stoichiometry due to the high substrate temperatures (500-700°C) were mentioned.

2) Tamura at Sony Labs showed me yttrium garnet films grown by liquid phase epitaxy on top of a gadolinium gallium garnet substrate. Tunable filters were built out of these and grooves in their surfaces were said to almost eliminate higher order responses. The films were said to find use in variable, high frequency oscillators in communications equipment. At the same time I was also shown the operation of a magnetic bubble memory in which bubbles were moved from one location to another and also obliterated, all using an argon laser beam. The preferred locations for the bubbles were generated in liquid phase epitaxially grown yttrium garnet films by etching small square depressions into the surface of such films. The introduction of bismuth into this garnet provided it with a high Faraday rotation angle. This permitted optical readout of the state of the memory.

4) Murata workers discussed a metallorganic CVD technique for the deposition of tantalum oxide films. Dielectric constants of 26, with 4-6 megavolt per

centimeter capability in a 100 Angstrom thickness were mentioned. Tantalum ethylide $Ta(OC_2H_5)_3$ vapor was used in the presence of titanium $O(C_3H_7)_4$ vapors, with the titania providing an acceptor in the tantalum oxide structure. Substrate temperatures above $650^\circ C$ caused film crystallization, but the dielectric strengths of the lower temperature amorphous films was said to be higher than of those that had been crystallized.

5) R. Vest reported on ferroelectrics from metallorganic precursors: Defect free lead titanate and lead strontium titanate films, covering 2 cm by 2 cm areas with near theoretical density were reported. He indicated that fast drying is necessary in these materials to obtain precipitation from the liquid without prior gel formation. They have to be made thin so as to prevent cracking from drying shrinkage. Multiple, superimposed film applications are possible.

6) D. Payne discussed spun-on and fired lead titanate alkoxide based films that he had made: Metal etoxide solutions were spin cast on smooth substrates and densified at $700^\circ C$. High quality ferroelectric properties were shown in 1 micrometer thin films. This demonstrates a high degree of order and crystallization after firing at relatively low temperatures. The films were said to withstand 100 volts per micrometer and this was said to permit their application as memory devices.

B) Processing

One of the more intriguing presentations at the seminar was by Shiosaki on laser activated grain boundary etching. More conventionally, there were some interesting analyses of surface chemistry phenomenae and their effects on dispersion and packing.

1) Shiosaki from Kyoto University told of a novel ceramic drilling technique. A KOH solution covering a PZT ceramic is excited by a laser and whole grains

are removed in the irradiated area. The progression rate with a 1 watt laser is more than 100 micrometers per second. It does not appear that there is damage in the ceramic constituting the walls of the hole. X-ray diffraction of the residue verified that whole grains had been removed out of the ceramic. A variety of ceramic formulations have been successfully drilled, using a self imaging focusing mechanism. The latter derived its input from the acoustic noise generated during laser irradiation in a PZT plate that supports the sample. The hole drilled is not fully cylindrical but a clean pattern can be generated.

2) Hirano (Univ. of Nagoya) reported on the synthesis of a 0.3 micrometer size mono-dispersed and mono-sized spherical particle suspension of zirconium titanium stannate, derived from alkoxides. These materials had been sintered in the past only with the help of sintering additives as zinc, nickel, iron or lanthanum oxides. They have desirable 10 GHz properties for applications in direct broadcast satellite receivers and telecommunications. Hirano's work on these materials was intended to make fine powders that could be sintered without sintering aids and hopefully thereby attain higher Q values.

He liquid mixed alkoxide derived precursors and a partial description is given of rather critical hydrolysis and multiple refluxing conditions that gave mono sized and mono dispersed spherical particles of the desired compositions. No small feat. The particles were dried by filtering on an 0.01 micro meter filter (made by the Toyo Rashi Company Ltd. in Tokyo) and fired to relative densities of >96% with Q values up to 5300 at 10 GHz, without any sintering aids. He felt that the application of high compacting pressures to deagglomerate fine particles can be counter productive, as it introduces strains in the material that give rise to excessive grain growth. The latter has been shown conclusively for hot pressed materials. The

application of zeta potential titrations and or other measurements indicate to him, that base acid surface reactions are not as reversible as is often assumed: For instance H^+ atoms that are attached to a bismuth oxide surface during acid treatment, are not replaced by OH molecules in a basic environment, but remain there and form "complexes" with OHs on adjacent sides. This model may be somewhat approximate, but evidence pointing to nonreversability of surface reactions has been observed elsewhere. This may well be the reason that most practical dispersant systems are of a steric nature, relying on a polymer rather than just on the surface charge for dispersion. The nonreversibility of surface reactions makes it necessary to control the electro chemical environment (i.e. the optimum pH level, as established by previous zeta potential titrations) right from the time a powder is originally synthesized through all stages of processing. This then permits purely electro-static repulsion to dominate and provide complete dispersion, negating the need for steric dispersion polymers.

3) Ueyama from Hitachi showed a linear increase in packing density of both alumina and barium titanate particles as agglomerate size is reduced. The theoretical green density calculated from mono size 8 coordinated spheres is obtained as agglomerates are eliminated. The primary particle size is then measured. The same mono size particles show a small decrease in packing density when the concentration of PMMA binder is reduced from the minimum void volume (approximately 12%) to lower values. The group at Hitachi also investigated the effect of agglomerate size and binder concentration on the sintered density of barium titanate. They found that elimination of agglomerates gave lower temperatures of surface densification. Agglomerate free barium titanate attained its final density of 5.8 gram/cm^3 at the surface

densification temperature, independent of binder concentration or of green packing density.

4) L. Levinson presented results from GE's laser patterning interconnecting work, pertaining to the optimum composition of the polymer that carries the wiring. This is to adjust its absorption coefficient for the laser light so as to maximize the etch rate. A peak in the etch depth per pulse versus absorption coefficient curve was found.

C. Barium Titanate Analysis and Dielectric Compositions

1) D. Smyth showed that the site occupation preference of tri-valent impurities in barium titanate depends both on ionic size as well as on the stoichiometry of the matrix. Yttrium and Erbium have the most intermediate ionic size and they show a variable site occupation preference, most strongly determined by the stoichiometry of the matrix. He showed some self compensation when barium titanate is doped with yttrium. This is indicated when the valley in the resistivity versus dopant concentration curve is shifted to significantly higher concentrations, also causing the curve itself to be significantly broader. On the other hand the full, theoretically expected self compensation due to simultaneous occupancy of both the A and B sites is only rarely observed. Simple and elegant.

2) R. Buchanan reported that the addition of zirconia to barium titanate gave (after firing below 1300°C) grain growth inhibited ceramic with the zirconia at the grain boundaries. At higher temperatures grains grew and zirconia was found in the lattice. The addition of calcium alumina borate flux gave sintering temperatures below 1175°C. Fluxing was said to allow diffusion of zirconia. He observed a Curie point shift, without grain growth above 1 μ m. Evidence of boron in the grain bulk under these conditions was also claimed.

3) I. Burn discussed a low fire K 10,000 Z5U formulation, that is said to be precalcined with a small amount of lead. It was said not to contain additions of bismuth, cadmium fluoride or other volatiles. His results are achieved through close control of A-B stoichiometry and a close donor-acceptor balance. Conduction is said to be electronic. He uses a new submicron barium titanate powder and the system is fired at 1100°C. 70% silver electrodes are used.

4) Takabatake from the Asahi Glass Company reported on glassy films having a dielectric constant of 6.5 at 100 KHz. They are intended to provide a low temperature firing multilayer technology for hybrid circuits. The glass-ceramic contains alumina, that does not react at 900°C. 2 MgO SiO₂ is added to this. When it dissolves, it causes the boron in the glass to react with the alumina, giving the glass a high resistance to corrosion by water. A similar system has been commercially sold in the United States for a considerable period.

5) Abe from Sakai Chemical prepared barium titanate powder using hydrothermal synthesis. The desired 1000°C sintering temperature was achieved through doping with additives.

D. Dielectrics for Nickel Electrode Multilayer Capacitors

The volume of nickel electrode multilayer capacitors made in quality conscious Japan tends to contradict U.S. claims that such devices cannot be made reliably. The history of this product (mentioned below) should certainly set one to think.

1) The paper by Sakabe from Murata on barium titanate based capacitors with internal nickel electrodes is a case of superior Japanese engineering in the application of U.S. science. One of his composition appears to be an acceptor doped, slightly barium rich, 10% calcium containing Z5U material, very similar

to that put together and patented by Smyth and Error in the late 60's. Murata got a patent (in 1976) on the calcium addition and the function and site occupancy of their 10% calcium addition has been described by Don Smyth. Murata fires at relatively low oxygen pressures (10^{-11} ATM PO_2) to prevent loss of capacitance control due to nickel oxide diffusion. The significant part about all of this is that at least 3 U.S. multilayer capacitor manufacturers tried to introduce nickel electrode capacitors into the U.S. market. Their lack of success has to be at least in part attributed to an insufficient willingness to make the required investment in engineering the system. This resulted in the premature marketing of devices that had inadequate life test performance. It appears that Japanese perserverance led in this case to a new product, i.e. to what they claim are economical and reliable substitutes for 1 to 100 mf tantalum capacitors.

Sakabe also mentioned a set of NPO and X7R formulations that are compatible with nickel electrodes. Again, a lot of early work was also done on these in the U.S.

2) Kishi from the Tayo Yuden Central Research Laboratory added 3% of an unspecified, alkaline earth containing lithium silicate glass to 1220°C solid state reacted barium titanate powder. It acted as a low temperature flux, lowering the sintering temperature to below 1200°C and also provided acceptor doping to the matrix. "Reliable" nickel electrode multilayer capacitors are presumably made from this. Both Z5U as well as X7R behavior are described. No post calcining milling is mentioned. This appears to be a rather ingeneous system.

3) Fujikawa reported on X7R nickel electrode multilayer capacitors containing $CaZrO_3$, Y_2O_3 and ~ 0.5% MnO .

E. Capacitor Reliability

Three U.S. papers on this subject illustrate the present U.S. concern and ONR sponsorship of this subject. It should be noted though that the first paper I ever saw discussing cracks leading to low voltage failures (blaming chlorine from CCl_4 degreasing fluid) came from Japan and also that at least TDK is doing in-house work on understanding delaminations (see below).

1) H. Anderson subjected multilayer capacitors to a 770° temperature gradient, whereupon they developed interelectrode cracks. These were then subjected to voltage and temperature testing. The currents he observed were strictly related to the presence of humidity and to voltages above .5 volts. Lower voltages or the elimination of humidity (either by heating or by drying) resulted in low currents. He therefore concluded that electrolytic conduction is responsible for "low voltage failures" since high voltages could dry out the cracks. No phenomena that could be related to the growth of metallic dendrites was observed.

2) L.C. Burton showed a conductivity peak in BaTiO_3 in the Ohmic (low voltage) regime, near the cubic to tetragonal inversion temperature.

3) J.P. Dougherty calculated the heat rise in a typical multilayer capacitor due to hysteresis losses from AC voltages. He finds that 12 volts rms can heat a typical capacitor chip at $>30^\circ\text{C}$ per second up to $130-140^\circ\text{C}$. In a cold ambient this was said to develop stresses up to 400 kilogram meter within 10 seconds.

F. Microwave Materials

The Japanese developments described in this section are a direct outcome of an initiative by the Japanese government, i.e. the previously noted installation of satellites for direct broadcast TV. These materials transcend

NO-A105 113

UNITED STATES - JAPAN WORKSHOP ON DIELECTRIC AND
PIEZOELECTRIC CERAMICS ((3RD)) HELD IN TOYAMA JAPAN ON
NOVEMBER (9)-(12) (1986)(U) KEIO UNIV TOKYO (JAPAN)

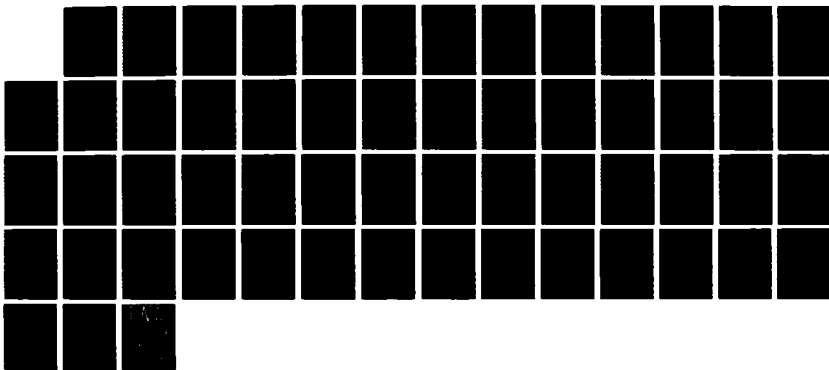
5/5

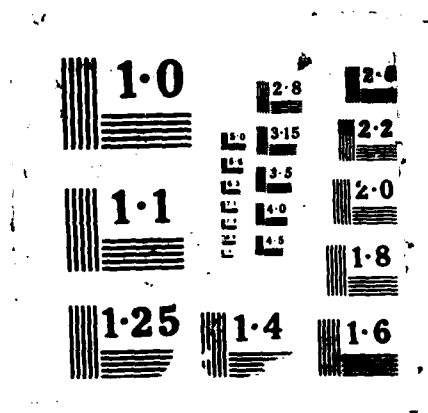
UNCLASSIFIED

30 JUL 87

F/G 11/2

NL





earlier U.S. developed microwave dielectrics, both in time as well as in performance.

1) Tamura (Murata) reported on $\text{Ba}(\text{Mg}_{1/3}\text{Ta}_{2/3})\text{O}_3$ that develops a high Q due to MgTa ordering, and the subsequent development of a hexagonal superstructure. It appears from infrared spectrum examinations that a strong c-a bond strength anisotropy contributes to the higher Q's. 10% BaSnO_3 was added to the material to provide more sinterability. This raised the Q even more, even though the superlattice lines tended to disappear. Q values of 20,000 with K's of 24 were seen at 10 GHz.

Murata is pioneering the application of infrared spectrum analysis to the improvement of electrical properties of electronic ceramics. For details see the Journal of the American Ceramic Society (1, 1986) and the Japanese Journal of Applied Physics (6, 1986).

2) Murano from Sony discussed the addition of <2% Co to PbZrO_3 to improve its properties as a dielectric resonator. Conventional solid state reaction techniques were used. After some materials optimization and after using a disc of $\text{SrTiO}_3\text{-NiO-Nb}_2\text{O}_5$ in series with it, a relatively high microwave K (170) device with a Q of 1200 was obtained.

3) Sato from Oki worked on a complex rare earth, barium poly titanate composition that gave a slightly higher Q (1800) with about half the dielectric constant than the material shown by Murano. He claimed etchability as an advantage for electrode plating.

G. Anisotropic Materials

In addition to what is shown here, there is also an effort on anisotropic materials in Dr. Yamagida's lab (see below).

1) Kemora and Yamaguchi from Keio University used molten salt synthesis to make rod-like potassium-strontium niobate crystallites. The spontaneous polarization in these is parallel to the major axis of the rods and after extrusion these rods were quite well aligned. X-ray diffraction of sintered compacts shows consequently a very high degree of anisotropy. Similar techniques had been applied to barium titanate and gave there a 40% improvement in maximum d_{33} .

2) Nagata (National Def. Acad.) prepared an oriented $Pb_5Ge_3O_{11}$ type ceramic by adding silica to the base composition. During hot pressing first a glass is formed; this then recrystallizes with the C axis normal to the pressing direction. A highly anisotropic ceramic results with a maximum pyroelectric coefficient of $15 \times 10^{-2} \mu C/cm C$, about 3 times that found in calcium stabilized $PbTiO_3$. A g_{33} response as high as in PZT was mentioned.

H. Relaxors and Piezoelectric Materials

Here dielectric constant as well as anisotropy of the coupling factors is a desired parameter, similar to what is being investigated in the U.S. (i.e. at Penn State). In addition, previous Japanese work tends to indicate that perovskite lead zinc niobate could exhibit rather high piezoelectric activity.

1) Harmer reported on transmission electron microscopy of lead scandium tantalate and lead magnesium niobates samples. Superlattice reflections, indicating short range order of magnesium and niobium ions over small regions, were found, even in what were thought to be disordered materials. The electrostatic charge imbalance was said to keep the ordered domains from growing.

2) W. Schulze analyzed lead magnesium niobate with excess magnesia and found a high dielectric constant, even though the excess magnesia seems to be concentrated near the grain boundaries. An effect of the magnesia on the ordering of the PMN structure is suspected.

3) Inagaki from Marcon Electronics Corp. showed barium and titanium to stabilize the perovskite structure in lead zinc niobate. Barium stabilization has been published previously by Penn State workers.

4) Ichinose (Waseda University) added as much as 35 mole% calcium (as well as Ba and Sr) to PbTiO_3 and found a peak in the spontaneous polarization of 42 $\mu\text{C}/\text{cm}$ with a K_t of 55% and a curie point downshift of 400°C. The maximum K_E/K_p ratio was at 25% calcium. Nice work.

5) Sakata (Science Univ. of Tokyo) investigated lead zirconate-lead tin zinc niobates and obtained relatively dense samples, having dielectric constants below 400 and a significant anisotropy of the coupling factors. Their d_{33} values were near 42, d_{31} values about 8.5 and d_{15} values were near 150. The material seems to be an improvement over lead titanate for high frequency pulse applications.

6) Honda (Mitsubishi) inhibited the grain growth and increased the sinterability of sodium lithium niobate through the addition of 1/2% alumina. Dielectric constants of 110 and coupling coefficients of 42% seem to make also this material useful for high frequency pulse applications.

7) Tashiro (Nat. Def. Acad.) investigated piezoelectric and mechanical properties of lead bismuth sodium iron niobate-lead titanate solid solutions as a function of lead titanate content. The material has a significant anisotropy of its electromechanical coupling factor. The behavior is very similar as that of lead titanate ceramic sintered through doping with calcium, samarium or lanthanum. The author finds a close correlation between K_p and

the Poisson's Ratio. The problem of trying to relate a ratio to a constant is acknowledged. The author was probably not aware of previous work in relating the Poisson's Ratio to the K_p/K_c ratio.

I. Piezoelectric Transducers

Only little U.S. research on bending elements has been reported recently. Japanese work on this is reported in the following 3 papers:

- 1) Uchino from Sophia University presented the construction of a monomorph that used barium titanate reduced to a resistivity of about 10^8 OHM-cm. When coated with a surface barrier electrode, it showed as much as 100 μ m deflection with an applied field and it exhibited mechanical resonances that make it also useful for buzzer and pump applications. This was one of the more ingenious devices shown at this meeting.
- 2) Saki (Toyo Soda) also showed a Barium Titanate based monomorph. It was initially reduced to semiconductivity and was then partially reoxidized-in from the surface, in so as to get a conductivity gradient and thereby (with voltage) a bending moment. The processing used is very similar to that applied to a high voltage fine grain barium titanate, surface-barrier type capacitor.
- 3) Tamura at Sony Central Labs showed me a piezoelectric bimorph that utilized a rather complex lead bismuth nickel zinc niobium titanium zirconiate as the driving material. A "shim plate" between the two piezoelectric driving plates was made out of oriented carbon fibers. This carbon fiber plate has more than an order of magnitude anisotropy in its modulus. This removes the mounting constraint from the driver plate to become narrower as its length increases (because of its Poisson ratio). As a result of this, a 35% to 50% increase in bimorph deflection was claimed. This appears to be a well thought-out remedy to a not always recognized limitation of bimorph operation.

4) Kikuchi, an engineer at TDK, evaluated the acoustic response of honeycomb-shaped PZT material. He found the radial resonance reduced by a factor of 8 in magnitude. Harmonics of these are almost completely absent and the thickness resonance was reduced in frequency by almost 30%. There is furthermore no indication of thickness harmonics. Stiffness and Q are also less than in solid disks. The application of honeycomb-shaped PZT devices as effective underwater acoustic sources is under consideration.

5) M. Kahn (the author of this report) discussed preparation and performance parameters of PZT 5A with photolithographically defined ordered void structures. A hydrostatic sensing gain of $199 \text{ db} \pm 3.5 \text{ db}$ up to 250 KHz was shown. The factors leading to enhanced tensile fracture strengths and fracture energies of these were also discussed.

6) Takeuchi (Hitachi) evaluated the response of 1-3 PZT/polymer composites as a function of the PZT pillar size and volume fraction. Coupling factors (K_p) as high as 0.38 appear to make this configuration useful in the planar vibrational mode as well as in the flexure mode. The latter could find use in a lower acoustic impedance piezoelectric speaker.

7) R.E. Ault discussed design parameters for composite transducers that can lead to the suppression of lateral resonances. This is done by utilizing a super-lattice period in the composite that gives rise to wide, lateral frequency stop bands.

8) Jomura from Hitachi Metals discussed mechanisms for increasing the available strains in a ceramic, as for instance by volume changes caused by phase transitions. Transverse strains as high as 0.1% at 10 kv/cm were mentioned.

9) Abe from Toshiba discussed a polynomial expansion of the electric field in terms of the polarization, applied to determine the temperature coefficient of the electrostriction for a "modified lead zinc niobate ceramic".

J. Piezoelectric Applications

1) H. Kamata at Oki showed me an assembly line where they are making about 20,000 Sonoboys a year. A substantial fraction of the assembly is done by hand, even though they have some automated materials handling equipment. They use monomorphs as omnidirectional sensors. These consist of a thin ceramic disc mounted on a brass shim in an aluminum or plastic cup. This was used in addition to other, more conventional configurations. The specifications of 10 different types of sonoboys that they have made are attached. HQS 6B is presently the most popular type (70% of their output). The sonoboys I saw in assembly used a seawater actuated battery that was able to power the buoy for up to 8 hours (shorter times were programmable). The construction of the bimorph sensing element as well as of the sonoboy itself did not appear to be hardened for elevated pressures or for shock loads.

2) R. Ting reported on a 6 foot by 6 foot hydrophone array which was made up of 5 inch square elements of PVDF encapsulated in flexible polyurethane. The difficulty with this material is in its loss of piezoelectric sensitivity at 60°C, its low dielectric constant and in its planar anisotropy. He also mentioned VDF -TRFE copolymers that are relatively stable up to 85°C. He also discussed the performance of a 1-3 composite made by Plessy that was said to have a g_h as high as 40mVm/N with changes of only 3 db under static pressures to 35 MPa.

3) Two papers on piezoelectric ceramic actuators, one by Takahashi and another one by Yoshura (both from the NEC) described the advantages of a piezoelectric tape puncher in which small size actuators are mounted in close proximity: at

is relatively silent and with the inductive source described by Takahashi requires only little energy for operation.

4) Chubachi (Tohoku Univ.) continues to develop his line focus beam acoustic microscope. It tests local variations in elastic properties of a surface at 225 MHz. Significant differences in propagation velocity were shown across a PZT ceramic wafer. This is a sophisticated system that appears essential to make high quality surface acoustic wave devices.

K. Varistors

1) Matsuyama (Tayo Yuden) discussed electrical properties of strontium calcium titanate based varistors, indicating that lower oxygen pressure results in lower bulk resistivities. After indiffusion of sodium oxide this gives varistors with higher alpha at larger currents and therefore a larger surge energy absorbing capability.

2) TDK are also making varistors, both out of reduced and grain boundary oxidized strontium titanate as well as out of TiO_2 . It appears that the TiO_2 based varistors have about twice the dissipation factor of strontium titanate based devices below 2 KHz, but at higher frequencies their loss is significantly less.

3) An interesting varistor application is a washer like structure made by TDK with segmented electrodes. It is designed to be mounted behind and connected to the collector of fractional horsepower universal motors to suppress arcing and prolong brush-life. Only a very reliability conscious user of small motors could be expected to pay the required premium for such a feature.

L. Substrates and Mechanical Properties

1) Takahashi from Toshiba showed data on the use of yttrium oxide as a sintering aid in aluminum nitrate. Its quantity has to be closely controlled

but it is claimed if that the oxygen content kept below 1%, 2 to 3 times the thermal conductivity of aluminum nitrate that is hot pressed without a sintering aid can be achieved.

2) Nihara (Nat. Def. Akad) discussed strength and fracture toughness of CVD prepared silicon carbide. There was no glassy phase in the grain boundaries and as a result the material had good high temperature strength. The CVD process conditions were manipulated to generate multiple stacking faults and these faults were found to deflect cracks and increase fracture toughness considerably. Very significant work.

3) Yamamoto (Nat. Def. Acad.) determined stress magnitudes and anisotropies in various poled lead titanate and PZT compositions by measuring indentations crack lengths.

M. Photovoltaics

1) Uchino (Sophia Univ.) described a relay that was activated by the photostrictive effect in PLZT: light generates charges at the surface of a bimorph. The charge accumulation causes a photovoltage and the high d_{33} of the poled PLZT then causes strain and a deflection of the PLZT. This was used to operate a snap switch. Illumination of an oppositely poled PLZT strip causes an opposite voltage that can be used to reverse the switch action. The high device impedance causes it to require 2 sec to 100 sec for equilibration. The behavior is described graphically. A nice piece of device engineering.

2) B. Koepke reported on a study of PLZT compositions designed to obtain optimum light switching. He found the lowest switching levels with Zr/ Ti ratios of $< 65/35$ and with $< 9.4\%$ La.

3) A. Haertlig reported on photoconductivity in biased PLZT; When a voltage is used to close a PLZT shutter to (block) strong light, polarization at the

JAPANESE SONOBUOYS

TYPE	IIQS 3 D	IIQS 5 D	IIQS 5 E	IIQS 6 B	IIQS 1 2	IIQS 2 1 B	IIQS 2 1 C	IIQS 3 1 C	IIQS 3 2	IIQS 4 1
PURPOSE	JULIE JEZEDEL	DT	DEEP BT	JEZEDEL	DIFAR	REF JEZEDEL	MEASURE SOUND PROP	ECHO RANGING	CASS I	VLA JEZEDEL
SIZE	A	A	A	A	A	A	A	A	A	A
AVERAGE WEIGHT (KG)	6	6.5	7.0	6	10	6	6	10.5	17.5	10
MAX LAUNCHIAS (KNOTS)	250	250	250	250	300	250	250	250	250	300
LIGHT LIGHT	NO	NO	NO	NO	NO	NO	NO	YES	NO	NO
EYE MARKER	NO	NO	NO	NO	NO	NO	NO	NO	NO	NO
HYDROPHONE DEPTH (m)	20 OR 90	PHONE TO 457	PHONE TO 1219	20 OR 90	30 OR 300	20 OR 90	20 OR 90	20 OR 250	20 OR 450	20 OR 90, 30 OR 300
TYPE (HR)	1	1/10	1/4	1, 3 OR 8	1 OR 3	3	3	1/2	1/2	3
VERAGE RP POWER (WATTS)	3/4	1/4	1/4	3/4	3/4	3/4	3/4	1/4	1/4	3/4
NUMBER OF CHANNELS	31	31	31	31	31	31	31	12	31	31
S. TYPE	AN/SSQ 41A	AN/SSQ 36	—	AN/SSQ 41B	AN/SSQ 53A	AN/SSQ 57A	—	AN/SSQ 47B	AN/SSQ 50	—
NOTES				2500000 1000000						DEVELP.

electrodes causes then an internal bias, that changes the resultant shutter characteristics.

N. Modeling

1) Banno (NEK) elaborated on his previously introduced cubes model for voids in ceramics. He introduced a shape factor to describe voids that are isotropic only in the X-Y direction and calculates electrical, mechanical and piezoelectric properties for ceramics having porosities up to 15%.

Interesting correlations to experimental data are shown for conventionally pressed materials, assuming nearly round pores and for hot pressed materials assuming an X-Y diameter twice times the Z thickness. This model could be applicable to the determination of average pore shape.

2) Kagegava (Chiba Univ.) showed a technique for determining compositional fluctuations from the width of x-ray diffraction lines. The calculation is based on the differences in line width obtained from different lattice spacings. Very elaborate and very interesting.

III. Panel Meeting on Piezoelectrics

Professor Newnham did an outstanding job at initiating and encouraging discussion. It would be my recommendation though to try to schedule the panel in the future for the second or third day, so as to give the participants a chance to become better acquainted first.

1. There were some comments about making geometries with graded impedances, as one could get from filler concentration gradients in 0-3 composites.

2. PVDF material apparently has been a disappointment. Some of the shortcomings quoted concern its high output impedance, its large transverse response and its excessive flexibility that were quoted to give rise to noise.

3. There was some discussion about the d_{31} parameter to have imaginary as well as a real components: Positive d_{31} values were measured in lead titanate at certain temperatures. There was also some discussion on the contribution of the electronic structure to the high polarization and Curie point of this material. Its anisotropy is particularly useful in high frequency piezoelectric 1-3 arrays where the interaction between the individual elements in the transverse mode has to be minimized.

4. There was some discussion of the mechanisms that control the d_{31} parameter. One is the Poisson ratio of the material and another one is, caused by a high c/a ratio that can give rise to microcracks or microfissures that reduce the d_{31}/d_{33} ratio. Excessive poling voltages can do the same.

5. NEC was specifically quoted as having a strong position in the manufacture of low cost piezoelectric motors.

Hard piezoelectric materials with low hysteresis, low aging and high mechanical toughness are generally preferable for this application. In addition, a high Q increases the potential efficiency of the motor. This is critical in battery powdered applications. In addition one of course wants the highest possible strains. Ceramic compositions near phase boundaries look therefore most attractive, except that materials with strains in excess of 6% (i.e. Bismuth Ferrite) are self destructing. Another approach is the utilization of electrostrictive phenomena and consideration is being given to strain magnification through the preparation of non-homogeneous devices.

6) Apparently there is a direct inverse relationship of the coupling factor (K_T/K_p) ratio to the ionic size of dopants in lead titanate. Doping with gadolinium gives the highest and with lanthanum gives the lowest anisotropy. Cobalt doping is an exception, it gives a relatively high anisotropy for its ionic size.

IV. Visit to Dr. Yamagida's Laboratory at the University of Tokyo

Dr. Yamagida and his coworkers are involved in a variety of activities:

- 1) They are trying to raise the anisotropy of barium titanate made from fibrous precursors (Journal of the American Ceramics Society, April, 1985) by doctor blading, stacking and firing thick films.
- 2) One of Dr. Yamagida's main interests is the development of materials for sensing applications. The attached table summarizes some of his efforts in this area. Their work on porous zinc oxide is continuing with various electronic dopants so as to increase its sensitivity and specificity.
- 3) They have investigated the PTCR effect and lattice parameters in barium titanate doped with neodymium. They have verified self-compensation (occupancy both of barium and titanium sites) at neodymium concentrations above .15%. (Journal Korean Ceramics Society, 1985).
- 4) They have looked at additions of .5% to 10% of alumina to ZnO, to zirconia and to strontium chloride to increase the conductivities of these systems. The responsible mechanisms range from lattice substitutions in ZnO to interfacial ionic conductivity of alumina particles in strontium chloride, as well as in calcium fluoride and in barium fluoride.
- 5) They have a program evaluating conductivity and weight loss behavior of single oxide systems (rock salt structures) as NiO, MgO, and MnO and others that are amenable to modelling.

SENSOR CONFIGURATIONS

Sensitivity to	Material	Sensor Configuration	Operating Temperature	Sensitivity	References (1)
CO	CuO-ZnO	Mechanically contacting surfaces	260°C	$\frac{1.5 \times \text{current}}{\text{decade of PCO}_2}$	Chem. Soc. of Japan 4/86
CO ₂	Beta Al ₂ O ₃ bulk	one electrode coated with LiCO ₃	500°C	$\frac{40 \text{ mV}}{\text{decade of PCO}_2}$	J. Mat. Sci. 5/86
Reducing gases	ZnO	Porous body Pt impregnated	400°C	25% Res. change with 400 ppm C ₃ H ₈	J. Am. Cer. Soc. 1/85
Relative humidity	(Zn _{0.8} Ni _{0.22})O	Sintered body ZnO exsolved around NiO grain cores (2)	25°C	4 x wet/dry voltage	Chem. Soc. Jap. 6/85
Relative humidity	ZnO-(Ni _{0.97} Li _{0.03})O	Mechanically contacting surfaces	25°C	100 x wet/dry current	J. Am. Cer. Soc. 7/86

- (1) All co-authored by H. Yamagida
(2) 800°C for 336 hrs.

6) Kishimoto from this laboratory presented at the Toyama meeting an excellent piece of work on pure BaTiO_3 tapes, that had been mechanically compressed after burnout. He showed that after firing he obtained a relatively flaw free material, in which both electrical breakdown and mechanical bending test failures originated in the grain boundaries. This work had been preceded by high temperature breakdown studies in MgO . There they found localized thermal breakdown channels (similar to what we are seeing in PTCR devices) and also lower breakdown strengths in single crystals in the presence of dislocations. They found even lower breakdown strengths in polycrystalline structures (Journal of Material Science, 1985).

Professor Yamagida's group contains 30 people. They have constructed some relatively sophisticated systems for heat treating and testing of devices under complex conditions of gas composition and gas flow. They also have set up a rudimentary tape casting facility. They seem to be quite strong on equipment they put together themselves.

V. Plant Visits

1) At the central laboratory of the Sony Corporation, they showed feasibility of increasing the memory capacity of a laser disk memory by three orders of magnitude. This requires cooling the storage media to the temperature of liquid helium and frequency modulating the laser beam, allowing a read out at each spot at 1000 different frequencies. This is made possible by the different environments of neighboring atoms into which die molecules in the storage media are frozen. The exact frequency response of each die molecule is determined by the force field generated by surrounding molecules.

They also had an impressive array of CVD reactors, designed to control the gas flow so as to permit abrupt changes in the compositions of the deposited films. More informally we discussed technical information transfer:

They were not complimentary at all on the scope and quality of technical information from Russia or China. Information generated in the United States was quoted as being very useful but information generated in Japan was said to have even more engineering content and show more applied results than that generated in the United States.

2) At the TDK capacitor plants in Akita, Mr. Furukawa explained that they are mixing their raw materials in high speed, plastic coated, continuous flow, disk mills, with the material recirculated two or three times until the right particle size is measured (on a Leeds and Northrop microtrack). The material is then filtered and calcined in Saggars. At least for disk capacitor preparation the material is then spray dried.

They make 560 million disks a month. Thinner disks are made by punching sheets, heavier parts by rotary pressing. On the surface their in-line lead forming and disk assembly machines look very similar to equipment used more than 20 years ago in the now almost defunct U.S. disk capacitor industry.

Some changes included a novel soldering approach where-in only the leads were dipped into the solder pot and the solder ball that accumulated on each lead end was used to provide solder when sweating the leads to the disks. Two cleaning and coating stations were also included with each assembly machine. An automatic outline inspection machine using video cameras, was also used. The only significant amount of manpower in the whole line was at final packaging where the capacitors strips were respooled from the large wheels used in the line to small packaging wheels. At that location a girl inserted capacitors by hand into the empty spots on the belt where previously rejects had been pulled out by the test machines.

One reason for their success in building and maintaining their disk manufacturing operation is probably in their local customer base. Disk capacitors are largely used in the assembly of entertainment equipment, of which there is practically none left in the U.S. It appears though that history has come a full circle, insofar as part of the Japanese disk manufacturing operations are being transferred elsewhere. Not only due to lower labor costs, but also because the market for disk capacitors that has developed in other countries.

TDK are using 3 different methods for making multilayer capacitors: I was shown their most mature activity in which the dielectric as well as the electrode layers are laid down by screening. The latter operation plus the drying ovens as well as a return belt and the required substrate handling fixtures were all in one integral unit, better than 15 feet long. Because drying is required after each screening cycle, the output of each machine is relatively low. I saw 32 of these machines. They use one operator for each 4 machines. The operators (who are fully gowned for dust reduction) seemed to spend most of their time in cleaning screens from old set-ups and setting up for new configurations. As in most capacitor manufacturing there is a significant number of different parts that have to be made. The equipment looked very clean, seemed to be running very smoothly with lots of chrome plated and clean, painted surfaces in evidence. As in all manufacturing operations that I visited, everybody removed their shoes at the main entrance.

They used diamond wheels for dicing the green pads. This is slower but makes cleaner cuts than the blade dicing technique commonly used in the U.S. Automation of the dicing machines for X and Y cutting on the same machine was still being set up. There was no smell from their binder solvent recovery

operation nor from their burn-out ovens. They use 2 day air burn-out in ovens, similarly to what is practiced in the U.S.

Multilayer capacitor firing is done on zirconia slabs onto which the chips are loaded in a dense, single layer from an automatic loader. For termination of chips, I saw them using 4 U.S. made Palomar terminators. This was one of the few activities where there were a significant number of technicians attending an operation.

They had a room full of automatic chip sorting and testing machines. In another area there was a number of automated visual inspection machines, in which dual video cameras hooked up to a computer were utilized to automatically inspect the outline of chip solder coverage from each side. They use cartridges to feed the chips to and from the machine. Very low reject rates were observed in both operations.

TDK are also making a range of positive temperature coefficient products including a line of honeycombs. They are trying to introduce these in clothes dryers and mentioned also baseboard heater-type applications.

In the afternoon Mr. Furukawa and Mr. Yahagi discussed their development work on compositions and grain size control for internal barrier layer strontium titanate based dielectrics (via adjustments of stoichiometry) and also by additions of manganese oxide and of 10% calcium titanate. In addition they seemed quite concerned about factors leading to delamination in multilayer capacitor: They are using exclusively 100% palladium electrodes with high fired dielectric compositons. There seems to be an incipient development of silver bearing internal capacitor electrode systems. They showed TGA curves and suggested that the rapid weight loss at the temperature that the palladium oxide becomes unstable may be responsible for their delamination problems. They had evolved a thermal shock testing technique

which was said to be able to detect delaminated capacitors. They seem to be well aware of U.S. publications in this area. TDK seem to be relatively strong in equipment design, their engineering manager seems to be an expert in this area. They claimed to be able to sell chips at 2 yen each and make a profit. Their equipment was constructed like money was no object, with extended unattended operation to be one of the foremost design parameters. As noted, low output rates were compensated for by more machines.

In a different location (near Tokyo) TDK has a substantial operation manufacturing hybrid circuits. They were said to use 1 1/2 ton of silver paints a month and an unspecified amount of Birox resistor material from Dupont. Low frequency as well as microwave hybrids are made there in an automated assembly line. It was said to have 30 automatic screeners with parts handled in cartridges, permitting automatic loading and feeding into processing equipment and kilns. The majority of these hybrids was said to go into telecommunications applications.

3) Dr. Banno gave me a tour through the NGK Spark Plug plant. This facility is heavily automated: They have a substantial metal working plant in which relatively old German and American-made equipment is automatically making the metal parts for spark plugs. The material here is handled in bulk with manned fork lifts moving large containers full of small parts. In the plating operation and in the ceramic preparation and assembly plant, 90% or more of materials handling is automated.

Their alumina is wet milled and spray dried. The spark plugs are hydrostatically pressed, go through a curing cycle, are cut and ground to shape, fired, marked, glazed and fired again with very little human intervention in the process. Copper electrodes are used in the spark plugs,

and nickel plating is applied to the business end of the electrode to provide erosion protection. Talcum is used for sealing the electrode to the insulator. A significantly larger fraction of the machinery on the floor is dedicated to handling, moving and aligning the parts than to the operations themselves. It appears that careful design, construction and upkeep of such equipment is at least in part responsible for the Japanese productivity. I saw relatively old equipment running unattended, having a multitude of interlocks and safety switches monitoring its operation. Apparently mechanical linkages and relay logic were broadly used to program the equipment.

NTK (an affiliate) is marketing a wide range of "fine" ceramic products. They have a broad line of 455 KHz piezoelectric band pass filters and fm discriminators, 7-15 MHz frequency-control resonators and piezoelectric ceramic-metal, as well as ceramic-ceramic bymorph elements for audio tone generators. They also have an extensive line of piezoelectric ignitors. They also make a variety of piezoelectric transducers: Some are finished into hydrophones, others are assembled into transmitters in what appear to be both military as well as civilian applications. They are also making piezoelectric oil level detectors, engine knock sensors as well as both TiO_2 and zirconia oxygen-pressure measuring elements. They furthermore have an extensive line of alumina insulators, heater supports, thread guides, metallized substrates for microcircuit packages as well as silicon carbide cutting tools, bearing elements, compressor rotors plus a variety of ceramic parts for air-cooled internal combustion engines. They also showed me beta alumina, solid electrolyte batteries presumably designed for load leveling applications in electric power grids. Altogether a very respectable product line.

VI. Summary

A U.S. manufacturer would find it nearly impossible to make at a profit from a broad line of new devices with special materials, as I saw at NGK, without a more extensive and costly incubation time than is usually found acceptable. One has therefore to conclude that the Japanese implementation of some of these technologies is due to their use of other than early profitability criteria when they make decisions on the introduction of new products. The wide spread of their decision making process may contribute to this: a midlevel manager who (at least in Japan) is looking at a 15 year future with his employer, is more apt to take the long view than a senior executive who is concerned with the reaction of stockholders, most of whom may have only little longterm commitment to their corporation.

Notwithstanding a low unemployment rate, (by U.S. standards) there appears to be quite a sense of competition in Japan. It is not certain that people in Japanese industry work any harder than in the U.S., but Japanese professionals seem to be putting in longer hours. One cannot fail to be impressed by their factories. It appears that they have set out to do things the "right way" with a willingness to spend rather substantial amount of money to obtain properly designed manufacturing equipment. It appears that because of a conceived high labor cost (that still may well be lower than in the U.S.) the Japanese have improved their productivity by beating on banks and on machine designers in preference to beating on their production force:

They have automated many hard to mechanize materials-handling operations that manufacturers in the U.S. often find it more profitable to perform with manual labor. One is led to the conclusion that funds expended on equipment designers and model builders somehow carry much lower overhead adders than those expended for direct labor.

I saw numerous Japanese items that are sold in the United States at lower prices than in Japan. This would imply that at least in 1986 Japanese manufacturers and traders exported merchandise at significantly lower profit margins than were extracted from sales within Japan.

The support of advanced technologies by the Japanese government takes many forms; for instance as suitable sensors are being developed, their use is mandated universally, as for instance sensors for the presence of escaping cooking gas. Right now there seems to be some discussion on mandating the use of ceramic PTCR heaters instead of nichrome in laundry dryers and even in space heaters. The lower surface temperatures of PTCR heaters reduce the fire hazard posed by dried lint, paper scraps, etc. These applications have been considered in the United States more than 10 years ago but were rejected then, largely due to the high material costs. There are a number of Japanese manufacturers who have now built up a significant PTCR manufacturing capability and if the use of ceramic PTCR heaters is legislated, one could expect roughly a doubling in the tonnage of electronic ceramics produced in Japan (PTCR devices have a much larger mass than multilayer or even disk capacitors).

When looking at the scope of Japanese research, the breadth of their product lines (specifically in high tech ceramics) and at their investment in automation and materials handling, one is forced to conclude that many decisions on expenditures and investments are made with only small regard to the immediate return on the investment. One can easily infer that centralized funds are made available for the sole purpose of advancing technology and raising productivity. The government then has a vested interest in supporting the market for new products, i.e. by legislation or by policies that lead to increased exports. With the recent downturn in Japanese exports one can

expect increased encouragement of internal Japanese consumption. The decision to initiate for instance direct satellite broadcasting in Japan, has given rise to a considerable amount of activity towards the development and manufacture of microwave home satellite receivers: 10 GHz frequencies allow receiving dishes only a little above 2 feet in diameter and stable small resonators are needed for local oscillator frequency control. They are presently transmitting on two channels, giving excellent pictures. The use of even higher frequencies is envisioned. As noted, a significant amount of research in ceramic dielectrics is directly attributable to this decision.

Japan is still a land of contrasts. One sees people using abacuses, but in many areas one notices penetration of advanced technology in consumer areas which are more advanced than those found in the U.S: One sees for instance hand calculators with graphics programs and displays, pay television in the back seat of taxi cabs, computerized wake-up calls in hotels and other sophisticated consumer electronics. The quality of their train system has no equal in the U.S.

~~_____~~

~~_____~~

26P

JAN 14 1987₁

REPORT ON U.S.-JAPAN SEMINAR
ON DIELECTRIC AND PIEZOELECTRIC CERAMICS

R. E. Newnham
Materials Research Laboratory
Pennsylvania State University
University Park, PA 16802

My trip to Japan was very brief because of teaching commitments at Penn State. I spent just one week in Japan with air flights on two consecutive weekends. On Sunday, November 9 through Wednesday, November 12 I attended the Seminar at Toyoma, after which I visited N.E.C. on Thursday and spoke at the Satellite Symposium Friday.

I was favorably impressed with the quality of the Seminar on Dielectric and Piezoelectric Ceramics. The setting at Toyoma was conducive to extensive interaction between the U.S. and Japanese delegations. The auditorium at YKK was excellent and the meeting organizers (Prof. Yamaguchi and Dr. Freiman) did a fine job in selecting participants and laying out the program.

My only regret is that there were not enough U.S. industrial participants. About 80% of the U.S. delegation was from university and government laboratories, while 80% of the Japanese were from industry. This is not meant as a criticism of the selection process. I know that Dr. Freiman and Dr. Pohanka tried very hard to recruit more industrial scientists for the meeting. A change in policy involving guidelines for the meeting needs to be invoked before the next symposium. Both delegations should be more evenly balanced between industry, university, and governmental scientists.

In regard to the technical content of the meeting, it is difficult to comment on all the papers presented but I discuss a few highlights from the Japanese poster sessions in the following paragraphs.

CAPACITORS

Since the last U.S.-Japan symposium, several Japanese capacitor manufacturers have commenced production of MLC with base-metal electrodes. The papers by Kishi (Taiyo Yuden), Sakabe (Murata) and Fujikawa (Kyocera) described BaTiO_3 -based dielectrics modified by Sr, Ca and Zr. The presence of excess calcium in the titanium site seems to be critical in preserving high resistivity during firing cycles under low oxygen pressure. Capacitors meeting X7R and Y5V specifications are in production. One wonders whether or not copper electrodes will be used next.

MICROWAVE RESONATORS

Several papers describing microwave dielectric resonators were presented at the Toyama meeting. $\text{Pb}(\text{Zr,Ce})\text{O}_3$ ceramics developed by a team of scientists from Sony and Narumi China has an unusually high value of dielectric constant ($K \sim 170$) and electrical Q (~ 1200) at 3 GHz. The K value is about eight times larger than other resonator ceramics, allowing significant reduction in resonator dimensions. The use of antiferroelectric ceramics was anticipated by others but this is the first production lot.

The temperature coefficient is not quite as small as some dielectric resonators, nor is its Q as large as the $\text{Ba}(\text{Mg,Ta})\text{O}_3$ - BaSnO_3 ceramics reported by Murata. The dielectric constant of

this material is only 24.5 but the Q at 10 GHz is 20,000, a new record!

TRANSDUCERS AND ACTUATORS

Laser-induced chemically etching of PZT was demonstrated by Shiosaki and Kawabata of Kyoto University. This appears to be an extension of Susan Troler's work at Penn State on etched tape-cast transducers. Shiosaki showed a lot of interest in the paper she gave at the ISAF meeting in Lehigh, although he did not credit her work. By irradiating the ceramic in a cool etchant he greatly increased the rate of etching, which is a useful way of "customizing" the transducer design.

The two papers given by Uchino's group were excellent. The photodriven relay using PLZT ceramics produces deflections of more than 100 μm . A monomorph actuator using a ferroelectric semiconductor layer was also described. When a voltage is applied, the field builds up on the piezoelectric layer causing a sizable deflection of the bilayer device.

The green-sheet punch made by NEC was also impressive. More than 1600 holes per minute were punched by the piezoelectric actuator.

COMPOSITE PIEZOELECTRICS

Takeuchi (Hitachi Central Research Laboratory) described some experiments on planar mode vibrations of 1-3 diced PZT-

epoxy composites. Surprisingly large coupling factors of 35% were observed for samples containing 20 to 60 volume % PZT. The materials look to be useful for piezoelectric speakers and other flexure mode devices.

The paper by Varaprasad (Naval Dockyard, Bombay) was interesting. He has been experimenting with various polymer matrices for 0-3 composites. There were some unexpected changes in the polymer dielectric spectrum with and without PZT filler. It is not clear why the spectrum changes. Dr. Gillman gave an interesting poster on the composite hydrophones made by Plessey Australia. The sensitivity surpasses any other commercial hydrophone material.

NEC VISIT

On Thursday, November 13 I visited the Central Research Laboratories of Nippon Electric Research with Dr. Pohanka, Prof. Schulze, Dr. Haertling and Prof. Burton. The visit was disappointing in the sense that we were not shown the research laboratory or the pilot plant operation for integrated ceramics. Instead, we received a cordial welcome and taken to the showroom for electronic products.

After lunch there were talks by NEC scientists and the U.S. visitors. The NEC staff gave good reviews of recent progress on AlN substrates for high power transducers. Remarkable thermal conductivities are achieved with fully-dense aluminum nitride ceramics.

Dr. Utsumi went over the work on monolithic multicomponent ceramics (MMC). Considerable progress has been made since I last visited the lab in December 1985. At that time they had just announced the interstratified packages containing high-and low-permittivity tapes with screen-printed circuitry and ruthenium oxide resistors, a four-phase co-fired system.

Four new advances were reported during our visit: display panels, ink jet printers, UV curable dielectrics, and controlled space processing. Luminescent display panels make use of the high K layers in an MMC package. By placing a high permittivity layer just below the electroluminescent phosphor, considerable field enhancement and brightness is achieved. The phosphor display layer on the outer surface makes good use of the area cleared by burying capacitors and resistors inside the package.

Ink jet printers can also be added to the package. The miniature multilayer printers described at the Toyama meeting appear to be compatible with MMC technology. Symmetric electrode configurations were found to be superior to the one-sided arrangement reported earlier. With printers and display the MMC technology will find many additional applications.

Integrated ink jets make use of controlled space technology. This is a way of incorporating patterned channels and cavities inside ceramic bodies by utilizing shaped pieces of fugitive phase. The processing is similar to the porous PZT composites made at Penn State and NRL but extensive use is made of photolithography. This makes it possible to generate

intricate porosity patterns inside the ceramic without time-consuming processing steps.

The fourth advance is a UV-curable dielectric paste made from lead borosilicate glass and alumina powders embedded in an organic photopolymer matrix. Using patterned masks, it is possible to build complex 3-D circuitry with via holes as small as 40 microns.

MMC technology is advancing very fast at NEC.

My last day in Tokyo was spent at two meetings. At the request of Prof. Yamaguchi and Dr. Freiman, organizers of the Toyama meeting, Prof. Vest, Dr. Pohanka, Prof. Harmer and I spoke at a satellite meeting in Tokyo. The same day I took part in a second meeting with Japanese industrial and government leaders. The second meeting was organized by Dr. Shirasaki of the National Institute for Research on Inorganic Materials. There were no Japanese presentations at either meeting.

A Review of the 3rd U.S.:Japan Seminar
on Dielectric and Piezoelectric Ceramics

Prepared by

Walter A. Schulze

of

Alfred University

The following is a series of observations and highlights on the poster session and plant visitations resulting from this interaction. There is no attempt made to analyze the "big picture" concerning long range US or Japanese superiority in this market area except to reinforce the conclusion from the meeting four years ago. The Japanese companies appear to be committing a considerably larger fraction of their gross revenues into research and development than their US counterparts. It appears that the emphasis is still on development and that products are stressed considerably above understanding. My personal projection is that the Japanese industrial research and development is progressing more rapidly and is definitely ahead of their US counterparts. This is visually intensified by the willingness of Japanese companies to let their personnel publish.

The visitation to facilities represented a considerable change from four years ago. I understand that there were still some exceptions, but the visitations to NEC and Hitachi offered no observations of production, and in the case of NEC, not even viewing research facilities was permitted. This may be a response to the very limited number of tours offered to Japanese participants after the second US:Japan Seminar.

The principal question that must be addressed is if this seminar series is worth the expense? My feeling is that the answer is yes, if the goal is to expose a broader group of US workers to the progress of the Japanese than would normally exist and also foster knowledge of and interaction with the key Japanese workers in piezoelectric and dielectric ceramics. The interactions every two years serve a number of educational and social functions. They allow a broader view of the Japanese technology than most of us could afford to accumulate. This was most dramatic in the first seminar when the unanimous conclusion was that we were even further behind than we thought. The other educational benefits are the obvious lead time derived from presentations well before publication and the somewhat unpredictable flow of information during personal conversations. The social interactions between individual researchers allow the development of an understanding of why some of the work is conducted and how the results are derived. These processes are roughly construed as "reading between the lines", and in some cases, can add considerably to technical results. Other bits of technical information continue to flow throughout the years in the form of notes, Christmas cards, technical preprints, and exchange of

samples.

The above benefits are real and functioning for the University participants but are tragically lacking for most of our industrial friends since they chose not to participate. This may be attributed to their inability to fully participate in presentations and plant visitations due to corporate policy. This is also attributed to a few oversights as evident by the omission of Transelco. I personally feel saddened by the lack of US industrial participation but can offer neither reasons or solutions. If the Japanese industries withdraw in the same percentage, the series will become useless. An alternative to a formal series would be to make equivalent funds available to send small groups to selected Japanese conferences and trade shows with the purpose of gathering information, visiting facilities and developing personal contacts.

The following are comments and additional information on the posters presented at the seminar listed by day and number as given in the abstracts.

M-1

It is very nice that this paper is of US origin since it is one of the first demonstrations of electrically usable sol-gel derived ferroelectric film. The ferroelectric properties are comparable to bulk properties and the processing is compatible with Si substrates.

M-4

This paper represents the exploration of a different approach to the preparation reactive, high purity BaTiO_3 . The hydrothermal derived powder showed good sintering at 1200C and developed predictable dielectric properties without sintering aids.

M-6

This work was unknown to me and represents a significant advancement in the preparation of complex shapes and composites. The technique opens up many possibilities for the preparation of devices at higher frequencies (higher than are currently possible). The fact that this has already been shown to be useful on ferrites suggests that it may also be significant in producing micro and millimeter wave devices.

M-15

This is an important statement because of the tendency of workers to consider MLCs as purely electrical devices. Thermomechanical relations should be considered in any complete analysis.

M-16

As usual, Martin Harmer's observations continue to add to the understanding and confusion (things are more complex than we perceive) of relaxor dielectrics. I found the statement that he has observed differences in ordering near the grain boundaries particularly interesting since we observe ordering changes as viewed by the dependence of the dielectric constant on temperature. It appears the material formed later by the expanding grain boundary may be more ordered.

M-22

Yamashita's work demonstrates the continued progress made by many Japanese researchers on relaxor dielectrics. Conversations with the author indicate that this system is very convenient in that it can be modified (as with BaTiO_3) to fit many of the normal temperature classifications from a single base system.

T-1

I found it very interesting to see a group pursuing antiferroelectrics as a high K, high frequency dielectric. The losses should be much lower since the domain walls should not couple with field. This is similar to work started at Penn State 3 to 4 years ago.

All these microwave studies demonstrate the continued willingness of the Japanese to chase formulations on empirical grounds. The advances must be very expensive and show their resolve to dominate a specific market segment.

T-3

Dr. Wakino's group appears to be one of the few which has programs that utilize high frequency spectrographic analysis to project dielectric response and to approach the problem of a low loss in a high frequency dielectric in a scientific fashion.

T-4

Dr. Nishigaki's high frequency dielectric material, like his low frequency material, is extremely complex but works. This, again, suggests an intense empirical study.

T-18

Photostriction in its present form represents a laboratory curiosity. These interesting and obscure phenomena should be remembered to be considered for the odd application. What they do indicate is that Dr. Uchino is a very intelligent and imaginative worker with good industrial contacts. He will surely be one of the major players in Japanese ferroelectric research for the following decades.

W-4

It was rewarding to see the pressure stable hydrostatic response from the lead titanate based ceramic. A good test of the usefulness of this seminar series would be to see if Bob Ting's appeal for new hydrophone samples elicits a good response from the Japanese participants.

W-12

This device may or may not be important in its own right, but again shows the range of Uchino's interests and his industrial contacts.

Roundtable on piezoelectrics

Tuesday evening I attended the roundtable on piezoelectric materials and devices. The attendance was sufficient to fill the room with a few late comers having to sit away from the "Japanese" table. The following is most of the list of topics chosen by polling the participants; no information was recorded as to how many votes were for each topic.

1. Why does modified lead titanate have a low transverse coupling and what are the latest models?
2. What are the latest miniaturization techniques?

3. Is there any recent information on high displacement actuators?
4. A request for more information on piezoelectric motors and their applications.
5. What activates a high d coefficient in piezoelectrics?
6. How are d" and k" increased in porous material?
7. Are there any new composites with large hydrostatic response?
8. A request for discussion on the strong piezoelectric response of tungsten-bronze material.
9. A request for discussion of artificial symmetry.
10. What are the latest advances in thin film piezoelectrics?

My notes on the discussion are very broken, but the impression is still very clear that the roundtable was well attended, had good participation by both groups, and was definitely worthwhile. Probably more than half of the time was spent discussing the piezoelectric response of modified lead titanate. The discussion centered on trying to understand the recent Wersing model. As usual, there was a heated debate as to the role of microcracking in decoupling. The consensus still seems to be an admission that every piezoelectric ceramic has some microcracking, but it is not significant in modified lead titanate. There is still a strong interest in increasing the k of lead titanate.

Other observations are the following:

Americans do not generally understand piezoelectric motors, probably because we do not have the markets.

Laser enhanced etching may open new approaches to the fabrication of high frequency resonators.

There are now five manufacturers of 0-3 composite in Japan and it is

probably better than PVDF. Also, "someone" now has a 0-3 that works at 13 MHz. Ask Dr. Cross!

In conclusion, I felt that this roundtable was very helpful and would recommend this format for other meetings. One improvement would be the addition of a large writing area.

Company Visitations

I do not use the common term plant trips because I saw no manufacturing.

NEC

The NEC format was very disappointing, but we were treated very well. The principal interaction was 15 minute talks by both US and Japanese participants. All the technology discussed has, I believe, been previously presented before this meeting. I personally found three things very interesting.

There is a Canadian exchange student working at the NEC Central Lab. I believe he said he was from Dr. Sayers group.

The glass fluxed fully integrated interconnect substrates are impressive when you can actually handle them. When I asked about their availability, I was told that the technology was being transferred to production. I believe US schools and industry are just starting in this area (excluding IBM).

They have been working on combinations of antiferroelectric and relaxor ferroelectric materials for dielectric applications. The results look very similar to the PLZT work.

Hitachi Central Laboratory

The Hitachi tour was more interesting in that we were allowed to visit some research areas. I have only two observations that may be useful.

The high frequency 1-3 composites seem to be struggling for production level applications. The medical arrays do not seem to be significantly

superior to displace current technology, and applications such as speakers are only laboratory exercises. Also, the exhibit on 1-3 composites has been removed from the Hitachi Laboratory Exhibition Hall.

Hitachi has produced very good quality PbTiO_3 thin film epitaxed on SrTiO_3 single crystal. The Pt electrode strips disturb the crystallinity. When I asked why the SrTiO_3 was not reduced in an electrode pattern by local diffusion of dopant, they wanted to drop the subject and then admitted they had applied for a patent in that area.

TRIP REPORT

1986 JAPAN-U.S. STUDY SEMINAR ON
DIELECTRIC AND PIEZOELECTRIC CERAMICS, AND
RELATED LABORATORY VISITS, NOVEMBER 8-19, 1986

Donald M. Smyth
Materials Research Center
Building #32
Lehigh University
Bethlehem, PA 18015

THE THIRD U.S.-JAPAN SEMINAR ON
DIELECTRIC AND PIEZOELECTRIC CERAMICS, AND RELATED
LABORATORY VISITS, NOVEMBER 8-19, 1986

I. INTRODUCTION

This third joint seminar gave another outstanding opportunity to exchange information and ideas with our Japanese colleagues. The professional relationships developed during these three meetings have given valuable insight into the Japanese technical operation and planning. As in the case of the earlier meeting in Japan in 1982, this meeting offered the added attraction of visits to various laboratories and production facilities.

The seminar was again characterized by a Japanese delegation that was mostly industrial and a U.S. group that was almost entirely academic. The very meager participation by U.S. industrial scientists was extremely disappointing. The presentations reflected this imbalance in that the U.S. posters tended to be more basic. As before, I found the Japanese scientists very much interested in the application of our more basic approach to their problems. I was particularly interested in the development of multilayer ceramic capacitors (MLCs) with base metal electrodes (BMEs). I first heard about the work at Murata at the 1982 seminar, and at least three Japanese companies are now manufacturing these devices in significant quantities. In the larger sizes these capacitors have the potential for replacing solid tantalum capacitors for some applications. I have emphasized the discussion of this area in this report.

I am also interested in the progress in Japan in applying the principles of defect chemistry. While the group at Murata does this quite successfully in their work on dielectric compositions for BMEs, the effort at the National Institute for Research in Inorganic Materials (NIRIM) has its problems. I could not agree with the interpretations offered for any of the three separate projects described to me.

The visits to laboratories and production facilities were notable for their openness and candor. For example, we were given a very

thorough tour of Murata's main production plant for multilayer capacitors. The work in progress in various laboratories was discussed in detail, and while it is unrealistic to expect to learn about their latest hot ideas, the discussions were reasonably up to date. Questions about future directions and plans were not obviously avoided. I thought that this attitude was quite remarkable, and quite a contrast to the response of U.S. industry on the other side of this exchange. Frankly, I feel that I now know more about the Japanese ceramic capacitor industry than I do about the U.S. counterpart.

The Seminar and the visits were very well organized. The meeting facilities made available by YKK were outstanding. The cochairmen, Dr. Freiman and Professor Yamaguchi deserve congratulations for a very well-run meeting, and the Office of Naval research and Dr. Pohanka should be commended for their foresight in making these joint meetings possible.

The report is divided into two major parts: a section on the seminar presentations of particular interest to me, and the discussions concerning them; and a section describing visits to laboratories at Murata, NEC, NIRIM, and Sumitomo, and to the Murata multilayer capacitor plant.

II. PRESENTATIONS AT THE JOINT SEMINAR

M-20 Sakabe, Takagi, and Wakino
Murata

This was an update of the work presented at the 1982 Joint Seminar about a dielectric having the general formula $(\text{Ba}_{1-x}\text{Ca}_x\text{O})_m (\text{Ti}_{1-y}\text{Zr}_y\text{O}_2)$. The materials retained a high resistivity when fired in a reducing atmosphere compatible with Ni electrodes if $x > 0$ and $m > 1$. My suggestion at that time, that some Ca was then forced onto octahedral sites where it serves as an acceptor impurity, Ca_{Ti}'' , is now generally accepted.

Murata has been manufacturing these BME multilayers for 3 years and is now producing 20 million per month. They expect this rate to

increase substantially and are constructing a new building for this purpose (see Section III).

This start-up and rate of production is very modest compared with the predictions heard in 1982. The delay seems to have been caused by problems with the high temperature leakage current, and that has now been solved by the addition of a low temperature anneal after sintering. This application of basic defect chemistry reduces the oxygen-excess, p-type conduction caused by the high acceptor dopant concentration. This has now opened the way to a large market in the 0.1-100 μf range. It is only at 0.1 μf and above that the cost-saving in electrode metal is sufficient to justify the additional production costs of the BME process.

M-19 Kishi, Wada, Murai, Chazono, and Yamaoka
Taiyo Yuden

Taiyo Yuden is now producing 5 million/month of their own version of a BME multilayer. Their composition is described as $(\text{Ba}_{1-x-y}\text{Sr}_x\text{Ca}_y)(\text{Ti}_{1-z}\text{Zr}_z)\text{O}_3$, and an alkaline earth lithium silicate glass is added as a sintering aid. Contrary to the Murata approach, there is no attempt to make the ceramic composition rich in alkaline earths. Yamaoka indicated, however, that the Ca content is necessary, and the glass must contain alkaline earths. The result, I believe, is that the ceramic takes up additional alkaline earths from the glass phase, making it alkaline earth rich, and forcing some of the Ca onto the Ti-sites. Thus in a rather indirect way, a composition very similar to the Murata dielectric is achieved. The low firing temperature (1100-1200°C) makes it unnecessary to give these units a separate anneal to reduce the hot leakage.

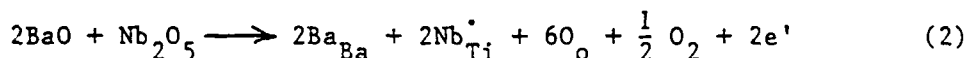
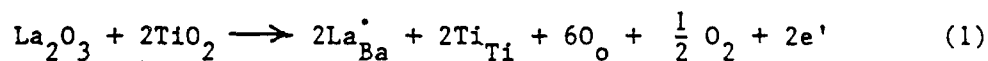
M-21 Fujikawa, Yokoe, and Hamano
Kyocera

Kyocera described their own version of a dielectric for BME multilayers and are apparently producing a few million/month. Their major dopants are MnO and Y_2O_3 . The MnO serves as a conventional acceptor dopant while Y_2O_3 helps to flatten the TC curve. The use of

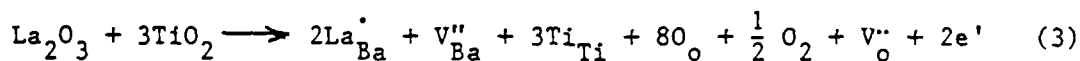
Y_2O_3 is a little tricky, as we have shown that Y can act as a Ba-site donor, Y_{Ba}^{\bullet} , in the presence of excess TiO_2 . That would tend to cancel out the acceptor effect of the MnO and could even lead to semiconduction, but it appears that their compositions contain more Mn than Y, so that there is still a net acceptor excess no matter where the Y resides.

W-21 Shirasaki and Haneda
NIRIM and TDK

This poster summarized Dr. Shirasaki's personal explanation of semiconduction in donor-doped $BaTiO_3$. This has been published before and is based on his assertion that the generally accepted model cannot explain some observed phenomena. The usual model is that the donor impurity substitutes for one of the host cations, depending on its size, and gives a positively charged impurity center that is compensated by free electrons



This is in agreement with a wide variety of experimental evidence. Dr. Shirasaki proposes that the donor centers are compensated by cation vacancies and that because this "loosens the lattice", a corresponding amount of oxygen is also lost leaving oxygen vacancies and electrons:



Available thermodynamic evidence does not confirm the "loosening of the lattice", and it is very unlikely that the system would choose to form so many more defects than necessary. Purported difficulties with the usual model can be traced to misinterpretations of published results. I believe that the proposed model is clearly incorrect.

III. PLANT AND LABORATORY VISITS

Murata: Tour of MLC Plant in Takefu

The capacitor division of Murata is known as the Fukui Murata Manufacturing Co., Ltd., and is located primarily in Fukui Prefecture near the Japan Sea north of Kyoto. Four major plants in that area produce ceramic capacitors of various types:

Takefu: monolithic chips, 1400 employees
Miyasaki: monolithic epoxy coated radial axial and molded types
(a "new" plant), 450 employees
Ozawara: feed through and wedge shapes, 100 employees
Shirayama: barrier layer, 230 employees

The Takefu plant produces 1.2 billion MLCs/month(!), mostly chips. They also produce 0.4 billion very small chips/month in a new plant in Izumo, further west along the coast. This plant is described as having twice the area of the Takefu plant. They also manufacture 0.4 billion MLCs/month in Singapore, and 0.6 billion discs/month at Yokaichi near Kyoto. The engineering staff in the three main Fukui plants totals 620, almost all college graduates. This includes a substantial number who design almost all of their product equipment.

Capacitor sales by Murata totaled \$322,000,000 in 1985, an increase of 40% over the previous year (!). This is 38% of total Murata sales. 39% of their total sales are outside of Japan; 17% go to North and South America. Murata claims to have 50% of the world market in MLCs.

On November 13, we toured the main MLC plant in Takefu. This is a very well maintained complex of about eight buildings. We were given a complete and open tour of all phases of the production process. Up to the firing step, everything was done under Class 10,000 clean room conditions. We could not enter these areas, but there were sufficient windows to give a good view.

There was nothing particularly remarkable about their production process; the procedures were quite traditional. It was all done, however, in a very neat and well-organized environment, and, of course,

on an enormous scale. As indicated earlier, they design and build most of their production equipment. I was particularly impressed by their test facility, where chips were being automatically loaded into each test stand at the rate of 5/second. Each chip is tested for capacitance, dissipation factor, leakage current at two voltage levels, and subjected to a flash voltage. They had 100 test stands giving a total capacity of 1.8 million chips/hour.

The BME units are fired in N_2-H_2 atmospheres with the oxygen activity being measured with zirconia sensors. They are constructing a new building that will be devoted to BME production. It appears that they will be producing about 100 million/month within 2-3 years. It is obvious that Murata is very serious about the BME market. They see these units in the higher capacitance range as low-cost replacements for solid tantalum capacitors.

BME capacitors are also produced by Murata-Erie in the U.S. Interestingly enough, they use a totally different composition that is not initially acceptor-doped. They fire near the Ni-NiO equilibrium condition with the result that some Ni is oxidized and dissolved into the ceramic where it becomes the acceptor dopant.

Murata feels that the more highly conducting Cu would be necessary only in high frequency NPO units. They are working on a $(Mg-Ca)TiO_3$ composition with a k of 20, but it is not yet in production.

They profess to have no reliability problems with the BME units, and expect that they will soon be able to guarantee a failure rate below 10 ppm/1000 hours. At that point customers will not need to use an incoming inspection test.

On November 14, we visited the Murata Research Laboratory at Nagaokakyo-shi, near Kyoto. Once again we had a very open tour and saw a very well-equipped laboratory. I was asked to give a presentation of the material included in my poster from the Joint Seminar.

My hosts for the Murata visit were Dr. K. Wakino and Mr. Y. Sakabe.

NEC: Visit to Research Laboratory

On November 17 we visited the Central Research Laboratories of NEC in Kawasaki City. The hosts were Drs. M. Yonezawa and T. Ohno. About

five months ago, a Materials Development Center under the direction of Dr. Ohno was formed separately from the Fundamental Research Laboratory. Dr. Yonezawa heads the Materials Research Laboratory in the latter organization. The organization and topics covered are summarized as follows:

A. Fundamental Research Laboratories

1. Exploratory

III-V compounds, molecular beam epitaxy
Bioelectronics
Ultrafine structures, focused ion beams
Computational physics and chemistry
Radiation sensitive organic materials

2. Semiconductor Research Laboratory

Si crystals
III-V crystals
Material and device process evaluation

3. Materials Research Laboratory (M. Yonezawa)

a. Electronic ceramics

i. Low firing X7R MLC composition

$\text{Pb}(\text{Mg}_{1/2}\text{W}_{1/2})\text{O}_3\text{-PbTiO}_3\text{-PbZrO}_3$, modified
with about 2 mol % $\text{Pb}(\text{Mn}_{1/3}\text{Nb}_{2/3})\text{O}_3$
to meet X7R

k = 2300

DF = 0.9%

IR = 3800 Megohm μF (25°)

1000 (125°)

Firing temp. 980°

No failures with 50 volts on 18 μm layers at 145°

Now moved to production (80 million/month)

ii. Ultrafine powders

RF plasma CVD

Nitrides (AlN), carbides, oxides

iii. New functional thin films

High thermal conductivity

diamond

amorphous carbon

Ferroelectric thin films

BaTiO_3

$\text{Ba}(\text{Ti}_{1-x}\text{Zr}_x)\text{O}_3$

PbTiO_3

PLZT

iv. Metals

Rapid quench

(Ta-W)-Si-B, Nb_3Ge high crystallization

temperatures for ICs, to survive processing

without crystallization

Artificial superstructure

Mo/Ni, Co/Cr, metal/insulation

B. Materials Development Laboratory (Ohno)

1st Development Department (Takahashi)

1. Optoelectronics

Laser hosts

Nd-YAG

$\text{Gd}_3\text{Sc}_2\text{Ga}_3\text{O}_{12}:\text{Nd,Cr}$

2. Piezoelectric devices

Sonar (broad band) for Mn modules

Multilayer actuator for ink jet printer head -

will be on the market soon

Ceramic filter for 1.544 Mhz. communication system

$\text{Sr}_2\text{Nb}_2\text{O}_7$ and $\text{Sr}_2\text{Ta}_2\text{O}_7$ single crystals. (This was of interest to me because we are studying the defect chemistry of these materials.)

2nd Development Department (Takamizawa)

1. Low firing multilayer substrates for high speed computers

Pb borosilicate glass: Al_2O_3 45:55 weight %

Firing temp. 900°

$k = 7.5$

DF = 0.3%

$\rho = 3 \times 10^{14} \Omega\text{cm}$

Strength 3000 kg/cm² ($\sim \text{Al}_2\text{O}_3$)

Thermal cond. 0.01 cal/deg cm sec ($< \text{Al}_2\text{O}_3$ but OK
for high speed computers)

Metallization: Au, Ag-Pd, Ag

2. Monolithic multicomponent ceramic substrate

Insulator - same as above

Dielectric: $\text{Pb}(\text{Fe}_{2/3}\text{W}_{1/3})\text{O}_3 \cdot \text{Pb}(\text{Fe}_{1/2}\text{Nb}_{1/2})\text{O}_3$

$k = 7000$

Resistor: RuO_2

Important to match the shrinkage, especially of
insulator and dielectric

Capacitance and resistance as an integral part of
the substrate

3. AlN

Multilayer structures with 3 metallized layers

C. Optoelectronic Research Laboratories

1. Basic OE Research

crystal growth and processing, quantum effect optical
devices

2. OE Device Research Laboratory

optical single-crystal devices for communication and
information processing

3. OE Equipment Research Laboratory

systems research lab

optical communication and switching

gas lasers

4. Display Device Research Lab

National Institute for Research in Inorganic Materials (NIRIM)

NIRIM was the first organization to be located in Tsukuba Science
City (1972), where 46 national laboratories and universities are

currently located, about 40 miles northeast of Tokyo. It is a major national laboratory, devoted mostly to research on ceramic materials. They work closely with industries, including a system for Visiting Research Officers, and their main goal is to transfer technology from the laboratory to an industry. NIRIM is one of six national research laboratories "attached" to the Science and Technology Agency that reports directly to the Office of the Prime Minister. A number of other laboratories are part of the Agency of Industrial Science and Technology, part of MITI (Ministry of International Trade & Industry).

NIRIM operates on a "group system". Groups are formed to attack a specific problem, usually for a period of five years. The project is then reviewed and either terminated or extended for a fixed period. Thus the staff is in a constant state of flux as groups are started up and terminated. The distribution of groups in 1986 is indicated on the following page.

My host was Dr. S. Shirasaki and we quickly agreed not to discuss the defect chemistry of perovskites because "we have a difference" (see the earlier discussion of paper W-21). Instead, I had technical discussions with four groups:

1. ZnO varistor. It was observed that ZnO doped with Li_2O is an insulator, while when doped with Al_2O_3 it is a semiconductor. This is exactly what is expected for a reduction-type semiconductor; Al is a donor impurity $\text{Al}_{\text{Zn}}^\bullet$ compensated by electrons. Once again, however, the semiconduction is attributed to a combination of oxygen vacancies and electrons. Actually the concentration of oxygen vacancies will be suppressed by donor impurities, since they are both positively charged.

2. Effect of impurities on the anatase-rutile transition in TiO_2 .

Dy, among others, was found to affect the transition temperature, and this was attributed to its presence as an interstitial donor $\text{Dy}_\text{T}^{\bullet\bullet}$. I would expect it to be a substitutional acceptor, Dy_{Ti}' , since that is a less highly charged defect.

3. Easily sintered perovskite. This was reported to be in use by 50 companies. The concept seems to be to accomplish a two-phase precipitation. For PZT, for example, a solution of Pb + Zr is precipitated with NH_3 to give PZ with residual Pb in solution. TiCl_4 is then added to precipitate PT. The mixture is calcined at $700-900^\circ$ to give a particle size of $0.02 \mu\text{m}$. When made in this way, PLZT can be sintered in air to transparency, and $\text{Ba}(\text{Zn}_{1/3}\text{Nb}_{1/3})\text{O}_3$ can be sintered at 1200° with near theoretical density being achieved at 1400° .

It is not clear to me how or why this works.

4. Electron microscopy. NIRIM has a very well equipped laboratory with very competent staff (Drs. Bando and Horiuchi). They have had a 1.25 MeV microscope for about 10 years. It has a resolving power of 1.6 \AA , and has been heavily used to obtain some excellent lattice images for a variety of materials. It is interesting to note that a 400 keV microscope that they have had for about 3 years (JEM-4000EX) gives equivalent results. We will be receiving a similar instrument (Phillips 430) at Lehigh in about four months.

Sumitomo Metal Mining - Ichikawa

My final visit was on November 19 to the Central Research Laboratories of Sumitomo Metal Mining Co. My host was Mr. Ko Takada, who had just returned after spending nearly two years in our laboratory. This is a very well equipped laboratory working on a variety of ceramics-related projects.

Mr. Nishii described the activities of the Applied Chemistry Team that is working on powder preparation and applications. They are investigating ceramics (Si_3N_4 , PSZ, ZrO_2), electronic ceramics (PZT Ba-ferrite), monodispersed spherical powders (TiO_2 , ZrO_2 , PSZ, SiO_2 , Ta_2O_5 , Nb_2O_5 $0.2-0.7 \mu\text{m}$), and ultrafine powders (Ta, W, Nb, Si_3N_4 , BN, borides, carbides). They use wet processes:

controlled precipitation and sol-gel, including multistage
precipitation (see visit to NIRIM)
hydrolysis of alkoxides

hydrothermal,
hybrid DC + RC plasma.

Mr. Nomura described his work on microwave ceramics. With the addition of 1% Mn, they can sinter $\text{Ba}(\text{Mn}_{1/3}\text{Ta}_{2/3})\text{O}_3$ to 98.47% of theoretical density. This gives a Q of 16,800 and k of 25 at 10.5 GHz with a temperature coefficient of 3 ppm/°C. Dr. Matsumoto and Mr. Hiuga described a rapid sintering process for BMT without addition of impurities. They lower the sample into the furnace at 1650° for 5 min. This gives a cubic structure without pyrochlore phase, although a small amount of $\text{Ba}_5\text{Ta}_4\text{O}_{15}$ is sometimes detected. An anneal in O_2 for 100 hours at 1450°C gives an ordered structure. Q goes up with density and ordering. They make about 100 units/month for special, high-priced applications, such as satellites.

PURDUE
UNIVERSITY TURNER LABORATORY FOR
ELECTROCERAMICS

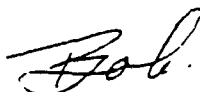
December 29, 1986

Dr. Stephen W. Freiman
National Bureau of Standards
Gaithersburg, MD 20899

Dear Steve:

Enclosed is my trip report for the Third U.S.-Japan Seminar
on Dielectric and Piezoelectric Materials. It was a long trip for
me but I feel it was worthwhile.

Sincerely,



Robert W. Vest
Turner Professor of
Engineering

RWV:t1e

Enclosure



A. A. Potter Engineering Center
West Lafayette, Indiana 47907

TRIP REPORT - Robert W. Vest

Third U.S.: Japan Seminar on Dielectric and Piezoelectric Ceramics.
November 9-12, 1986, Toyama, Japan

Summary and Recommendations

My overall impression was very favorable and I think this seminar should be continued. The primary benefits to the U.S. are in the contacts established between individual scientists, which will lead to closer liaison in the future; the technical aspects alone would not justify the expense involved. The hospitality shown the American attendees was outstanding, and we should try very hard to reciprocate in 1988.

The format of 4 minute presentations followed by the poster sessions worked reasonably well and I cannot think of a better way to handle that many papers. Certainly, there should not be parallel sessions. The conference organizers should try harder to get accurate information to the authors on the size of the posters; there was much more space available than we had been told. The program chairmen should also try harder to only solicit papers covering research done during the previous 2 years. For example, Banno's paper was essentially the same one he presented at Williamsburg in 1984. Some changes should be made if roundtable discussions are to be kept as part of the format. The one on Processing turned out to be a semi-circular table; it was only the American half that said anything. Perhaps it would help if one representative from each country prepared a short list of topics which he knows scientists from his country will address in order to get the discussion started.

We should seriously consider organizing a Satellite Symposium for scientists and managers from U.S. industry to follow the 1988 Seminar. If

done right, this could also get more representatives from U.S. industry to participate in the Seminar. The format of the Symposium in Tokyo on November 14, 1986 was good and should be followed, and we should treat the Japanese lecturers at least as well as the four Americans were treated this fall.

Technical Aspects

The majority of the materials and processing papers had been previously presented in more depth at other conferences, and so I saw very little that was new. Perhaps I attend too many conferences. I did get excited about some of the applications papers by the Japanese, particularly the session on actuators. Several of these contained ideas that were new to me; the monomorph structure discussed by the researchers at Sophia University and Toyo Soda (W-12 and W-15) was very intriguing. I was also struck by the absence of any U.S. papers in the actuator session, but I suppose this is a reflection of the lack of participation by U.S. industrial laboratories.

LIST OF U. S. PARTICIPANTS

Anderson, H. U.	University of Missouri-Rolla
Auld, B. A.	Stanford University
Brown, A. E.	Union Carbide Corp.
Buchanan, R.	University of Illinois at Urbana-Champaign
Burn, I.	E. I. du Pont de Nemours & Co.
Burton, L. C.	Virginia Polytechnic Institute and State University
Cross, L. E.	Pennsylvania State University
Diness, A. M.	Office of Naval Research
Dougherty, J.	Advanced Materials Technologies
Freiman, S. W.	National Bureau of Standards
Gillman, C. B.	Weapons Systems Research Laboratory
Haertling, G.	Motorola, Inc.
Harmer, M. P.	Lehigh University
Holman, R. L.	Battelle Columbus Laboratories
Kahn, M.	U. S. Naval Research Laboratory
Koepke, B.	Honeywell Inc.
Levinson, L. M.	General Electric Corporate Research and Development
Neurgaonker, R. R.	Rockwell International Science Center
Newnham, R. E.	Pennsylvania State University
Payne, D. A.	University of Illinois at Urbana-Champaign
Pohanka, R. C.	Office of Naval Research
Schulze, W. A.	Alfred University
Smyth, D.	Lehigh University
Ting, R.	U. S. Naval Research Laboratory
Vest, R. W.	Purdue University
Wright, B. G.	Office of Naval Research

LIST OF JAPANESE PARTICIPANTS

Abe, K.	Toshiba Corp.
Abe, K.	Sakai Chemical Industry Co., Ltd.
Adachi, H.	Matsushita Electric Ind. Co., Ltd.
Adachi, M.	Kyoto University
Aoki, M.	Sakai Chemical Industry Co., Ltd.
Baney, R. H.	Nagoya University
Banno, H.	NGK Spark Plug Co., Ltd.
Chubachi, N.	Tohoku University
Enomoto, T.	Central Glass Co., Ltd.
Fujikawa, N.	Kyocera Corp.
Hamano, F.	Kyocera Corp.
Hidaka, K.	Sakai Chemical Industry Co., Ltd.
Hikita, K.	Mitsubishi Mining & Cement Co., Ltd.
Hirano, S.	Nagoya University
Honda, T.	Mitsubishi Electric Corp.
Ichinose, N.	Waseda University
Inagaki, K.	Marucon Electronics Co., Ltd.
Igarashi, H.	National Defense Academy
Jomura, S.	Hitachi Metals Co., Ltd.
Kakegawa, K.	Chiba University
Kimura, T.	Keio University
Kishi, H.	Taiyo Yuden Co., Ltd.
Kishimoto, A.	University of Tokyo
Murata, K.	Hitachi Metals Co., Ltd.
Matsubara, S.	NEC Corp.
Mitsuyu, T.	Matsushita Electric Ind. Co., Ltd.
Murano, K.	Sony Corp.
Nagata, K.	National Defense Academy
Niihara, K.	National Defense Academy
Nishigaki, S.	Narumi China Corp.
Ogasawara, T.	TDK Corp.
Ohmura	Yoshida Kogyo K. K.
Okamoto, A.	TDK Corp.
Okazaki, K.	National Defense Academy
Sakabe, Y.	Murata Manufacturing Co., Ltd.
Sakai, N.	Toyo Soda Manufacturing Corp.
Sakata, K.	Science University of Tokyo
Sato, H.	OKI Electric Industry Co., Ltd.
Shiosaki, T.	Kyoto University
Sirasaki, S.	National Institute for Research in Inorganic Materials
Takabatake, M.	Asahi Glass, Co.
Takahashi, K.	Hitachi Ltd.
Takahashi, S.	NEC Corp.
Takahashi, T.	Toshiba Corp.
Takeuchi, H.	Hitachi Ltd.
Tamura, H.	Murata Manufacturing Co., Ltd.
Uchino, K.	Sophia University
Ueyama, T.	Hitachi Chemical Co., Ltd.
Varaprasad, A. M.	Sophia University
Wakino, K.	Murata Manufacturing Co. Ltd.
Wasa, K.	Matsushita Electric Ind. Co., Ltd.
Yamauchi, T.	Keio University
Yamamoto, T.	National Defense Academy
Yamamura, H.	Toyo Soda Manufacturing Corp.
Yamana, S.	Hitachi Chemical Co., Ltd.
Yamaoka, N.	Taiyo Yuden Co., Ltd.
Yamashita, Y.	Marucon Electronics Co., Ltd.
Yanagida, H.	University of Tokyo
Yano, S.	Narumi China Corp.
Yokoe, N.	Kyocera Corp.
Yoshiura, T.	NEC Corp.

END

11-87

DTIC